# Summarization and Interpretation of Historical Physical Oceanographic and Meteorological Information for the Mid-Atlantic Region

## Final Report to the Bureau of Land Management U.S. Department of the Interior

October 1977

**U.S. DEPARTMENT OF COMMERCE**
**National Oceanic and Atmospheric Administration**
Environmental Data Service
Center for Experiment Design and Data Analysis

# Summarization and Interpretation of Historical Physical Oceanographic and Meteorological Information for the Mid-Atlantic Region

## Final Report to the Bureau of Land Management U.S. Department of the Interior

### Interagency Agreement AA550-IA6-12

Robert G. Williams and Fredric A. Godshall
Eugene M. Rasmusson, Project Supervisor

October 1977
Washington, D.C.



**U.S. DEPARTMENT OF COMMERCE**
**National Oceanic and Atmospheric Administration**
Environmental Data Service
Center for Experiment Design and Data Analysis

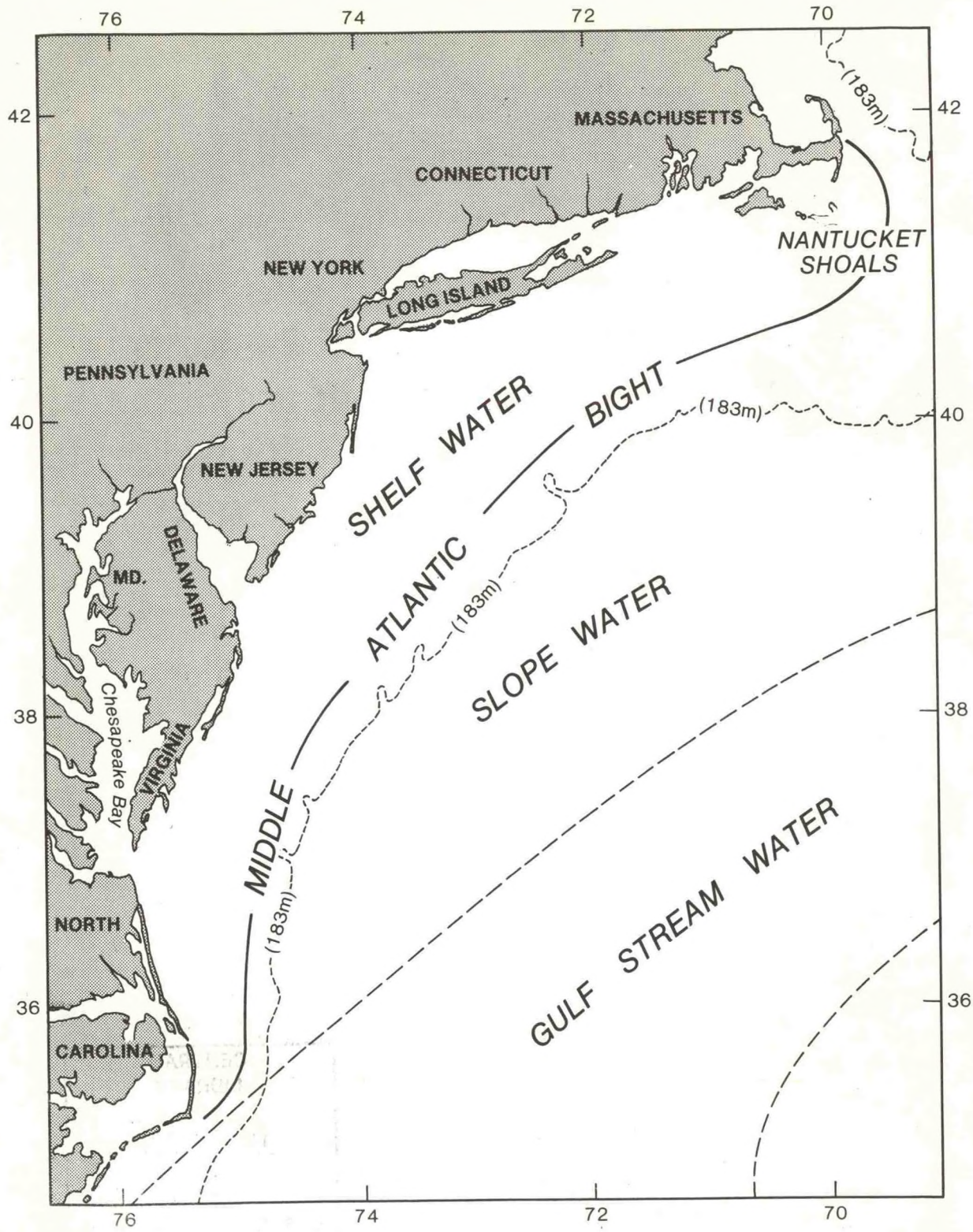
76
74
72
70
42
40
38
36
MASSACHUSETTS
CONNECTICUT
NEW YORK
LONG ISLAND
PENNSYLVANIA
NEW JERSEY
DELAWARE
MD.
VIRGINIA
Chesapeake Bay
NORTH
CAROLINA
(183m)
NANTUCKET
SHOALS
SHELF WATER
BIGHT
ATLANTIC
SLOPE WATER
MIDDLE
GULF STREAM WATER

## EXECUTIVE SUMMARY

This report describes the results of an environmental study of the Mid-Atlantic region of the Outer Continental Shelf performed under inter-agency agreement AA 550-IA6-12 between the Bureau of Land Management, U.S. Department of the Interior, and the Environmental Data Service, National Oceanic and Atmospheric Administration, U.S. Department of Commerce. The Mid-Atlantic region as defined for this study is the area extending northward from 38°N to 41°N between the coast and the 2,000 m isobath.

The study consisted of three tasks:

- To summarize historical meteorological and oceanographic data for the region.
- To analyze the historical data summaries.
- To draw conclusions from the analysis and to recommend design for future field programs to fill existing data gaps.

The meteorological data used were obtained primarily from the National Climatic Center, Asheville, North Carolina. They include National Weather Service coastal station records and standard shipboard marine surface observations, supplemented by ocean weather station and meteorological buoy measurements. Most of the oceanographic data were obtained from the National Oceanographic Data Center, Washington, D.C., with complementary data sets provided by private institutions.

### Meteorological Factors

The surface wind field, which affects the movement of spilled pollutants, as analyzed on the basis of passing-ship, or "Marine Deck," observations is similar to that documented in the literature. In winter, the mean flow over the Mid-Atlantic region is from the WNW-NW, with winds at around 7.0 to 9.0 kt; in summer, winds are from the SSW-SW at 3.3 to 4.5 kt. Variability of the surface wind, described in terms of wind "constancy," is highest during these two seasons. Comparisons with ocean weather station data and buoy measurements indicate that the Marine Deck observations may be biased toward low wind speeds on the order of 10 percent, and a comparison between these observations and coastal-station data showed that the latter wind speeds were generally 30 to 80 percent less than the wind speeds over adjacent ocean areas. A method is described by which adjustment factors can be applied to shoreline data to overcome these discrepancies, but a more reliable description of the land-sea differences will have to await the availability of data now being acquired by meteorological buoys deployed in the area.

Visibility is often restricted in early spring because of advection fog, but icing potential, i.e., ice accretion on ship superstructures, was found to be slight.

Adequacy of data. The Marine Deck observations are quite adequate for defining the major statistical features of the surface wind field, but better

estimates of extreme wind speeds and return periods depend on many more years of wind records or an improved statistical estimation method.

## Characteristics of Water Masses

Water masses, whose structure and variability are particularly relevant to the dispersion and advection of pollutants, were analyzed by dividing the Mid-Atlantic region into 12 areas of relatively homogenous water characteristics. Statistical summaries of water properties at various depths are presented for these areas and a quasi-objective analysis was done for a 1/2° grid covering the region.

In winter, water temperatures on the shelf are nearly uniform, at 5 to 7°C with a slight increase with depth. The shelf-slope water front, a major hydrographic feature in the region, is delineated by the 10°C isotherm. Warming begins in late March to April, leading to a weakening of horizontal gradients and the development of a seasonal thermocline, usually located at a depth of 15 to 25 m. Summer temperatures increase somewhat with decreasing latitude, but cold "winter" water still persists on the bottom. Salinity increases seaward, is highest in winter, and increases with depth in all seasons. As with temperature, the salinity distribution attains maximum vertical stratification in summer, when river runoff in the spring has had time to spread out over the shelf and lower near-surface salinity, while bottom salinity remains high. Temperature and salinity combine to enhance the vertical density stratification in summer, when density increases rapidly with depth because of lower temperature and higher salinity. The higher density in winter is controlled mainly by the increasing salinity gradient, which overrides the effect of the temperature gradient.

Water mass classification by quasi-objective analysis of temperature-salinity profiles shows that features indicative of major physical processes in the Mid-Atlantic region can be inferred from historical salinity-temperature-depth (STD) and Nansen cast data. The primary process is the shoreward movement of higher density oceanic water wedging itself beneath the near-surface seaward flux of fresher, lighter shelf water by advection and mixing. The magnitude of volume transport from these residual flows cannot, however, be estimated from the data available.

Dissolved oxygen and nutrient concentrations, which are important in evalutating potential degradation of ocean pollutants, shows dissolved oxygen concentrations to vary seasonally, with the water in the surface layer always being saturated and large vertical differences being found in the midshelf area. Low summer concentrations of dissolved phosphate are attributed to biological uptake; high winter concentrations to reduced biological uptake, aided by normal land and river runoff, which carries the phosphate concentrations into the shelf area. Runoff is also a significant factor in determining the silicate concentrations in the area.

Adequacy of data. Although the data base is in general adequate to document the seasonal means and variations on the space scale of the 12 oceanographic areas, they are not sufficient for an analysis on the scale of 1/2° squares. The following was also concluded from an evaluation of the data:

(1) The Marine Deck observations provide a good description of the temperature field.

(2) Mechanical bathythermograph (MBT) and expendable bathythermograph (XBT) data constitute the largest source of subsurface temperatures and are useful after careful editing, but the STD-Nansen cast data were used in most of the analyses because of their inherently greater accuracy.

(3) Salinity data for most of the Mid-Atlantic region cannot be used to reliably describe the physical processes taking place.

(4) The historical data base is of limited use in estimating mean seasonal geostrophic currents in the region. These could best be computed from the data on a cruise-by-cruise basis, rather than from seasonal averages.

(5) Data on dissolved oxygen and nutrient concentrations allow delineation of differences only in terms of the winter and summer seasons, and are not adequate for establishing a benchmark of water quality with which future water quality measurements could be compared.

## Circulation Patterns

Surface currents, which act directly to advect and disperse pollutants, were analyzed from ship-drift data, and current vectors and variability statistics were computed. Mean southwesterly flow on the order of 5 cm/s (0.1 kt) was found to occur parallel to the coast during all seasons. Seasonal variability was found to be not as pronounced as variability reported in the literature from surface-drifter studies. Recent evidence from direct current measurements indicates that the variability may, indeed, be small. The ship-drift observations do not, however, show the uniform increase in mean current strength with distance from the coast inferred from surface-drifter statistics and current-meter measurements.

Subsurface currents were analyzed from current-meter records, which showed that (1) mean subsurface current components are of the same order of magnitude as those derived from ship-drift data; (2) variability is much larger than the mean value; (3) maximum subsurface currents are generally an order of magnitude larger than the mean vector magnitude; (4) the most frequent values of subsurface current speed are larger than the mean vector magnitude; (5) semidiurnal tides are a major component of the current close to shore, decreasing in magnitude rapidly with distance from the coast; (6) inertial currents appear prominently in shallow, nearshore areas, in contrast to results reported in the literature; (7) under conditions of strong vertical gradients, bottom currents are often decoupled from surface currents; and (8) most of the energy occurs at subtidal frequencies in the midshelf and outer shelf areas.

Adequacy of data. The ship-drift data base was found to be a good source of data for study of seasonal mean surface currents at 1/2° resolution, but the number of observations is insufficient for generating reliable monthly summaries. The number and duration of direct current measurements are

inadequate for accurate determination of the time and space scales of motion in the region, except in the New York Bight apex.

## Vertical Mixing

Vertical mixing is strong in winter, when nearly homogenous water is found from the surface to the bottom. Seasonal warming that begins in spring and, in some nearshore areas, surface layer intrusion by river flow and land runoff create vertical density gradients that inhibit vertical mixing in late spring and summer. Hence, there is a barrier to vertical mixing in summer, although even under these conditions vertical current shear and turbulent flow fields associated with internal gravity waves can produce some mixing.

Adequacy of data. The historical data base is useful for indirect assessment of seasonal mixing patterns from temperature-salinity characteristics and mean vertical density profiles, but it is inadequate for direct study of dispersion of pollutants on time scales of days to weeks.

## Ocean Waves

The seasonal wave climatology compiled from visual shipboard observations shows that sea states in the Mid-Atlantic region are maximum in winter and minimum in summer. Strong northwest winds in winter produce waves that increase in height and length with distance from the coast. Weak southwest summer winds produce a predominant southwest direction for ocean waves, with heights and periods again increasing with distance from the coast. The relative frequency of high waves from the east is lower than expected, while extreme wave height as estimated in this study are thought to be too high.

Adequacy of data. Biases and errors in shipboard observations are often found in the published literature, but comparison of these observations with published lightship statistics and coastal wave measurements revealed no differences directly attributable to shipboard observer errors. These data were found to be useful for a general description of "typical" wave contitions. Return periods of extreme wave heights cannot be estimated reliably, however, without an adequate storm climatology for the Mid-Atlantic region and a wave hindcasting model that includes the effects of refraction and limited fetch.

## Conclusions and Recommendations

The oceanographic data base currently available is insufficient for reliable analysis of the variability of motion and mixing at the small time and space scales needed for further development of pollutant trajectory prediction models. A primary task in such modeling efforts is to identify and estimate the relative magnitudes of the atmospheric forcing functions and the magnitudes and phase delays of the ocean response. Analysis of this forcing and the response of shelf waters should have highest priority, followed by similar analysis of the slope water, and of the exchanges between shelf and slope water and the associated dynamics of the shelf-slope water front.

To obtain the extended time-series data needed, a 5-year observation program is proposed, consisting of the deployment of meteorological-oceanographic buoys at fixed locations along the continental shelf, with oceanographic vessels to be used for servicing the buoys as well as for taking closely spaced hydrographic casts. The program should include intensive study of internal waves and mixing processes, and of the cross-shelf gradients and shelf-slope water interactions. Details of the observation program would be developed with the participation of individual scientists, who would take the responsibility for planning the various data analyses and specify the data requirements for these analyses.

ACKNOWLEDGMENTS

The authors are indebted to several staff members of the Environmental Data Service (EDS) in the preparation of this report, particularly to the following: Jerome Ziemianski, who assisted in the data analyses and provided indispensable overall help in assembling the report; John B. Jalickee and Douglas Hamilton, whose asymptotic singular decomposition (ASD) technique was used in the water mass analysis; and to Donald T. Acheson and Thomas Carpenter, who provided advice and technical support in the analysis of current measurements. Helpful discussions were also held with Joseph Bishop and Robert Dennis of EDS and with Marshall Earle of the National Ocean Survey.

The oceanographic data summaries were produced by Gary Falk and his colleagues of the National Oceanographic Data Center, and the meteorological data were furnished by Robert Quayle and William Brower of the National Climatic Center. V. Goldsmith, E. P. Ruzecki, and C. Welch of the Virginia Institute of Marine Science, and staff members of the Woods Hole Oceanographic Institution, the Massachusetts Institute of Technology, and the Chesapeake Bay Institute provided valuable aid in some of the oceanographic analyses.

Acknowledgment is also due May Laughrun for editing and layout and Gloria Thompson and Clementine Edwards for typing the final copy.

CONTENTS

CONTENTS (Continued)

# 1. INTRODUCTION

Within the goals for marine minerals management of the Department of the Interior, the Bureau of Land Management is required to consider protection of the marine and coastal environment in submerged Federal land leasing. In order to meet this requirement, the Bureau of Land Management has established broad objectives for environmental studies programs (U.S. Department of the Interior, 1976) which include the establishment of a baseline for describing the existing physical characteristics of the marine environment and the capability for predicting potential impacts associated with hazards related to the exploration and development of petroleum and natural gas deposits. In partial fulfillment of these objectives, this report describes the results of environmental studies of the Mid-Atlantic region of the Outer Continental Shelf under Interagency Agreement AA 550-IA6-12 between the Bureau of Land Management, U.S. Department of the Interior, and the Environmental Data Service, National Oceanic and Atmospheric Administration, U.S. Department of Commerce. The Mid-Atlantic region of the Outer Continental Shelf as defined for this study is the area extending northward from 38°N to 41°N latitude between the coast and the 2,000 m isobath.

This report was prepared with the following objectives:

(1) To summarize historical meteorological and oceanographic data for the Mid-Atlantic region.

(2) To analyze the summarized data.

(3) To draw conclusions from the analysis and offer recommendations for future work.

The data used in producing the summaries were obtained primarily from the National Climatic Center and the National Oceanographic Data Center of NOAA's Environmental Data Service. Meteorological data used include historical records from National Weather Service coastal stations and standard marine surface observations from transient ships, as well as some meteorological buoy data. The main body of oceanographic data consist of salinity-temperature-depth (STD) and Nansen casts, supplemented by ship-drift observations and current meter records. The various types of data are described in section 2.

The surface wind field, which plays an important role in determining the movement of spilled oil and other pollutants, is dealt with in detail in section 3. Seasonal means and variability of surface winds are illustrated, a method is described by which coastal-station wind data can be adjusted to approximate conditions over adjoining ocean areas, wind trajectory patterns are calculated, and visibility restrictions and the potential for superstructure icing are discussed.

A major part of this report, section 4, is devoted to the physical characteristics of the water masses in the Mid-Atlantic region, whose structure and variability are particularly relevant to the dispersion and advection of pollutants. Since diffusion, mixing, and advection are seldom measured directly, the potential for these processes must be inferred from

analysis of such variables as water temperature, salinity, and density. The vertical density, which is dependent on temperature and salinity and which determines the rate of vertical mixing and momentum exchange from the surface, is considered in detail. In addition to an analysis of the surface and subsurface water temperature and salinity, data on dissolved oxygen and nutrient concentrations are presented, since these data are important for an evaluation of potential degradation rates of ocean pollutants.

Circulation features analyzed in section 5 include the mean surface current field and its variability, which act directly to advect and disperse pollutants; subsurface currents and their tidal constituents; and subtidal flows, which produce large water-mass transports. From these circulation features and from the water-mass characteristics, some inferences concerning vertical mixing are drawn in section 6. Ocean waves are discussed in section 7, which includes estimates of return periods of extreme wave heights in the region.

In the final section of this report, the data used are evaluated in terms of reliability and deficiencies and recommendations are made for the design of future field programs to fill existing gaps in the data needed for an adequate environmental assessment.

# 2. SOURCES OF DATA

## 2.1 Meteorological Data

The meteorological data used in this study were obtained primarily from the National Climatic Center (NCC), Asheville, North Carolina, and are described below. Other records for the area studied exist, but were not used. For example, additional data for the New York Bight have been prepared by NCC for the MESA New York Bight Project (Lettau et al., 1976), but these data are generally of lower quality; many are based on fragmentary observations or exist only in manuscript form.

Validation of the data received from NCC was limited to the following:

(1) Winds were checked for directions greater than 360° and for directions reported during calm winds.

(2) Extremely high wind speeds were checked against reported weather activity.

(3) Obvious errors in air temperature were deleted.

(4) Restricted visibility observations were checked against reported weather.

### 2.1.1 Coastal Station Surface Observations

These data are derived from routine hourly observations of surface meteorological parameters at the National Weather Service stations. They were provided by NCC in the form of: (1) hourly observations on magnetic tape for approximately 20 years, and (2) standard statistical summaries for the same time period. Statistical summaries were obtained for Nantucket, Massachusetts; Westhampton and Kennedy International Airport, Long Island, New York; Atlantic City, New Jersey; Dover, Delaware; and Norfolk, Virginia. Only the data from Westhampton, Kennedy Airport, and Atlantic City (table 2.1) were used in this analysis because of deficiencies in the other data records.

Table 2.1.--National Weather Service summary records used

| Station | Lat.N (deg) | Long.W (deg) | Time Period |
|---|---|---|---|
| Westhampton, L.I., N.Y. | 40.9 | 72.6 | May 1951 – Dec. 1969 |
| Kennedy International Airport, N.Y. | 40.7 | 73.8 | July 1948 – Dec. 1974 |
| Atlantic City, N.J. | 39.5 | 74.6 | Jan. 1945 – Dec. 1974 |

### 2.1.2 Standard Ship Marine Surface Observations

This data base, often referred to as the "Marine Deck" or "Tape Deck File 11," consists of observations acquired, over several decades, by ships in transit. From these data monthly statistical summaries were derived for 15 areas, roughly paralleling the coastline, which were chosen in order to estimate the horizontal gradients of meteorological parameters perpendicular to the coast (fig. 2.1.). Table 2.2 lists the number of observations used in deriving the summaries.

Table 2.2.--Ship observations used for climatological summaries

| Area | No. of observations | Area | No. of observations |
|---|---|---|---|
| 1 | 2,983 | 9 | 12,006 |
| 2 | 1,158 | 10 | 13,349 |
| 3 | 4,629 | 11 | 13,554 |
| 4 | 6,577 | 12 | 8,971 |
| 5 | 14,794 | 13 | 13,173 |
| 6 | 19,187 | 14 | 24,343 |
| 7 | 10,540 | 15 | 14,218 |
| 8 | 9,201 | | |

### 2.1.3 Ocean Weather Station "H"

Data obtained by a ship serving as Ocean Weather Station "H" at the following locations and over the following time periods were used in this study: (1) 36.0°N, 70.0°W, from May 1944 to April 1952; (2) 36.7°N, 69.7°W, from May 1952 to June 1954; and (3) 38.0°N, 71.0°W, from February 1970 to December 1975. The station was closed from July 1954 to February 1970 and during the 1970-75 summer seasons from April to August. Although these data fall outside the region of primary interest, they proved useful for comparison with other wind records, as discussed in section 3.1.2.1.

### 2.1.4 Meteorological Buoys

A limited amount of data was available from the meteorological buoys listed in table 2.3 and shown in fig. 2.1. The data from these buoys also were useful for comparison with other wind data.

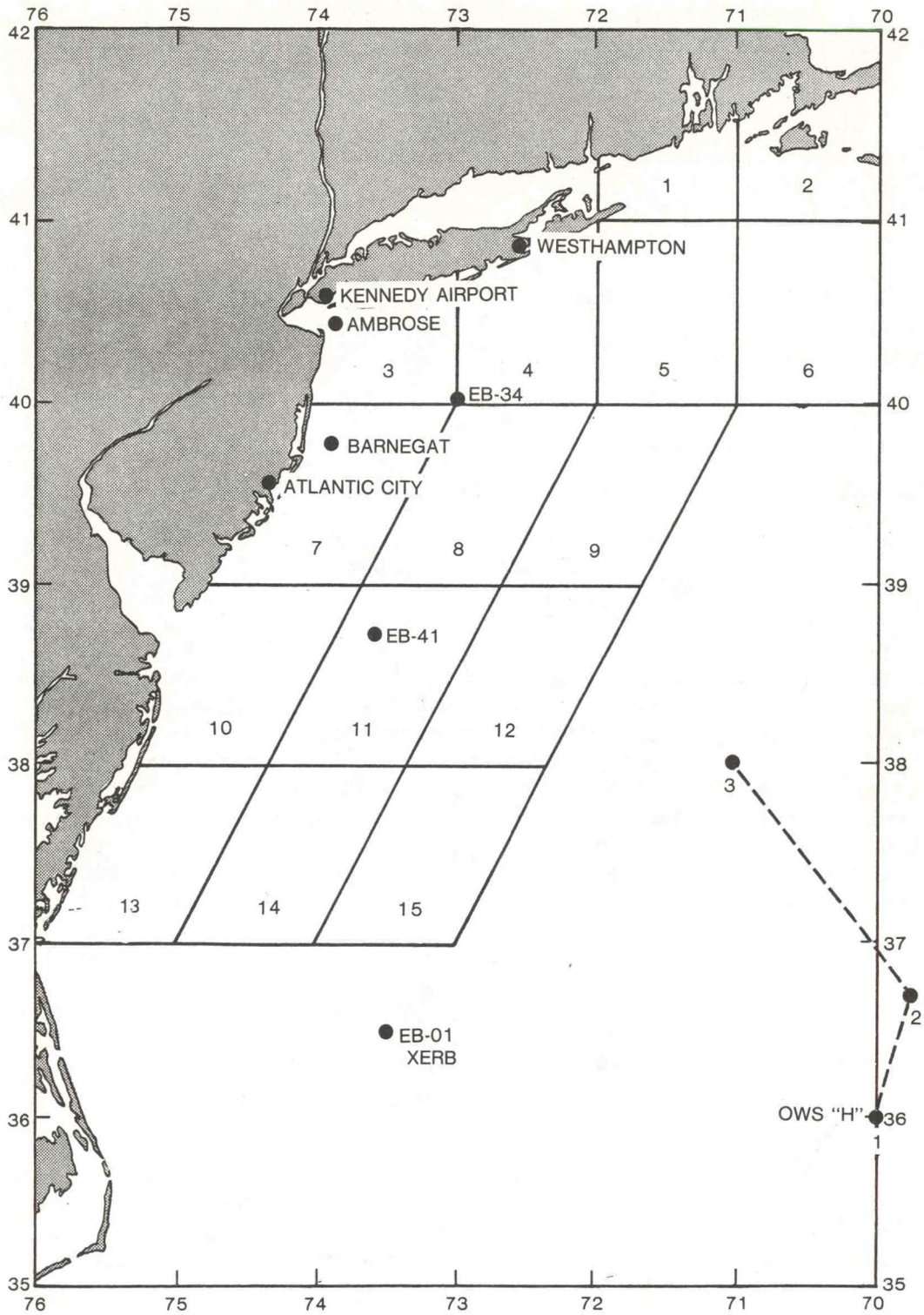


Figure 2.1.--Meteorological observation stations, instrumented buoys, and offshore areas used for climatological summaries.

Table 2.3.--Meteorological buoy data used

| Buoy | Lat.N (deg) | Long.W (deg) | Time Period |
|---|---|---|---|
| XERB | 36.5 | 73.5 | Feb. 1970 - July 1970<br>Sept.1970 - June 1972 |
| EB-01 | 36.5 | 73.5 | Oct. 1972 - Apr. 1973<br>Aug. 1973 - Mar. 1974<br>Dec. 1974 - Mar. 1975 |
| EB-34 | 40.1 | 73.0 | Oct. 1975 - Jan. 1976 |
| EB-41 | 38.7 | 73.6 | Oct. 1975 - Dec. 1975 |

## 2.2 Oceanographic Data

### 2.2.1 Data Used

The main body of oceanographic data used in this study was obtained from NOAA's National Oceanographic Data Center (NODC), Washington, D.C. The number, type, and time period of observations are listed in table 2.4. The NODC data were summarized over the areas shown in figure 2.2, which are irregular in shape and were tailored to the spatial distribution of distinctive water masses and to specific lease areas. Also used were two types of observations from passing ships provided by NCC: visual surface wave observations and sea surface temperatures. The latter data were summarized for the meteorological areas shown in figure 2.1.

At the inception of this study, approximately 2,500 salinity-temperature-depth (STD) and Nansen casts were available from the NODC archive. Subsequent efforts to supplement these data resulted in an additional 5,300 casts of temperatures and salinities. The ship-drift observations on file at NODC were compiled primarily from the extensive files at the U. S. Naval Oceanographic Office, but some data were obtained from the Netherlands.

A major source of data on surface and bottom currents is the surface and seabed drifter file at NODC. Comprehensive studies of these data in their original form have been made by Bumpus and Lauzier (1965) and Norcross and Stanley (1967), and it was therefore deemed sufficient for this analysis to review the work of these authors.

Subsurface current meter data are generally archived at NODC in the various formats in which they were submitted by individual investigators, which makes ready use of these data difficult. However, a considerable amount of these data put into a common format by NOAA's Marine Ecosystems Analysis (MESA) Program Office was used in this study.

Table 2.4--Oceanographic data for the Mid-Atlantic region available at NODC

| Observation system | No. of casts or observations | Measured quantity | Expected accuracy | Remarks |
|---|---|---|---|---|
| Mechanical bathythermograph (MBT) | 28,000 | Temperature (T) | On the order of ± 0.5°C and ± 3 m | Cover period 1944 to present; accuracy highly dependent on calibration methods and handling; being replaced by XBT. |
| Expendable bathythermograph (XBT) | 10,000 | Temperature (T) | ± 0.1°C<br>± 2 m | Cover period 1962 to present; repeatability of the digitized XBT record is ± 0.2°C and ± 2 m. |
| Nansen cast | 7,764 | Temperature (T)<br>Salinity (S)<br>Oxygen ($O_2$)<br>Nitrate ($NO_3$)<br>Phosphate ($PO_4$)<br>Silicate ($Si O_3$) | ± 0.02°C<br>± 0.02%<br>± 0.04 ml/l<br>± 5%<br>± 10%<br>± 8% | NODC does not distinguish between temperatures and salinities from Nansen casts or from STD sensors. |
| Electronic salinity-temperature-depth (STD) sensor | | Temperature (T)<br>Salinity (S) | ± 0.02°C<br>± 0.03% | Accuracies approximate; depend on manufacturer. |
| Subsurface current meter | 133 | Current speed (V)<br>Current direction (Θ)<br>Pressure (P) | ± 10%<br>± 5%<br>± 1% | Accuracies depend on manufacturer and mooring configuration; accuracies given here are for the Aandera meter. |
| Surface currents from ship drift | 75,661 | Ship drift | | Cover period 1850 through 1974; relies on large numbers of observations to reduce error. |

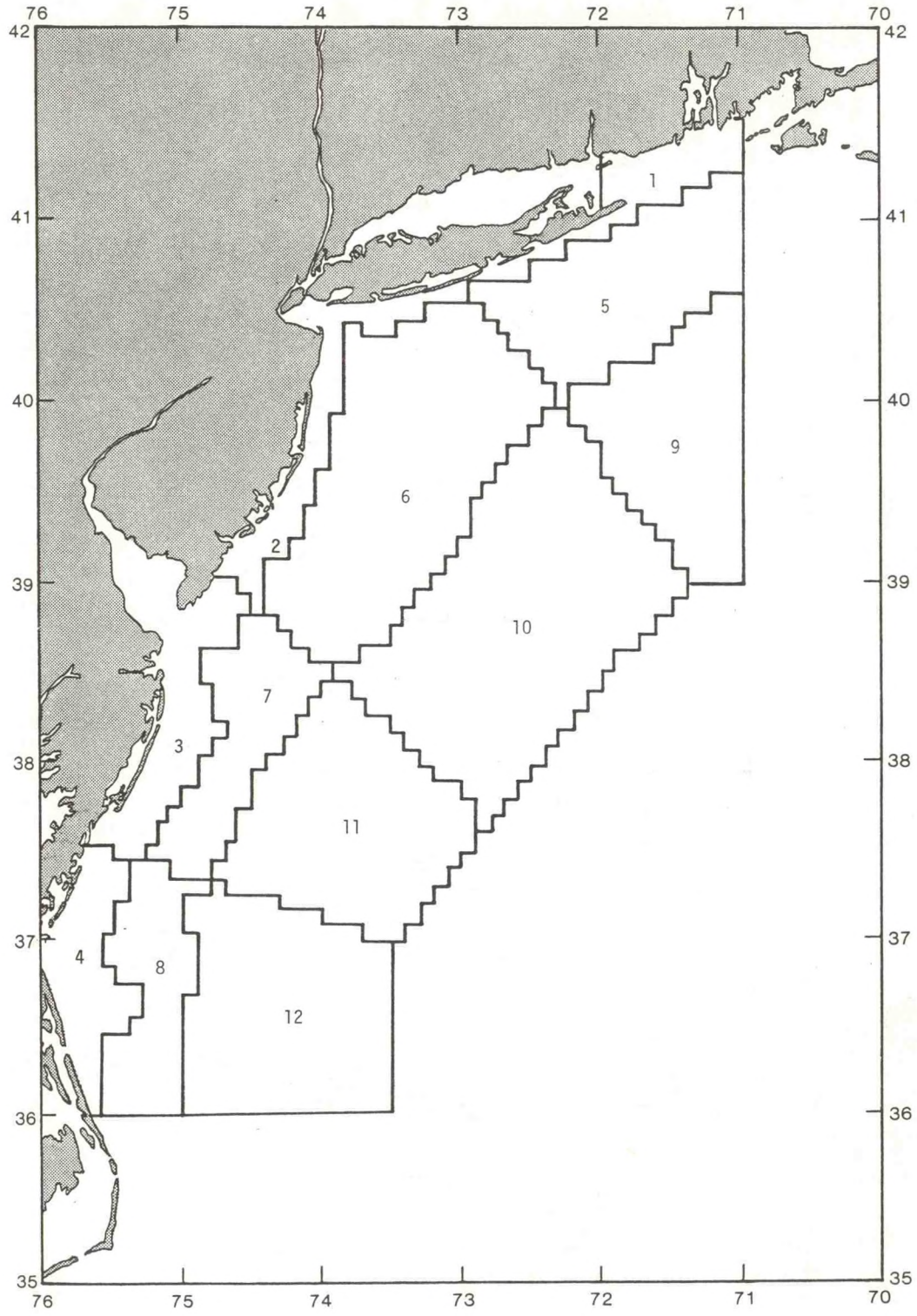


Figure 2.2.--Areas used for summaries of oceanographic data.

amount of these data put into a common format by NOAA'S Marine Ecosystems Analysis (MESA) Program Office was used in this study.

2.2.2 Data Not Used

Time was insufficient for acquiring and incorporating hydrographic (STD) and current meter data obtained by the Lamont Geological Observatory, current meter data acquired by the Chesapeake Bay Institute, and additional current meter data recently shipped from the MESA Program Office to NODC.

Surface wave data not used include the following:

(1) A large amount of data on the results of wave gage deployments along the U. S. east coast published by the Coastal Engineering Research Center (CERC) of the U. S. Army Corps of Engineers (Thompson, 1974). Extrapolation of these data, which were collected mostly from installations on piers along the beach, might provide a good basis for comparison with visual surface observations.

(2) Data on surface wave height and direction now becoming available through NODC from NOAA Buoy Office deployments of instrumented buoys in the Mid-Atlantic Bight. These data should prove a valuable addition to the data base.

(3) Surface wave measurements recently made and reported by the EG&G Corporation (1976) in connection with an environmental site survey of the proposed nuclear power plant at Atlantic City, New Jersey. These observations may be a good source for summarizing the wave climate in the area.

# 3. METEOROLOGICAL FACTORS

In the analysis of the meteorological data, answers were sought to the following questions:

(1) What are the general characteristics and seasonal variations of the surface wind field over the Mid-Atlantic region?

(2) How do the various sources of data describing the surface wind field yield comparable statistics? Can biases be identified and corrected for the various data sets? How useful are shoreline station wind data for describing the overwater wind field, and are they an adequate source of time-series data for overwater trajectory computations?

(3) To what extent can the distribution of extreme wind speeds be determined?

(4) What are the probabilities of various classes of visibility over the area?

(5) What is the potential for superstructure icing, determined as a function of meteorological parameters?

## 3.1 Surface Wind Field

Surface winds play a critical role in determining the movement of spilled oil and other pollutants in the marine environment. Through frictional drag, they have a direct effect on the movement of pollutants at the sea surface, and through the forcing of the current field over the shelf they play an important indirect role in subsurface transports.

The major source for surface wind data is the historical file of surface ship observations, referred to as the "Marine Deck" observations. These data were used to characterize the wind fields over the region, and the results are summarized in section 3.1.1. Section 3.1.2 gives the results of intercomparison studies of wind speed statistics from several different sources of data. The surface trajectory climatology, derived from coastal-station wind data corrected for the systematic bias between the land and sea wind statistics, are illustrated and discussed in section 3.1.3. Estimates of extreme wind speeds, as obtained from the Marine Deck observations, are presented in section 3.1.4. Visibility restrictions and icing potential are discussed in sections 3.2 and 3.3.

### 3.1.1 Seasonal Means and Variability

The salient features of the mean wind fields are illustrated in figures 3.1 to 3.4, which show the mean wind vector for each of the averaging areas for the four mid-season months.

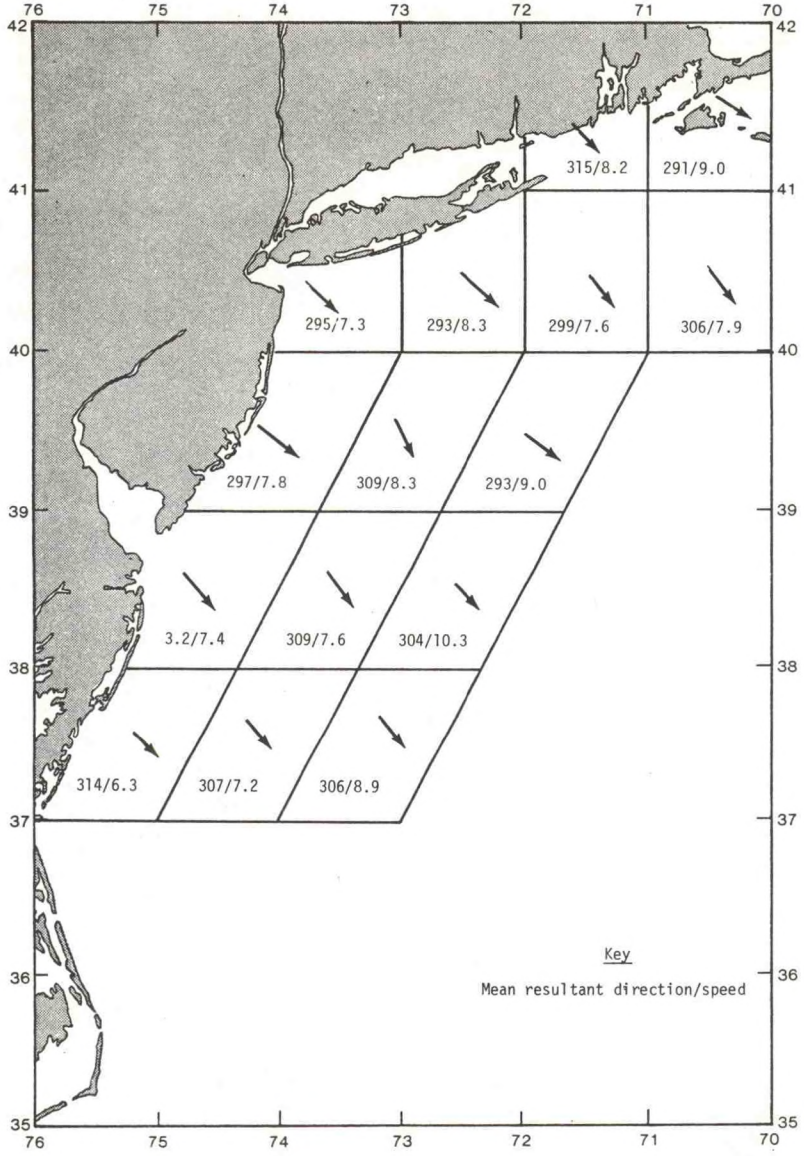


Figure 3.1.--January mean vector wind.

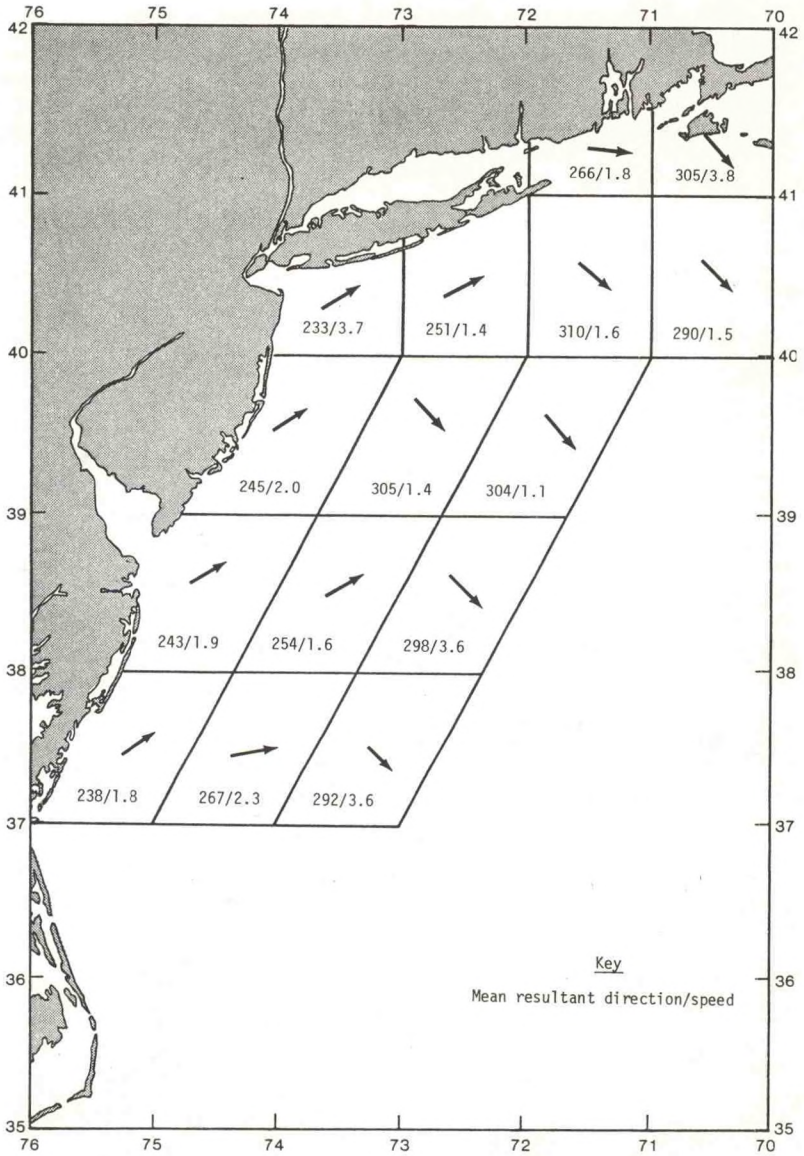


Figure 3.2.--April mean vector wind.

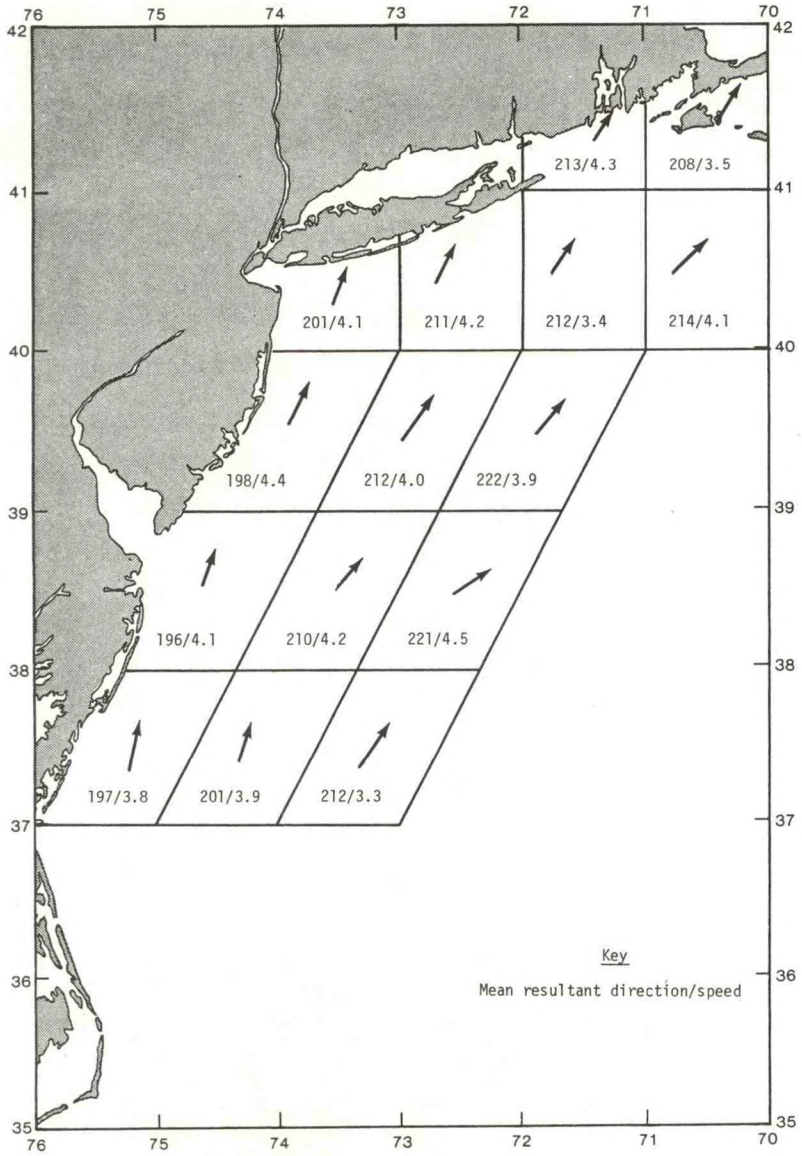


Figure 3.3.--July mean vector wind.

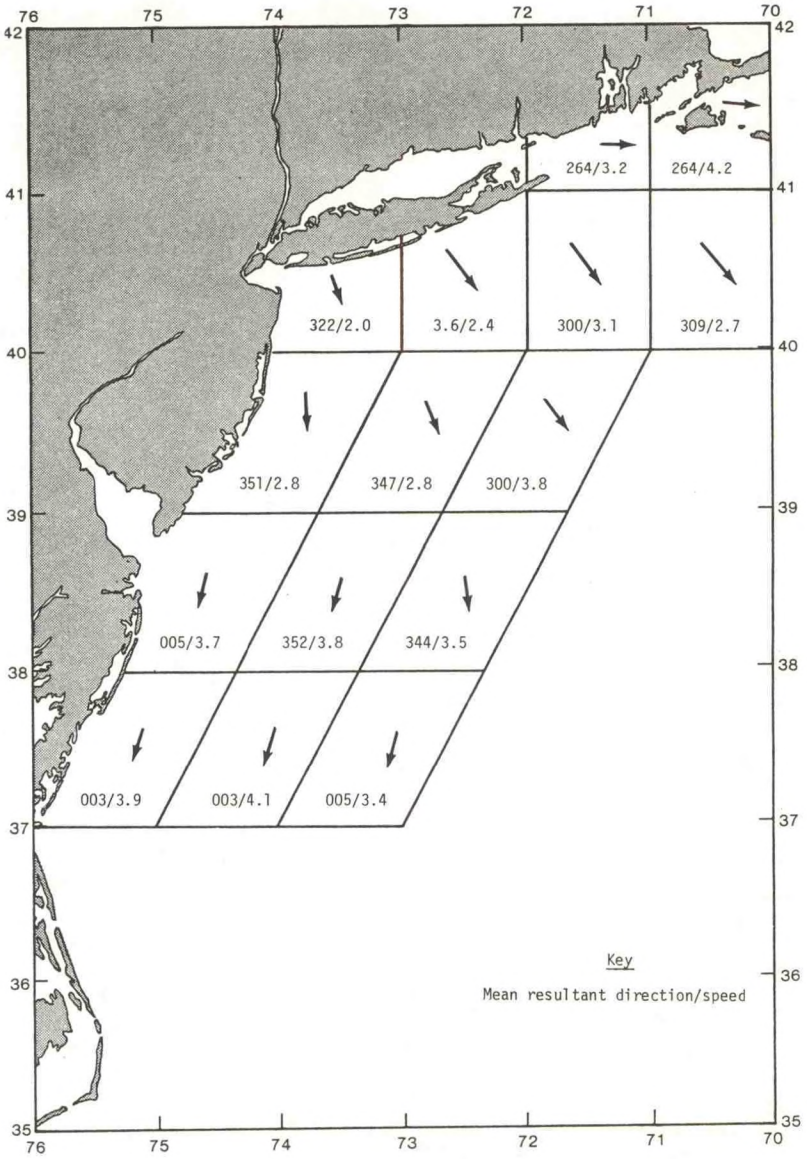


Figure 3.4.--October mean vector wind.

During January, the mean flow field over the North Atlantic is dominated by the Icelandic Low, with mean SW flow over the eastern North Atlantic and mean NW flow over the western North Atlantic. Thus, the January mean wind vectors over the Mid-Atlantic region (fig. 3.1) are from the WNW-NW at around 7 to 9 kt.

The July wind field (fig. 3.3) is in sharp contrast to that observed in January. The summertime Icelandic Low is greatly diminished in intensity and influences only the area north of about 55°N. The remainder of the North Atlantic is dominated by an expanded Bermuda Subtropical High, which results in SSW-SW flow over the Mid-Atlantic area. The April and October wind fields (figs 3.2 and 3.4) represent conditions during the transition seasons.

The variability of the surface wind is described in terms of the wind "constancy," defined as

$$C = \frac{\vec{V} \times 100\%}{\bar{S}} ,$$

where C is the constancy, expressed as a percentage, $\vec{V}$ is the vector mean wind, and $\bar{S}$ is the scalar mean wind speed. Constancy for each meteorological area for each mid-season month are given in table 3.1.

Table 3.1.--Surface wind constancy (%)

| Area | January | April | July | October |
|---|---|---|---|---|
| 1 | 50.0 | 13.5 | 41.7 | 23.0 |
| 2 | 57.3 | 26.8 | 36.8 | 29.4 |
| 3 | 47.7 | 29.4 | 40.6 | 15.4 |
| 4 | 48.8 | 10.8 | 40.4 | 17.6 |
| 5 | 42.7 | 12.2 | 34.7 | 22.3 |
| 6 | 47.0 | 12.3 | 48.8 | 20.3 |
| 7 | 49.1 | 16.3 | 42.3 | 20.4 |
| 8 | 45.6 | 12.0 | 37.0 | 19.2 |
| 9 | 51.1 | 9.2 | 38.2 | 26.4 |
| 10 | 46.5 | 15.7 | 39.8 | 26.8 |
| 11 | 44.2 | 14.0 | 40.4 | 26.4 |
| 12 | 54.8 | 24.0 | 40.9 | 24.3 |
| 13 | 40.9 | 13.4 | 35.2 | 28.1 |
| 14 | 43.4 | 17.4 | 35.8 | 29.5 |
| 15 | 50.0 | 24.5 | 30.8 | 23.9 |

As seen in the table, the constancy values are highest in winter (January average, 47.9). Summer is next highest (July average, 38.9). Values for the transition months are considerably lower, indicating more variable winds in the spring and fall.

Note that the mean scalar wind speeds for each of the areas can be computed from the values of constancy in table 3.1 and the mean vector speeds given in figures 3.1 to 3.4, i.e.,

$$S = |\bar{\vec{V}}| \times 100\%/C \quad .$$

The mean scalar wind speeds during the summer and winter are about 2 to 2.5 times the mean vector wind speed. In the fall, the mean scalar wind speed is around 4 to 5 times the vector speed,while in April, when the mean vector speed is lightest, the mean scalar speed is 4 to 10 times larger than the mean vector speed.

The consistency of these results indicates that apart from the possibility of systematic bias, which will be discussed in the next section, the Marine Deck observations available for the Mid-Atlantic region are quite adequate for defining the major statistical features of the surface wind field.

### 3.1.2 Intercomparison of Wind Data

The Marine Deck observations are widely used for meteorological studies over the oceans, but it is generally recognized that they may have certain deficiencies because (1) they are normally made by crew members who are not trained meteorological observers and for whom the observation routine often represents a diversion from their principal duties, (2) the sensors on the ship may be improperly exposed and maintained, and (3) the ships may systematically avoid areas of bad weather, e.g., high winds.

The large number of these observations, derived from different ships, and taken by different observers at different times, provides good reason to expect that averaging will eliminate most random errors. However, the possibility of a bias toward low wind speeds in these measurements remains. In an effort to determine whether a significant bias does exist, wind statistics obtained from the Marine Deck data were compared with data obtained from Ocean Weather Station "H" and from the meteorological buoy EB-01. These comparisons are discussed in sections 3.1.2.1 and 3.1.2.2.

Observations from National Weather Service coastal stations represent another potential source of wind data for describing conditions over the Mid-Atlantic area. Comparison of statistics derived from these data with those obtained for the nearshore areas from meteorological buoys and from the Marine Deck observations are described in sections 3.1.2.3 and 3.1.2.4, respectively.

3.1.2.1 Ocean Weather Station "H" - Marine Deck Observations. Wind observations obtained at Ocean Weather Station (OWS) "H" from May 1949 to January 1976 (25,071 observations) were compared with transient ship observations acquired within a 1° square centered at the nominal position of the ship "H." The results are summarized in table 3.2.

Table 3.2.--Comparison of frequency of wind speeds (%) observed at ship "H" with those computed from the Marine Deck data

| | Wind speed (kt) | | | | | | | | | |
|---|---|---|---|---|---|---|---|---|---|---|
| | 0-3 | 4-6 | 7-10 | 11-16 | 17-21 | 22-27 | 28-33 | 34-40 | 41-47 | > 47 |
| OWS "H" | 4.0 | 8.7 | 14.9 | 25.1 | 17.7 | 14.3 | 7.8 | 5.5 | 1.3 | 0.6 |
| Transient ships | 3.9 | 9.1 | 18.6 | 25.8 | 19.4 | 11.7 | 6.6 | 3.7 | 0.6 | 0.4 |

The mean wind speeds are 17.3 kt for ship "H" and 16.2 kt for the Marine Deck observations, with ship "H" reporting consistently greater frequencies of wind speeds exceeding 21 kt (29.6% vs. 23.8%). Ownbey (1975) in a similar study found that transient ships regularly reported higher wind speeds than ship "H" when the wind was less than 9 kt, and lower wind speeds when the wind was greater than 20 kt.

The mean wind speed differences (ship "H" minus Marine Deck) for the entire period is 1.1 kt. However, for the period before 1970, the difference is 1.3 kt, while the difference for observations since that time is 0.8 kt, suggesting a possible improvement in the transient-ship observations in later years.

3.1.2.2 Buoy EB-01 - Marine Deck Observations. The availability of a small amount of data recorded from October 1972 to March 1975 by meteorological buoy EB-01, located at 36.5°N, 73.5°W, allows further comparison with the transient ship wind data. The results are given in table 3.3. Because the buoy data cover a relatively short period, while the transient ship data were acquired over a much longer time, these results should be interpreted with some caution. Nevertheless, it is apparent that the differences in the distributions for EB-01 and the Marine Deck observations are quite similar to those found in the ship "H" - Marine Deck comparisons, with the buoy showing a higher frequency of wind speeds exceeding 16 kt.

Table 3.3.--Comparison of frequency of wind speeds (%) based on buoy EB-01 and Marine Deck observations (area 15)

| | Wind Speed (kt) | | | | | | | | | |
|---|---|---|---|---|---|---|---|---|---|---|
| | 0-3 | 4-6 | 7-10 | 11-16 | 17-21 | 22-27 | 28-33 | 34-40 | 41-47 | >47 |
| Buoy EB-01 (8,794 obs.) | 3.3 | 7.6 | 21.2 | 24.0 | 18.6 | 16.6 | 6.8 | 1.6 | 0.4 | 0 |
| Transient ships (14,236 obs.) | 6.3 | 11.3 | 23.1 | 17.9 | 15.9 | 9.0 | 3.8 | 2.0 | 0.4 | 0.2 |

More definitive results await the accumulation of longer records from EB-01 and other buoys recently deployed in the area, e.g., EB-41 (38.7°N, 73.6°W) and EB-34 (40.1°N, 73.0°W).

3.1.2.3 Coastal-Station - Buoy Observations. Systematic differences between the low-level wind fields over land and over adjacent marine areas create problems in the direct use of wind data from coastal stations to describe conditions over adjacent marine areas, but the lack of marine data from fixed observation platforms leaves little choice but to make the best possible use of the shoreline station data. For example, the direct computation of a surface trajectory climatology requires a long and relatively complete time series of wind observations, taken at intervals of a few hours. Such a time series cannot be derived from randomly distributed ship observations, or from the relatively short series of buoy data currently available.

Some indication of the systematic land-sea differences in wind can be obtained, however, by comparing the coastal station data with the buoy data now available. Figure 3.5 is a bivariate plot of wind speed frequencies based on simultaneous observations at Westhampton, Long Island, and buoy EB-34, located approximately 53 miles to the southwest, for October 1975 to January 1976. Figure 3.6 is a similar plot for Atlantic City, New Jersey, and buoy EB-41, approximately 77 miles to the southeast, for October to December 1975. The pattern of stronger winds over the water is apparent, with an average difference between EB-34 and Westhampton of 9.0 kt, and between EB-41 and Atlantic City of 8.4 kt. Less consistency was found in wind direction changes, with EB-34 showing a mean counterclockwise shift of 12° from the direction at Westhampton, and EB-41 showing a mean counterclockwise shift of only 0.7° from the direction at Atlantic City.

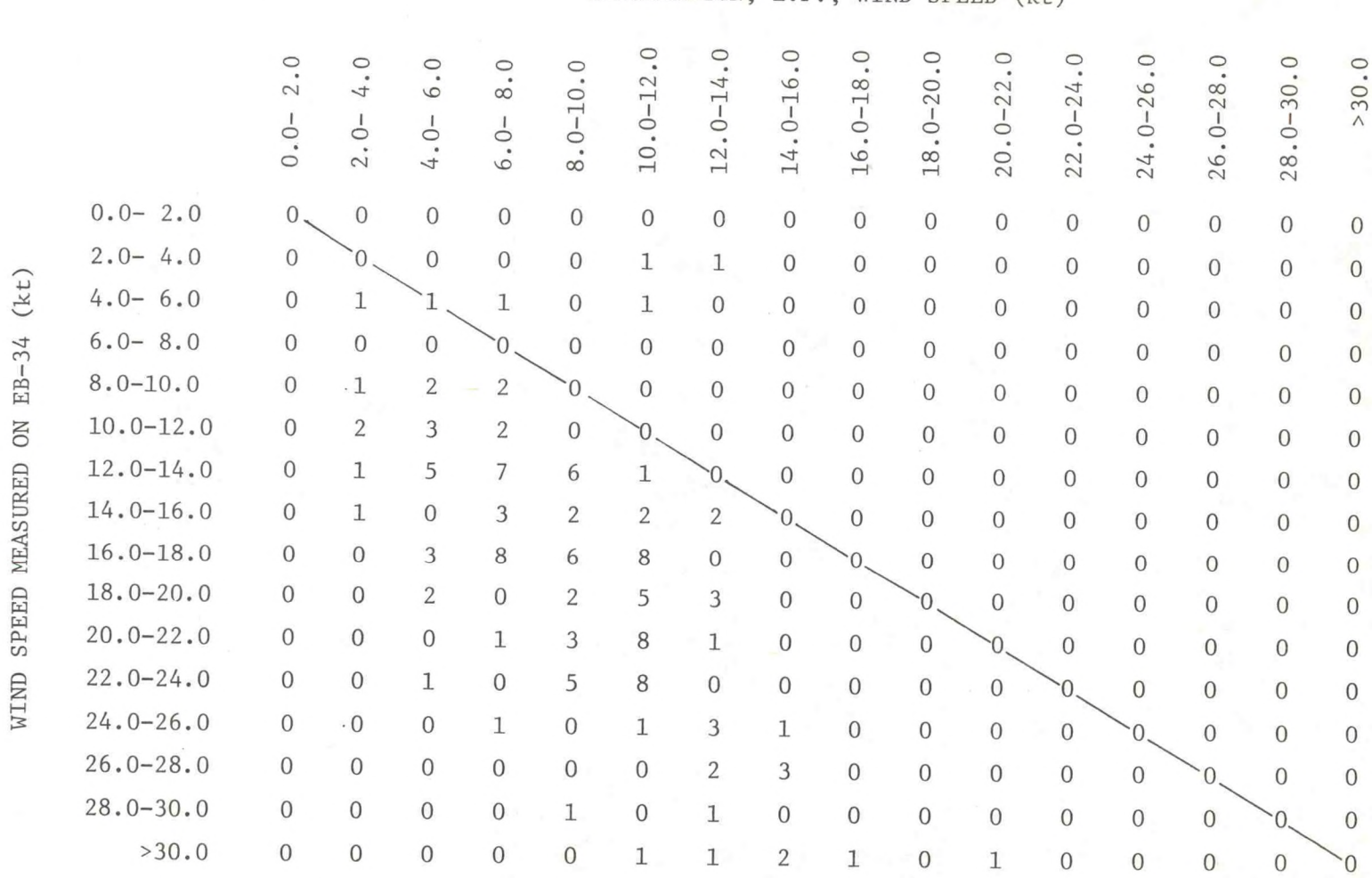


| | 0.0- 2.0 | 2.0- 4.0 | 4.0- 6.0 | 6.0- 8.0 | 8.0-10.0 | 10.0-12.0 | 12.0-14.0 | 14.0-16.0 | 16.0-18.0 | 18.0-20.0 | 20.0-22.0 | 22.0-24.0 | 24.0-26.0 | 26.0-28.0 | 28.0-30.0 | >30.0 |
|---|---|---|---|---|---|---|---|---|---|---|---|---|---|---|---|---|
| 0.0- 2.0 | 0 | 0 | 0 | 0 | 0 | 0 | 0 | 0 | 0 | 0 | 0 | 0 | 0 | 0 | 0 | 0 |
| 2.0- 4.0 | 0 | 0 | 0 | 0 | 0 | 1 | 1 | 0 | 0 | 0 | 0 | 0 | 0 | 0 | 0 | 0 |
| 4.0- 6.0 | 0 | 1 | 1 | 1 | 0 | 1 | 0 | 0 | 0 | 0 | 0 | 0 | 0 | 0 | 0 | 0 |
| 6.0- 8.0 | 0 | 0 | 0 | 0 | 0 | 0 | 0 | 0 | 0 | 0 | 0 | 0 | 0 | 0 | 0 | 0 |
| 8.0-10.0 | 0 | 1 | 2 | 2 | 0 | 0 | 0 | 0 | 0 | 0 | 0 | 0 | 0 | 0 | 0 | 0 |
| 10.0-12.0 | 0 | 2 | 3 | 2 | 0 | 0 | 0 | 0 | 0 | 0 | 0 | 0 | 0 | 0 | 0 | 0 |
| 12.0-14.0 | 0 | 1 | 5 | 7 | 6 | 1 | 0 | 0 | 0 | 0 | 0 | 0 | 0 | 0 | 0 | 0 |
| 14.0-16.0 | 0 | 1 | 0 | 3 | 2 | 2 | 2 | 0 | 0 | 0 | 0 | 0 | 0 | 0 | 0 | 0 |
| 16.0-18.0 | 0 | 0 | 3 | 8 | 6 | 8 | 0 | 0 | 0 | 0 | 0 | 0 | 0 | 0 | 0 | 0 |
| 18.0-20.0 | 0 | 0 | 2 | 0 | 2 | 5 | 3 | 0 | 0 | 0 | 0 | 0 | 0 | 0 | 0 | 0 |
| 20.0-22.0 | 0 | 0 | 0 | 1 | 3 | 8 | 1 | 0 | 0 | 0 | 0 | 0 | 0 | 0 | 0 | 0 |
| 22.0-24.0 | 0 | 0 | 1 | 0 | 5 | 8 | 0 | 0 | 0 | 0 | 0 | 0 | 0 | 0 | 0 | 0 |
| 24.0-26.0 | 0 | 0 | 0 | 1 | 0 | 1 | 3 | 1 | 0 | 0 | 0 | 0 | 0 | 0 | 0 | 0 |
| 26.0-28.0 | 0 | 0 | 0 | 0 | 0 | 0 | 2 | 3 | 0 | 0 | 0 | 0 | 0 | 0 | 0 | 0 |
| 28.0-30.0 | 0 | 0 | 0 | 0 | 1 | 0 | 1 | 0 | 0 | 0 | 0 | 0 | 0 | 0 | 0 | 0 |
| >30.0 | 0 | 0 | 0 | 0 | 0 | 1 | 1 | 2 | 1 | 0 | 1 | 0 | 0 | 0 | 0 | 0 |

Figure 3.5.--Frequency of wind speeds measured by buoy EB-34 and Westhampton coastal station.

ATLANTIC CITY, N.J., WIND SPEED (kt)

| WIND SPEED MEASURED ON EB-41 (kt) | 0.0- 2.0 | 2.0- 4.0 | 4.0- 6.0 | 6.0- 8.0 | 8.0-10.0 | 10.0-12.0 | 12.0-14.0 | 14.0-16.0 | 16.0-18.0 | 18.0-20.0 | 20.0-22.0 | 22.0-24.0 | 24.0-26.0 | 26.0-28.0 | 28.0-30.0 | >30.0 |
|---|---|---|---|---|---|---|---|---|---|---|---|---|---|---|---|---|
| 0.0- 2.0 | 0 | 0 | 2 | 0 | 0 | 0 | 0 | 0 | 0 | 0 | 0 | 0 | 0 | 0 | 0 | 0 |
| 2.0- 4.0 | 0 | 1 | 1 | 0 | 1 | 0 | 0 | 0 | 0 | 0 | 0 | 0 | 0 | 0 | 0 | 0 |
| 4.0- 6.0 | 0 | 0 | 5 | 1 | 0 | 0 | 0 | 0 | 0 | 0 | 0 | 0 | 0 | 0 | 0 | 0 |
| 6.0- 8.0 | 0 | 1 | 4 | 2 | 0 | 1 | 0 | 0 | 0 | 0 | 0 | 0 | 0 | 0 | 0 | 0 |
| 8.0-10.0 | 0 | 1 | 6 | 2 | 0 | 0 | 0 | 0 | 0 | 0 | 0 | 0 | 0 | 0 | 0 | 0 |
| 10.0-12.0 | 0 | 3 | 5 | 2 | 2 | 2 | 0 | 0 | 0 | 0 | 0 | 0 | 0 | 0 | 0 | 0 |
| 12.0-14.0 | 0 | 1 | 7 | 6 | 2 | 2 | 0 | 0 | 0 | 0 | 0 | 0 | 0 | 0 | 0 | 0 |
| 14.0-16.0 | 0 | 0 | 5 | 3 | 2 | 1 | 1 | 1 | 0 | 0 | 0 | 0 | 0 | 0 | 0 | 0 |
| 16.0-18.0 | 0 | 0 | 2 | 2 | 3 | 1 | 3 | 1 | 0 | 0 | 0 | 0 | 0 | 0 | 0 | 0 |
| 18.0-20.0 | 0 | 0 | 3 | 5 | 0 | 2 | 0 | 1 | 0 | 0 | 0 | 0 | 0 | 0 | 0 | 0 |
| 20.0-22.0 | 0 | 0 | 3 | 5 | 1 | 4 | 2 | 1 | 0 | 1 | 0 | 0 | 0 | 0 | 0 | 0 |
| 22.0-24.0 | 0 | 0 | 2 | 2 | 4 | 4 | 0 | 1 | 0 | 0 | 0 | 0 | 0 | 0 | 0 | 0 |
| 24.0-26.0 | 0 | 0 | 0 | 0 | 4 | 3 | 3 | 0 | 0 | 0 | 0 | 0 | 0 | 0 | 0 | 0 |
| 26.0-28.0 | 0 | 0 | 0 | 1 | 1 | 0 | 0 | 1 | 0 | 0 | 0 | 0 | 0 | 0 | 0 | 0 |
| 28.0-30.0 | 0 | 0 | 0 | 0 | 0 | 0 | 3 | 1 | 0 | 0 | 0 | 0 | 0 | 0 | 0 | 0 |
| >30.0 | 0 | 0 | 0 | 0 | 0 | 0 | 3 | 1 | 2 | 1 | 0 | 0 | 0 | 0 | 0 | 0 |

Figure 3.6.--Frequency of wind speeds measured by buoy EB-41 and Atlantic City coastal station.

3.1.2.4 Coastal-Station - Marine Deck Observations. As noted earlier, the degree to which the systematic wind differences between land and sea can be determined from currently available buoy data is quite limited. It is therefore useful also to compare the shoreline data with the Marine Deck observations, keeping in mind the indications of a bias toward low wind speeds in the Marine Deck observations discussed in sections 3.1.2.1 and 3.1.2.2 above.

The mean wind speeds for Atlantic City, New Jersey, for Kennedy Airport and Westhampton, Long Island, and for the adjacent ocean areas, based on Marine Deck observations, are listed in table 3.4. As seen, the wind speeds at the land stations are consistently lower than those over the adjacent ocean areas but the differences vary between 2.5 and 6.2 kt, which is not surprising since they are a function of station exposure and the ship's distance from the coast.

Table 3.4.--Mean wind speeds and differences derived from coastal-station and Marine Deck observations

| | Atlantic City | Marine Deck (area 7) | Kennedy Airport | Marine Deck (area 3) | Westhampton | Marine Deck (area 4) |
|---|---|---|---|---|---|---|
| Mean speed (kt) | 9.1 | 13.2 | 10.5 | 13.0 | 7.9 | 14.1 |
| Difference (kt) | 4.1 | | 2.5 | | 6.2 | |

To further examine the consistent differences between the coastal-station and the transient-ship observations, adjustment factors for speed and direction were calculated. These factors are determined from comparison of the mean winds from the two sets of data, i.e., the ratio of the speed of the mean coastal wind to the speed of the mean offshore wind defines the speed factor, while the difference in direction of the two mean winds defines the direction factor. A detailed description of the method for computing these adjustment factors is given in appendix A. The model used gives a good picture of the systematic difference between the two sets of observations if their distributions are similar, and differences in speed and direction are independent of wind direction. The speed and direction adjustment factors computed for the three coastal stations are given in table 3.5.

Figure 3.7 shows the results of a computation in which the Westhampton data were adjusted based on the Marine Deck observations and compared with simultaneous data recorded by buoy EB-34. The mean wind speed difference is 2 kt, compared with 9 kt if unadjusted Westhampton data had been used. This suggests that the adjustments are useful for computations over short periods of time. The underestimate by 2 kt may be due to the fact that the adjustment factors were derived from the Marine Deck observations, which have been shown to be biased toward low wind speeds.

ESTIMATED WIND SPEED (kt)

| WIND SPEED MEASURED ON EB-34 (kt) | 0.0- 2.0 | 2.0- 4.0 | 4.0- 6.0 | 6.0- 8.0 | 8.0-10.0 | 10.0-12.0 | 12.0-14.0 | 14.0-16.0 | 16.0-18.0 | 18.0-20.0 | 20.0-22.0 | 22.0-24.0 | 24.0-26.0 | 26.0-28.0 | 28.0-30.0 | >30.0 |
|---|---|---|---|---|---|---|---|---|---|---|---|---|---|---|---|---|
| 0.0- 2.0 | 0 | 0 | 0 | 0 | 0 | 0 | 0 | 0 | 0 | 0 | 0 | 0 | 0 | 0 | 0 | 0 |
| 2.0- 4.0 | 0 | 0 | 0 | 0 | 0 | 0 | 0 | 0 | 1 | 0 | 1 | 0 | 0 | 0 | 0 | 0 |
| 4.0- 6.0 | 0 | 0 | 1 | 1 | 0 | 1 | 0 | 0 | 1 | 0 | 0 | 0 | 0 | 0 | 0 | 0 |
| 6.0- 8.0 | 0 | 0 | 0 | 0 | 0 | 0 | 0 | 0 | 0 | 0 | 0 | 0 | 0 | 0 | 0 | 0 |
| 8.0-10.0 | 0 | 0 | 1 | 1 | 1 | 2 | 0 | 0 | 0 | 0 | 0 | 0 | 0 | 0 | 0 | 0 |
| 10.0-12.0 | 0 | 0 | 2 | 3 | 0 | 2 | 0 | 0 | 0 | 0 | 0 | 0 | 0 | 0 | 0 | 0 |
| 12.0-14.0 | 0 | 0 | 1 | 4 | 1 | 7 | 0 | 6 | 1 | 0 | 0 | 0 | 0 | 0 | 0 | 0 |
| 14.0-16.0 | 0 | 0 | 1 | 0 | 0 | 3 | 0 | 2 | 2 | 0 | 2 | 0 | 0 | 0 | 0 | 0 |
| 16.0-18.0 | 0 | 0 | 0 | 3 | 0 | 6 | 2 | 6 | 8 | 0 | 0 | 0 | 0 | 0 | 0 | 0 |
| 18.0-20.0 | 0 | 0 | 0 | 1 | 1 | 0 | 0 | 2 | 5 | 0 | 3 | 0 | 0 | 0 | 0 | 0 |
| 20.0-22.0 | 0 | 0 | 0 | 0 | 0 | 1 | 0 | 3 | 8 | 0 | 1 | 0 | 0 | 0 | 0 | 0 |
| 22.0-24.0 | 0 | 0 | 0 | 0 | 1 | 0 | 0 | 5 | 8 | 0 | 0 | 0 | 0 | 0 | 0 | 0 |
| 24.0-26.0 | 0 | 0 | 0 | 0 | 0 | 1 | 0 | 0 | 1 | 0 | 3 | 0 | 0 | 1 | 0 | 0 |
| 26.0-28.0 | 0 | 0 | 0 | 0 | 0 | 0 | 0 | 0 | 0 | 0 | 2 | 0 | 1 | 2 | 0 | 0 |
| 28.0-30.0 | 0 | 0 | 0 | 0 | 0 | 0 | 0 | 1 | 0 | 0 | 1 | 0 | 0 | 0 | 0 | 0 |
| >30.0 | 0 | 0 | 0 | 0 | 0 | 0 | 0 | 0 | 1 | 0 | 1 | 0 | 1 | 1 | 1 | 1 |

Figure 3.7.--Frequency of wind speeds measured by buoy EB-34 and estimated wind speeds based on adjusted Westhampton coastal-station data.

Table 3.5.--Wind speed and direction adjustment factors for coastal stations

| | Atlantic City (area 7) | Kennedy Airport (area 3) | Westhampton (area 4) |
|---|---|---|---|
| | | Winter (November-April) | |
| Wind speed (ratio) | 1.5 | 1.4 | 1.8 |
| Wind direction (deg) | 5.3 | 1.4 | -4.8 |
| | | Summer (May-October) | |
| Wind speed (ratio) | 1.7 | 1.2 | 1.5 |
| Wind direction (deg) | -7.8 | -6.5 | -19.4 |

3.1.2.5 Gradient Wind Computations. Estimates of gradient wind* that are made from the spacing and curvature of isobars on a surface atmospheric pressure field analysis are another potential source of wind data for the continental shelf area. Comparisons were made between wind speeds measured by buoy EB-34 and gradient wind estimates obtained from the objective analyses used by the National Weather Service in its limited fine mesh boundary layer model (LFM model) to generate synoptic weather maps. The average difference between the estimated gradient wind speed for the buoy site and the wind speed recorded by the buoy from November to December 1975 was 7 kt (an RMS difference of 11 kt). These differences are probably the result of deficiencies in the gradient wind approximation, in which the effect of friction on the wind speed and direction is neglected.

3.1.2.6 Summary. The Marine Deck wind observations are adequate for defining the major features of the mean monthly surface wind field, as well as for providing a statistical description of its variability. However, comparative studies, based on wind data from Ocean Weather Station "H" and a short record of wind data from buoy EB-41, show strong evidence of bias toward low wind speeds in the Marine Deck statistics. This negative bias, on the order of 10 percent, could be due to a systematic error in the transient-ship observations, but more likely results from a tendency by the ships to avoid areas of bad weather or to "miss" observations under bad weather conditions.

* The theoretical meteorological wind that results from a balance between the horizontal forces from the pressure gradient, from centripetal acceleration, and the Coriolis acceleration.

Comparison of shoreline-station wind data with buoy and Marine Deck observations in adjacent ocean areas showed the expected bias toward lower wind speeds at the coastal stations. The magnitude of the bias depends on the specific coastal station and its exposure, but overwater wind speeds are generally from 30 to 80 percent higher than those at adjacent coastal stations. A method has been developed, however, by which wind speed and direction adjustment factors can be derived from Marine Deck observations and applied to coastal station wind data in order to approximate conditions over adjoining ocean areas. The time-series data being acquired from meteorological buoys deployed in the area, when paired with synoptic coastal station observations, will allow a more complete description of the land-sea wind differences. Only short records of buoy data were available for this study, but the accumulation of 2 to 3 years of shoreline-station and buoy data should be sufficient for determining these differences.

### 3.1.3 Surface Trajectory Climatology

The distribution of surface wind trajectories varies from one point of origin to another within the Mid-Atlantic area, but the major features of the surface wind climatology over the area vary relatively little. One can therefore obtain a fairly good estimate of the trajectory climatology from wind records at Westhampton, Long Island, and Atlantic City, New Jersey, by using the method described in section 3.1.2.4 and appendix A for adjusting these coastal-station data. The adjusted data can then be assumed to be representative of the climatic characteristics of the northeast and southwest portions, respectively, of the area under study.

Application of the appropriate adjustment factors to the Westhampton hourly observations produced time-series wind data for each of the northern marine areas (see fig. 2.1). The wind record covered 10 years and permitted generation of multiple wind trajectories, which can be used to simulate the motion of drifting oil on the sea surface under the effect of wind alone (Schwartzberg, 1970).

In generating a wind trajectory, 3 percent of the first wind speed and direction data in the record was applied for a 3-hr period. The next 3-hourly wind report was then used to compute the end point of a second 3-hourly leg of the trajectory, and so on, until the path of the parcel had been estimated for a specified length of time. The wind data record was then advanced 72 hr and another trajectory computation begun. The process was repeated for trajectory time limits of 1, 2, 4, 8, 16, and 32 days until the entire data record had been used. The region of the trajectory computations was subdivided into 10-mi$^2$ areas. In the course of computing each trajectory, the number of trajectory traverses of each area was retained. The resulting trajectory climatology based on the adjusted Westhampton and Atlantic City data is shown in figures 3.8 and 3.9, respectively. The isolines in these figures enclose the areas traversed by at least 20 percent of the trajectories that began at the origin and were followed for the indicated time spans. For example, the outermost contours in these figures enclose the 10-mi$^2$ ocean areas traversed by at least 20 percent of the trajectories followed


Figure 3.8.--Coverage of wind trajectories for 1, 2, 4, 8, 16, and 32 days based on adjusted Westhampton data.


Figure 3.9.--Coverage of wind trajectories for 1, 2, 4, 8, 16, and 32 days based on adjusted Atlantic City data.

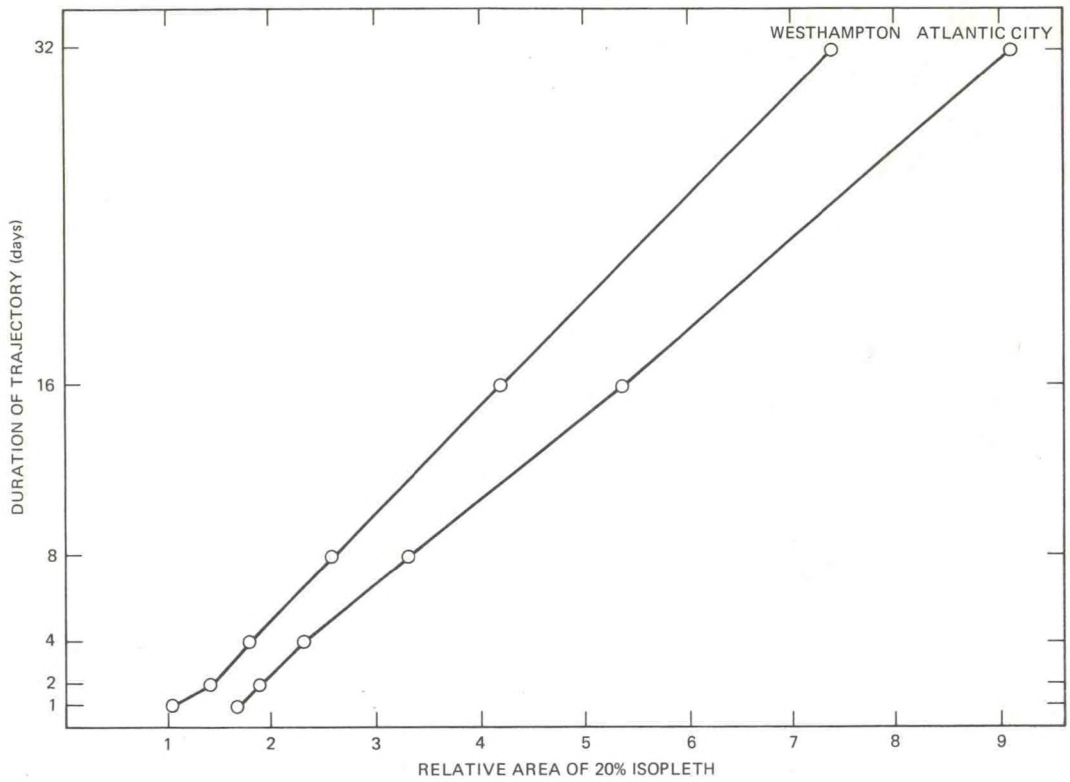


Figure 3.10.--Variation in trajectory coverage with duration of trajectory.

for 32 days. The area within each of the isolines in these figures was measured with a planimeter, and the relative sizes of the measured areas were plotted against the duration of the trajectory paths, as shown in figure 3.10. The linear increase in area with time is similar to a "random walk" process (Moore, 1962), but the lack of symmetry of the contours around the point of origin is suggestive of such a process superimposed on a large-scale transport vector. This finding suggests that it may be possible to construct a fairly good surface trajectory climatology by characterizing it in terms of two parameters: the slope of the curve in figure 3.10, and a parameter defining the departure from symmetry, i.e., the large-scale transport vector.

In the trajectory computations described above, the adjustment factors derived from the Marine Deck observations were used, and the computations therefore reflect the effect of the negative wind speed bias in these observations. Since, however, the bias appears to be on the order of only 10 percent, it will not affect the general conclusions of this analysis.

### 3.1.4 Extreme Wind Speeds

Extreme wind speed return periods of 5, 10, 25, 50, 100, and 200 years were estimated for each of the 15 climatological areas (fig. 2.1) by fitting the extreme wind observations by a Fisher-Typpitte Type II distribution, and then estimating the wind speed corresponding to each return period from the theoretical distribution.

The use of a Fisher-Typpitte Type II distribution to estimate the return period of occurrence frequency of extreme winds has been proposed by Thom (1966). By this method, the distribution is fitted around the maximum average monthly wind speed, and estimates of the return period (frequency) of high wind speeds are then derived from the distribution curve. The return period of hurricanes is also considered for the site in question, and estimates of extreme winds made from the Fisher-Typpitte distribution are adjusted empirically according to the frequency of hurricanes. Results of such an analysis for the Mid-Atlantic climatological areas used here are shown in figure 3.11, where maximum wind values, read from the top within each area, are indicated for return periods of 5, 10, 25, 50, 100, and 200 years.

## 3.2 Visibility Restrictions

Criteria for selecting visibility limitation ranges were developed on the basis of stopping and maneuverability distances required for large ships to avoid collision. This information was available for the Universe Ireland, a tanker of 326,000 dwt. This ship has a turning radius of about 1/2 mi, and requires about 2 mi to stop when travelling at its full speed of 14.8 kt. Since it is unlikely that a captain would drive his ship at full speed under poor visibility conditions, and since avoidance of collision would require engine reversal as well as maneuvering, visibility ranges of $\leq$ 1 mi and $\leq$ 1/4 mi were chosen to indicate frequencies of poor visibility conditions that could restrict ship operations. The monthly frequencies in percent for each of the areas are shown in figures 3.12 to 3.23. Note that variation in the air and water temperature differences over the year produces a considerable variation in the expected frequency of low visibility ranges. During periods when the air temperature is warmer than the sea surface, heavy fog is often found over the cold-water areas.

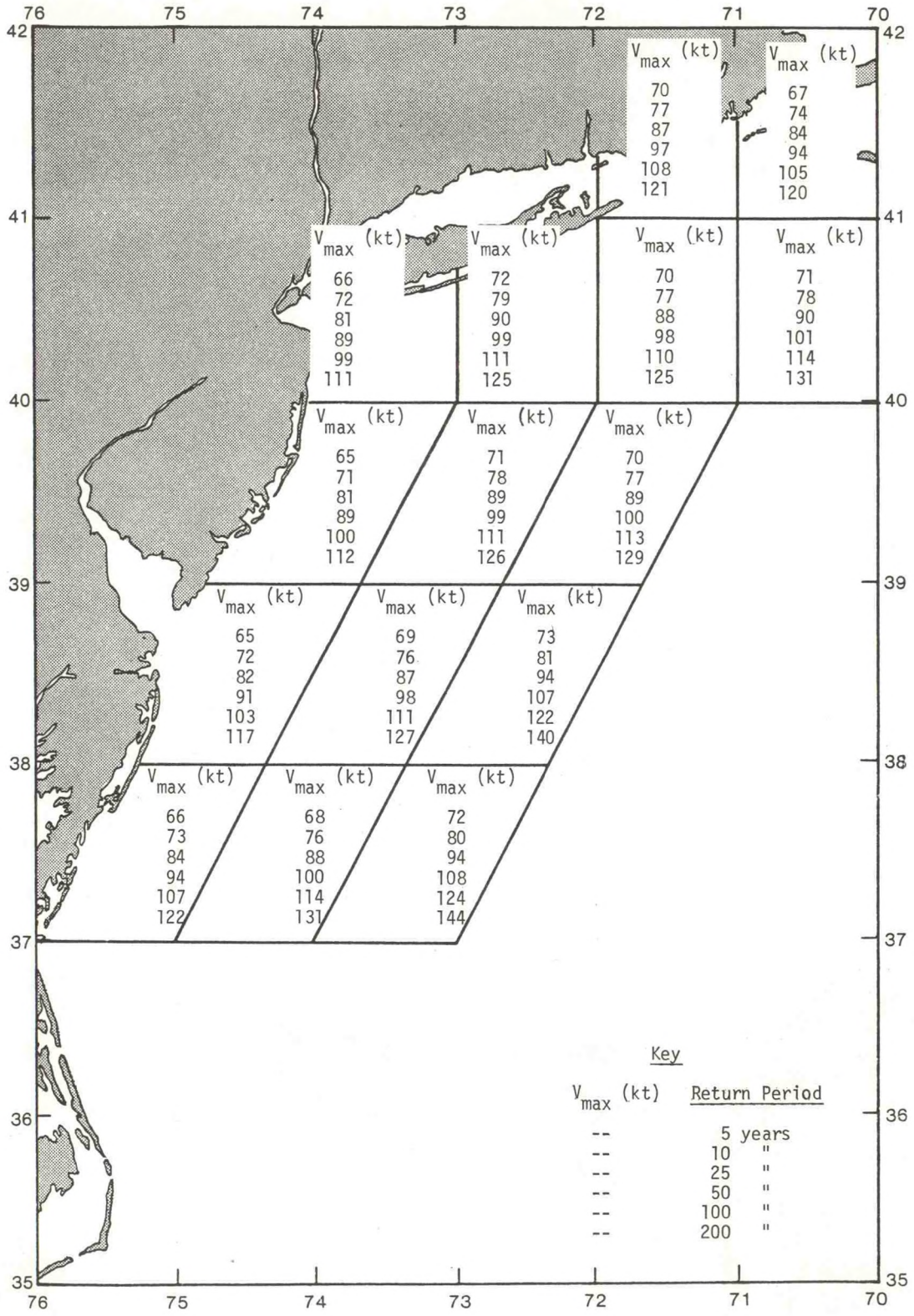


Figure 3.11.--Extreme wind speeds.

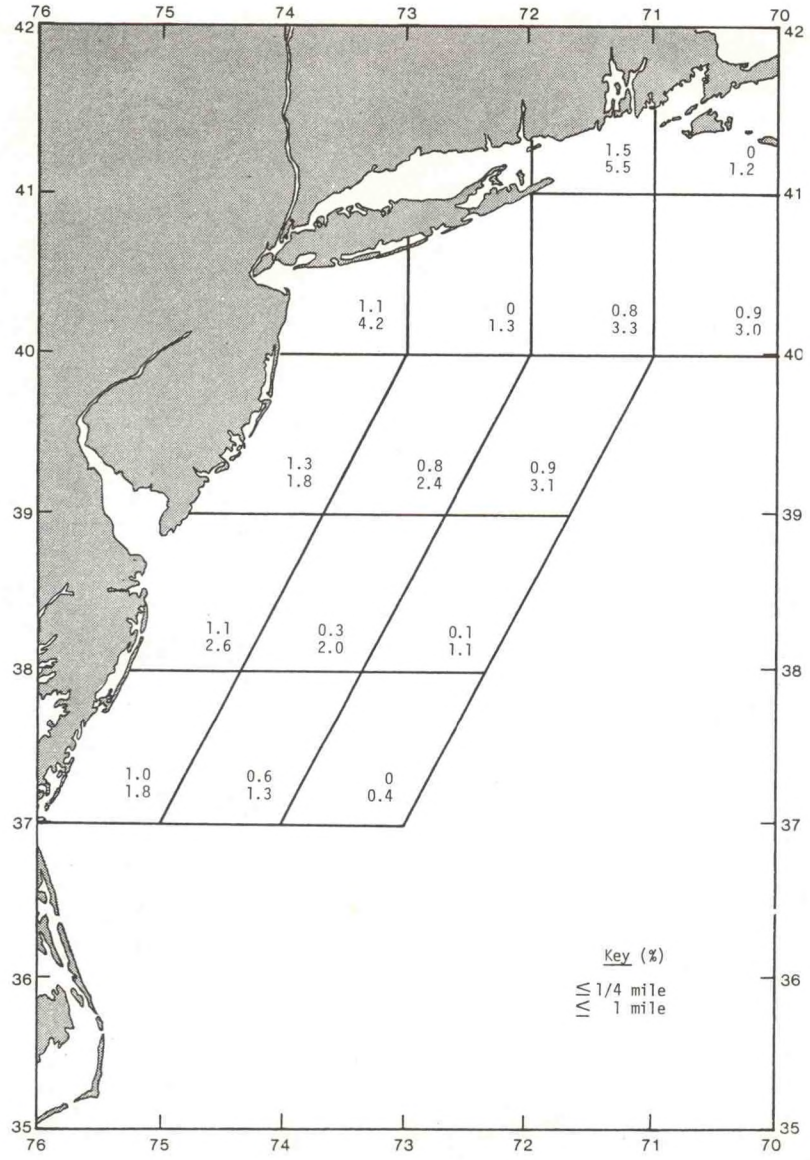


Figure 3.12.--January visibility range frequency.

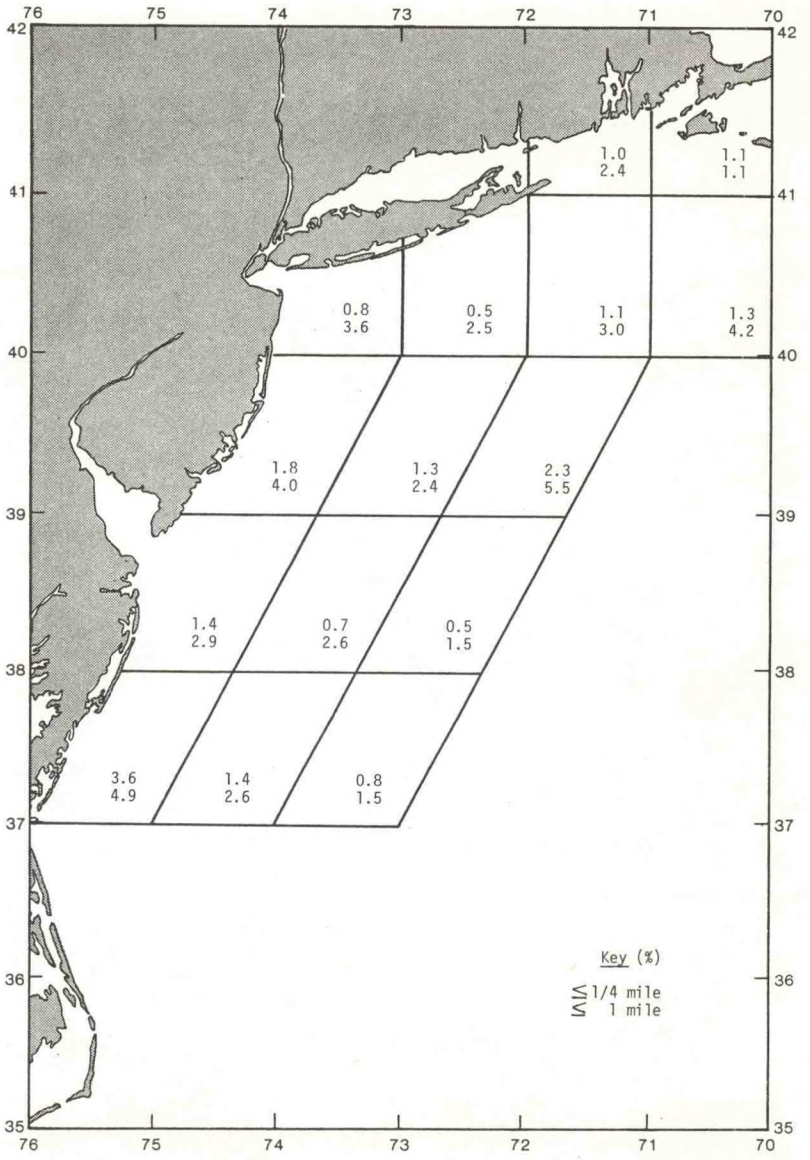


Figure 3.13.--February visibility range frequency.

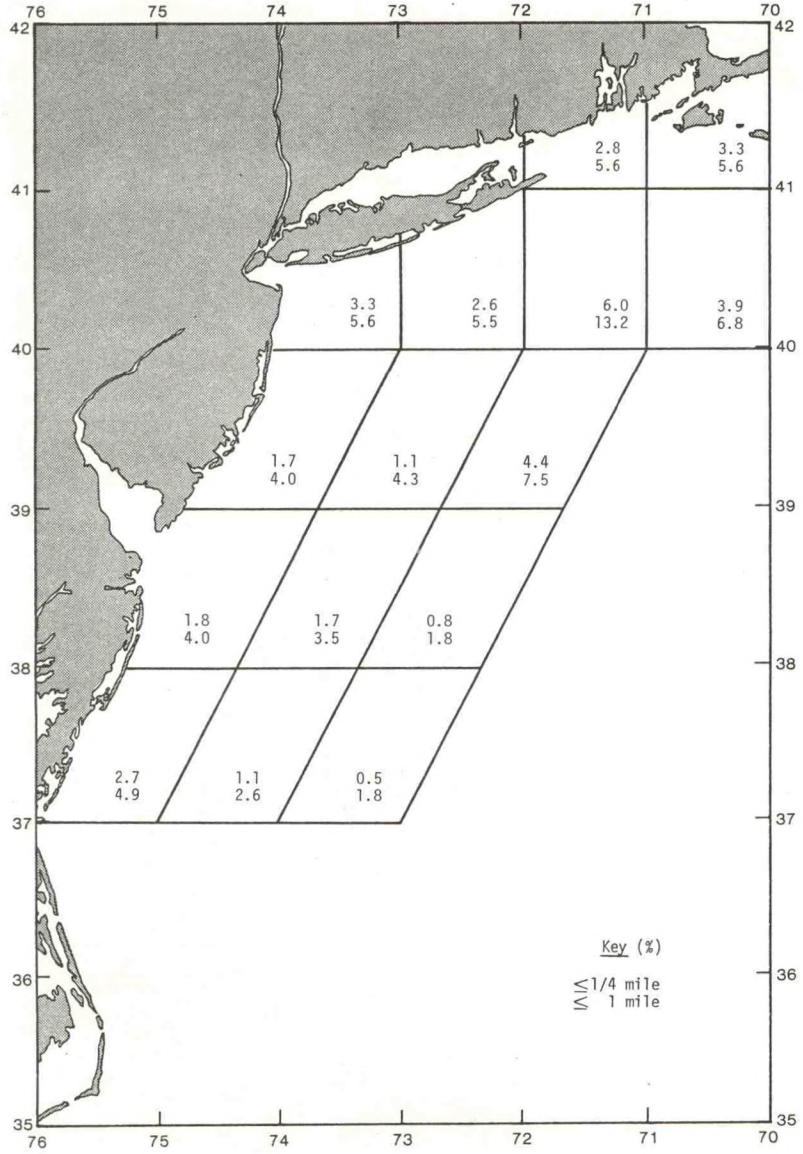


Figure 3.14.--March visibility range frequency.

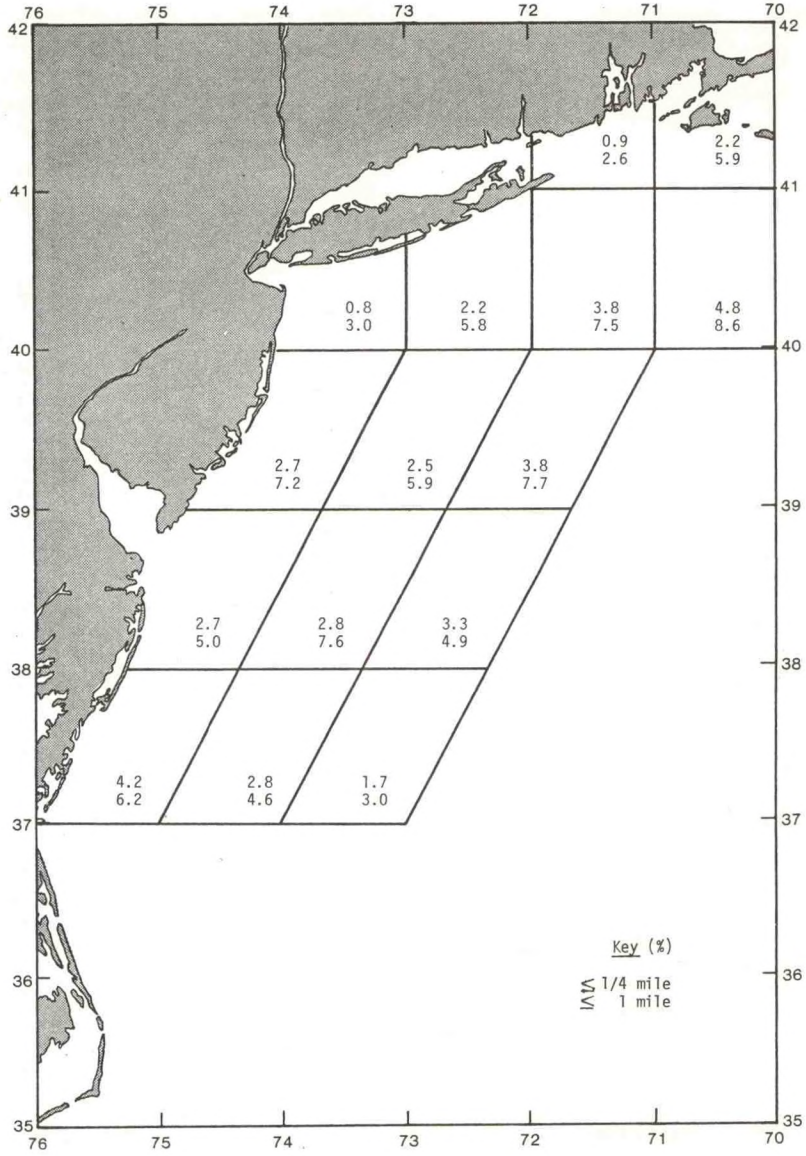


Figure 3.15.--April visibility range frequency.

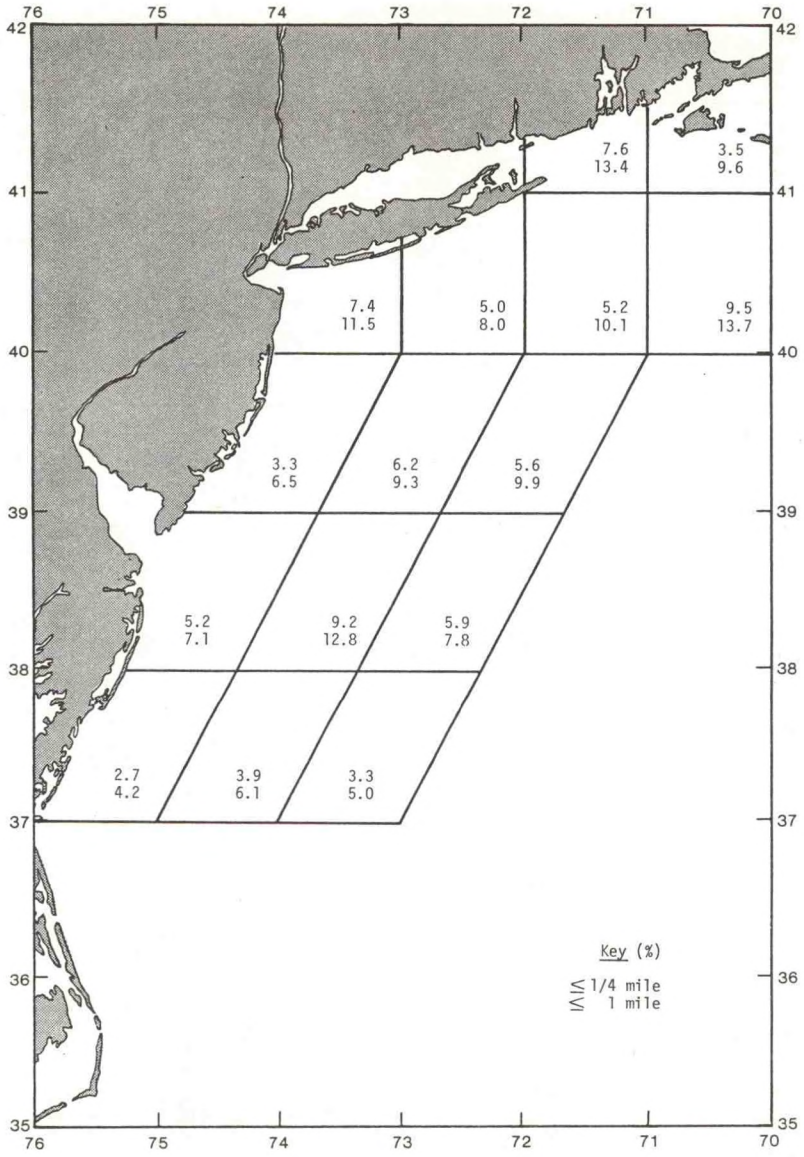


Figure 3.16.--May visibility range frequency.

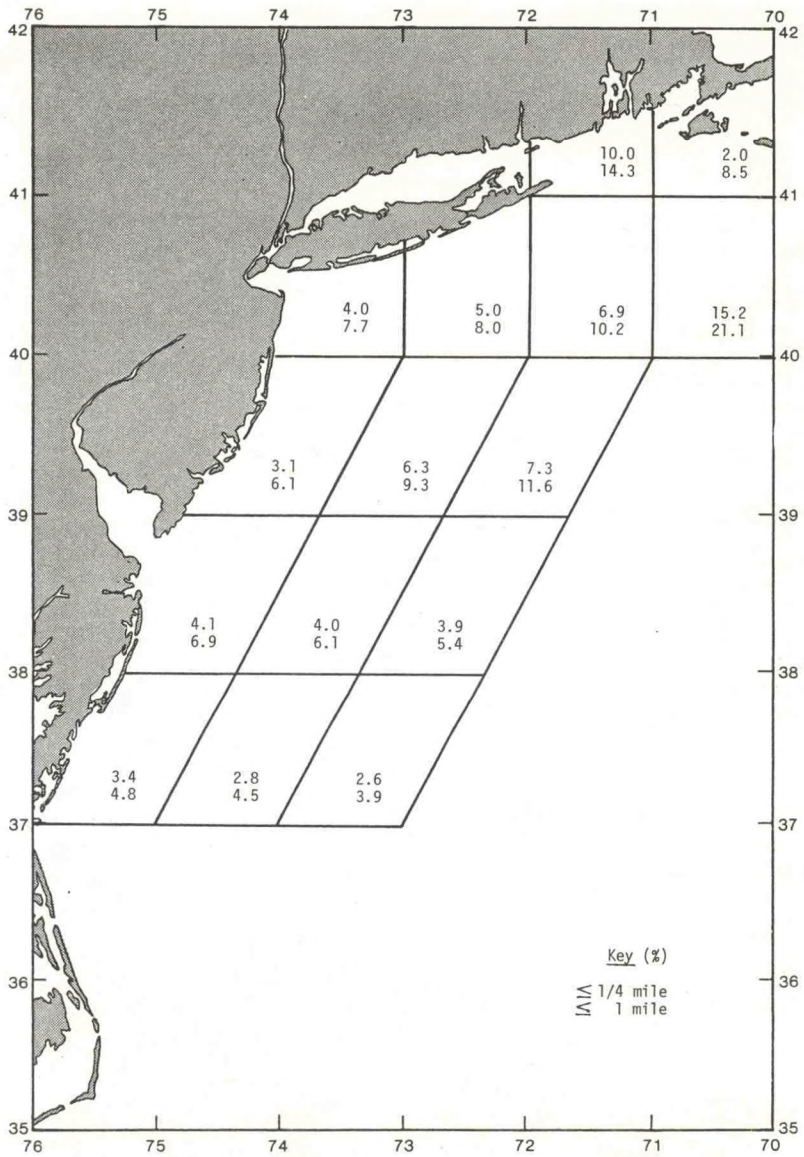


Figure 3.17.--June visibility range frequency.

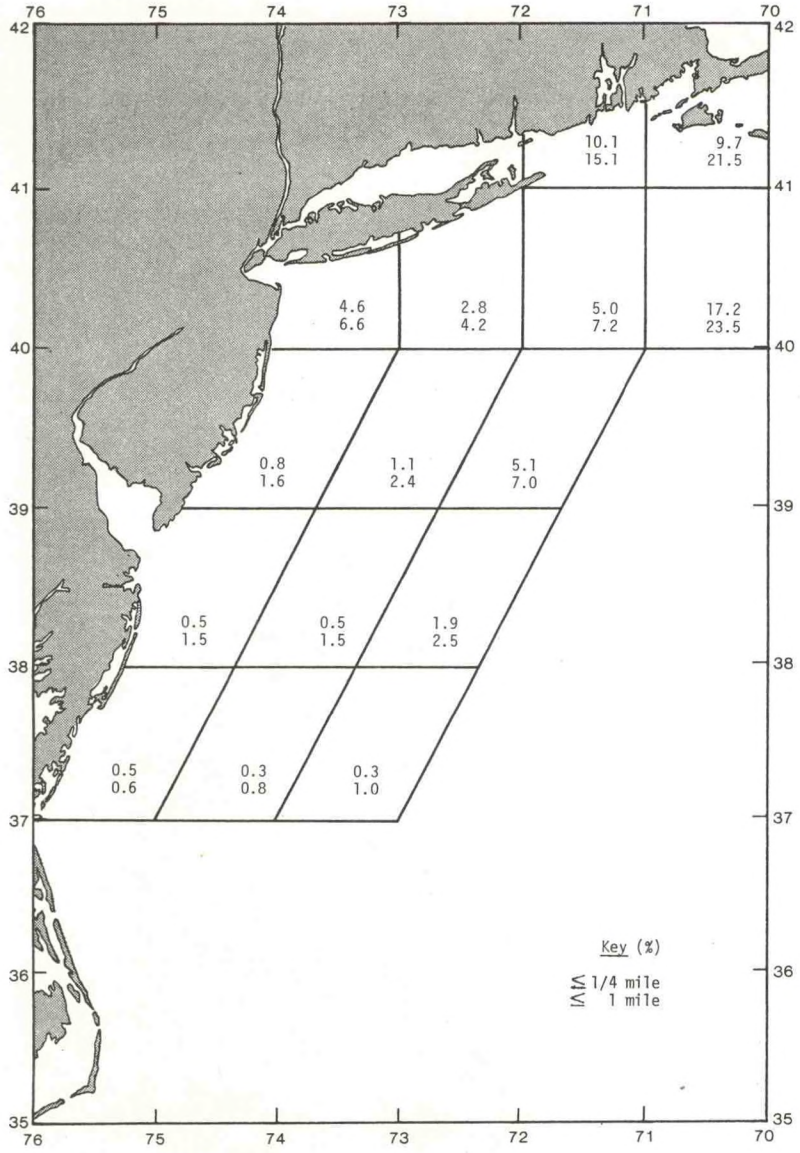


Figure 3.18.--July visibility range frequency.

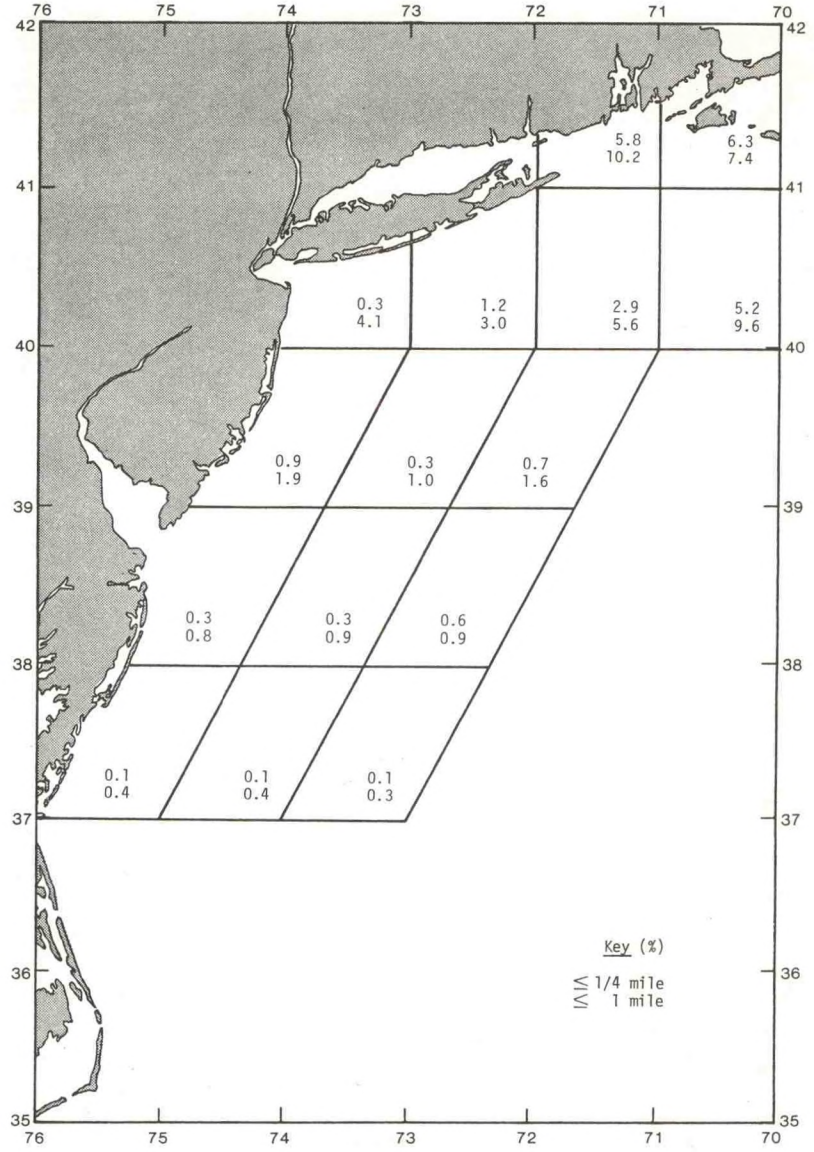


Figure 3.19.--August visibility range frequency.

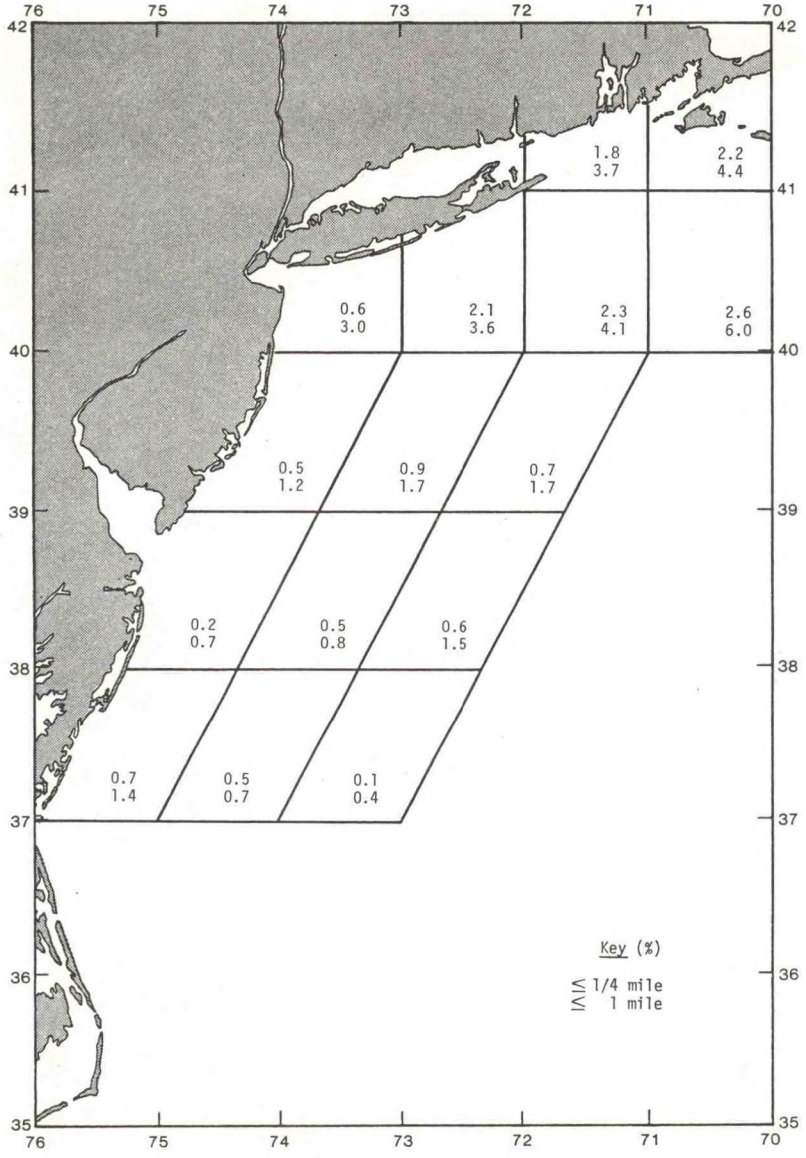


Figure 3.20.--September visibility range frequency.

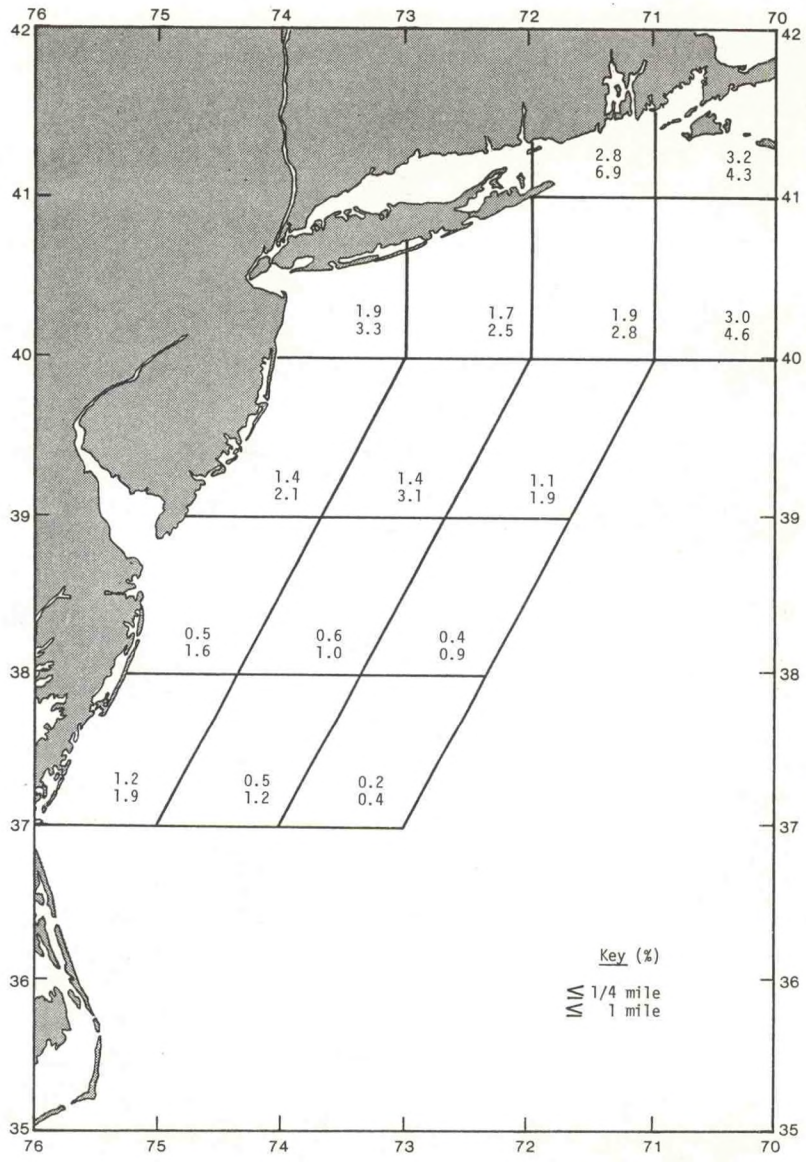


Figure 3.21.--October visibility range frequency.

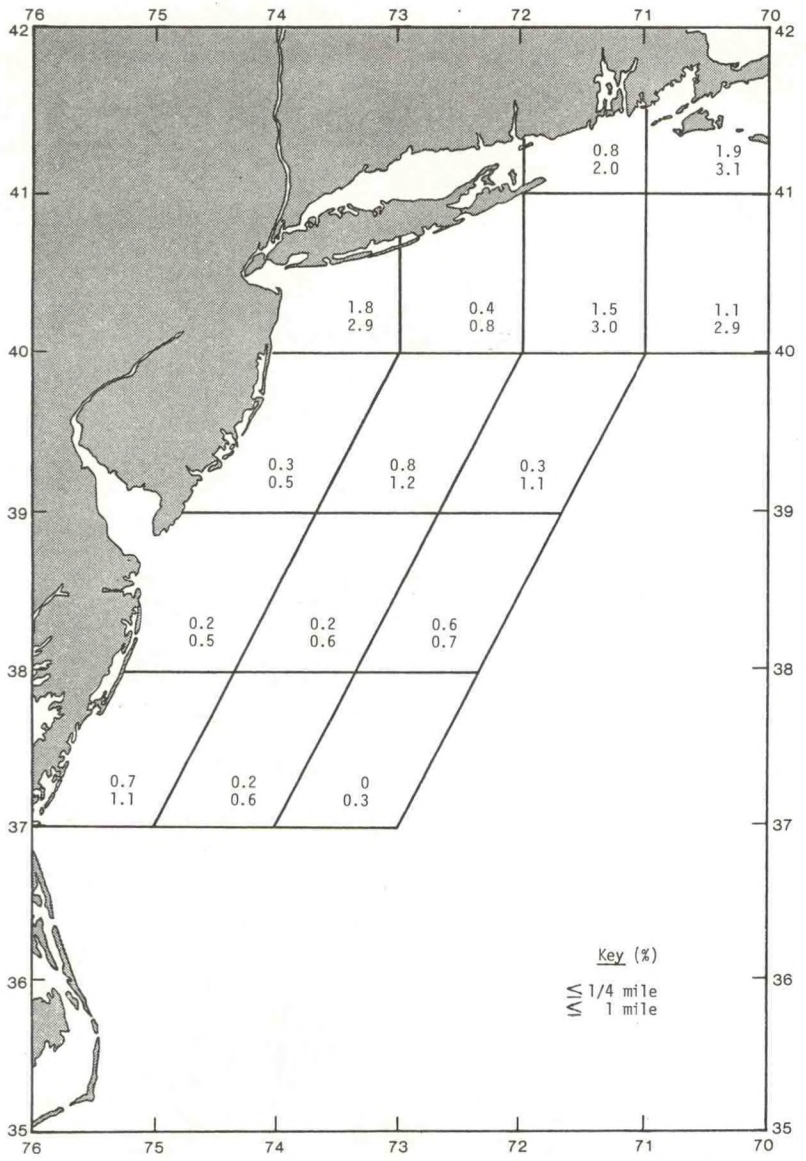


Figure 3.22.--November visibility range frequency.

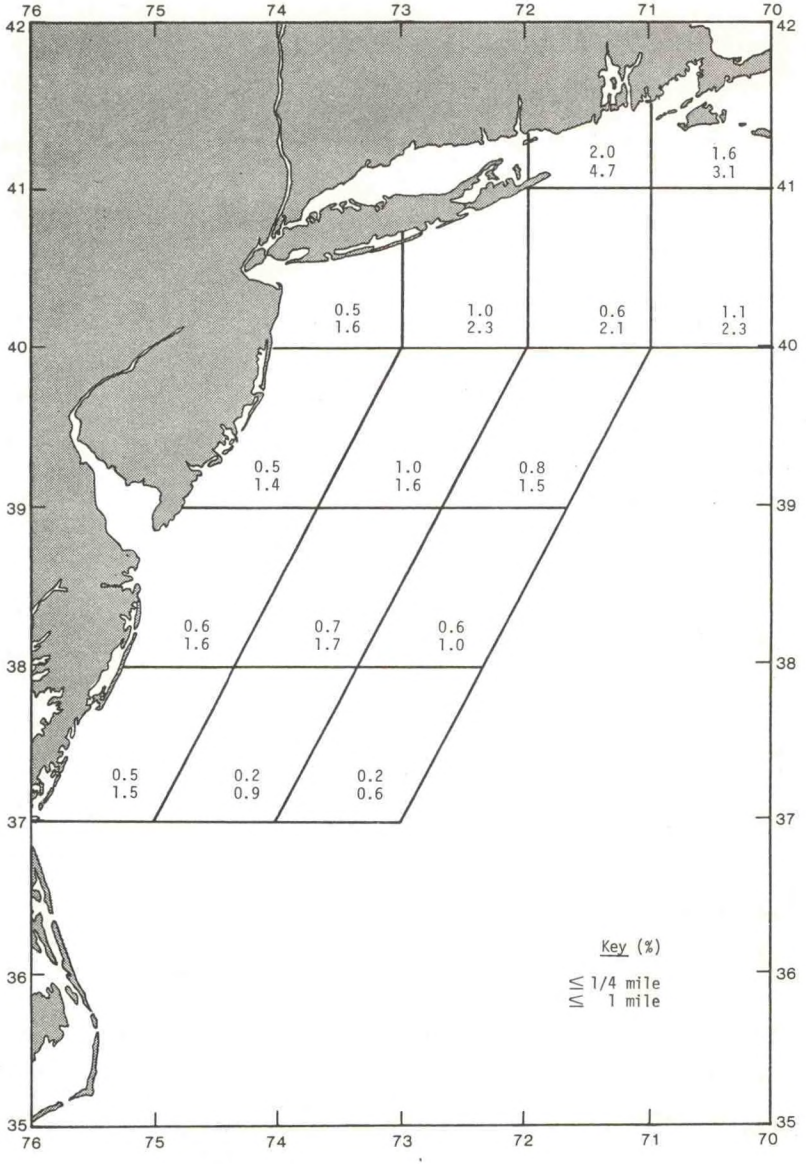


Figure 3.23.--December visibility range frequency.

## 3.3 Superstructure Icing

The potential for accretion of ice on the superstructure of a ship at sea depends on the forward speed of the ship in relation to the direction of wind and wave, the speed of the wind, and the air and water temperature. It also depends on the shape of the parts of the superstructure; hence, nonuniform ice accretion rates are expected on a ship. Further, since the direction of ship travel relative to wave direction is not predictable, any statistic that describes the potential for icing on a ship can do so only in terms of general conditions; ice accumulation rates can vary widely under similar meteorological and oceanographic conditions.

Empirical relationships between air temperature, wind speed, sea-surface temperature, and ice accumulation rates have been published by Minsk (1975). These relationships were used in this study for computing the frequency of light (1 to 3 cm/24 hr), moderate (4 to 6 cm/24 hr), and severe (7 to 14 cm/24 hr) icing potential for each of the 15 areas. Because of the extreme conditions required for appreciable ice accumulation, only a few of the areas were found to be affected. Potential icing conditions begin in the northern portions of the Bight in December (fig. 3.24). They increase in January (fig. 3.25); and reach maximum extent in February (fig. 3.26). By March (fig. 3.27), the potential for ice accumulation is limited to the immediate coastal areas. These findings indicate that icing of a ship's superstructure is less significant in risk assessment than other parameters because of the lower frequency of conditions that create a potential for icing.

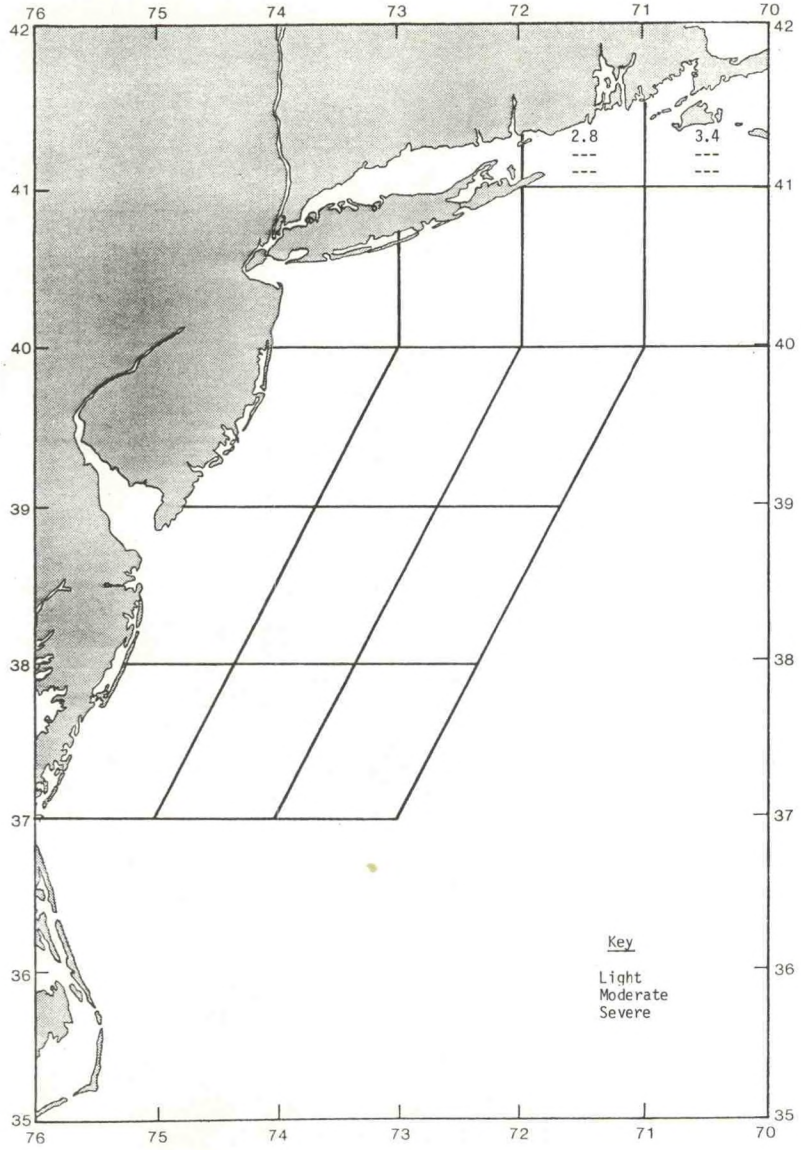


Figure 3.24.--December icing potential frequency.

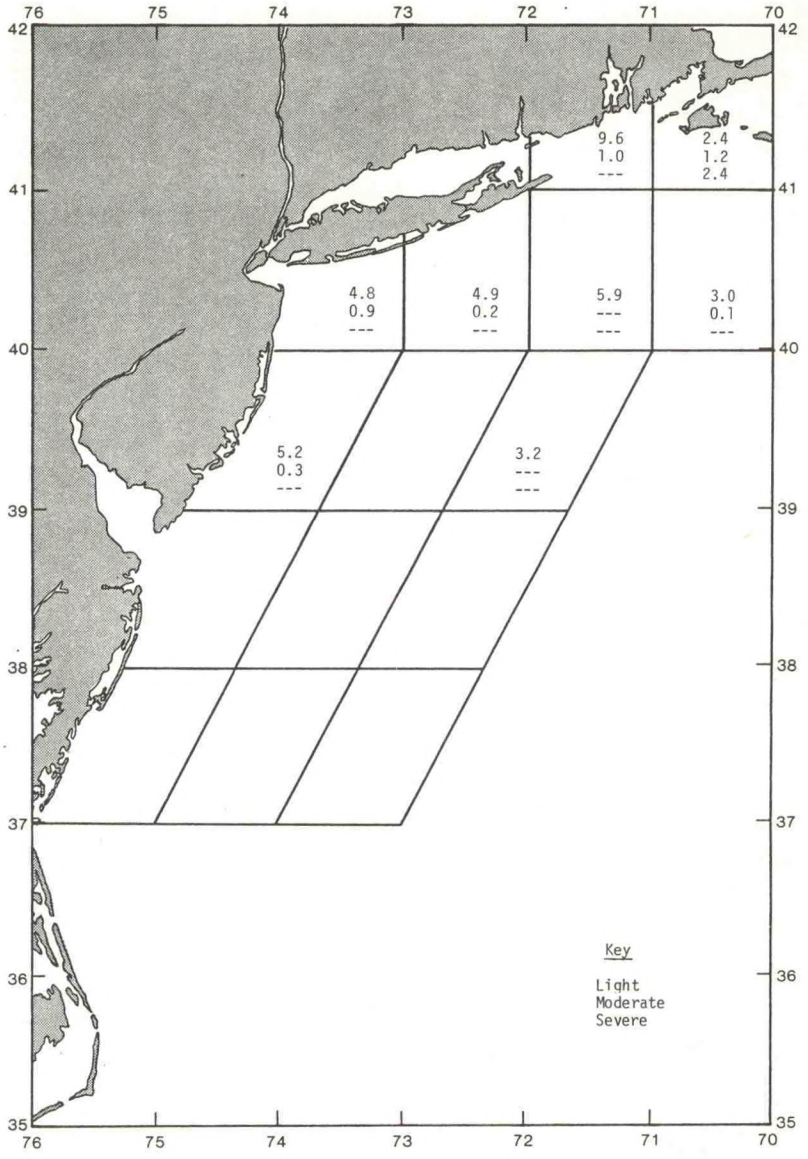


Figure 3.25.--January icing potential frequency.

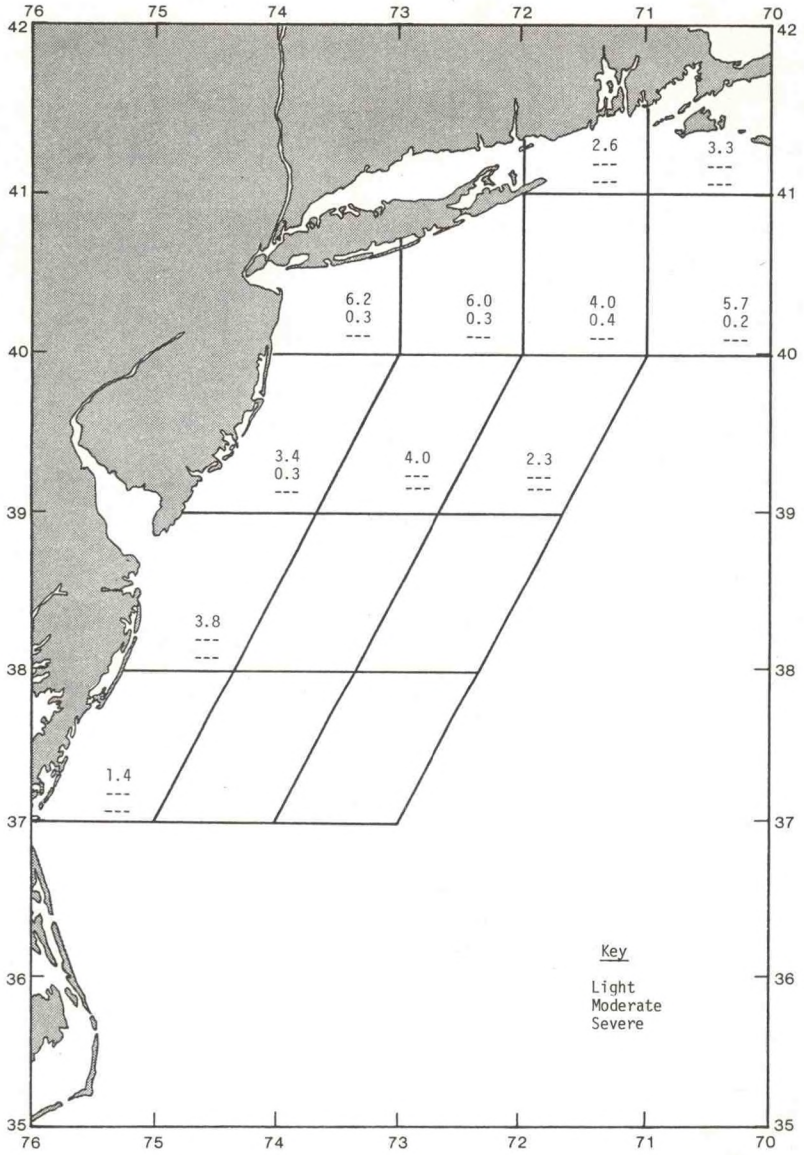


Figure 3.26.--February icing potential frequency.

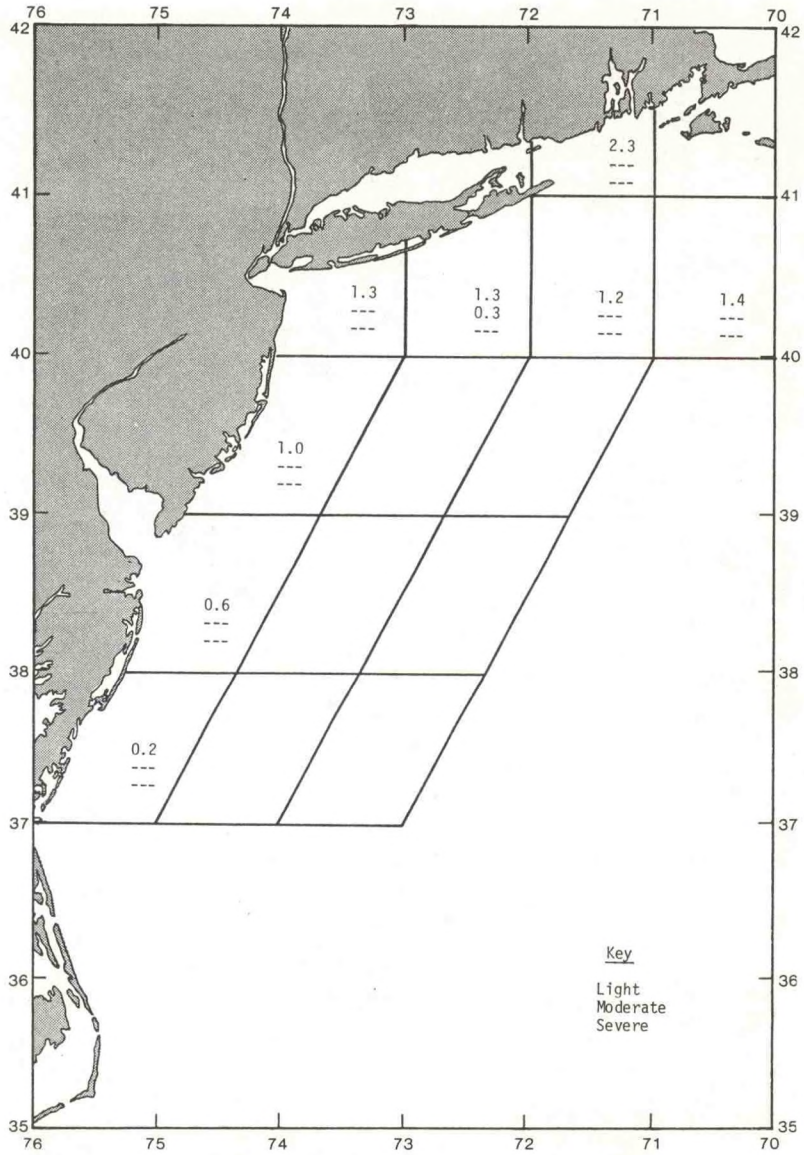


Figure 3.27.--March icing potential frequency.

# 4. CHARACTERISTICS OF WATER MASSES

Water masses are generally classified according to temperature and salinity characteristics. As applied to the deep ocean, the term "water mass" connotes a conglomerate of water having a specific temperature and salinity range, e.g., Pacific Deep Water, salinity = 34.66 to 34.69 parts per thousand (ppt), temperature = 1.5 to 2.0°C. Classification by temperature-salinity (T-S) characteristics has proved to be very useful, because it makes it possible to determine the water types that comprise the water masses and their origin. Hence, inferences can be drawn regarding circulation patterns within a given region from T-S characteristics. Knowledge of the distribution of dissolved oxygen and nutrients and of the resident biota is a valuable supplement to the T-S distributions in characterizing water masses in the oceans.

In shallow coastal waters and transition (slope) waters, the situation is far more complex than that found in the deep ocean. River drainage, continental extremes of atmospheric temperature, and biological activity lead to a much larger physical and chemical variability. As applied to the coastal environment, the term "water mass" must therefore be given a much more liberal interpretation, and the T-S analysis is correspondingly less precise. Nevertheless, studies of T-S correlations and distributions in coastal waters are indispensible in diagnosing coastal water structure.

The variables described in this study are those requisite for determining the behavior of pollutants, such as spilled oil, and the response of the environment to those pollutants. They include temperature, salinity, density, and specific volume anomaly, which is a good descriptor of the mass and pressure fields. The static stability E, i.e., the vertical space derivative of density, is also computed, since it provides one measure of the likelihood of vertical mixing.

The seasonal march of these variables is presented for the 12 oceanographic summary areas (see sec. 2.2, fig. 2.2), and means and variations are discussed. Spatial fields of temperature, salinity, density, and specific volume anomaly for selected depths are also presented for the oceanographic seasons, defined as:

Winter - January, February, March.
Spring - April, May, June.
Summer - July, August, September.
Fall - October, November, December.

## 4.1 Data Reduction and Analysis

The primary salinity-temperature-depth (STD) data, which include Nansen casts, from the National Oceanographic Data Center (NODC) were complemented by data obtained directly from Virginia Institute of Marine Science, Chesapeake Bay Institute, Massachusetts Institute of Technology, and NOAA's Marine Ecosystems Analysis (MESA) Program. Mechanical bathythermograph (MBT) and expendable bathythermograph (XBT) records and data on dissolved oxygen and nutrients were also provided by NODC. The latter constitutes a very small data base, from which only an outline of mean distributions could be obtained.

For the most part, the various types of data are summarized individually in order to facilitate comparative studies. A twofold approach was used in the characterization of water masses, and the concomitant evaluation of the data base:

(1) The Mid-Atlantic region was subdivided into 12 physically consistent areas for convenient summarization of hydrographic properties. In determining the shape of these areas (see sec. 2.2, fig. 2.2), an effort was made to limit the number of water masses in each area as much as possible. An aid in this effort was the quasi-objective analysis technique discussed below.

(2) Quasi-objective analysis of the physical parameters was made, and isopleths of these parameters at up to four depths for each season were prepared. The amount of data is minimal for this purpose but adequate for highlighting the major features of the area, as well as useful for evaluating the limitations of the current data base.

### 4.1.1 Quasi-Objective Analysis Technique

The quasi-objective method used to implement the twofold approach is called asymptotic singular decomposition (ASD), and is a method of empirical orthogonal function analysis. In ASD classifications several subjective judgments are necessary; hence the term "quasi-objective." The method was applied in this study to both the temperature-salinity (T-S) profiles for water mass classification, and to the temperature, salinity, density, and specific volume anomaly depth profiles in smoothing the data for the field analysis described in section 4.1.3. A very brief description of the ASD method is given here; the details of the technique, as well as examples of its application to coastal waters, are given in an article by Jalickee and Hamilton (1978), which is included as appendix B to this report. The method has also been described in more popular terms by Hamilton and Jalickee (1977).

The basic ASD procedure is to decompose a data set into a table of multiplicative factors that, when combined, can recreate the original data set to any desired degree of approximation. The factors are ordered so that, when the approximation is expressed as a sum, the first term accounts for the largest amount of the variance explained by any term in the sum, the second term for the second largest amount of variance,

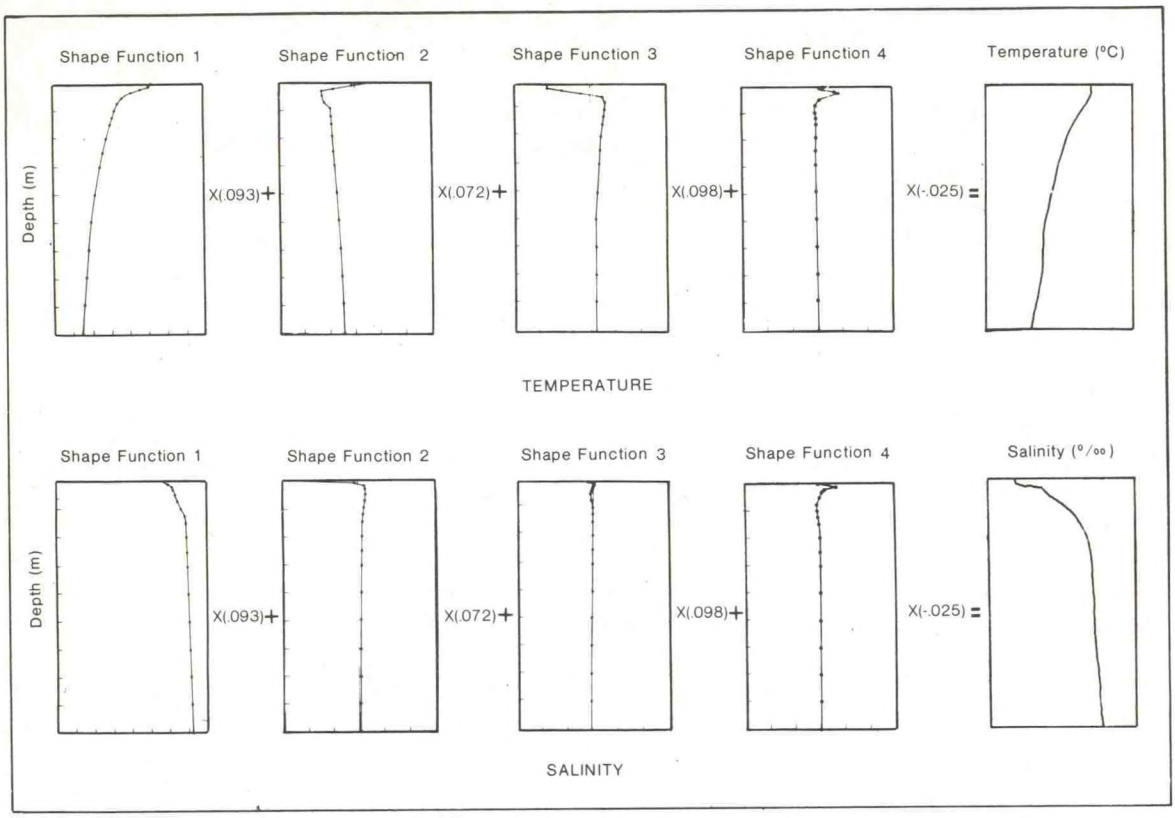


Figure 4.1(a).--Examples of "shape" functions that give the characteristic shapes of the temperature and salinity profiles (Hamilton and Jalickee, 1977)

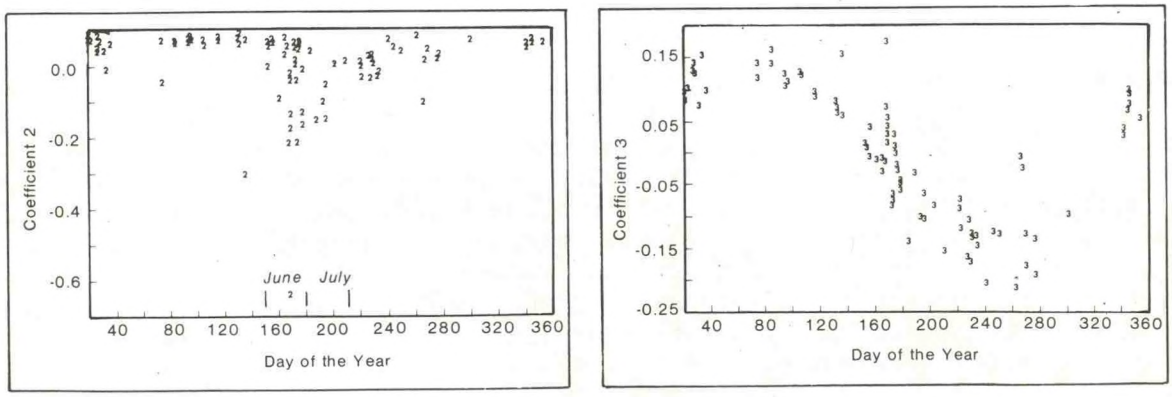


Figure 4.1(b).--Examples of station coefficients that relate "shape" functions to individual stations (Hamilton and Jalickee, 1977).

and so forth. This is useful in data smoothing, as explained in section 4.1.2. In contrast to other approximating expansions, such as the Fourier series or polynomial series, the factors are completely characterized by the data set and are not specified beforehand. In addition, they are an optimum representation of the data in the sense of least squares.

The terms in the expansion of the hydrographic data set consist of products of two types of terms: "shape functions," which give the characteristic shapes of the temperature and salinity profiles; and "station coefficients," which relate the shape functions to individual stations. Stations with similar T-S profiles have similar coefficients; stations with dissimilar profiles do not. This is what makes the classification possible. To proceed with the station classification, station coefficients and shape functions are rearranged, or rotated, by ASD to optimize the groupings (something like finding the principal axes of a rigid body). Then, each new shape function represents the T-S profile for one of the groups.

These procedures, illustrated in figures 4.1 and 4.2, were used to delineate the types and locations of water masses based on STD data for the Mid-Atlantic Bight, where the number of water masses is large and the hydrographic structure often is complex.

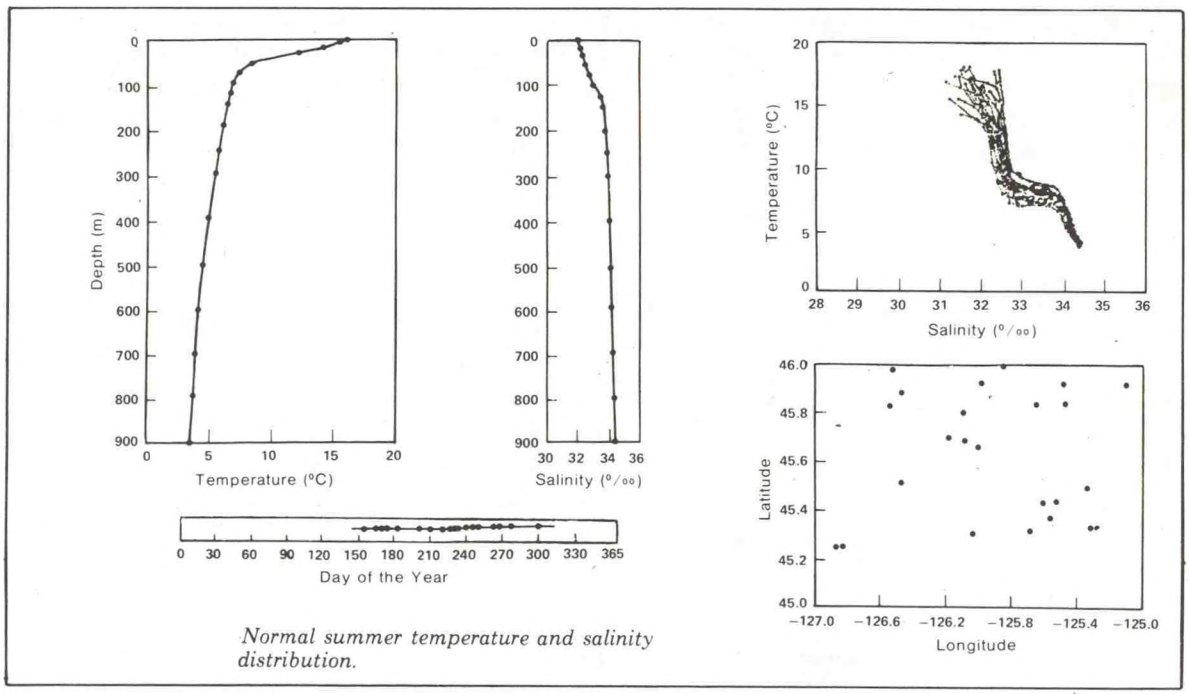


Figure 4.2.--Example of a group obtained by rotation of the factors to emphasize group distinctiveness (Hamilton and Jalickee, 1977).

### 4.1.2 Area Statistics

After the oceanographic areas had been identified, statistics -- including means, numbers of observations, extreme values, standard deviations, and histograms -- were computed from the MBT and XBT data by standard NODC software. The scatter in both data sets was very large for the individual frequency distributions at depth increments of 10 m, as seen in figure 4.3 for winter, area 6. Since it would be difficult to associate a unique distribution function with such histograms, the data were summarized over the following depth intervals:

| | |
|---|---|
| Mixed layer | 0 to 25 m |
| Upper thermocline | 25 to 50 m |
| Lower thermocline | 50 to 75 m |
| Subthermocline | 75 to 150 m |

The possibility of using temperature as a predictor of density was examined, but was not explored further; it was apparent from these data that salinity is often the predominating factor in determining density of Mid-Atlantic Bight waters.

A summary area analysis of the STD-Nansen cast data (similar to the one shown in figure 4.3) was done, but the results revealed large scatter in the data. Because it was suspected that this large scatter was due primarily to the presence of erroneous data, an editing and validation procedure was developed by the Applications Design Branch of NODC. This procedure consisted of decomposing the data for each area by the ASD method, identifying outliers in the station coefficients, and examining the T-S diagrams on the cathode ray tube of the NODC interactive computer system. Stations with obviously erroneous T-S characteristics were deleted from the data base. Soundings that did not reach a specified minimum depth, or contained an inadequate density of observations in depth for application of the ASD method, were deleted from the data base.

Subsequent recomputation of the summary statistics revealed, however, that many errors still remained, including misplaced decimal points and incorrect navigation data. Hence, it was necessary to manually review and validate the data for some areas. Details of this validation, and an accounting of data kept and rejected for this study, are given in appendix C. In future work, it is recommended that ASD editing be performed separately for temperature and salinity, since many types of errors are not evident from the T-S plots alone.

The statistical summaries were again rerun with the edited data for temperature and salinity, and also for the computed quantities of density ($\sigma_t$) and specific volume anomaly ($10^5\delta$).

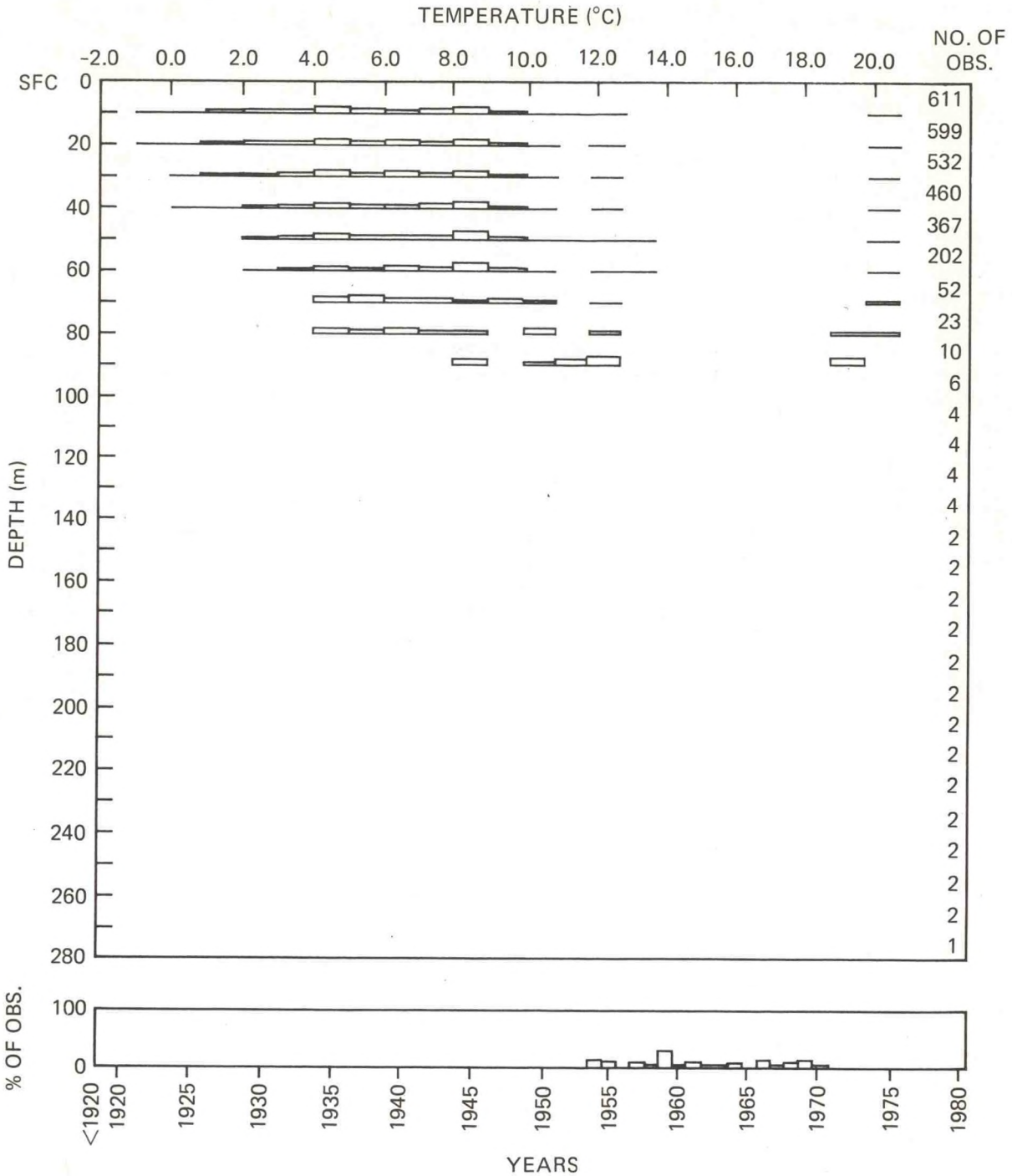


Figure 4.3.--Frequency distribution histogram based on MBT and XBT data, area 6, winter.

4.1.3 Field Analysis - Seasonal Means and Variability

The fields of temperature, salinity, density, and specific volume anomaly were analyzed and mapped for selected depth intervals of 0, 10, 50, 100, and 200 m. The procedure for generating these maps consisted of the following:

(1) The edited temperature and salinity data for each area were decomposed by the ASD method, interpolated points were generated where necessary, and only the first three terms of the decomposition were retained and used to regenerate the data. This process acts as a low-pass filter in reducing the noise in the data, while retaining the characteristic features.

(2) The ASD-smoothed soundings were basketed in ½° squares, and interpolations were made where necessary to obtain data at 5-m depth increments. Means and standard deviations were then computed for each ½° square.

(3) A data grid was prepared by entering the means and standard deviations within the ½° squares along with the number of observations used. Contours were drawn using a contour interval greater than the mean standard deviation over the entire Mid-Atlantic Bight to take into account the effects of internal waves and errors in the measurements, as explained in section 4.3.

## 4.2 Case Studies

Case studies, consisting of an analysis of individual quasi-synoptic hydrographic surveys, are useful in describing "typical" conditions when data are inadequate for a more comprehensive statistical description, or when one wishes to examine the characteristics of the individual events from which the statistics derive. In this section, data from four cruises are used for comparison of winter and summer conditions during 1967 and 1974 in the area under study.

### 4.2.1 Cresswell's Summer Synoptic Cruises (1958)

Cresswell (1967) conducted five monthly cruises during the spring and summer of 1958 for a detailed investigation of temperature and salinity distributions. Although these cruises were slightly to the east of the area under study here, his results are of interest, since many of the same features can be found in the Mid-Atlantic Bight. From analysis of his data Cresswell concluded the following:

(1) Continental shelf water exhibits marked seasonal variability, extends over the shelf edge, and intrudes into the slope water.

(2) The core of this shelf water is the winter-cooled shelf bottom water, which irregularly detaches from its parent water mass and moves across the salinity front (halocline) at the shelf break and into the slope water. This process, that of a "bubble" of cold shelf water detaching and moving into the slope water, is called "calving" and is believed to be the result of heavy shelf water at the shelf break, which is potentially unstable, being agitated by shoreward propagating internal waves.

(3) Calving is an important mechanism to induce mixing, and provides an outlet for the excess of fresh water acquired by river outflow.

Cresswell's hydrographic sections clearly showed the main features of the area in summer:

(1) The temperature and salinity front, which occurs at the region of the shelf break (depth = 100 m), separates fresh shelf water from more saline slope water, and slopes upward and seaward from the bottom in the region of the 100-m bathymetric contour.

(2) The seasonal thermocline intensifies as summer progresses, and very complex temperature structures develop on space scales of tens of kilometers. The seasonal march of temperature structure as depicted by Cresswell is shown in figure 4.4.

(3) Very cold water is found on the shelf on the bottom. This is the residual "winter" bottom water, which has been discussed in detail by Ketchum and Corwin (1974).

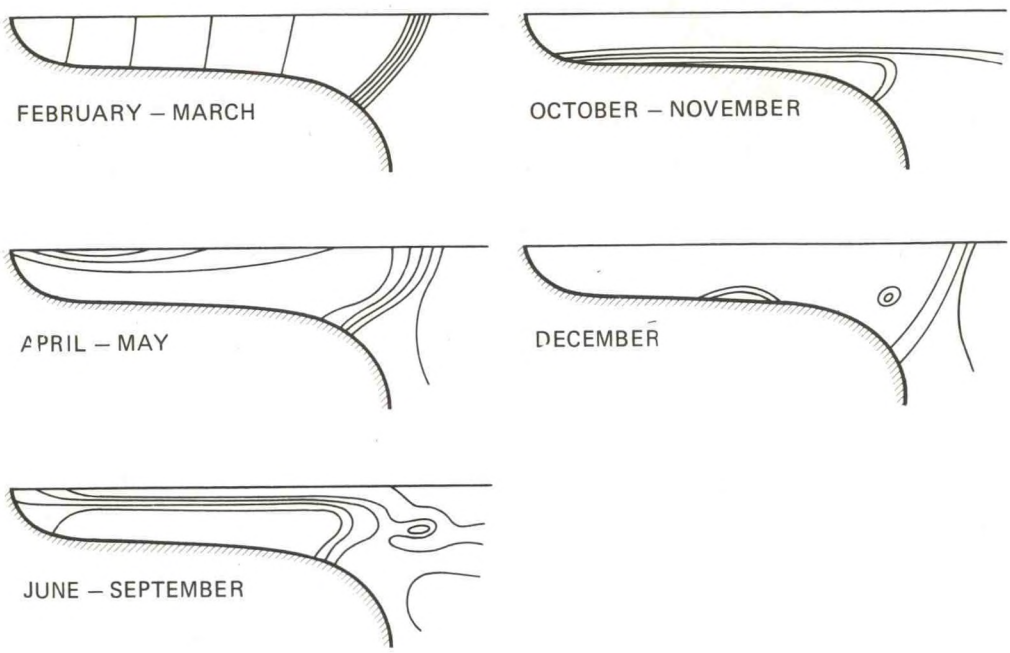


Figure 4.4.--Generalized development and deterioration of northwestern Atlantic shelf and slope temperature structure (Cresswell, 1967).

### 4.2.2 ICNAF Expeditions (1967)

As part of a study by the International Commission for the Northwest Atlantic Fisheries (ICNAF) of environmental conditions in the Bight, the USCGC Evergreen made two hydrographic surveys, one in September 1967 and the other in December 1967 (Whitcomb, 1970).

Water column structure can be studied from Whitcomb's vertical sections of temperature, salinity, and density, which are oriented approximately normal to the coast. Main temperature features in September were: (1) a strong seasonal thermocline, separating warm shelf surface water from the residual "winter" bottom water; and (2) an increase of mixed layer temperature, from 16.0°C near the coast to 21.0°C just seaward of the shelf break.

The vertical structure of salinity in summer included a strong salinity front at the shelf break, separating the coastal water with salinity of less than 34 parts per thousand (ppt) from the slope water with salinity of more than 35 ppt. On the shelf, the stratification was nearly horizontal and increasing seaward; seaward of the shelf break, it was vertical. The density slope front in summer resulted primarily from the salinity structure rather than from the temperature structure,

with an upward bulge of isopycnals in the shelf break region indicating motion with possible upwelling. This slope of the isopycnals on the shelf produced a geostrophic flow to the southwest, which agrees with observations of the mean flow in this area (Bumpus, 1973).

The winter temperature structure consisted of nearly homogeneous water on the shelf of 7 to 9°C, with a steeply inclined front at the shelf break. Water temperature increased by about 4°C over a distance of 20 nmi, and increased downward at the shelf break from about 9°C at the surface to 11°C at the bottom. Salinity increased slowly over the shelf, from 31.7 ppt near the shore to 32.7 ppt just north of the salinity front. These values were higher than in September, increasing across the front by 2 ppt (from 33 to 35 ppt) over a distance of about 20 nmi. The December density ($\sigma_t$) structure was nearly homogeneous on the shelf, with $\sigma_t$ = 26.25.

The following major conclusions were reached by Whitcomb from study of all September and December data:

(1) The cold core of "winter" water, which he defines as being 8°C or less, prevailed in September from Cape Cod to just offshore Chesapeake Bay.

(2) A warm core layer with temperatures exceeding 14°C was found in December along the shelf break from the waters off Maryland northward.

(3) Evidence of "calving" was found in these data.

(4) A counterflow inshore of the Gulf Stream, to the southwest, was deduced from the density field.

### 4.2.3 MIT New England Shelf Dynamics Experiment (1974)

Another winter cruise in the area made in late February and early April 1974 by the USCGC Dallas as part of the MIT New England Shelf Dynamics Experiment has been reported on by Flagg and Beardsley (1975). The second leg of this cruise was fairly close to the path followed in 1967 during the ICNAF expeditions by the USCGC Evergreen (Whitcomb, 1970) along the 72nd meridian southeast of Montauk Point, New York. The eastern legs of the Dallas cruise were essentially repeated during March and April 1974 by the R/V Verrill, and Flagg and Beardsley note that only slight changes in the hydrographic structure took place during the 3-month period.

### 4.2.4 U.S. Coast Guard Mid-Atlantic Bight Survey (1974)

The Mid-Atlantic Bight was surveyed by the USCGC Evergreen in August 1974, and the results have been reported by Morgan et al. (1976). Stations 32-36 during this cruise also cut across the 72nd meridian.

### 4.2.5 Comparisons of Conditions in 1967 and 1974

The ICNAF, MIT, and USCG Mid-Atlantic Bight cruises make close comparison of both winter and summer conditions in 1967 and 1974 possible.

The locations of the hydrographic sections compared below are shown in figure 4.5. Vertical sections of temperature, salinity, and density were redrawn on a common scale to make the comparisons easier.

Winter. As seen from the vertical temperature structures in figure 4.6, the slope front occurs in about the same place (above the 100-m isobath) and could be denoted by the same isotherm (10°C). Temperatures on the shelf are shown to be somewhat colder in the 1974 MIT Dallas section than in the 1967 ICNAF Evergreen section, but this may be due partly to seasonal changes, since the Dallas section was made in February, while the Evergreen section was made in December. Temperature is seen to increase slightly with depth in both sections on the shelf, and more rapidly with depth as the slope front is crossed. The salinity patterns are also similar, as seen in figure 4.7, but the Dallas salinities are higher, with the 34-ppt isohaline reaching the bottom at the 60-m isobath. In the case of the Evergreen, the intersection depth is over 100 m. The major feature on the shelf is the small positive salinity gradient, which increases as the shelf break is approached. The density sections on both cruises show similar patterns in the isopycnals (fig. 4.8), but the Dallas values are higher on the shelf by about 0.5 $\sigma_t$ units. The topography of the $\sigma_t$ = 26.5 surface from the Dallas cruise exhibits wavelike behavior, typical of the slope front (Flagg and Beardsley, 1975).

On the R/V Verrill cruise in March and April 1974, the slope of the front increased, but its center remained within $\pm$ 5 km of its initial position. The same isotherms and isohalines seemed to define the front.

Summer. Figure 4.9, which shows the vertical temperature sections, indicates that much warmer surface waters and slightly warmer bottom waters were found in the summer of 1974 than in 1967. The predominant vertical stratification is evident in both sections, but is much more intense in the August 1974 section. Winter bottom water is present in both sections, but was colder in September 1967. The seasonal thermocline extended further seaward in 1974 than in 1967, when this region appeared to be occupied by an eddy (Whitcomb, 1970). The salinity structure for the 1974 cruise shown in figure 4.10 appears rather different from the 1967 section. The 1974 section shows higher salinities on the shelf, but lower salinities seaward on the shelf break. Both sections show salinity inversions in the frontal region. Indications of a core of low salinity water of less than 34 ppt in the 1974 section might be evidence of a calved "bubble." The 1974 density section, when compared with the 1967 section (fig. 4.11) shows a similar pattern of isopycnals sloping upward in the offshore direction, but the stratification is more intense in the August 1974 than in the September 1967 section.

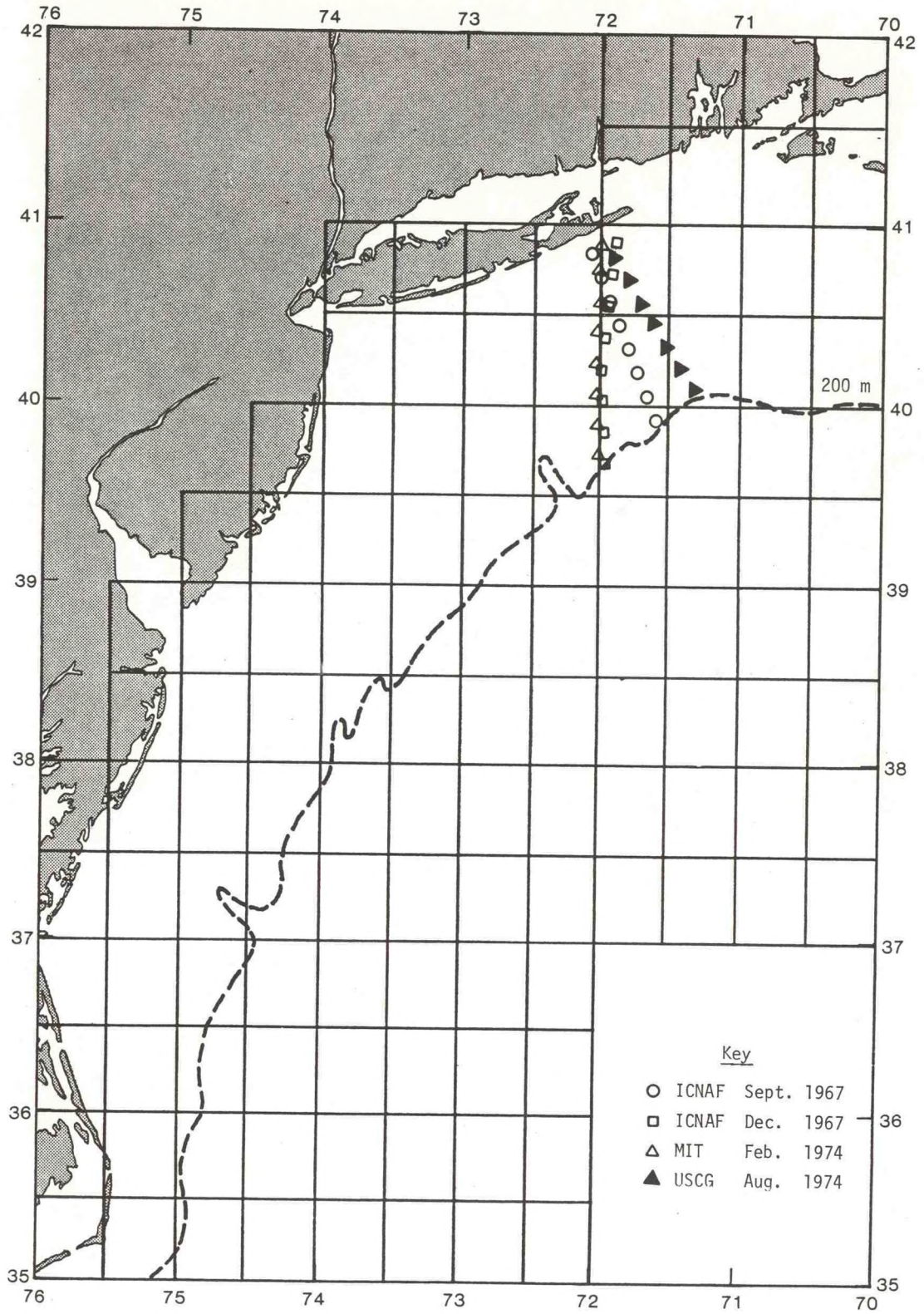


Figure 4.5.--Locations of hydrographic sections compared in text.

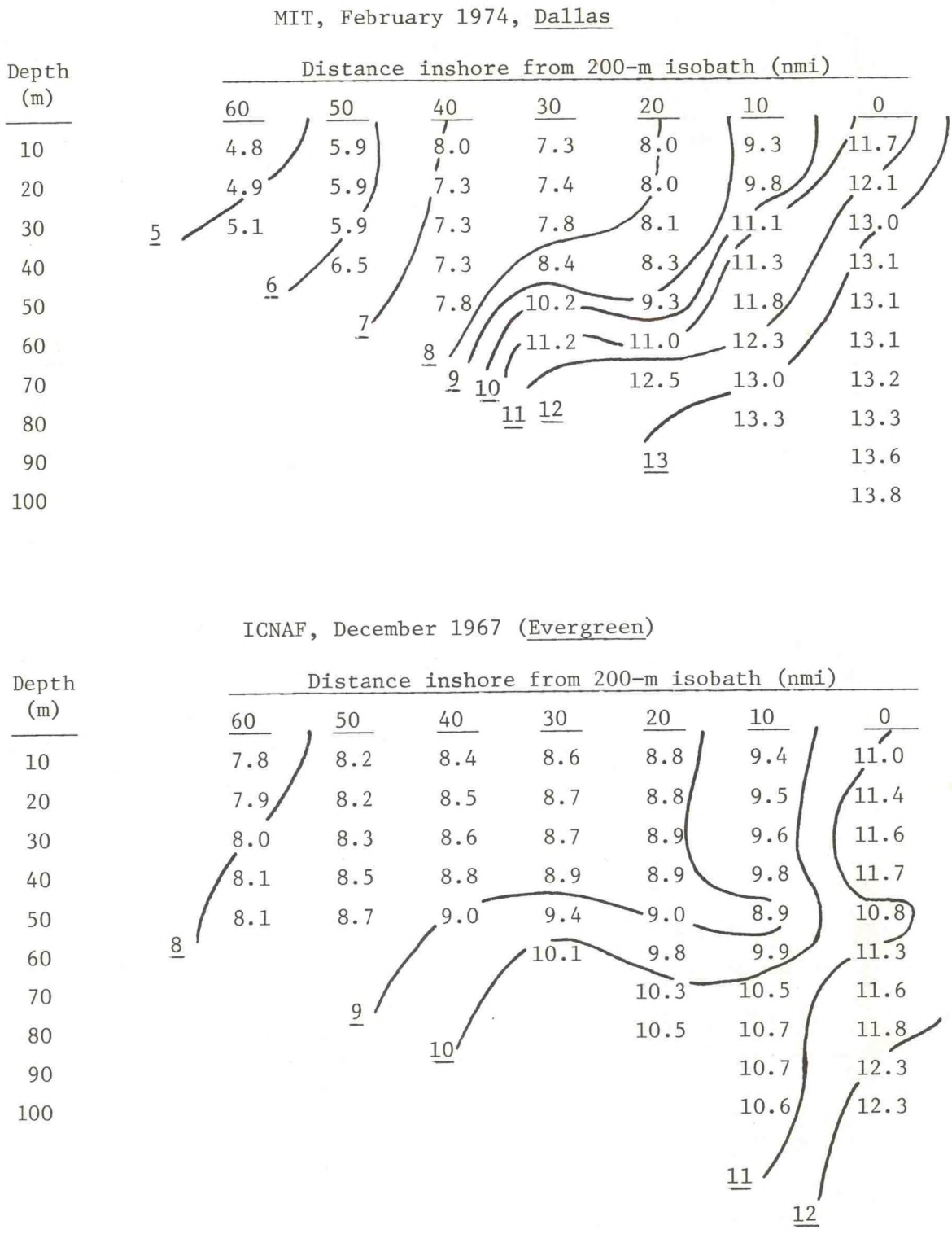


Figure 4.6.--Comparative vertical temperature sections southeast of Montauk Point, New York, in winter 1967 and 1974.

MIT, February 1974, (Dallas)

| Depth (m) | Distance inshore from 200-m isobath (nmi) | | | | | | |
|---|---|---|---|---|---|---|---|
| | 60 | 50 | 40 | 30 | 20 | 10 | 0 |
| 10 | 32.1 | 32.7 | 33.0 | 33.3 | 33.7 | 34.0 | 35.0 |
| 20 | 32.6 | 32.8 | 33.1 | 33.4 | 33.7 | 34.0 | 35.1 |
| 30 | 32.7 | 32.8 | 33.4 | 33.6 | 33.7 | 34.2 | 35.2 |
| 40 | | 33.1 | 33.6 | 33.7 | 33.8 | 34.9 | 35.2 |
| 50 | 33 | | 33.8 | 33.8 | 34.1 | 35.1 | 35.5 |
| 60 | | | | 33.9 | 34.4 | 35.1 | 35.5 |
| 70 | | | | 34 | | 35.1 | 35.5 |
| 80 | | | | | | 35.2 | 35.5 |
| 90 | | | | | | 35 | 35.5 |
| 100 | | | | | | | 35.5 |

ICNAF, December 1967 (Evergreen)

| Depth (m) | Distance inshore from 200-m isobath (nmi) | | | | | | |
|---|---|---|---|---|---|---|---|
| | 60 | 50 | 40 | 30 | 20 | 10 | 0 |
| 10 | 32.2 | 32.5 | 32.6 | 32.6 | 32.7 | 33.1 | 34.0 |
| 20 | 32.2 | 32.5 | 32.6 | 32.6 | 32.7 | 33.2 | 34.1 |
| 30 | 32.3 | 32.5 | 32.6 | 32.6 | 32.7 | 33.2 | 34.2 |
| 40 | 32.4 | 32.6 | 32.6 | 32.6 | 32.7 | 33.2 | 34.2 |
| 50 | | | 32.6 | 32.7 | 32.7 | 33.3 | 34.3 |
| 60 | | | | 32.7 | 32.7 | 33.4 | 34.3 |
| 70 | | | | | 32.7 | 33.5 | 34.4 |
| 80 | | | | | 32.7 | 33.7 | 34.5 |
| 90 | | | | | | 33.9 | 34.6 |
| 100 | | | | | 33 | | 34.8 |
| | | | | | | 34 | |

Figure 4.7.--Comparative vertical salinity sections southeast of of Montauk Point, New York, in winter 1967 and 1974.

MIT, February 1974, Dallas

| Depth (m) | Distance inshore from 200-m isobath (nmi) | | | | | | |
|---|---|---|---|---|---|---|---|
| | 60 | 50 | 40 | 30 | 20 | 10 | 0 |
| 10 | 5.30 | 5.79 | 5.95 | 6.13 | 6.25 | 6.35 | 6.57 |
| 20 | 5.60 | 5.80 | 6.03 | 6.16 | 6.26 | 6.38 | 6.72 |
| 30 | 5.65 | 5.87 | 6.19 | 6.22 | 6.28 | 6.53 | 6.72 |
| 40 | | 6.02 | 6.25 | 6.30 | 6.31 | 6.64 | 6.72 |
| 50 | | 26.0 | 6.28 | 6.32 | 6.50 | 6.67 | 6.73 |
| 60 | | | | 6.38 | 6.62 | 6.70 | 6.75 |
| 70 | | | | | 6.63 | 6.71 | 6.75 |
| 80 | | | | 26.5 | | 6.70 | 6.77 |
| 90 | | | | | | | 6.80 |
| 100 | | | | | | | 6.83 |

ICNAF, December 1967 (Evergreen)

| Depth (m) | Distance inshore from 200-m isobath (nmi) | | | | | | |
|---|---|---|---|---|---|---|---|
| | 60 | 50 | 40 | 30 | 20 | 10 | 0 |
| 10 | 5.15 | 5.30 | 5.35 | 5.40 | 5.45 | 5.65 | 6.00 |
| 20 | 5.15 | 5.30 | 5.35 | 5.40 | 5.45 | 5.60 | 6.00 |
| 30 | 5.20 | 5.30 | 5.35 | 5.40 | 5.45 | 5.60 | 6.00 |
| 40 | 5.20 | 5.30 | 5.35 | 5.40 | 5.45 | 5.65 | 6.00 |
| 50 | | 5.30 | 5.35 | 5.40 | 5.45 | 5.70 | 6.15 |
| 60 | | | | 5.50 | 5.50 | 5.80 | 6.20 |
| 70 | | | 25.5 | | 5.80 | 6.00 | 6.25 |
| 80 | | | | | 5.90 | 6.20 | 6.45 |
| 90 | | | | | | 6.45 | 6.70 |
| 100 | | | | | 26.0 | 6.60 | 6.80 |
| | | | | | | 26.5 | |

Figure 4.8.--Comparative vertical density ($\sigma_t$) sections southeast of Montauk Point, New York, in winter 1967 and 1974.

USCG, August 1974, (Evergreen)

| Depth (m) | Distance inshore from 200-m isobath (nmi) | | | | | | |
|---|---|---|---|---|---|---|---|
| | 60 | 50 | 40 | 30 | 20 | 10 | 0 |
| 10 | 20.0 | 20.5 | 20.5 | 21.5 | 22.5 | 23.0 | 23.0 |
| 20 | 16.0 | 15.0 | 16.0 | 20.0 | 21.0 | 22.5 | 22.3 |
| 30 | 14.5 | 11.0 | 11.0 | 14.0 | 18.0 | 20.0 | 20.0 |
| 40 | 13.0 | 10.0 | 10.0 | 10.0 | 15.0 | 17.0 | 14.0 |
| 50 | | 10.0 | 9.5 | 10.0 | 13.5 | 15.5 | 12.0 |
| 60 | | | 9.5 | 9.5 | 12.0 | 14.5 | 13.0 |
| 70 | | | | 9.5 | 11.0 | 14.0 | 13.0 |
| 80 | | | | | | 13.5 | 13.5 |
| 90 | | | | | | 13.5 | 13.8 |
| 100 | | | | | | | 13.9 |

ICNAF, September 1967 (Evergreen)

| Depth (m) | Distance inshore from 200-m isobath (nmi) | | | | | | |
|---|---|---|---|---|---|---|---|
| | 60 | 50 | 40 | 30 | 20 | 10 | 0 |
| 10 | 15.5 | 16.0 | 15.4 | 16.2 | 17.8 | 18.7 | 19.5 |
| 20 | 14.7 | 15.2 | 14.5 | 14.6 | 16.2 | 18.0 | 18.5 |
| 30 | 14.3 | 13.0 | 13.0 | 13.0 | 13.2 | 13.9 | 15.5 |
| 40 | 11.7 | 10.0 | 9.0 | 9.6 | 10.0 | 10.0 | 12.5 |
| 50 | 9.8 | 9.2 | 8.5 | 8.2 | 8.0 | 8.5 | 11.0 |
| 60 | | 9.2 | 8.5 | 7.8 | 7.8 | 8.5 | 10.9 |
| 70 | | | | | 7.8 | 8.5 | 11.0 |
| 80 | | | | | | 8.7 | 11.2 |
| 90 | | | | | | 8.7 | 11.2 |
| 100 | | | | | | 9.2 | 11.9 |

Figure 4.9.--Comparative vertical temperature sections southeast of Montauk Point, New York, in summer 1967 and 1974.

USCG, August 1974 (Evergreen)

| Depth (m) | Distance inshore from 200-m isobath (nmi) | | | | | | |
|---|---|---|---|---|---|---|---|
| | 60 | 50 | 40 | 30 | 20 | 10 | 0 |
| 10 | 31.5 | 32.0 | 32.5 | 33.5 | 34.4 | 35.2 | 35.2 |
| 20 | 32.5 | 32.3 | 32.6 | 33.0 | 34.1 | 35.2 | 35.0 |
| 30 | 32.3 | 32.4 | 32.6 | 33.1 | 34.0 | 35.2 | 34.5 |
| 40 | | 32.6 | 32.7 | 33.2 | 34.4 | 35.4 | 34.3 |
| 50 | | 32.6 | 32.7 | 33.3 | 34.4 | 35.3 | 34.6 |
| 60 | | | 32.8 | 33.3 | 34.4 | 35.6 | 34.9 |
| 70 | | | | 33.3 | 34.3 | 35.6 | 35.3 |
| 80 | | | | | 34.0 | 35.6 | 35.5 |
| 90 | | | | | | 35.6 | 35.6 |
| 100 | | | | | | | 35.6 |

32 33 34 35 35

ICNAF, September 1967 (Evergreen)

| Depth (m) | Distance inshore from 200-m isobath (nmi) | | | | | | |
|---|---|---|---|---|---|---|---|
| | 60 | 50 | 40 | 30 | 20 | 10 | 0 |
| 10 | 32.0 | 32.3 | 32.6 | 33.2 | 33.8 | 34.2 | 34.8 |
| 20 | 31.8 | 32.2 | 32.5 | 33.0 | 33.8 | 34.1 | 34.6 |
| 30 | 31.8 | 32.2 | 32.4 | 32.8 | 33.3 | 33.7 | 34.2 |
| 40 | 32.0 | 32.2 | 32.4 | 32.6 | 32.9 | 33.5 | 34.2 |
| 50 | 32.1 | 32.3 | 32.4 | 32.6 | 32.9 | 33.6 | 34.3 |
| 60 | | | 32.5 | 32.7 | 33.1 | 33.6 | 34.3 |
| 70 | | | | | 33.2 | 33.6 | 34.3 |
| 80 | | | | | | 33.7 | 34.4 |
| 90 | | | | | | 33.8 | 34.6 |
| 100 | | | | | | 34.2 | 34.8 |

32 33 34

Figure 4.10.--Comparative vertical salinity sections southeast of Montauk Point, New York, in summer 1967 and 1974.

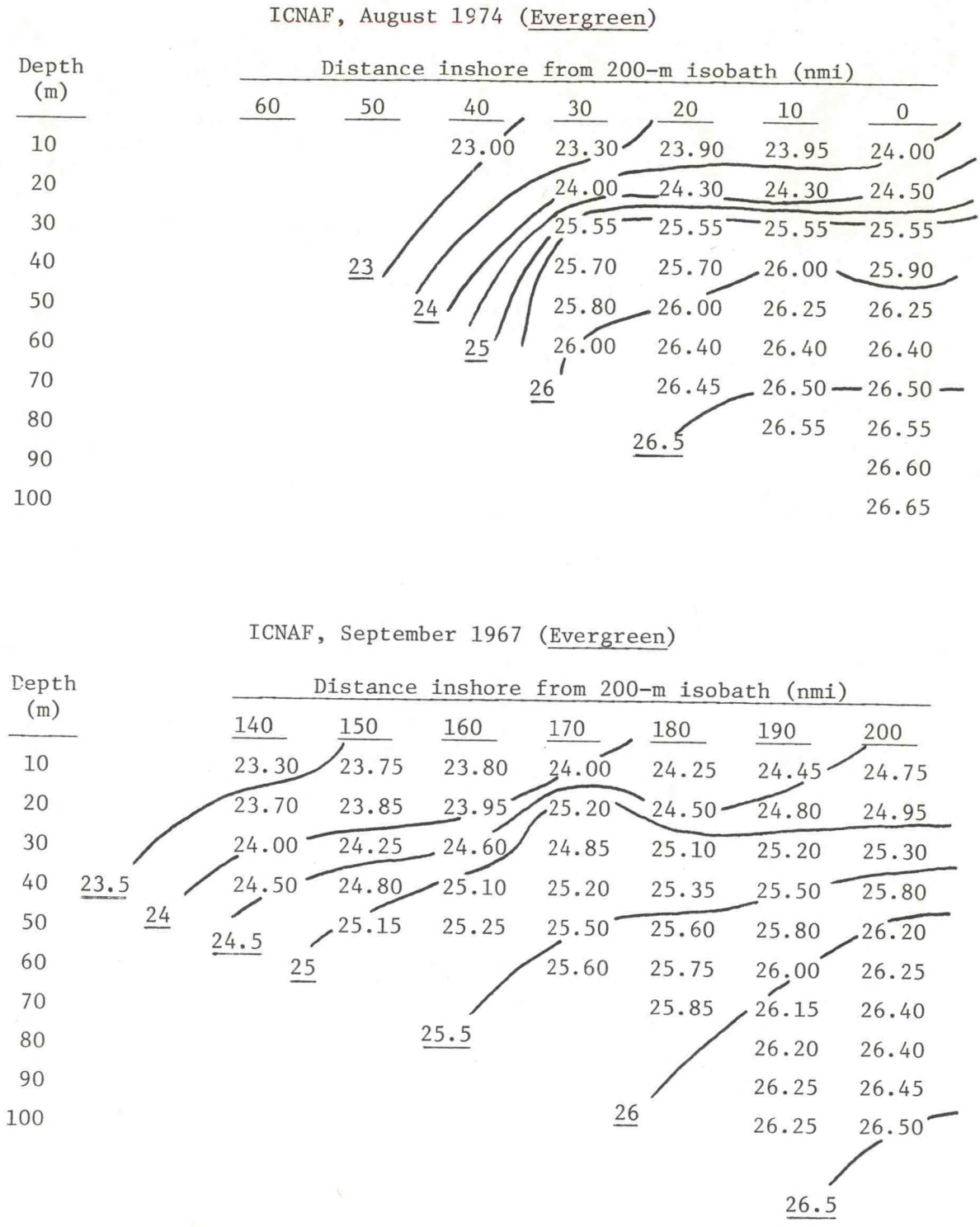


Figure 4.11.--Comparative vertical density ($\sigma_t$) sections southeast of Montauk Point, New York, in summer 1967 and 1974.

### 4.2.6 Summary

Vertical sections of oceanographic properties in the same area have been examined based on results from four cruises, two in 1967 and two in 1974. The major features are similar in all cases, but there are some significant differences both in magnitudes of mean quantities and in detailed characteristics. From this sampling, the differences between summer and winter temperatures and water densities are seen to be larger than between the two years for the same season. Year-to-year salinity variations, however, appear to be the same order of magnitude as summer-to-winter variations (see sec. 4.4.6). In general, however, the magnitudes of the errors encountered by combining data grouped by season over several years seem to be acceptable for delineating seasonal variability.

## 4.3 Internal Waves

The internal waves of the ocean encompass a broad spectral range of phenomena, ranging from oscillations at the Brunt-Väisalä frequency with periods of a few minutes to topographic Rossby waves with periods of a month or more. In this section internal waves between the Brunt-Väisalä frequency and the diurnal tidal frequency are considered, since this is the band that is potentially most troublesome, distorting hydrographic observations. Some observations of internal waves made in the Mid-Atlantic Bight are reviewed in section 4.3.1. The effects such waves could have on the analysis presented in this report are discussed in section 4.3.2.

### 4.3.1 Measurements of Internal Waves in the Mid-Atlantic Bight

Internal waves are difficult to measure and to positively identify. Unless experiments are specifically designed for such measurements the waves will manifest themselves as noise in the hydrographic data. One of the few internal wave experiments conducted in the Mid-Atlantic Bight was that by Apel and colleagues (Apel et al., 1975a; Proni and Apel, 1975; Apel et al., 1975b), who observed internal waves in the Bight simultaneously with the Earth Resources Technology Satellite (ERTS) and with a shipboard high frequency acoustic sounder. These observations depended on two properties of internal waves: (1) under calm conditions, internal waves are accompanied by slicks on the sea surface, which change the optical surface reflectivity; and (2) either through an accumulation of plant and animal material on the thermocline, or by density differences, internal waves create an acoustically reflecting surface (for resonant acoustic frequencies) that can be used to monitor the wave profiles. The following results were obtained from these experiments:

(1) Internal waves were detected as groups or "packets" propagating shoreward from the edge of the continental shelf. These packets were separated by distances of 15 to 30 km.

(2) The waves appeared to be of tidal origin, i.e., the generating mechanism is hypothesized to be the diurnal barotropic tide (surface tide) that is scattered into baroclinic (internal) modes at the edge of the continental shelf.

(3) The wave crests were nearly always parallel to shore, with some focusing of wave energy at Hudson Canyon.

(4) The wavelengths of the waves within the packets were between 300 and 4,000 m with phase speeds of about 0.25 m/s to 0.35 m/s.

(5) The amplitudes of the waves were estimated to be on the order of 15 to 20 m from crest to trough.

(6) Internal waves with wavelengths of about 500 m were observed, with periods about 20 min and phase speeds of about 0.35 m/s.

(7) Typical packet lengths were on the order of 3 km.

(8) The waves seemed to disappear near the 50-m depth contour.

(9) The waves were observed only in summer and fall.

An earlier internal wave experiment was conducted by Gaul (1961a and b), who deployed taut-moored buoys with platinum resistance thermometers within 100 m of Texas Tower No. 4., located about 70 mi southeast of New York City. Measurements were made in the early fall of 1959 and late spring of 1959 (May 13 to June 4). His conclusions are as follows:

(1) Internal temperature disturbances, resembling solitary waves, were quite common under conditions of vertical stability (temperature decreasing with depth).

(2) The waves occurred in groups of one to four and moved shoreward at about 0.5 m/s.

Gaul does not discuss the amplitudes of the waves, but he shows temperature fluctuations as high as 5°C at a single depth. From his mean temperature vs. depth profiles, this would require a displacement in the isothermal surfaces on the order of 20 m in depth.

Griscom (1968) monitored temperature at several depths, also at Texas Tower No. 4. His measurements covered the period from October 14 to 25, 1959, when stratification would not be expected to be strong. A rather weak tidal connection was found in his temperature data at 30-m depth (15 percent of the total variance), and 35 percent of the variance at 40 m was associated with the semidiurnal tidal frequency. The magnitude of these variations was $\pm$ 0.8°C at 30 m and $\pm$ 1.5°C at 40 m. The spectra of the temperature deviations indicated large, unresolved, very low frequency variances of weeks or more with no distinguishable peaks. The spectrum was relatively flat at frequencies above 1 cycle/hr, indicating that wave activity was slight during the observation period. The strongest temperature fluctuations at the site appeared to be associated with wind shifts, rather than with internal waves.

Flagg et al. (1976) used taut-moored arrays southeast of Long Island (40°54.0'N, 70°4.3'W) to measure current and temperature on the continental shelf from late February to early April 1974 during the time of weak vertical stratification. They found that tidal components were not dominant in the temperature spectra, with most of the variability occurring at very low frequencies. More energetic fluctuations were found at 70-m depth further out on the shelf (40°18.2'N, 70°51.4'W), but the preponderance of energy was still at the very low unresolved frequencies, corresponding to periods of 100 hr or more.

Evidence from the above observations and from observations by Wunsch and Hendry (1972) and Halpern (1971) just north of the area

under study indicate that tidally related internal waves in the Mid-Atlantic region occur predominantly during periods of strong vertical stratification of the outer and midshelf regions in the late spring, summer, and early fall. The waves propagate in groups or "packets," with, perhaps, 3 to 10 waves per packet, and travel toward the shore at speeds of 0.2 to 0.5 m/s. Amplitudes of the waves range from 4 to 20 m in crest-to-trough distance. Observed wavelengths range from 300 to 4,000 m.

### 4.3.2 Effects of Internal Waves on Hydrographic Data

Since this study is a statistical one, and incorporates data from several years and from a variety of measuring systems, the only practical approach to the problem of the effect of internal waves on hydrographic data is to attempt to estimate error bounds on the data that could result from internal wave activity, and to compare the size of these errors with the errors expected from other sources. Except for the shelf break region, the seasonal march of vertical stratification in the Bight is such that internal waves of significant intensity are generally found during the warm half of the year only. During late fall, winter, and early spring, internal wave activity is weak and typical errors in hydrographic data summaries associated with each station should be small (1°C in temperature) compared with other sources, such as the variation in mean water column temperature from year to year, which may be several degrees at any given location. Hence, when data from several years are combined, year-to-year variability will most probably overpower any errors caused by internal wave activity.

During the warm half of the year, however, errors in measurement at specific depths introduced by internal wave activity can be of the same order of magnitude as the errors generated by combining data from several years. Consider figure 4.12, which is a plot of temperature vs. depth for the USCGC Evergreen station 44 (40° 14.0'N, 70° 29.8'W) in 1974 (Morgan et al., 1976). It is assumed that the data on which the profile is based do not show the effect of internal waves. If internal waves were present, with maximum amplitude of 20 m at the thermocline, the profile might be distorted as in figure 4.12(a) if the crest of a wave were under the ship, and as in (b) if the trough were under the ship. This is a highly simplified picture of the situation, but it does show an error band on the order of ± 5°C in the thermocline region. Internal wave effects would be much reduced away from the thermocline. The possible variation in this profile can be compared with year-to-year variability by noting temperature vs. depth for the USCGC Evergreen station 15 at a nearby position (40° 00'N, 71° 00'W) measured in September 1967 (fig. 4.13). It is seen that variability within the thermocline during the warm season due to internal waves could be of the same order of magnitude as year-to-year variability. Note also that the error would probably be more serious for STD casts than for Nansen casts, because an STD cast is a near-instantaneous profile of temperature and salinity, whereas Nansen bottles are allowed to "soak" at a given depth and provide an average temperature over about a 10-min interval.

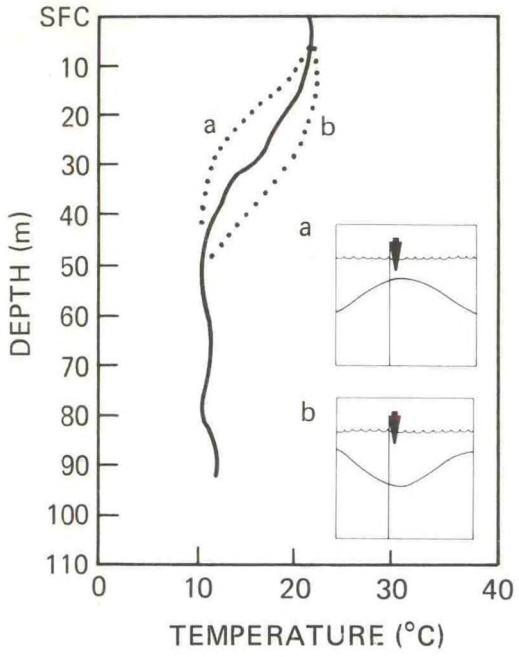


Figure 4.12.--Temperature vs. depth, Evergreen station 44, August 1974.

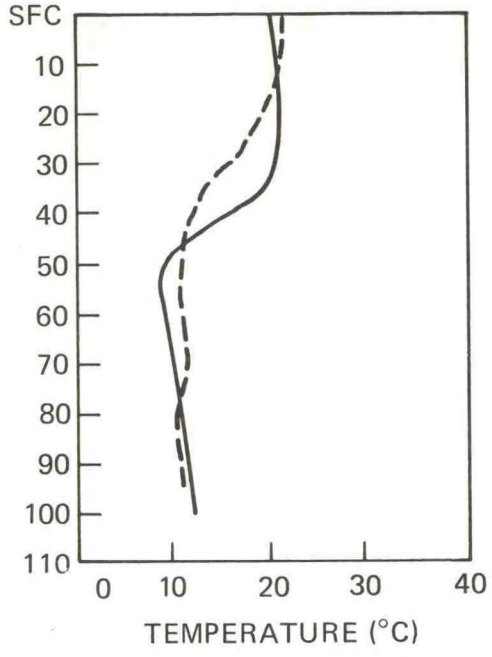


Figure 4.13.--Temperature vs. depth, Evergreen station 15, September 1974 (dashed line = station 44).

The question remains as to what procedures can be used to account for the variability due to internal waves in attempting to provide the best estimate of parameter means at given depths. Three methods are potentially available:

(1) "Isentropic" analysis--mapping the oceanographic properties on density ($\sigma_t$) surfaces (Montgomery, 1938). This procedure corrects for internal waves, since the parameter in question, say temperature, is assigned its correct density rather than nominal depth, and the analysis then proceeds in density coordinates. The problem with applying this method to the Mid-Atlantic data is that it is best suited to the main oceanic thermocline--away from such surface effects as heating, cooling, and bottom friction--since the assumptions made in the formulation of "isentropic analysis" prohibit strong local sources and sinks. The method could conceivably be used here, but several problems regarding relaxation of the assumptions and incorporation of boundary conditions would have to be solved first.

(2) Vertical averaging--taking vertical averages over depth intervals larger than the amplitudes of the internal waves. This procedure gives accurate averages, but obscures detail in the vertical structure. It has been used in two types of analyses for this report: the ASD method (sec. 4.1.1) smooths the data in the vertical, and the frequency-parameter histograms

(sec. 4.1.2) cover intervals that should be large enough to "average over" internal wave effects.

(3) Constant level analysis--mapping oceanographic properties at discrete depths. Wyrtki (1971), in preparing constant-level charts for the Indian Ocean, notes that internal waves, as well as other periodic and nonperiodic disturbances, contribute to the variability of oceanographic properties at any given depth. All this variability is summed as one number: the standard deviation of the parameter at a given depth. This standard deviation then determines the contour interval to be applied in the analysis of the data, i.e., the contour interval should be at least as large as the standard deviation. The maps thus prepared show contours that reflect the uncertainty in the data, and give a measure of the mean structure of the fields only, not of their variability. Wyrtki also allowed the isopleths to deviate from observations by an amount equal to the standard deviation of the charted property in the corresponding area.

Wyrtki's procedures were adopted for the field analysis presented in the next section of the physical variables at chosen, fixed depths. The contour intervals were obtained by averaging the standard deviations for all areas, and using the mean standard deviation for each chart.

## 4.4 Seasonal Means and Variability

The results of the water analysis are presented in this section. Area statistics for temperature and salinity are given, followed by the results of the temperature-salinity (T-S) classification study, which highlights the most important features of the T-S distribution in the Mid-Atlantic region. The derived quantities of water density ($\sigma_t$) and specific volume anomaly ($\delta$) are presented next, and conclusions are drawn regarding the adequacy and utility of the historical hydrographic data base.

### 4.4.1 Sea-Surface Temperature

Knowledge of sea-surface temperature is important in determining the behavior of spilled oil, since it affects the "weathering" of the oil, as well as in determining whether the spilled oil will be in a purely liquid or liquid-solid state. The Marine Deck observations from transient ships on file at the National Climatic Center (NCC) is a major source of sea-surface temperature data, and constitutes a much larger data base than is available for subsurface temperatures. These data should be used with some care, however, because of the lack of standardized observation methods used aboard ships. Many measurements are obtained by reading engine room injection temperatures. In other cases, a water sample is simply drawn with a bucket and temperature is read with a mercury thermometer before, it is hoped, evaporation can have too great an effect. Uniform standards for thermometer calibration, are in general, not applied.

Nevertheless, it is generally assumed that random errors tend to cancel and that a meaningful average can be obtained when a sufficient number of observations is used. In a recent study based on Marine Deck surface temperature data, Fieux and Stommel (1975) examined long-term temperature trends in the North Atlantic east of Bermuda, and the general suitability of Marine Deck temperatures for climatological studies. They showed that in the area between 50°W and 60°W a cold period prevailed between 1910 and 1920, followed by a warming between 1925 and 1930, cooling from 1935 to 1940, warming during the 1950's, and cooling up to 1972. They compared Marine Deck temperatures and temperatures obtained at 32°20'N, 64°45'W once or twice a month from 1954 to 1974 by a research vessel from the Bermuda Biological Station. Variations in sea-surface temperature were found to be similar in the two data sets except for one period in 1962.

A second comparison made by Fieux and Stommel between Marine Deck temperatures and temperatures observed by Ocean Weather Station (OWS) ECHO at 35°N, 48°W did not show good agreement. The temperatures at OWS ECHO were sometimes much colder, and the fluctuations were not well correlated. In a third comparison, between Marine Deck temperatures and bathythermograph (BT) data on file at Woods Hole Oceanographic Institution, individual BT's showed a large spread, even during a single month. In general, however, the values centered on the Marine Deck temperatures.

The comparison with the temperatures obtained by the research vessel from the Bermuda Biological Station was considered to be the most significant

of the three, since these data, although small in number, were acquired with great care.

Fieux and Stommel found the standard deviation of an individual Marine Deck observation to be on the order of ± 0.8°C. With 50 observations, the 95 percent confidence interval was found to be ± 0.28°C; with 100 observations, ± 0.19°C. Also, the confidence interval improved with time; in 1970 it was ± 0.09°C. In the analysis presented here, the 95 percent confidence intervals ranged from a high of ± 0.61°C for area 2 in summer to a low of ± 0.11°C for areas 6, 10, and 15 in summer.

Monthly averaged values and standard deviations for representative months as computed from Marine Deck sea-surface temperatures are shown in figures 4.14 to 4.17. The number of observations used in computing these averages is listed, by area, in table 4.1.

Table 4.1.--Number of observations of sea-surface temperature used in computing representative monthly averages

| Area | No. of observations | | | |
|---|---|---|---|---|
| | February | May | August | November |
| 1 | 169 | 320 | 353 | 206 |
| 2 | 78 | 97 | 81 | 141 |
| 3 | 327 | 426 | 281 | 259 |
| 4 | 560 | 459 | 361 | 417 |
| 5 | 1,489 | 1,783 | 1,143 | 924 |
| 6 | 1,174 | 1,687 | 2,008 | 853 |
| 7 | 890 | 795 | 749 | 725 |
| 8 | 714 | 998 | 580 | 583 |
| 9 | 1,781 | 787 | 583 | 562 |
| 10 | 1,161 | 1,037 | 1,061 | 961 |
| 11 | 884 | 1,555 | 905 | 914 |
| 12 | 536 | 642 | 731 | 739 |
| 13 | 1,022 | 1,138 | 1,038 | 955 |
| 14 | 1,675 | 2,147 | 1,965 | 1,913 |
| 15 | 926 | 1,129 | 1,152 | 1,057 |

Large horizontal gradients are observed from December through March, with temperature and temperature variability increasing toward the southeast over the Mid-Atlantic Bight as the slope water is encountered. The high standard deviations in the southeastern part of the area are probably the result of perturbations in the slope front. In the spring, the effects of warming in the very shallow coastal waters are evident, with mean temperatures north of 39°N decreasing toward the east, except for the southernmost areas.

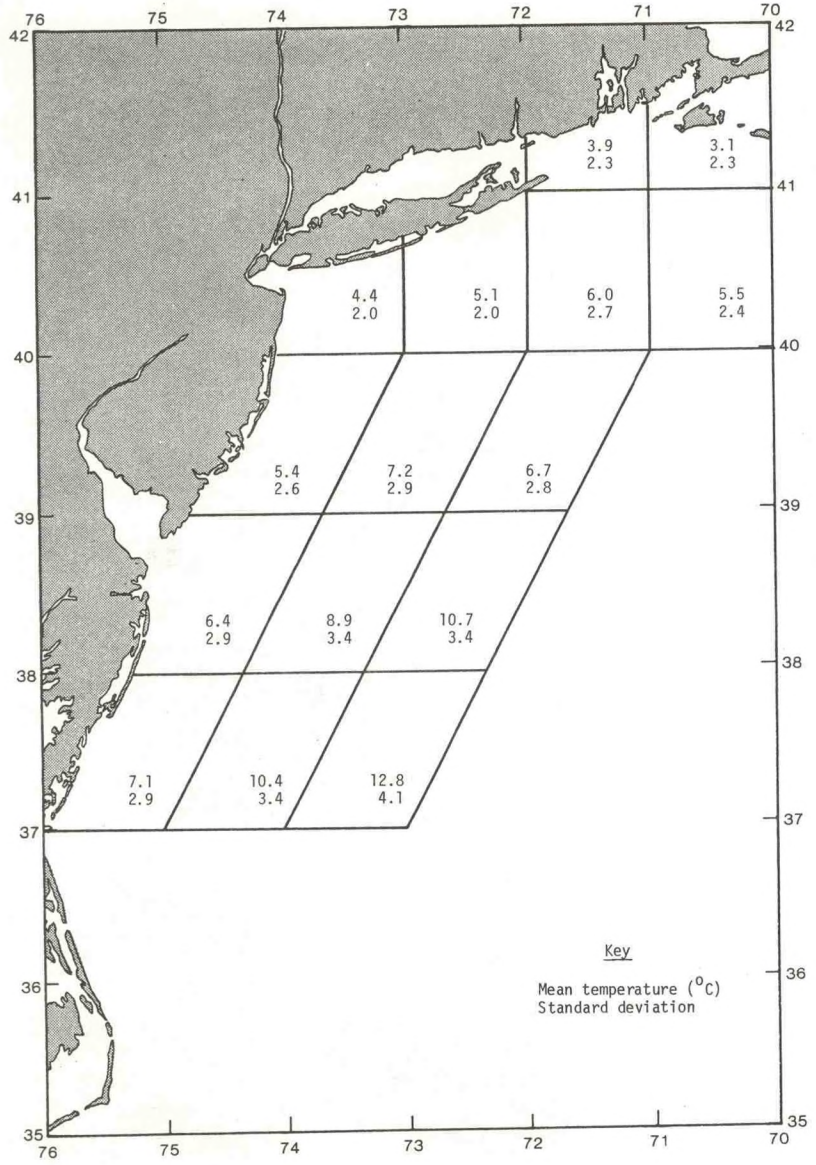


Figure 4.14.--February mean sea-surface temperature.

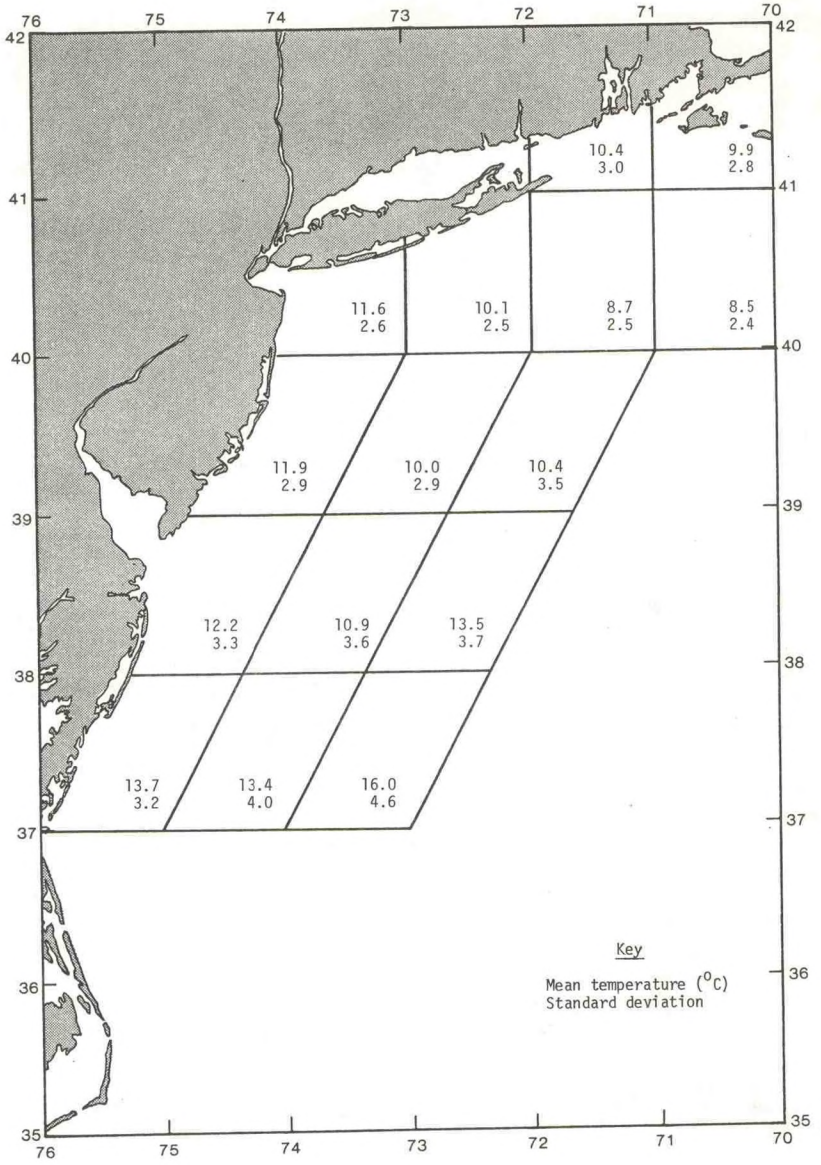


Figure 4.15.--May mean sea-surface temperature.

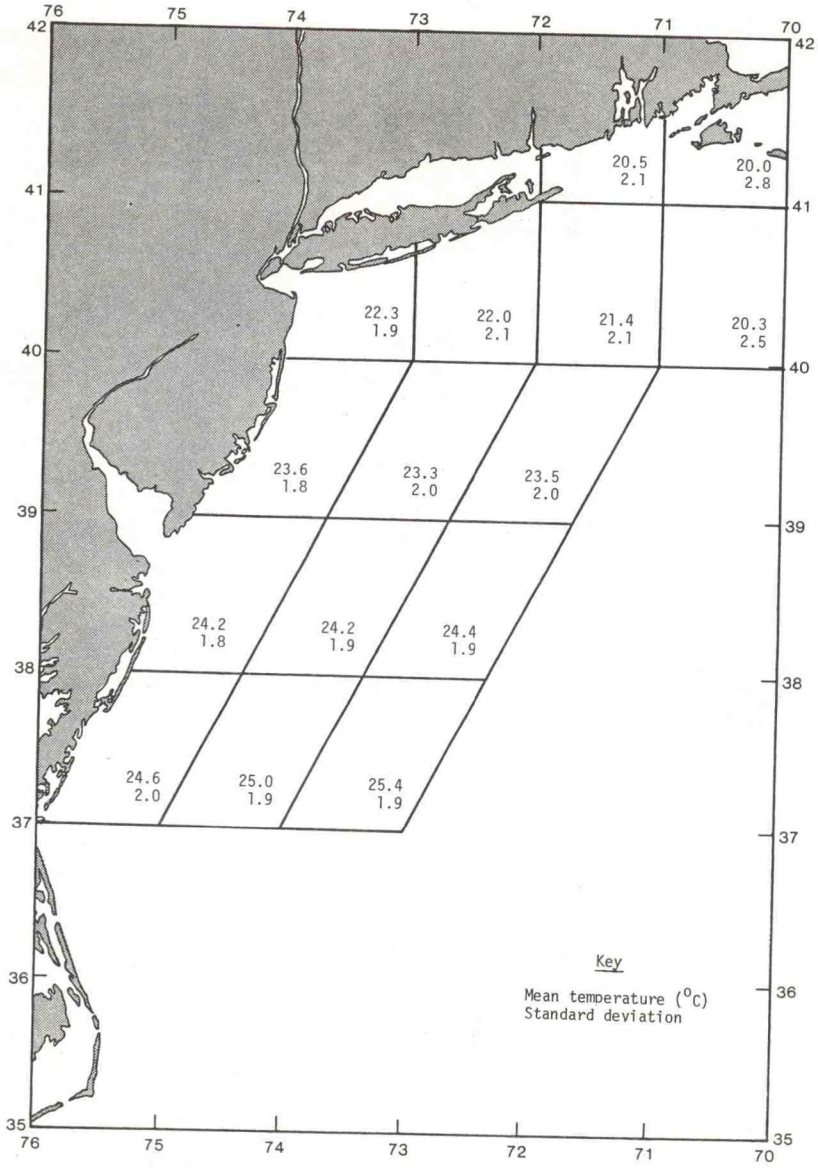


Figure 4.16.--August mean sea-surface temperature.

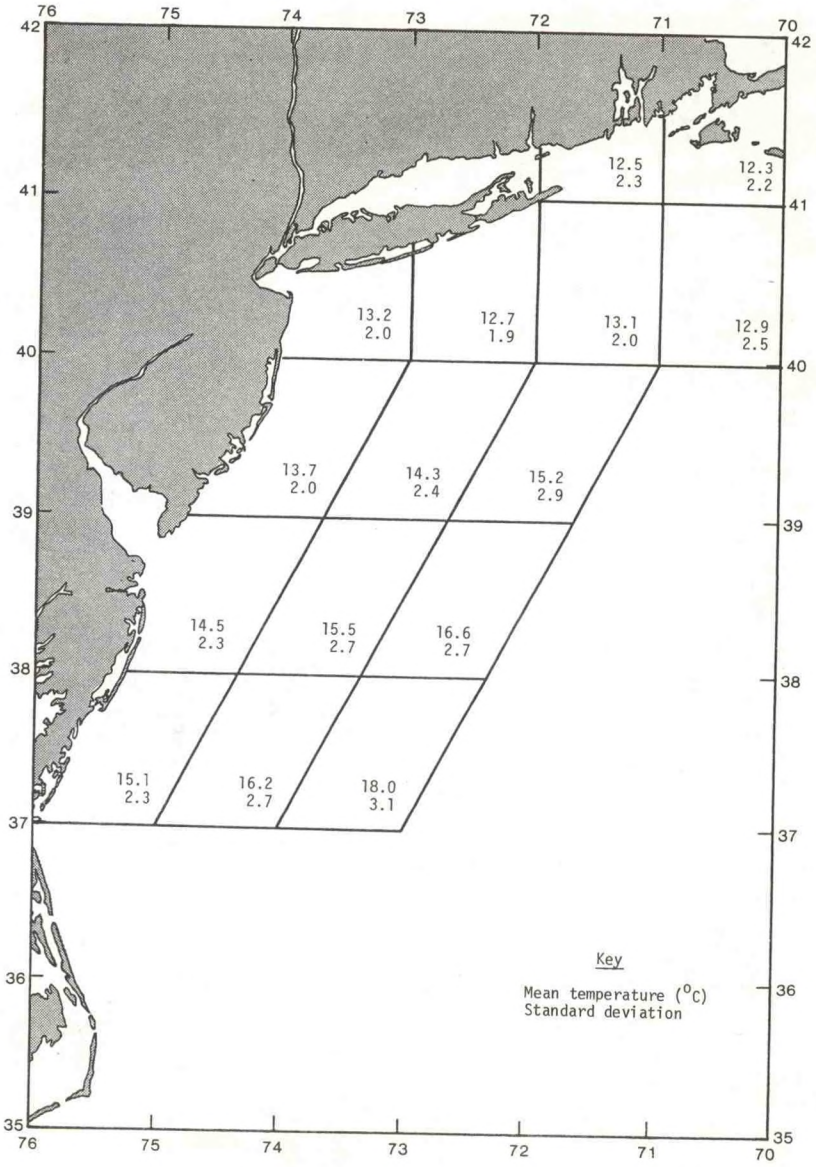


Figure 4.17.--November mean sea-surface temperature.

The gradient in the summer reflects primarily the latitudinal effects of increasing temperature with decreasing latitude. Variability, as evidenced by the standard deviation, is rather uniform over the area, and is highest in the southeast. Standard deviations are at a minimum in August, except in the northeast area. The tendency in October and November is for temperatures again to increase toward the southeast.

In summary, consistent and useful sea-surface temperature statistics appear to be obtainable from the Marine Deck observations over the Mid-Atlantic region.

### 4.4.2 Subsurface Temperature

Subsurface temperatures in the ocean are measured from ships by four different types of systems:

(1) Mechanical bathythermograph (MBT)
(2) Expendable bathythermograph (XBT)
(3) Reversing thermometers (Nansen casts)
(4) Electronic (resistance) temperature probes (STD casts)

The accuracies of these systems are quite different (see table 2.4, sec. 2.2.1), as are the procedures used in making the measurements. In general, STD and Nansen casts are made from a research vessel occupying an oceanographic station; MBT's and XBT's are used from a vessel underway, often from a ship of opportunity. The accuracy of the data is highly dependent on the knowledge and motivation of the observers, since large differences can result from improperly calibrated instruments.

The MBT is now being phased out. The XBT, which came into general use after 1967, was developed primarily for U.S. Navy destroyers to make profiles of temperature vs. depth while moving at high speed. It is easier to calibrate than the MBT, but its use in shallow water has been limited, since it depends on a wire that breaks when 450 m or more are payed out. This makes it difficult to define the ocean bottom in shallow water, since there is no depth sensor on the probe. Time and "known" rate of fall are used to estimate depth. Hence, errors can occur if the probe lies on the bottom when the ship is steaming forward.

Electronic salinity-temperature-depth (STD) data began to be acquired by research institutions in significant quantities during the mid-1960's. These data, as well as the Nansen reversing thermometer data, are approximately an order of magnitude more accurate than BT data. Modern research vessels use reversing thermometers mainly to calibrate the STD probes.

Because of the major differences in the observation systems and the lack of uniform calibration procedures, it was decided to treat each data set separately. The resulting means and standard deviations of temperature are presented in section 4.4.3. In view of the greater accuracy of the STD-Nansen cast data, the greater care usually taken in their acquisition, and the need for both temperature and salinity data to compute water density, STD-Nansen cast data are used in most of the

subsequent analyses discussed in this report.

Note: NODC does not distinguish between STD and Nansen cast data; both are archived in the NODC "station" data file. In the remainder of this report, they will be referred to simply as STD data.

### 4.4.3 Temperature Intercomparisons

The number of MBT and XBT data for the Mid-Atlantic region currently available from NODC is shown in figure 4.18. An inventory of the MBT, XBT, and STD data used for the temperature intercomparisons is given in table 4.2.

Table 4.2.--Number of MBT, XBT, and STD observations, by areas and season, used in this study

| Area | Winter | | | Spring | | | Summer | | | Fall | | |
|---|---|---|---|---|---|---|---|---|---|---|---|---|
| | MBT | XBT | STD | MBT | XBT | STD | MBT | XBT | STD | MBT | XBT | STD |
| 5 | 164 | 115 | 76 | 245 | 161 | 62 | 413 | 76 | 31 | 316 | 104 | 71 |
| 6 | 306 | 78 | 121 | 702 | 79 | 90 | 720 | 66 | 175 | 463 | 95 | 132 |
| 7 | 510 | 18 | 6 | 770 | 22 | 7 | 706 | 12 | 7 | 554 | 15 | 10 |
| 8 | 73 | 77 | 17 | 62 | 107 | 71 | 120 | 114 | 101 | 88 | 59 | 43 |
| 9 | 273 | 208 | 72 | 421 | 150 | 34 | 546 | 180 | 130 | 343 | 198 | 58 |
| 10 | 169 | 251 | 78 | 343 | 251 | 140 | 208 | 384 | 91 | 190 | 475 | 45 |
| 11 | 210 | 206 | 37 | 377 | 239 | 30 | 191 | 232 | 56 | 245 | 354 | 47 |
| 12 | 296 | 250 | 95 | 716 | --- | 134 | 426 | --- | 199 | 344 | --- | 103 |

Means and standard deviations were plotted for 8 of the 12 oceanographic areas chosen for this study (see sec. 2.2, fig. 2.2). Computations were not made for areas 1 to 4, because of their extreme shallowness and the complications involved in comparing data sets from these estuarine outflow areas. Means and standard deviations were also plotted for two deepwater North Atlantic "control" areas, located away from coastal influences. These are referred to here as area 55 (35-36°N, 65-66°W) and area 39 (33-34°N, 69-70°W).

As seen in figures 4.19 to 4.22, when relatively isothermal conditions prevail the mean profiles of all systems are nearly equal above 40 m in areas 5 to 8. Below 40 m, where the number of observations decreases markedly, the spread increases and large differences in standard deviation result. Greater variability is seen in the profiles for spring and fall than in the winter profile. In summer the shapes of the profiles are again more nearly similar above 40 m, and absolute differences are smaller than for spring and fall. For the offshore areas 9 to 12, shown in figures 4.23 to 4.26, the profiles are generally similar, except in spring for areas 10 and 12. In nearly all offshore areas, the XBT profiles are the warmest over most of the

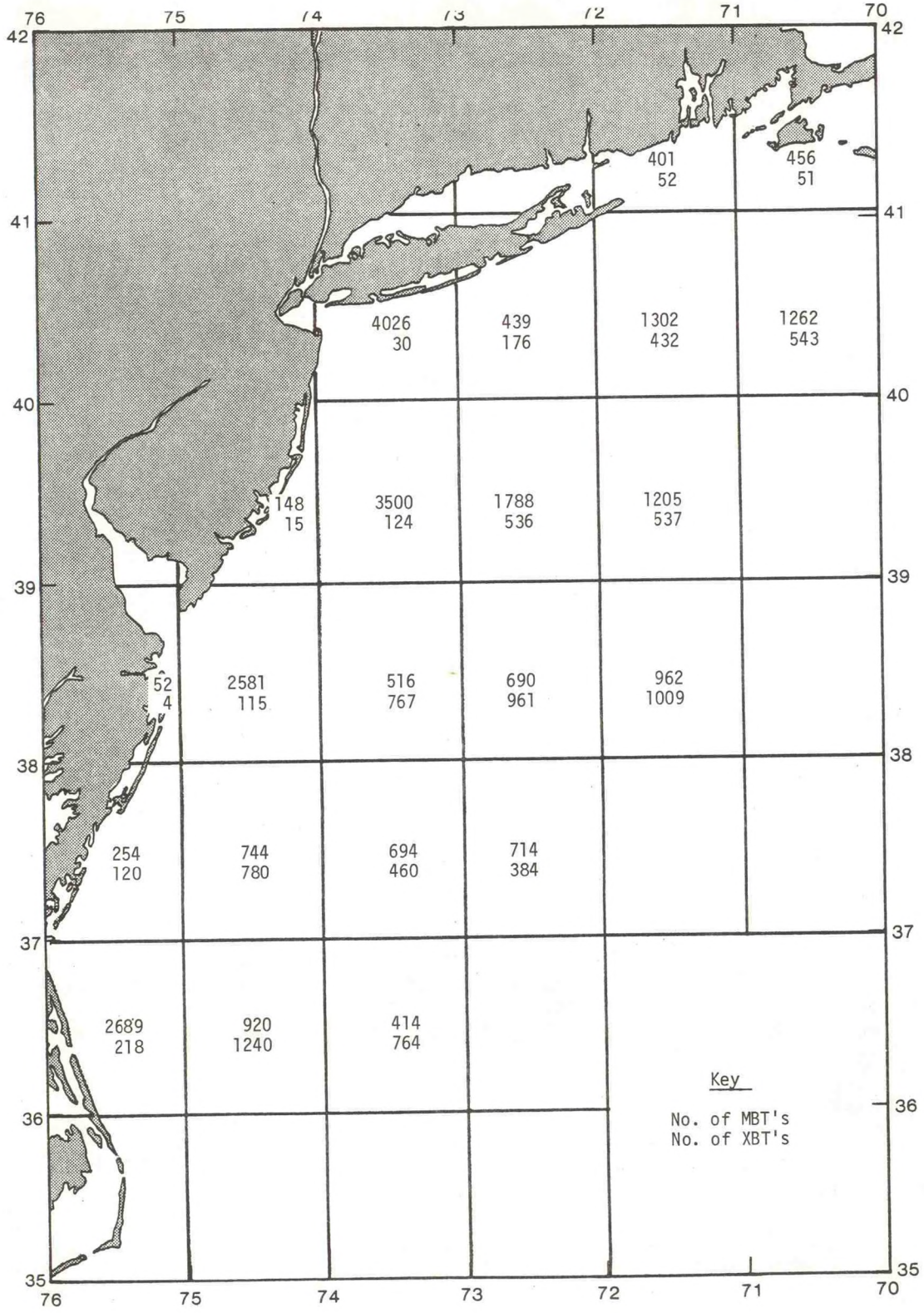


Figure 4.18.--Inventory, by $1^{o}$ squares, of MBT and XBT data archived at NODC.

water column. There seems to be no pattern in the magnitudes of the standard deviations except on the shelf, but the largest standard deviations are often associated with the largest number of observations (hence, the largest number of environmental conditions). The deepwater areas (figs. 4.27 and 4.28) show reasonable uniformity, except for area 55 in summer, where major differences are seen between the MBT and XBT profiles.

In an attempt to determine whether differences are the result of a real trend in water temperatures, temperatures at selected depths were plotted as a function of time for area 8 based on XBT and MBT data, and for area 55 based on all three types of data. As many near-simultaneous MBT and XBT casts as could be obtained were plotted, but the time and space distributions of the observations remained so scattered that this procedure yielded no useful results.

The problem was further examined by separate histograms for area 8 of temperature in water layers 25 m thick, based on each set of data (figs. 4.29 to 4.31). In the 0- to 25-m layer, the largest spread occurs in the MBT observations; the second largest, in the XBT data; and the smallest in the STD data. This may simply be a reflection of the differences in the sizes of the three data sets. In the 25- to 50-m layer, the distributions cover about the same range, although the XBT observations are more numerous.

Differences in mean temperatures for several depth levels above, within, and below the thermocline were examined for areas 6, 8, and 10 by testing for all seasons the hypotheses that (1) the MBT means and XBT means, respectively, are equal to the STD data means, and (2) they are unequal. The results of the tests, using Student's distribution, showed for all cases, except area 10 in summer, a statistically significant difference in the means, at the 90 percent level of significance. In this test, however, random sampling of independent observations from a normally distributed population is assumed, making the results suggestive rather than conclusive.

Surface MBT and XBT temperatures for two areas were compared with the Marine Deck observations of sea-surface temperatures from transient ships, with the following results: Marine Deck = 8.19°C, XBT = 7.46°C, and MBT = 7.32°C. Since neither the MBT nor XBT temperature sensors begin functioning properly until 1 or 2 m below the sea surface, the measurements by these sensors might be biased toward cooler surface temperatures.

Royer (1976) made a comparison of sea-surface temperatures using monthly means of both bathythermograph (BT) and bucket-ship intake data from Ocean Weather Station "P" (50°N, 145°W) for 1952 to 1965. He found the differences between the monthly means to be time-dependent, e.g., during 1952 the BT mean surface temperatures were higher than bucket-ship intake surface temperatures, while in 1954 to 1956 they were lower. A seasonal dependence was also observed, with a minimum difference in the measurements occurring in summer and a maximum in winter. The mean annual differences between the two types of measurements was more than 0.2°C before 1956; after 1956, when more careful procedures were instituted on board ship, the differences were less than 0.2°C.

In summary, large differences are observed in mean temperature profiles of MBT, XBT, and STD data. Visual comparisons of profiles and frequency distributions, as well as hypothesis tests, suggest that there are significant differences in the means of these data sets. The consistently higher temperatures recorded by the XBT's in the slope water is a factor to be considered, and there is a question as to whether these data sets can be combined without adjusting for relative biases. The conclusion reached is that, until a more comprehensive comparative analysis of the MBT, XBT, and STD data can be made, the three data bases should be analyzed separately. Subsequent analyses presented in this report are based on STD data.

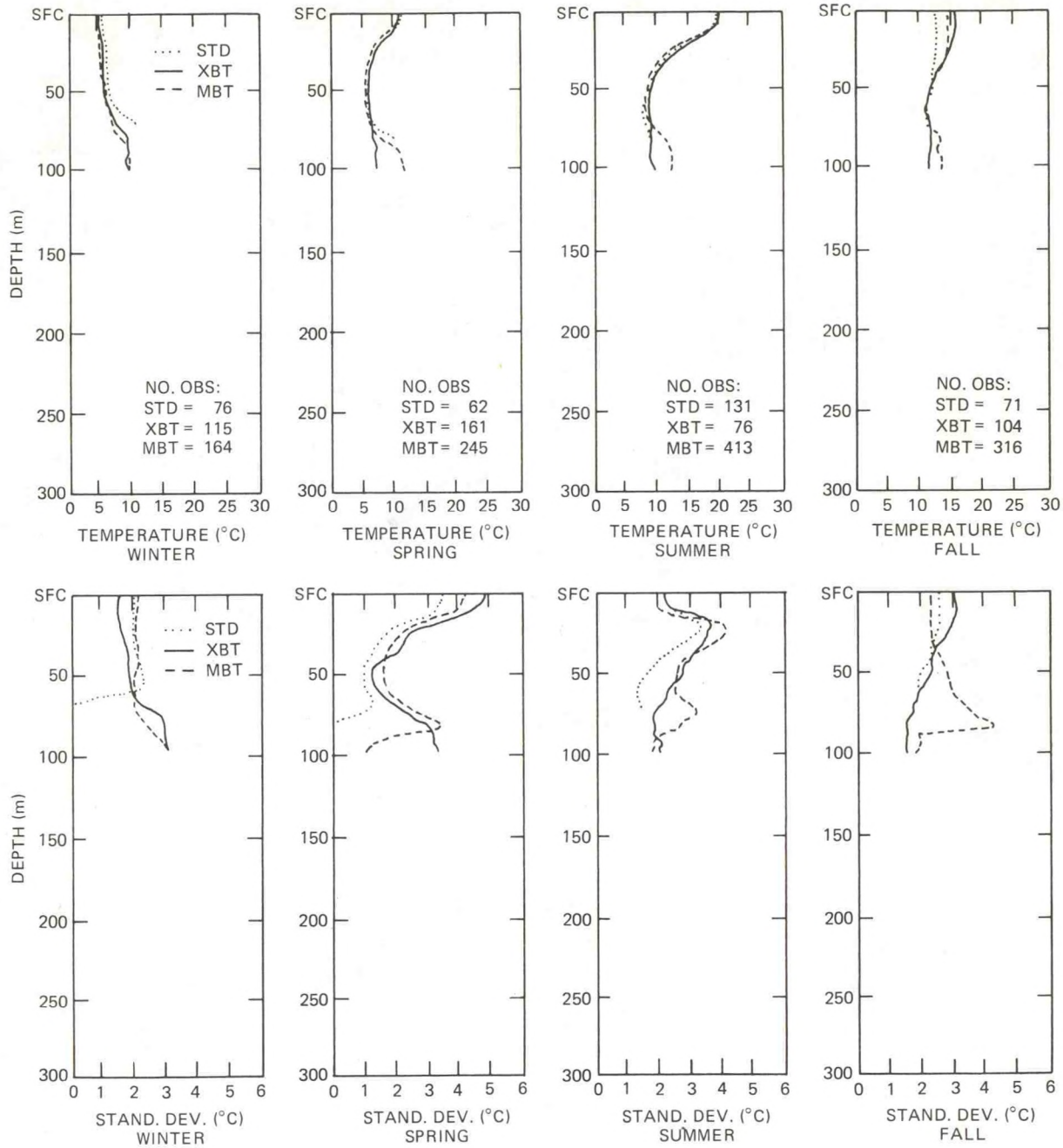


Figure 4.19.--Seasonal mean temperatures and standard deviations, area 5.

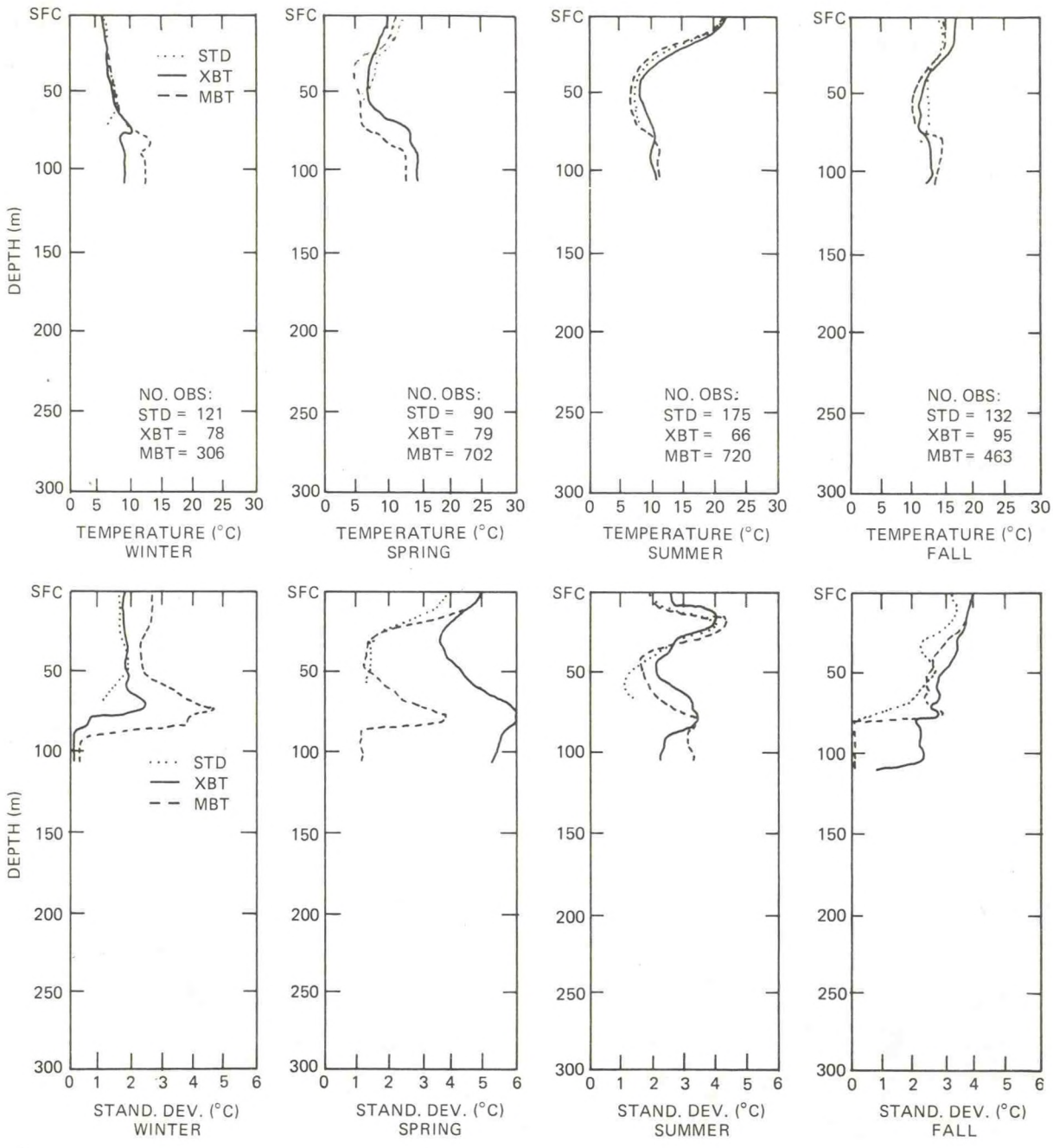


Figure 4.20.--Seasonal mean temperatures and standard deviations, area 6.

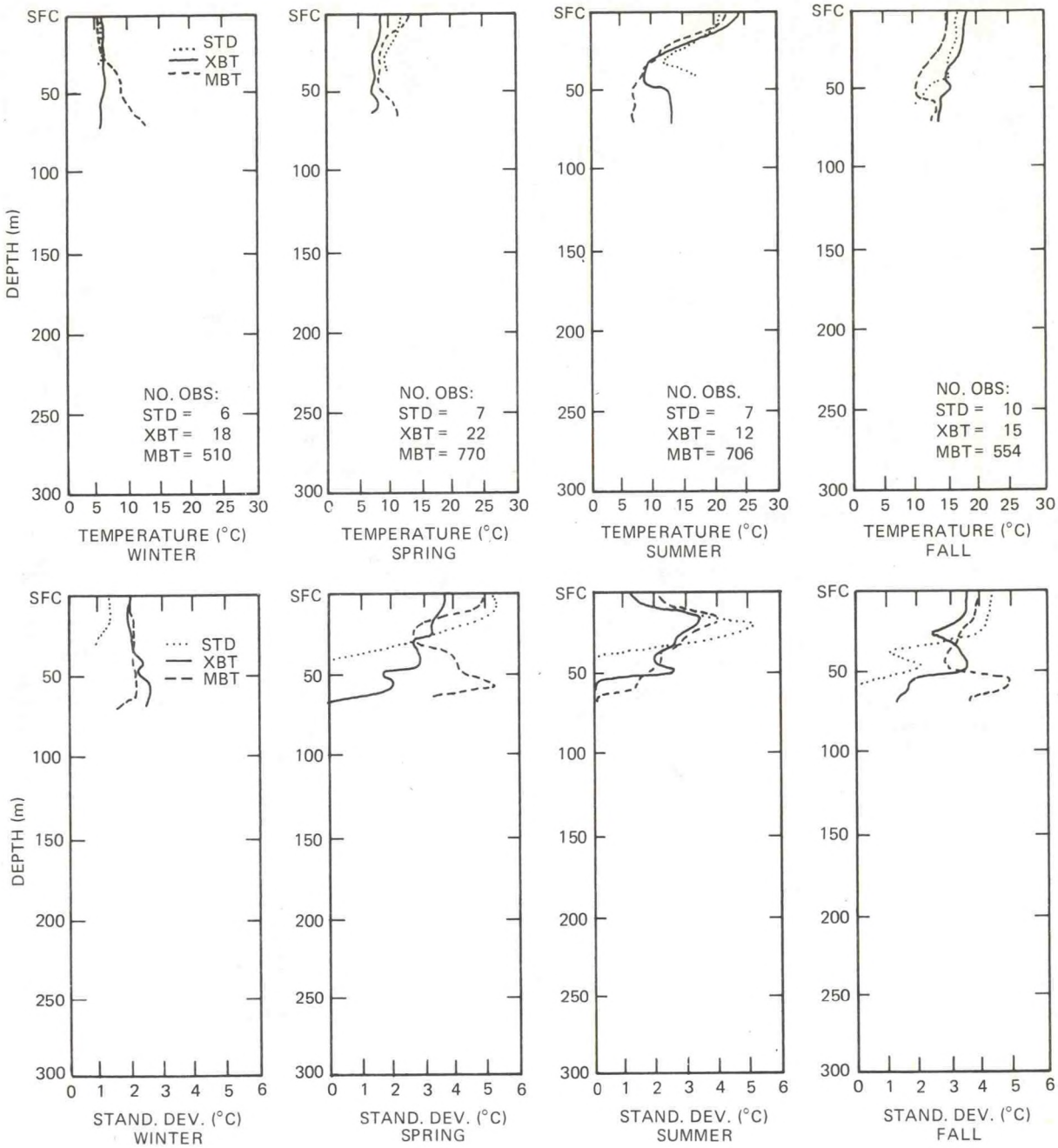


Figure 4.21.--Seasonal mean temperatures and standard deviations, area 7.

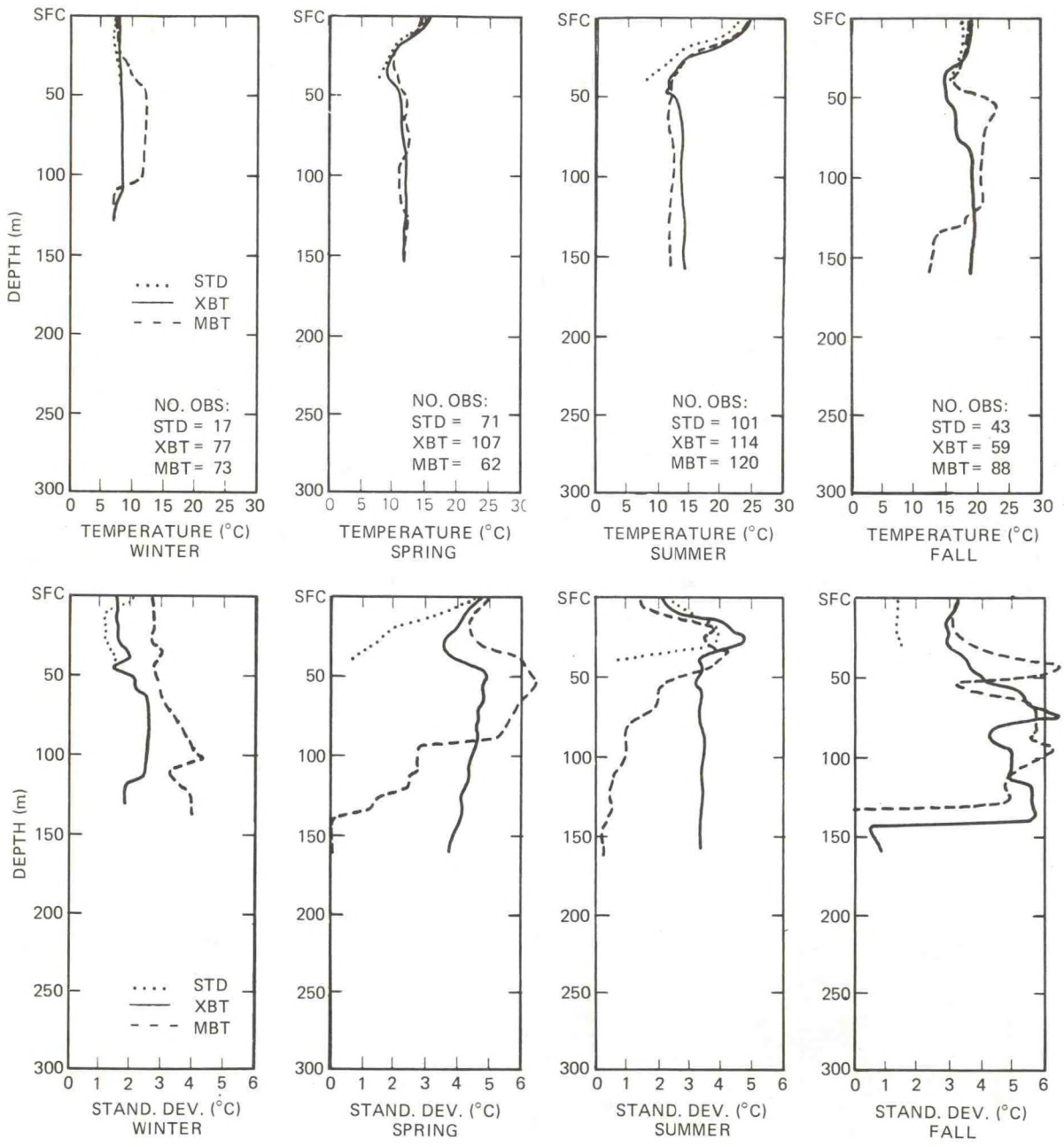


Figure 4.22.--Seasonal mean temperatures and standard deviations, area 8.

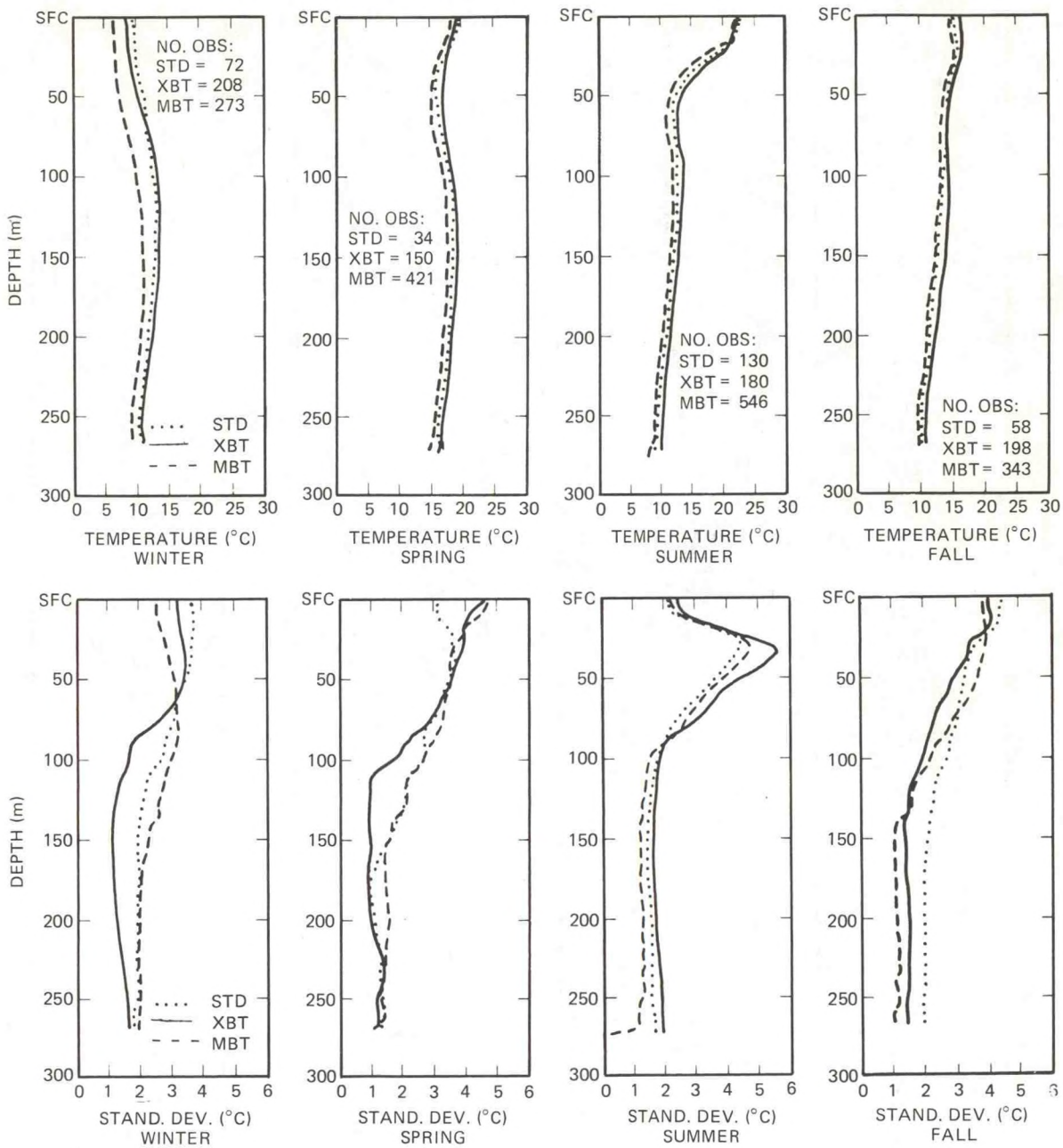


Figure 4.23.--Seasonal mean temperatures and standard deviations, area 9.

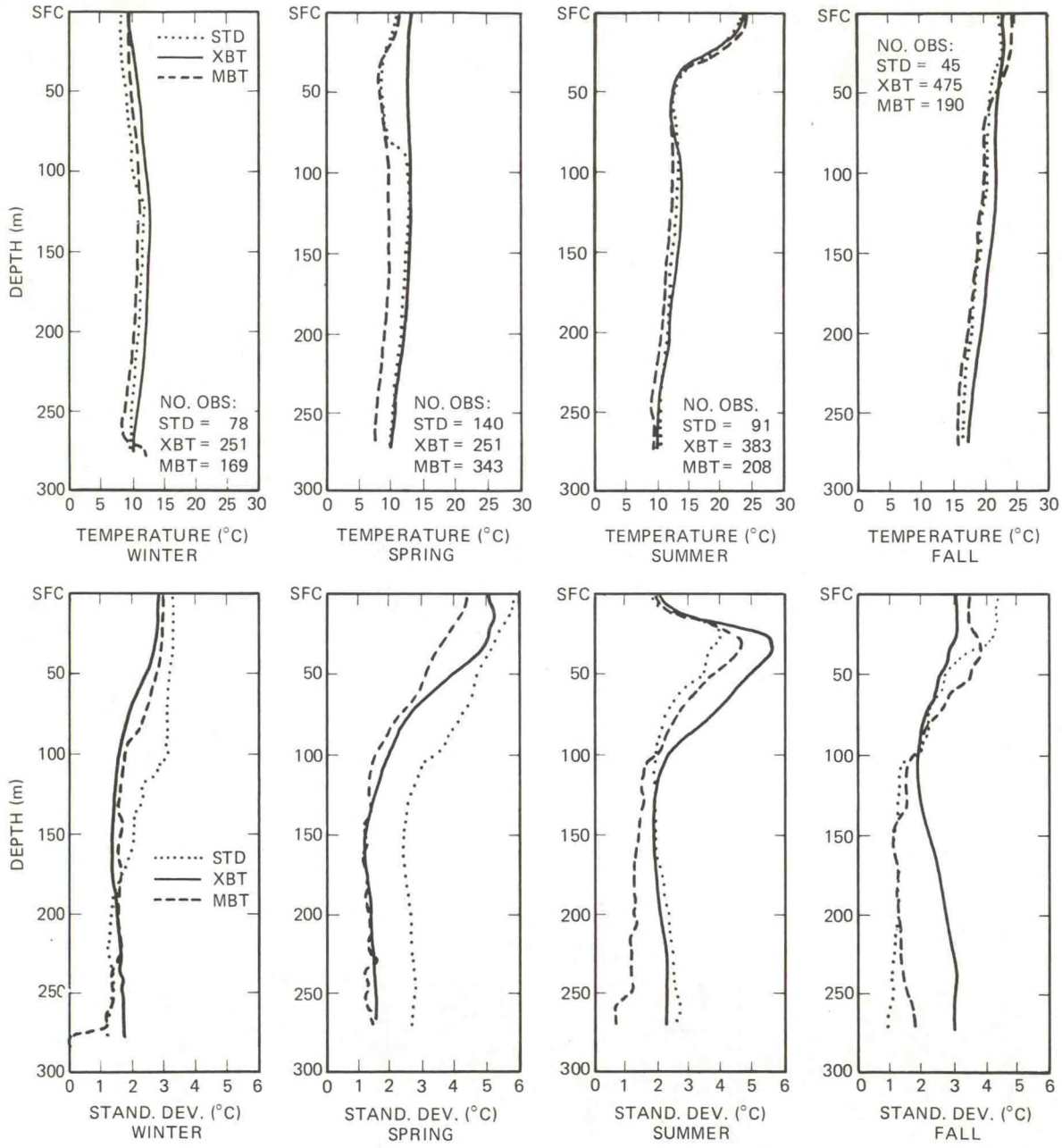


Figure 4.24.--Seasonal mean temperatures and standard deviations, area 10.

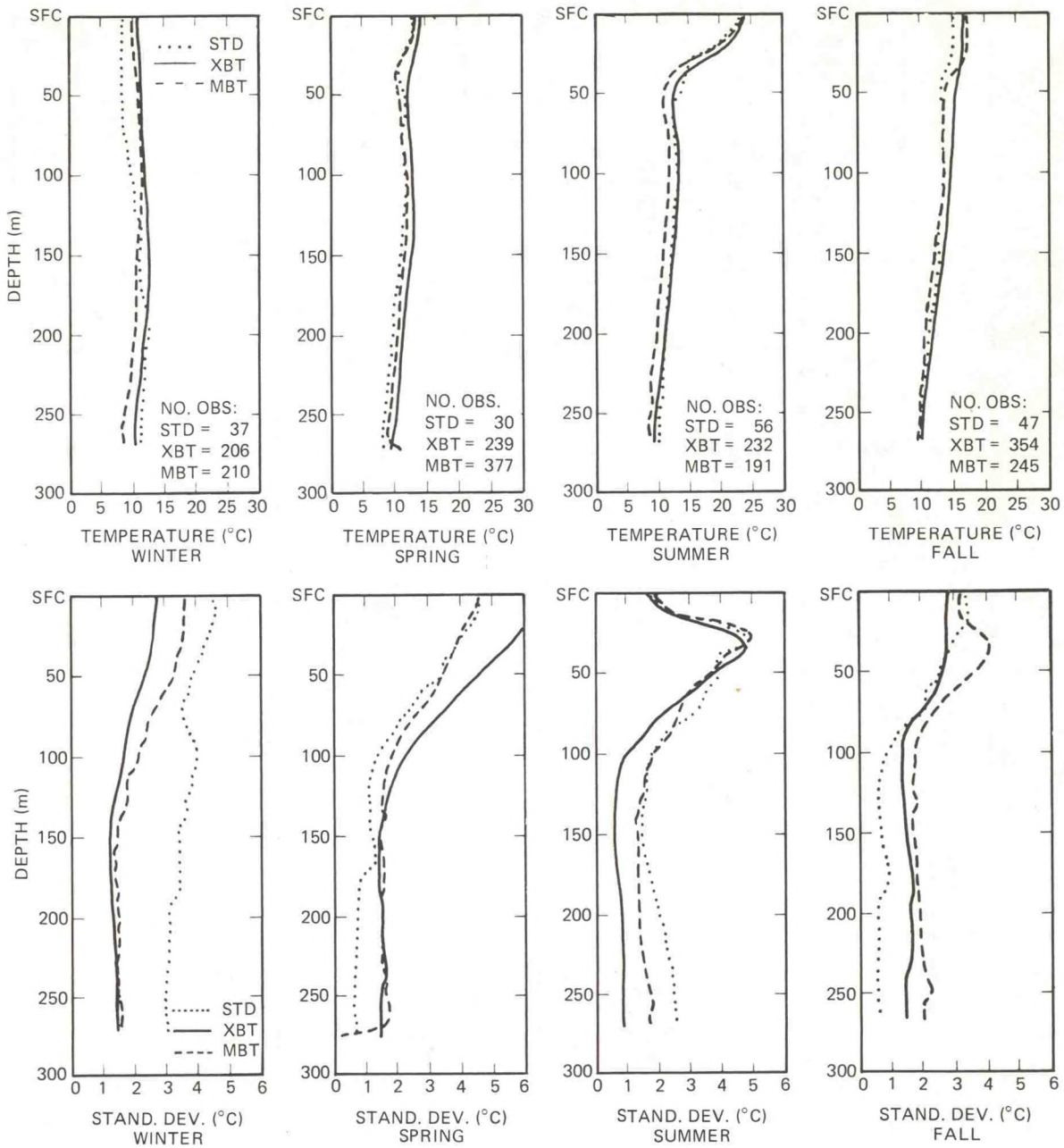


Figure 4.25.--Seasonal mean temperatures and standard deviations, area 11.

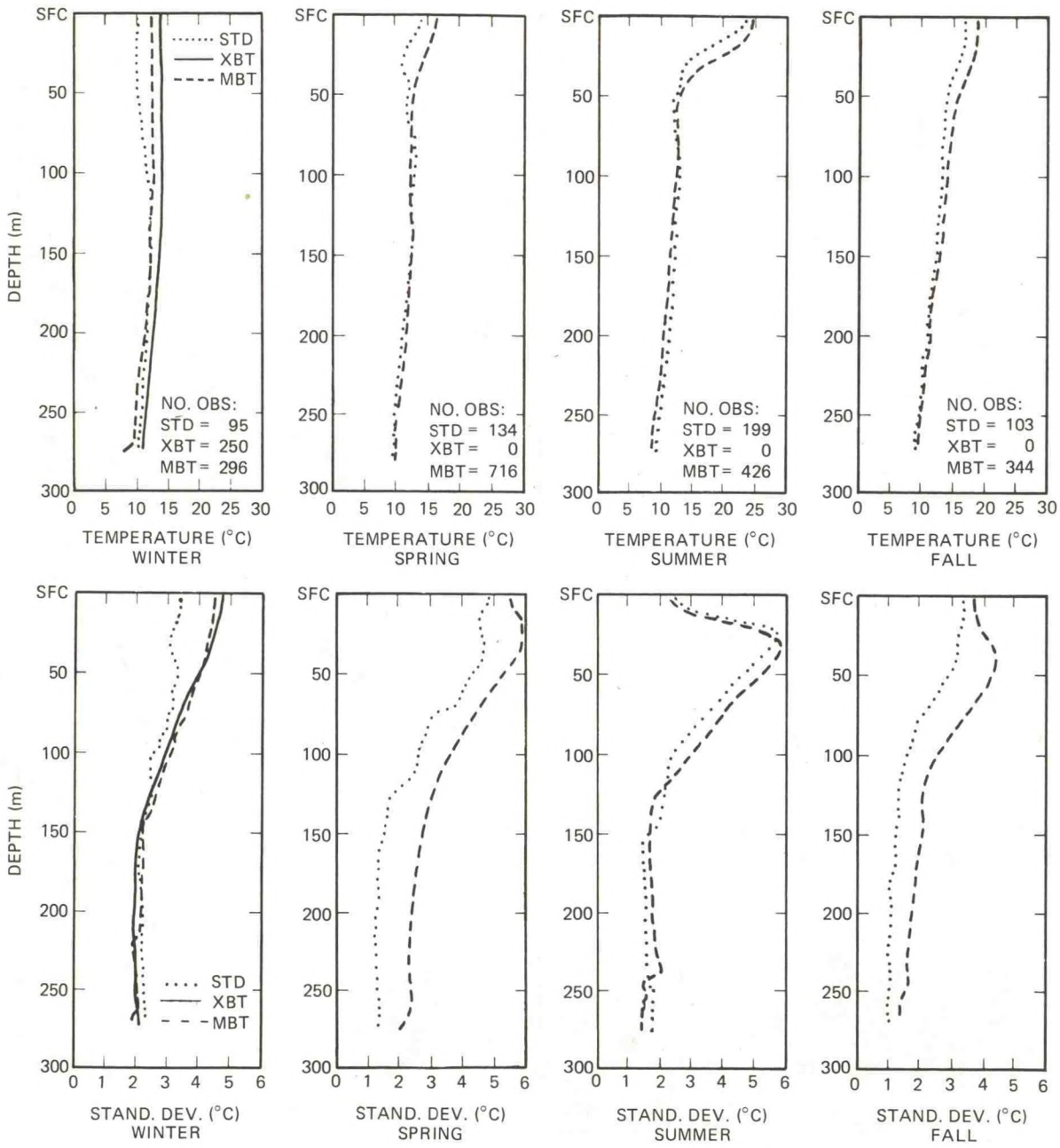


Figure 4.26.--Seasonal mean temperatures and standard deviations, area 12.

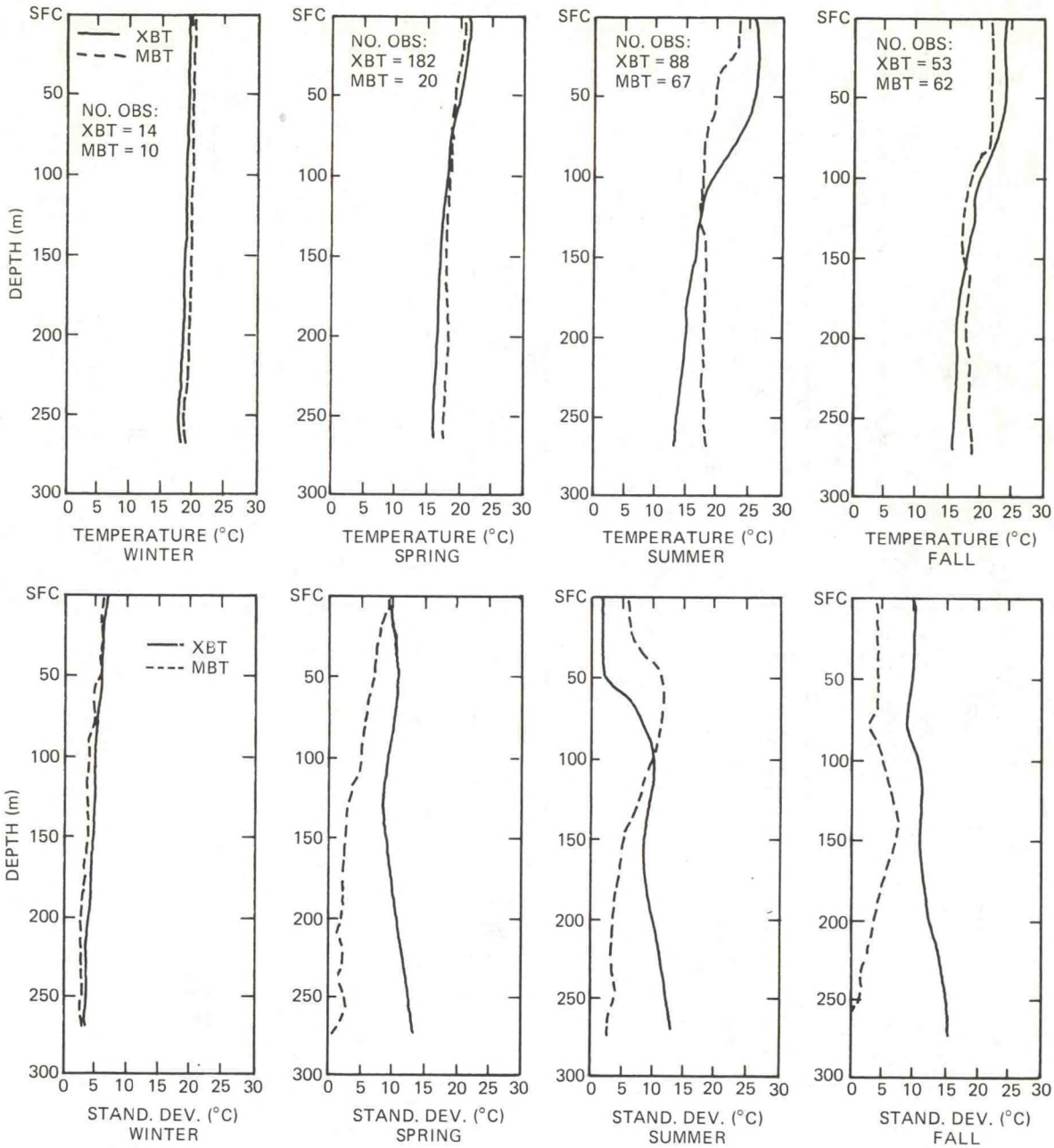


Figure 4.27.--Seasonal mean temperatures and standard deviations, area 55.

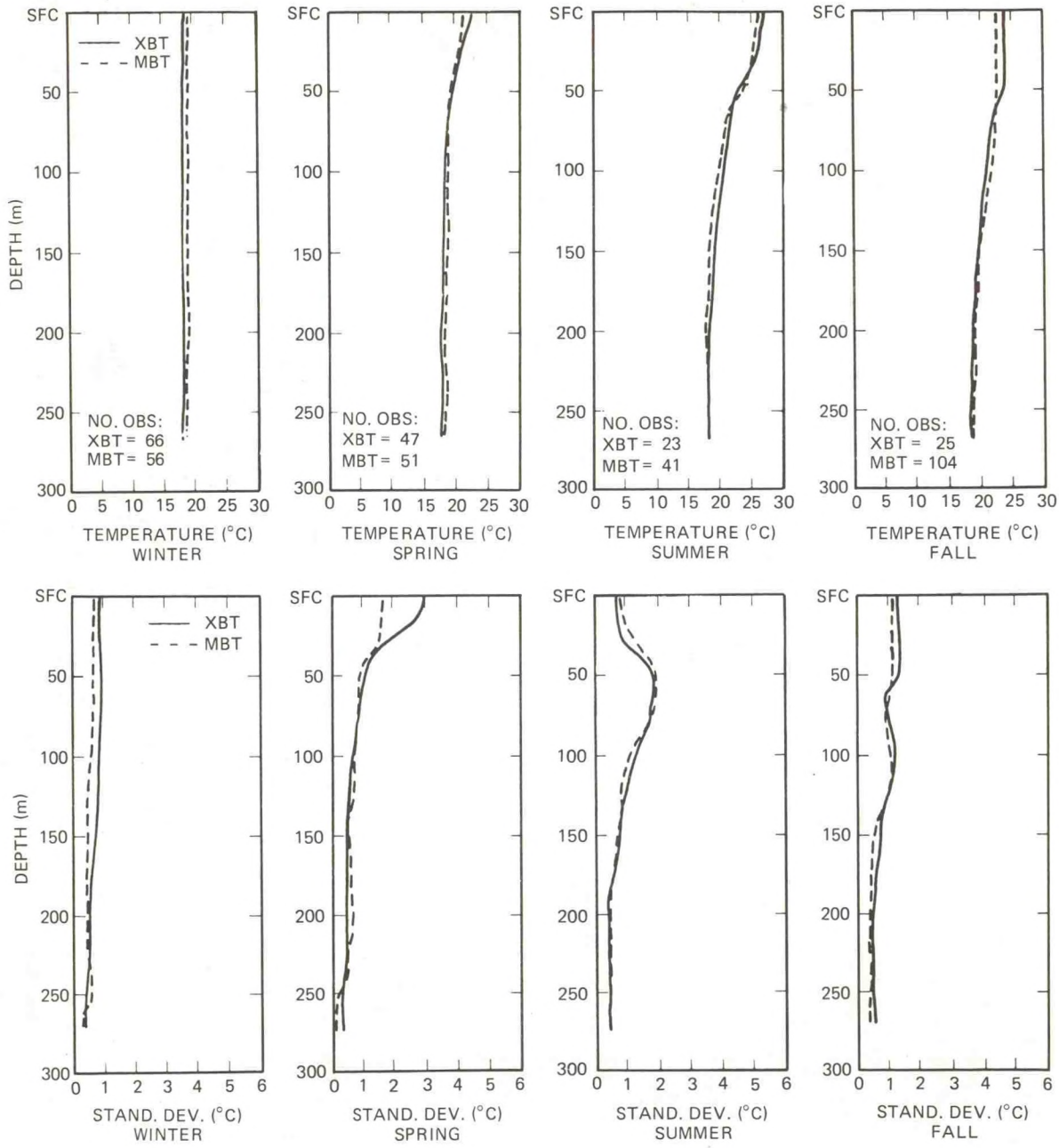


Figure 4.28.--Seasonal mean temperatures and standard deviations, area 39.

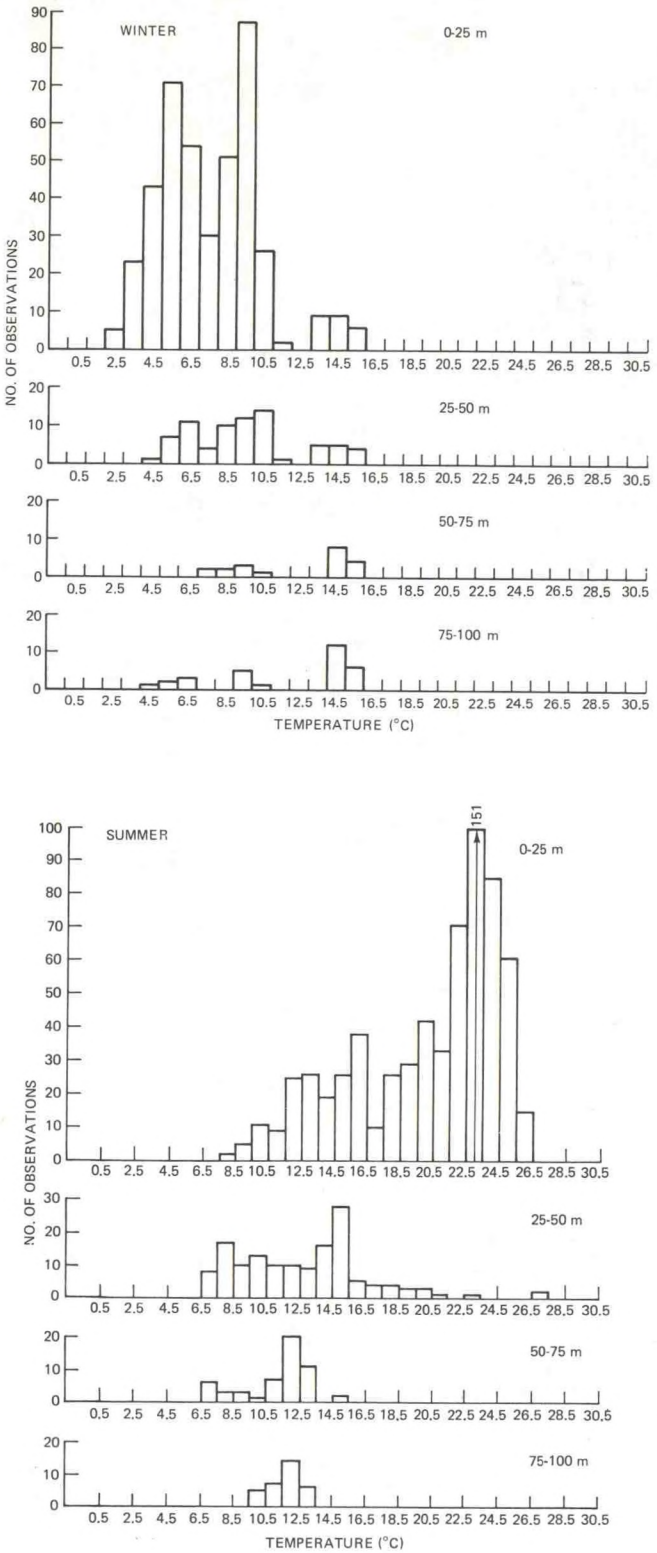


Figure 4.29.--Histograms of temperature based on MBT data, area 8, winter and summer.

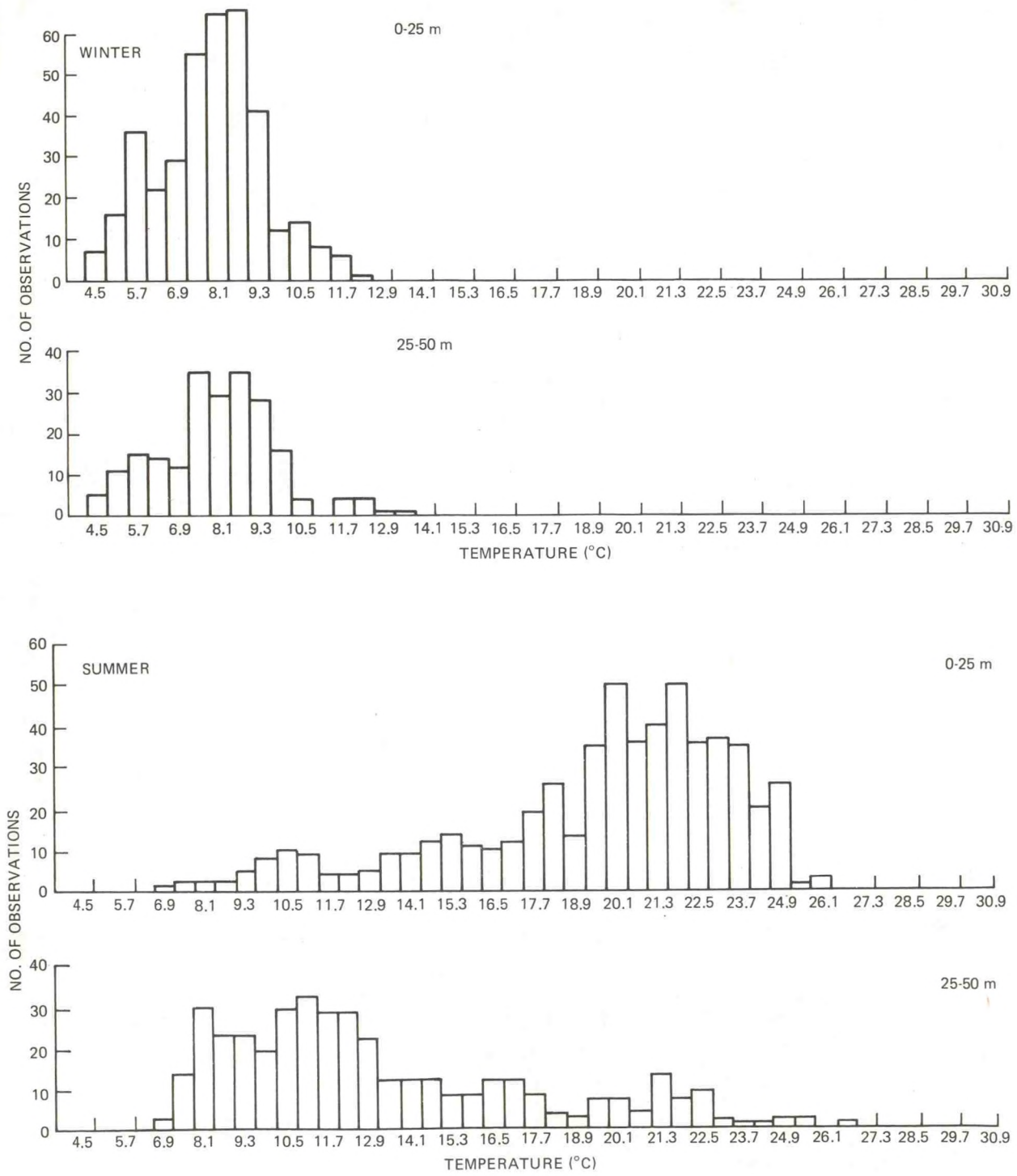


Figure 4.30.--Histograms of temperature based on XBT data, area 8, winter and summer.

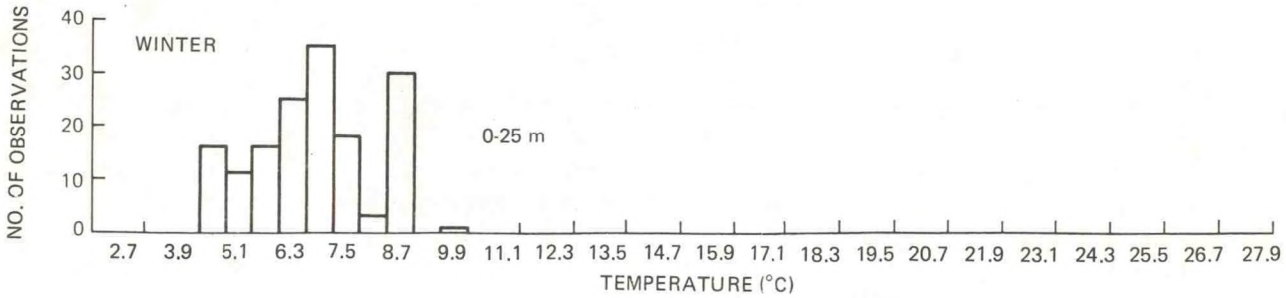


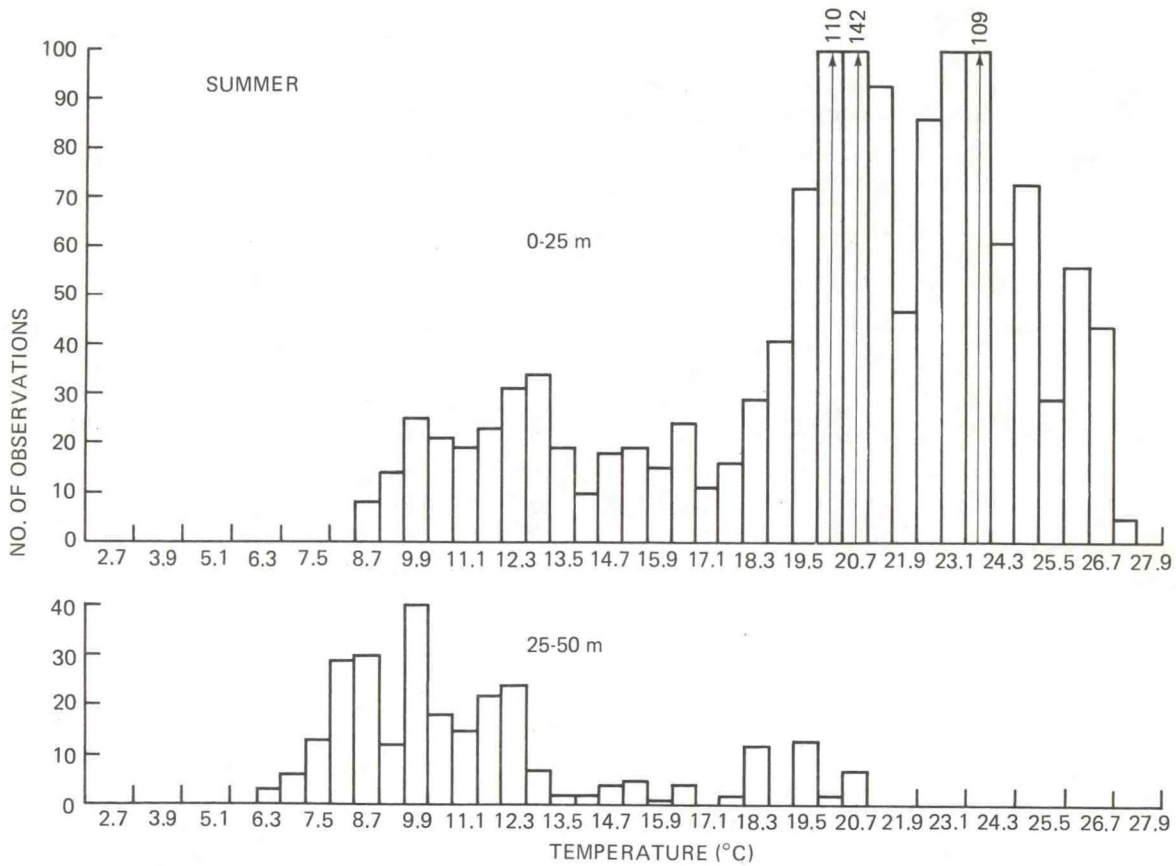


Figure 4.31.--Histograms of temperature based on STD data, area 8, winter and summer.

### 4.4.4 Seasonal Temperature Variations

Preliminary editing of the STD data used in this study was done primarily in terms of location to eliminate obviously erroneous positions or data taken in estuaries. In final editing, the criteria for ASD analysis of the data were used, i.e., measurements that were too shallow or had too low a vertical sampling density were eliminated. The final editing procedure is discussed in more detail in appendix C. An inventory of the data showing the number of observations both after preliminary and final editing is given in table 4.3. The number of observations available was not equal for every depth, generally decreasing rapidly with increasing depth.

Table 4.3.--Inventory of STD data used, showing number of observations before and after final editing

| Area | After preliminary editing | | | | | Total after final editing |
|---|---|---|---|---|---|---|
| | Winter | Spring | Summer | Fall | Total | |
| 1 | 11 | 10 | 17 | 12 | 50 | 45 |
| 2 | 116 | 130 | 162 | 158 | 566 | 423 |
| 3 | 1 | 20 | 19 | 8 | 48 | 35 |
| 4 | 38 | 67 | 96 | 49 | 250 | 81 |
| 5 | 76 | 62 | 131 | 71 | 340 | 262 |
| 6 | 121 | 66 | 175 | 132 | 494 | 254 |
| 7 | 6 | 7 | 7 | 10 | 30 | 18 |
| 8 | 17 | 71 | 101 | 42 | 231 | 126 |
| 9 | 70 | 34 | 126 | 58 | 288 | 214 |
| 10 | 78 | 140 | 91 | 45 | 354 | 189 |
| 11 | 30 | 56 | 47 | 95 | 228 | 42 |
| 12 | 95 | 134 | 199 | 103 | 531 | 106 |

Winter. Figure 4.32 shows mean "surface" temperatures (which, as noted earlier, may be a meter or more below the surface) and standard deviations based on STD data. Contours of ½° square averages of the same data smoothed by the ASD method (sec. 4.1.1) are shown in figure 4.33. Following the procedure used by Wyrtki (1971; see sec. 4.3.2), the countour intervals were made slightly larger than the average standard deviations. As seen, the maximum horizontal temperature gradients in winter are nearly normal to the coastline, with mean temperatures increasing from less than 5°C very near the coast to 5 to 7°C across most of the shelf, and rising rapidly at the shelf-slope water front. The 10°C isotherm appears to denote the center of the front, which agrees with findings by Wright (1976). Area 7 does not contain enough data for estimating the mean with any degree of confidence. (MBT data for this area indicate a mean surface temperature of 4.98°C.) The temperature distribution at 10 m is very similar to that at the surface, but at a depth of 50 m (figs. 4.34 and 4.35) temperatures are slightly

higher than at the surface and 10 m. The position of the 10° isotherm relative to the surface charts shows that the front slopes upward and seaward, as noted by Wright (1976).

At 100 m (figs. 4.36 and 4.37), temperatures are warmer than at 50 m, and average temperature variability is maximum at this depth. At 200-m depth, temperatures in the slope water are comparable to those at 100 m, consonant with the concept of a wedge of warmer water driving in under the cold shelf water. The number of observations is too small, however, to allow the definition of any details.

The vertical distribution of temperature is seen in the histograms for area 6 in figure 4.38. A slight temperature increase with depth on the midshelf is characteristic of the area. Combining data from both warm and cold winters results in temperatures ranging from about 3 to 10°C in the top layer. Figure 4.39 shows the complex vertical distribution of temperature for area 10 in the region of the shelf-slope water front. Maximum temperatures are observed in the layer between 100 m and 200 m, with surface temperature ranging from about 3 to 14°C.

The vertical temperature structure is seen in more detail for areas 6, 8, and 10 in figure 4.40, which shows data midlines (medians) and envelopes. The midline is in some respects a better measure of central tendency (Panofsky and Brier, 1965) than the mean in distributions that depart significantly from normality, as does ocean temperature. As seen in figure 4.40, temperature generally increases with depth, and an inversion is evident in area 6. The bulge of temperatures greater than 10°C indicates intrusion of slope water at the shelf-slope water front.

Spring. Vernal warming on the shelf is known to begin typically in late March, with heating of the near-surface water. As warming increases, vertical stratification develops and inhibits vertical mixing. By late May, the development of the thermocline is well underway. The residual "winter" water persists into summer, while the thermal front at the shelf-slope water interface weakens as spring progresses.

Figure 4.41 shows surface warming in the shallow waters near the coast. The latitudinal effect is evident in that the waters of the southern half of the Bight are warmer than the northern half. Figure 4.42 shows that the orderly winter pattern of a seaward increase in temperature normal to the coast has been succeeded by a more patchy distribution. The thermal front between shelf and slope water is still evident. Variability, expressed by the standard deviations, is much larger in spring than in winter. At 50-m depth (fig. 4.43), temperatures are only slightly warmer than during winter and in some cases, as in area 6, actually colder. Figure 4.44 shows the pattern of isotherms typical of the shelf-slope water thermal front. Vertical distributions in spring can be quite complex, expressing the high variability in the time of onset and intensity of vernal warming.

Summer. A marked thermocline develops in summer on the shelf at a depth of 15 to 20 m, with temperatures as low as 7.5°C in the pool of residual "winter" water. Figure 4.45 shows area means and standard deviations, and

contours of data smoothed by the ASD method are plotted in figure 4.46. Temperatures generally decrease toward the southeast, with smaller standard deviations than either in winter or spring. At 10 m (figs. 4.47 and 4.48), some effects of summer vertical stratification are already evident. At 50 m, variability is larger, indicating the thermocline region and the influence of internal waves (figs. 4.49 and 4.50). Temperatures are relatively constant at 100 m, as seen in figures 4.51 and 4.52.

Histograms of temperatures in the upper layer, from the surface to 25 m, for area 8 (fig. 4.53) show a range from 9 to 27°C, with strong skewness toward low temperatures. These variations could be due to internal waves on the thermocline, which is found at roughly 25 m. They could also simply reflect variations in temperature from year to year. The histograms for areas 6 and 10 (figs. 4.54 and 4.55) are skewed left at most depths. The vertical structure for areas 6, 8, and 10 is illustrated by the midlines and envelopes in figure 4.56. A strong thermocline is evident in all areas, with temperatures on the shelf decreasing from 20°C at the surface to 7°C or so at 50-m depth. The most intense thermocline appears to be located at a depth of about 25 m. The depth of the thermocline, as determined by NODC by calculating the depth of the maximum second deviative of the mean temperature vs. depth profile for ½° squares, is shown in figure 4.57. It is seen to be very shallow, 15 to 25 m, in almost all areas of the continental shelf.

Fall. Bottom temperatures continue to rise into September and sometimes early October, but surface temperatures drop. By late October to mid-November, surface cooling and strong winds effect convective overturn and destruction of the thermocline on the midshelf and inner shelf. Fall surface temperatures tend toward the winter pattern of temperature increasing seaward, normal to the coast (figs. 4.58 and 4.59), although the patterns are more complex than during winter. At 100-m depth, temperatures are nearly uniform (figs. 4.60 and 4.61).

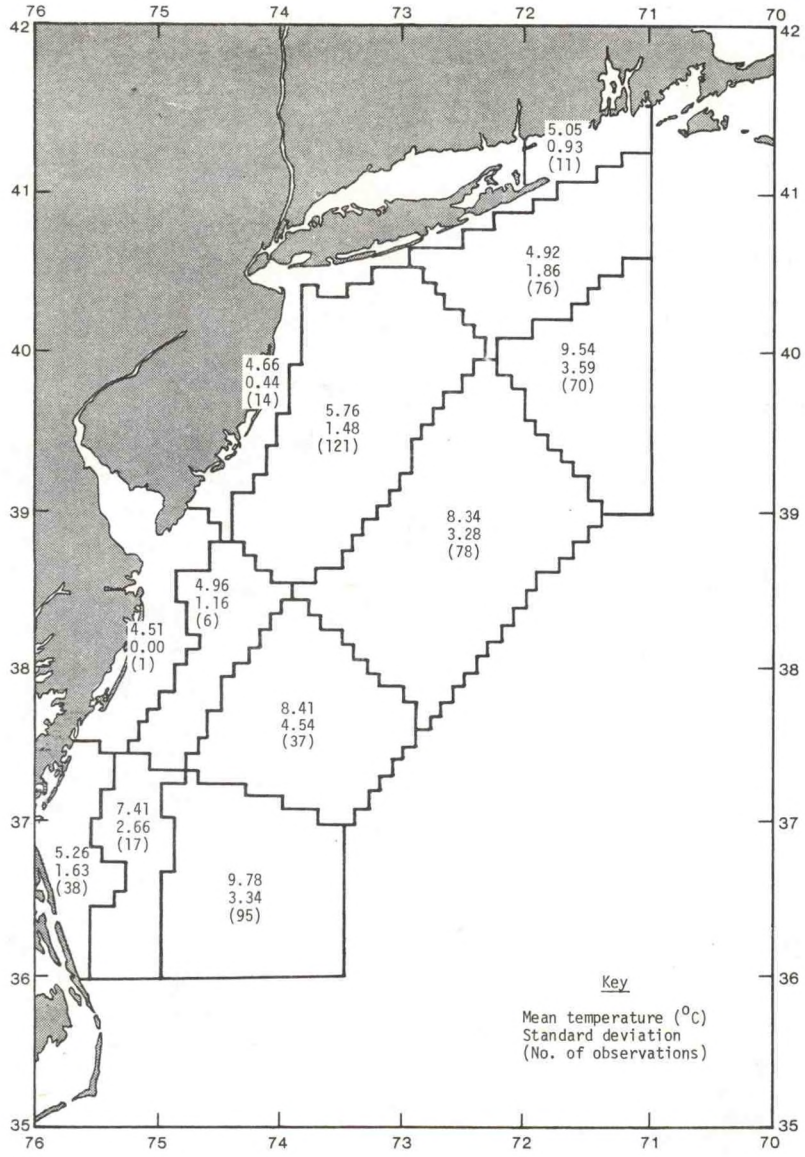


Figure 4.32.--Winter mean sea-surface temperatures.

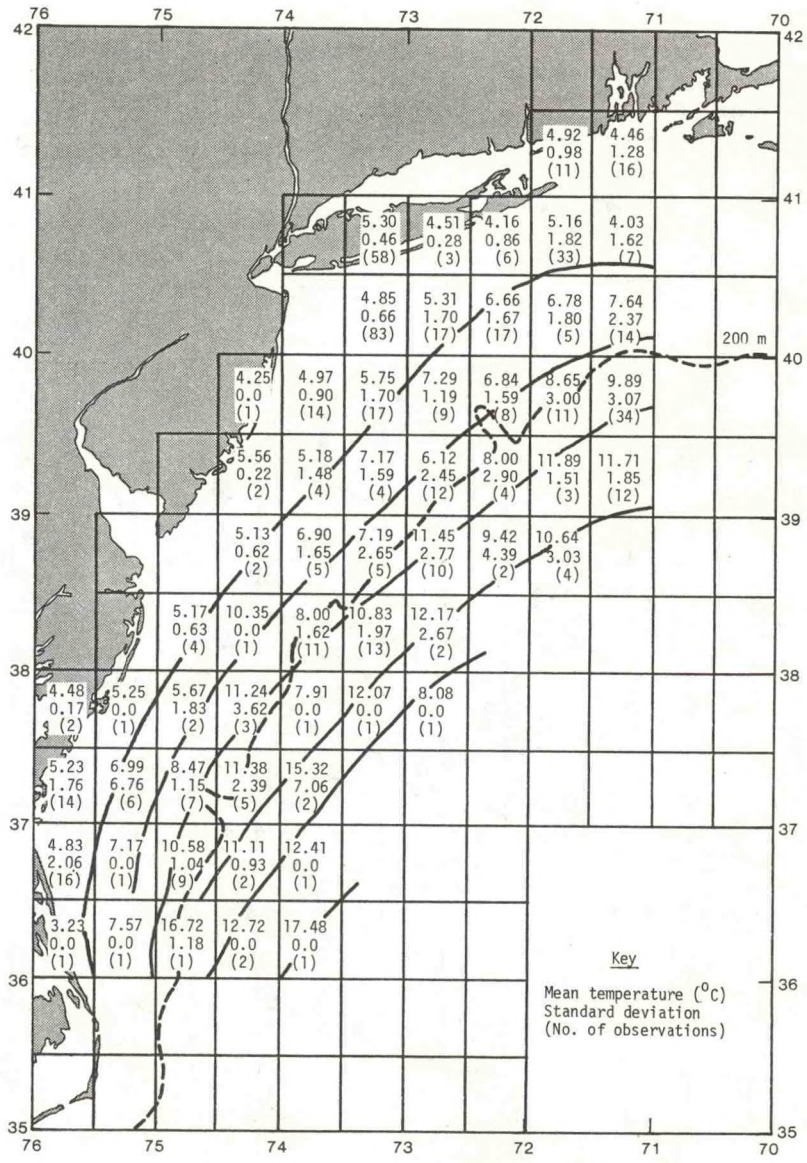


Figure 4.33.--Winter mean sea-surface temperature field.

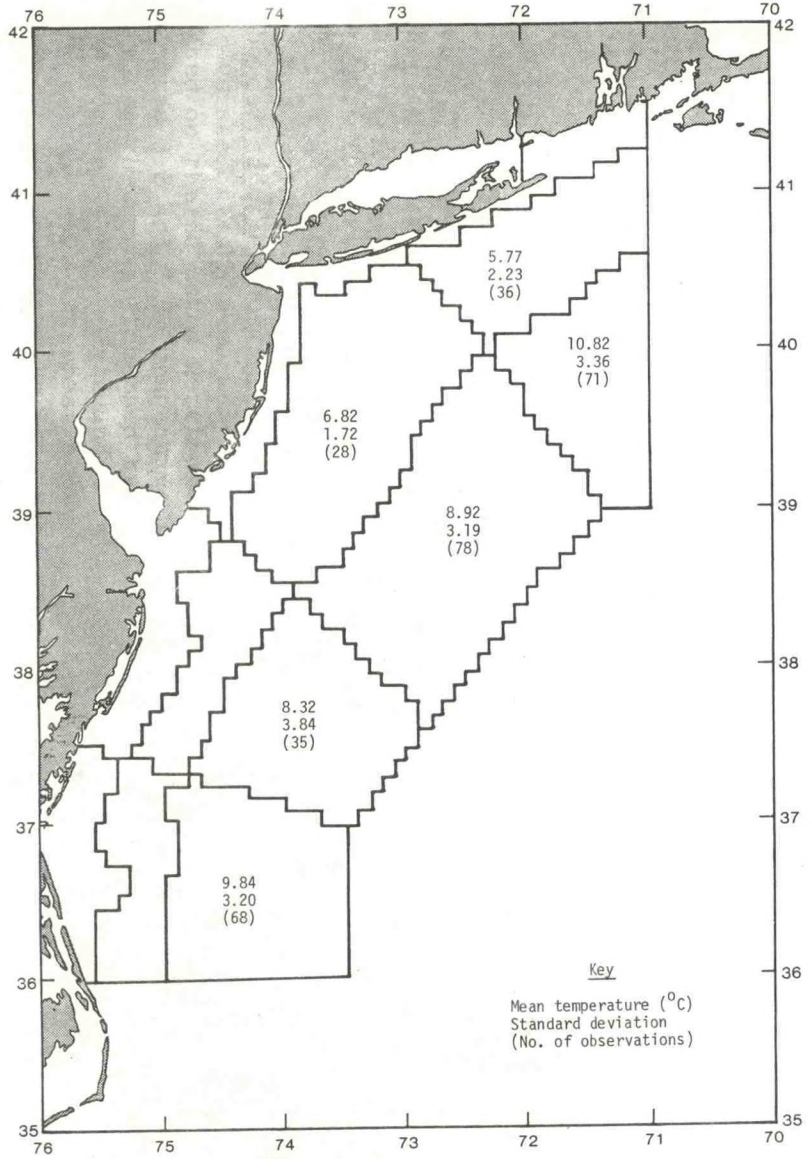


Figure 4.34.--Winter mean temperatures at 50-m depth.

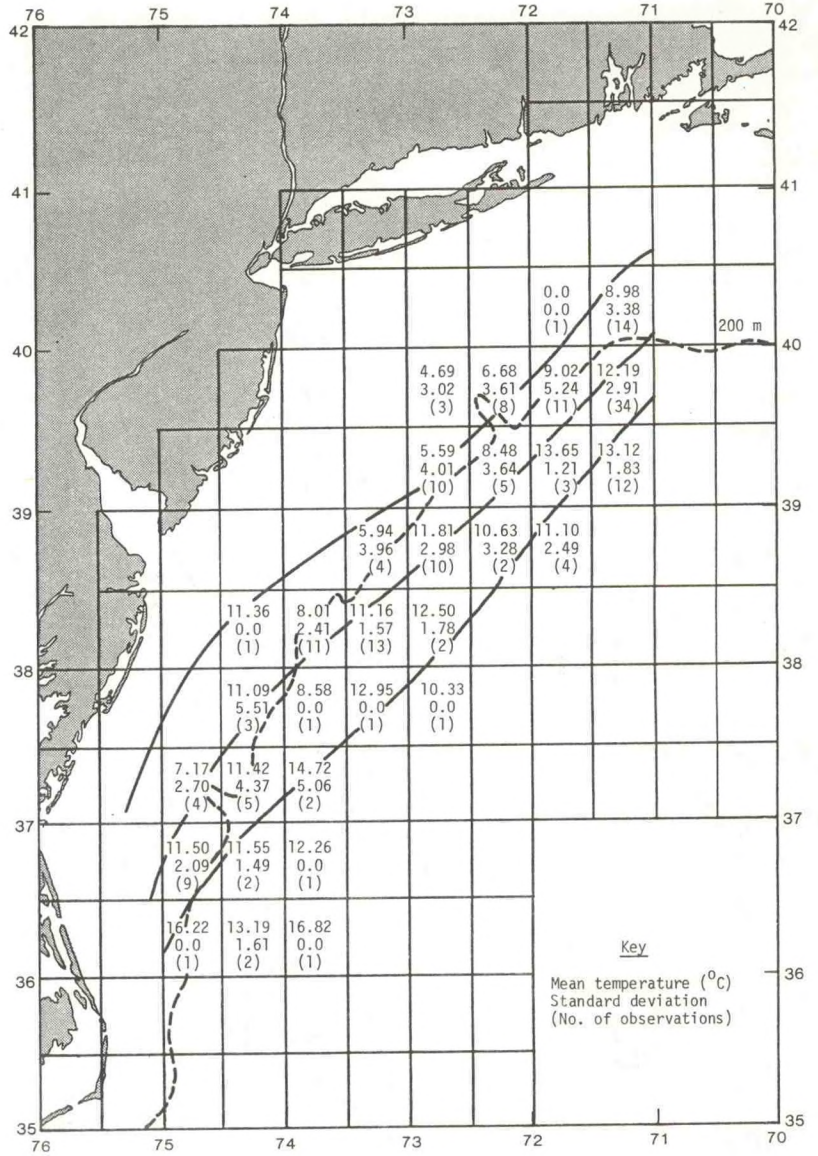


Figure 4.35.--Winter mean temperature field at 50-m depth.

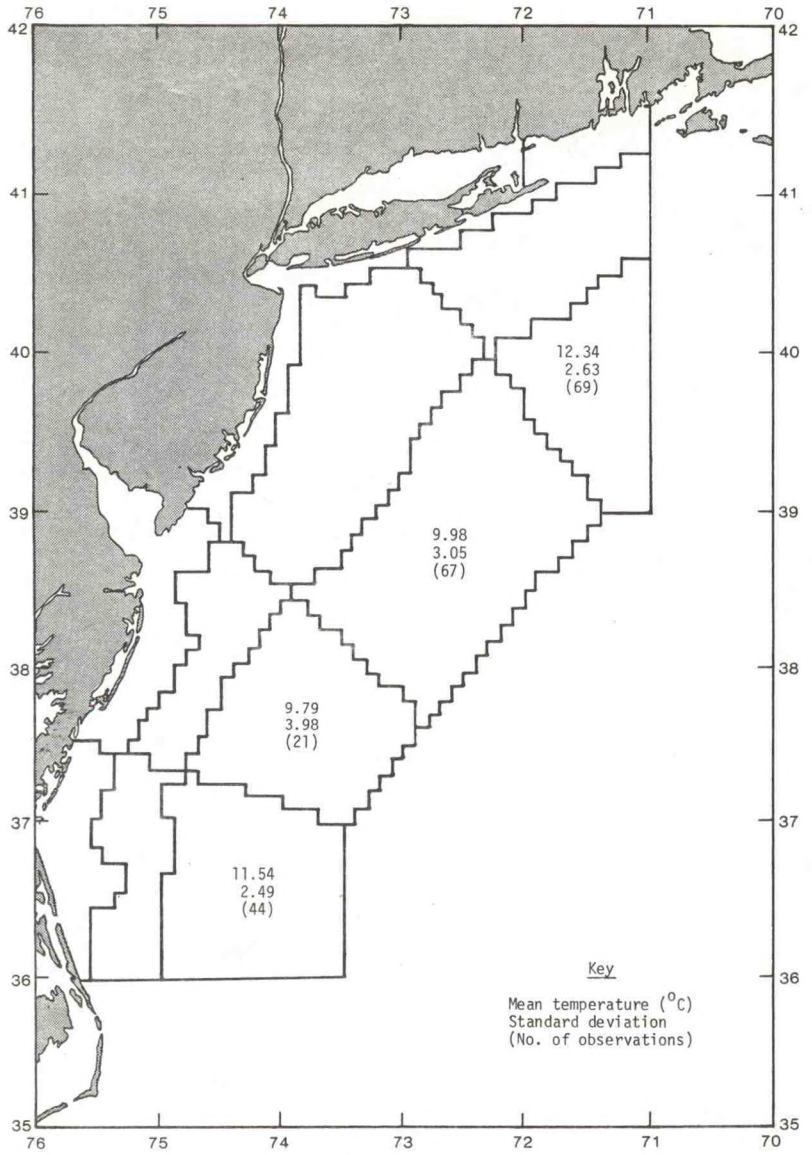


Figure 4.36.--Winter mean temperatures at 100-m depth.

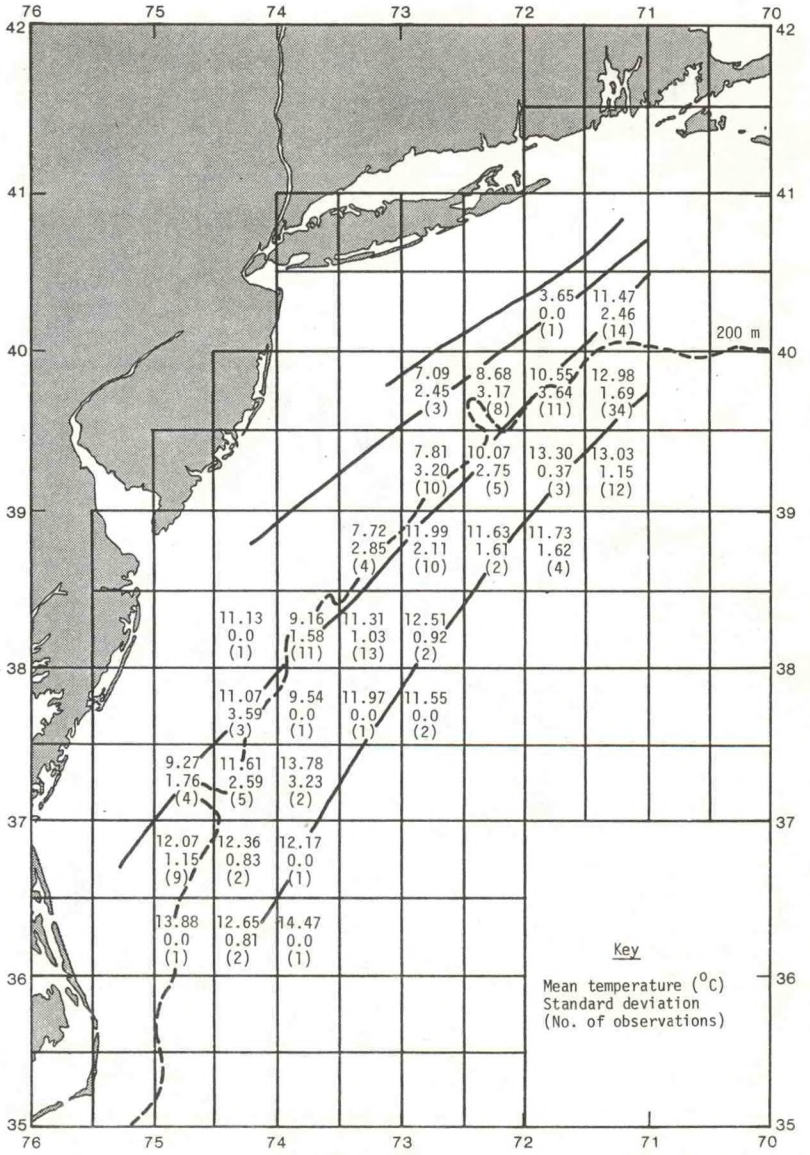


Figure 4.37.--Winter mean temperature field at 100-m depth.

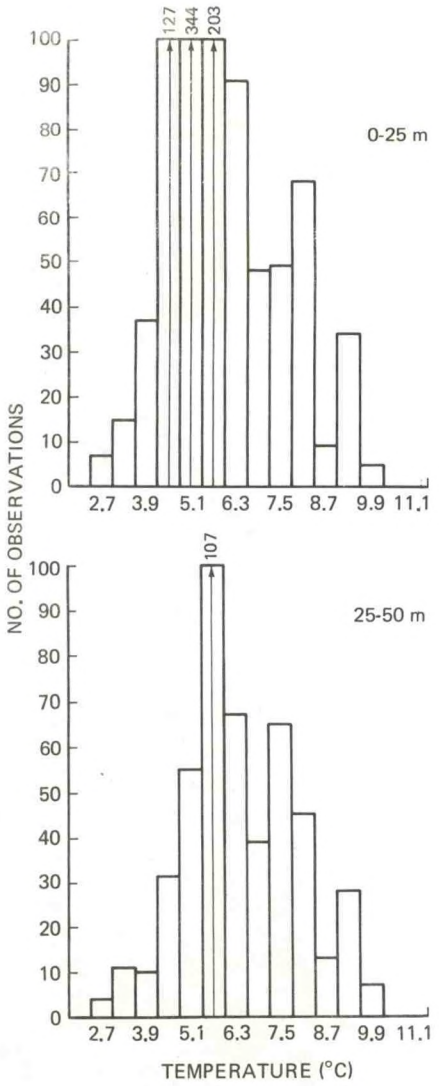


Figure 4.38.--Histograms of winter temperature, area 6.

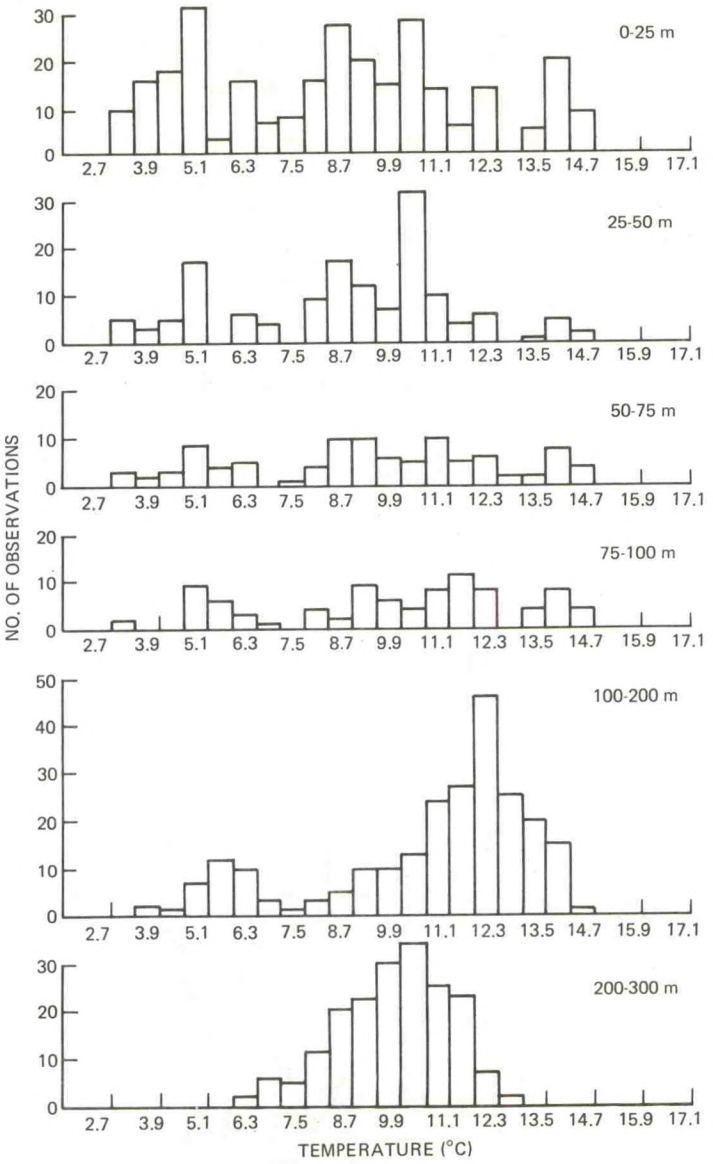


Figure 4.39.--Histograms of winter temperature, area 10.

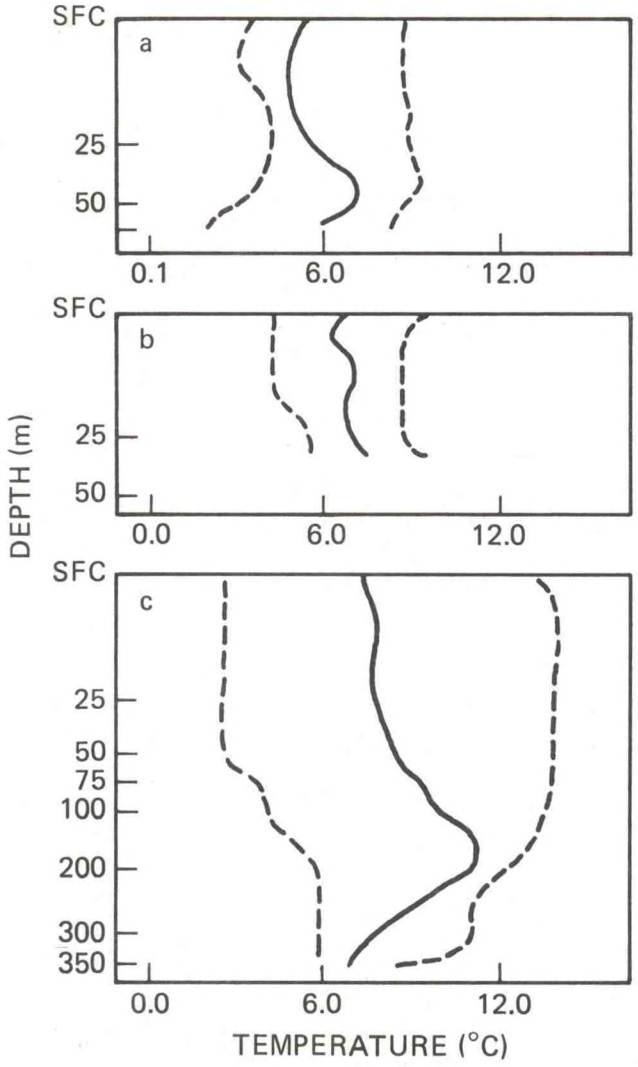


Figure 4.40.--Midlines (medians) and envelopes (2.5 and 97.5 percentiles) of winter temperatures for (a) area 6, (b) area 8, and (c) area 10.

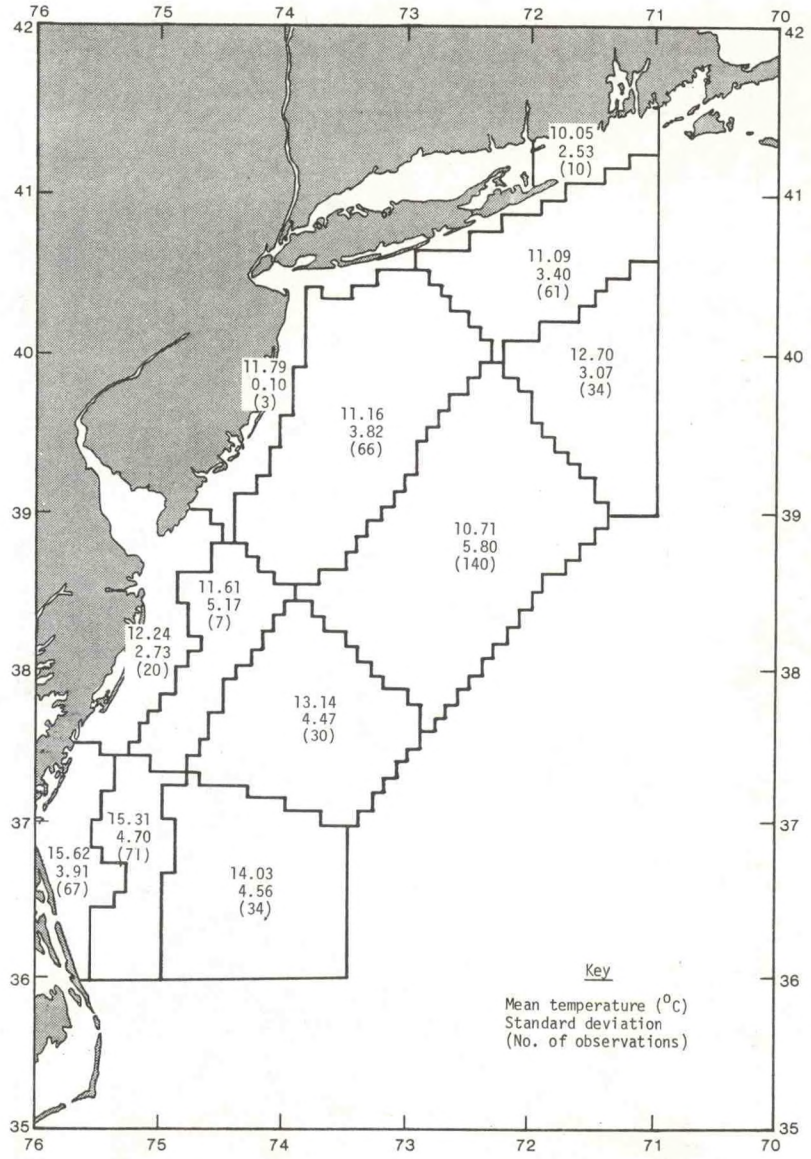


Figure 4.41.--Spring mean sea-surface temperatures.

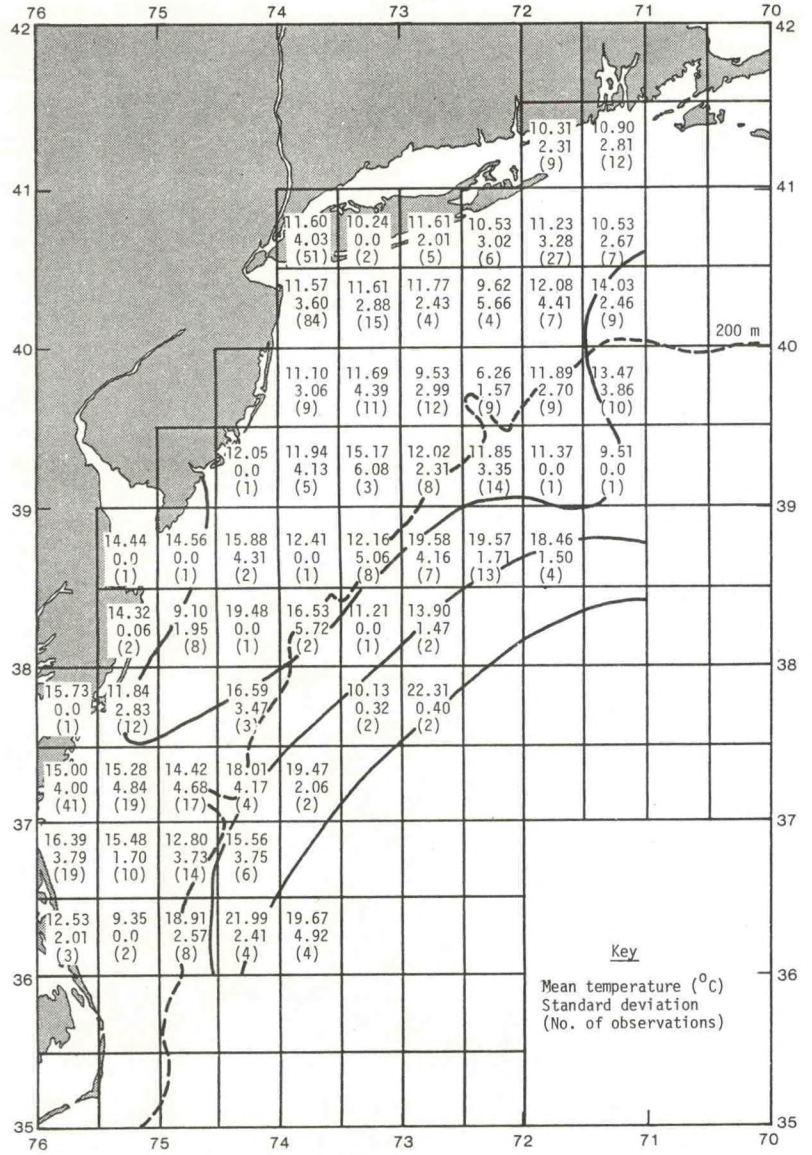


Figure 4.42.--Spring mean sea-surface temperature field.

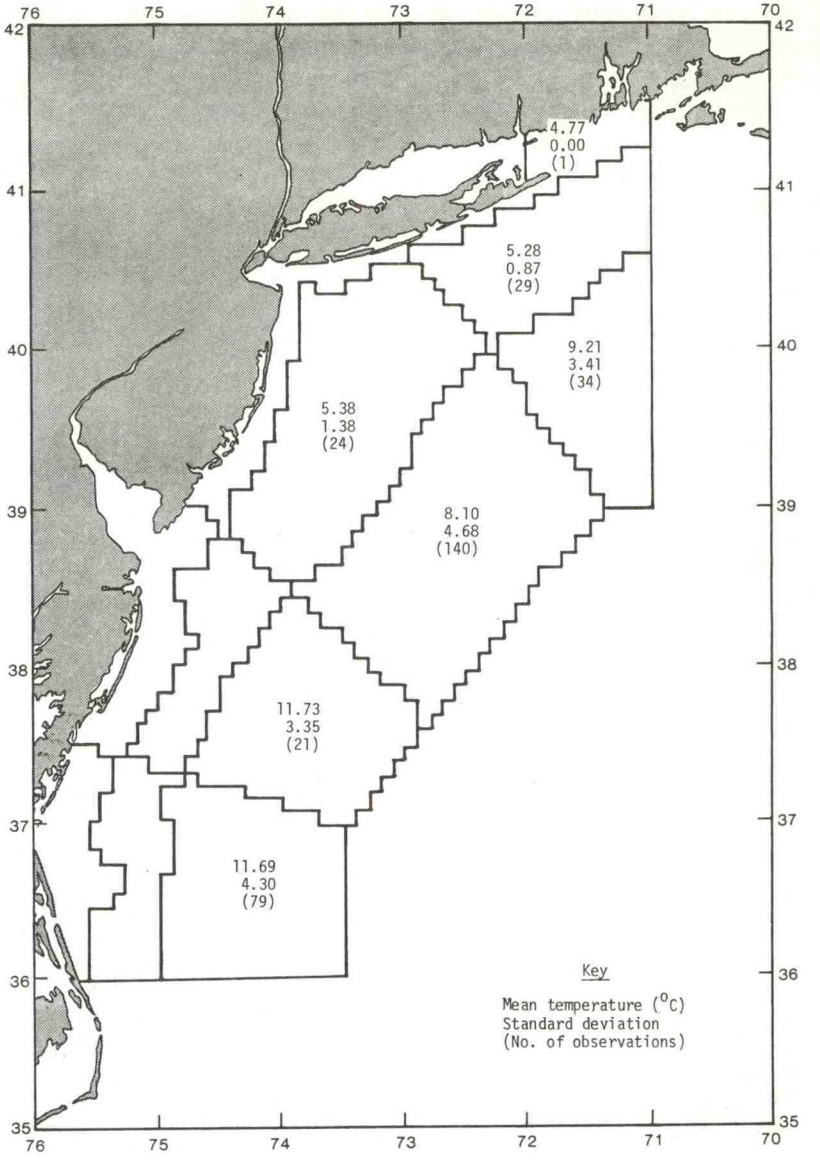


Figure 4.43.--Spring mean temperatures at 50-m depth.

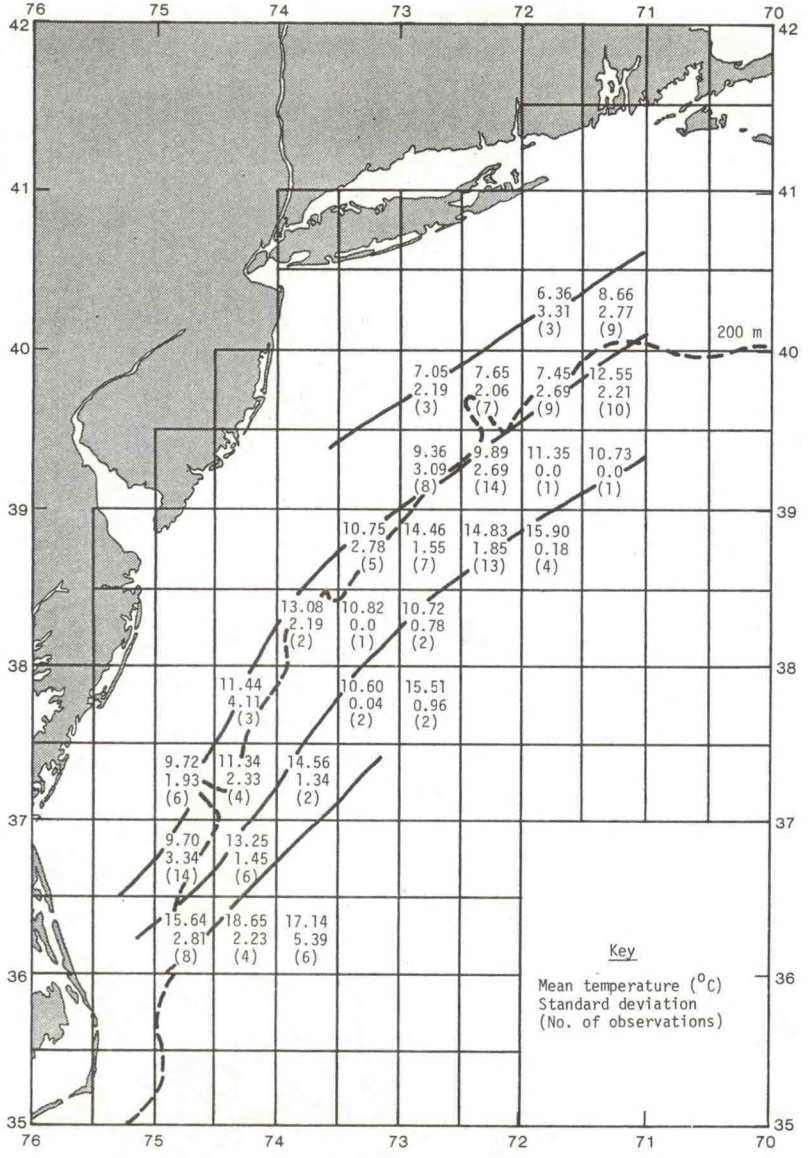


Figure 4.44.--Spring mean temperature field at 50-m depth.

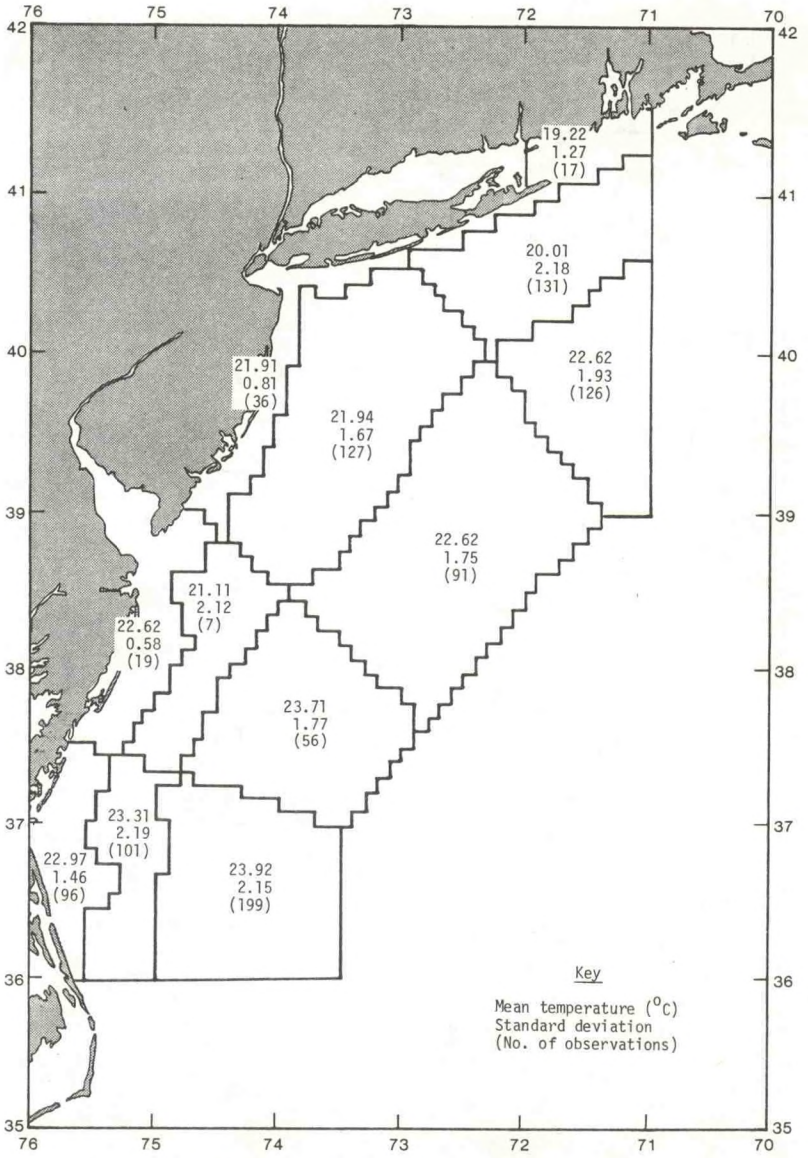


Figure 4.45.--Summer mean sea-surface temperatures.

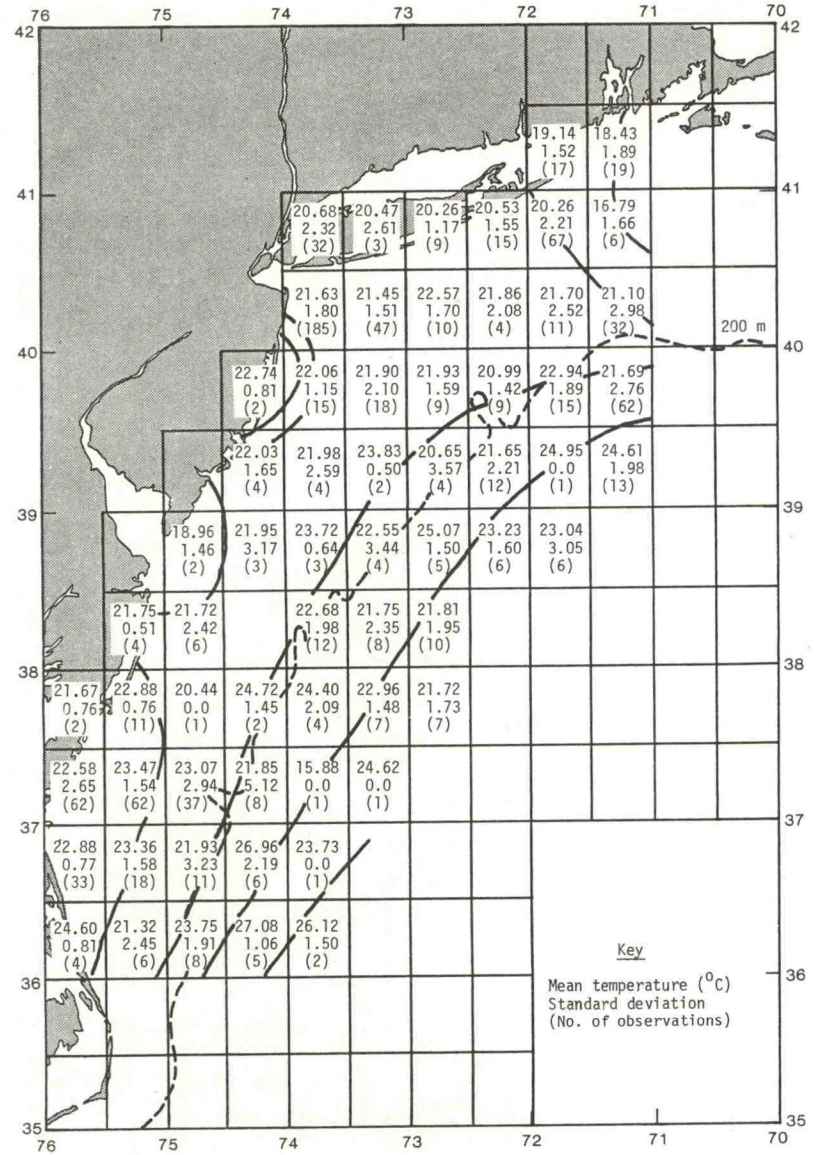


Figure 4.46.--Summer mean sea-surface temperature field.

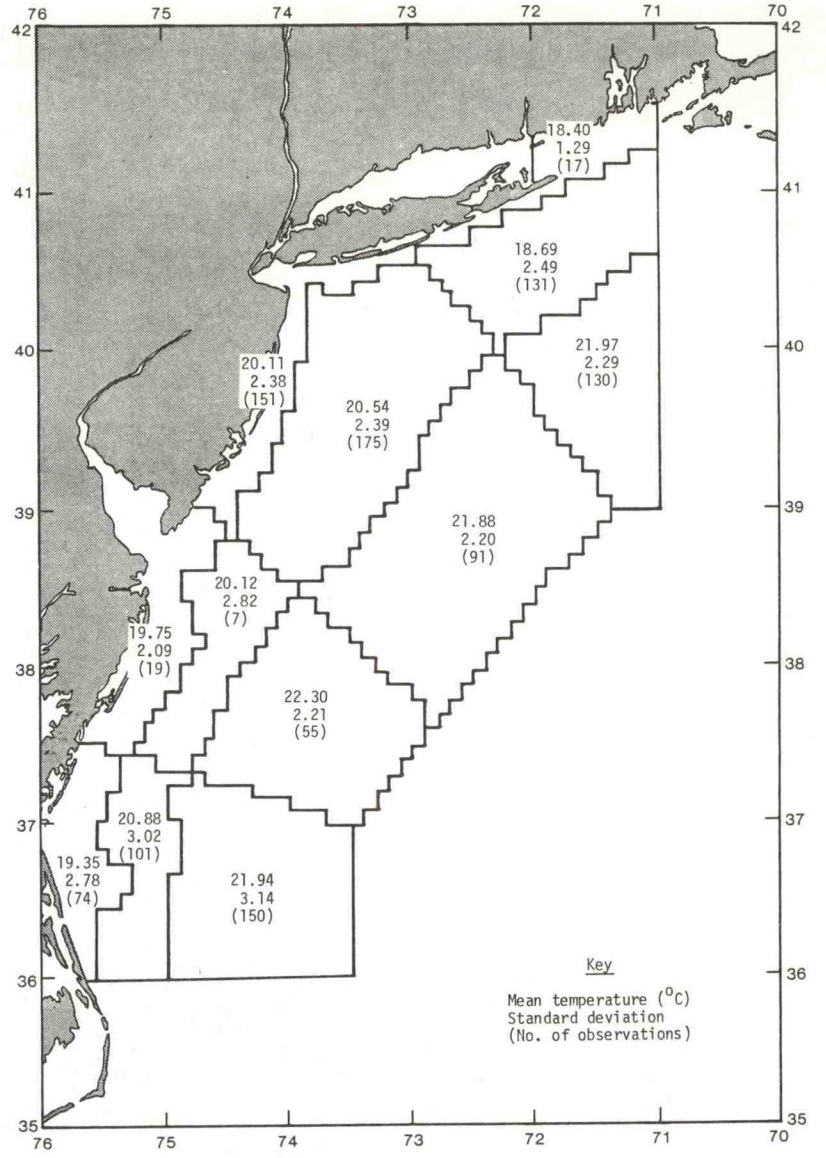


Figure 4.47.--Summer mean temperatures at 10-m depth.

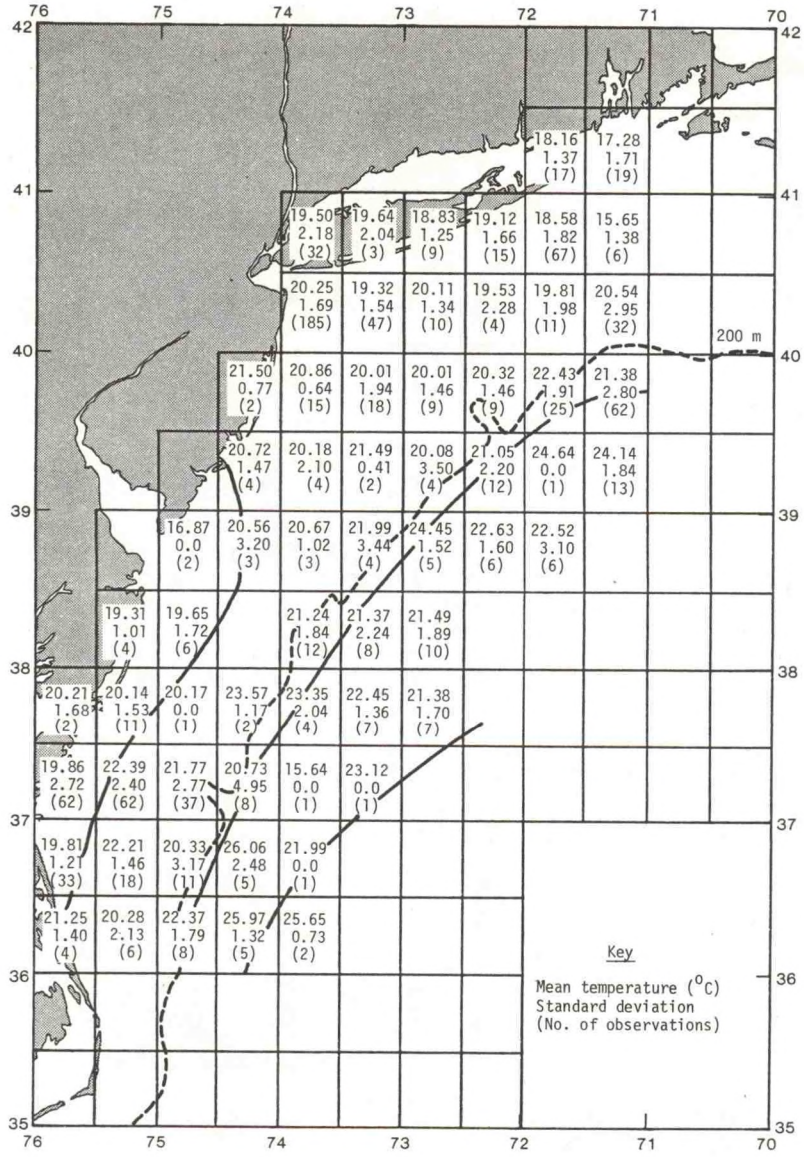


Figure 4.48.--Summer mean temperature field at 10-m depth.

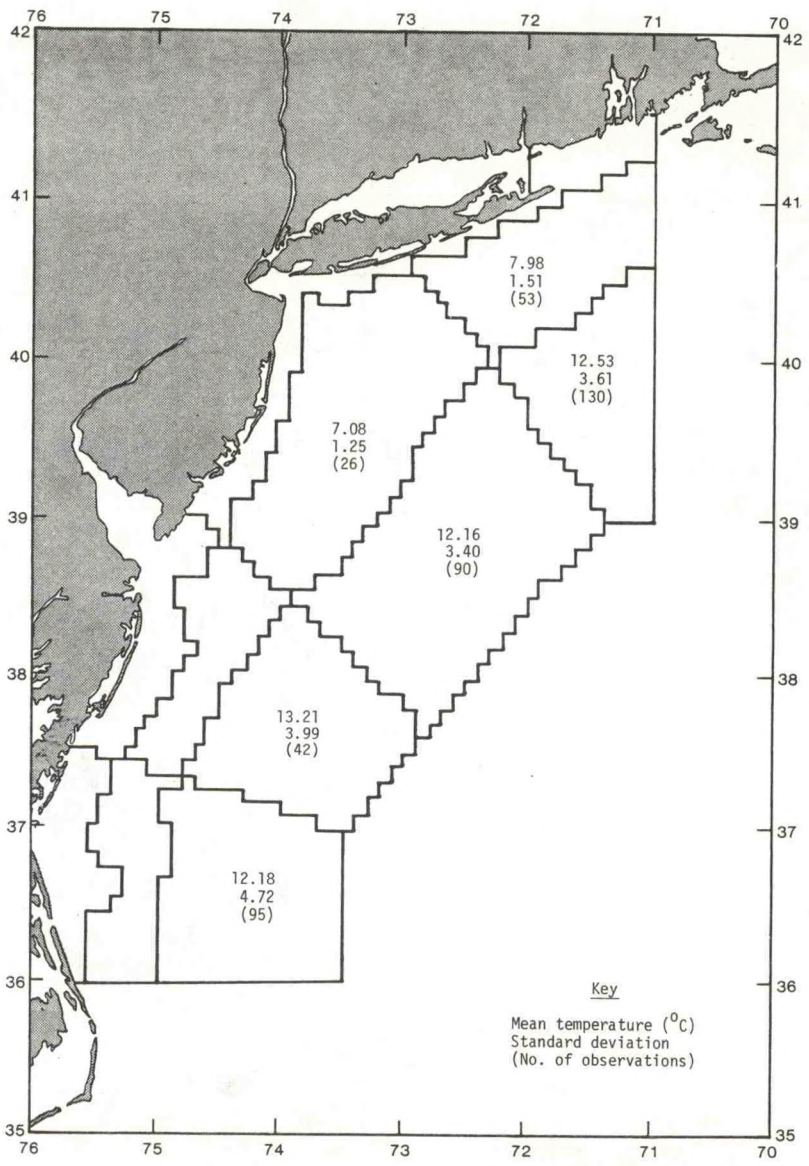


Figure 4.49.--Summer mean temperatures at 50-m depth.

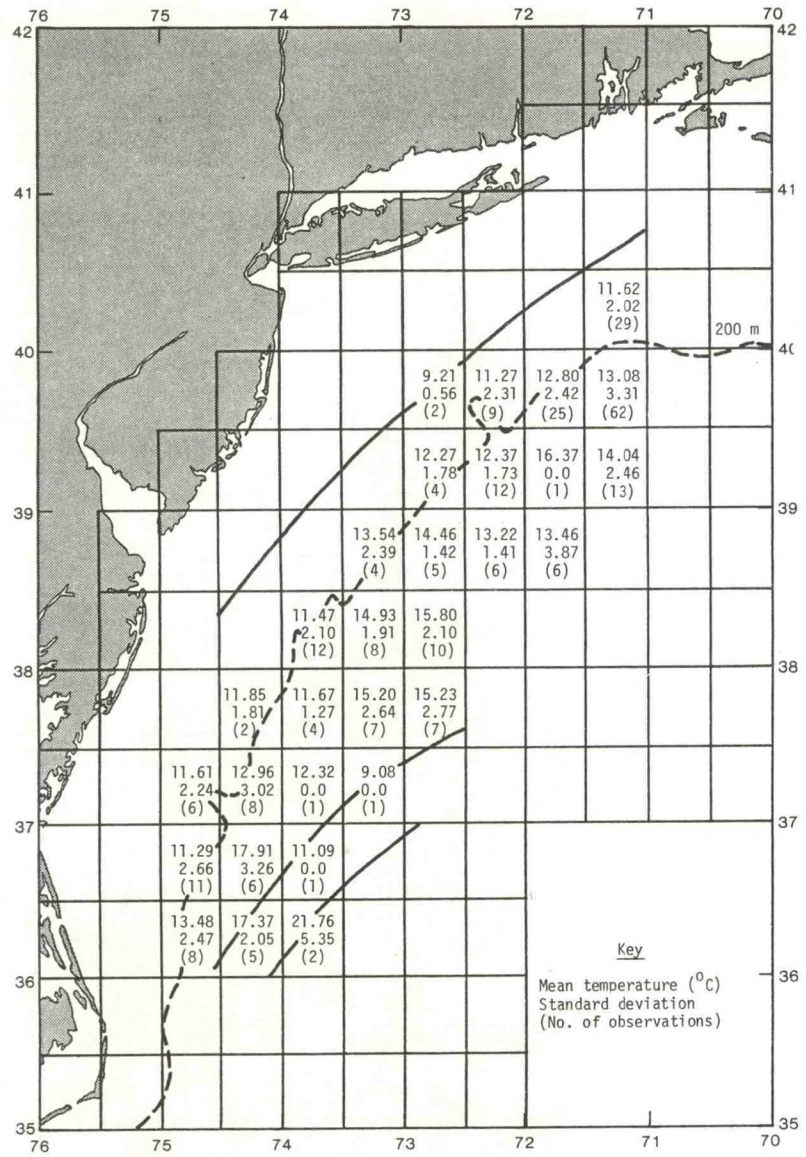


Figure 4.50.--Summer mean temperature field at 50-m depth.

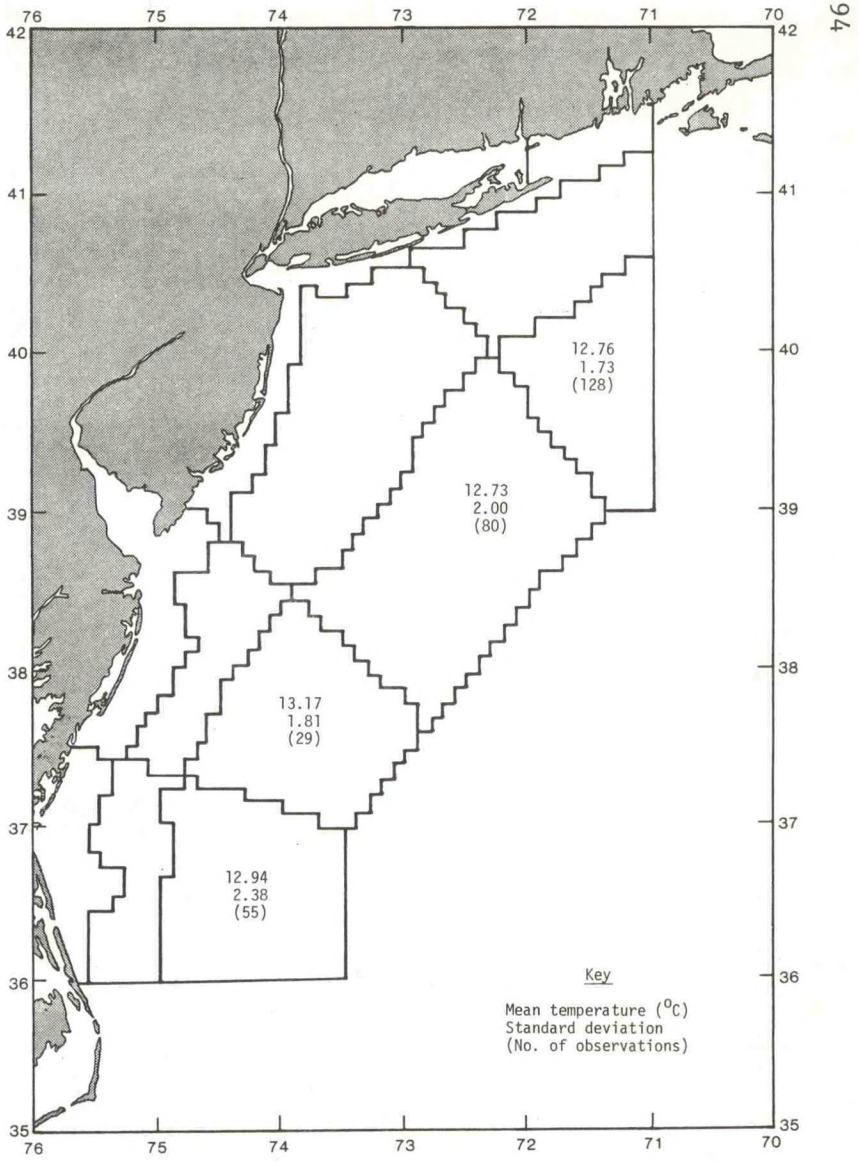


Figure 4.51.--Summer mean temperatures at 100-m depth.

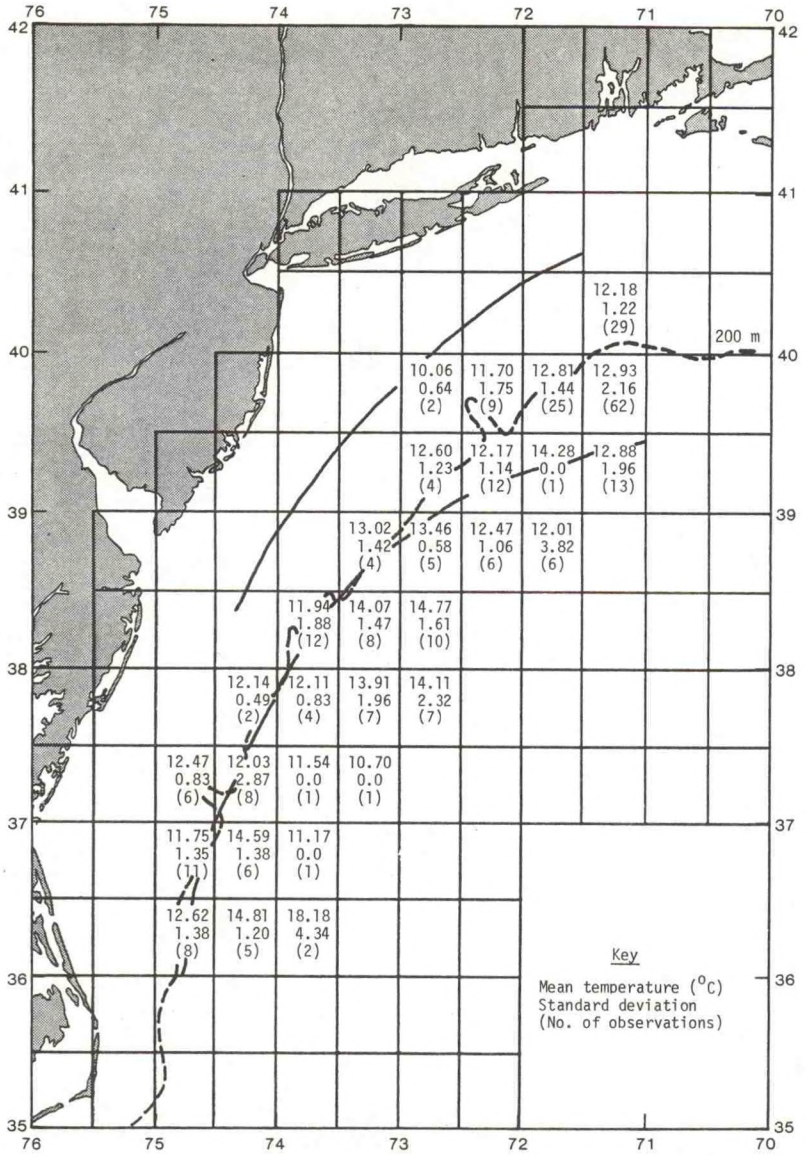


Figure 4.52.--Summer mean temperature field at 100-m depth.

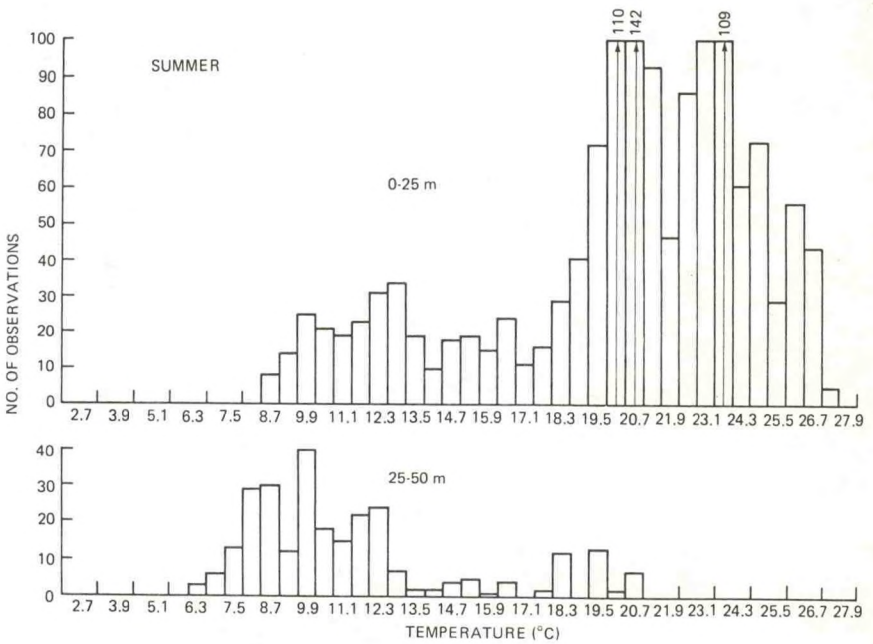


Figure 4.53.--Histograms of summer temperature, area 8.

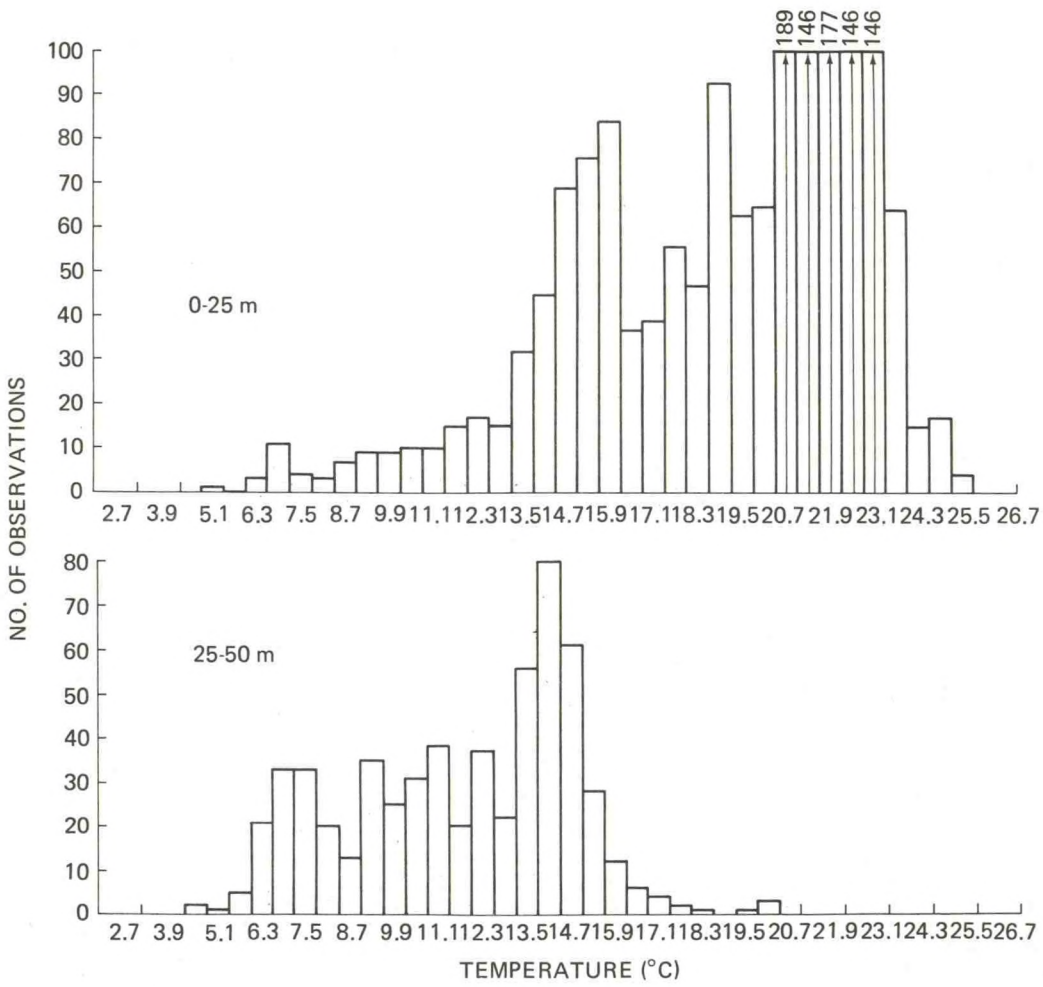


Figure 4.54.--Histograms of summer temperature, area 6.

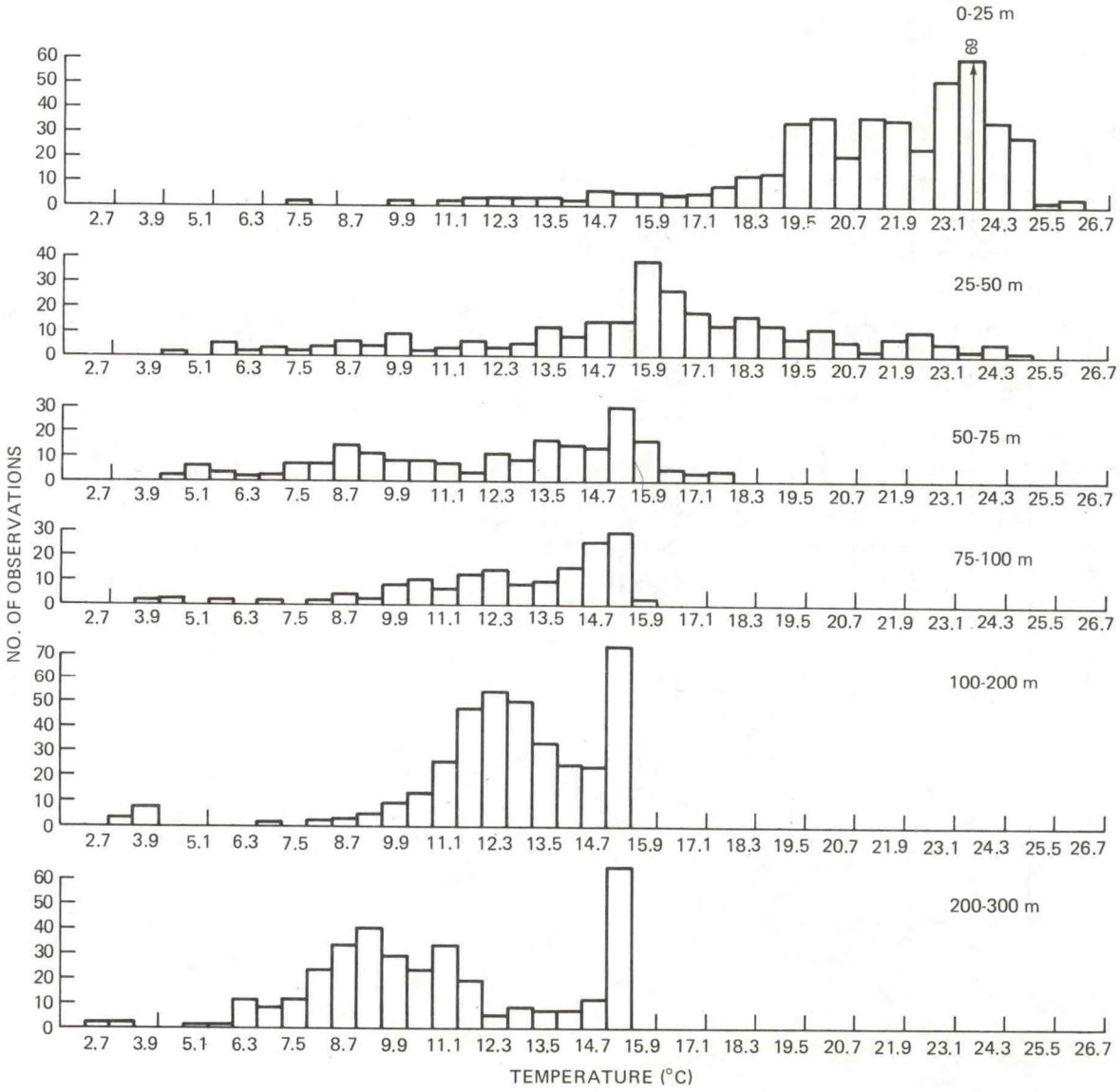


Figure 4.55.--Histograms of summer temperature, area 10.

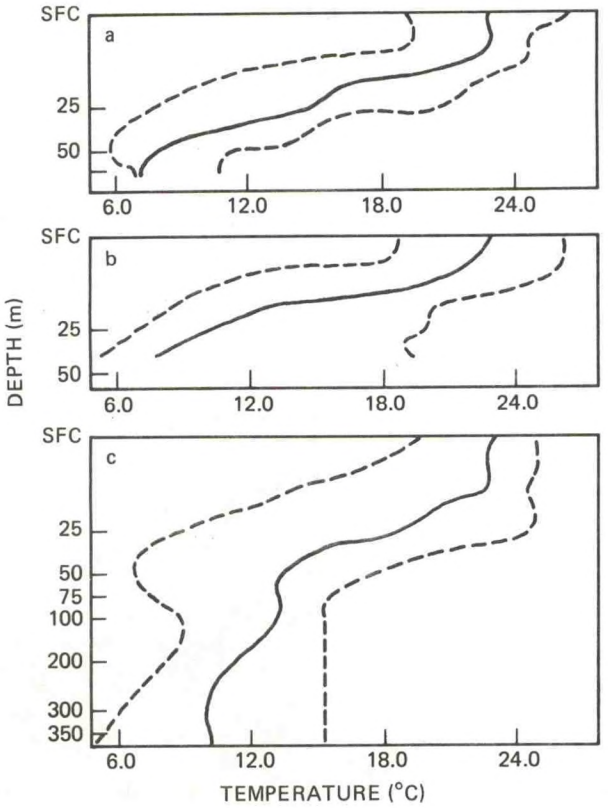


Figure 4.56.--Midlines (medians) and envelopes (2.5 and 97.5 percentiles) of summer temperatures for (a) area 6, (b) area 8, and (c) area 10.

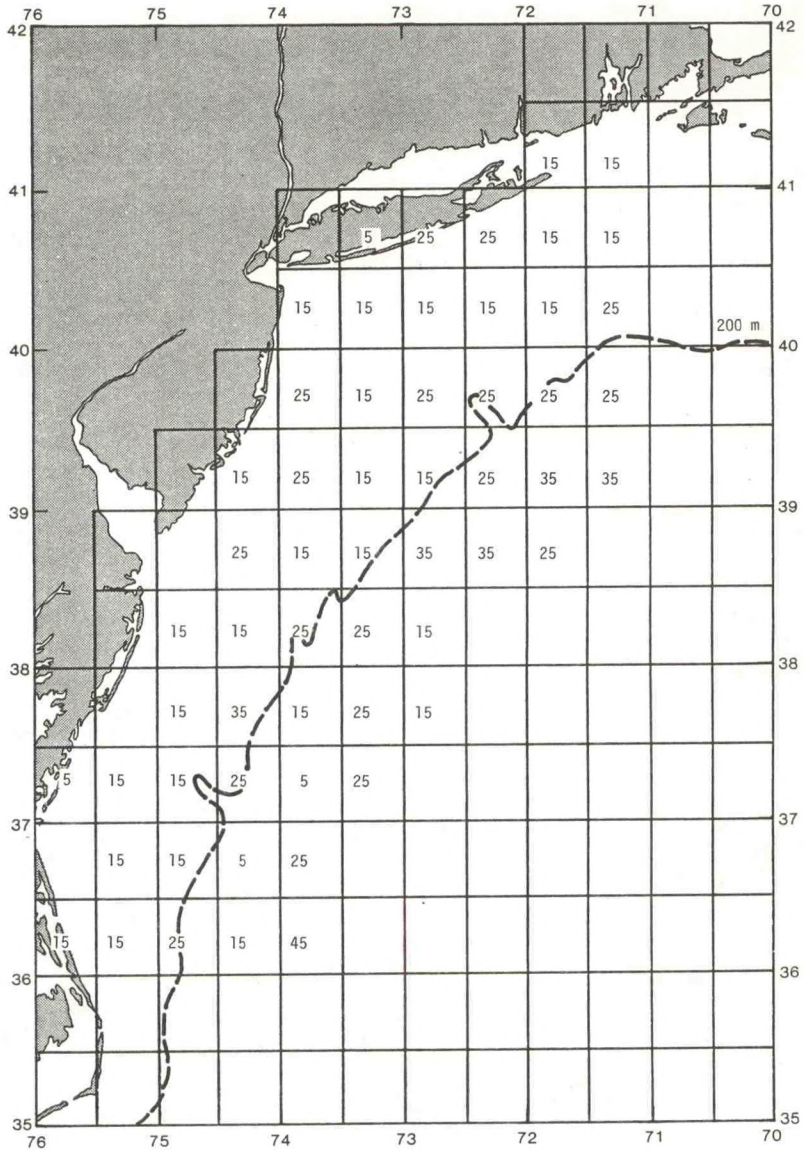


Figure 4.57.--Summer mean depths (m) of thermocline.

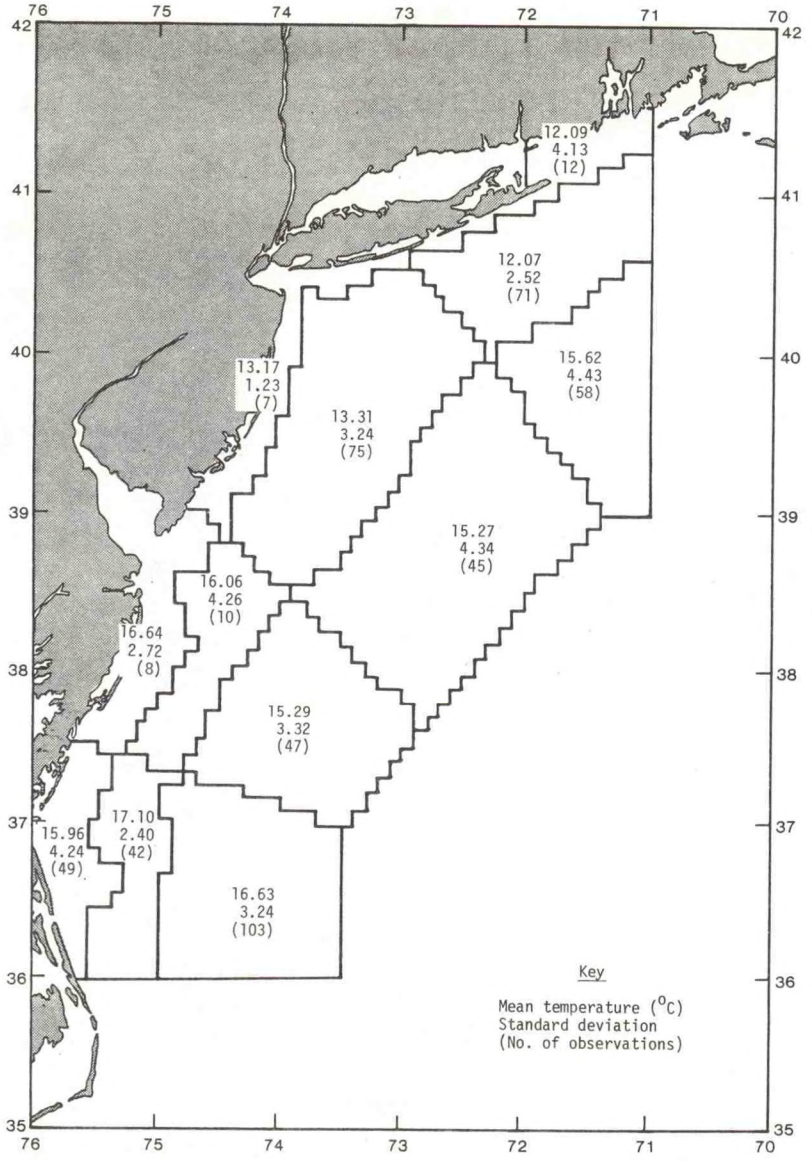


Figure 4.58.--Fall mean sea-surface temperatures.

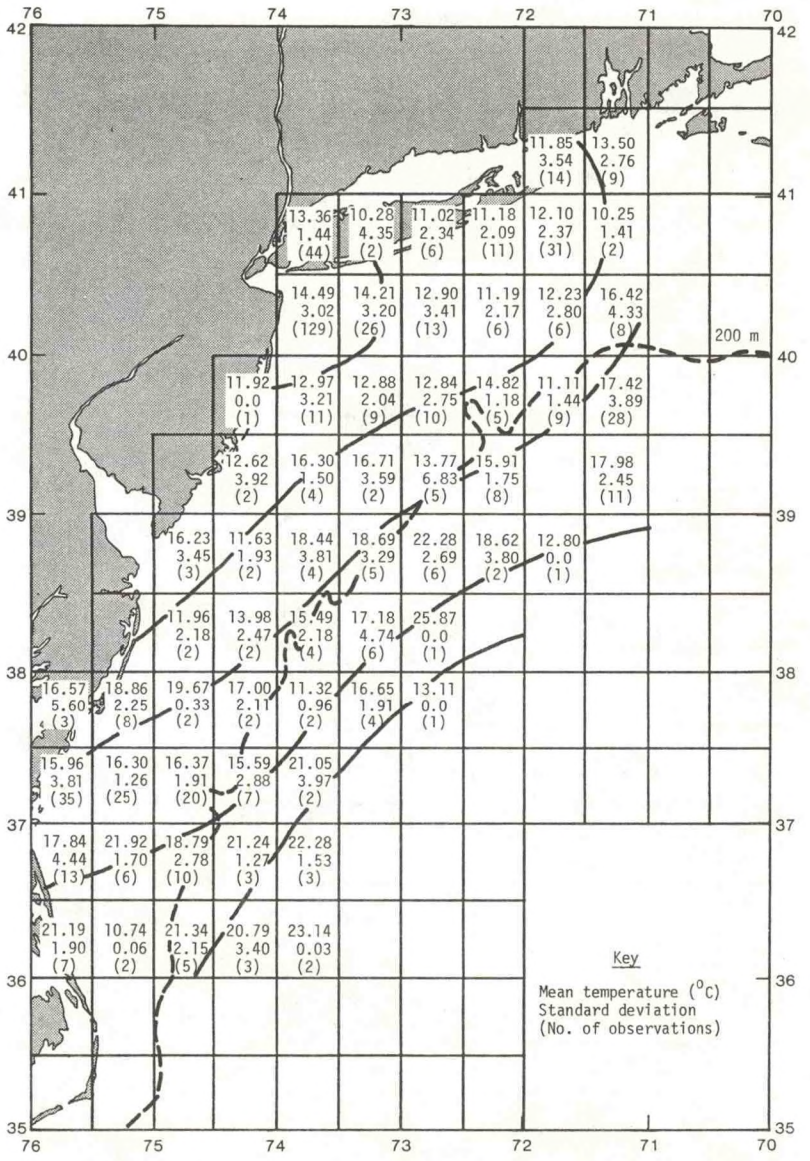


Figure 4.59.--Fall mean sea-surface temperature field.

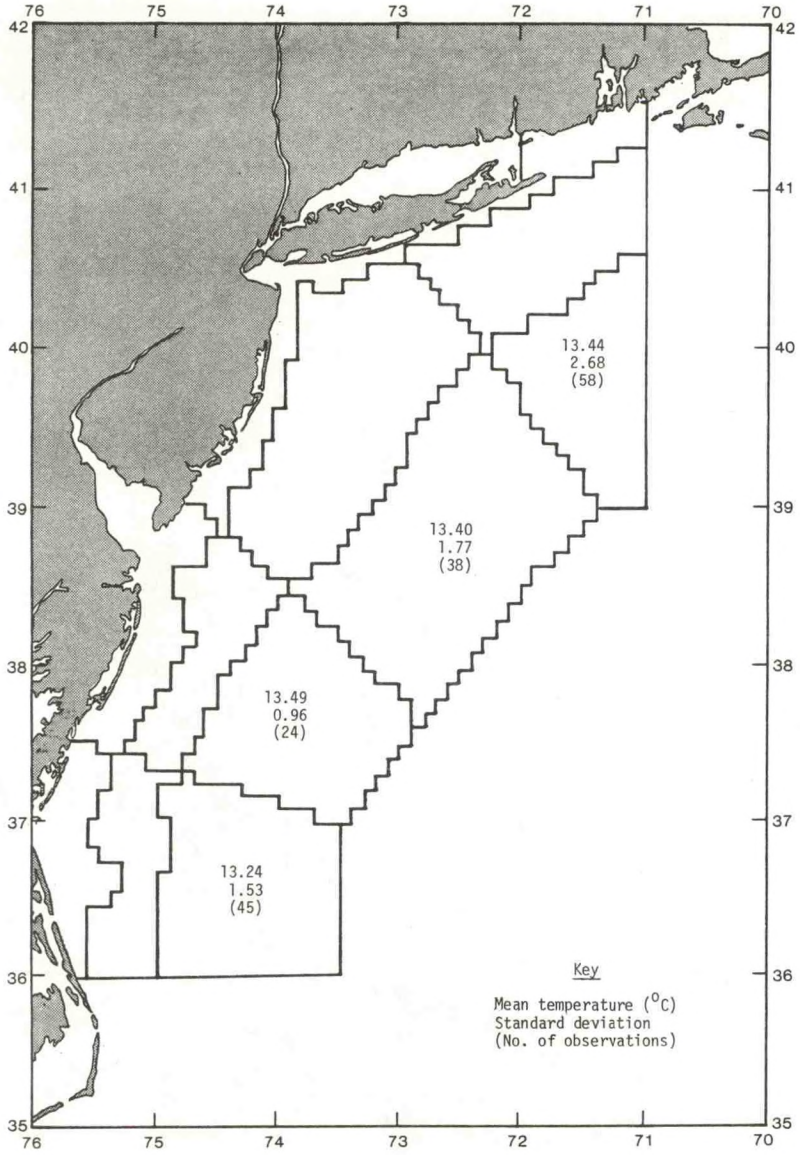


Figure 4.60.--Fall mean temperatures at 100-m depth.

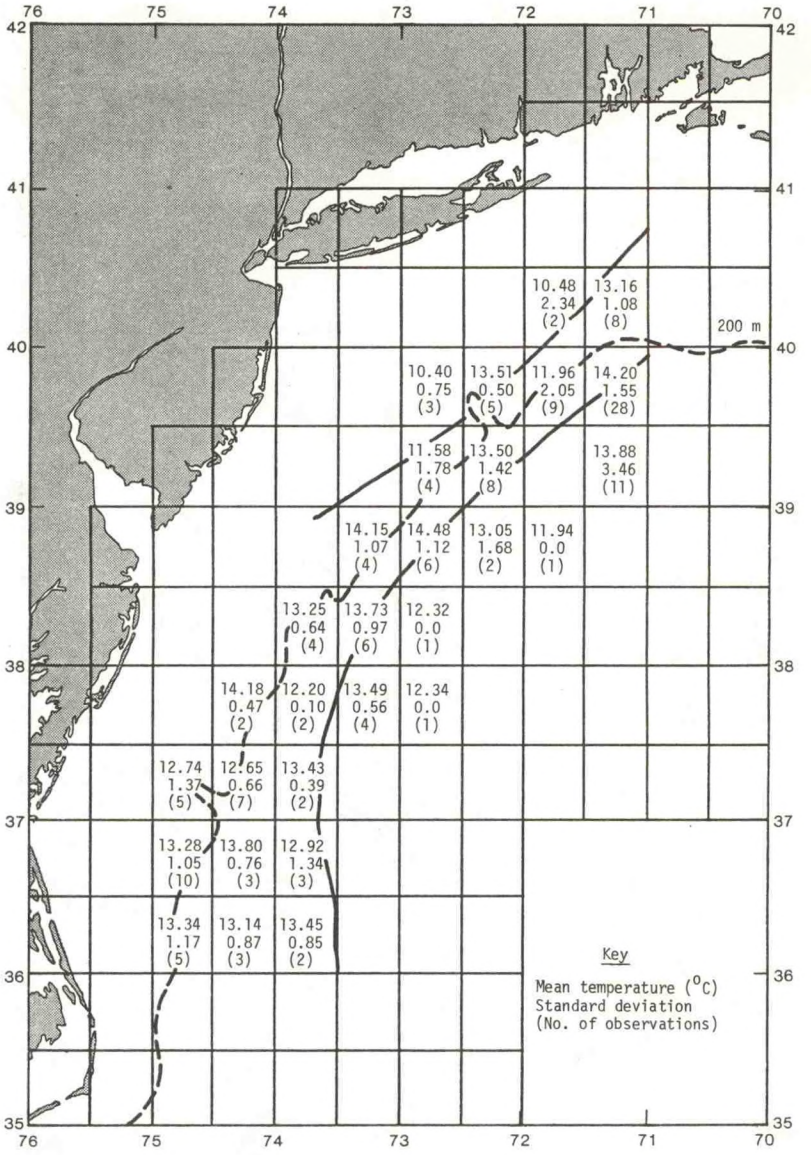


Figure 4.61.--Fall mean temperature field at 100-m depth.

### 4.4.5 Summary of Temperature Analysis

The results presented in the preceding sections show general agreement with previous studies (e.g., Walford and Wicklund, 1968). Winter temperatures over the shelf are nearly uniform spatially at 5 to 7°C, with a slight increase with depth. The major feature is the shelf-slope water front delineated by the 10°C isotherm. Vernal warming begins in late March to April, leading to a weakening of horizontal gradients and the development of a seasonal thermocline. Summer temperatures increase somewhat with decreasing latitude, but cold "winter" water still persists on the bottom. In the fall, increasingly strong winds aid surface cooling and cause convective overturn of the water column, and a return to winter conditions. Below 200-m depth, seaward on the shelf break, temperatures decrease rather uniformly to just above 3.7°C at a depth of 1,500 m in all seasons.

Comparison of the number of STD observations used in preparing the temperature charts for the 12 oceanographic areas with the observations used for the field analysis by ½° squares shows that the editing and validation criteria employed in the latter reduced the STD data base to the point where contour analysis is barely possible. The reason lies in the fact that many of the STD casts contain surface and bottom observations only, with very few measurements made in the water column. The STD data base is adequate, however, for documenting the seasonal means and variations on the space scale of the 12 oceanographic areas, except for area 7 where MBT data had to be used. The uneven distribution of the STD observations also makes their use difficult in any objective analysis scheme or in numerical models that require input at ½° resolution.

A detailed temperature-depth analysis from data summarized by month and ½° areas would be valuable in following chronologically the annual development of water mass structure, i.e., the development of the thermocline and variations in strength of the shelf-slope water front. Such an analysis would make it possible to describe the expected internal circulation of the shelf water, and the motion of pollutants in the water mass. Vertical mixing could then be related to that description.

### 4.4.6 Salinity

Although salinity in the ocean may not have a major effect on the dispersion of spilled pollutants at sea (e.g., Otto, 1973), the description of the distribution of salinity is important in risk assessment for the following reasons:

(1) Salinity distributions in coastal waters have a major influence on the density distributions, which, in turn, have an effect on circulation.

(2) In case of a pollutant spill, salinity will affect its severity in terms of resident pelagic and benthic organisms.

(3) Salinity is often used as a tracer in determining horizontal and vertical mixing rates, and in testing pollutant dispersion models.

The distribution of salinity on the continental shelf is controlled by river runoff and by the influx of saline ocean water. Two major features are apparent from previous work (e.g., Bigelow and Sears, 1935): a horizontal gradient normal to the coastline, with salinity increasing seaward, and an increase of salinity with depth. The seasonal march of salinity is forced by river runoff, which reaches a maximum in April and May. The cycle of runoff and subsequent mixing usually results in a minimum of salinity in summer and a maximum in winter. Complicated processes occur at the shelf-slope water front, which is marked by the 34.5-ppt isohaline, as has been shown by Bigelow and Sears (1935).

Winter. Surface mean salinities by area (fig. 4.62) and by ½° squares (fig. 4.63) show a seaward increase from 31 to 32 ppt inshore of the 20-m isobath, to 33 ppt across the midshelf, and to 34 ppt at the shelf break, roughly along the 200-m isobath. Plumes of low-salinity water are seen near the mouths of the Hudson and Delaware Rivers, and in the vicinity of Chesapeake Bay. Variability in salinity is relatively small, the standard deviation being generally less than 1 ppt. The 50-m depth charts (figs. 4.64 and 4.65) show a decrease in variability, and an increase in salinity over the entire area. The histograms in figure 4.66 for area 6 show unimodal vertical distributions without apparent skewness, but with a slight increase of mean salinity with depth. Figure 4.67, on the other hand, shows a skewed distribution for area 8, which probably results from pulses of freshwater outflow from Chesapeake Bay. In the midline plots for areas 6, 8, and 10 (fig. 4.68), the vertical salinity gradient is apparent. In the shelf-slope water front, salinity reaches a maximum at about 200-m depth, which is the wedge of slope water associated with the warm temperature wedge noted earlier. Below this depth, variability decreases greatly.

Spring. Increased river runoff lowers salinities on the inner continental shelf, and the effects of this freshwater discharge is apparent from a comparison of figures 4.69 and 4.70 with figures 4.62 and 4.63. These effects are also seen in the water column in figure 4.71, which shows a skewness to the left in the distribution for the level from the surface to 25 m, probably reflecting large freshwater runoff from the Hudson River. The mean salinity at the surface is lower, enhancing the vertical gradient.

Summer. By summer, fresh water from spring runoff has had time to mix with coastal waters in most areas, resulting in the lowest salinities of the year, as seen in figures 4.72 and 4.73. Variability is also highest in spring and summer. Beardsley and Flagg (1975) have noted that in summer the salinity rather than the temperature distribution delineates the shelf-slope water front. As seen in figures 4.74 and 4.75, higher salinity values and smaller variability are found at 50-m depth than at the surface. The vertical distributions (figs. 4.76 and 4.77) show the influence in areas 6 and 8 of freshwater discharge from rivers overlying heavier, saltier shelf water. In area 10 (fig. 4.78), the increase of salinity with depth, and a decrease in variability with depth in the slope water, are apparent. The midlines and envelopes plotted in figure 4.79 for the three areas show the increased vertical gradients and greater variability of salinity in summer.

Fall. Lower river discharge and stronger winds in the fall lead to a trend toward winter conditions, with higher values and decreased variability of salinity (figs. 4.80 and 4.81). Areas 10 and 5 show highest seasonal average of salinity in the fall, rather than in winter, in contrast to the other areas in the Bight. Cresswell (1967) has suggested that exchange of slope and shelf water may reach a maximum in summer, which could result in high salinities in the fall, but the number of observations is insufficient to examine this phenomenon, as seen from the analysis at 100-m depth (fig. 4.82), where the expected significant intrusions of slope water are not apparent.

Summary. Salinity increases with depth in all seasons, with differences between surface and bottom salinity of over 1 ppt commonly occurring on the shelf. The vertical salinity gradient is generally a maximum in summer and a minimum in winter in most locations. The horizontal gradient is generally perpendicular to the coast, with salinity increasing seaward.

The seasonal march of salinity generally shows a maximum in winter, with values of surface salinity reaching 33 ppt across the midshelf and 34 ppt at the shelf break. Exceptions are areas 10 and 5, where salinity is highest in the fall. The minimum occurs generally in summer, with salinities of 32 to 33 ppt prevailing on the shelf. Variability in salinity is lowest in winter, and highest in late spring and early summer near the coast. The number of observations in many parts of the Bight, however, is barely adequate to define either seasonal means or variability. According to Beardsley and Flagg (1975) the seasonal variability in salinity is of the same order of magnitude as the year-to-year variability. This assertion is examined below.

Figure 4.83 shows mean vertical profiles and standard deviations for area 6. It is seen that the lower limit of standard deviation in summer overlaps the higher limit of standard deviation in winter, making it difficult to identify a mean profile for each of the four seasons. The situation on the shelf break is illustrated in figure 4.84 for area 10, where the seasonal differences are seen to be small compared with year-to-year

fluctuations.

Many more observations than those currently available are needed to adequately describe the physical processes involved, especially because the salinity variations, rather than those of temperature, determine the density variations in some locations, e.g., the midshelf in winter, and the shelf-slope water front in summer. The requirement for reliable observations on the shelf has been strongly advocated by Wright (1976). Such observations would be helpful in analyzing the extent to which river runoff overrides the shelf waters and stabilizes the surface layers. The presence of a freshwater surface layer is an important factor in determining vertical momentum transport through the water column and the ensuing water circulation, forced by surface wind stress. Furthermore, an adequate set of salinity measurements would make it easier to estimate horizontal mixing rates, based on methods already developed and applied to a limited data set (Ketchum and Keen, 1955).

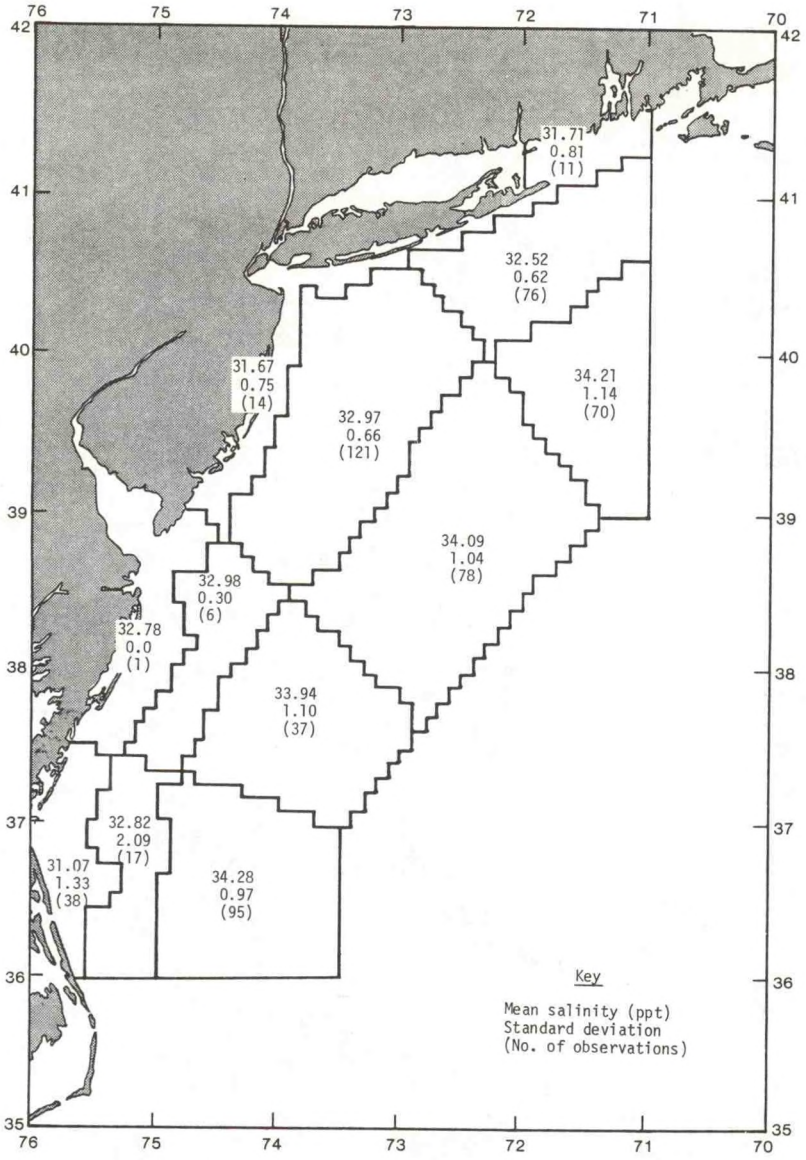


Figure 4.62.--Winter mean sea-surface salinities.

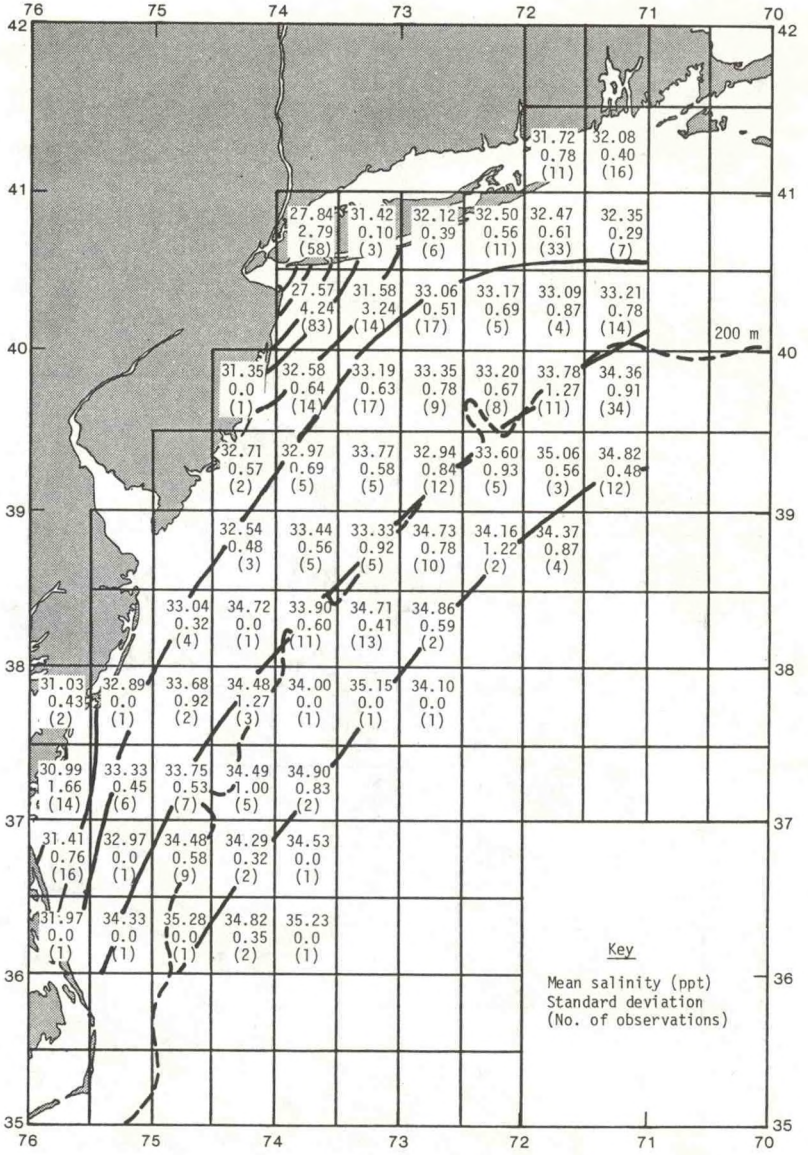


Figure 4.63.--Winter mean sea-surface salinity field.

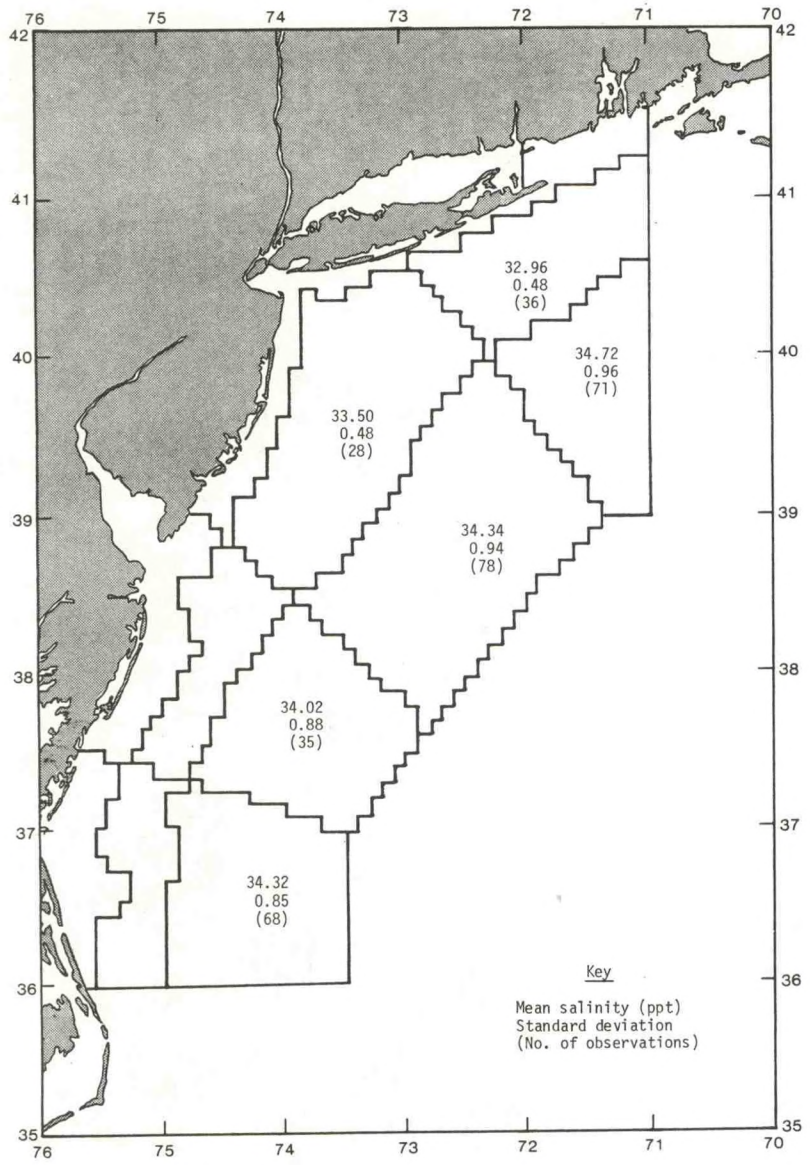


Figure 4.64.--Winter mean salinities at 50-m depth.

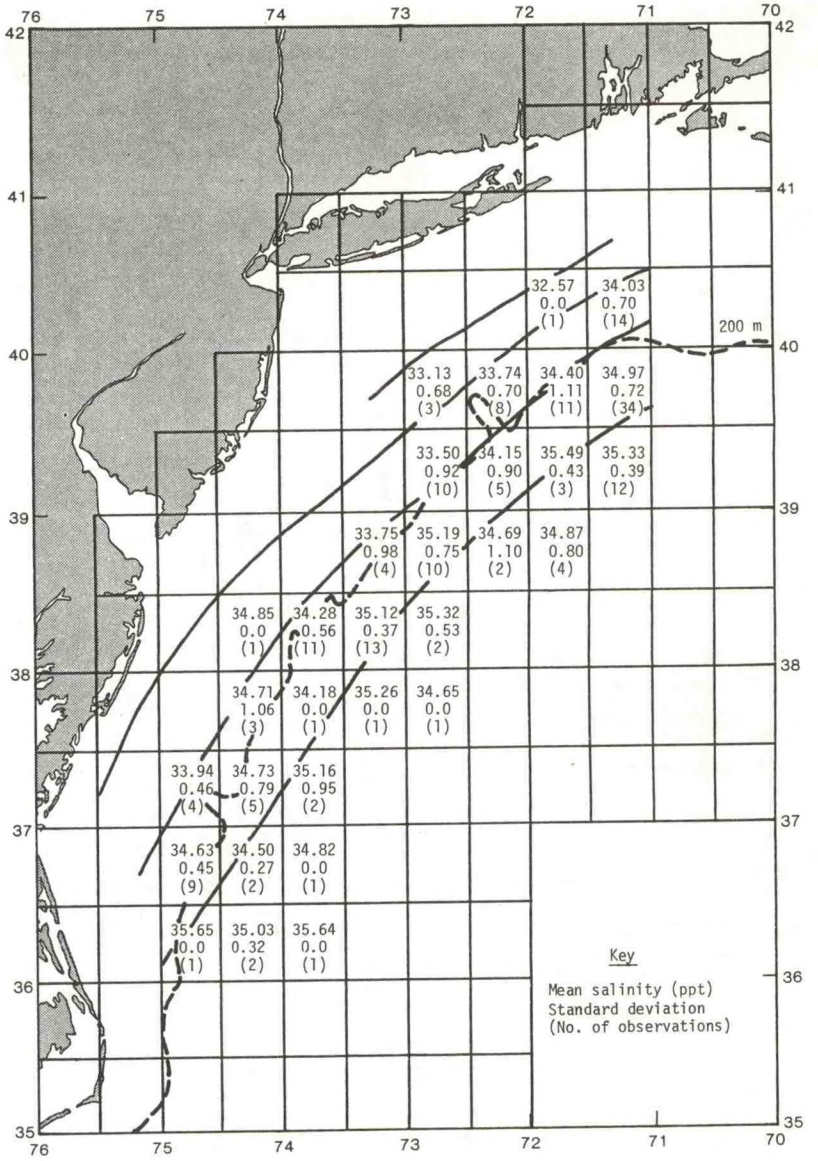


Figure 4.65.--Winter mean salinity field at 50-m depth.

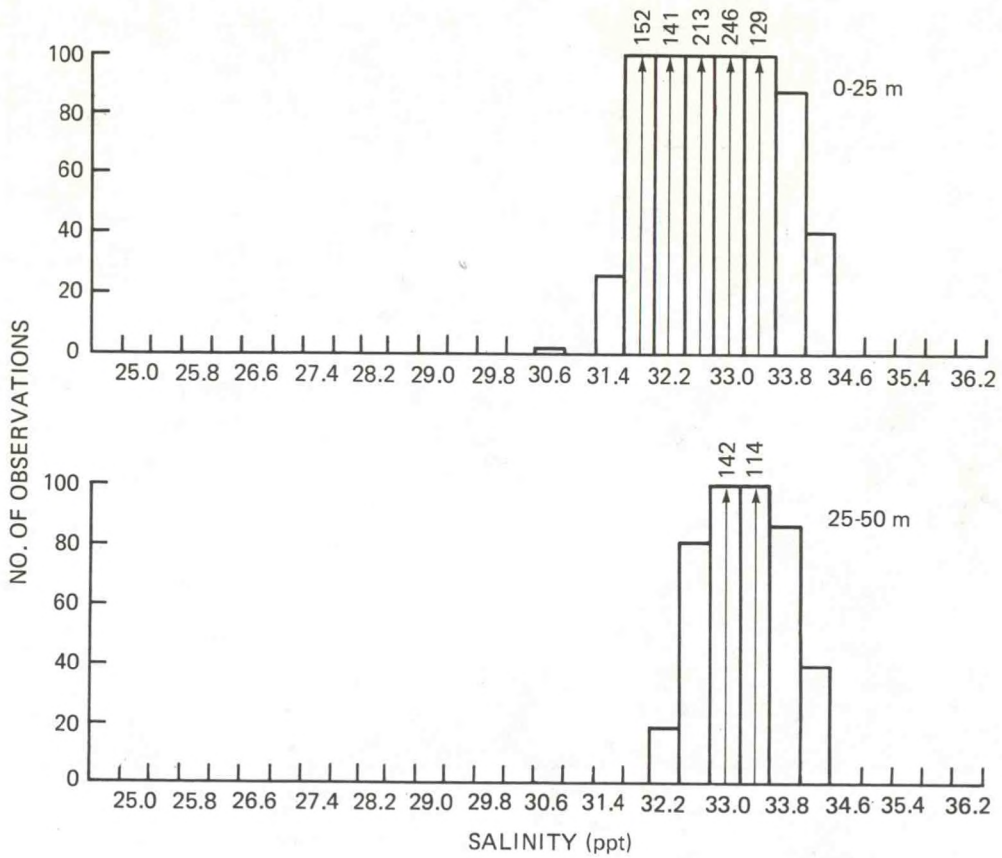


Figure 4.66.--Histograms of winter salinity, area 6.

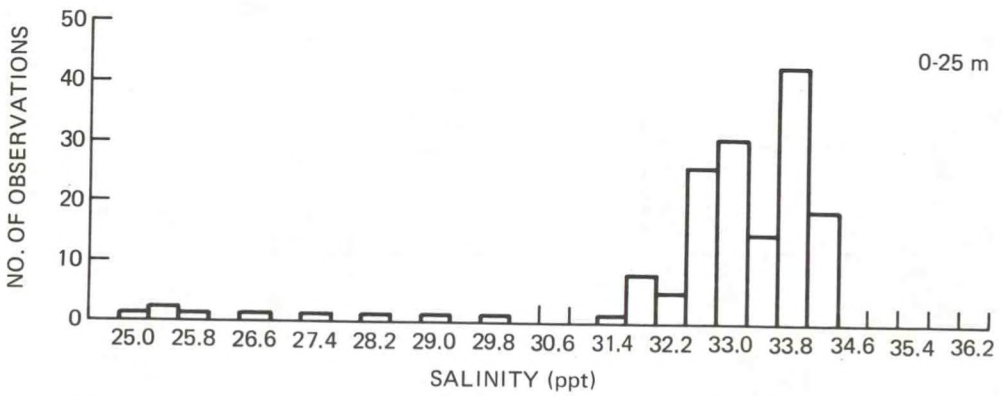


Figure 4.67.--Histograms of winter salinity, area 8.

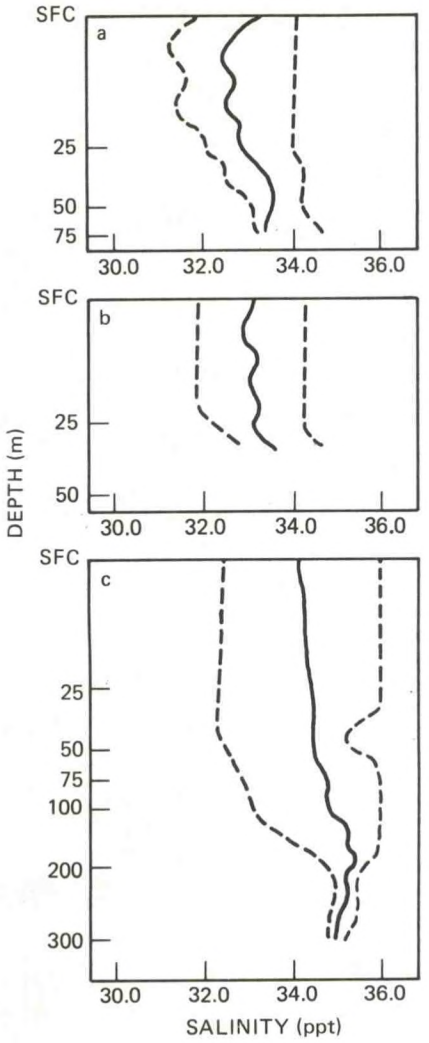


Figure 4.68.--Midlines (medians) and envelopes (2.5 and 97.5 percentiles) of winter salinities for (a) area 6, (b) area 8, and (c) area 10.

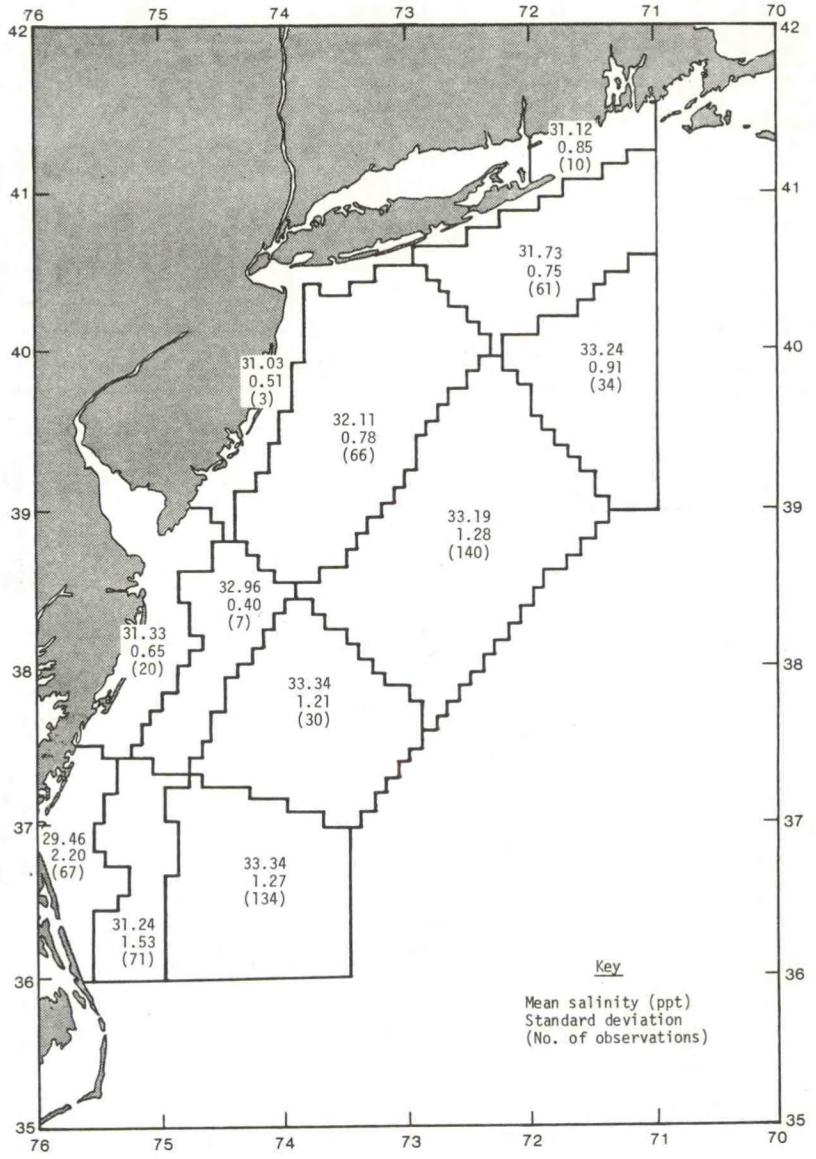


Figure 4.69.--Spring mean sea-surface salinities.

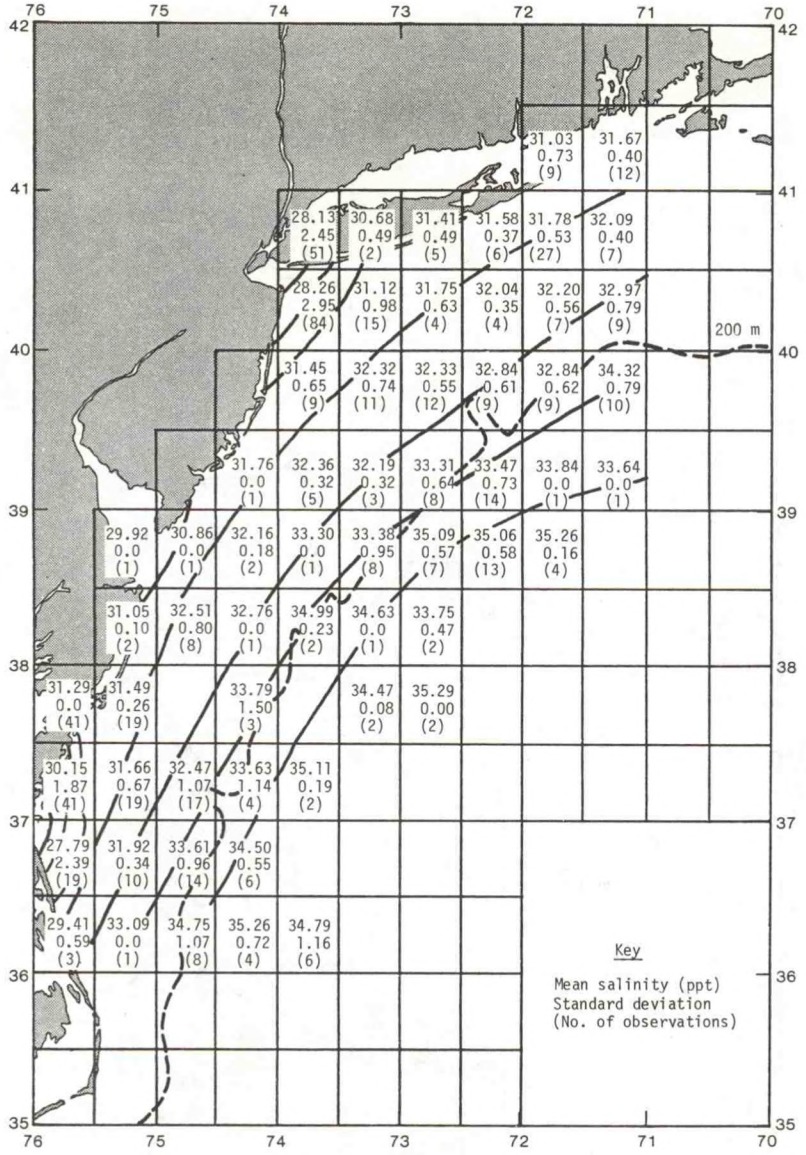


Figure 4.70.--Spring mean sea-surface salinity field.

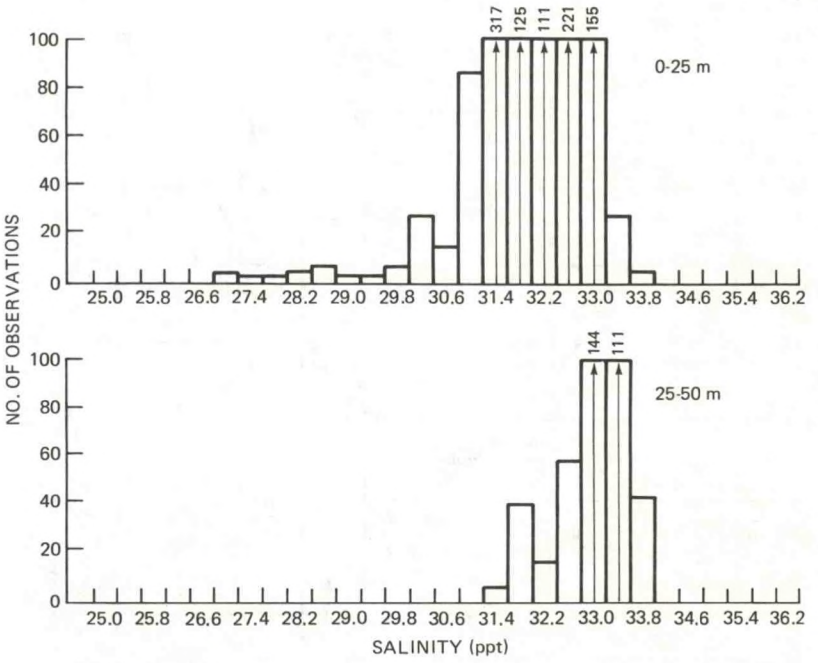


Figure 4.71.--Histograms of spring salinities, area 6.

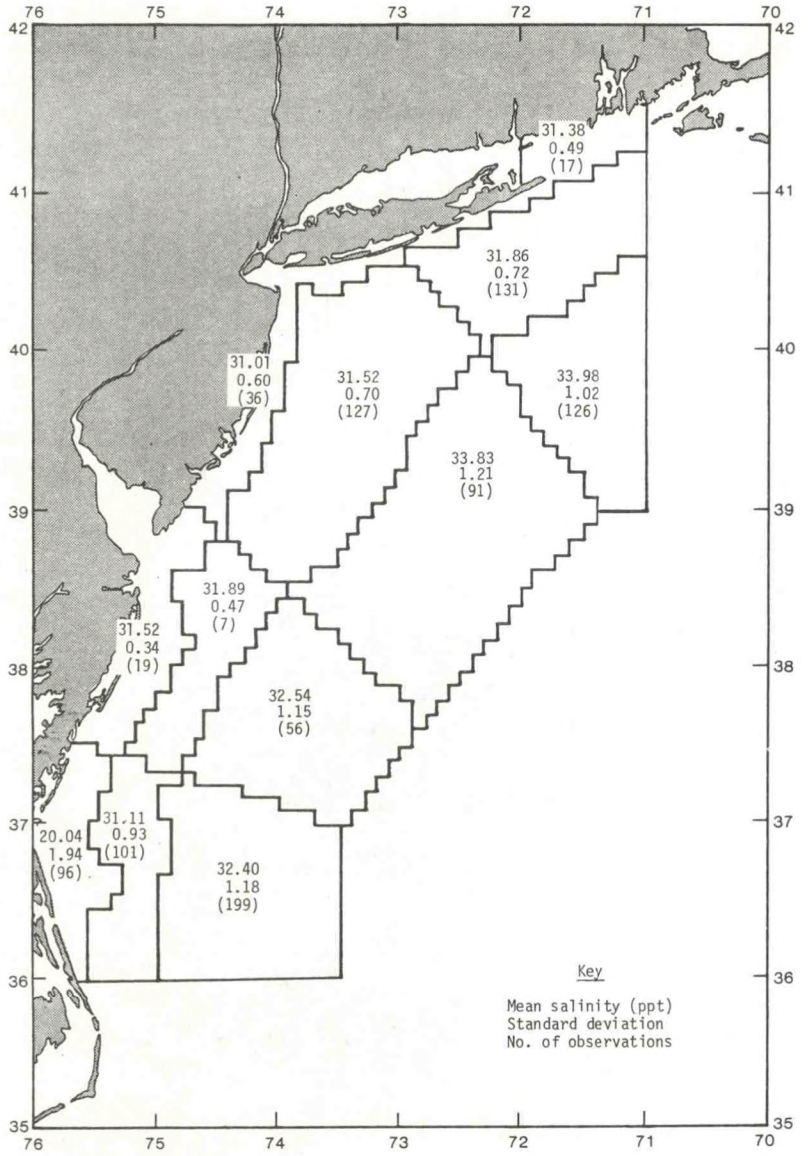


Figure 4.72.--Summer mean sea-surface salinities.

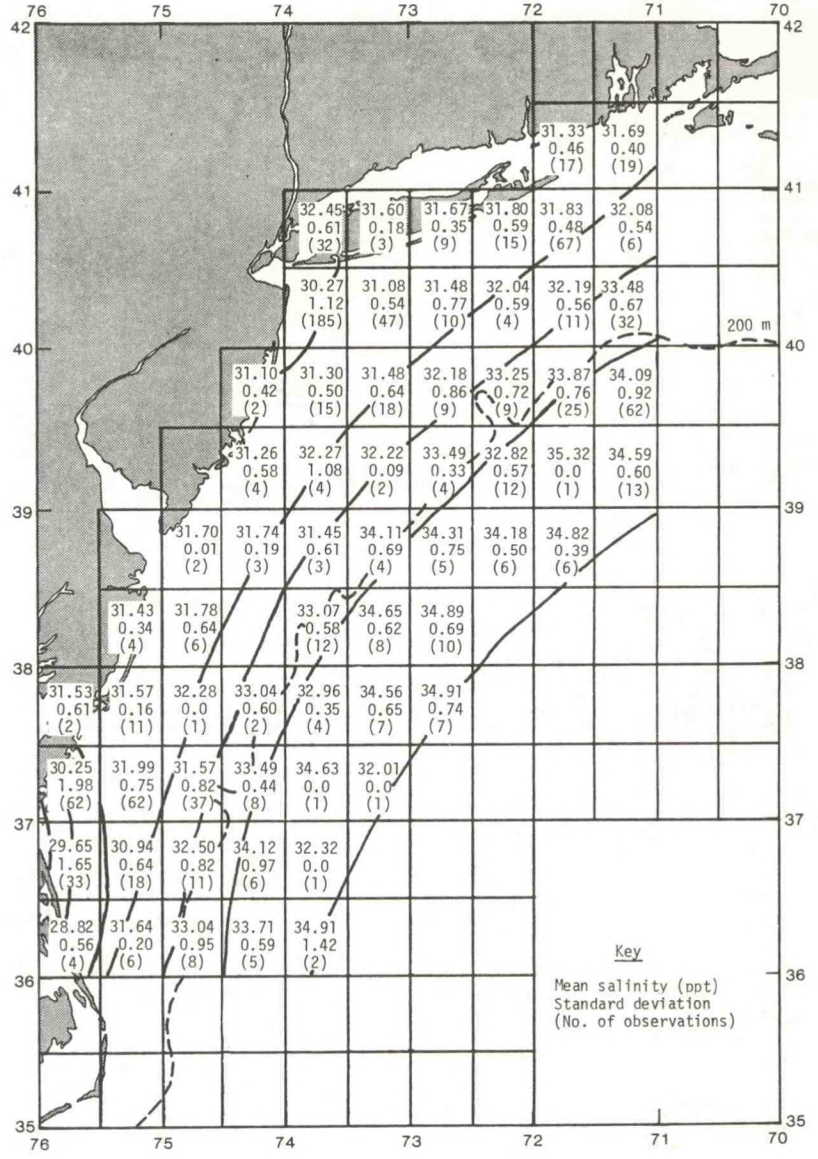


Figure 4.73.--Summer mean sea-surface salinity field.

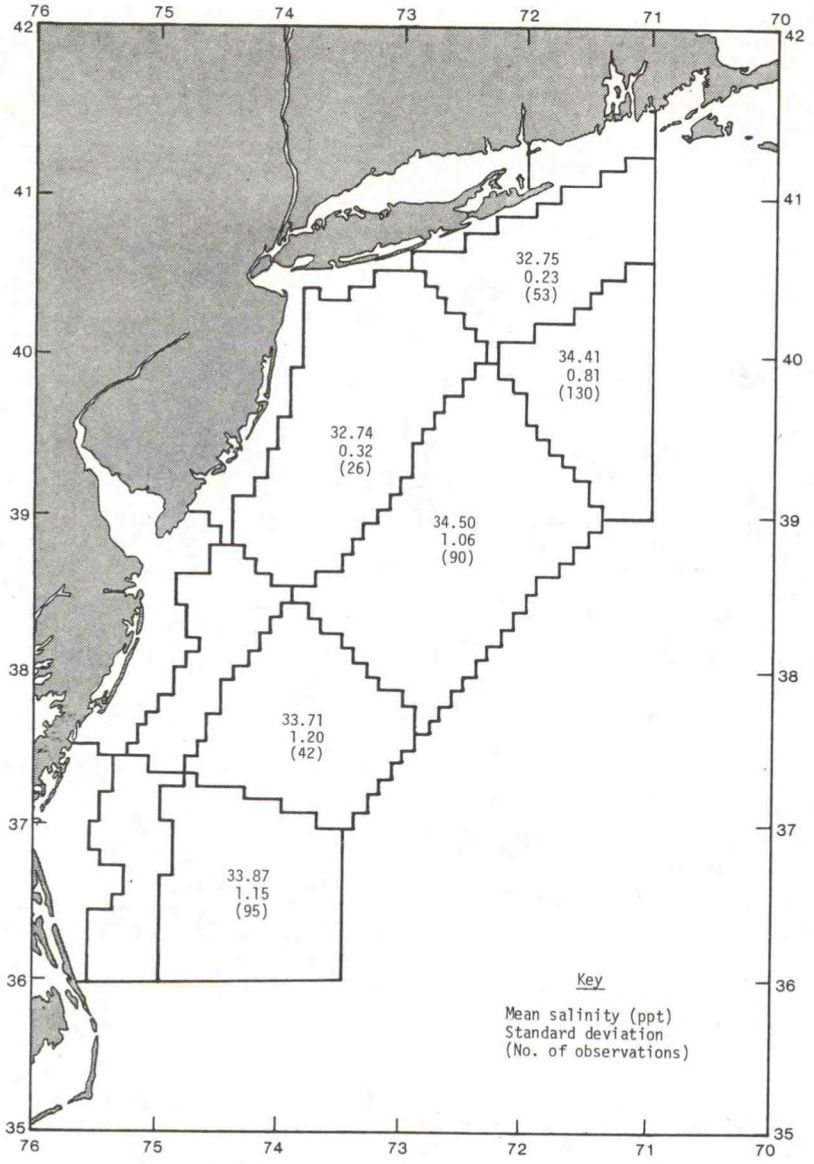


Figure 4.74.--Summer mean salinities at 50-m depth.

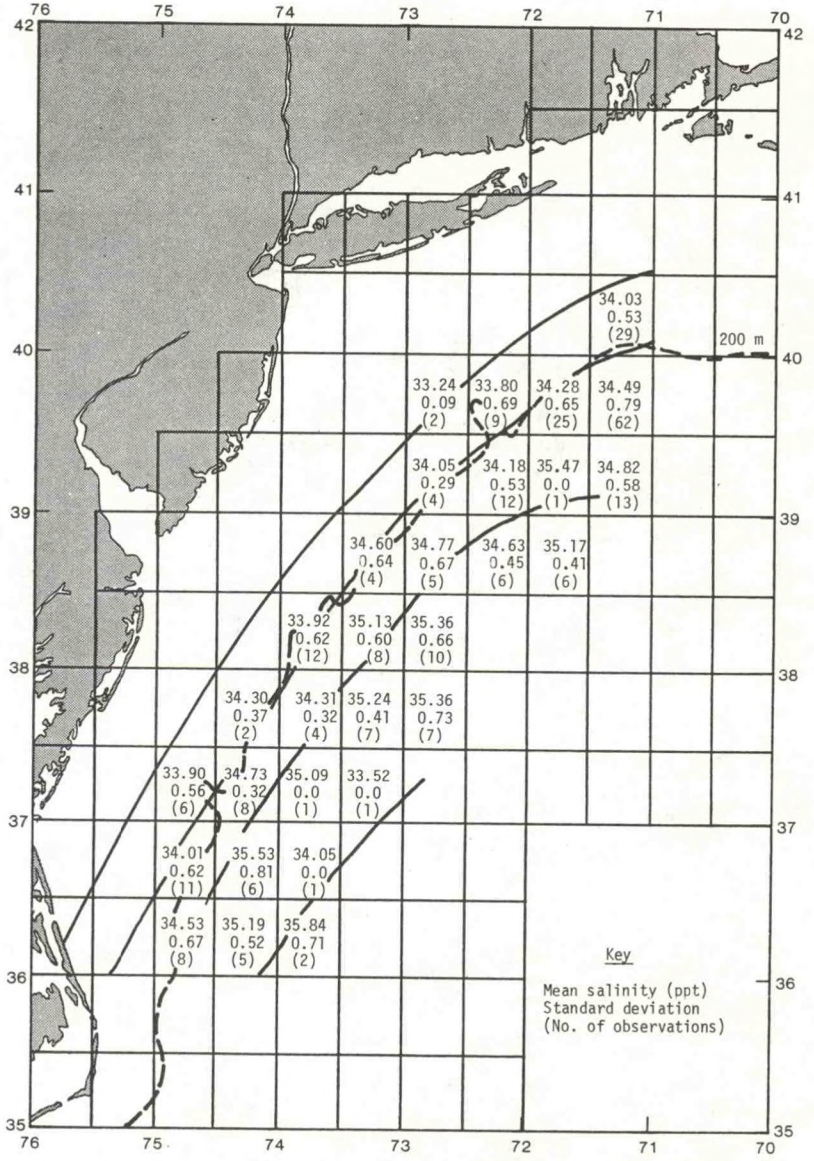


Figure 4.75.--Summer mean salinity field at 50-m depth.

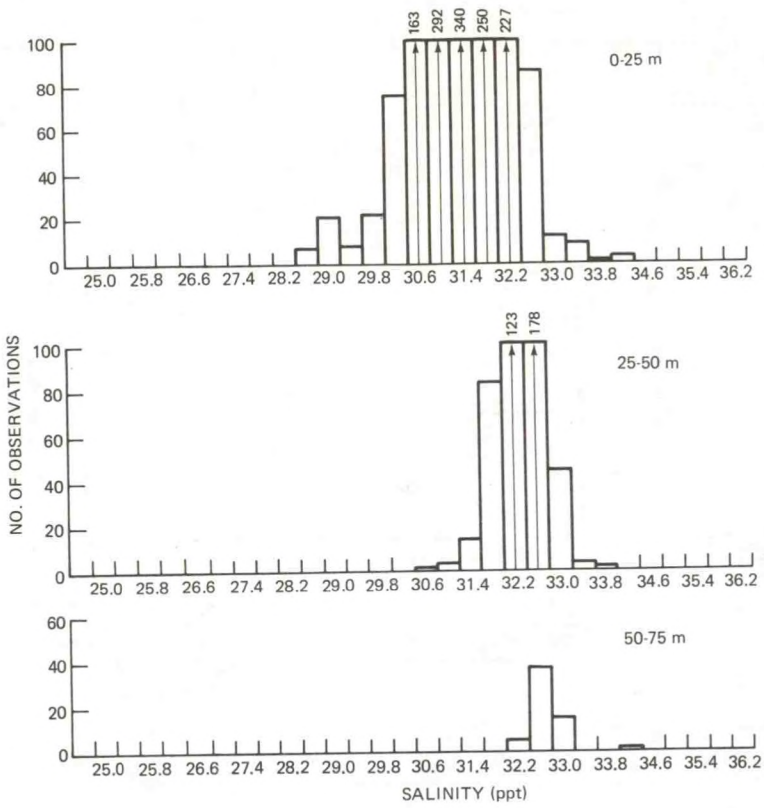


Figure 4.76.--Histograms of summer salinity, area 6.

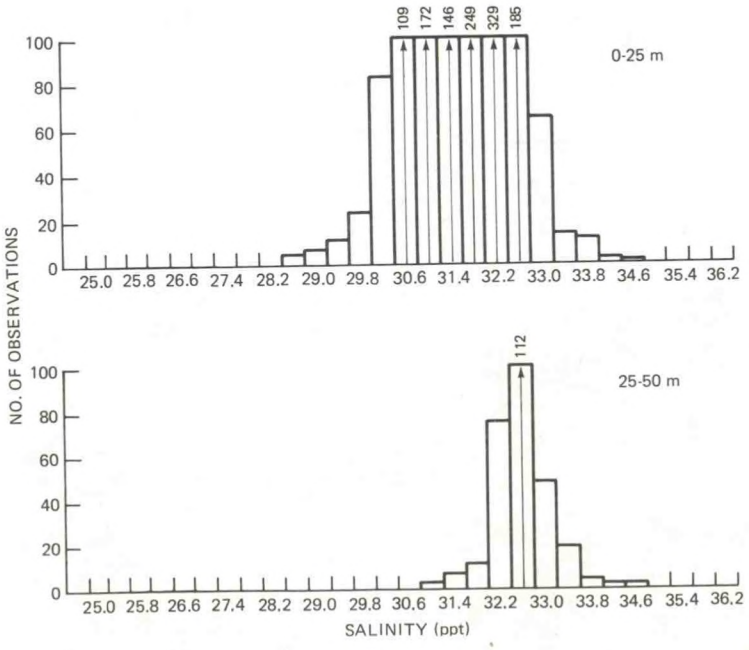


Figure 4.77.--Histograms of summer salinity, area 8.

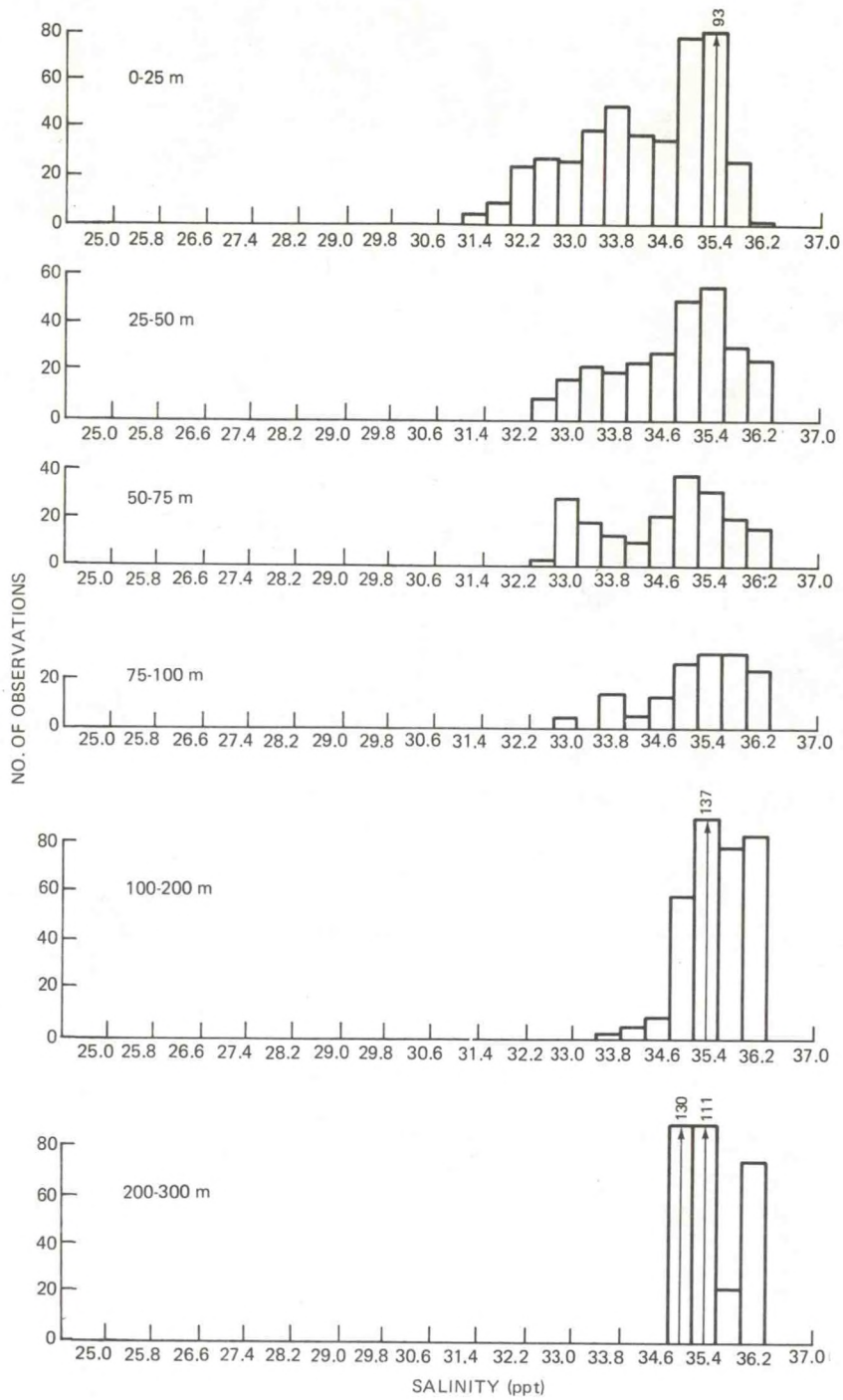


Figure 4.78.--Histograms of summer salinity, area 10.

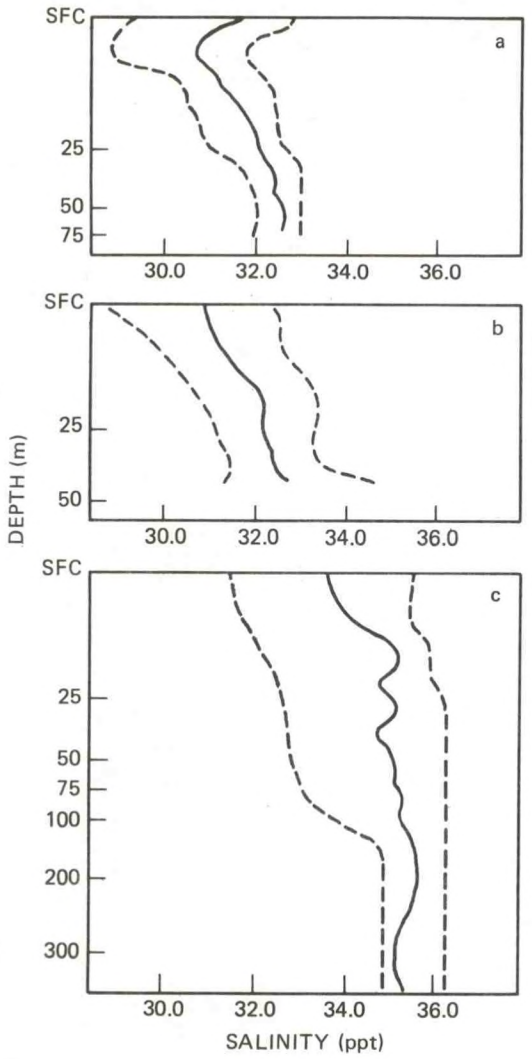


Figure 4.79.--Midlines (medians) and envelopes (2.5 and 97.5 percentiles) of summer salinities for (a) area 6, (b) area 8, and (c) area 10.

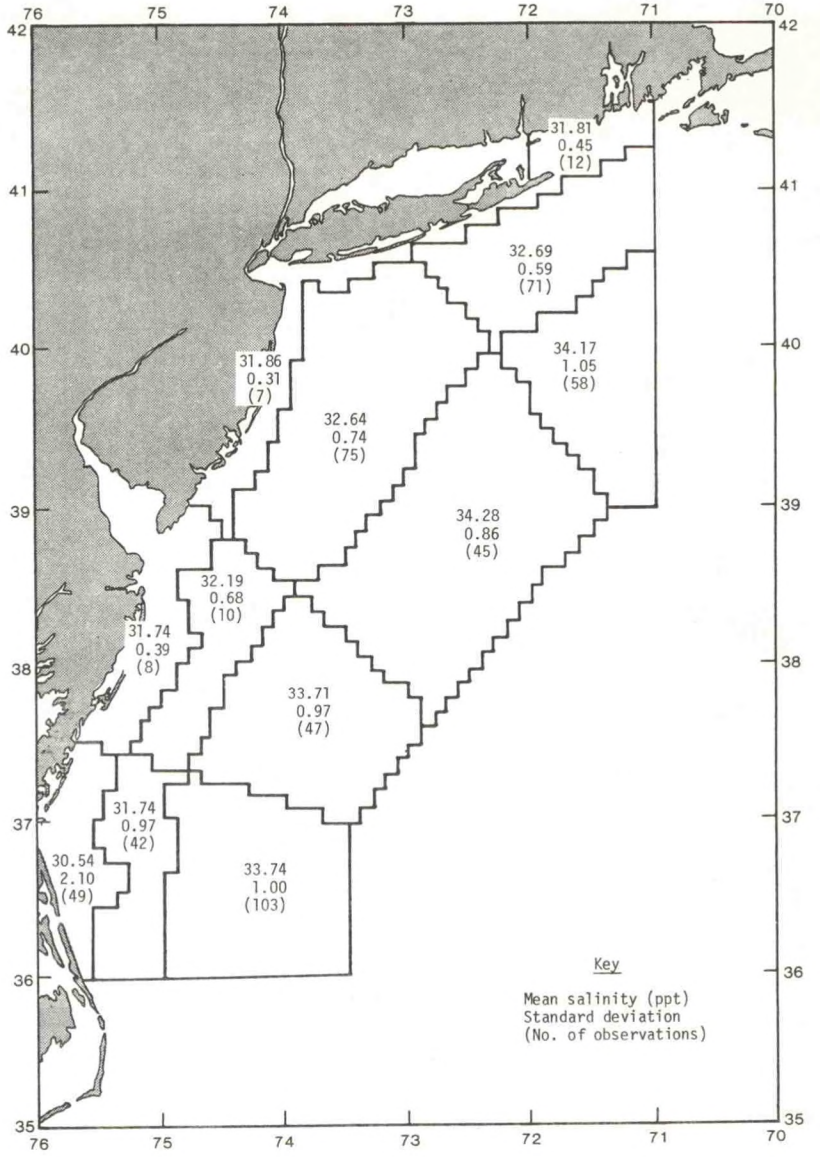


Figure 4.80.--Fall mean sea-surface salinities.

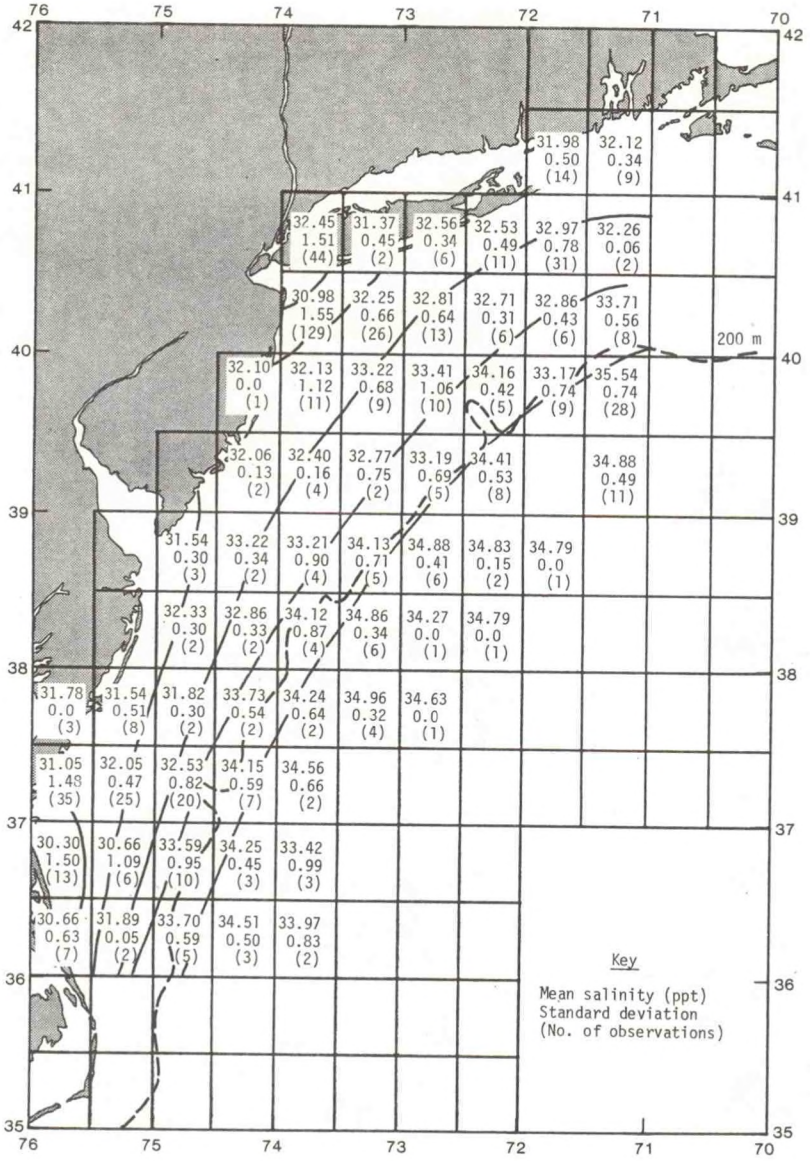


Figure 4.81.--Fall mean sea-surface salinity field.

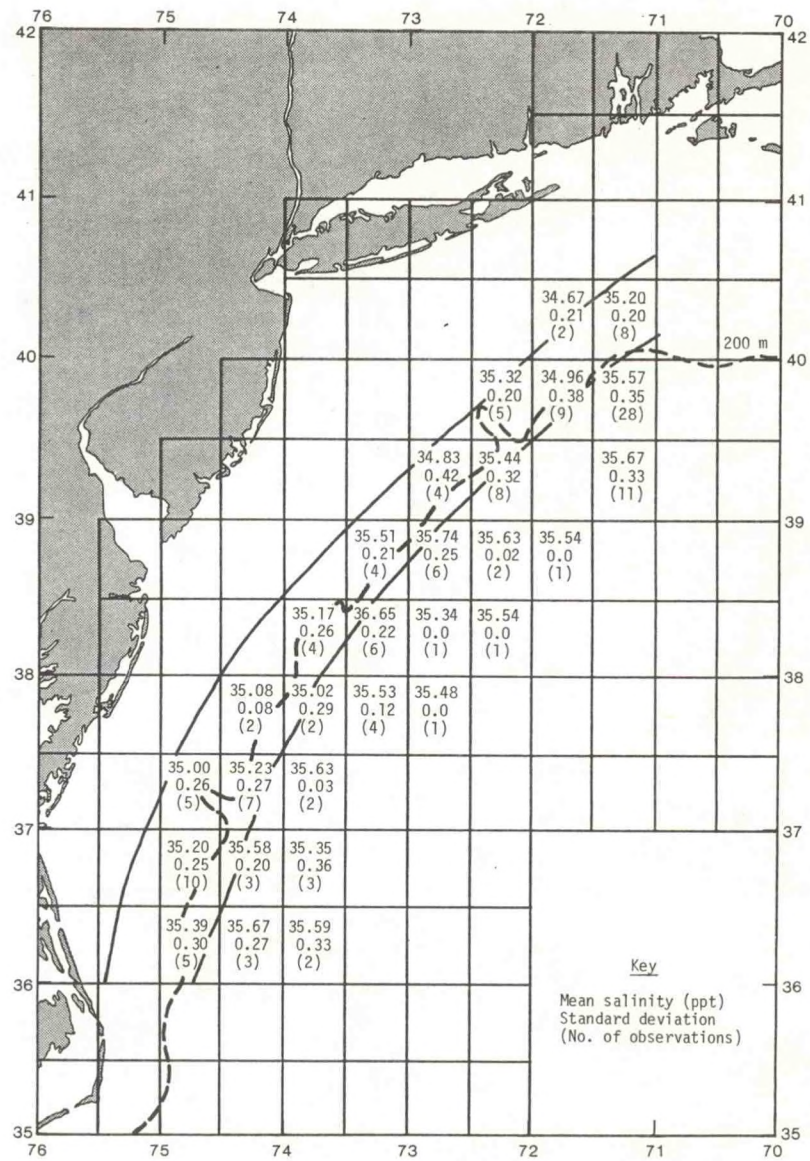


Figure 4.82.--Fall mean salinity field at 100-m depth.

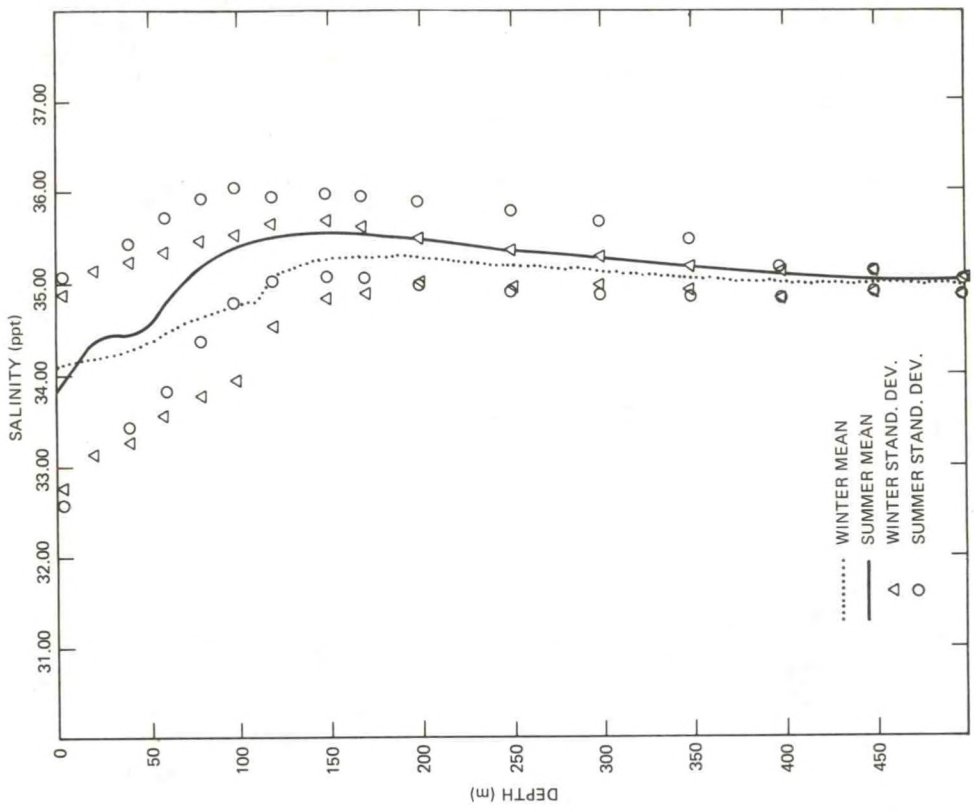


Figure 4.84.--Winter and summer mean vertical salinity profiles, area 10.

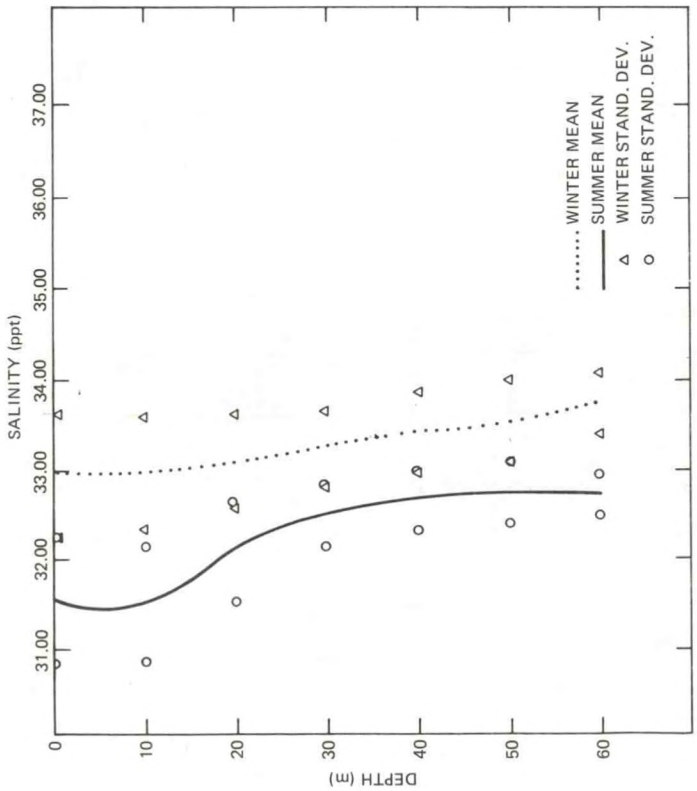


Figure 4.83.--Winter and summer mean vertical salinity profiles, area 6.

### 4.4.7 Temperature-Salinity Classification

The principal features discussed in the preceding two sections can be highlighted by temperature-salinity (T-S) classification according to T-S correlations. Although the T-S diagram has been applied primarily in studies of the deep ocean, it is a useful tool also for classifying water masses in the Mid-Atlantic Bight (Wright and Parker, 1976). However, the term "water mass" must be interpreted more liberally here, since, as has been shown, shallow coastal waters, being adjacent to atmospheric and terrestrial sources and sinks of water types, undergo very large fluctuations.

Presented below are the results of the classification of Mid-Atlantic water masses by the asymptotic singular decomposition (ASD) method discussed in section 4.1.1 and appendix B. The classification is limited to the outer continental shelf area, to depths of 900 m or more, because rapidly decreasing depth shoreward in the midshelf and inner-shelf regions made application of the ASD method difficult. However, since the main body of shelf water extends seaward well beyond the 200-m isobath (Wright and Parker, 1976), it is highly probable that the most important water masses of the area are covered by the classification work done for this study.

The geographical distribution of the number of STD casts used for the T-S classification is shown in figure 4.85. Six characteristic water groups were delineated by the analysis. Each group appears to be made up of at least three water masses, since a T-S curve with one approximating linear segment connotes two water masses; with two linear segments, three water masses; and so on (Neumann and Pierson, 1966). The results are summarized in figure 4.86, which shows the six T-S groups, their vertical profiles, and the regions in which they are found. Most of the literature on the Mid-Atlantic Bight (e.g., Norcross and Stanley, 1967) describes the water in terms of three primary groups, based on salinity:

Gulf Stream water - salinity > 36.0 ppt.

Slope water - salinity > 35.00 ppt and < 36.0 ppt.

Shelf water - salinity < 34 ppt.

As seen in figure 4.86, groups 2 and 6 are predominantly Gulf Stream water, with type 2 being the warmer and more saline at depths between 100 and 1,000 m. This water group is unlikely to be encountered often on the shelf. Group 6 is found in the shelf break region; note the characteristic subsurface salinity maximum at a depth of about 150 to 200 m, which occurs at the slope-shelf water front. Group 1 is quite similar to 6, but more southern and inshore in character, being warmer and less saline. Water group 3 shows the effect of low-salinity shelf water moving offshore from the midshelf region and overlying the heavier slope water, which agrees with the findings by Wright and Parker (1976).

Shelf water is also evident in group 5, which is found in winter and seems to be characteristic of the coastal waters south of New England (Voorhis et al., 1976; Wright and Parker, 1976). Beardsley and Flagg (1975)

found this T-S correlation pattern on several cruises southeast of Nantucket in late winter and early spring of 1974. However, the low-salinity portion of their curve was lower in salinity, as well as temperature, than was found in this study, because their cruise path was farther north and closer to the coast. They note that the upper branch of the T-S curve, toward T = 13.5°C and S = 35.5 ppt, consists of water that makes up the midshelf and inner-shelf regions out to the shelf-slope water front. The near-linearity of this part of the curve indicates a uniformity in the mixing processes of coastal and oceanic waters, and a lack of major intrusions of waters of either type. The "knee" of the curve, the very high temperature and salinity portion, is indicative of the warmer and more saline upper slope water, which has variable T-S characteristics as a result of the complicated mixing processes that occur in the zone of the shelf break. The lower branch of the curve moves close to T = 4.5°C and just under S = 35.00 ppt, in agreement with Beardsley's and Flagg's findings, and represents slope water lying seaward of the front and deeper than 250 m.

Water group 4 shows the effects of spring-warmed slope water mixing with colder deep water, probably the residual "winter" bottom water (Ketchum and Corwin, 1964). Both this group and group 5 exhibit subsurface temperature inversions and salinity maxima.

In summary, the water classification has shown that characteristic features indicative of major physical processes in the Mid-Atlantic region can be inferred from water mass analysis of historical STD data. The primary factor determining gross distribution is the shoreward movement of oceanic water of higher density wedging itself beneath the near-surface seaward flux of fresher, lighter shelf water by advection and mixing. The magnitude of volume transports of these residual flows cannot be estimated, however, without additional assumptions. Ketchum and Keen (1955) have estimated the renewal time of water on the Mid-Atlantic continental shelf to be 16 months, using T-S and land runoff data.

The seasonal march of temperature and salinity can be deduced from the analysis presented here, showing vernal warming and autumnal cooling effects to a depth of about 150 to 200 m, and salinity fluctuations due to spring runoff to about the same depth. If sufficient salinity data were available, it would be possible to estimate parameters describing vertical mixing, such as eddy diffusion coefficients, based on the T-S correlations (e.g., Mamayev, 1975).

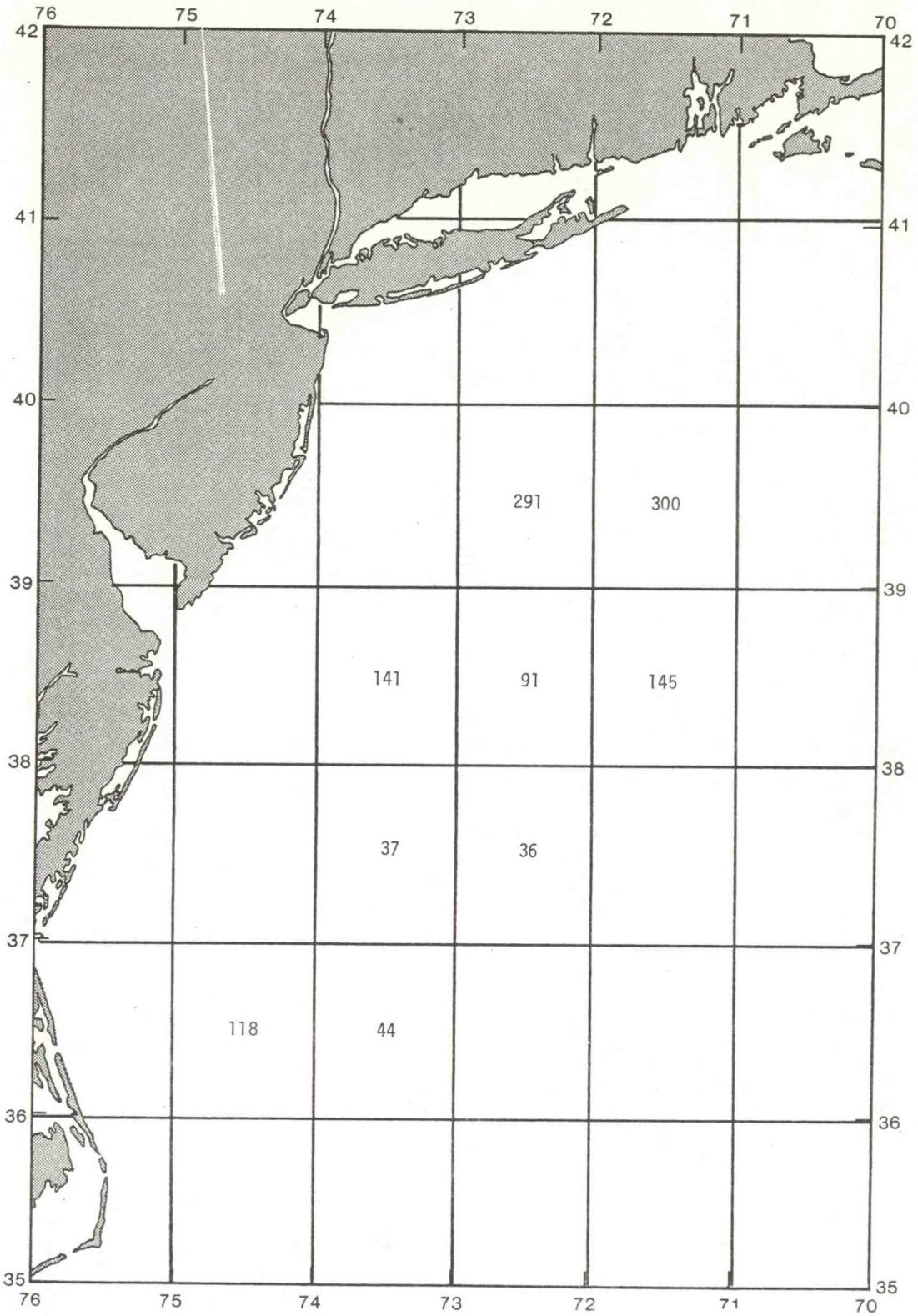


Figure 4.85.--Inventory, by $1^{o}$ squares, of STD casts used in the ASD water mass classification.

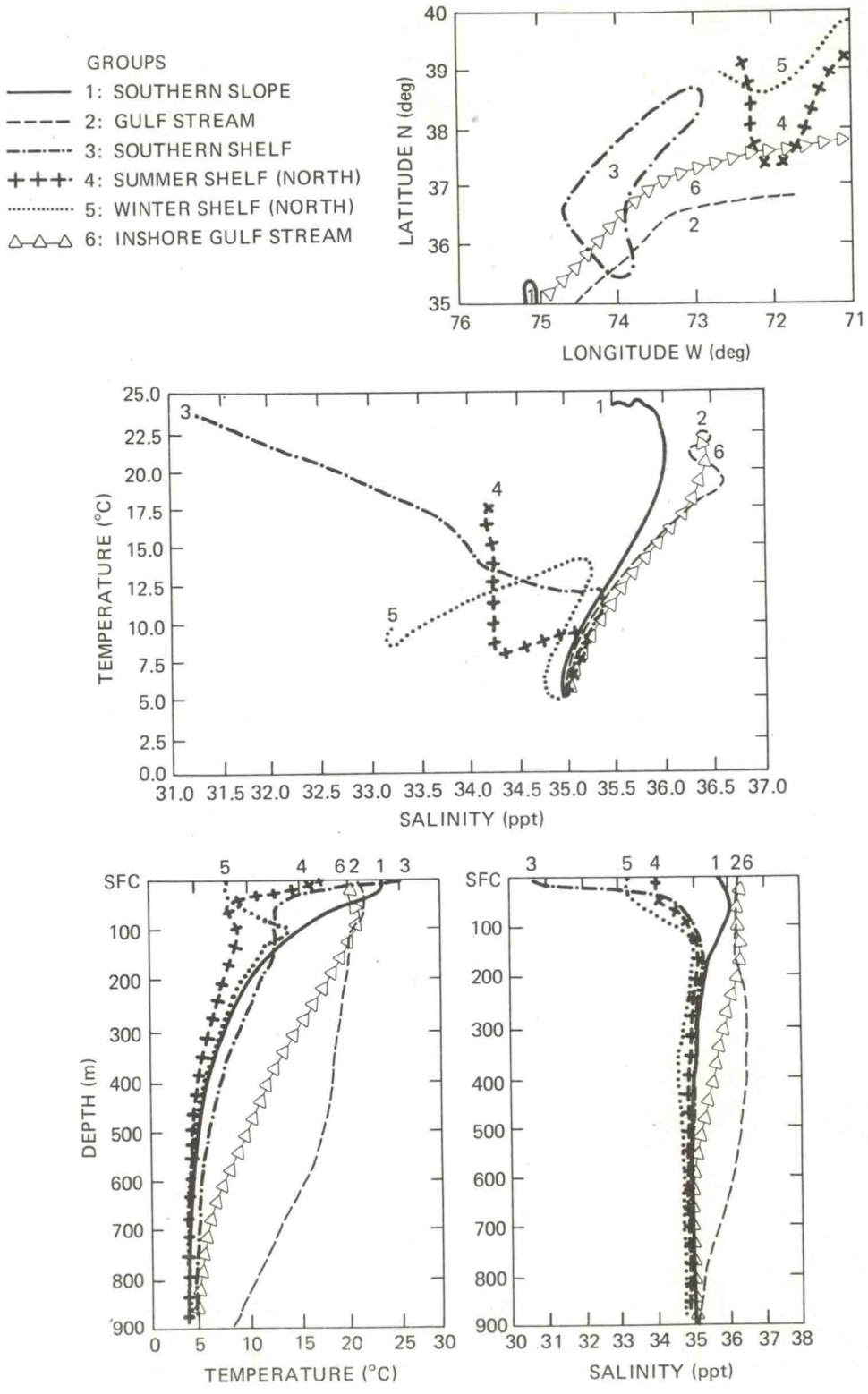


Figure 4.86.--Water mass classification by the ASD method based on STD data.

### 4.4.8 Density

The density structure on the continental shelf is similar to the salinity structure in that density ($\sigma_t$) increases downward and seaward throughout the year ($\sigma_t$ = water density at sea-level pressure minus 1 multiplied by 1,000). Density is low near the coast, where low salinity estuarine water is discharged, and high near the eastern boundary of the region, where high-density oceanic water interacts with shelf water. Maximum density is observed in late winter, resulting from low temperature and high salinity, and minimum density is observed in summer, resulting from high temperature and low salinity. During the winter, the density front at the shelf-slope water interface is maintained by the salinity, against the temperature gradient, since both temperature and salinity increase seaward, but the effect of increasing salinity overrides the effect of increasing temperature. In summer, the density gradient is also maintained by the salinity gradient, since horizontal temperature changes across the front are small.

Winter. The historical data used in this study indicate winter surface densitites of about $\sigma_t$ = 25.0 in the inshore waters, increasing to about $\sigma_t$ = 25.6 at the 200-m isobath, as shown in figures 4.87 and 4.88. A major density front between shelf water and slope water is not evident from these data, but rather a more gradual transition. Plumes of low-density water (as low as $\sigma_t$ = 22.0) are seen to emanate from the river mouths. Variability in density is seen on the order of half a $\sigma_t$ unit, increasing from north to south close to the coast, an effect of low-salinity river water from the Hudson and Delaware Rivers and Chesapeake Bay. Densities are higher and variability is smaller at 50-m depth (figs. 4.89 and 4.90). The horizontal density gradients are perpendicular to the coast. At the bottom, densities increase from about $\sigma_t$ = 26.0 on the inner shelf to $\sigma_t$ = 26.6 on the outer shelf. The vertical distributions in winter (figs. 4.91 to 4.93) show relatively homogeneous conditions over the northern part of the area, with a slight increase in mean density with depth. Area 8 (fig. 4.92) shows a skewness toward low density values near the surface, following the salinity distribution. In the shelf-slope water frontal zone (fig. 4.93, area 10) mean density is seen to increase steadily with depth, despite the inversions on both the temperature and salinity profiles discussed earlier. The midlines and envelopes in figure 4.94 show inversions over the water column in the shelf areas 6 and 8, followed by a smooth increase with depth below 25 m. These inversions cannot be termed significant, in view of the large envelope. In area 10, the density increases steadily with depth.

Spring. Surface densities in all areas are lower in spring than in winter (figs. 4.95 and 4.96), with evidence of plumes of low-density water coming from the major rivers. Variability in density is much larger than during the winter, as are the cross-shelf density gradients. As seen in figure 4.97, variability at 50-m depth is also higher than in winter in offshore areas 11 and 12, but not in areas 5, 6, 9, and 10.

Summer. Surface density is at a minimum on the shelf in summer, with typical values of $\sigma_t$ = 23.0 near the 200-m isobath (figs. 4.98 and 4.99). Variability is high, but the cross-shelf density gradient is less than in

spring. The isopycnals are generally parallel to the coast, but tend to follow fluctuations in the complex summer temperature field. Densities near the base of the mixed layer are seen to be more nearly uniform across the shelf than are surface densities (fig. 4.100). Estuarine outflow effects are reflected in the low densities near the coast and in the vertical density distributions for areas 6 and 8 (figs. 4.101 and 4.102). Figure 4.101 shows a change in area 6 to lower values from the winter distribution (cf. fig. 4.91), which is also true for temperature. The 50- to 75-m layer is high in density due to the cold bottom water. Figure 4.102 shows an even broader distribution of density in area 8, resulting from outflow of low-salinity water in Chesapeake Bay. The slope water distributions for area 10 (fig. 4.103) are more nearly symmetrical, with a shift of the density mean toward higher values with depth, and surface variability is seen to be much larger than variability below the pycnocline. The vertical structure in figure 4.104 for areas 6, 8, and 10 shows density increasing rapidly with depth in all cases, with the highest variability near the surface.

Fall. In the fall, density increases from the summer values in response to cooling of the surface waters and increasing salinities (figs. 4.105 and 4.106). A bimodal vertical distribution of density is found in area 6 in the 0- to 25-m layer, as shown in figure 4.107. This is a transition period during which conditions move from the strong summer stratification to mean homogenity on the shelf.

Summary. In winter, surface water density increases from about $\sigma_t$ = 25.0 in inshore waters to $\sigma_t$ = 25.6 at the 200-m isobath. In summer, it increases from about $\sigma_t$ = 21.5 inshore to $\sigma_t$ = 23.0 at the 200-m isobath south of Block Island. In the vertical, variability is highest at the surface, and decreases toward the bottom during all seasons. On the shelf in winter, nearly homogeneous water prevails, with only a slight increase in $\sigma_t$ from the surface to the bottom. In summer, however, differences as large as four $\sigma_t$ units between the surface and the bottom are not unusual. Some areas show a small mean density inversion, especially near the surface. Variability is highest in spring and summer, and lowest in winter. Based on the data used in this study, the density discontinuity at the shelf-slope water front does not appear as strong as expected from analysis of individual cruise data reported in the literature (e.g., Beardsley and Flagg, 1976). The reason is that the data were averaged from both sides of the front, and, since the density front is not as pronounced as the salinity front, discontinuities tend to be lost in the averaging. Another contributing factor is that the salinity and temperature gradients are often opposed, thus reducing the density gradient.

The numbers of observations in two areas--area 7 in all seasons, and area 3 in the fall--are insufficient for deriving a reliable estimate of mean density and density variability. Examination of the smoothed field analyses for ½° squares has shown that the amount of data is also insufficient for reliably delineating the shelf-slope water front.

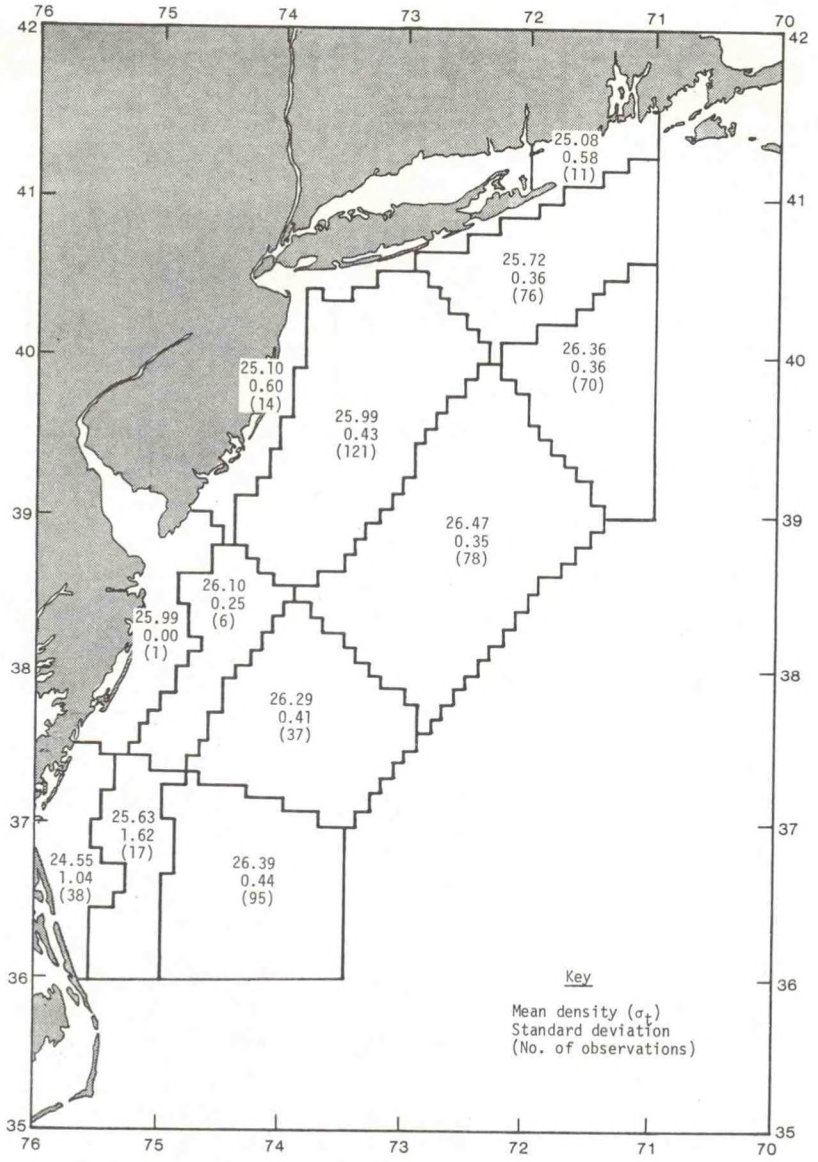


Figure 4.87.--Winter mean sea-surface densities.

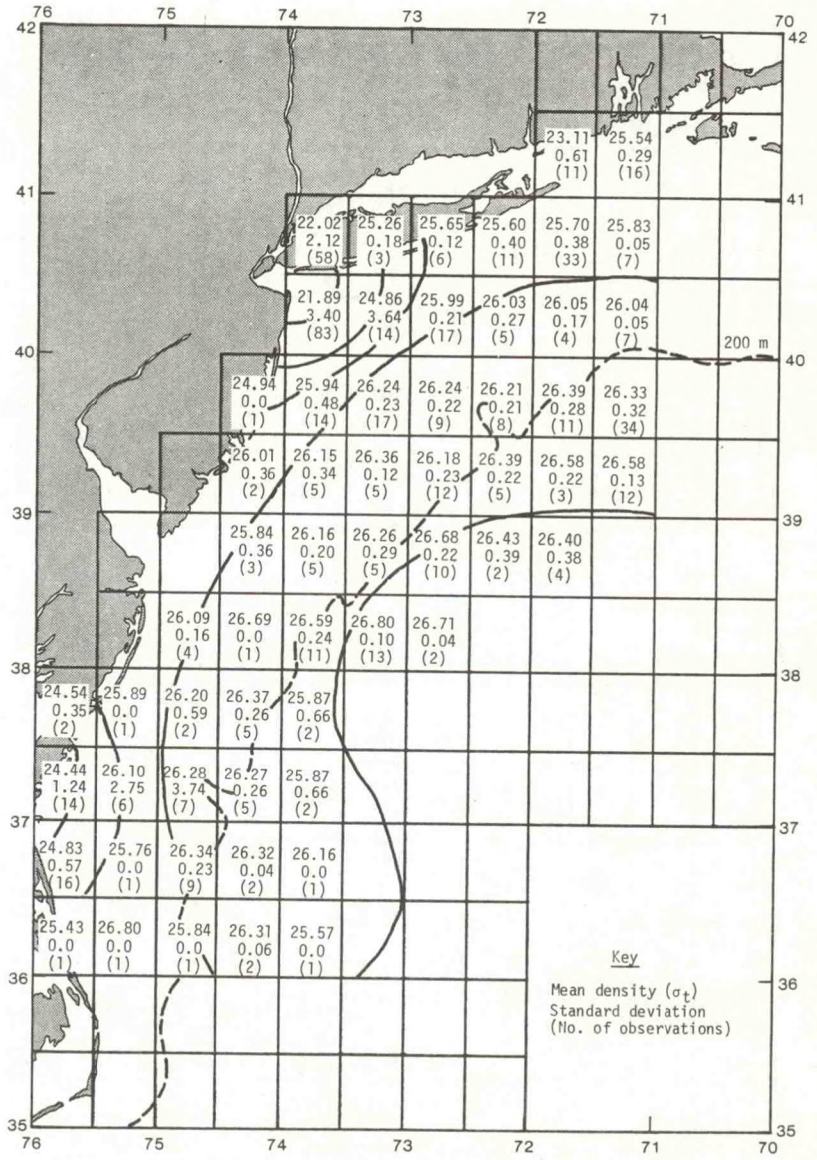


Figure 4.88.--Winter mean sea-surface density field.

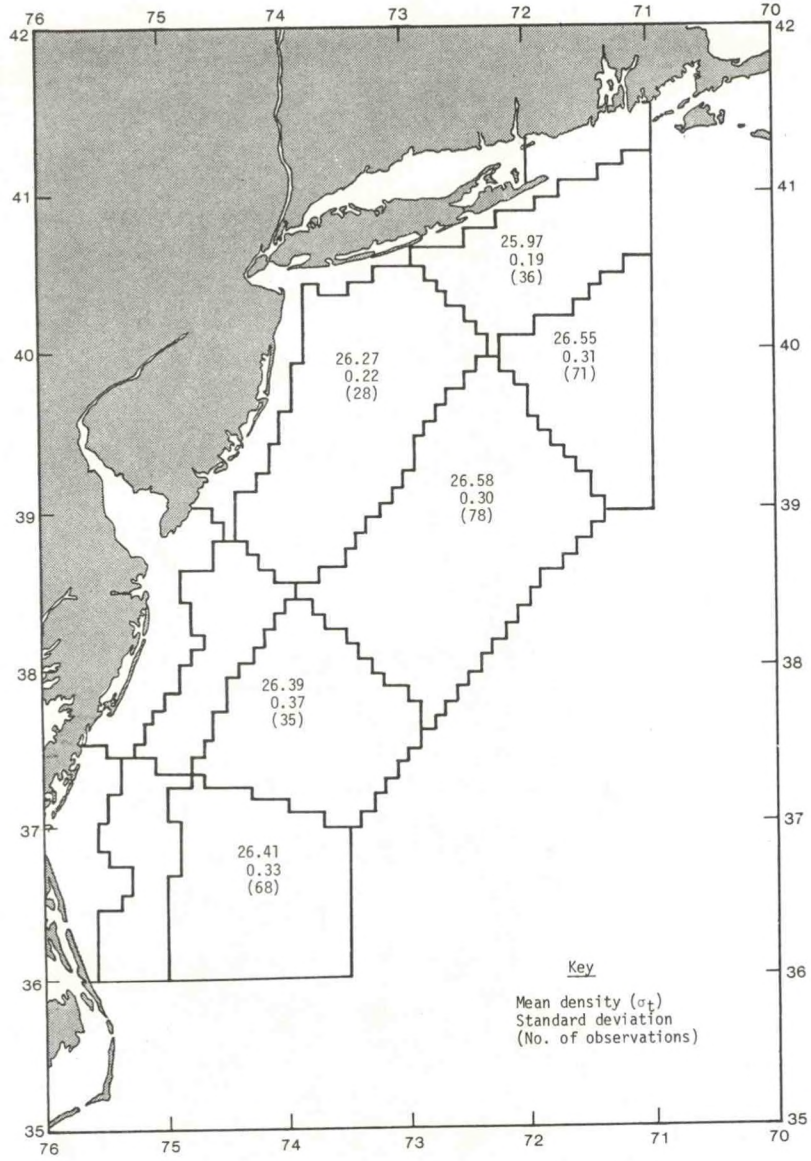


Figure 4.89.--Winter mean densities at 50-m depth.

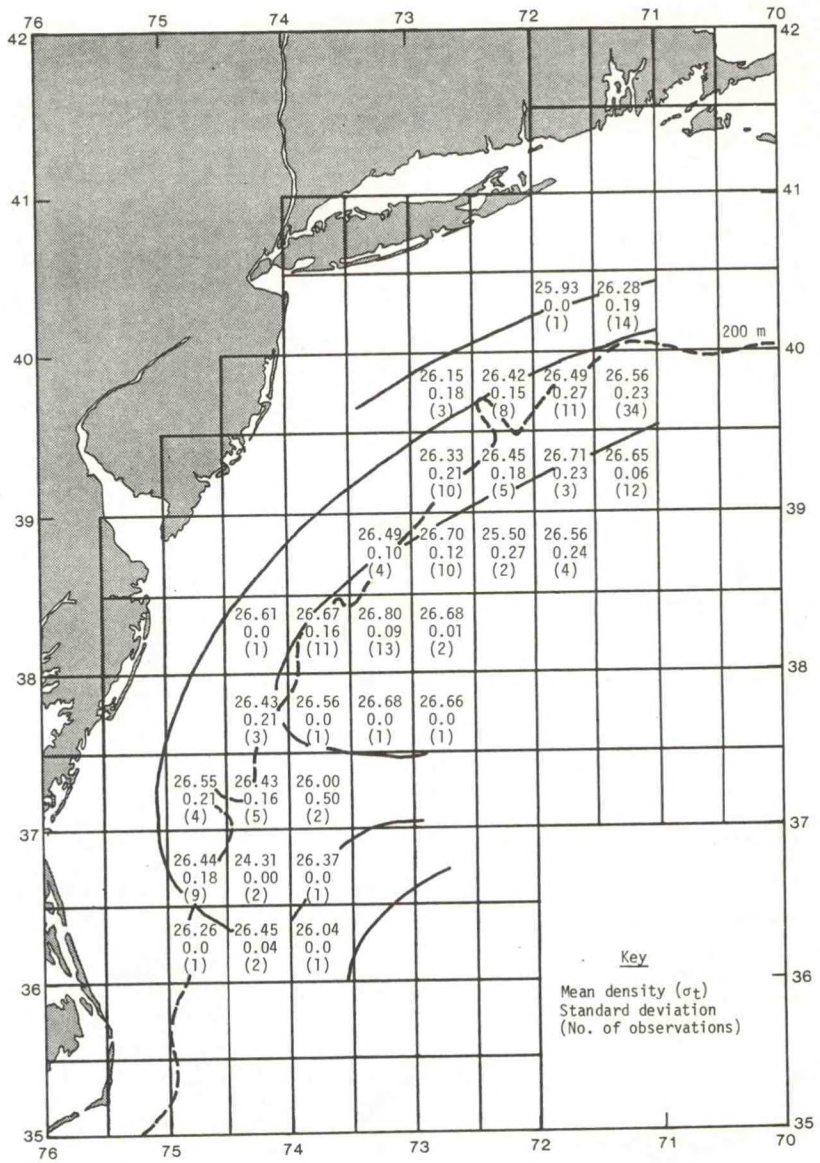


Figure 4.90.--Winter mean density field at 50-m depth.

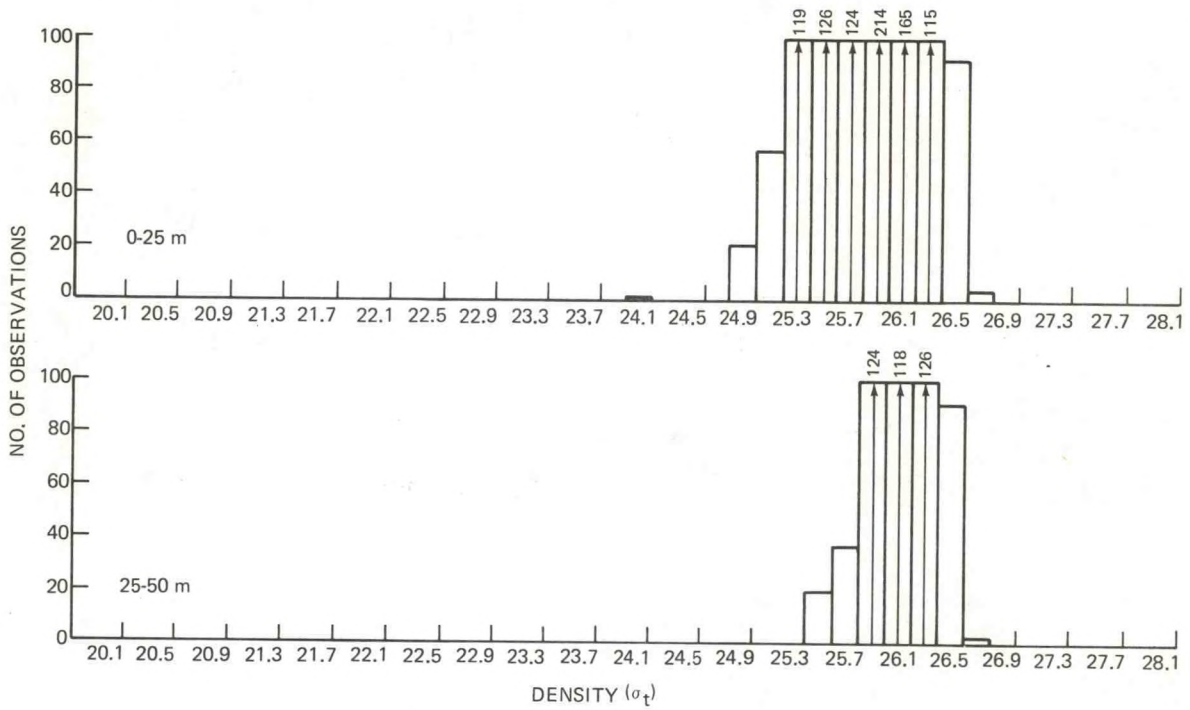


Figure 4.91.--Histograms of winter density, area 6.

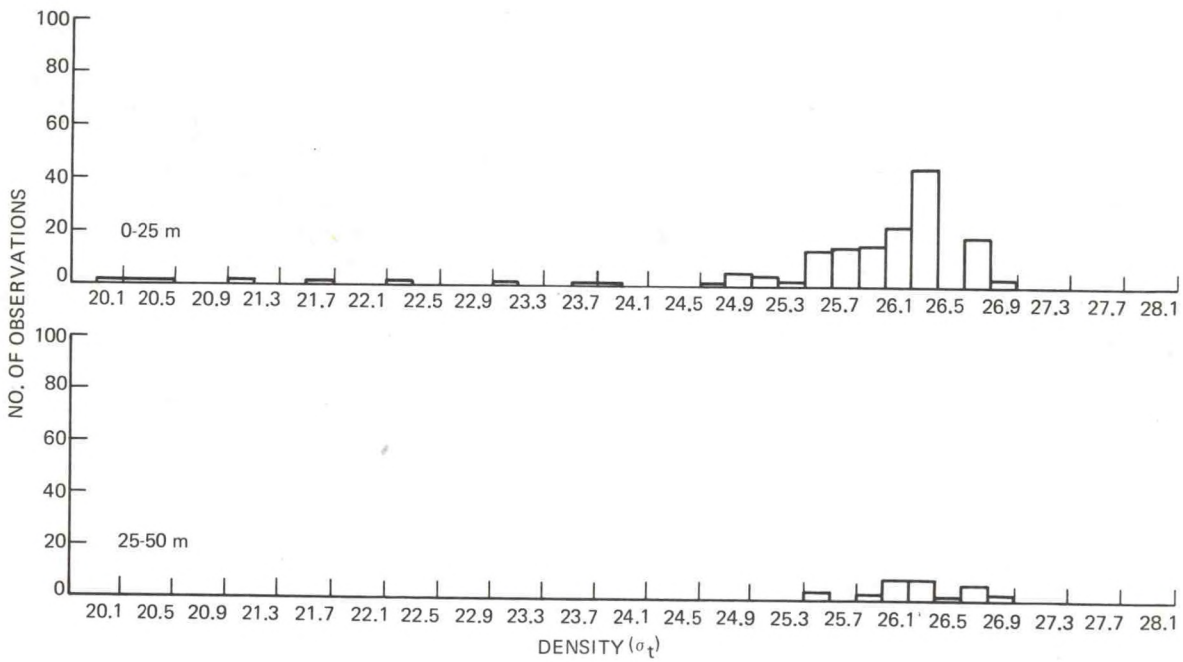


Figure 4.92.--Histograms of winter density, area 8.

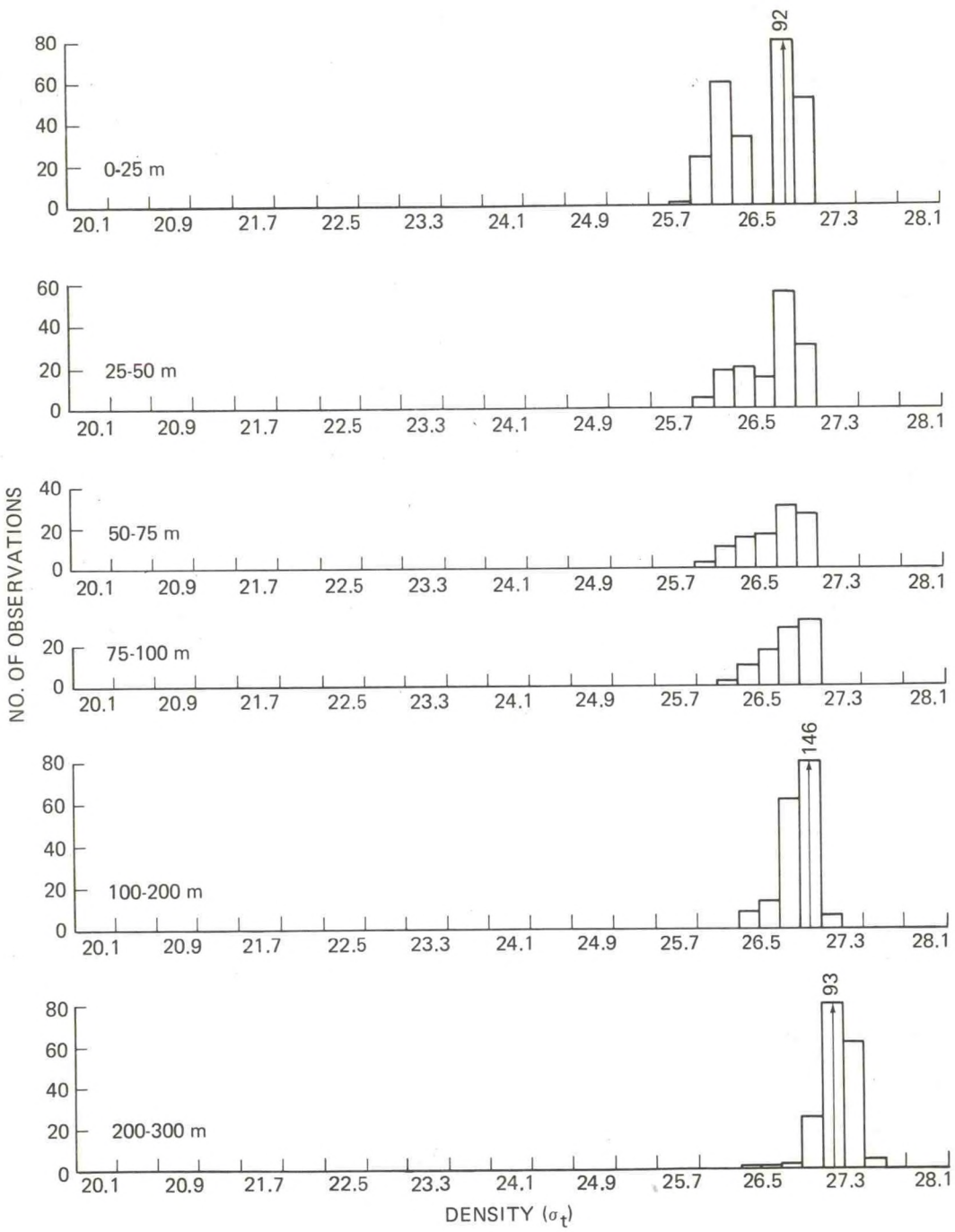


Figure 4.93.--Histograms of winter density, area 10.

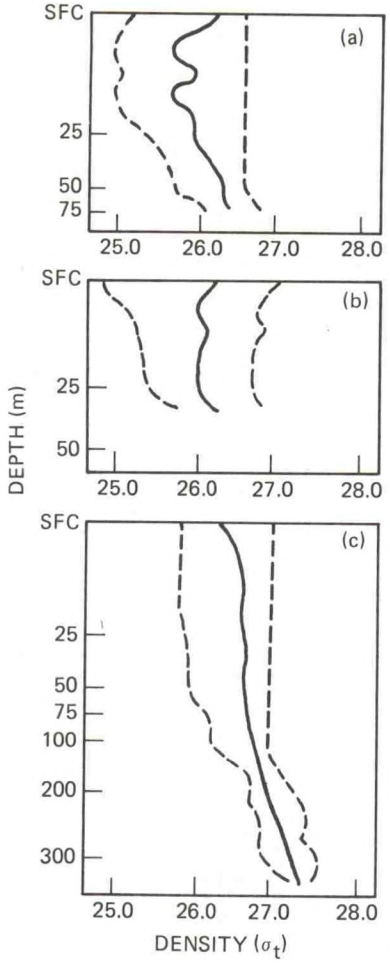


Figure 4.94.--Midlines (medians) and envelopes (2.5 and 97.5 percentiles) of winter densities for (a) area 6, (b) area 8, and (c) area 10.

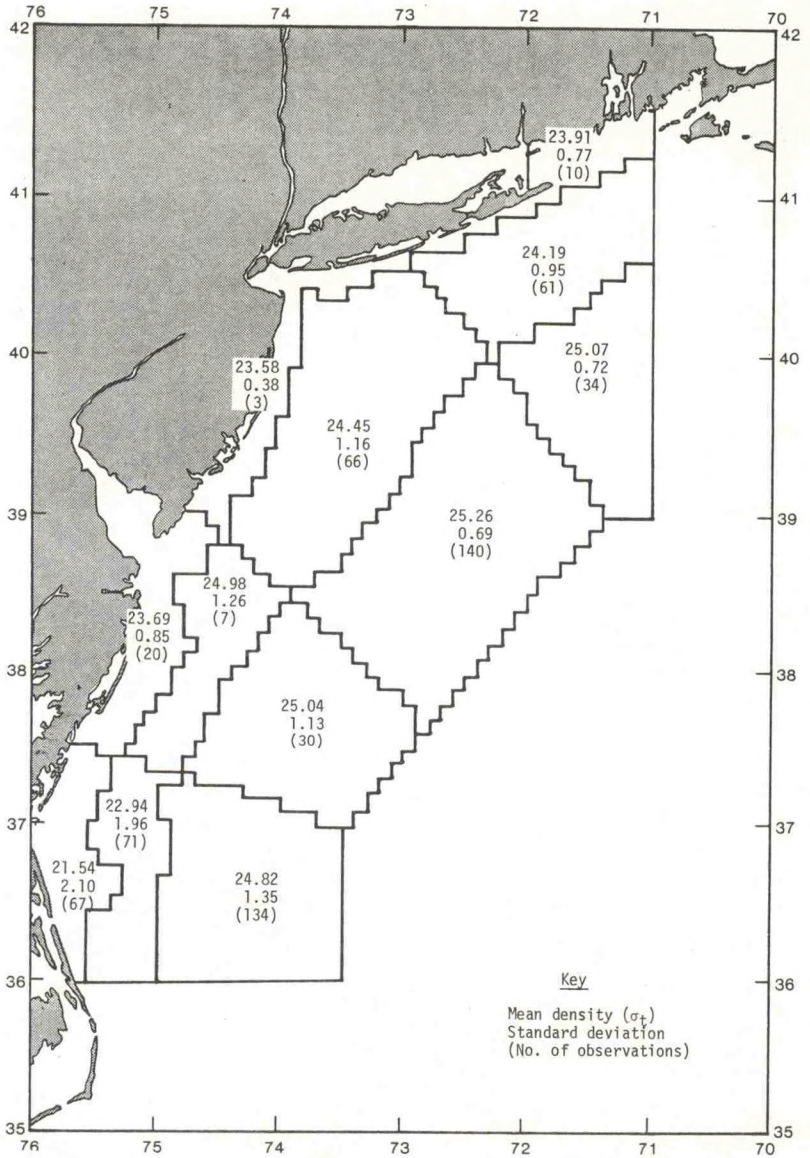


Figure 4.95.--Spring mean sea-surface densities.

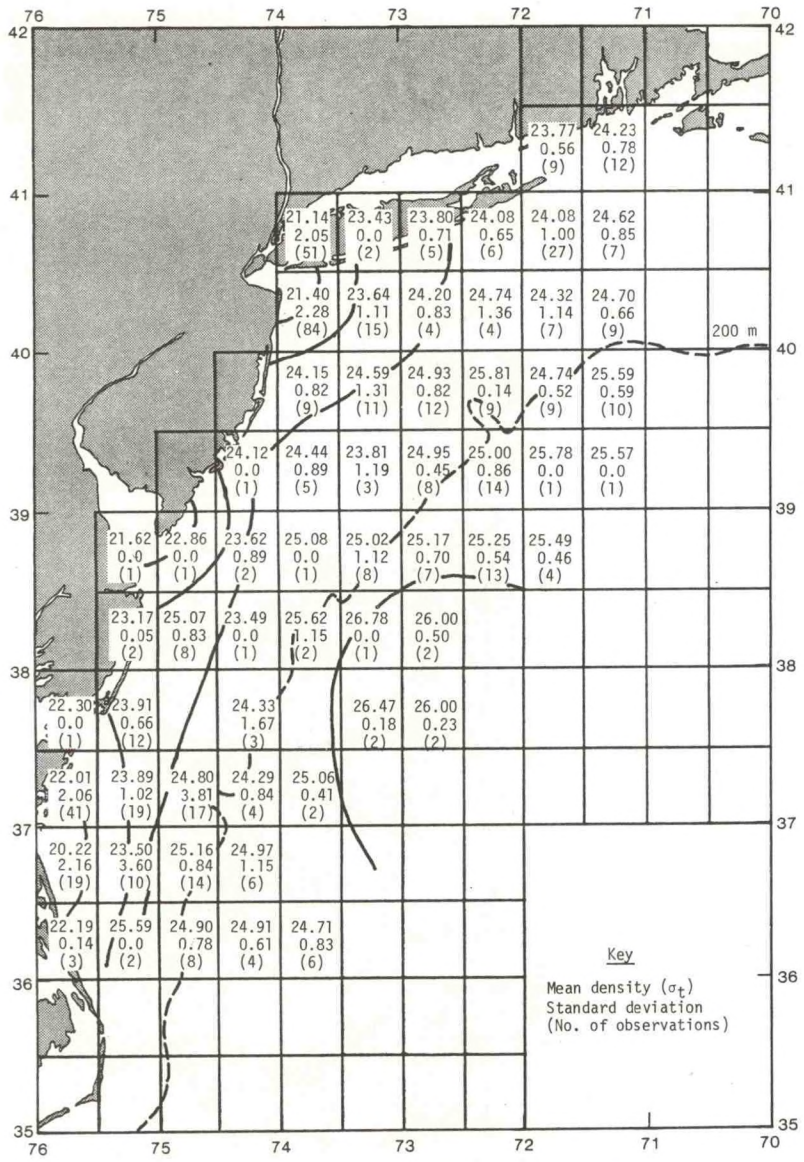


Figure 4.96.--Spring mean sea-surface density field.

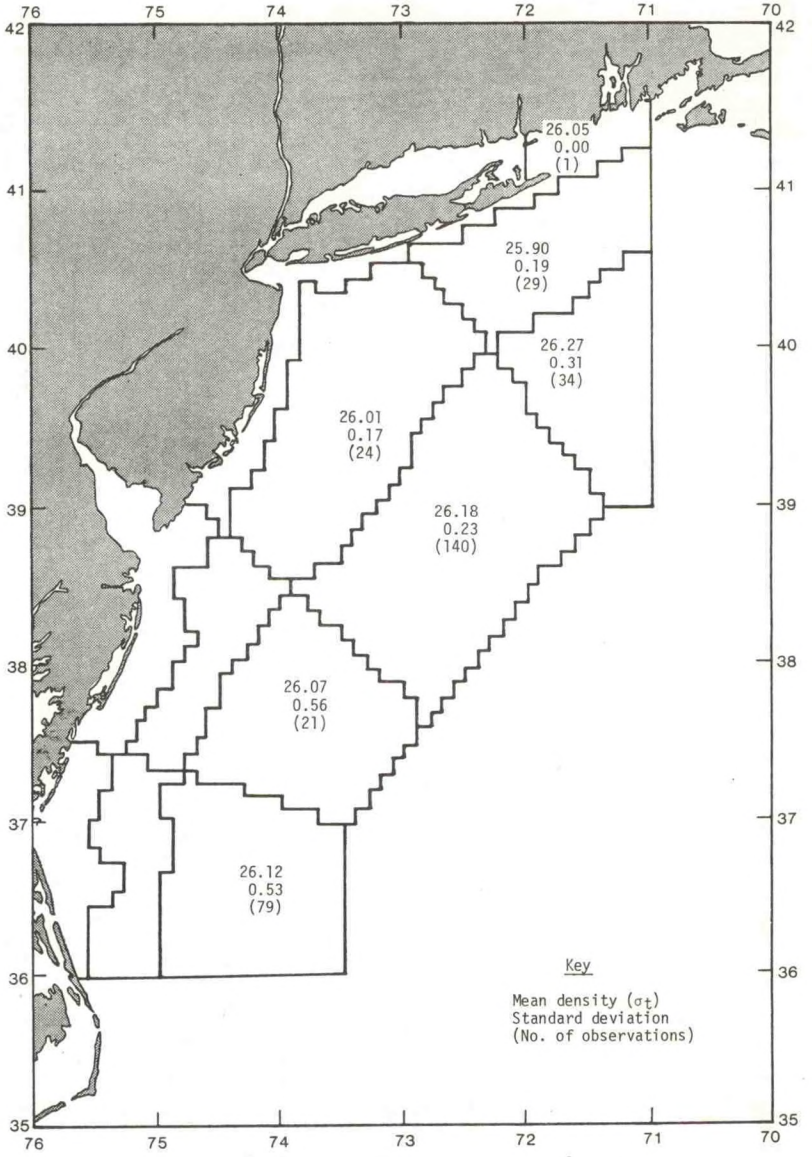


Figure 4.97.--Spring mean densities at 50-m depth.

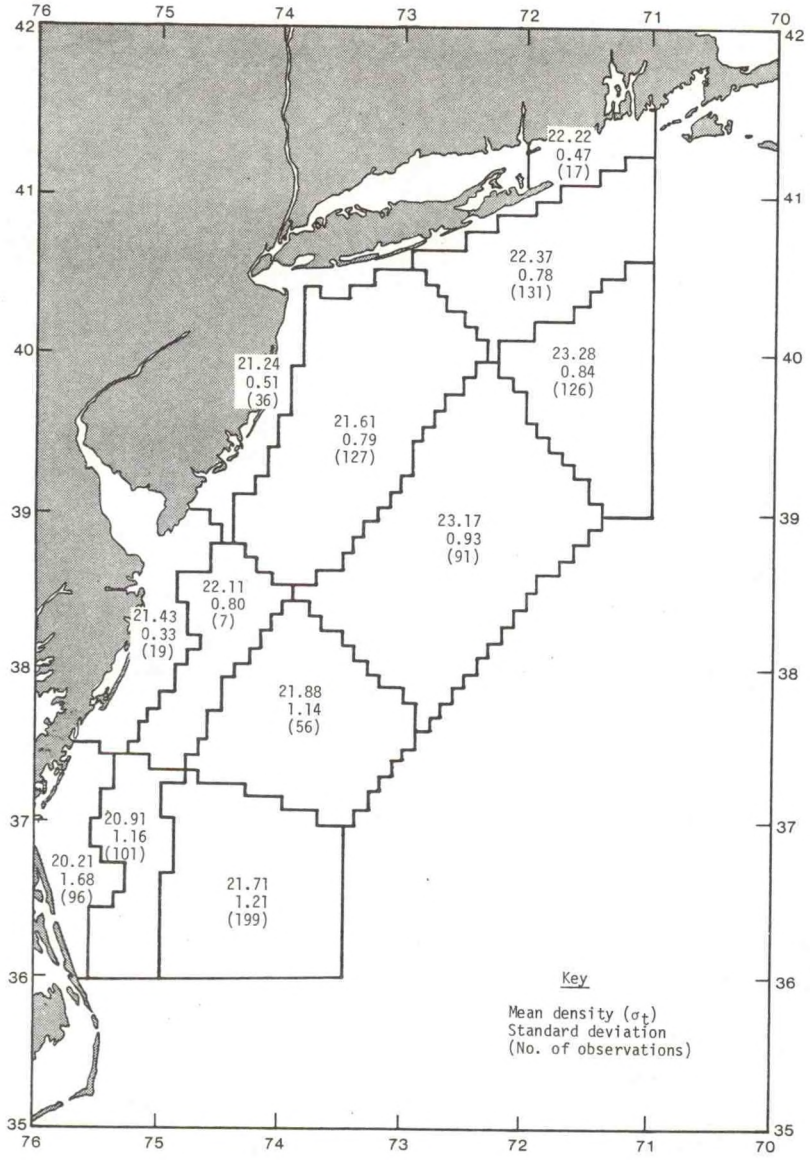


Figure 4.98.--Summer mean sea-surface densities.

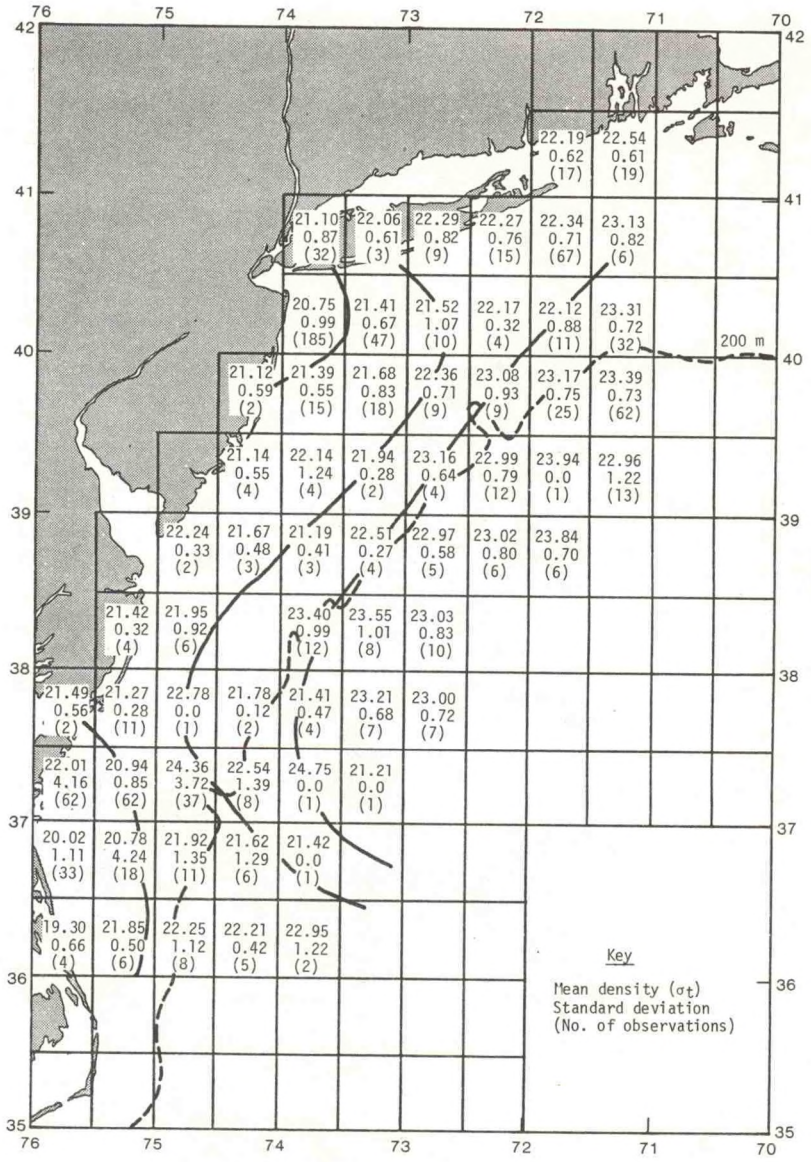


Figure 4.99.--Summer mean sea-surface density field.

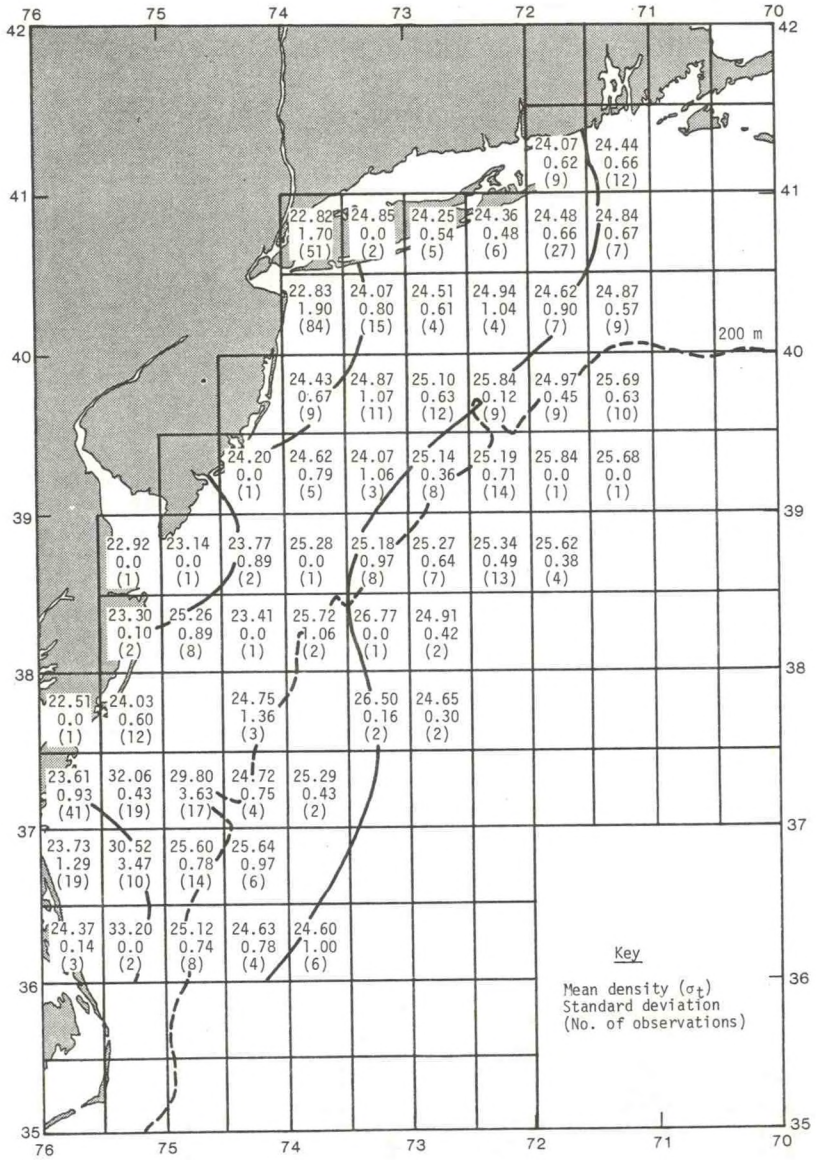


Figure 4.100.--Summer mean densities at 10-m depth.

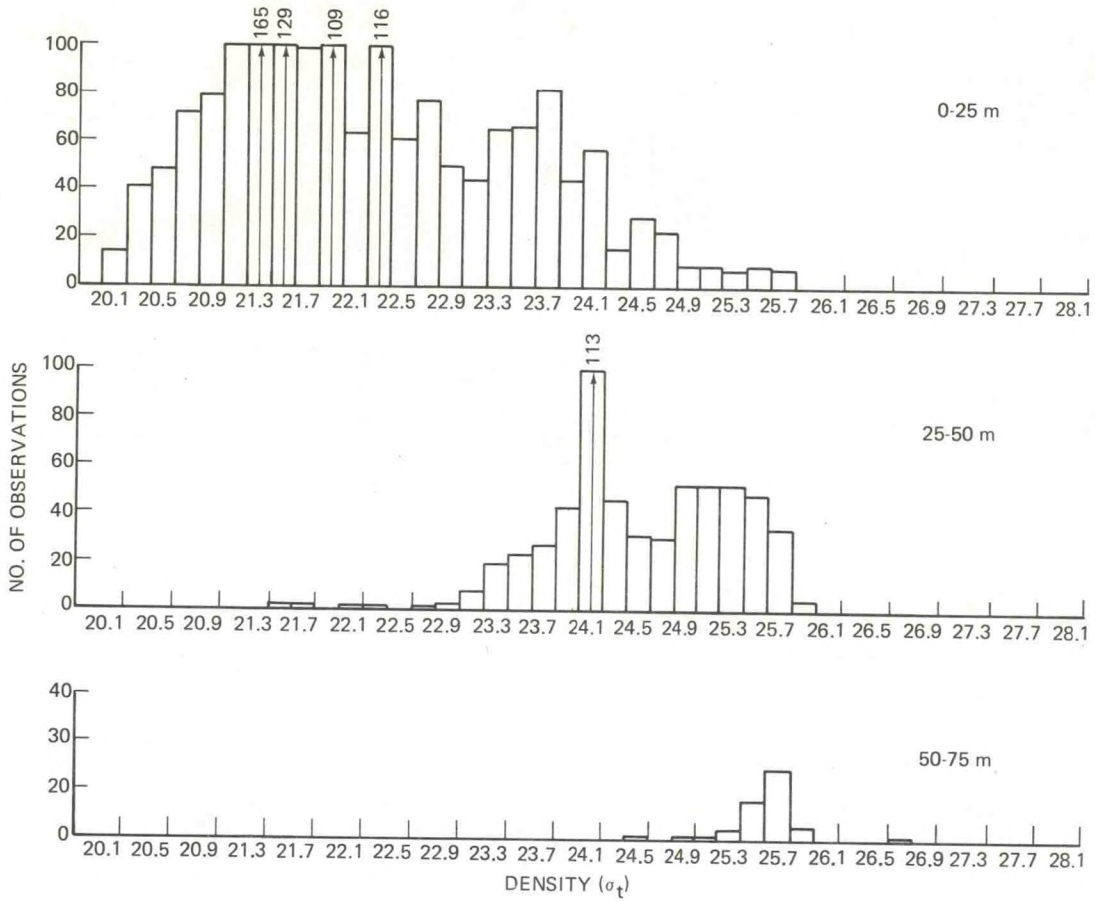


Figure 4.101.--Histograms of summer density, area 6.

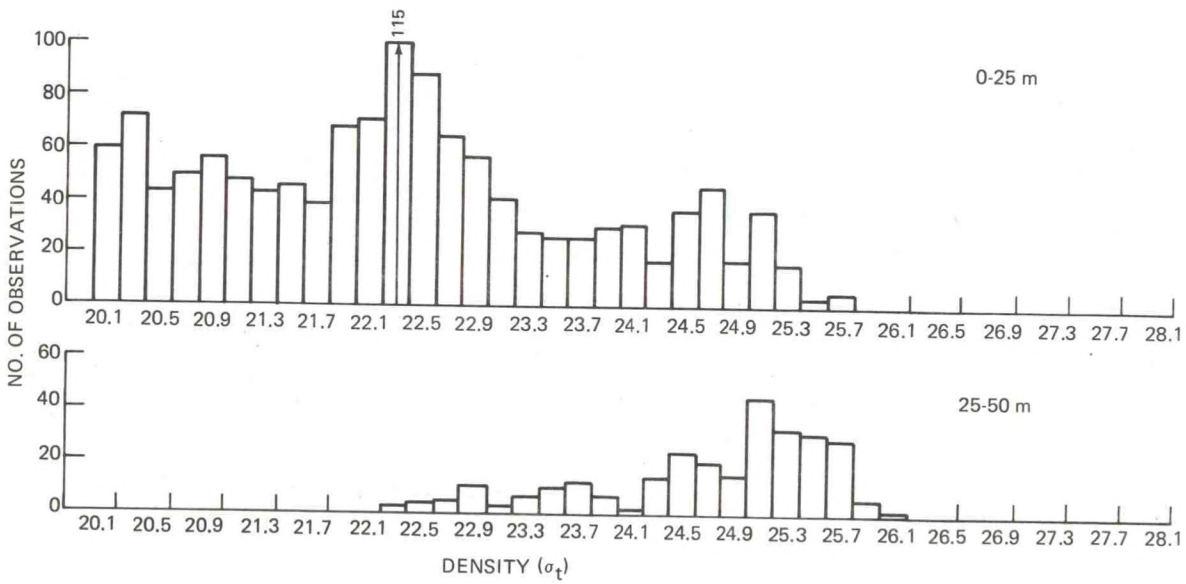


Figure 4.102.--Histograms of summer density, area 8.

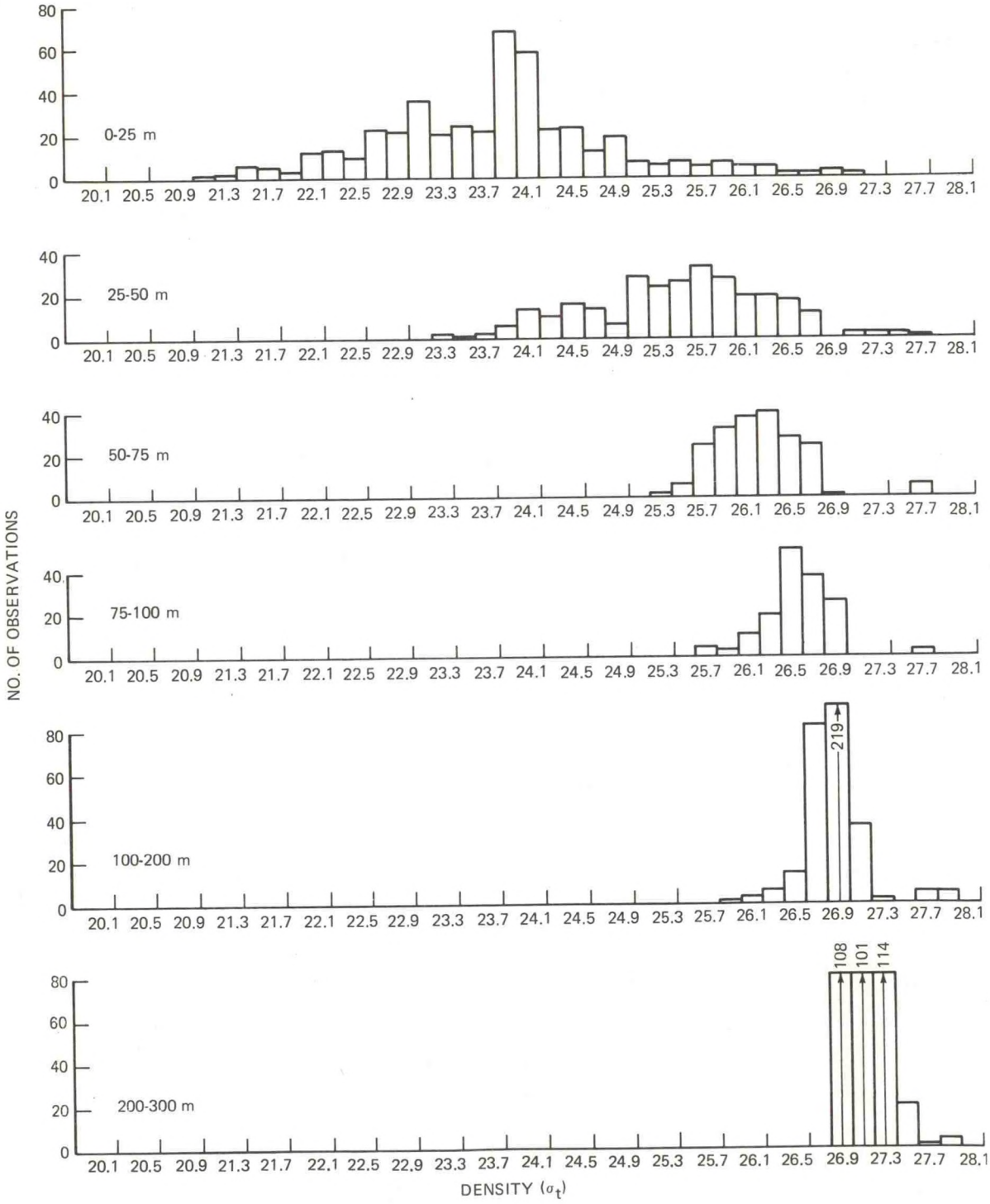


Figure 4.103.--Histograms of summer density, area 10.

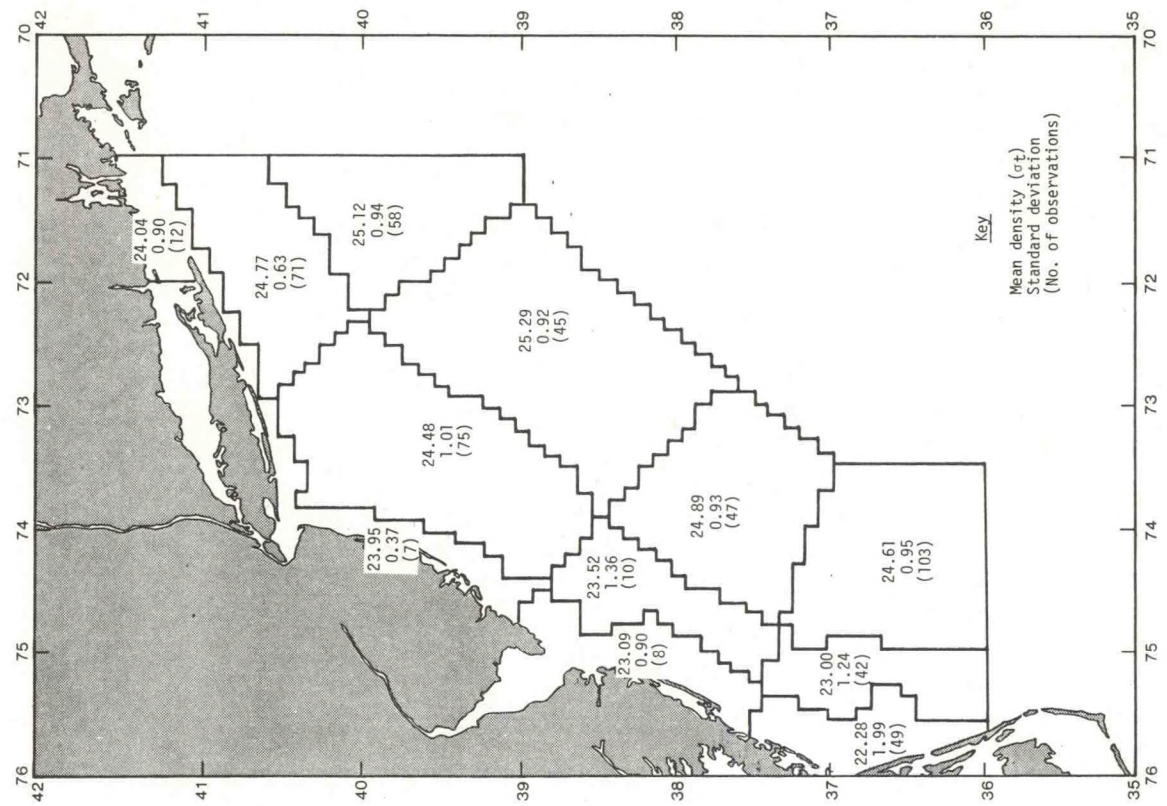


Figure 4.105.--Fall mean sea-surface densities.

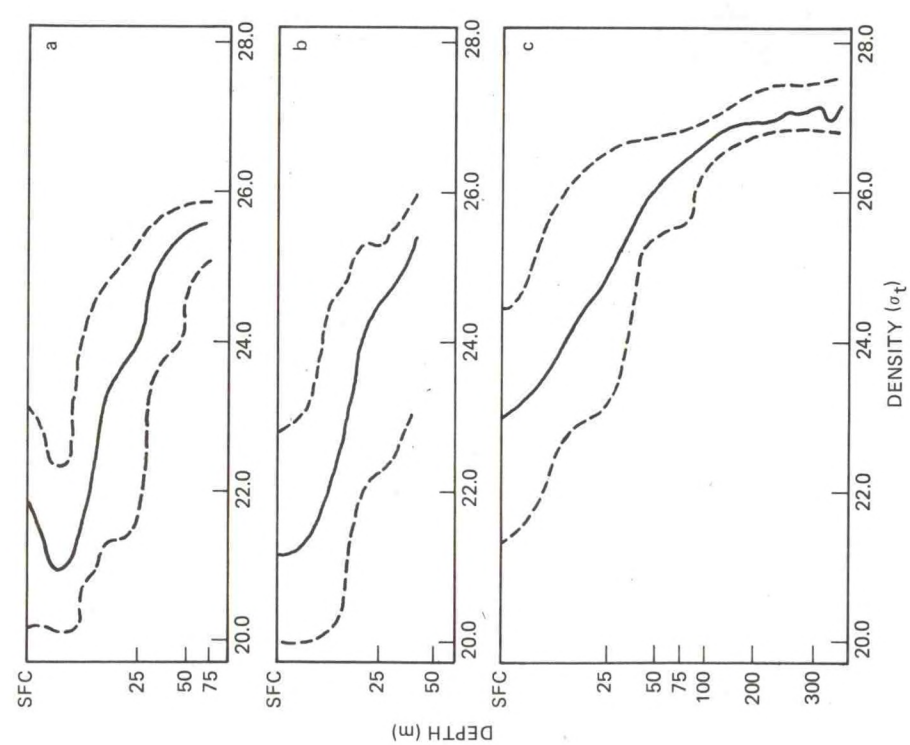


Figure 4.104.--Midlines (medians) and envelopes (2.5 and 97.5 percentiles) of summer densities for (a) area 6, (b) area 8, and (c) area 10.

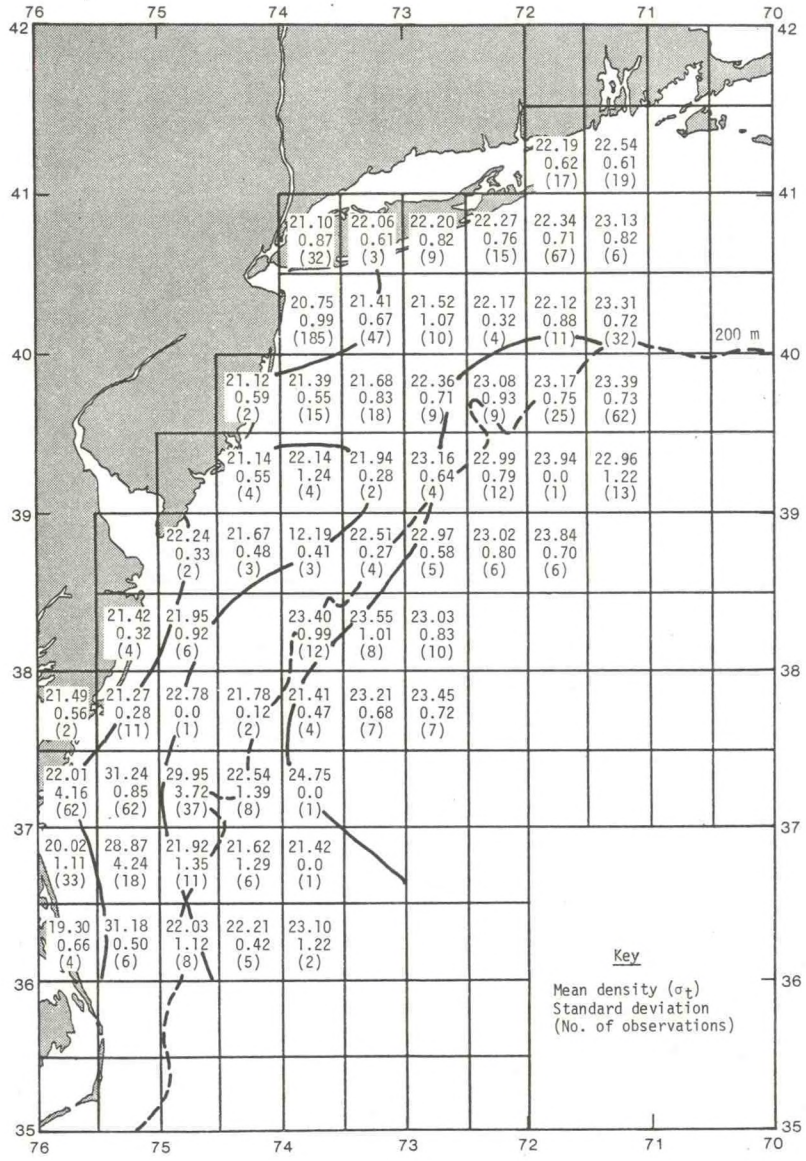


Figure 4.106.--Fall mean sea-surface density field.

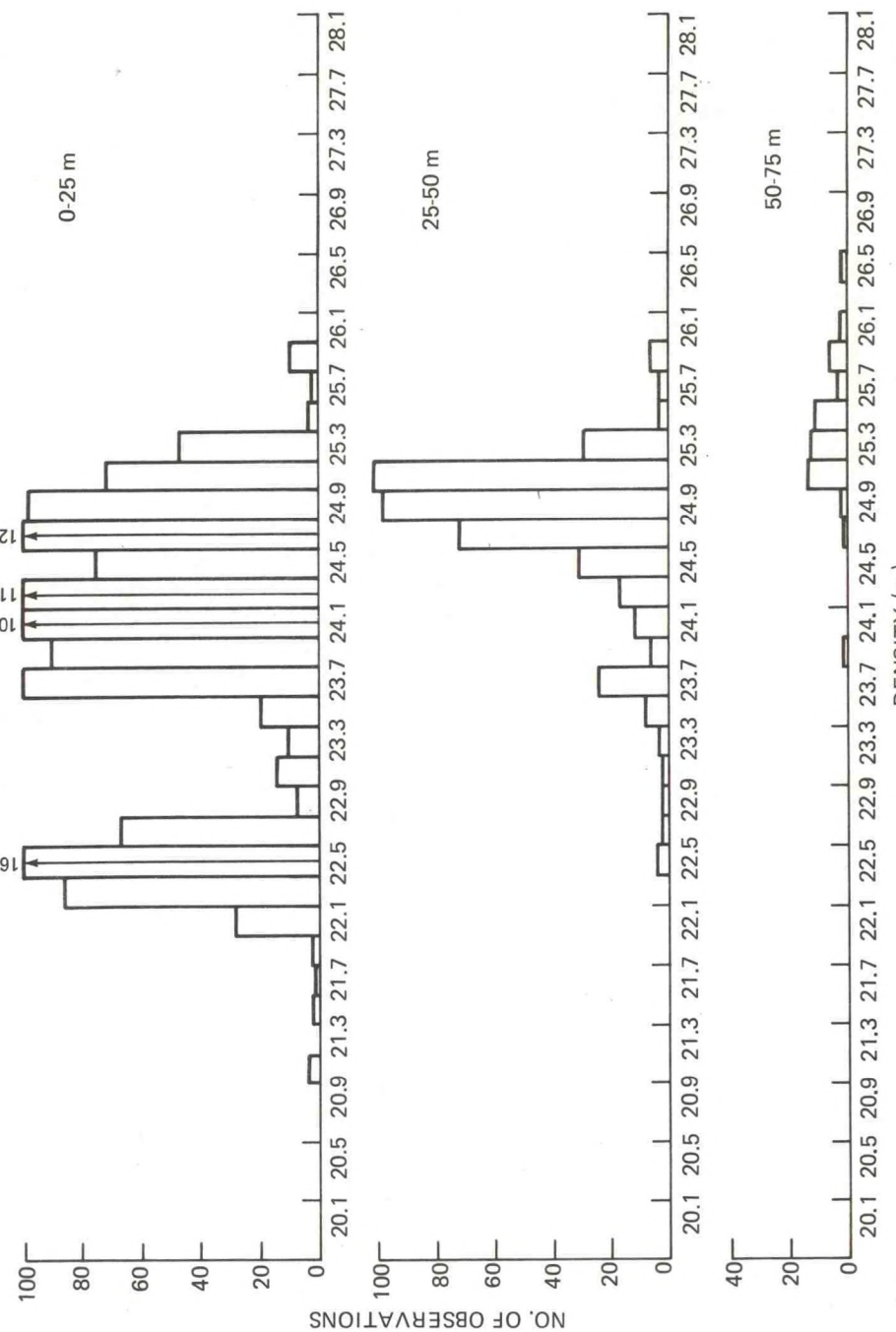


Figure 4.107.--Histograms of fall density, area 6.

### 4.4.9 Specific Volume Anomaly

Specific volume (steric) anomaly ($\delta$), computed from temperature and salinity, is the excess of the actual specific volume of seawater over the specific volume of seawater at 0°C and 35 ppt at the same pressure. The specific volume anomaly is the principal building block used by physical oceanographers to determine the dynamic behavior of an ocean area. In deep water, the vertical integral of specific volume anomaly yields the geostrophic currents. In shallow water, geostrophic currents can still be computed from the specific volume anomalies, but only after additional, controversial assumptions have been made.

Since specific volume is the reciprocal of density, the distribution of specific volume anomaly should be in opposition to density; that is, during the period of spring runoff and warm temperatures, specific volume anomaly should be high on the inner shelf, while during the winter it should be relatively low.

Winter. As shown in figures 4.108 and 4.109, specific volume anomaly in winter more or less parallels density but with opposite magnitudes (cf. figs. 4.87 and 4.88), with values being highest at the mouths of estuaries and lowest values in the slope water. The small number of observations makes it difficult to define the pattern of distribution in the southeastern part of the area (fig. 4.109). The distribution of specific volume anomaly at 50-m depth is shown in figures 4.110 and 4.111, where the horizontal gradients are seen to be smaller than at the surface. The shelf-slope water front is more apparent from these charts than from the density charts. Again, the small number of observations in the southeastern region makes interpretation very difficult. The vertical distribution of specific volume anomaly for area 6 (fig. 4.112) shows a relatively homogeneous mass field in winter, ranging from $10^5\delta$ = 140 to 300. The vertical structure for areas 6, 8, and 10 is shown in figure 4.113, where specific volume anomaly is seen to decrease rather uniformly with depth. The greatest variability is near the surface, and decreases markedly below 100-m depth.

Spring. Relatively large horizontal gradients of specific volume anomaly are evident in spring (fig. 4.114), with values of $10^5\delta > 600$ at the mouths of estuaries. Few observations during this season are available for the central part of the Bight, making it difficult to draw any conclusions about the mass field in that area. The vertical distribution (fig. 4.115) shows the effect of the vernal decrease in density associated with warming and river outflow.

Summer. The surface pattern of specific volume anomaly that can be derived from the STD data is rather incoherent and not amenable to interpretation. At 10-m depth (figs. 4.116 and 4.117), the increase of specific volume anomaly in the southern part of the Bight is evident, a result of summer heating and the low densities associated with the outflow from Chesapeake Bay. The broad range in specific volume anomaly values on the shelf in summer is evident in figures 4.118 and 4.119, where values from 250 to 900 are found in the 0- to 25-m layer. Between 25 and 50 m the range is much smaller. In the upper layers of the slope water, as seen in area 10

(fig. 4.120), surface values are widely distributed, but below 75 m the range is relatively narrow. The vertical structure (fig. 4.121) shows a rapid decrease in specific volume anomaly with depth, with high variability in the upper layers. The higher values of specific volume anomaly of the shelf water compared with the slope water are evident.

Fall. The data are too scattered for a meaningful analysis of specific volume anomaly distributions in the central and southern portions of the Bight (fig. 4.122). In the northeastern part of the Bight, the main feature is the decrease of specific volume anomaly with distance from the coast. As in the case of density, the vertical distribution (fig. 4.123) shows a tendency for bimodal specific volume anomaly distributions in the upper layer.

Summary. Relatively high values of specific volume anomaly are found near the coast and low values offshore, decreasing with depth during all seasons. A north-south gradient is evident in summer, with high values in the southern half of the region. The number of observations is insufficient for a description of the mean mass field by ½° squares during the summer and fall seasons, when the variability in specific volume anomaly is highest.

The combination of large variability in specific volume anomaly, particularly during summer, and the relatively small number of edited observations available suggests that the historical data base can best be used for estimating the geostrophic flow field, or to provide input to models on a cruise-by-cruise basis, after careful manual editing of the data and judicious interpretation of all information associated with each cruise.

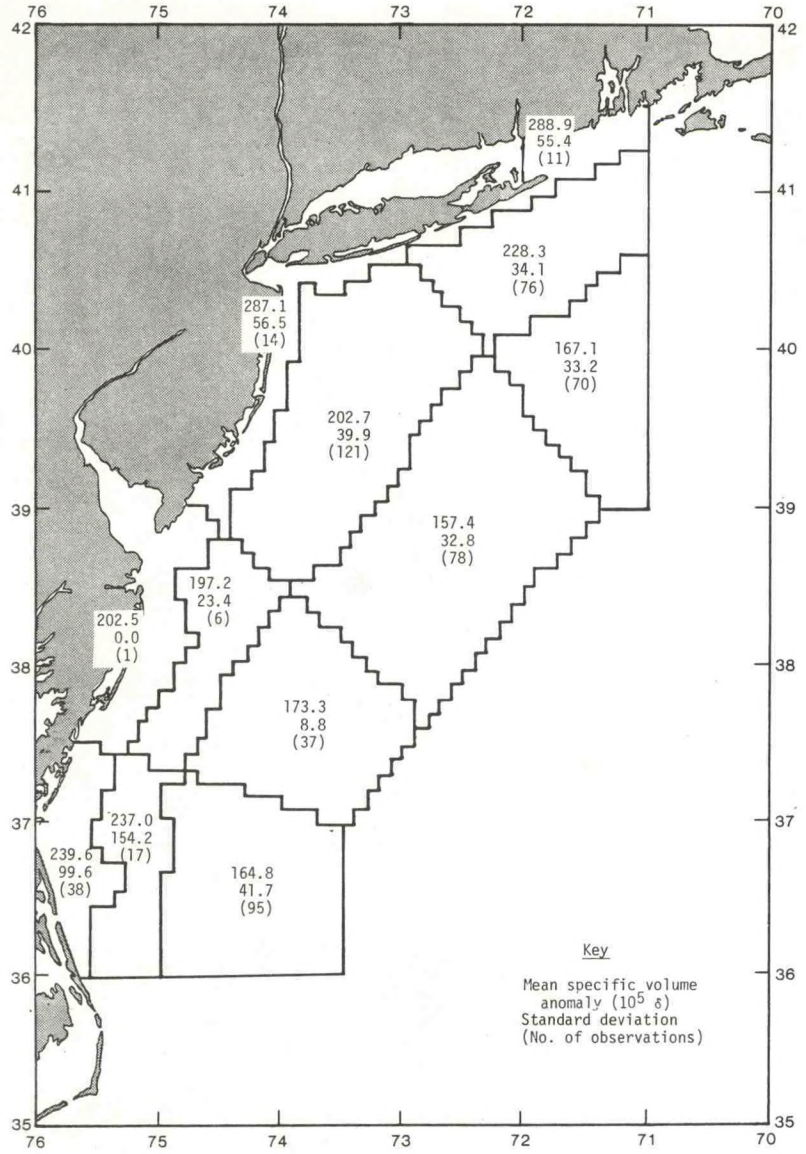


Figure 4.108.--Winter mean sea-surface specific volume anomalies.

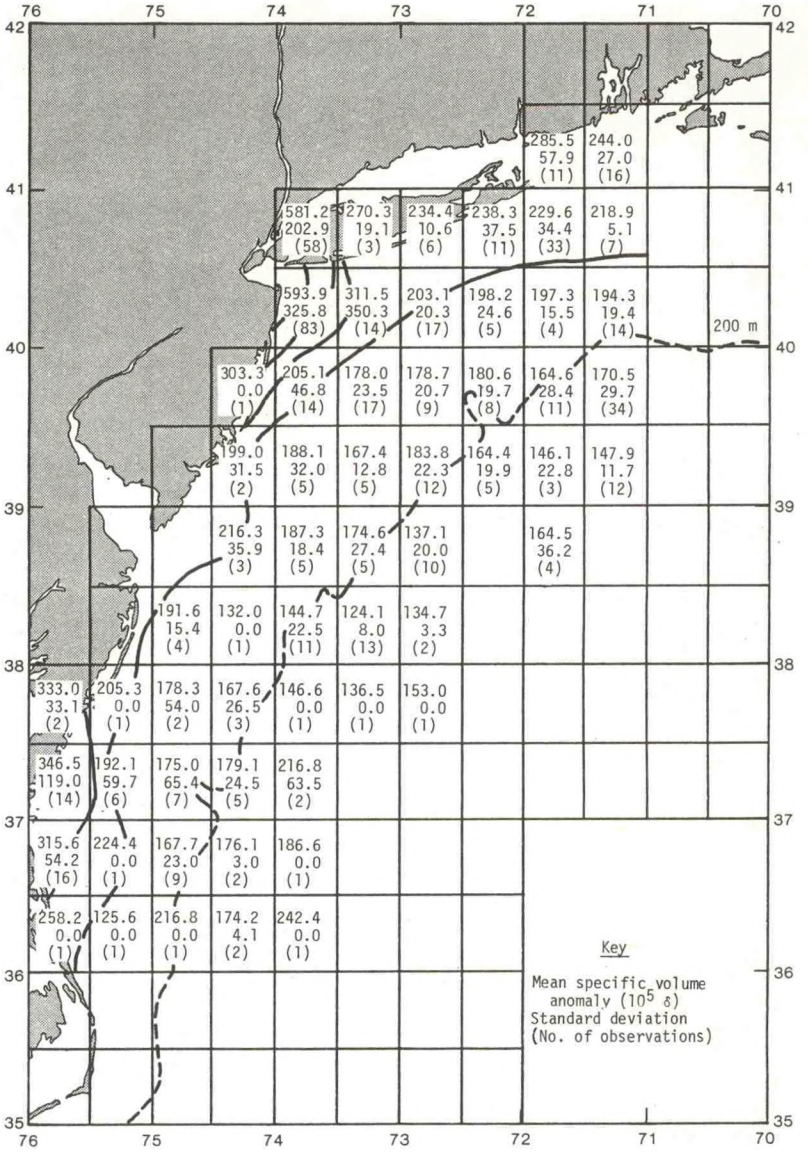


Figure 4.109.--Winter mean sea-surface specific volume anomaly field.

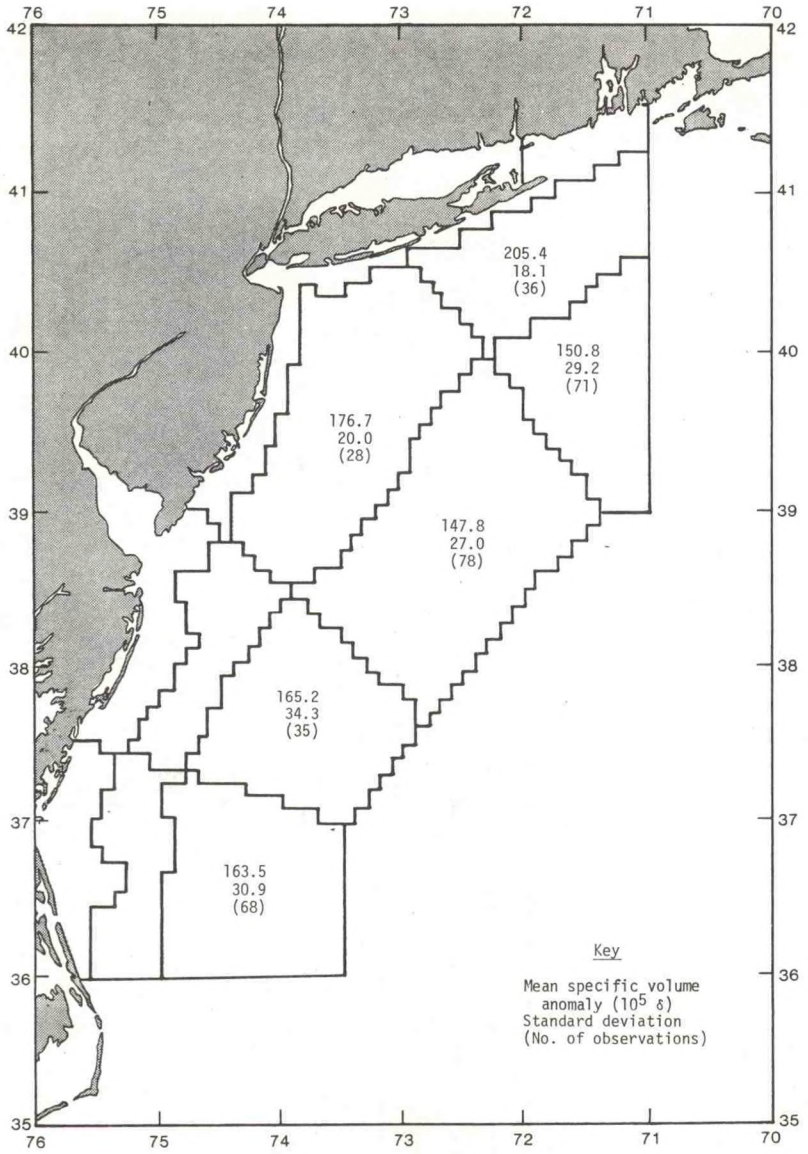


Figure 4.110.--Winter mean specific volume anomalies at 50-m depth.

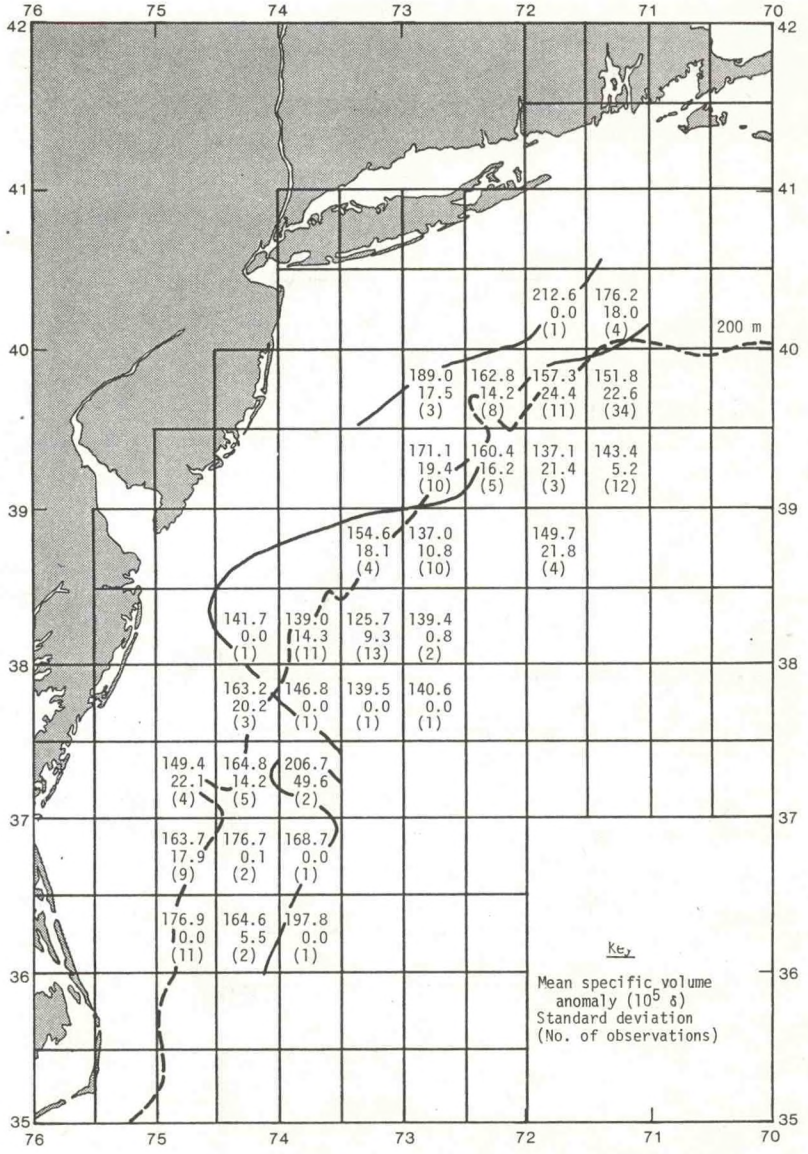


Figure 4.111.--Winter mean specific volume anomaly field at 50-m depth.

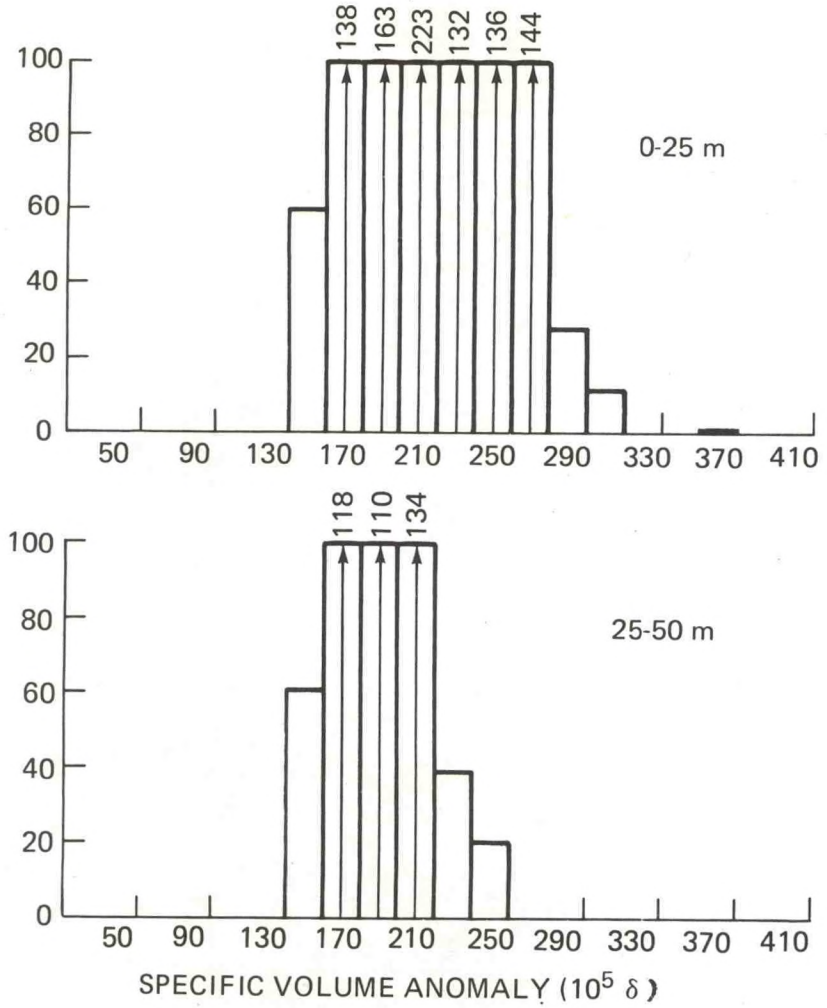


Figure 4.112.--Histograms of winter specific volume anomaly, area 6.

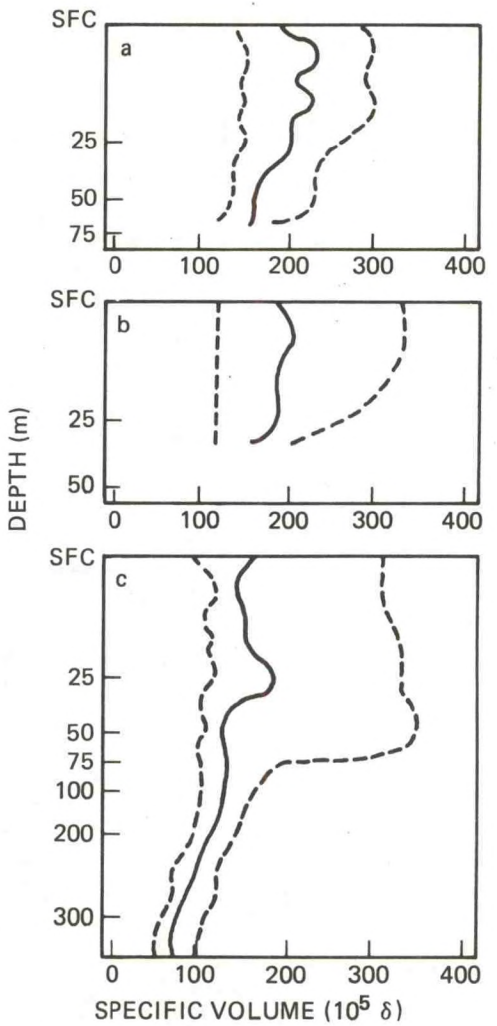


Figure 4.113.--Midlines (medians) and envelopes (2.5 and 97.5 percentiles) of winter specific volume anomalies for (a) area 6, (b) area 8, and (c) area 10.

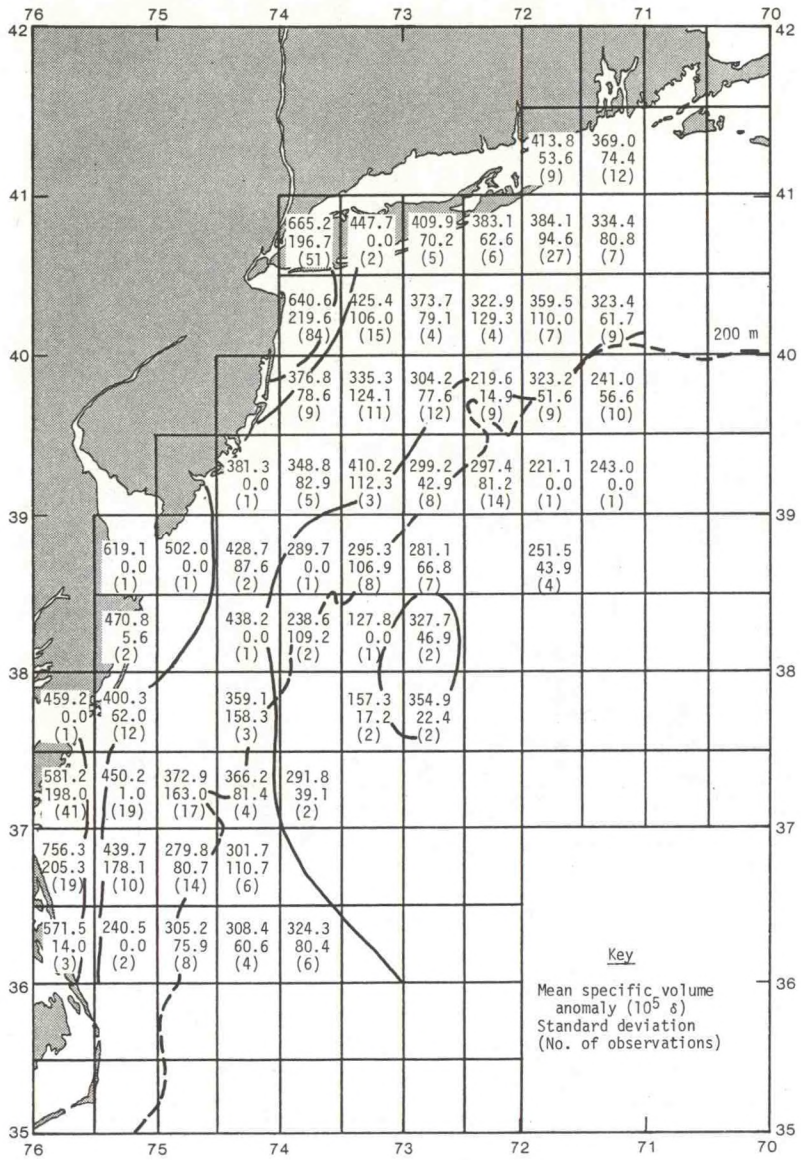


Figure 4.114.--Spring mean sea-surface specific volume anomalies.

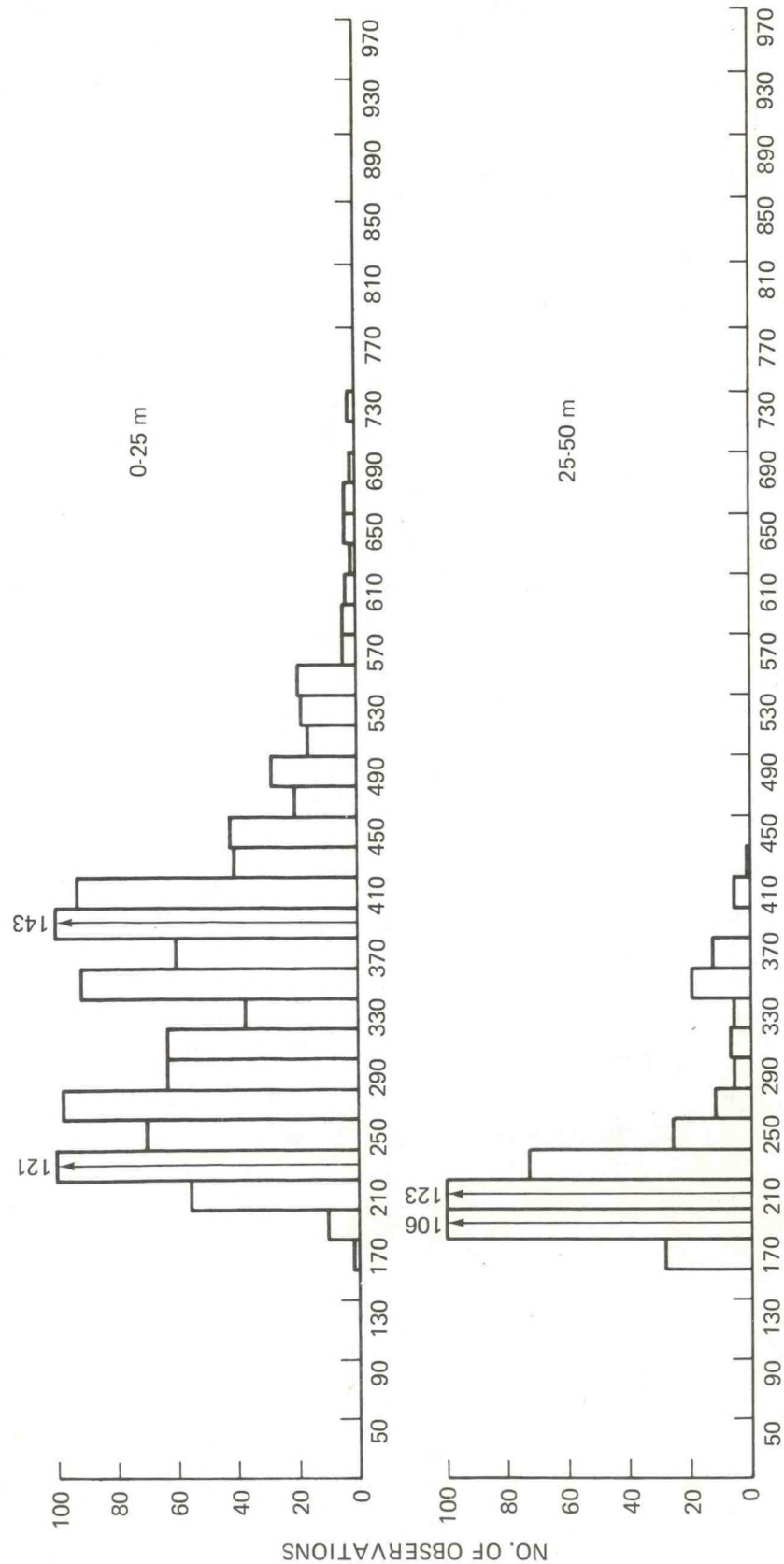


Figure 4.115.--Histograms of spring specific volume anomaly, area 6.

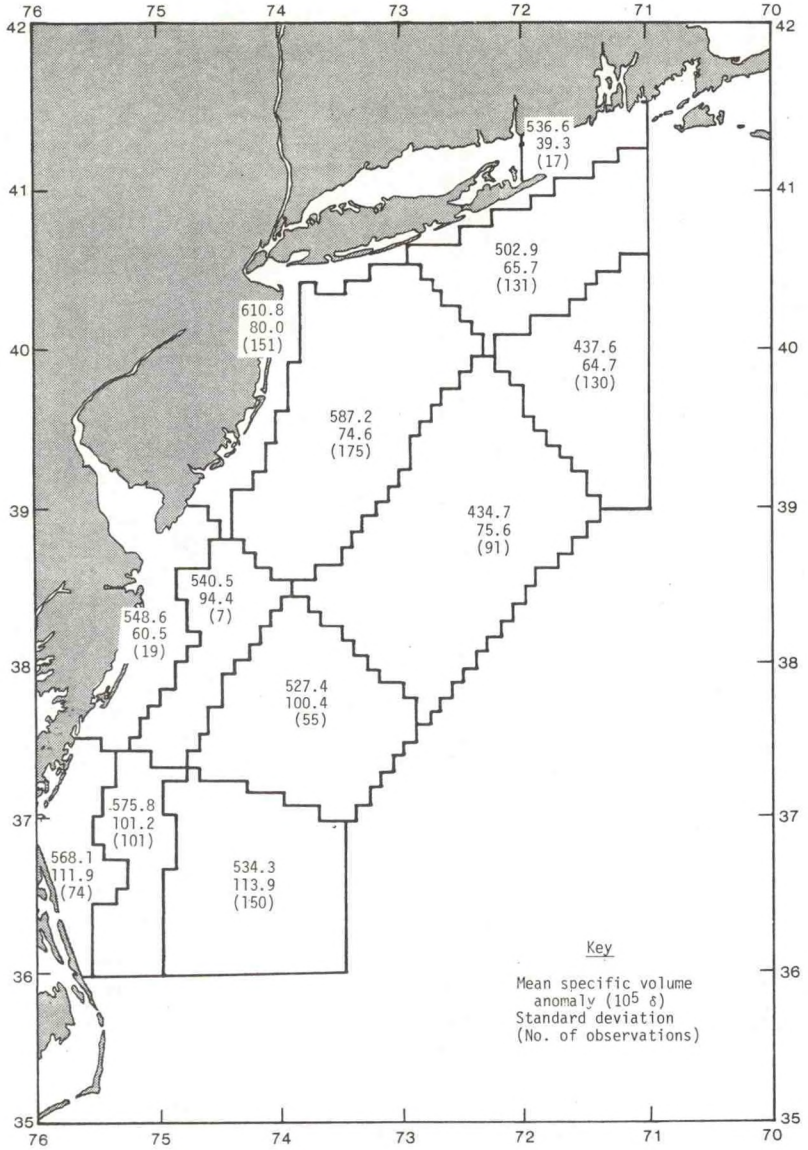


Figure 4.116.--Summer mean sepcific volume anomalies at 10-m depth.

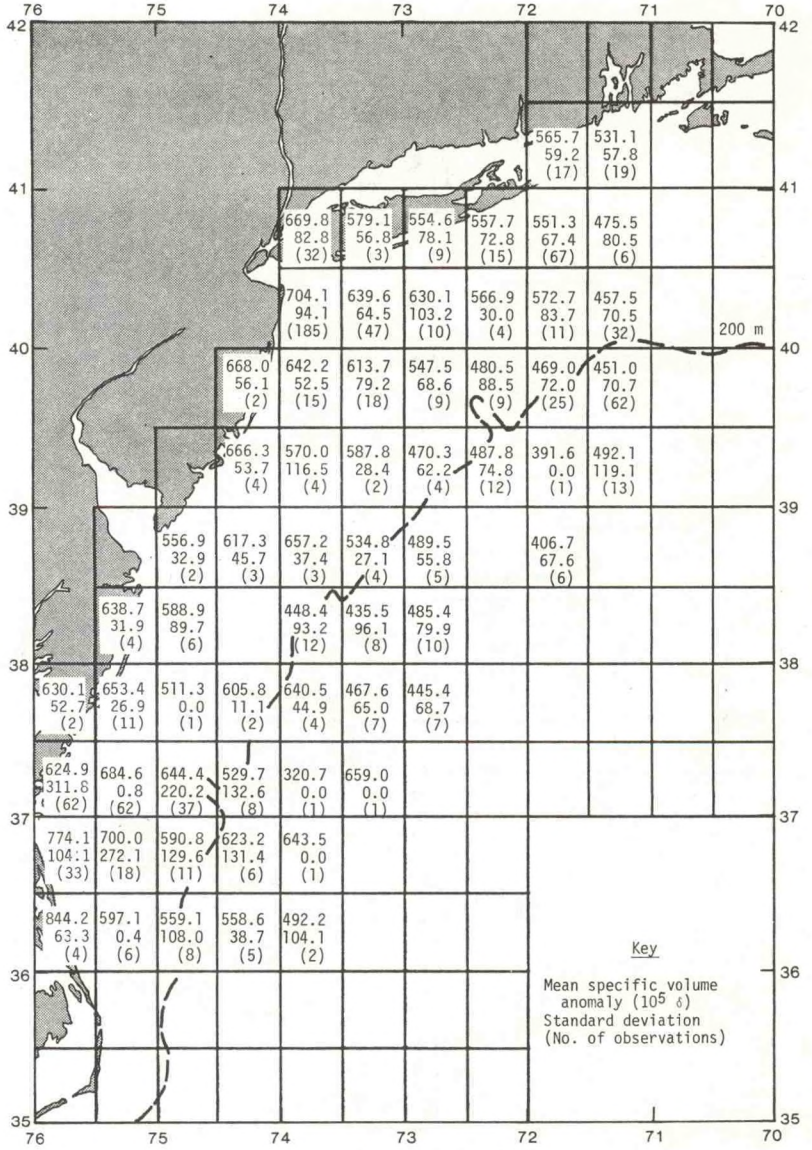


Figure 4.117.--Summer mean specific volume anomaly field at 10-m depth.

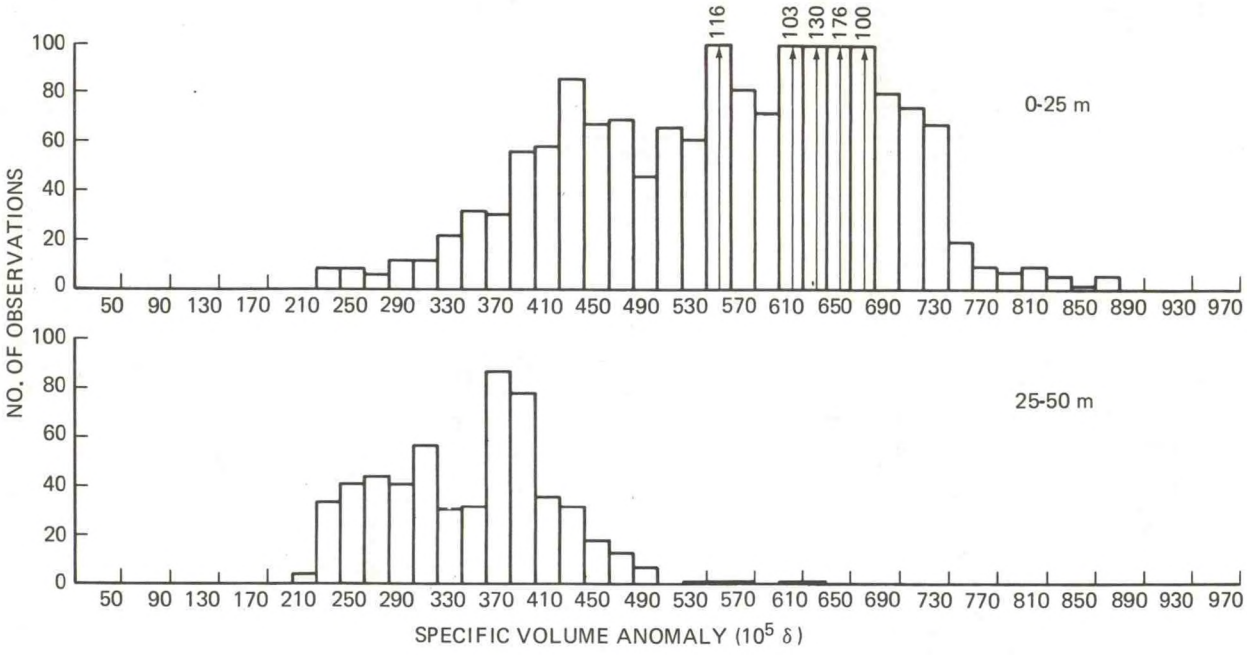


Figure 4.118.--Histograms of summer specific volume anomaly, area 6.

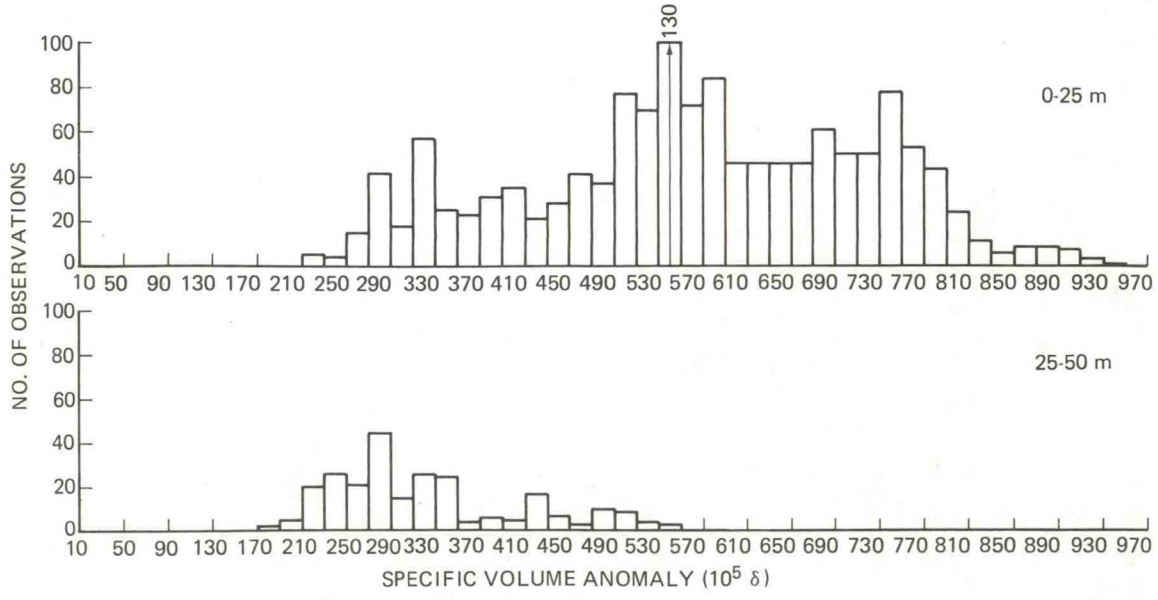


Figure 4.119.--Histograms of summer specific volume anomaly, area 8.

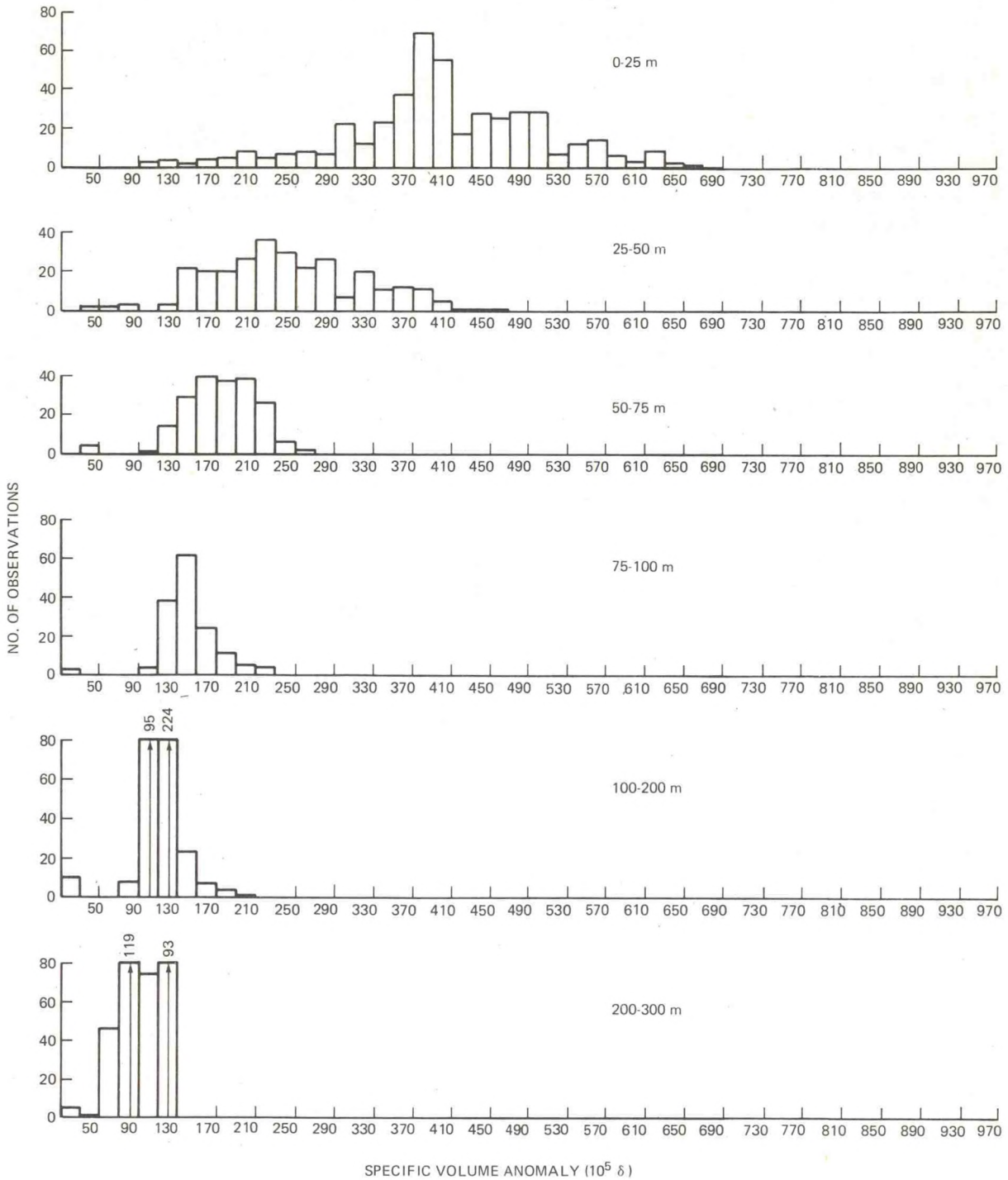


Figure 4.120.--Histograms of summer specific volume anomaly, area 10.

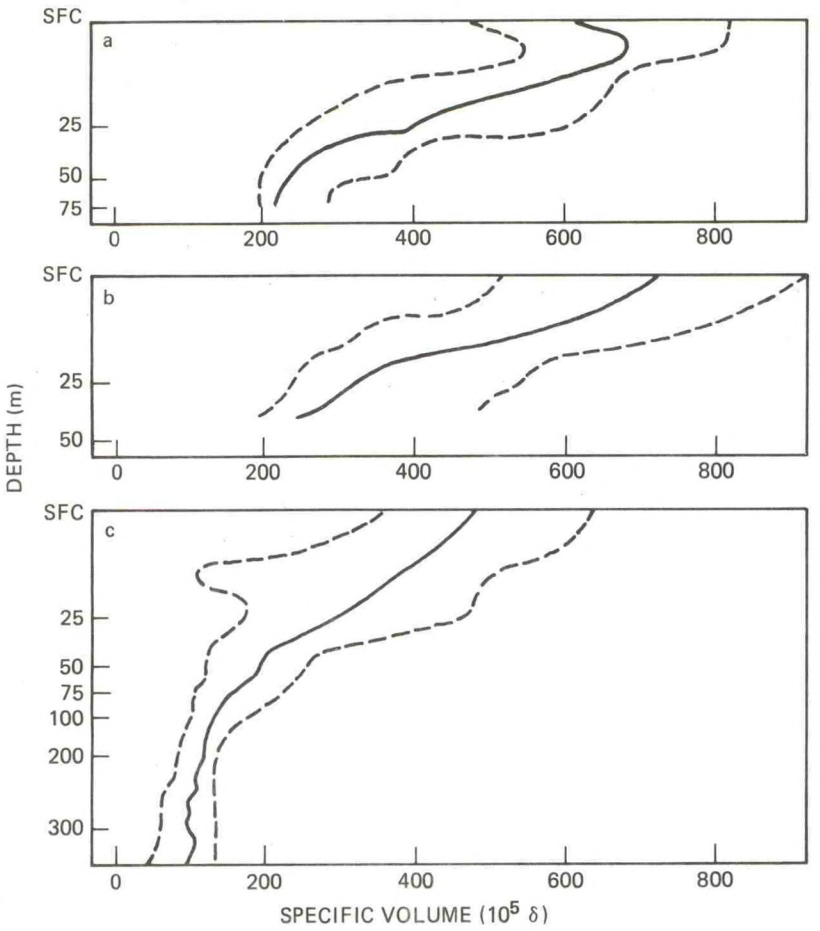


Figure 4.121.--Midlines (medians) and envelopes (2.5 and 97.5 percentiles) of summer specific volume anomalies for (a) area 6, (b) area 8, and (c) area 10.

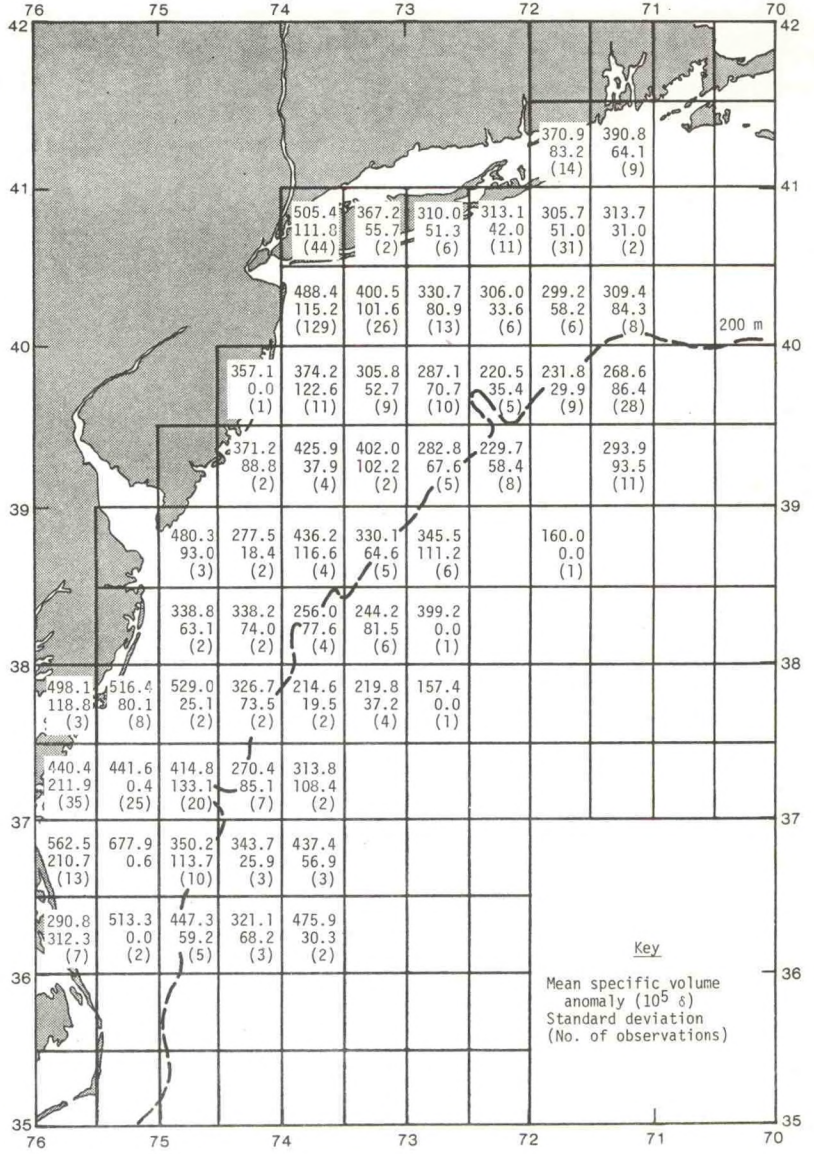


Figure 4.122.--Fall mean sea-surface specific volume anomalies.

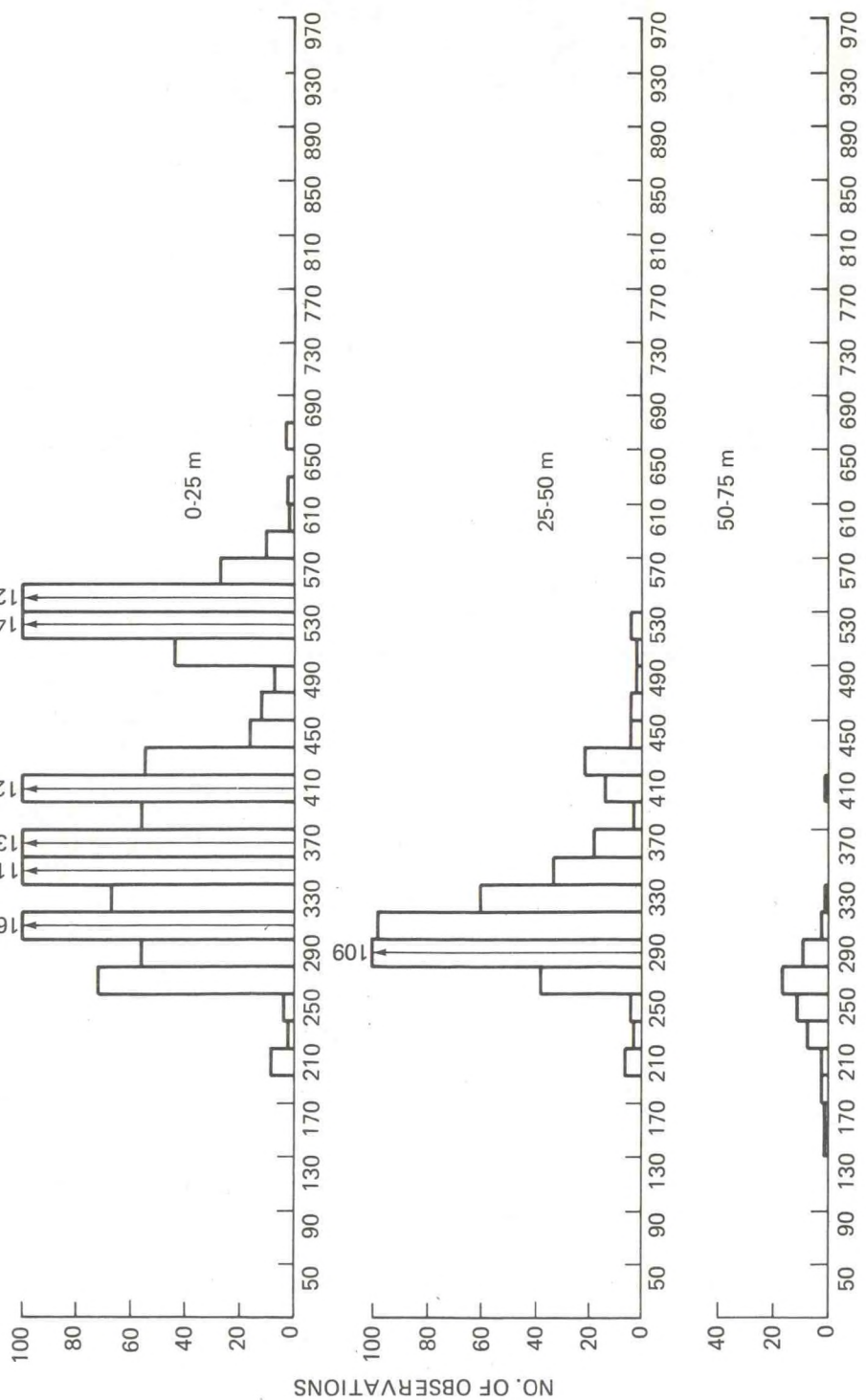


Figure 4.123.--Histograms of fall specific volume anomaly, area 6.

## 4.5 Dissolved Oxygen and Nutrient Concentration

Because few data are available for analyzing concentrations of dissolved oxygen or nutrients, only general characteristics of the distribution and variability of these variables could be determined for some of the oceanographic areas under study.

### 4.5.1 Dissolved Oxygen

Oxygen in seawater comes from atmospheric oxygen dissolved at the sea surface and the dissolution of oxygen released during photosynthetic processes within the photic zone. In the deepwater areas 9, 10, 11, and 12, concentration of dissolved oxygen is close to saturation throughout the year, and is dependent upon the normal partial pressure of atmospheric oxygen and monthly average surface water temperatures. Corresponding to an annual surface temperature variation of about 9.5°C, the variation of average monthly dissolved oxygen concentration is about 1.5 ml/l in area 9. In terms of environmental impact, a critical period for oxygen requirements for biological activity is the summer season, when warmer water is saturated with dissolved oxygen at a lower concentration, producing less oxygen for aerobic processes. The analyses discussed below therefore pertain primarily to summer conditions. An inventory of the data used is given in figure 4.124.

The distribution of dissolved oxygen concentrations over depth layers of 25 m is shown in figure 4.125 for area 9 in summer (July, August, September). The increase seen in concentrations from the surface through the 50-m level is a result of the increase in saturation concentration, while the decrease with depth below 50 m is commonly associated with biological oxygen demands and the lack of dissolved oxygen transported downward from the surface. The vertical profile for area 9 during summer is given in figure 4.126, and the March profile for the same area is shown in figure 4.127, where the nearly uniform concentrations in the surface layers reflect the effect of vertical mixing. Although the summer profile of oxygen concentration in area 12 (fig. 4.128) looks similar to the profile for the more northern area 9, the surface layer concentrations are lower in area 12. The reason lies in the warmer surface waters, by about 2°C, and, perhaps, in a phosphate limited plant growth and less photosynthetic oxygen production. Only dissolved phosphates are considered here (sec. 4.5.2), and phosphate concentrations of about 0.0 to 0.4 µg atoms/l seem to be typical (Koblentz-Mishke et al., 1970). The summer distribution of dissolved oxygen over 25-m layers in area 12 is shown in figure 4.129.

Figure 4.130 shows the March profile of dissolved oxygen concentration for area 6, which is illustrative of the winter-spring vertical variation. The effect of cooler Hudson River waters mixing with slope waters is apparent. The oxygen concentration is higher in the surface layers in this area than in either areas 10 or 9. In addition, the wide range and grouping of concentration measurements may be the result of the large west-to-east variation in dissolved oxygen over the area, or may suggest the vertical transport of deep waters to the surface. The summer profile for area 6 (figure 4.131) shows the strong influence of Hudson River intrusion in

the surface layer, where very low concentrations of dissolved oxygen are found at about 20-m depth.

Surface water temperature in much of area 6 is slightly lower, and the biochemical productivity higher, than in area 9 (Koblentz-Mishke et al., 1970), which may account for the higher dissolved oxygen concentration in the surface layer in area 6 during the summer (fig. 4.132).

In area 5, the vertical distribution in summer (fig. 4.133) is similar to the distribution to the east in area 9 of deeper water (cf. fig. 4.126). There is no indication of the strong vertical stratification as suggested by the dissolved oxygen concentration distribution found in area 6 during the summer, and the similarity between oxygen distribution in the 0- to 25-m and 25- to 50-m layers also illustrates the absence of stratification in area 5 (fig. 4.134).

In area 2, a coastal area, strong vertical stratification is established as early as June, but the lowest dissolved oxygen concentration in the surface layer does not occur until later in the season. Figure 4.135 shows the vertical distribution in August, which is illustrative of summer conditions. Considering the large differences in the characteristics of the dissolved oxygen profiles in areas 6 and 2, a large scatter in the magnitude of concentrations in area 6 could be expected. The diagram in figure 4.136 gives evidence of the problem of data scatter for large geographical areas, such as area 6. The data points in the surface layer in the left portion of the diagram reflect June measurements in the western portion of area 6; the other data, measurements in the eastern portion of the area.

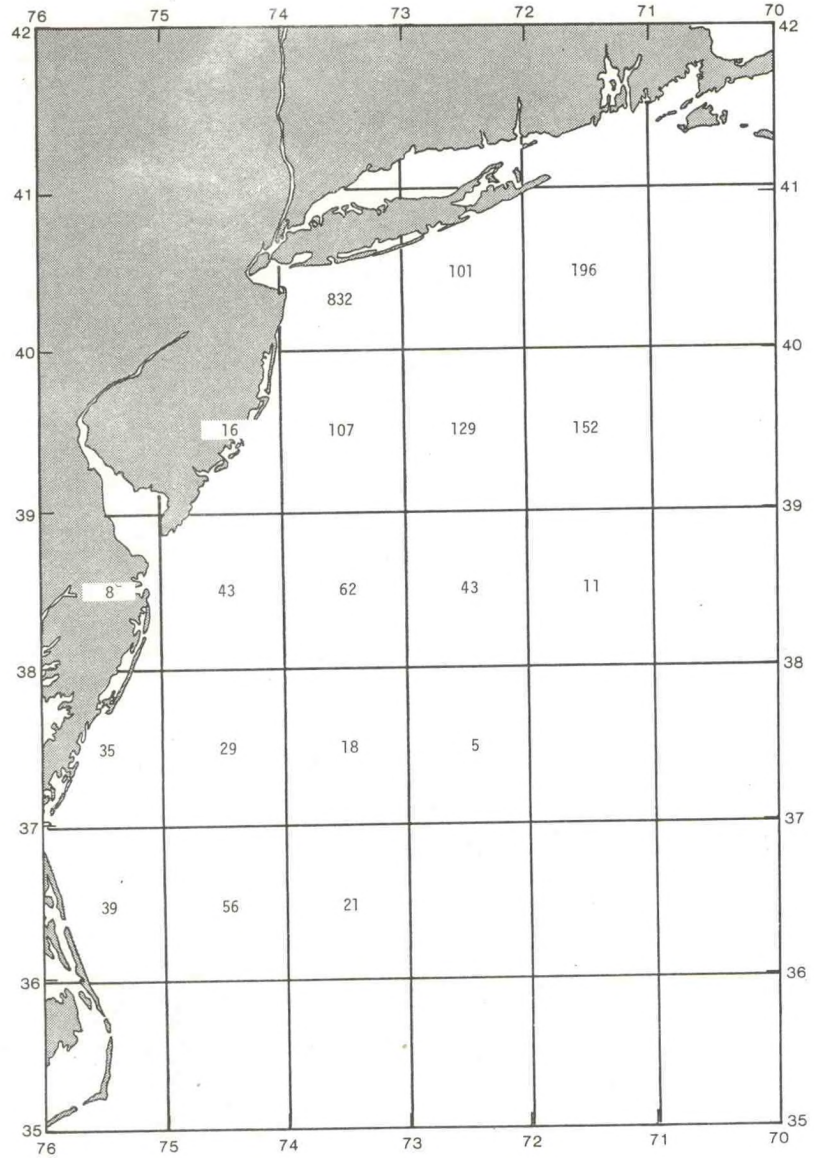


Figure 4.124.--Inventory, by $1^{o}$ squares, of STD data containing oxygen measurements.

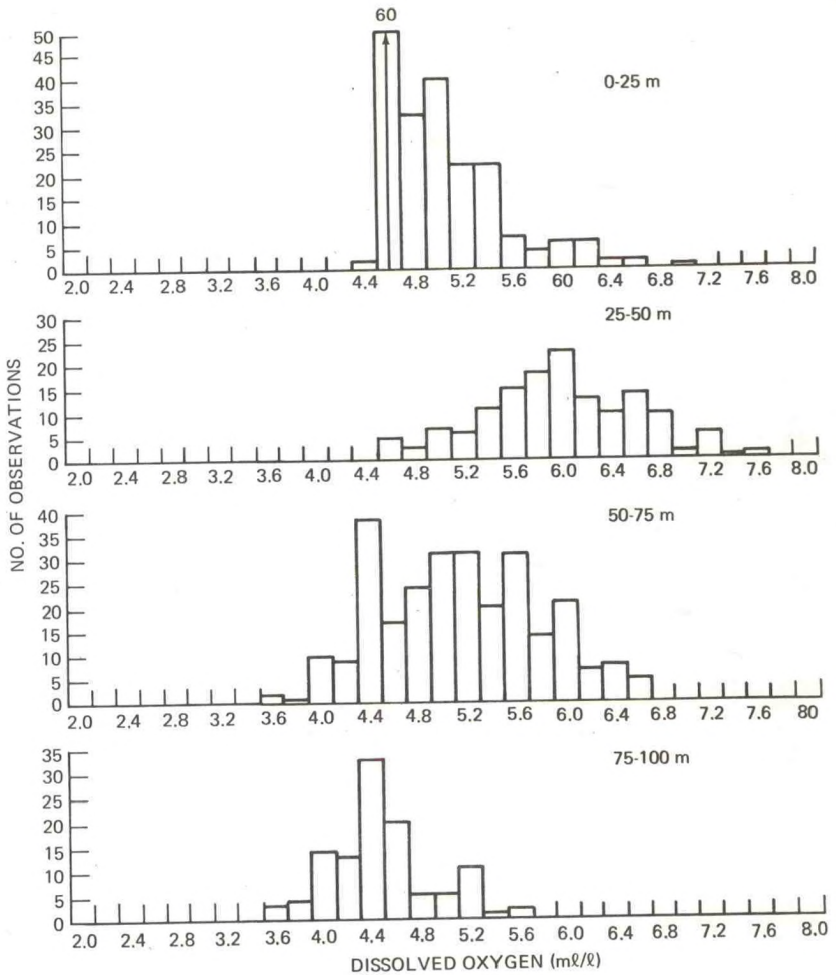


Figure 4.125.--Histograms of summer dissolved oxygen concentrations, area 9.

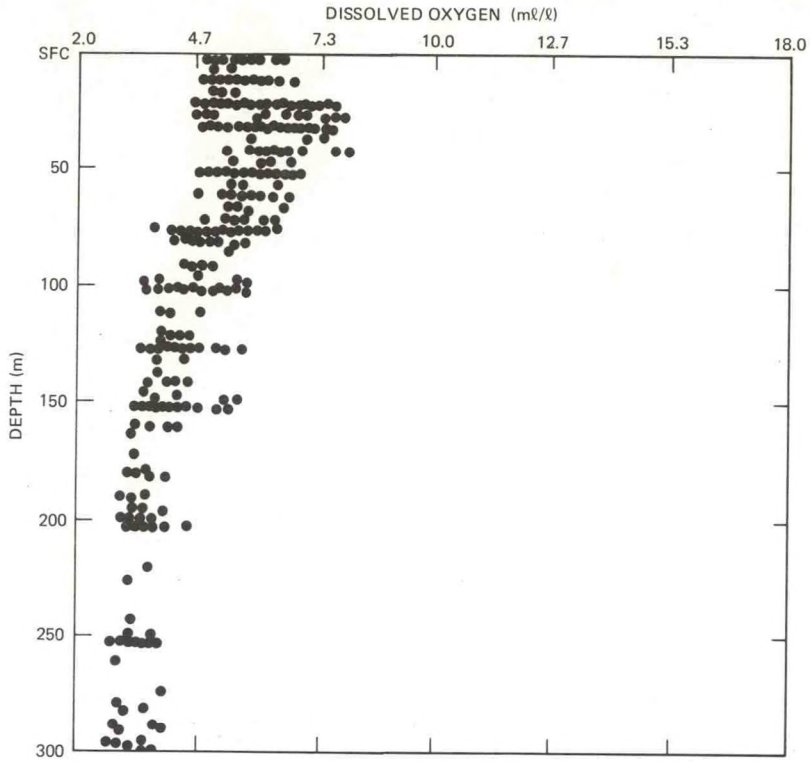


Figure 4.126.--Summer vertical profile of dissolved oxygen, area 9.

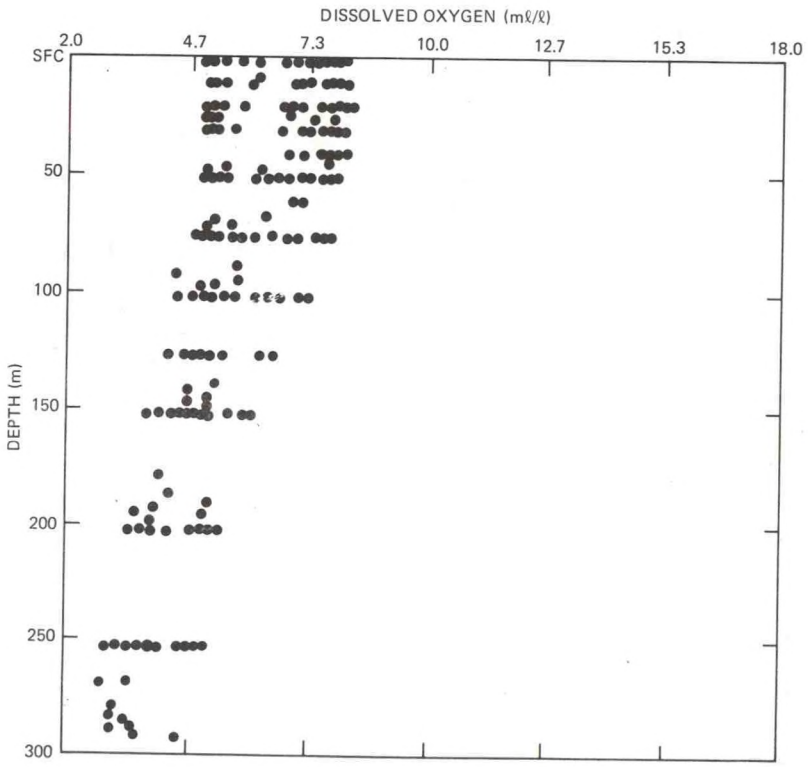


Figure 4.127.--March vertical profile of dissolved oxygen, area 9.

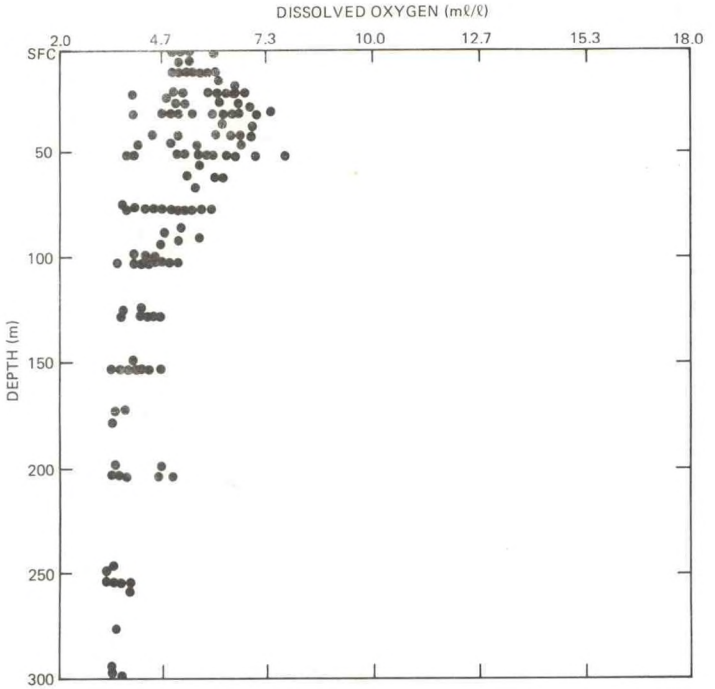


Figure 4.128.--Summer vertical profile of dissolved oxygen, area 12.

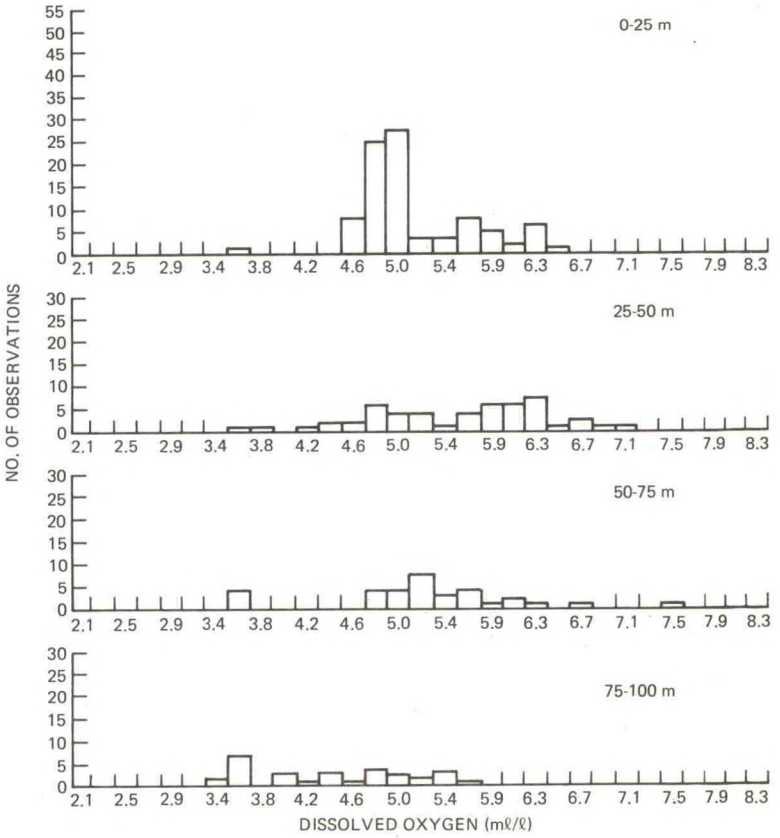


Figure 4.129.--Histograms of summer dissolved oxygen concentration, area 12.

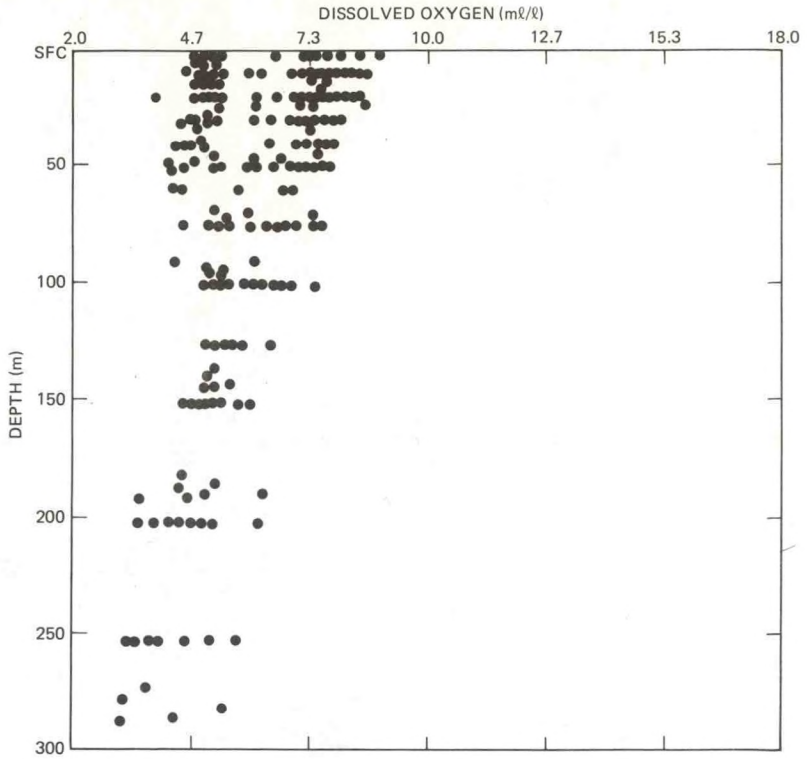


Figure 4.130.--March vertical profile of dissolved oxygen, area 6.

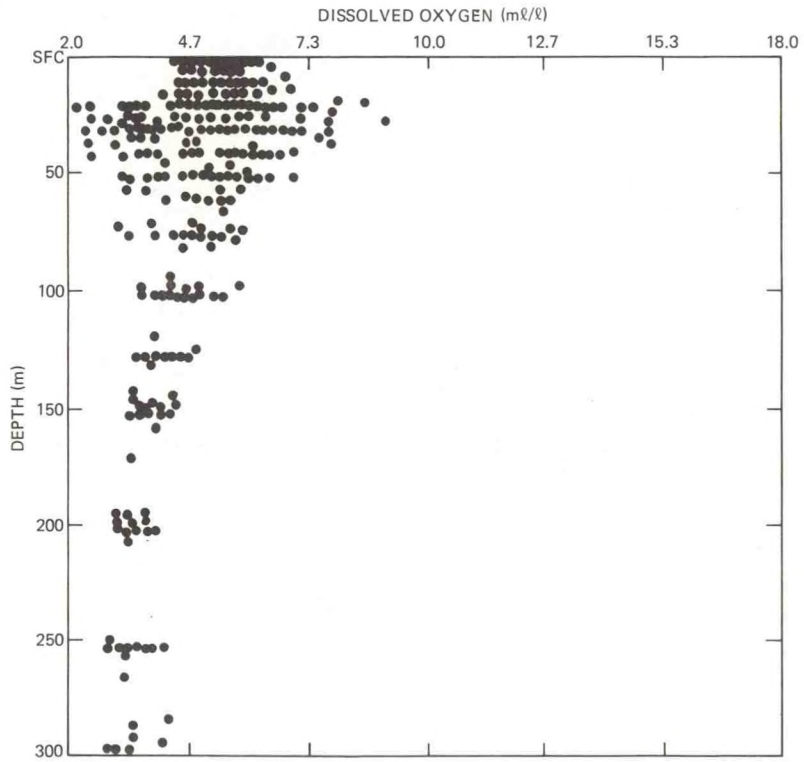


Figure 4.131.--Summer vertical profile of dissolved oxygen, area 6.

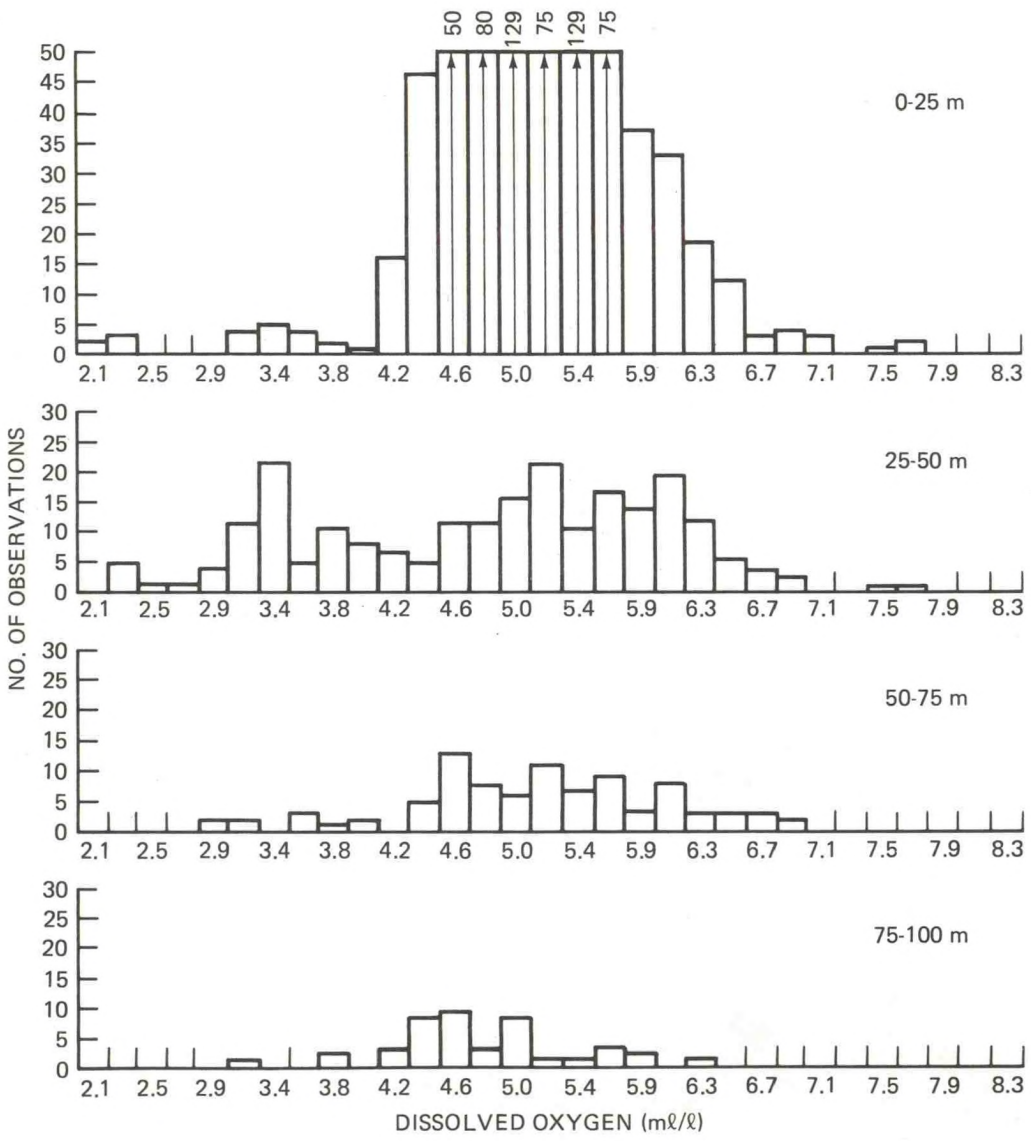


Figure 4.132.--Histograms of summer dissolved oxygen concentration, area 6.

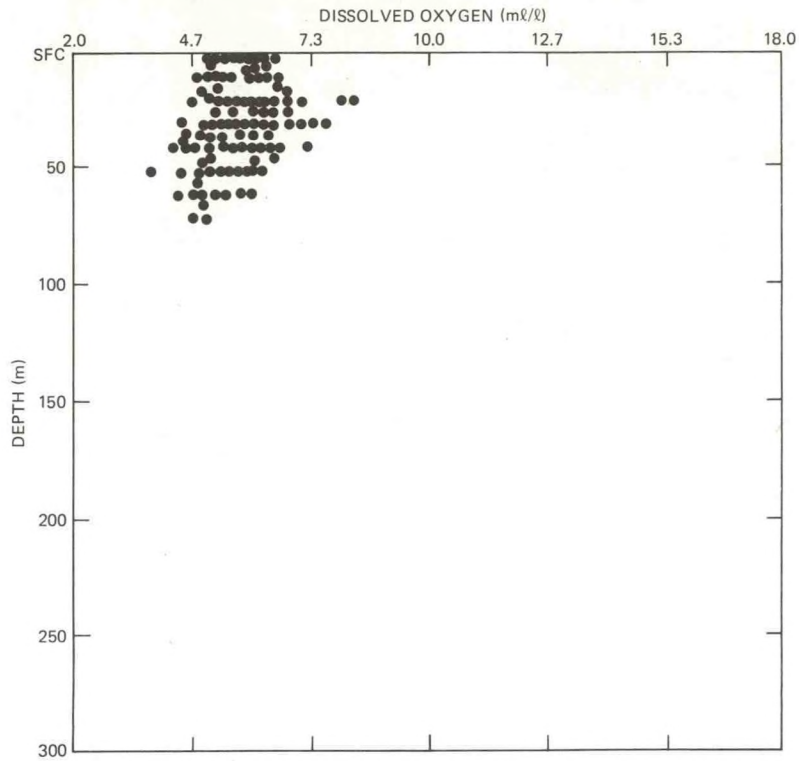


Figure 4.133.--Summer vertical profile of dissolved oxygen, area 5.

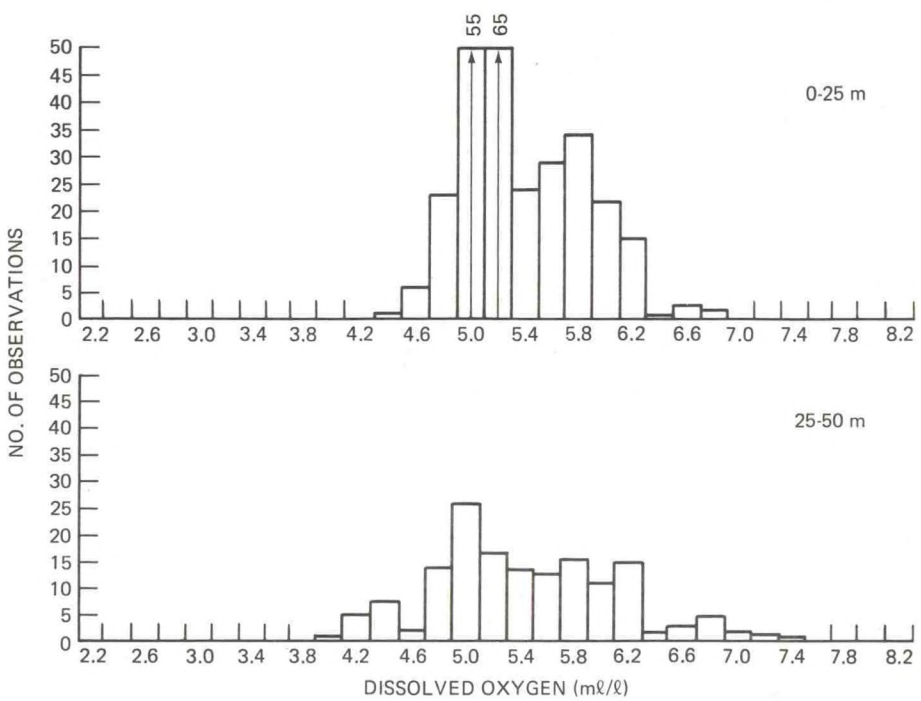


Figure 4.134.--Histograms of summer dissolved oxygen concentration, area 5.

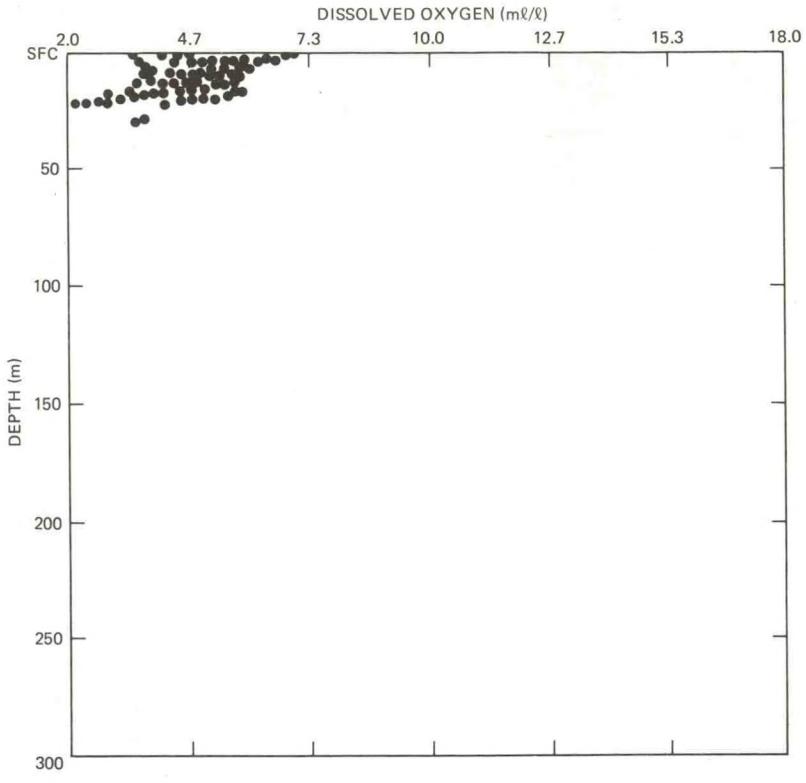


Figure 4.135.--August vertical profile of dissolved oxygen, area 2.

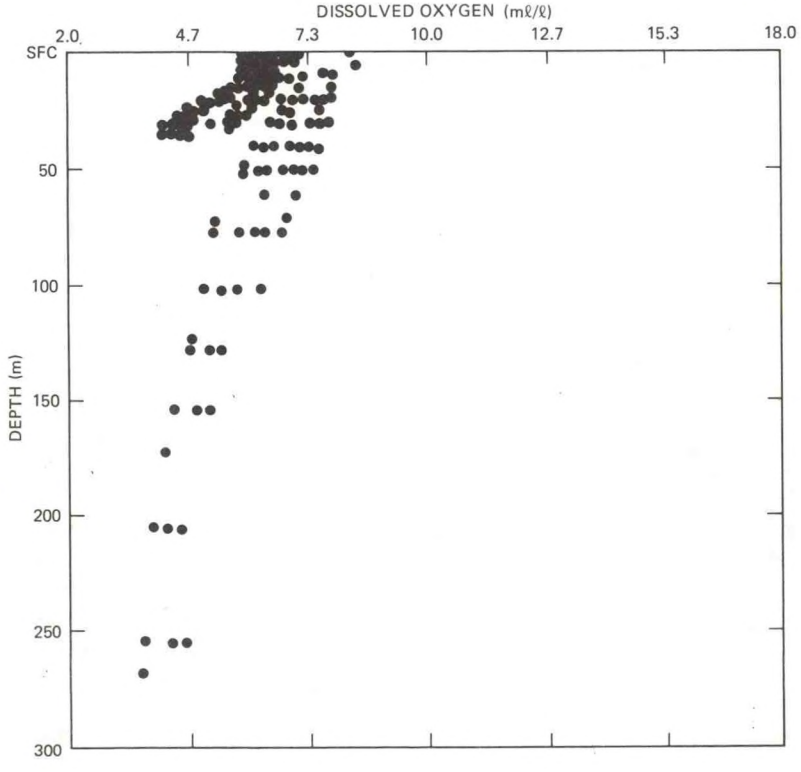


Figure 4.136.--June vertical profile of dissolved oxygen, area 6.

4.5.2 Phosphate

Phosphates are assimilated into organic material during biological processes within the water column, and the rate of this uptake is dependent upon the rate of biological activity. The dissolved phosphate concentration would therefore be expected to be minimum during warm periods. When biological uptake of phosphates decreases, decay processes acting on dead organic matter are expected to release phosphates to the water, causing higher concentrations during cold periods. Because of runoff from land and river discharges, which carry relatively large concentrations of phosphates, the concentrations of phosphates are expected to be higher and to vary more widely in nearshore areas than in areas farther away from the coast. The brief analysis presented below is based on the data shown in figure 4.137.

The average surface layer concentrations found in the eastern areas (areas 9, 10, 11 and 12) are similar to the concentrations reported in the literature (Riley and Chester, 1971; Yentsch, 1975; Amos, 1976). An example of the distribution of phosphate concentrations in area 9 in winter (January, February, March) is shown in figure 4.138. The histogram of the frequency of dissolved phosphate concentrations for 25-m layers in this area indicates very little variation in concentration with depth during the winter (fig. 4.139). An example of the phosphate concentrations in summer is given in figure 4.140, which shows the concentrations within the first 50 m to be much lower than in winter. The histogram in figure 4.141 also illustrates this decrease. Comparison of the phosphate distribution at depths from 75 to 100 m in summer and winter indicates little seasonal change. The few observations of phosphate concentrations of less than 0.46 µg atoms/l between 75 and 100 m during the summer is apparently caused by infrequent vertical mixing reaching this layer. Values were not plotted below 300 m because of the very few data available for layers below this depth.

The winter and summer phosphate distributions plotted in figures 4.142 and 4.143 for area 6, an intermediate area, seem to be a mixture of the characteristics of the deeper, eastern regions and those along the shore. The vertical variation in phosphate concentration in the first 50 m is probably due to the runoff from the Hudson River* and to water density stratification from temperature and salinity differences between the intruding river water and prevailing shelf waters. Phosphate concentration being a function of the amount of input from the deeper water masses and the intruding river water, a wide variation in surface layer concentrations is expected in a "mixed" water mass, as in area 6 (fig. 4.144), where the vertical distribution in winter (fig. 4.145) differs little from the winter distribution found in area 9 (cf. fig. 4.138).

Phosphate concentration in area 5 also seems to reflect the influence of coastal runoff, but the water is relatively shallow and not much variation

* Representative of the magnitude of dissolved phosphate concentration in the lower Hudson estuary is 2.7 µg atoms/l (Simpson et al., 1975).

in the vertical structure is evident. In figure 4.146, the profile for area 5 superimposed on the plotted concentrations for area 6 illustrates the similarity in phosphate distribution in the two areas. The vertical structure of the distribution in area 5 is shown in figure 4.147.

The strong influence of land and river runoff on the coastal phosphate concentration in area 2 in January is seen in figure 4.148. The shallow water produces a vertically mixed water mass in the area, preventing development of any significant vertical structure in the phosphate distribution. A comparison of the phosphate concentrations in July in area 2, shown in figure 4.149, with the concentrations in winter (fig. 4.148) shows that the uptake of phosphates by biological processes significantly reduces the concentrations in summer.

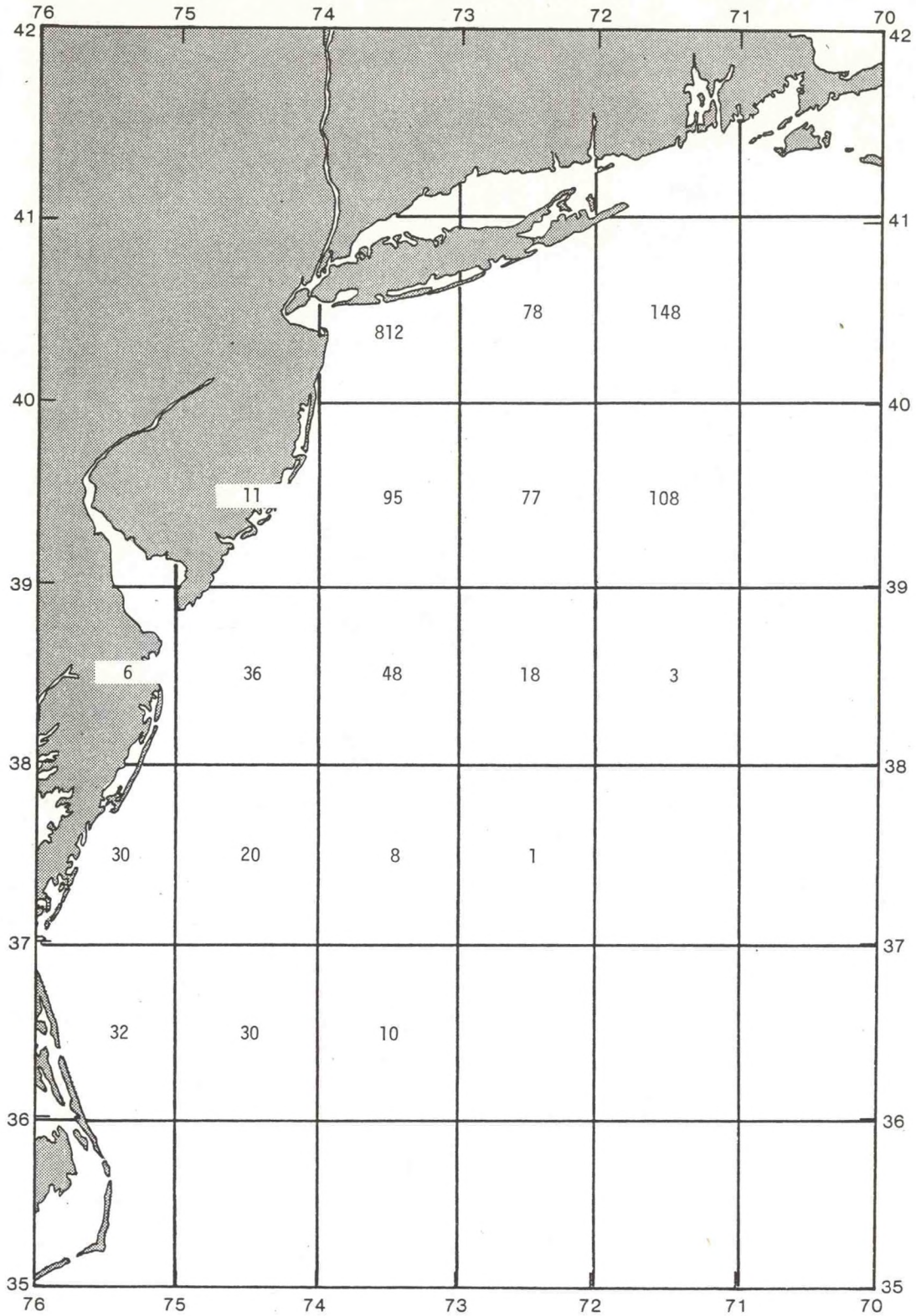


Figure 4.137.--Inventory, by $1^{o}$ squares, of STD data containing phosphate measurements.

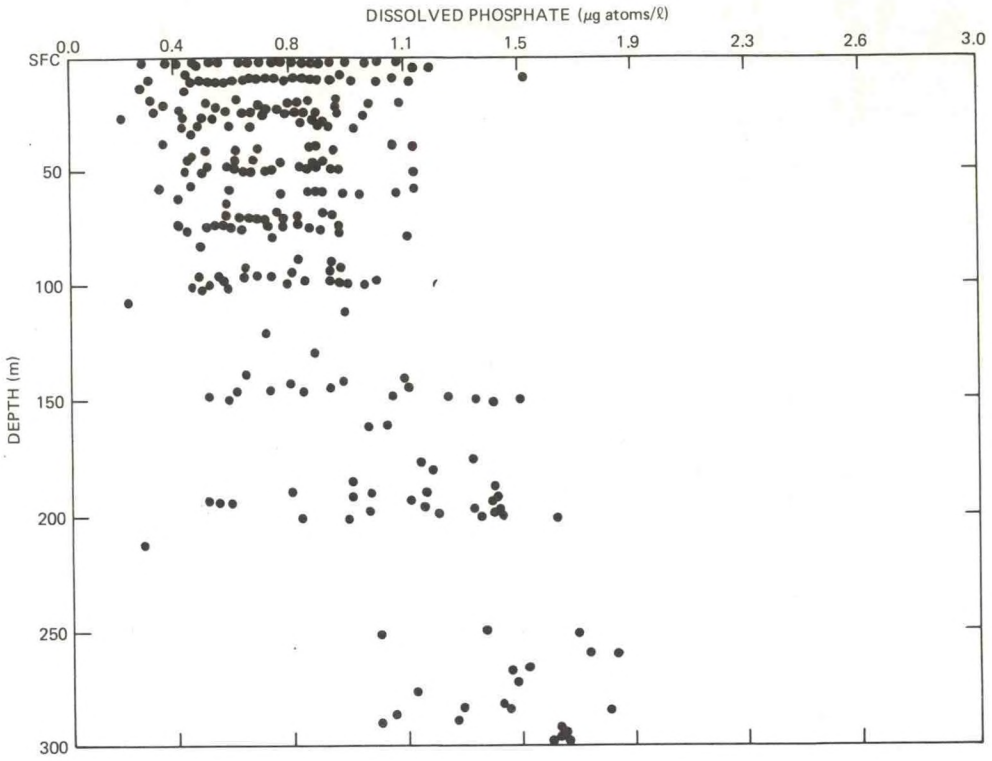


Figure 4.138.--Winter vertical profile of dissolved phosphate, area 9.

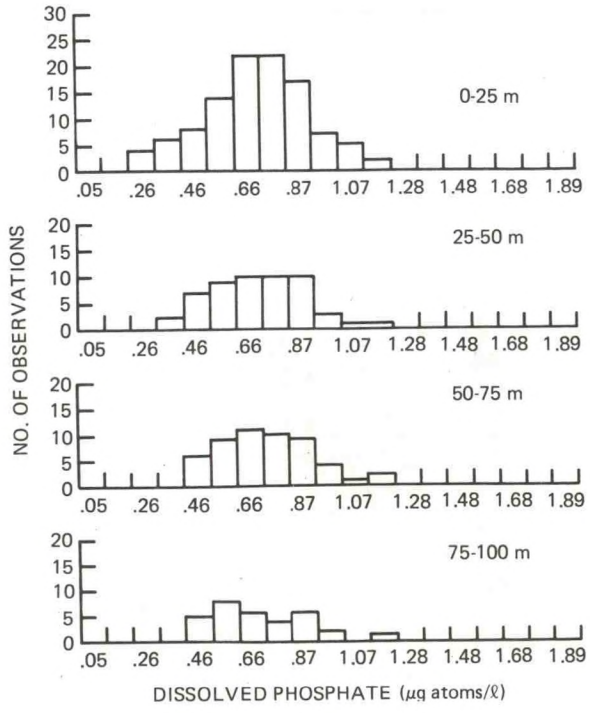


Figure 4.139.--Histograms of winter dissolved phosphate concentration, area 9.

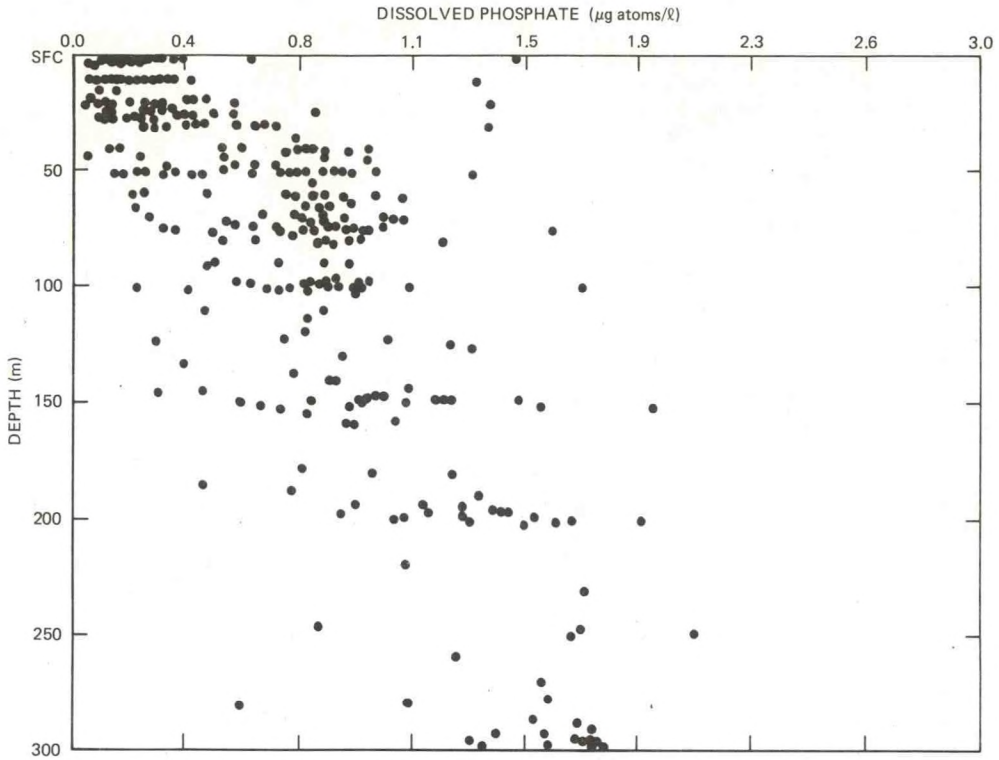


Figure 4.140.--Summer vertical profile of dissolved phosphate, area 9.

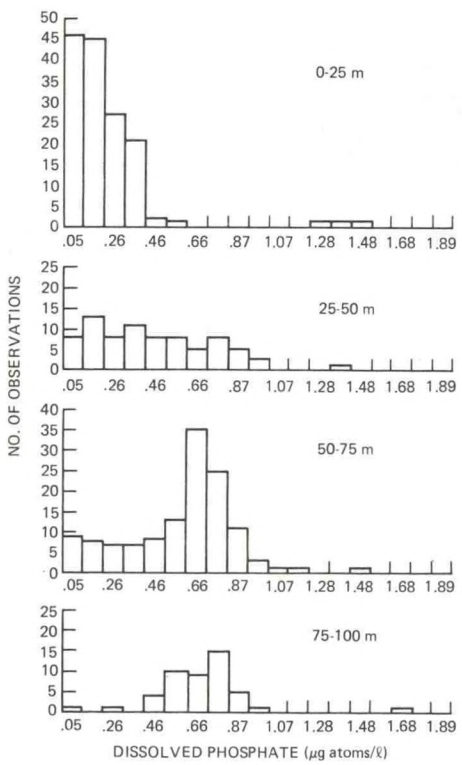


Figure 4.141.--Histograms of summer dissolved phosphate concentration, area 9.

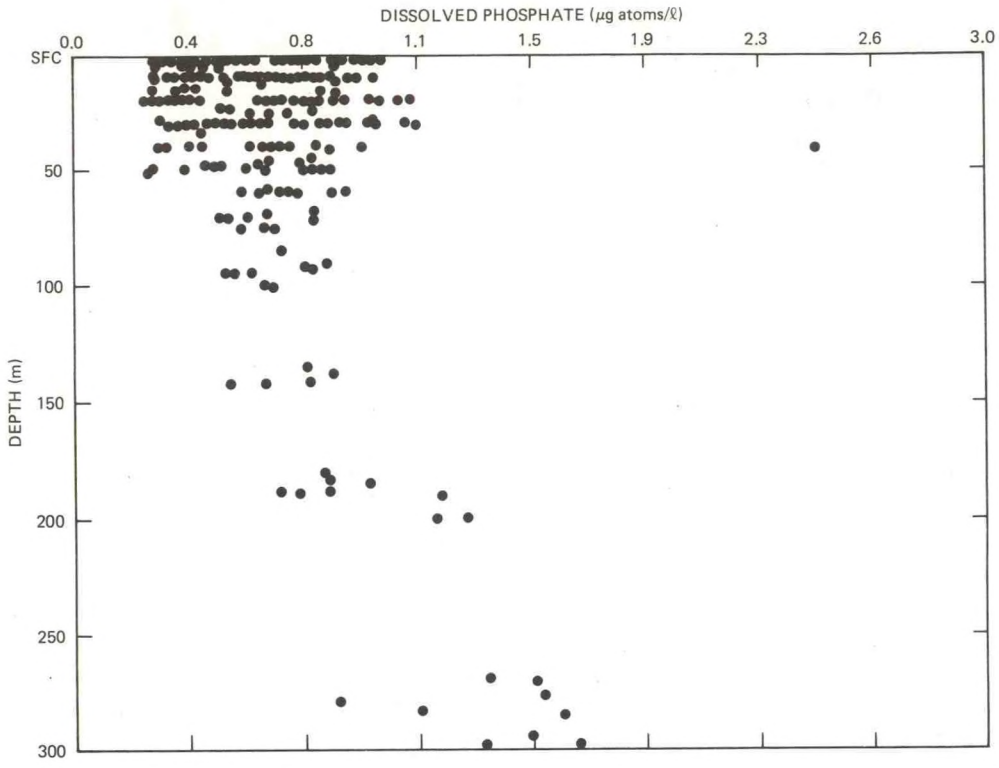


Figure 4.142.--Winter vertical profile of dissolved phosphate, area 6.

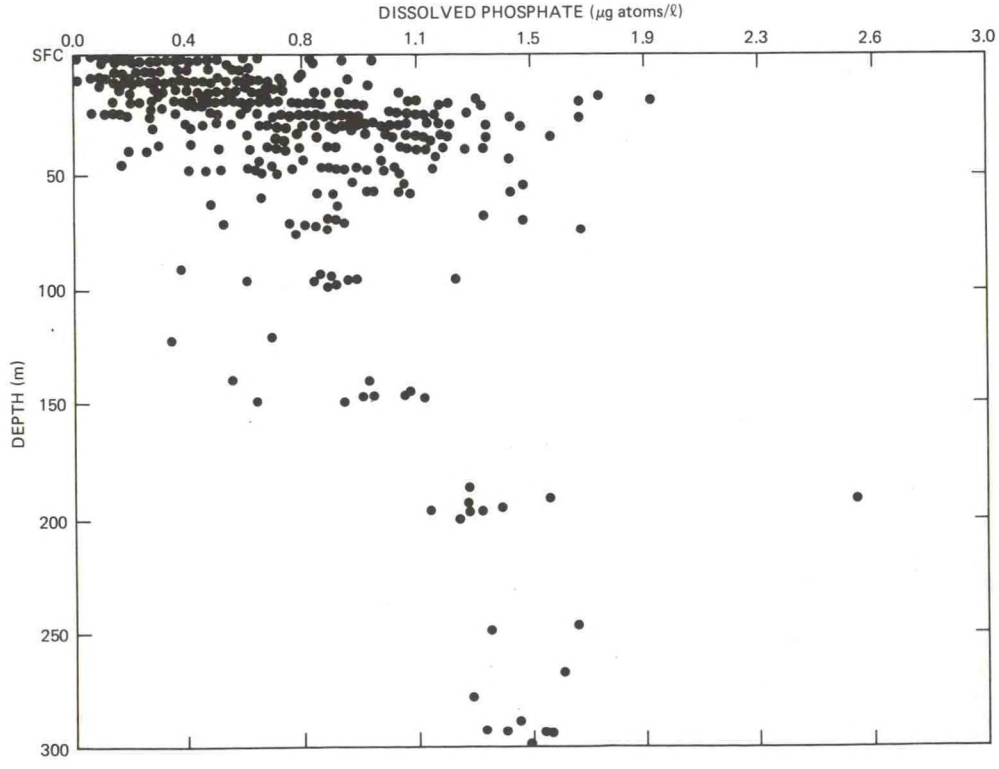


Figure 4.143.--Summer vertical profile of dissolved phosphate, area 6.

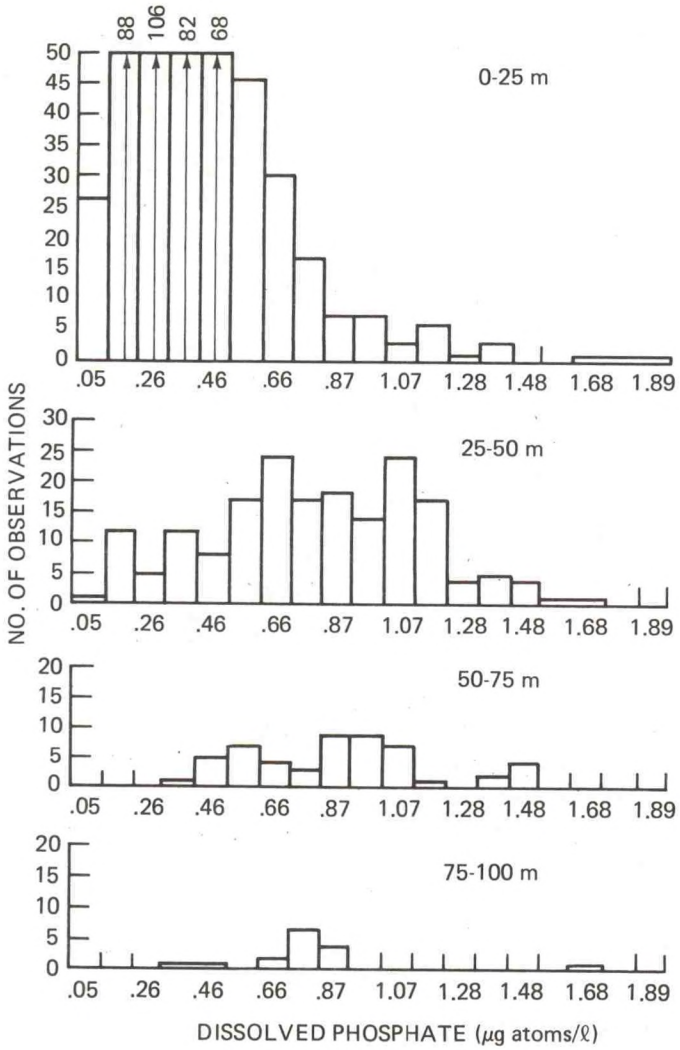


Figure 4.144.--Histograms of summer dissolved phosphate concentration, area 6.

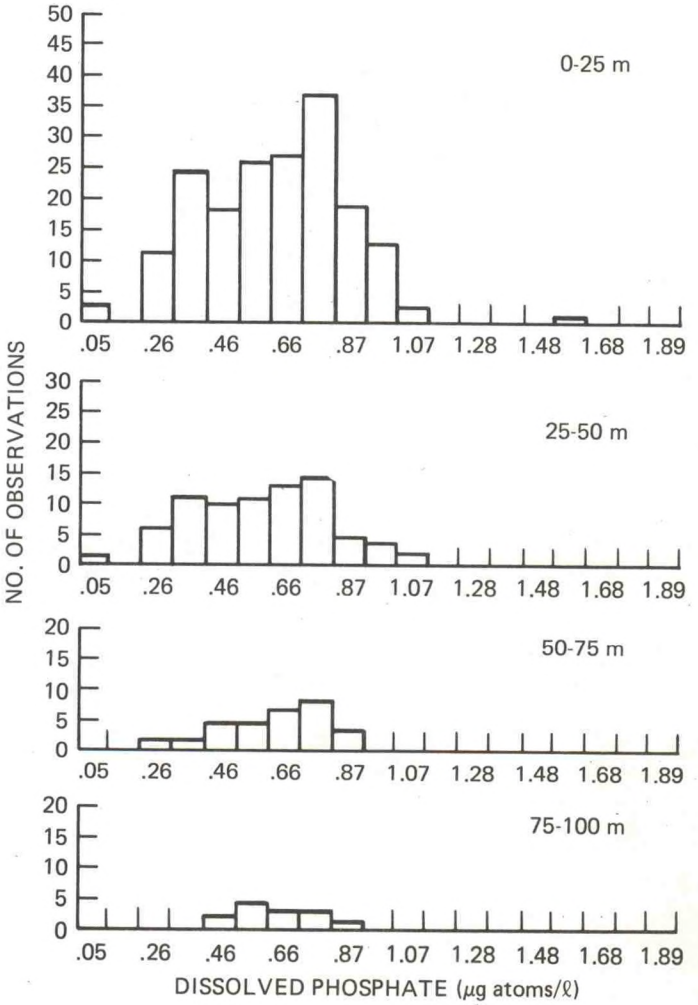


Figure 4.145.--Histograms of winter dissolved phosphate concentration, area 6.

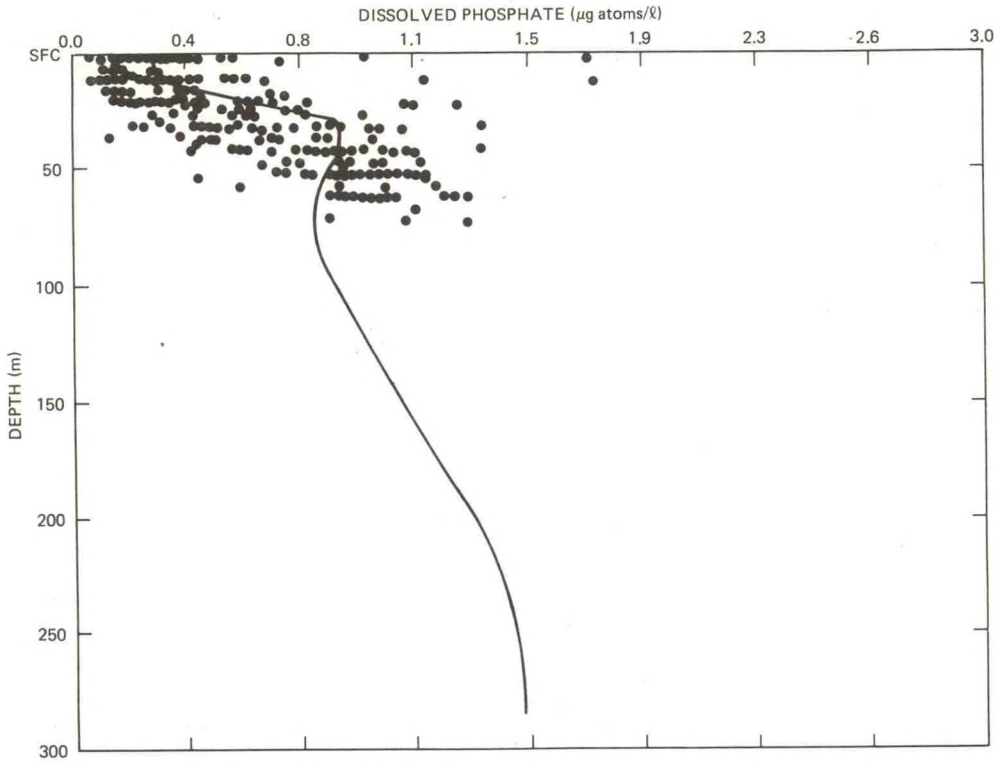


Figure 4.146.--Summer vertical profile of dissolved phosphate, area 6, with summer profile for area 5 shown as solid line.

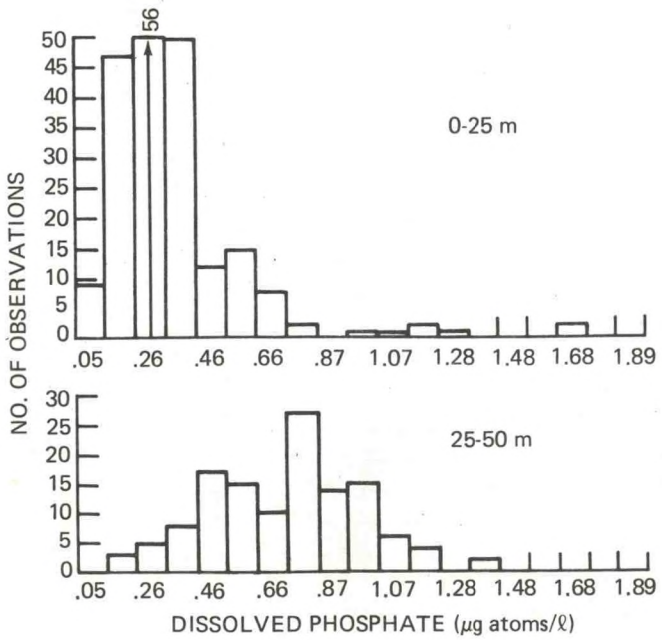


Figure 4.147.--Histograms of summer dissolved phosphate concentration, area 5.

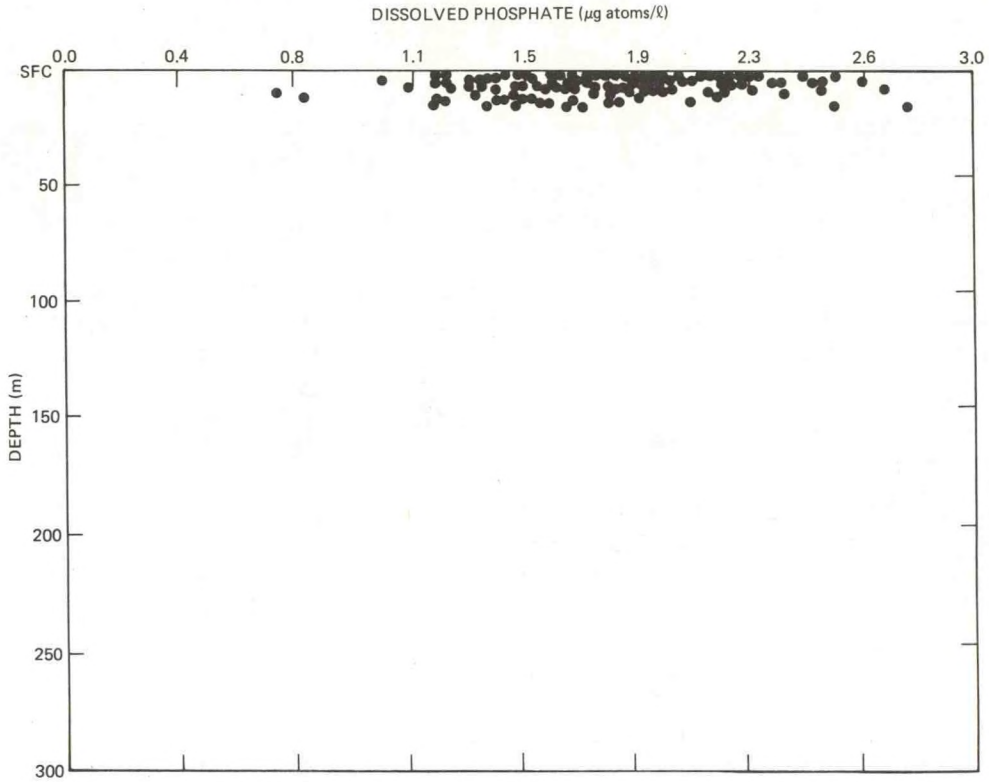


Figure 4.148.--January vertical profile of dissolved phosphate, area 2.

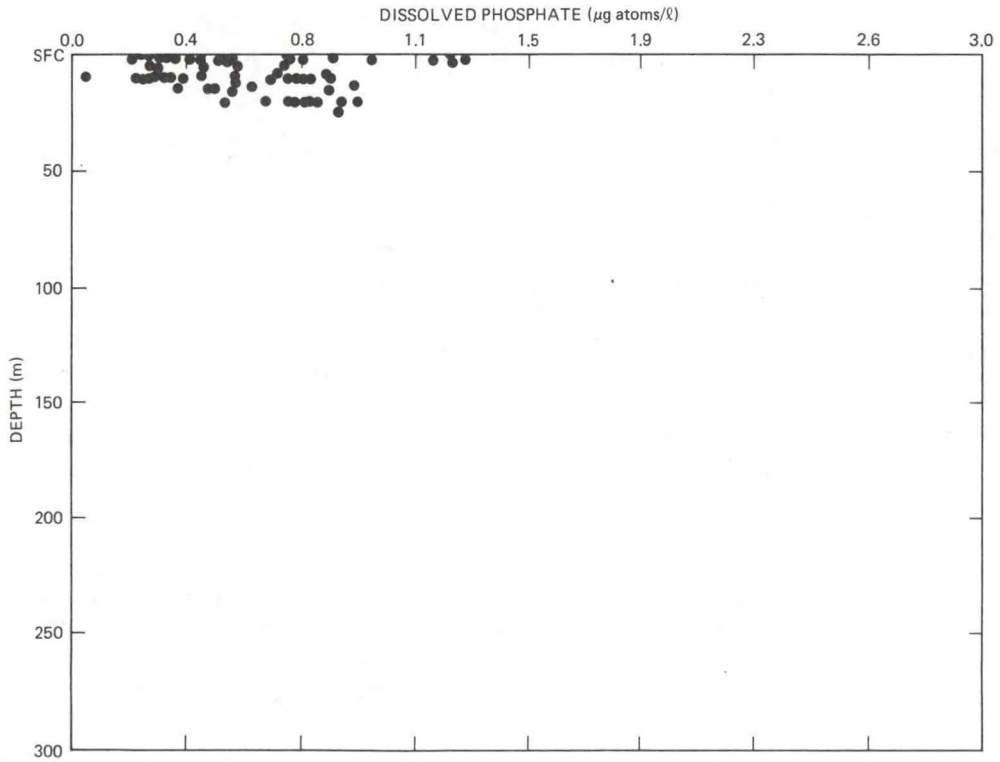


Figure 4.149.--July vertical profile of dissolved phosphate, area 2.

### 4.5.3 Silicate

Silicates enter coastal waters primarily from land runoff and river waters. In deepwater regions, upwelling brings them to the upper layers. Silicates are assimilated by diatoms in the surface layer, and the skeletal material of these organisms, which sinks, redistributes the silicates in the deep water and on the bottom. One would expect, therefore, that in the immediate coastal areas dissolved silicate concentrations would be relatively high, and that the vertical profiles of concentration in the eastern, deepwater areas would show low concentrations near the surface, with general increases in concentration with greater depth below the surface. That this is the case is substantiated by the published literature (Armstrong, 1965; Horne, 1969; Simpson et al., 1975; Amos, 1974).

Silicate concentrations in the areas analyzed in this study show a considerable range in magnitude for monthly periods at all depths, from about 1.0 to 20.0 µg atoms/l in depths to 300 m. Data are sparse, as shown in figure 4.150, with fewer than 50 observations available per area for all depths for any month. The discussion below is therefore limited to general characteristics of the distribution of silicate concentrations.

In figure 4.151, the vertical profile of dissolved silicate concentration in area 9 for July and August shows the general characteristics of a deepwater area. The data are very widely scattered, and insufficient for further analysis. The vertical profile of silicate concentrations in the same area 9 for the winter months (December, January, February) is shown in figure 4.152. The considerable differences between the two profiles is attributed to the uptake of silicates in the surface layers in summer by diatoms and other organisms.

Analysis of dissolved oxygen and phosphate concentration distributions indicated the intrusion of Hudson River water into area 6 and subsequent stratification. Rapid decrease of dissolved oxygen concentration at depths below 50 m, plotted in figure 4.153, shows the presence of a stratification of the water mass, as was noted earlier (sec. 4.5.1). The rapid increase below the same depth in silicate concentration, also plotted in this figure, is probably associated with the stratification, the uptake of silicates apparently causing low concentration in the surface layer.

The poor quality of silicate concentration data available and their sparse distribution prevent further analyses of these data.

### 4.5.4 Nitrate

The nitrate concentration data for the Mid-Atlantic region are also very few, as shown in figure 4.154, and of very poor quality. Monthly plots of nitrate concentration at various depths for each of the 12 oceanographic areas showed that the data values were scattered over at least an order of the magnitude and that fewer than 10 observations were available for several months of the year over the entire water column from surface to bottom. No attempt was therefore made to analyze these data.

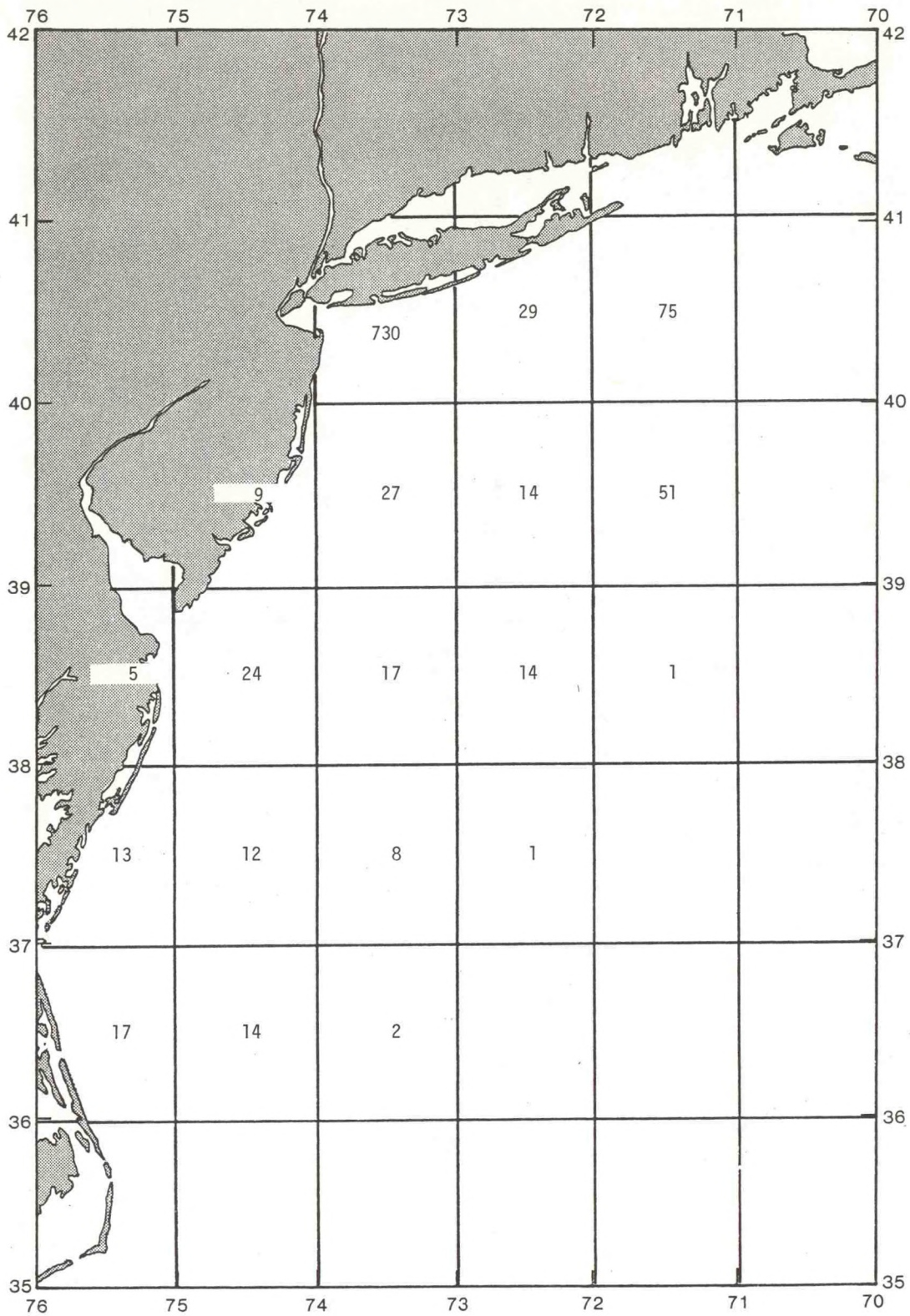


Figure 4.150.--Inventory, by $1^{o}$ squares, of STD data containing silicate measurements.

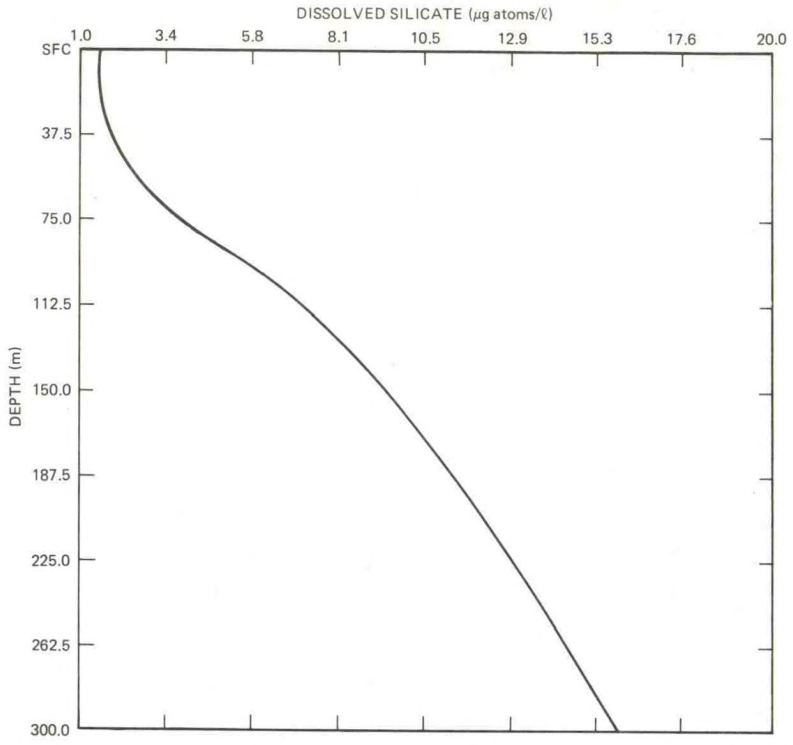


Figure 4.151.--July and August vertical profile of dissolved silicate, area 9.

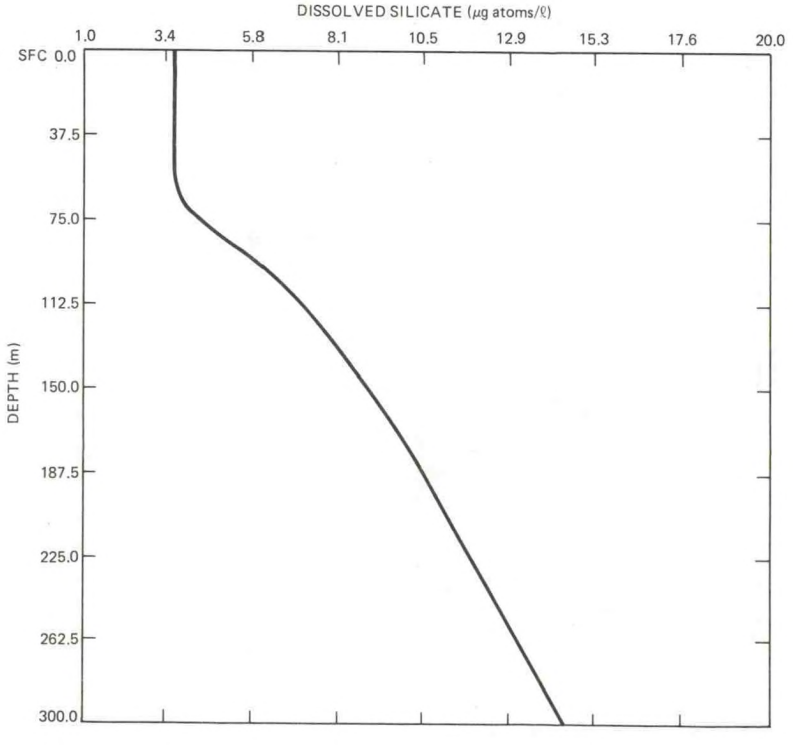


Figure 4.152.--Winter vertical profile of dissolved silicate, area 9.

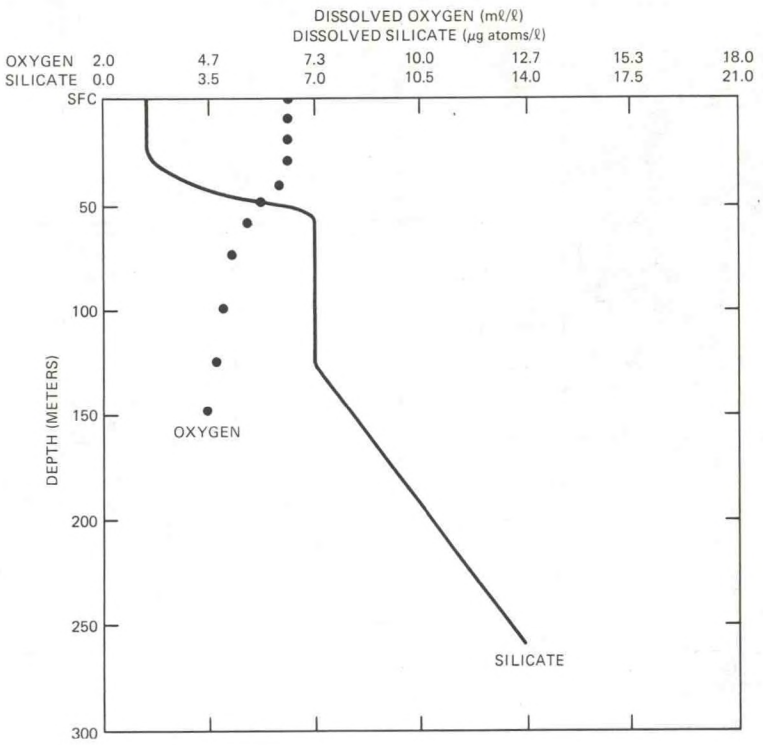


Figure 4.153.--May vertical profiles of dissolved oxygen and silicate, area 6.

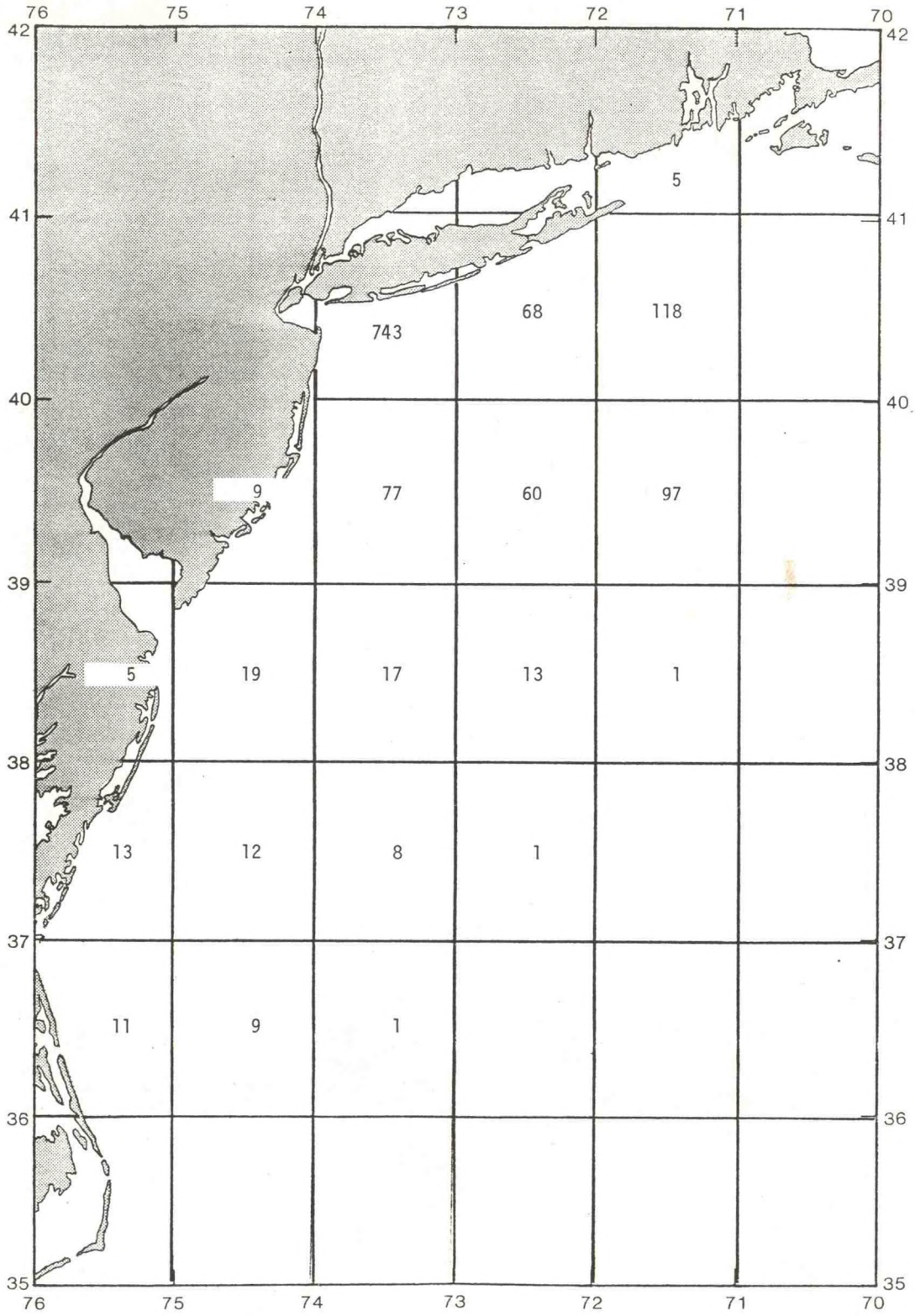


Figure 4.154.--Inventory, by $1^{o}$ squares, of STD data containing nitrate measurements.

### 4.5.5 Summary

Few dissolved oxygen and nutrient concentration measurements are available for the Mid-Atlantic region. To produce a set adequate for analysis, these data were examined in monthly and seasonal groups for each parameter. The range in concentrations found within each group often extended over an order of magnitude, which can be attributed to poor measurements, to the long periods of time over which the data were grouped, and to the wide spatial variation of the variables over the areas studied. Future change in the environment from the baseline concentrations shown here would have to be very large before the significance of new mean conditions could be established.

# 5. CIRCULATION PATTERNS

For this study, general seasonal circulation patterns were derived primarily from ship-drift observations archived at NODC, and from the published literature. The description given below of transient and tidal currents is based primarily on a review of the literature. A few examples of direct measurements are included to illustrate absolute magnitudes and variability of currents that have been observed in the Mid-Atlantic region.

## 5.1 Potentially Important Circulation Features

The question of the relative importance of the mean circulation compared with transient features is discussed in this section, with consideration given to the relative velocities to be expected from mean and transient features and to the evidence available for the existence of these features.

### 5.1.1 Gulf Stream

The existence of the Gulf Stream has been acknowledged since the time of Franklin (1786). This current flows "permanently" toward the northeast at speeds of over 2 kt (100 cm/s) within a band of about 50 km each side of an imaginary axis. Von Arx (1952), using towed electrodes, measured speeds as high as 4.4 kt (220 cm/s) at the surface.

### 5.1.2 Mean Coastal Currents

Shoreward of the Gulf stream, there is a strong velocity shear zone across the shelf-slope water interface. Water east of the front flows northeast, forming the north wall of the Gulf Stream. Water west of the front flows southwest. Neumann (1960) explains this mean coastal current as a compensation current. The shear zone creates an elongated cyclonic gyre of slope water between Cape Hatteras and Nantucket Shoals, separating shelf water from the Gulf Stream during all seasons of the year (Neumann and Schumacher, 1944). Direct current measurements in the slope water at 39°20'N, 70°00'W (site "D") have shown a long-term average surface current on the order of 0.2 kt (10 cm/s) toward the southwest (Beardsley et al., 1976).

There is a large amount of evidence that the "permanent" average flow in the coastal region is southwest at all depths. Extensive studies by Bumpus (1973) of the permanent flow inshore of the 100-m isobath indicate a mean flow on the order of 0.1 kt (5 cm/s) southwest from Nantucket Shoals to Cape Hatteras. During periods of prolonged southwest winds and low runoff, surface currents have been observed flowing northward in summer very near the coast. Bottom currents appear to be much weaker (0.008 to 0.02 kt; 0.4 to 1.0 cm/s) than surface currents south and southwest. A weak seasonal fluctuation in the permanent coastal current results from variations in wind stress and runoff.

### 5.1.3 Anticyclonic Eddies

From one to four large anticyclonic Gulf Stream eddies (Bisagni, 1976; Beardsley et al., 1976) pass through the eastern boundary of the Mid-Atlantic region each year. These eddies rotate clockwise, while their centers move slowly southwest at 0.1 to 0.2 kt (5 to 10 cm/s) along the shelf break. Eddy diameters vary from 100 to 200 km at the surface, and from 70 to 120 km at the 200-m isobath. Speeds within the eddies range from 0.6 to 1.6 kt (30 to 80 cm/s). Most values for the flow fields of these eddies are inferred from the surface temperature fields observed by satellite and aircraft infrared sensors, supplemented by XBT data. Computed geostrophic speeds have been checked by occasional direct drogue current measurements.

Long-term current meter records at 39°20'N, 70°00'W (site "D") indicate considerable energy over periods on the order of 30 days (Beardsley et al., 1976). The cause of these fluctuations is unknown, but they are believed to be attributable to Rossby waves propagating up the continental slope, to Gulf Stream meanders, or to anticyclonic eddies (see app. E).

### 5.1.4 Tides and Meteorologically Forced Transient Currents

Diurnal and semidiurnal tidal currents are weak on the outer continental shelf, but they increase in strength as the shoreline is approached. Current strength is determined largely by bottom topography. Low-frequency fluctuations in the coastal current near the shore appear to be strongly wind-driven (Beardsley and Butman, 1974). The response time of the shelf waters to meteorological transients is believed to be very rapid (Scott and Csanady, 1976). Inertial currents (inertial period = 18.5 hr at 40.5°N) resulting from fast-moving meteorological systems seem not to be reflected in most nearshore current meter records, but they are prominent in current meter data acquired at the shelf break and seaward (Beardsley et al., 1976). Strong meteorologically induced currents can prevail for several days, as in the case of the "northeasters." Under these conditions transport of surface water can be much greater than under meteorologically quiescent conditions (Boicourt and Hacker, 1976).

Comparison of mean current speeds with transient features indicates that the tidal and transient flows are typically an order of magnitude larger than the seasonal mean flow.

## 5.2 Data Used and Method of Analysis

The primary source of data for this study is the Surface Current Data System (SCUDS) file of ship-drift observations at NODC (Waters, 1976). These data are considered to be of high quality, and have been carefully screened for duplication and obvious navigation errors. Not included are observations made under conditions of high winds and waves (winds $\geq$ 33 kt, waves > 12 ft), or when the interval between observations exceeds 12 hr. Set is recorded to the nearest degree true; drift, to the nearest tenth of a knot.

Current meter data from NOAA's Marine Ecosystems Analysis (MESA) Program were obtained on magnetic tape from NODC. These data consist of 10-min averages of current speed and direction at several locations within the area under study.

Although surface and bottom drifter trajectory data are archived at NODC, these data were not analyzed, since the results from drifter studies have been well covered in the literature (e.g., Bumpus, 1973). Statistics compiled from the literature, from the "Gulfstream," a monthly summary issued by NOAA, and from periodic charts, based on satellite and aircraft infrared data, prepared by the U.S. Coast Guard, were used in evaluating eddy intrusions into the Mid-Atlantic region.

### 5.2.1 Ship-Drift Data

Ship drift is the result of the surface current and the action of the wind on the ship's superstructure. It is generally assumed that the wind effect is random and can be eliminated by averaging numerous observations. Since the ship-drift data represent a major source of information on large-scale flow in the Mid-Atlantic Bight, they were examined in some detail. Charts were prepared for the following:

(1) Current velocity vectors.

(2) Current "constancy" ([average velocity vector/average speed] x 100%); see Panofsky and Brier (1965).

(3) Frequency of occurrence and mean current speed by compass quadrant.

(4) Means and standard deviations of north and east current components.

The Applications Design Branch of NODC performed all computations using standard computational formulas.

Summaries of the ship-drift data are available from NODC for various area grids as small as 6-min squares and periods as short as 1 month. To determine the optimum grid for this analysis, partial summaries were obtained for 6-min, ½°, and 1° squares for monthly and seasonal periods. Six-minute summaries produced a noisy surface current field with numerous gaps, especially in the region of the shelf break at the 200-m isobath. One-degree summaries provided stable averages, but much useful detail was lost. These results, and the fact that the typical grid mesh of mean coastal circulation models is on the order of ½°, led to the choice of ½° squares as the optimum spatial grid for the analysis presented here. Similarly, examination of time-averaging scales showed that the monthly summaries contained numerous gaps, making the flow field difficult to interpret even on the ½° scale. Three-month seasonal summaries beginning with winter (January, February, March) were found to be the most appropriate for this study. Monthly summaries of current vectors and speed and direction at ½° resolution are provided in appendix D as supplementary information.

Distribution of the number of ship-drift observations by ½° squares and by season is shown in figure 5.1. The fewest observations, other than at mouths of estuaries, are in the northeast section of the Bight, north of 38°N and east of 73°W. Seasonally, the largest number of observations is in summer and the fewest in fall. In summer, the observations are sufficient for monthly analysis of reasonably stable averages (app. D).

### 5.2.2 Current-Meter Data

The current meter records obtained from NODC were acquired by NOAA's MESA Program Office in 1973-75. They consist of 120 time histories of current speed and direction measured in 10-min increments by Aanderaa current meters RCM-4 and RCM-5 (Patchen et al., 1974). Location and time of each observation are given, but data processing and quality control procedures are not documented in detail. However, Charnell and Mayer (1975) and Patchen et al. (1974) discuss some of the processing and editing procedures used.

For this study, the current meter records were screened for location and length of record, and 18 of the 120 records were identified as being of particular interest. Many of the records were acquired too close to shore to be considered in this study. East (u) and north (v) current components were first computed from the current speeds and directions, and the time histories of the u and v components were plotted and visually scanned for outliers and periods of time when the meter was inoperative. The following statistics were then computed:

(1) Means and standard deviations of the u and v components.

(2) Maximum currents in the north-south and east-west directions.

(3) Individual probability distributions (histograms) of the u and v components, and joint distributions of these components.

(4) Spectral densities of the u and v components.

(5) Coherence and phase of the u and v components.

(6) Autocorrelations and cross-correlations of the u and v components.

An analysis of these data is presented in section 5.4.

## 5.3 Analysis of Ship-Drift Data

The results of seasonal analysis of surface currents from ship-drift data are presented in this section. Mean seasonal surface currents derived from these data are compared with results from surface-drifter studies and direct current measurements, and comparisons are also made with published sources of historical mean current in the Mid-Atlantic region.

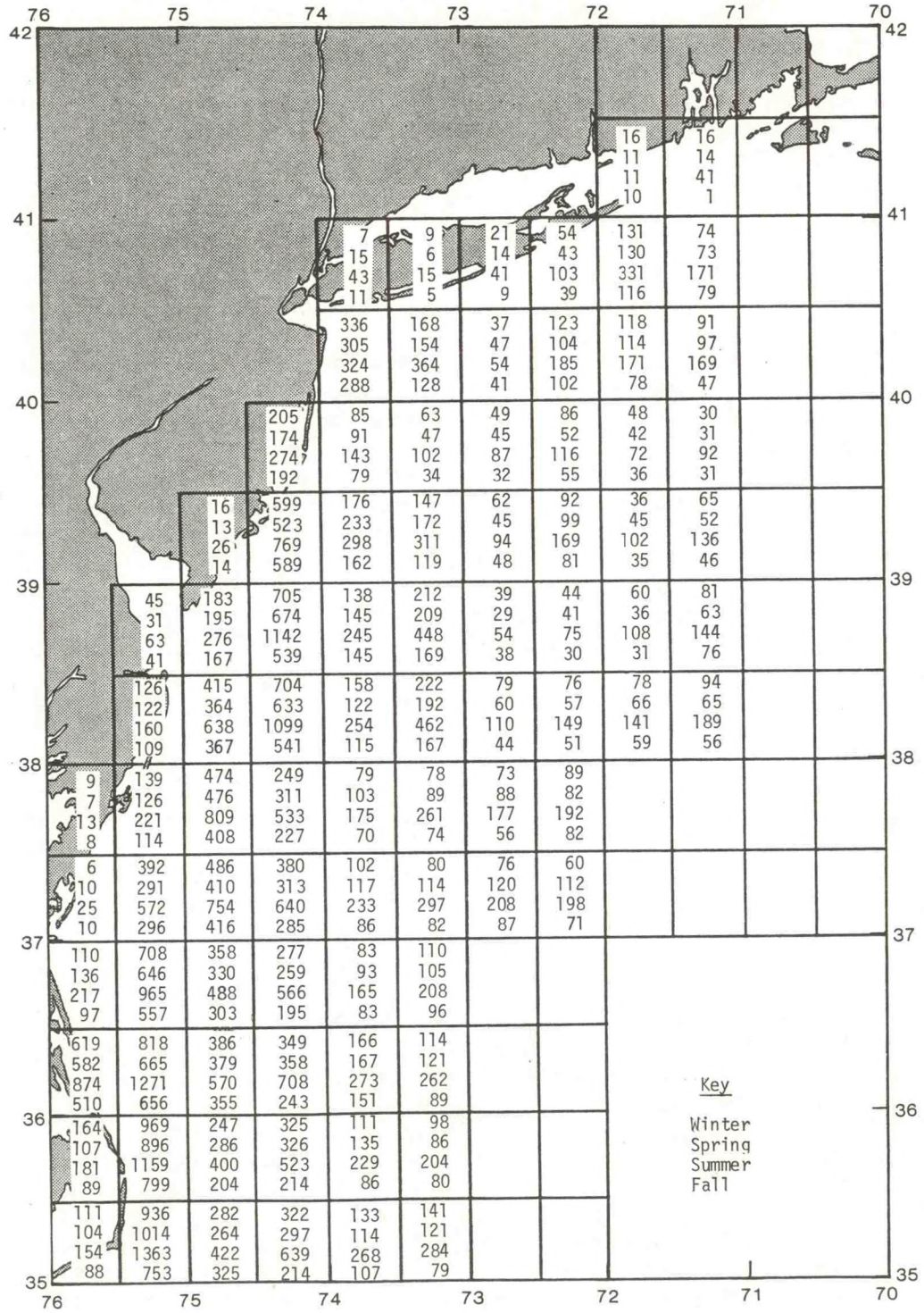


Figure 5.1.--Inventory of ship-drift observations.

### 5.3.1 Surface Currents Derived From Ship-Drift Data

Seasonal surface current vectors are presented in figures 5.2 to 5.5. Figure 5.2 clearly shows the well-documented mean southwest flow over the shelf (e.g., Bumpus, 1973), the turn to seaward just north of Cape Hatteras, and the northward flow seaward of the 200-m isobath along the northern edge of the Gulf Stream. Typical mean speeds are 0.1 kt (5 cm/s).

A striking feature in figures 5.2 to 5.5 is the lack of strong seasonal variability in the currents, except near the mouths of estuaries. In winter the primary driving force is the wind stress from the northwest, while in summer it is the cross-shelf pressure gradient generated by the outflow of low-salinity water from the mouths of estuaries, as pointed out in earlier studies by Bumpus (1973). More recent studies based on direct current measurements (e.g., Beardsley et al., 1976) show less seasonal variability than had been previously found, which may provide indirect support for the hypothesis advanced by Stommel and Leetmaa (1973) and Csanady (1976) that a long-shore pressure gradient possibly impressed by the large-scale ocean circulation is a driving force for the circulation on the shelf in all seasons. Sturges (1977) notes, however, that data from tide gages show that the slope may be very small in summer, although geodetic leveling cannot yet confirm results of oceanographic leveling.

The slight seasonal decrease in current strength during summer inferred from the ship-drift data is probably due to the prevailing southwest winds opposing the "coastal circulation" created by the distribution of the mass field and the longshore pressure gradient. It could, on the other hand, indicate a bias in the data, because the mean winter wind is codirectional with the residual current, whereas the mean summer wind opposes the current. The summer winds could exert forces on the superstructures of the observation vessels, causing displacements not due to current and thus result in errors in ship position (and hence current estimates) that would not be removed in seasonal averaging.

One difference between the results from the ship-drift data and from earlier drift-bottle studies and current meter observations (Beardsley and Flagg, 1975) is the absence of a discernable increase in current strength with distance from the coast. Another feature not evident in the ship-drift data is the current reversals close to shore, possibly because ships nearing port often make large course and speed changes that are not properly documented.

The current "constancy" was calculated to establish whether the relatively weak mean currents shown on the charts for the middle and northern part of the gyre are really weak but consistent currents, or whether the small mean values are primarily the result of highly variable current direction. The constancy value is the ratio, in percent, of the mean vector average of the current speed to the mean scalar average of the speed, i.e., a current that always flows in the same direction would have a constancy of 1, while a current of random direction would have a constancy approaching 0. The calculated values for each season are shown in the isopleths in figures 5.6 to 5.9. The areas of highest constancy are seen

in the southeastern part of the region along the northern edge of the Gulf Stream, and in the midshelf region, especially in the southern half of the area. Along the shelf break is an area of low constancy, i.e., high variability in current direction. There is little apparent seasonal variation in constancy.

Current variability along the shelf break can be seen in more detail in figures 5.10 to 5.13, where the distribution of data values is plotted by quadrant of the compass. Mean current speeds over the shelf break are generally as high as on the shelf. Directions over the shelf break are highly variable, which is to be expected since the shelf break region is frequently traversed by anticyclonic eddies passing southward (Bisagni, 1976). Current is also seen to be highly variable in the coastal region just south of Long Island, as has been reported in the literature (Charnell and Mayer, 1975). Note, however, that the shelf break and Long Island areas contain a relatively small number of observations.

Current variability is also illustrated in figures 5.14 to 5.17, which show the means and standard deviations of the east (u) and north (v) components of surface current. In almost all areas and seasons, standard deviations are as large or larger than the means, in some cases by almost an order or magnitude.

In an effort to examine the errors and biases in the ship-drift data, a technique developed for generating offshore wind climatology from coastal land stations (sec. 3.1.2.4) was applied to the surface wind data to determine whether ship-drift statistics can be predicted from shore-station surface wind statistics. Results were inconclusive, and the quality of the data was therefore evaluated by comparison with published atlases and direct current measurements.

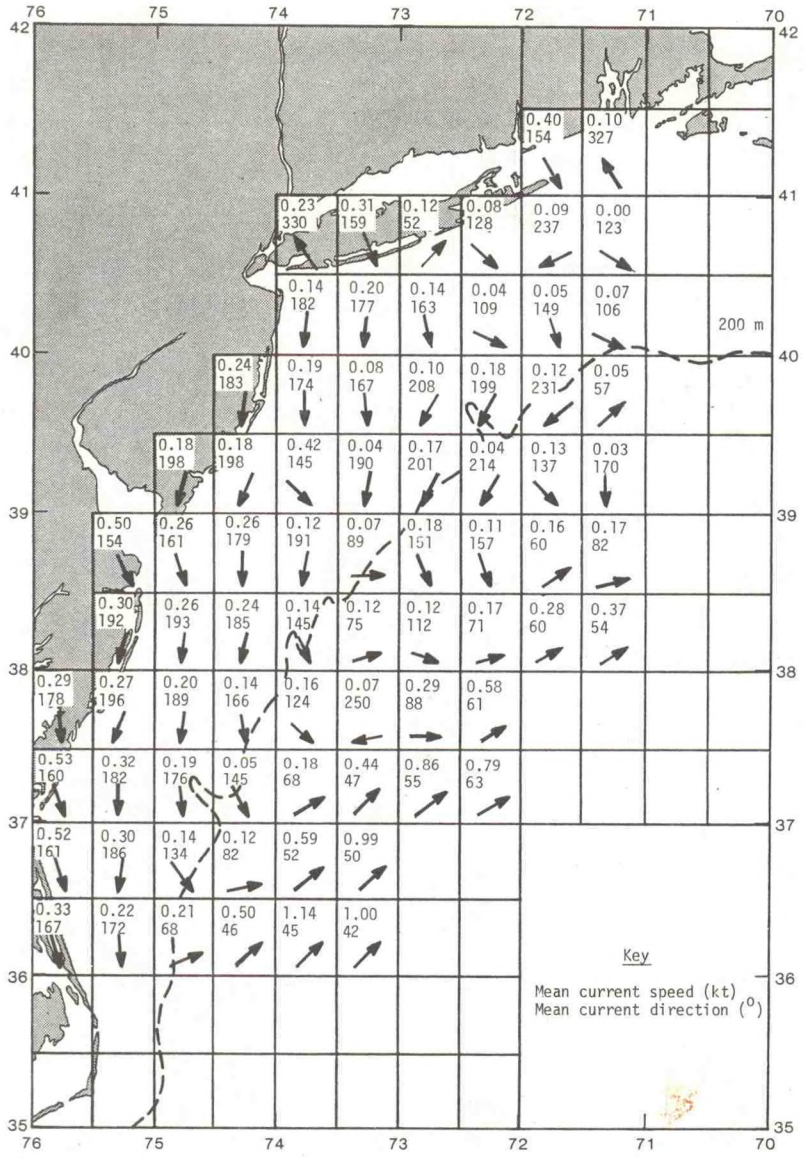


Figure 5.2.--Winter current vectors.

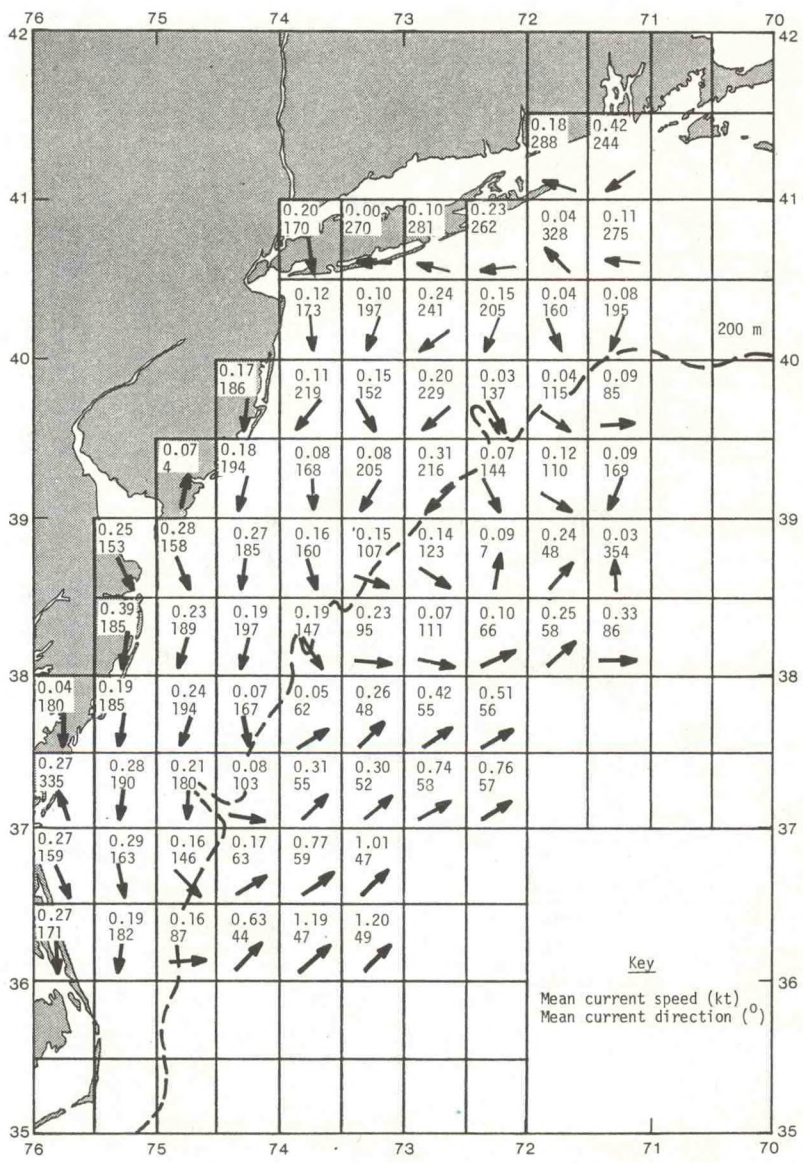


Figure 5.3.--Spring current vectors.

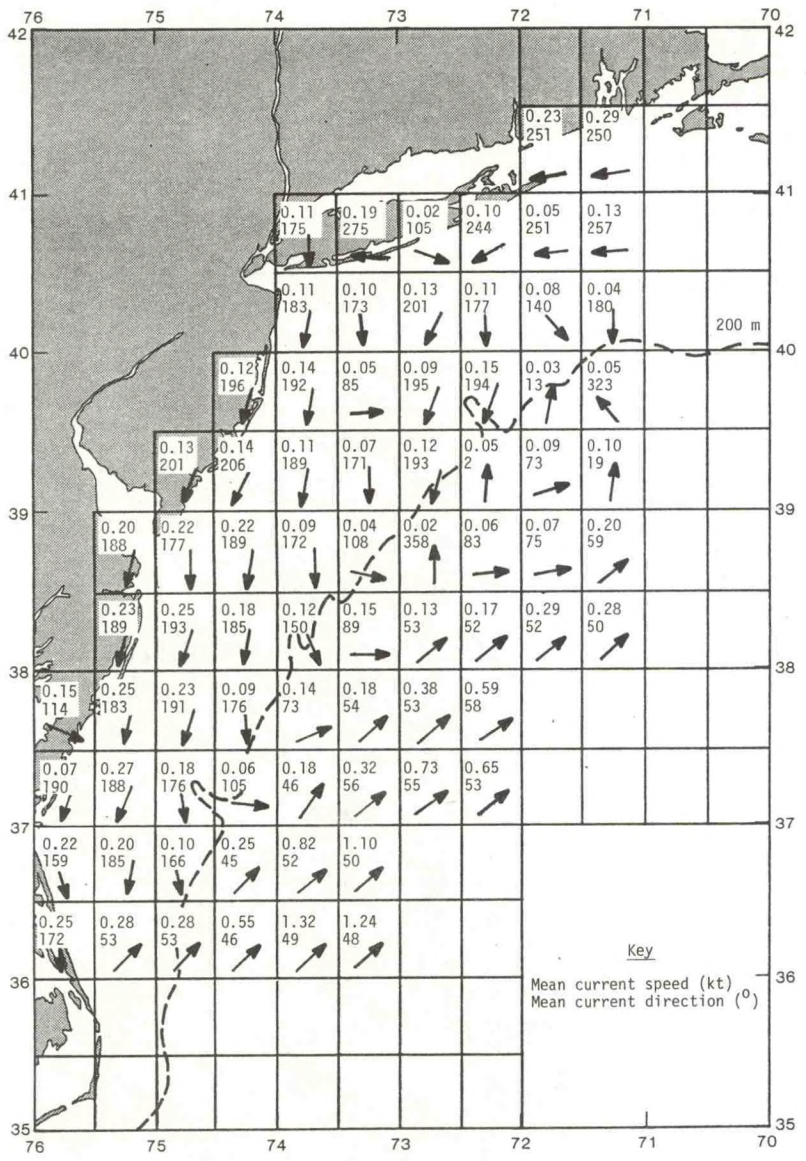


Figure 5.4.--Summer current vectors.

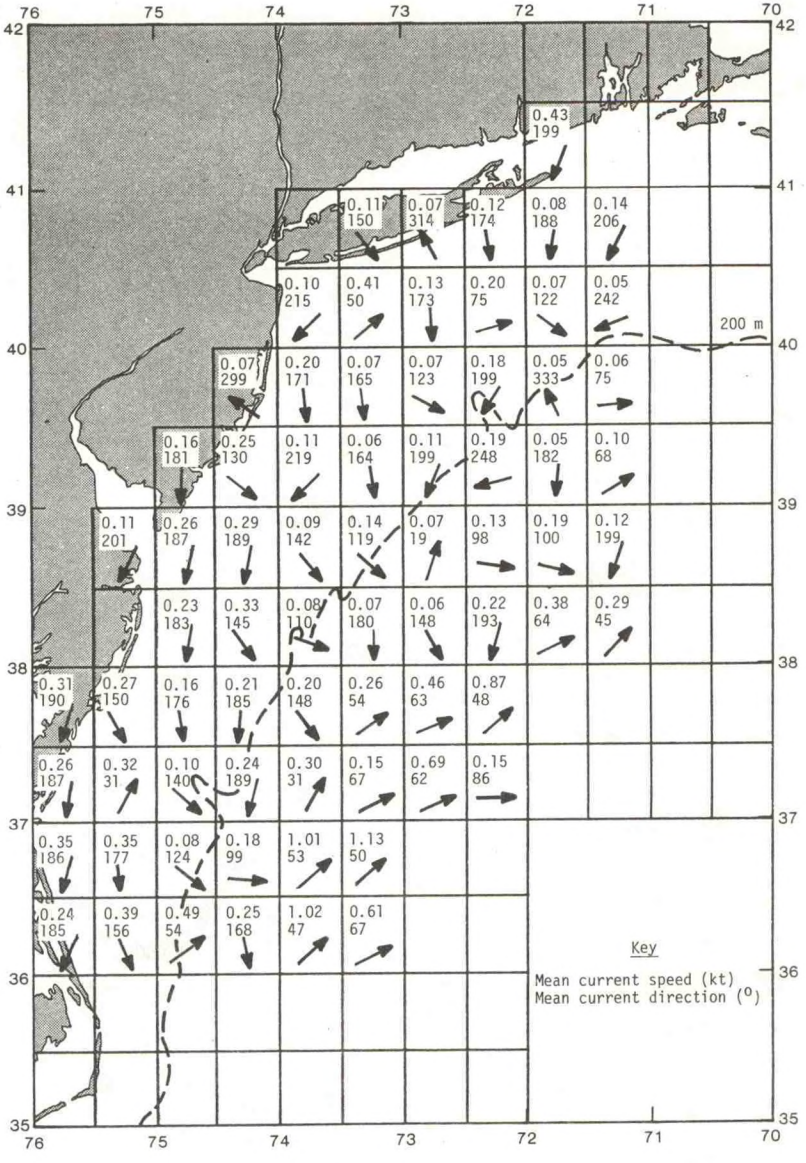


Figure 5.5.--Fall current vectors.

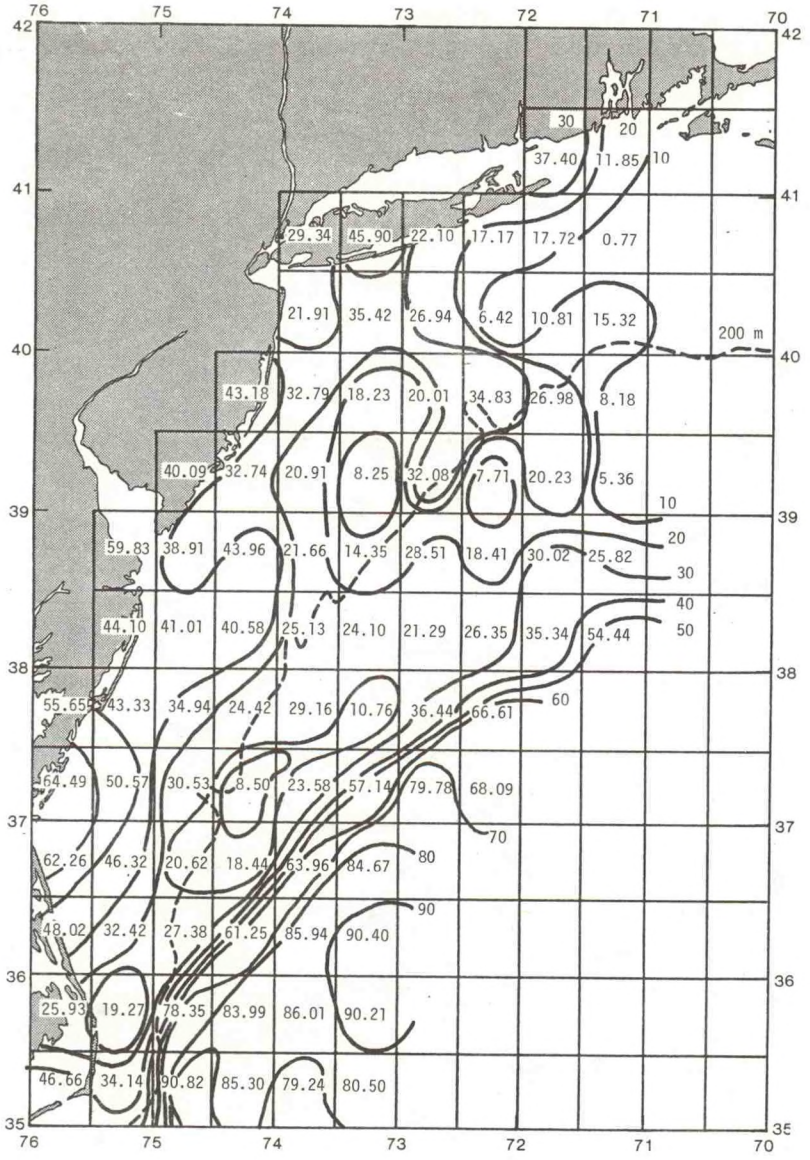


Figure 5.6.--Winter mean current constancy (%).

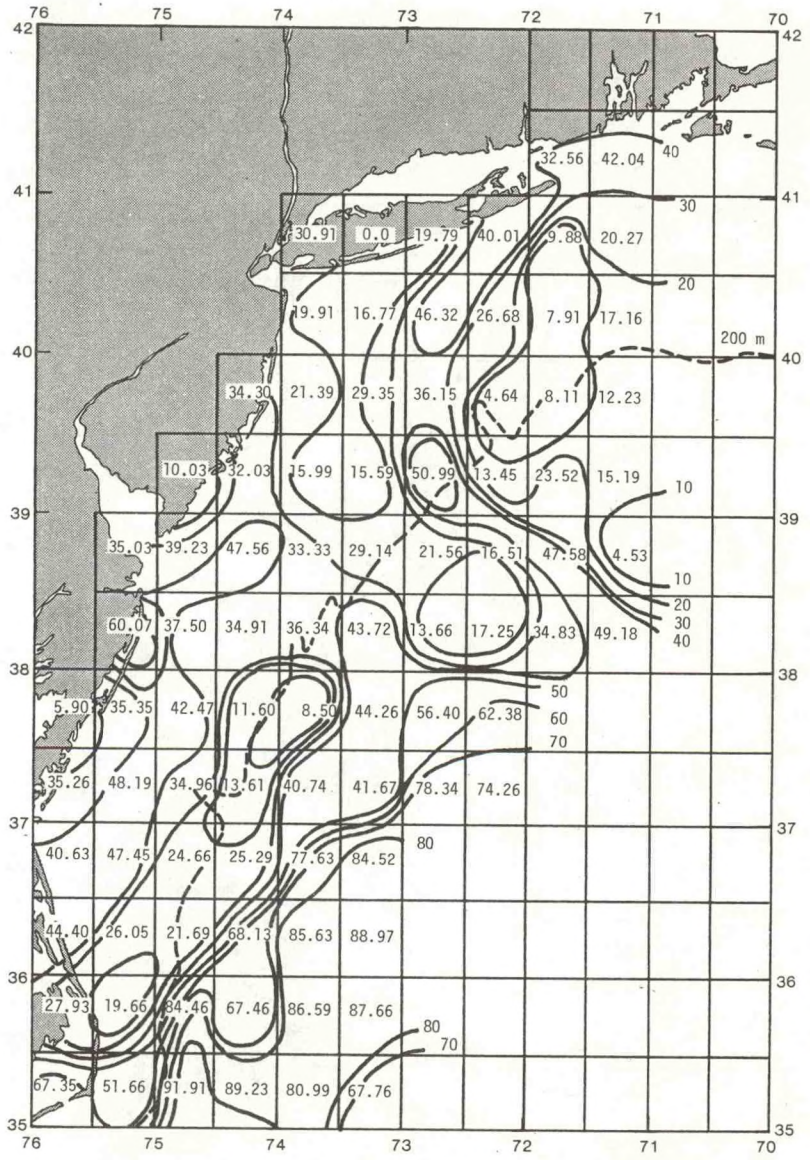


Figure 5.7.--Spring mean current constancy (%).

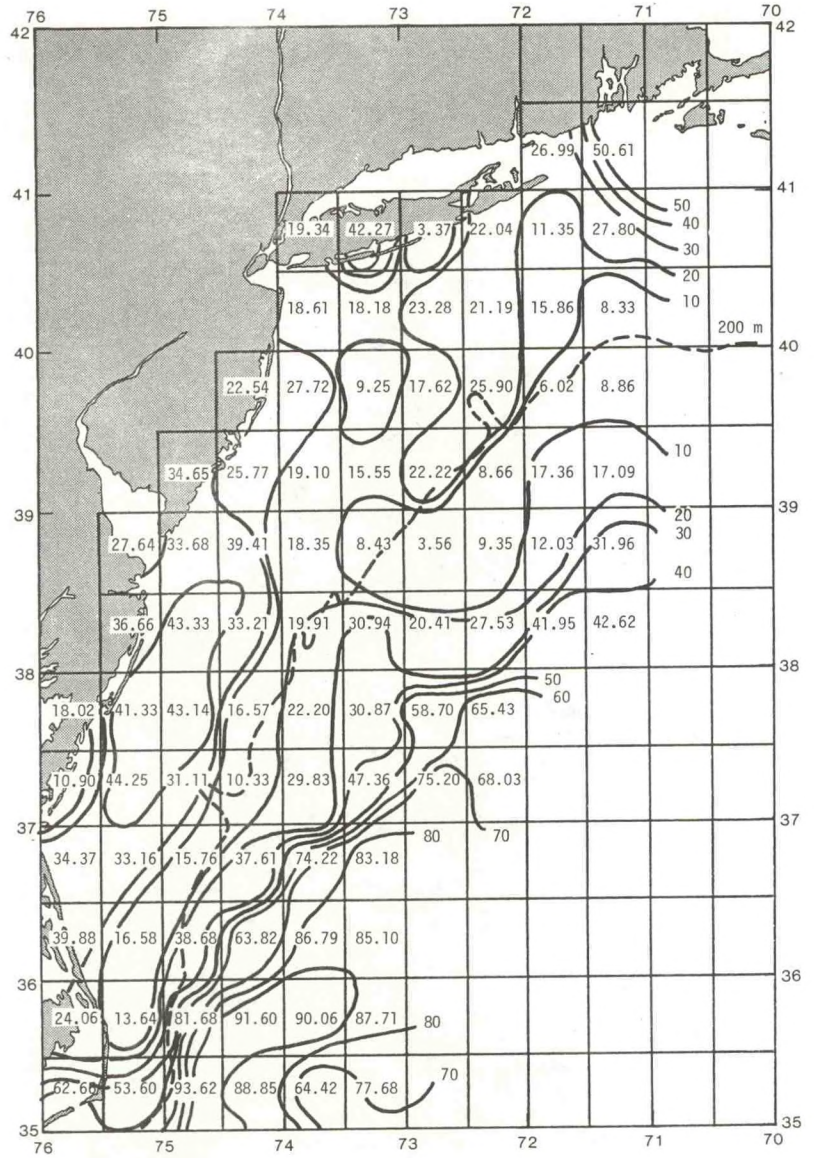


Figure 5.8.--Summer mean current constancy (%).

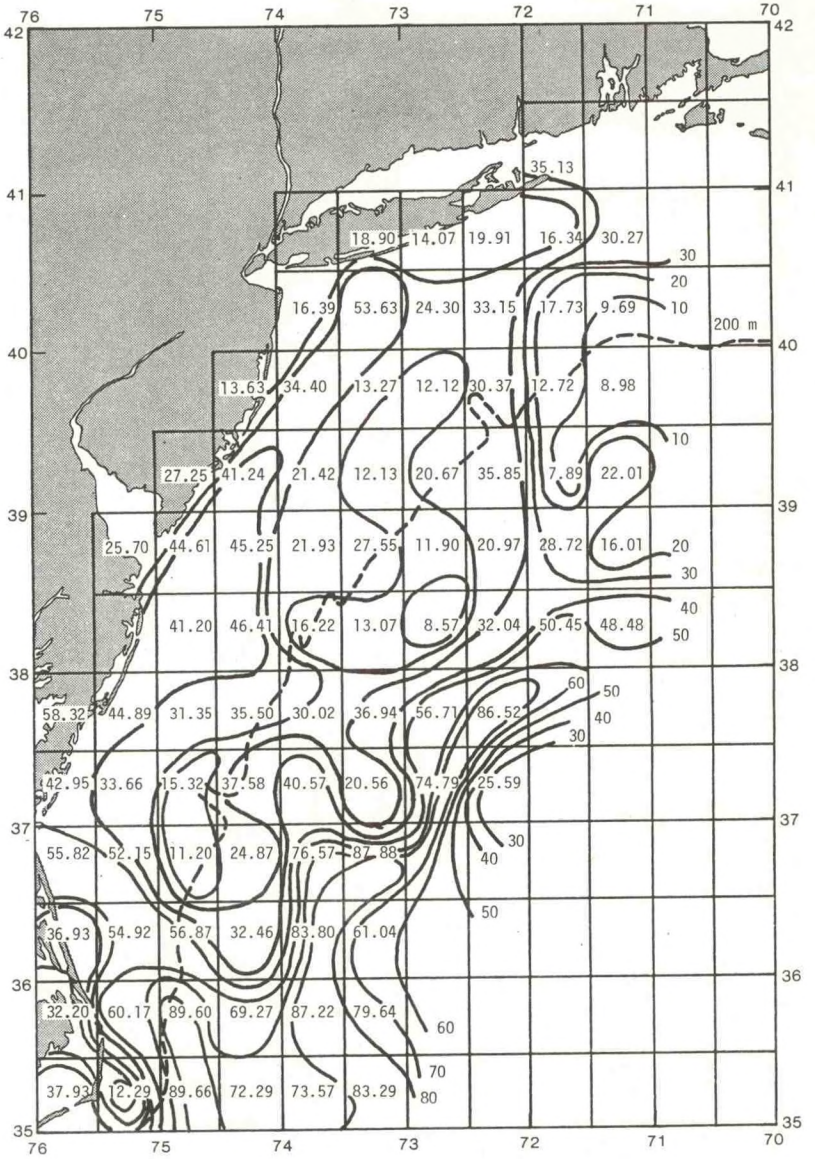


Figure 5.9.--Fall mean current constancy (%).

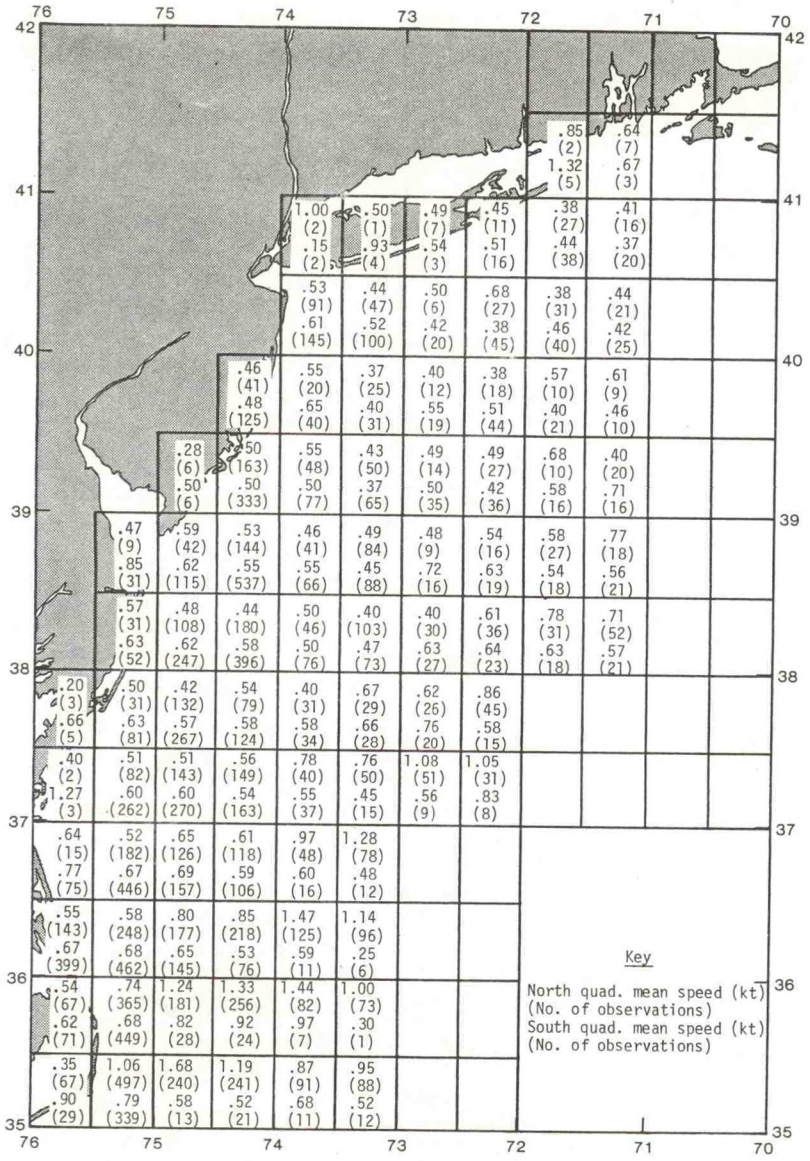


Figure 5.10a.--Winter mean sea-surface current speeds, north and south quadrants.

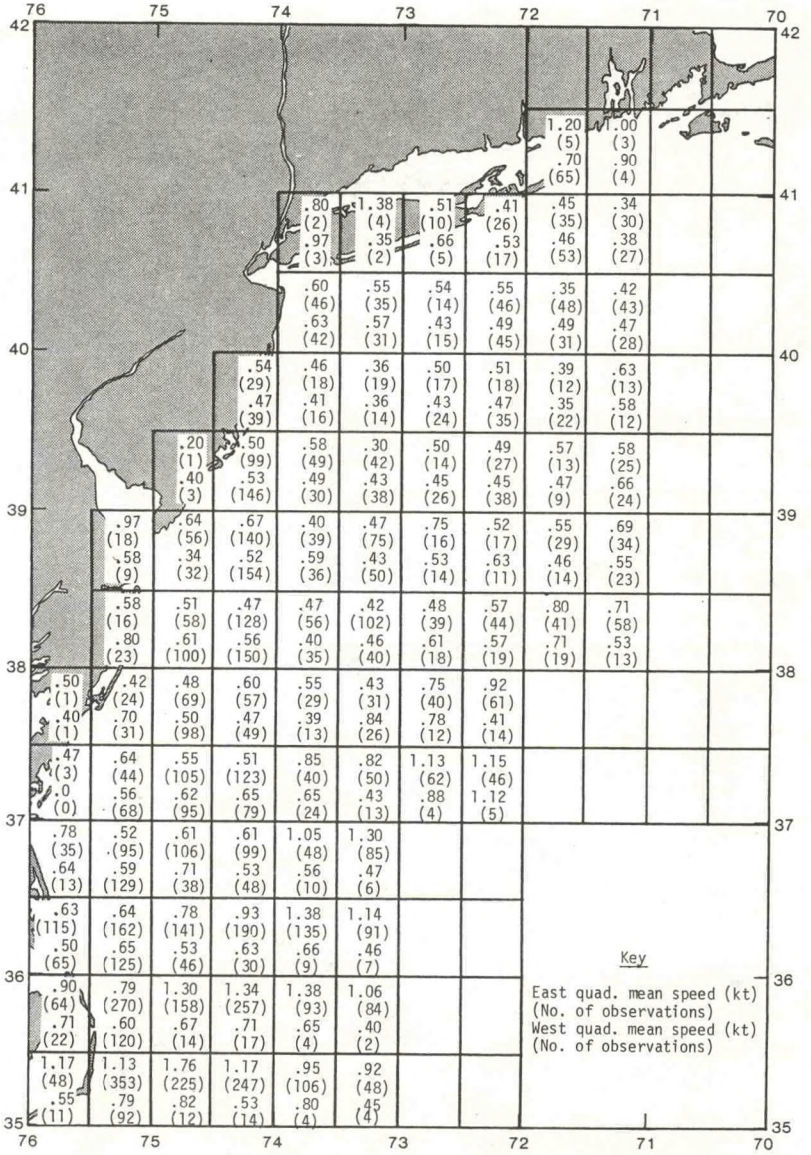


Figure 5.10b.--Winter mean sea-surface current speeds, east and west quadrants.

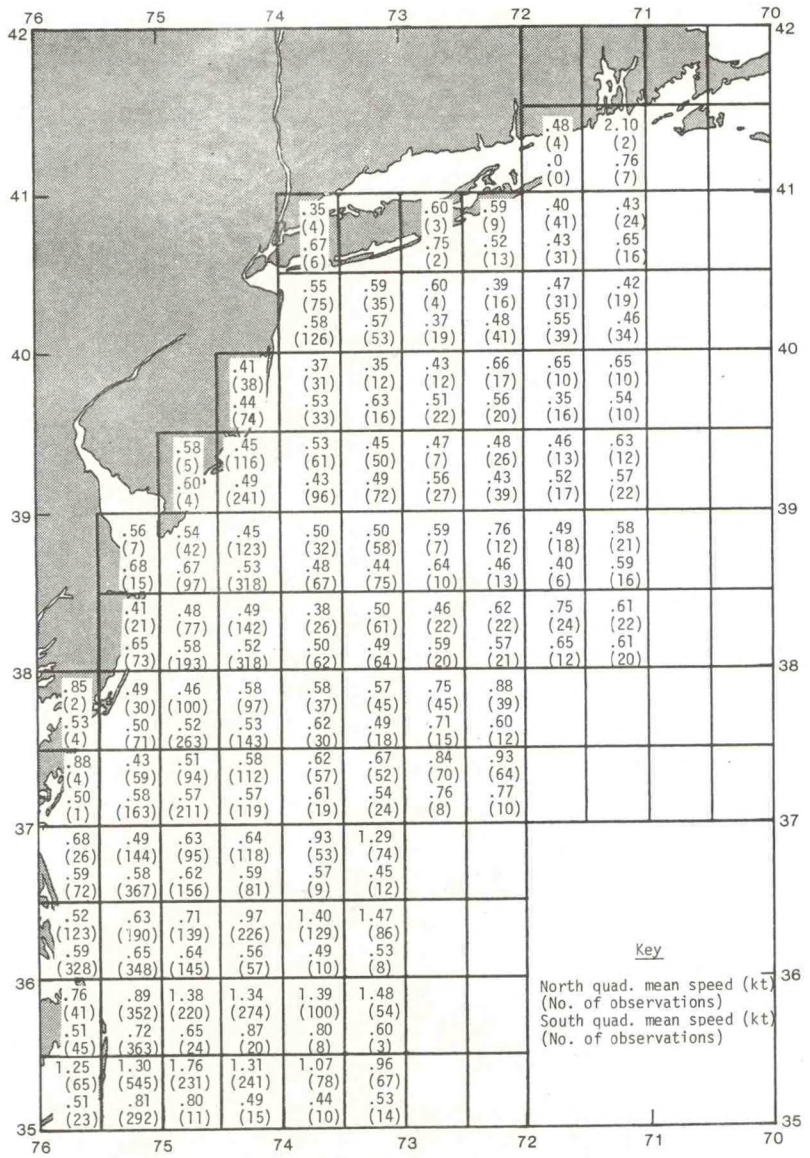


Figure 5.11a.--Spring mean sea-surface current speeds, north and south quadrants.

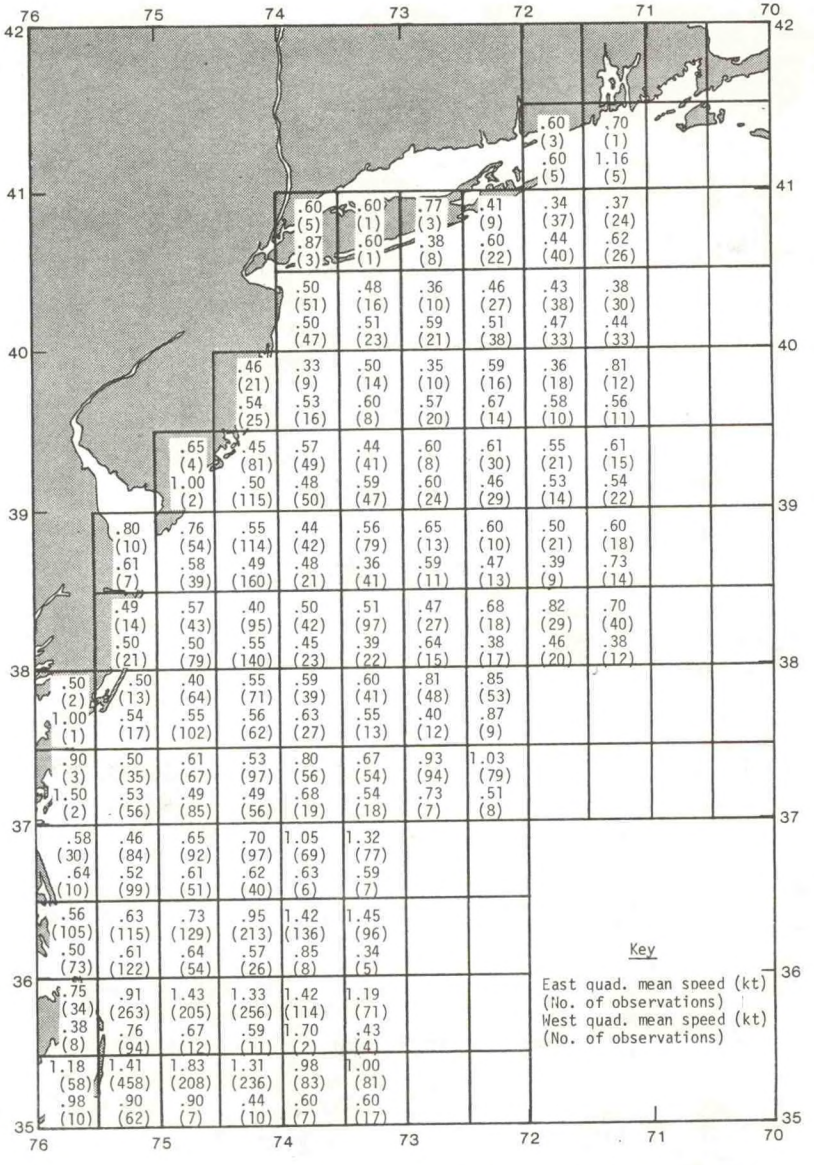


Figure 5.11b.--Spring mean sea-surface current speeds, east and west quadrants.

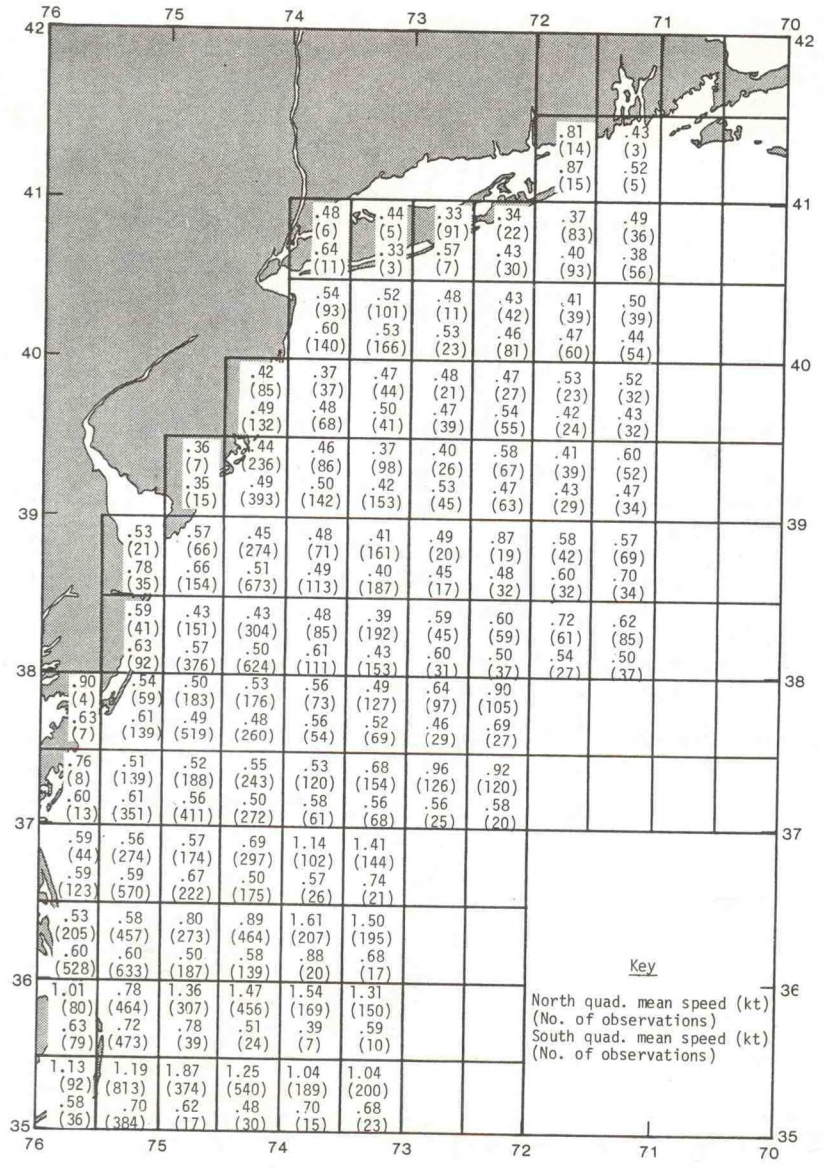


Figure 5.12a.--Summer mean sea-surface current speeds, north and south quadrants.

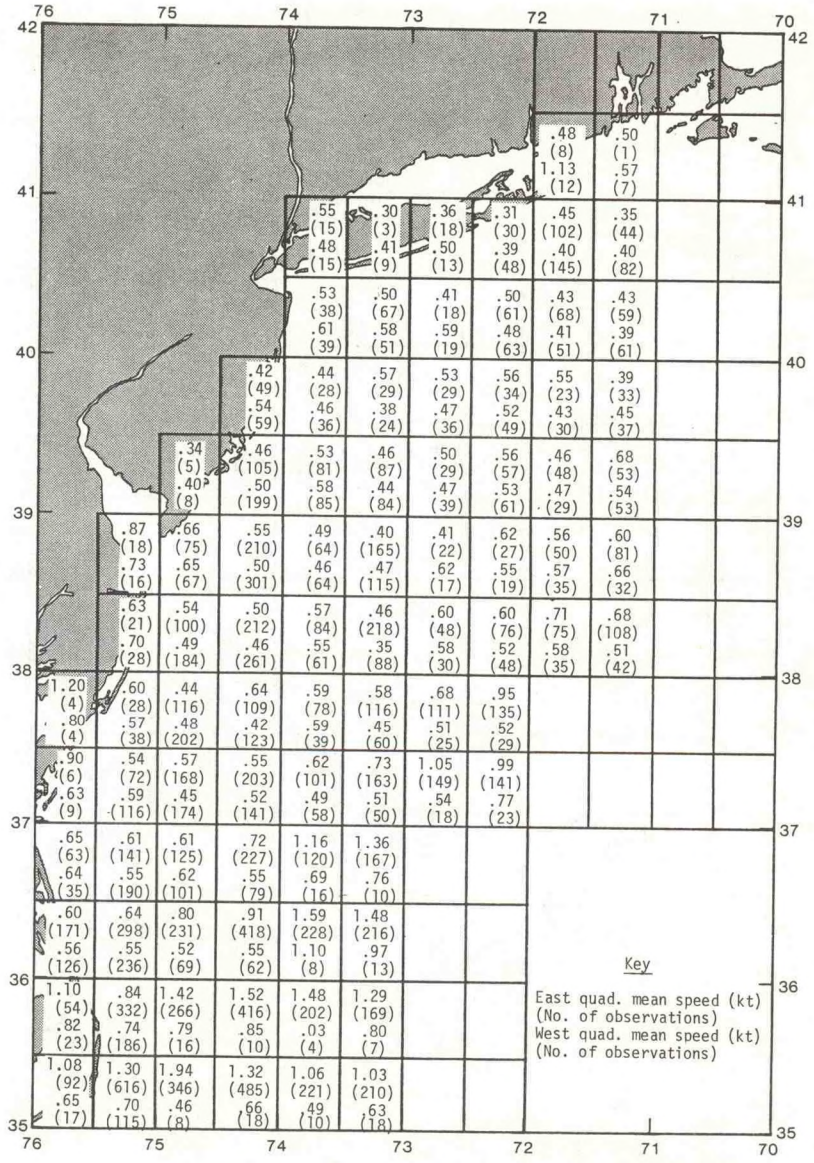


Figure 5.12b.--Summer mean sea-surface current speeds, east and west quadrants.

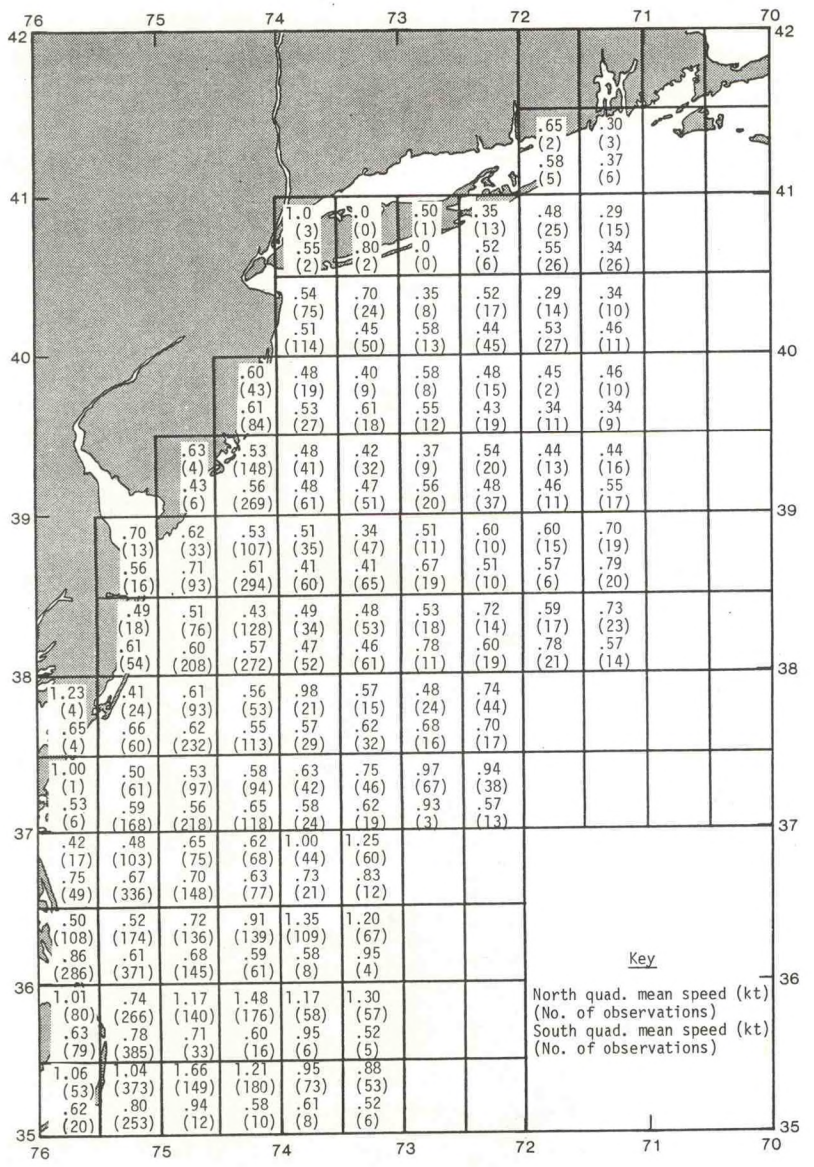


Figure 5.13a.--Fall mean sea-surface current speeds, north and south quadrants.

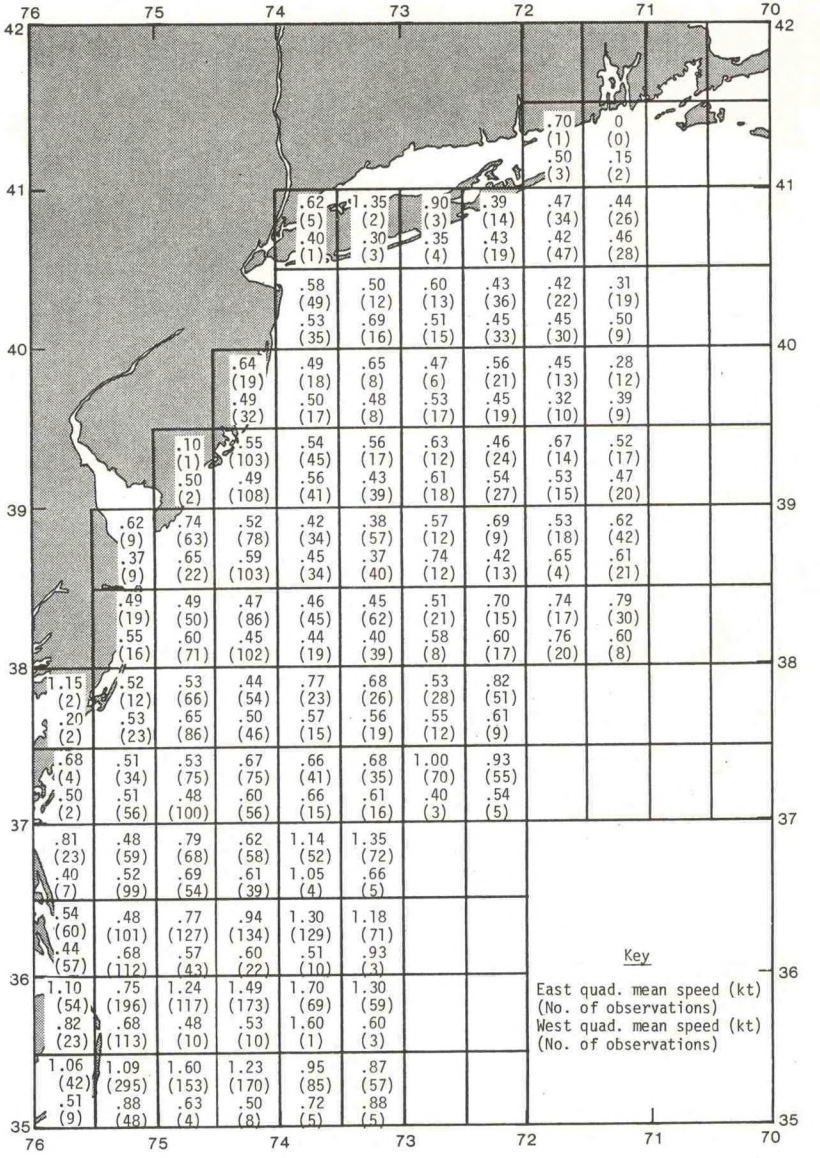


Figure 5.13b.--Fall mean sea-surface current speeds, east and west quadrants.

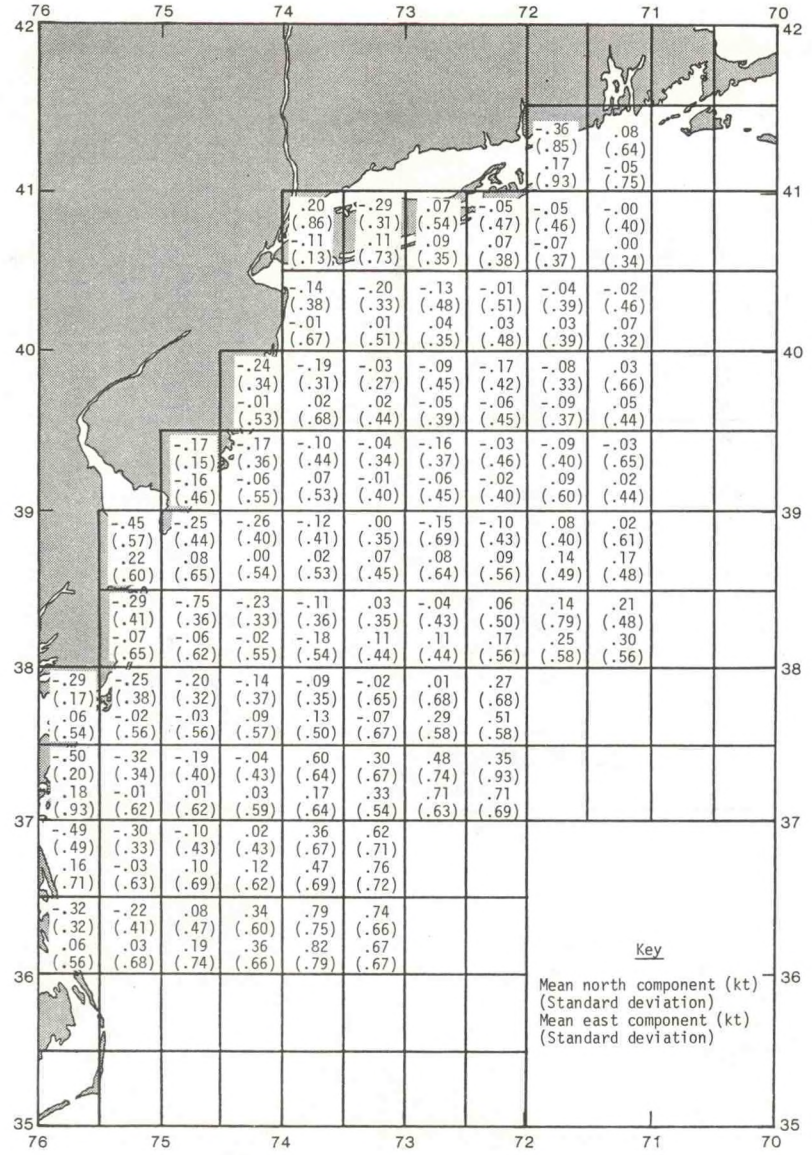


Figure 5.14.--Winter means and standard deviations of sea-surface current.

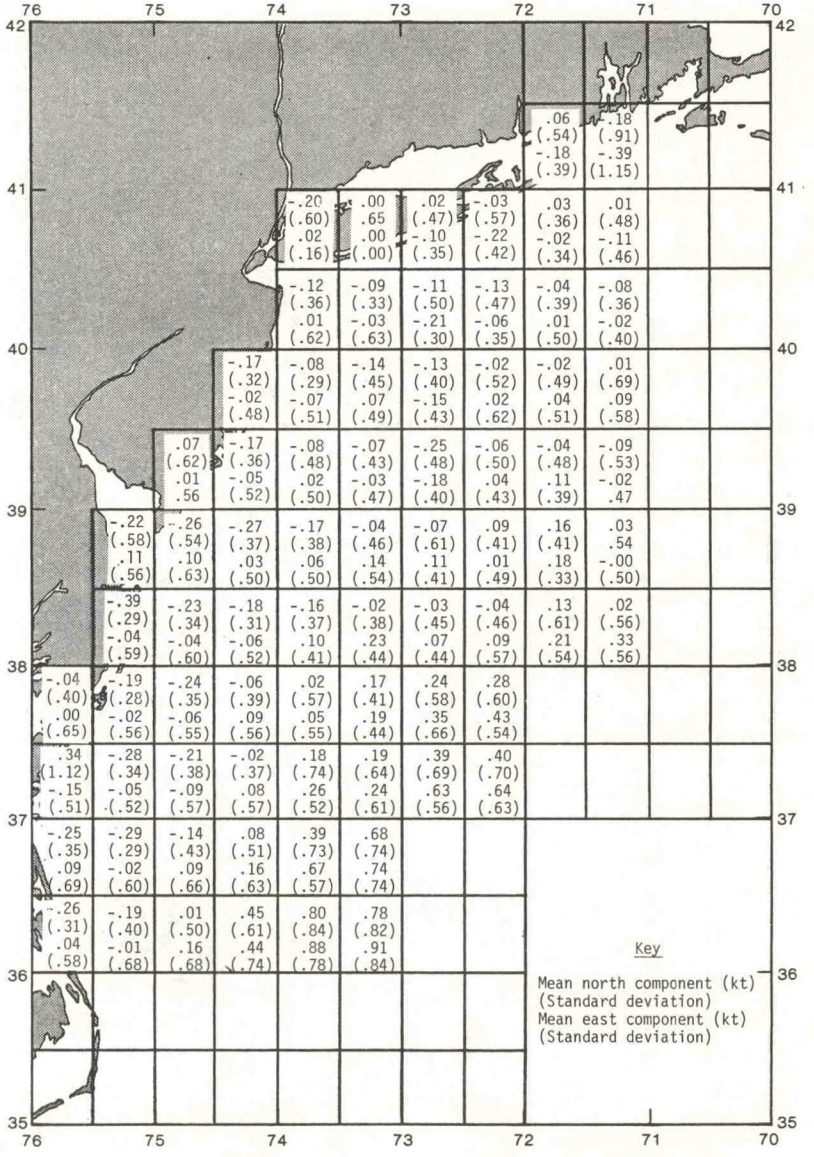


Figure 5.15.--Spring means and standard deviations of sea-surface current.

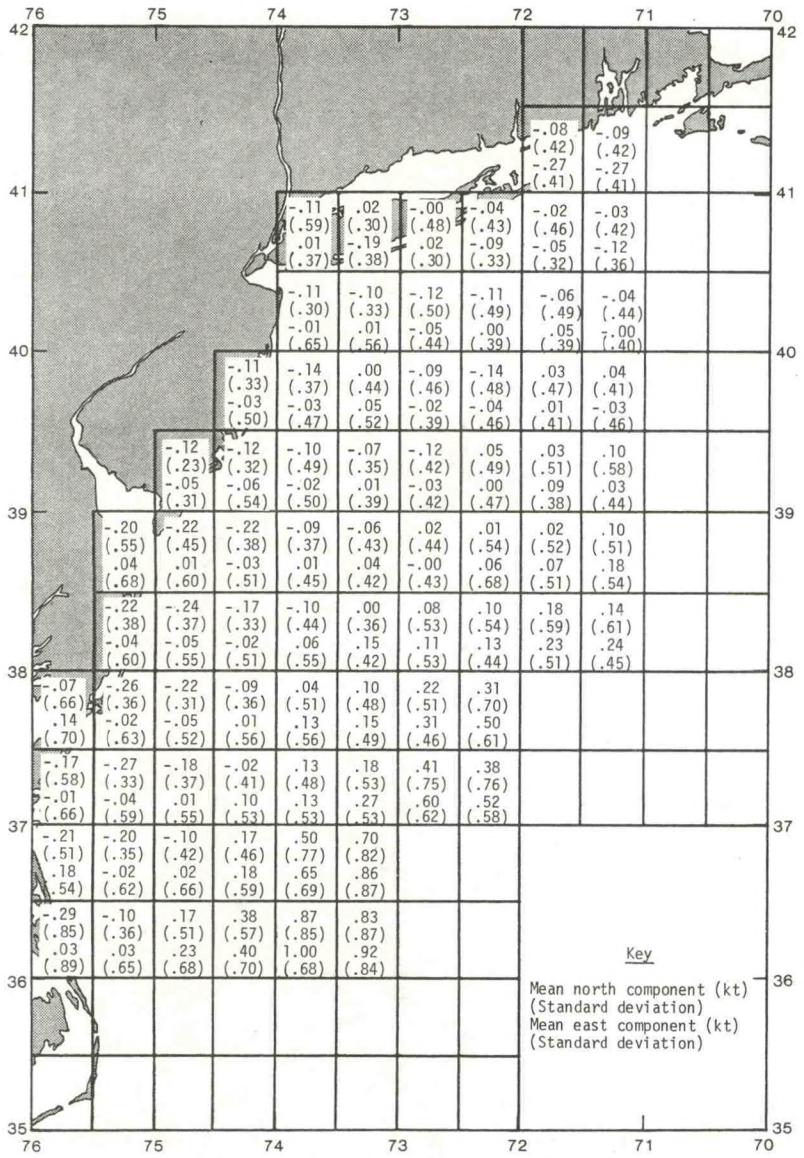


Figure 5.16.--Summer means and standard deviations of sea-surface current.

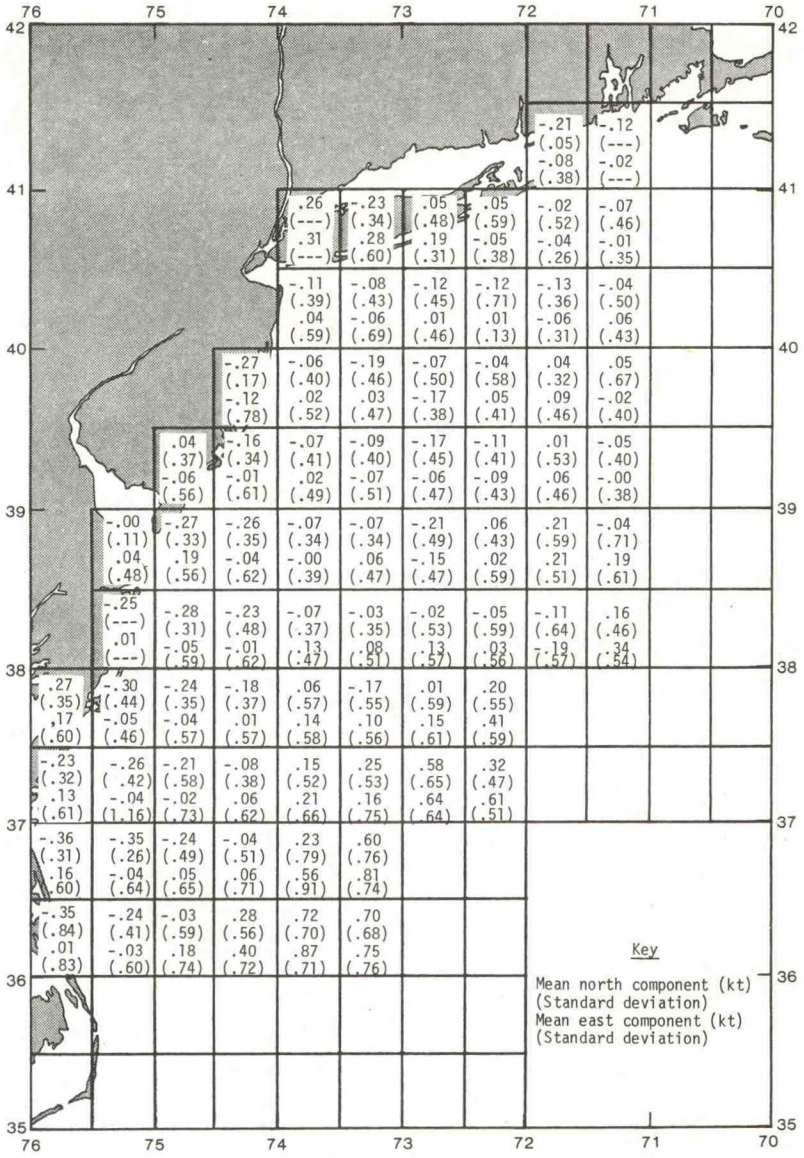


Figure 5.17.--Fall means and standard deviations of sea-surface current.

### 5.3.2 Comparison of Surface Currents from Ship-Drift and Surface-Drifter Observations

Extensive measurements of surface currents using surface drifters have been made by Bumpus and Lauzier (1965), who published their results in atlas form. Superposition of mean seasonal current vectors and speeds on a chart of mean seasonal currents obtained from the NODC ship-drift file shows a general south-to-southwest flow in all seasons along the continental shelf, with an offshore component along the shelf edge and an easterly component along the shelf edge south of 37°N. There are some major differences between the two data sets for the coastal waters along Long Island and the coastal and shelf areas of New England, where the differences in current direction are sometimes as large as 90 to 130°. In a few scattered areas along the shelf the differences are as large as 180°. Differences in current speed vary greatly, ranging from 0.0 to 0.3 kt (0 to 15 cm/s), with little correlation or overall pattern. Comparison by season is summarized below.

Winter (fig. 5.18). Major differences, of up to 130°, are found in winter in the coastal waters of Long Island and in the New England coastal and shelf areas. Speed differences over the shelf are highly variable and uncorrelated, ranging from 0.01 to 0.3 kt (0.5 to 15 cm/s).

Spring (fig. 5.19). The coastal waters of Long Island and New England show major differences in spring in both current speeds and directions from the area south of New England extending outward as far as the shelf edge from 39° to 40°N and between the 50- and 100-m isobaths. Differences in current direction derived from the two data sets are large, amounting to as much as 130° in the coastal waters north of the Chesapeake and Delaware debouchments. There is little correlation between differences in speed, which range up to 0.25 kt (13 cm/s).

Summer (fig. 5.20). Differences in direction are again noticeable in summer along the Long Island and New England coastal areas, and exceed 90° in scattered areas along the shelf. Differences in speed, of up to 0.21 kt (10.5 cm/s) are uncorrelated.

Fall (fig. 5.21). Current direction derived from the two types of data shows the largest differences in fall, amounting to as much as 180° and seen particularly off the embayments. Speed differences very from 0.01 to 0.2 kt (0.5 to 10 cm/s), again without consistent pattern.

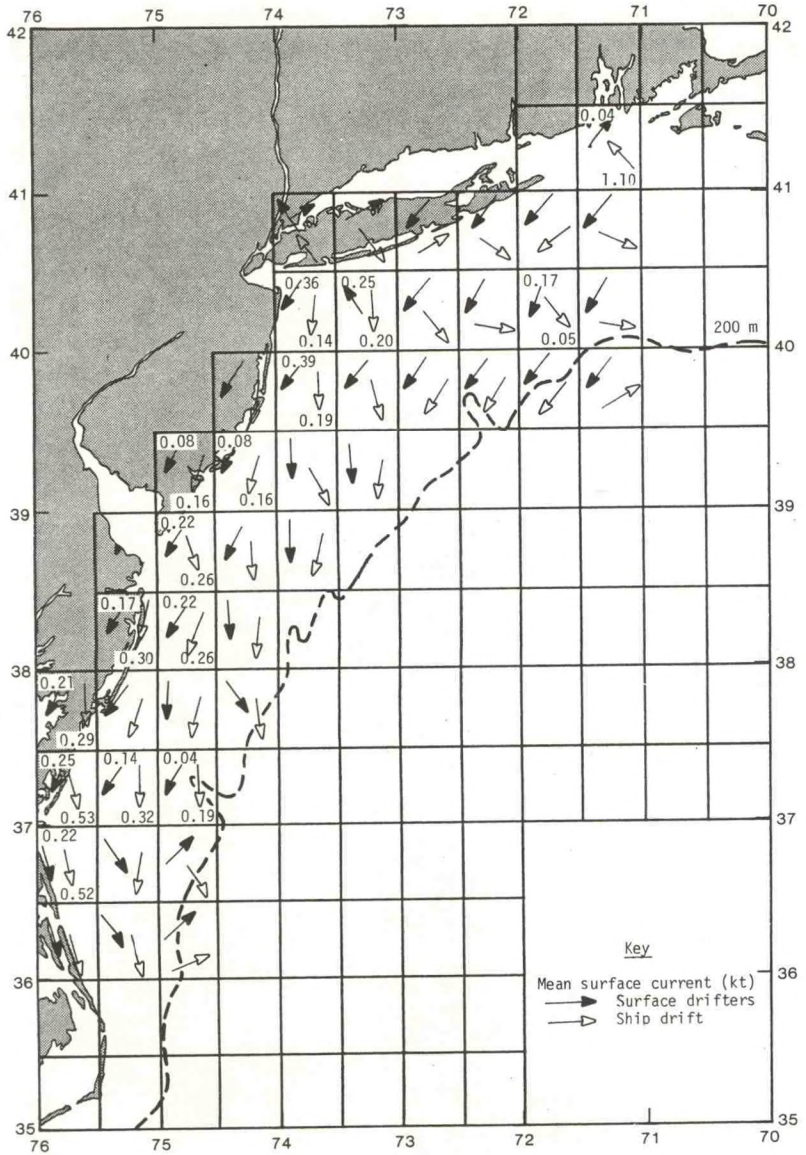


Figure 5.18.--Comparison of winter mean sea-surface currents based on ship-drift and surface-drifter observations.

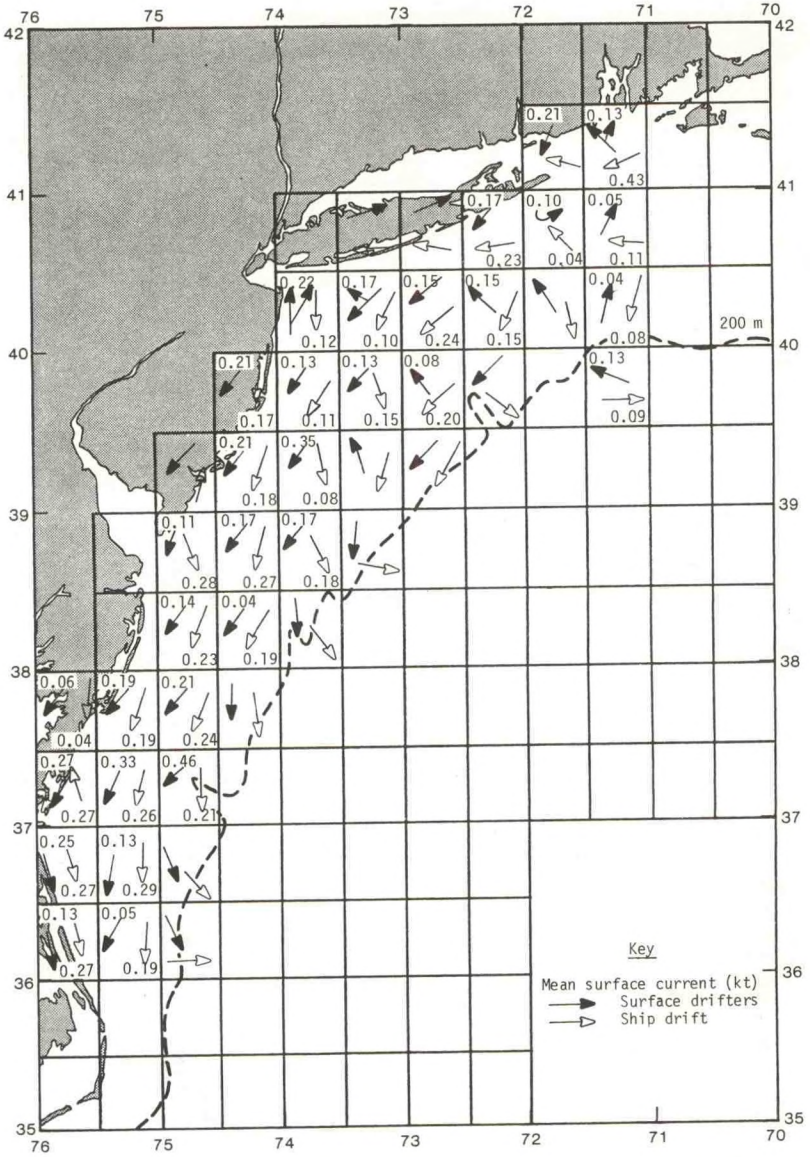


Figure 5.19.--Comparison of spring mean sea-surface currents based on ship-drift and surface-drifter observations.

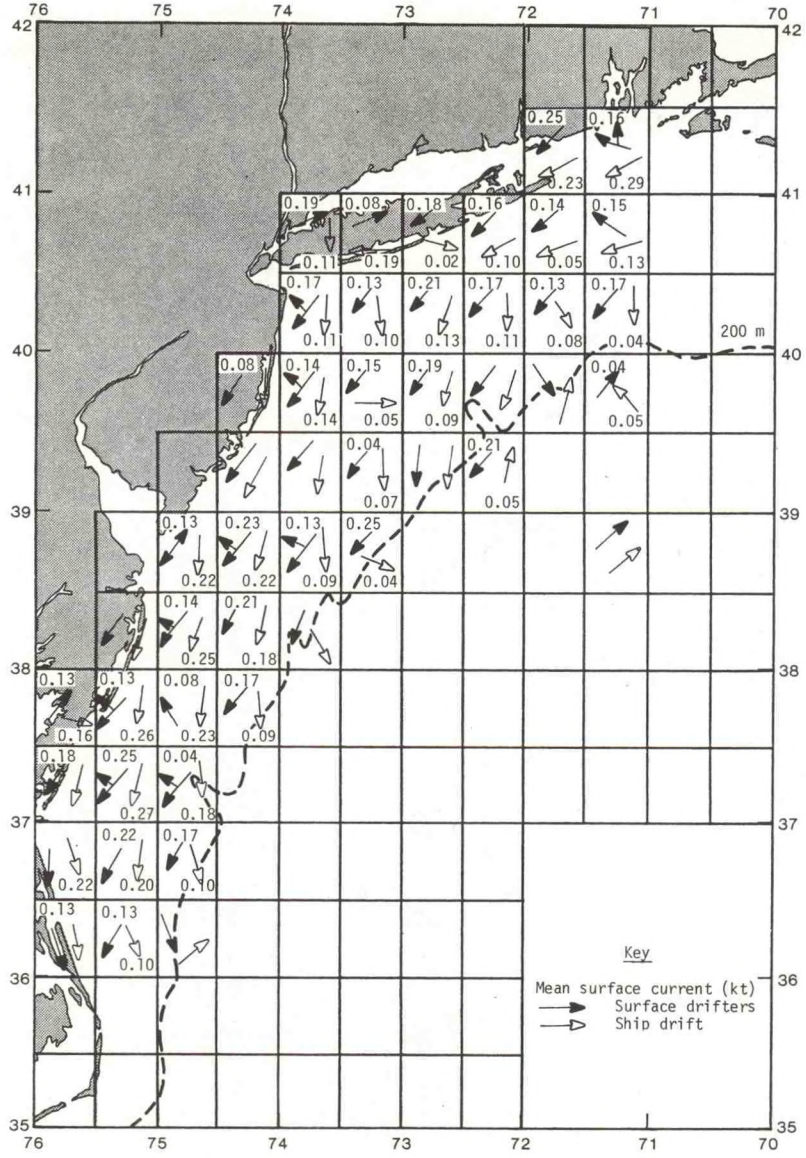


Figure 5.20.--Comparison of summer mean sea-surface currents based on ship-drift and surface-drifter observations.

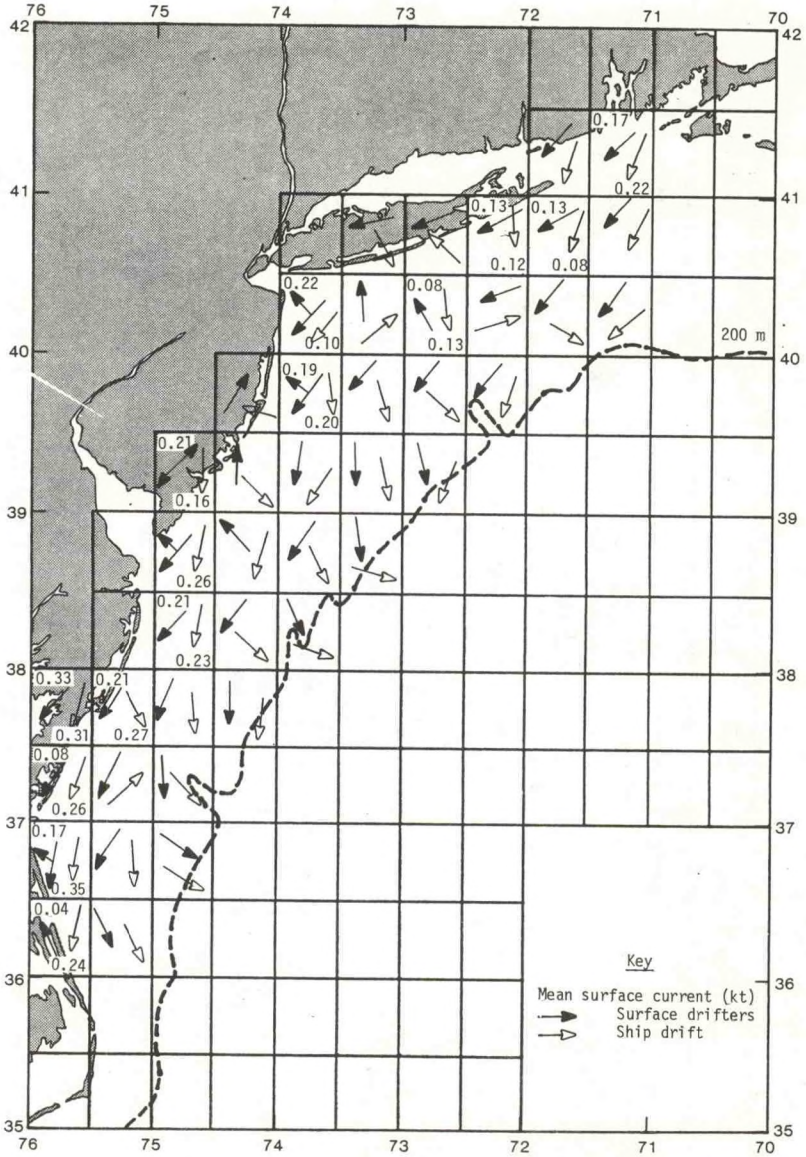


Figure 5.21.--Comparison of fall mean sea-surface currents based on ship-drift and surface-drifter observations.

### 5.3.3 Comparison of Surface Currents From Ship-Drift and Published Data

Table 5.1 lists mean values of u and v current components drawn from various published sources (Amos, 1976; Beardsley et al., 1976; Charnell and Mayer, 1975; Flagg et al., 1976). Mean values at depths of 20 m or less from this table, combined with near-surface averages computed from the current meter data archived at NODC, were compared with the ½° mean seasonal averages derived from the ship-drift observations. In all, 20 pairs of values for the u and v components were included in the comparison. The averages difference was found to be -0.0026 kt (-0.13 cm/s) for the u component and -0.0512 kt (-2.56 cm/s) for the v component. Although based on a limited number of observations, this comparison seems to indicate general agreement between current meter and ship-drift data.

In additional comparisons, the monthly current averages, contained in appendix D, were compared with measurements published by Haight (1942), by Bumpus and Lauzier (1965), and by the U.S. Naval Oceanographic Office (1947; 1970-76) in atlases and charts.

Haight's study was based on the following lightship data (fig. 5-22):

Ambrose Channel (40°27.1'N, 73°49.4'W), 13 months, 1936-38.
Barnegat Lightship (39°45.8'N, 73°56'W), 18 months, 1934-36.
Northeast End (38°57'N, 74°29.6'W), 17 months, 1912-19.
Winter Quarter Shoal (37°55.4'N, 74°56.4'W), 26 months, 1912-20.
Chesapeake Lightship (36°58.7'N, 75°42.2'W), 12 months, 1935-36.

Bumpus and Lauzier (1965) made measurements in the same area in 1963. The results of the two studies are compared in figure 5.23.

With minor variations, all these studies indicate southwesterly surface current flow in the Mid-Atlantic region. The speeds vary greatly, however, possibly because of differences in observation and computation methods, and because some observations were made in nearshore areas affected by freshwater outflow, winds, and tides. The "Pilot Charts of the North American Atlantic Ocean" (U.S. Naval Oceanographic Office, 1970-76) could be used in only a general way because these publications cover the entire North Atlantic Ocean. The NODC ship-drift data agree most closely with the atlas publication by the U.S. Naval Oceanographic Office (1947), and with the measurements made by Bumpus and Lauzier (1965). Fairly good agreement in most localities was also found with the results published by Haight (1942).

Although these comparisons cover a time span of over 40 years, there is general agreement concerning a mean south-to-southwest surface flow at speeds of somewhat less than 1.0 kt (50 cm/s) over the continental shelf, regardless of time or method of observation. Most current speeds are on the order of 0.1 to 0.2 kt (5 to 10 cm/s).

Table 5.1.--Means of north and east components of subsurface current obtained from the literature

| Lat.N (deg/min) | Long.W (deg/min) | Length of record (days) | Beginning date | Water depth (m) | Instr. depth (m) | East (u) comp. (kt) | East (u) comp. (cm/s) | North (v) comp. (kt) | North (v) comp. (cm/s) |
|---|---|---|---|---|---|---|---|---|---|
| | | | Instrument depth = 0-100 m | | | | | | |
| 39 28 | 74 15 | 60 | 7/1/72 | 12.0 | 5.0 | -0.042 | -2.10 | -0.058 | -2.90 |
| " | " | " | " | " | 10.0 | -0.034 | -1.70 | -0.046 | -2.30 |
| " | " | " | 7/1/73 | " | 5.0 | -0.042 | -2.10 | -0.058 | -2.90 |
| " | " | " | " | " | 10.0 | -0.026 | -1.30 | -0.036 | -1.80 |
| " | " | " | 12/1/73 | " | 5.0 | -0.040 | -2.00 | -0.056 | -2.80 |
| 40 45 | 71 03 | 33 | 3/8/73 | 60.0 | 42.0 | -0.128 | -6.40 | 0.000 | 0.00 |
| 40 19.4 | 73 47.8 | 41 | 8/27/73 | 44.9 | 36.0 | -0.007 | -0.33 | -0.022 | -1.11 |
| " | " | " | " | " | 30.0 | 0.038 | 1.88 | 0.005 | 0.26 |
| " | " | " | " | " | 19.9 | 0.084 | 4.22 | 0.035 | 1.75 |
| 40 18.4 | 73 51.5 | 40 | 8/28/73 | 23.8 | 21.1 | -0.009 | -0.43 | 0.002 | 0.12 |
| " | " | " | " | " | 15.2 | 0.110 | 5.49 | 0.031 | 1.55 |
| 40 29.7 | 73 56.7 | 34 | 9/3/73 | 10.0 | 9.1 | -0.021 | -1.03 | 0.079 | 3.93 |
| 40 32 | 73 56.7 | 35 | 9/4/73 | 16.5 | 8.9 | 0.020 | 1.01 | 0.207 | 10.36 |
| 40 28.2 | 73 40 | " | " | 23.5 | 22.4 | 0.007 | 0.34 | 0.017 | 0.86 |
| " | " | " | " | " | 14.4 | 0.009 | 0.44 | 0.128 | 6.40 |
| 40 10.2 | 73 24.8 | 30 | 9/22/73 | 37.6 | 34.5 | -0.018 | -0.90 | -0.019 | -0.94 |
| " | " | " | 9/8/73 | " | 22.4 | -0.080 | -3.99 | -0.144 | -7.19 |
| 40 33.4 | 73 10.6 | 29 | 9/9/73 | 24.7 | 15.8 | -0.040 | -2.01 | -0.004 | -0.18 |
| 40 25 | 73 45.1 | 11 | 9/28/73 | 28.4 | 25.7 | 0.094 | 4.70 | 0.063 | 3.14 |
| " | " | " | " | " | 17.4 | 0.132 | 6.62 | 0.139 | 6.94 |
| 40 19 | 73 48 | 42 | 10/27/73 | 46.1 | 45.2 | 0.097 | 4.83 | -0.015 | -0.77 |
| " | " | " | " | " | 37.2 | 0.141 | 7.06 | -0.045 | -2.25 |
| " | " | " | " | " | 31.2 | 0.335 | 16.76 | -0.064 | -3.22 |
| 40 18.4 | 73 50.9 | " | " | 22.9 | 14.3 | 0.184 | 9.22 | -0.009 | -0.45 |
| 40 29.7 | 73 56.7 | 38 | 10/28/73 | 10.3 | 9.4 | -0.075 | -3.73 | 0.054 | 2.71 |
| 40 32 | 73 41 | 41 | " | 16.5 | 13.8 | 0.042 | 2.10 | 0.155 | 7.24 |
| 40 28.4 | 73 40 | " | " | 22.9 | 14.0 | 0.016 | 0.79 | 0.265 | 13.26 |
| 40 18 | 73 55 | 42 | 10/27/73 | 20.1 | 19.2 | 0.054 | 2.70 | -0.039 | -1.96 |
| " | " | " | " | " | 11.2 | 0.155 | 7.74 | 0.033 | 1.67 |

Table 5.1.--Means of north and east components of subsurface current obtained from the literature (continued)

| Lat.N (deg/min) | Long.W (deg/min) | Length of record (days) | Beginning date | Water depth (m) | Instr. depth (m) | East (u) comp. (kt) | East (u) comp. (cm/s) | North (v) comp. (kt) | North (v) comp. (cm/s) |
|---|---|---|---|---|---|---|---|---|---|
| | | | | Instrument depth = 0-100 m | | | | | |
| 40 25 | 73 56 | 20 | 11/15/73 | 13.7 | 12.8 | 0.152 | 7.60 | 0.039 | 1.94 |
| 36 50 | 75 02 | 29 | 1/15/74 | 36.0 | 7.0 | 0.052 | 2.60 | -0.172 | -8.60 |
| " | " | " | " | " | 20.0 | 0.032 | 1.60 | -0.138 | -6.90 |
| " | " | " | " | " | 32.0 | 0.014 | 0.70 | -0.094 | -4.70 |
| 40 54 | 71 04 | 35 | 2/28/74 | 58.0 | 28.0 | -0.042 | -2.10 | -0.010 | -0.50 |
| 37 55 | 74 39 | 22 | 6/26/74 | 35.0 | 24.0 | -0.114 | -5.70 | -0.150 | -7.50 |
| 40 33 | 70 56 | 35 | 2/28/74 | 72.0 | " | -0.114 | -5.70 | 0.010 | 0.50 |
| " | " | " | " | " | 44.0 | -0.044 | -2.20 | 0.020 | 1.00 |
| " | " | " | " | " | 62.0 | -0.044 | -2.20 | 0.036 | 1.80 |
| " | " | " | " | " | 71.0 | -0.002 | -0.10 | -0.010 | -0.50 |
| 40 18 | 70 51 | 35 | 2/28/74 | 110.0 | 30.0 | -0.156 | -7.80 | 0.014 | 0.70 |
| " | " | " | " | " | 50.0 | -0.148 | -7.40 | 0.060 | 3.00 |
| " | " | " | " | " | 70.0 | -0.118 | -5.90 | 0.066 | 3.30 |
| 39 28 | 74 15 | 60 | 7/1/74 | 12.0 | 5.0 | -0.042 | -2.10 | -0.058 | -2.90 |
| " | " | " | " | " | 10.0 | -0.034 | -1.70 | -0.046 | -2.30 |
| " | " | " | 12/1/74 | " | 5.0 | -0.040 | -2.00 | -0.056 | -2.80 |
| " | " | " | " | " | 10.0 | -0.026 | -1.30 | -0.036 | -1.80 |
| 40 25 | 73 28 | 59 | 3/22/74 | 23.0 | 2.0 | -0.014 | -0.70 | -0.070 | -3.50 |
| " | " | 89 | " | " | 20.0 | -0.012 | -0.60 | -0.014 | -0.70 |
| 40 07 | 72 51 | 35 | 6/18/74 | 50.0 | 2.0 | -0.076 | -3.80 | -0.138 | -6.90 |
| " | " | " | " | " | 13.0 | -0.136 | -6.80 | -0.110 | -5.50 |
| " | " | " | " | " | 26.0 | -0.082 | -4.10 | -0.060 | -3.00 |
| " | " | " | " | " | 46.0 | -0.034 | -1.70 | -0.036 | -1.80 |
| 38 49 | 74 12 | 36 | 10/29/74 | 43.0 | 9.0 | -0.124 | -6.20 | -0.064 | -3.20 |
| " | " | " | " | " | 23.0 | -0.098 | -4.90 | -0.020 | -1.00 |
| " | " | " | " | " | 35.0 | -0.060 | -3.00 | 0.056 | 2.80 |
| 36 50 | 75 42 | 29 | 7/21/74 | 16.0 | 4.0 | -0.034 | -1.70 | 0.030 | 1.50 |
| " | " | " | " | " | 15.0 | -0.004 | -0.20 | 0.062 | 3.10 |
| 36 50 | 75 02 | 37 | 7/21/74 | 36.0 | 9.0 | -0.048 | -2.40 | -0.168 | -8.40 |

Table 5.1.--Means of north and east components of subsurface current obtained from the literature (continued)

| Lat.N (deg/min) | Long.W (deg/min) | Length of record (days) | Beginning date | Water depth (m) | Instr. depth (m) | East (u) comp. (kt) | East (u) comp. (cm/s) | North (v) comp. (kt) | North (v) comp. (cm/s) |
|---|---|---|---|---|---|---|---|---|---|
| | | | | Instrument depth = 0-100 m | | | | | |
| 36 50 | 75 02 | 37 | 7/21/74 | 36.0 | 20.0 | 0.052 | 2.60 | -0.110 | -5.50 |
| " | " | " | " | " | 30.0 | 0.048 | 2.40 | -0.026 | -1.30 |
| 36 50 | 74 48 | 26 | 7/21/74 | 70.0 | 11.0 | -0.074 | -3.70 | -0.214 | -10.70 |
| " | " | " | " | " | 30.0 | -0.046 | -2.30 | -0.332 | -16.60 |
| " | " | " | " | " | 58.0 | 0.000 | 0.00 | -0.262 | -13.60 |
| 36 50 | 74 40 | 18 | 7/21/74 | 70.0 | 76.0 | -0.062 | -3.10 | -0.252 | -12.60 |
| 40 54 | 70 04.3 | 35 | 2/27/74 | Unknown | 27.5 | -0.421 | -21.04 | -0.091 | -4.53 |
| " | " | " | " | " | 43.5 | -0.123 | -6.16 | 0.185 | 9.27 |
| " | " | " | " | " | 57.3 | -0.047 | -2.33 | 0.156 | 7.79 |
| 40 32.6 | 70 55.6 | 35 | 2/27/74 | " | 24.2 | -1.144 | -57.22 | 0.102 | 5.11 |
| " | " | " | " | " | 44.2 | -0.431 | -21.55 | 0.192 | 9.61 |
| " | " | " | " | " | 62.2 | -0.441 | -22.07 | 0.356 | 17.81 |
| " | " | " | " | " | 71.0 | -0.002 | -0.11 | -0.095 | -4.77 |
| 40 18.2 | 70 51.4 | 35 | 2/27/74 | " | 29.7 | -1.563 | -78.14 | 0.142 | 7.11 |
| " | " | " | " | " | 49.7 | -0.144 | -7.18 | 0.058 | 2.88 |
| " | " | " | " | " | 69.7 | -1.182 | -59.10 | 0.665 | 33.24 |
| " | " | " | " | " | 89.7 | -1.342 | -67.12 | 0.135 | 6.77 |
| 40 16 | 73 13 | 111 | 2/25/75 | 38.0 | 2.0 | -0.094 | -4.70 | -0.096 | -4.80 |
| " | " | 37 | " | " | 25.0 | -0.072 | -3.60 | -0.044 | -2.20 |
| " | " | 48 | 4/29/75 | " | 23.0 | -0.110 | -5.50 | -0.078 | -3.90 |
| " | " | 111 | 2/25/75 | " | 37.0 | -0.030 | -1.50 | -0.006 | -0.30 |
| 40 06 | 72 54 | 112 | 2/25/75 | 48.0 | 10.0 | -0.048 | -2.40 | -0.052 | -2.60 |
| " | " | 62 | " | " | 26.0 | -0.056 | -2.80 | -0.022 | -1.10 |
| " | " | 112 | " | " | 40.0 | -0.032 | -1.60 | -0.026 | -1.30 |
| 40 03 | 72 42 | 59 | 3/1/75 | 59.0 | 2.0 | -0.056 | -2.80 | -0.056 | -2.80 |
| " | " | " | " | " | 27.0 | -0.062 | -3.10 | -0.056 | -2.80 |
| " | " | 108 | " | " | 42.0 | -0.058 | -2.90 | -0.038 | -1.90 |

Table 5.1.--Means of north and east components of subsurface current obtained from the literature (continued)

| Lat.N (deg/min) | Long.W (deg/min) | Length of record (days) | Beginning date | Water depth (m) | Instr. depth (m) | East (u) comp. (kt) | East (u) comp. (cm/s) | North (v) comp. (kt) | North (v) comp. (cm/s) |
|---|---|---|---|---|---|---|---|---|---|
| | | | Instrument depth = 0-100 m | | | | | | |
| 39 39 | 72 38 | 64 | 2/24/75 | 76.0 | 2.0 | -0.052 | -2.60 | -0.034 | -1.70 |
| " | " | 25 | 5/23/75 | " | 2.0 | -0.108 | -5.40 | -0.182 | -9.10 |
| " | " | 64 | 2/24/75 | " | 26.0 | -0.098 | -4.90 | -0.014 | -0.70 |
| " | " | | " | " | 41.0 | -0.080 | -4.00 | -0.012 | -0.60 |
| " | " | 42 | 4/30/75 | " | 42.0 | -0.124 | -6.20 | -0.148 | -7.40 |
| " | " | 64 | 2/24/75 | " | 75.0 | -0.052 | -2.60 | 0.020 | 1.00 |
| 39 20 | 70 00 | Unknown | Unknown | 2640.0 | 10.0 | -0.250 | -13.00 | -0.012 | -0.60 |
| " | " | " | " | " | 100.0 | -0.114 | -5.70 | 0.022 | 1.10 |
| | | | Instrument depth = 101-500 m | | | | | | |
| 40 18 | 70 51 | 35 | 2/28/74 | 110.0 | 109.0 | -0.016 | -0.80 | 0.000 | 0.00 |
| 40 18.2 | 70 51.4 | 35 | 2/27/74 | Unknown | 108.5 | -0.149 | -7.46 | 0.007 | 0.37 |
| 39 20 | 70 00 | Unknown | Unknown | 2640.0 | 500.0 | -0.074 | -3.70 | -0.012 | -0.60 |
| 36 50 | 74 40 | 18 | 7/21/74 | 70.0 | 104.0 | 0.028 | 1.40 | -0.132 | -6.60 |
| | | | Instrument depth = 501-1000 m | | | | | | |
| 39 50 | 70 40 | 104 | 8/20/70 | 876.0 | 776.0 | -0.128 | -6.40 | 0.032 | 1.60 |
| 39 50 | 70 56 | 45 | 8/20/70 | 943.0 | 846.0 | -0.040 | -2.00 | 0.020 | 1.00 |
| " | " | " | " | " | 933.0 | -0.040 | -2.00 | 0.008 | 0.40 |
| " | " | " | " | " | 941.0 | -0.030 | -1.50 | 0.008 | 0.40 |
| 39 50 | 70 56 | 451 | 8/20/70 | 993.0 | 880.0 | -0.092 | -4.60 | 0.036 | 1.80 |
| " | " | 86 | " | " | 990.0 | -0.072 | -3.60 | -0.014 | -0.70 |
| 39 29.8 | 72 17.6 | 53 | 9/2/74 | 827.0 | 822.0 | -0.056 | -2.78 | 0.004 | 0.22 |
| 39 20 | 70 00 | Unknown | Unknown | 2640.0 | 1000.0 | -0.070 | -3.50 | 0.006 | 0.30 |

Table 5.1.--Means of north and east components of subsurface current obtained from the literature (continued)

| Lat.N (deg/min) | Long.W (deg/min) | Length of record (days) | Beginning date | Water depth (m) | Instr. depth (m) | East (u) comp. (kt) | East (u) comp. (cm/s) | North (v) comp. (kt) | North (v) comp. (cm/s) |
|---|---|---|---|---|---|---|---|---|---|
| | | | Instrument depth = > 1000 m | | | | | | |
| 39 23 | 70 59 | 46 | 8/20/70 | 2527.0 | 1504.0 | -0.056 | -2.80 | 0.006 | 0.30 |
| 39 35 | 70 58 | 111 | 8/20/70 | 2263.0 | 2163.0 | -0.128 | -6.40 | 0.004 | 0.20 |
| 39 37 | 71 15 | 111 | 8/20/70 | 2150.0 | 2052.0 | -0.102 | -5.10 | -0.008 | -0.40 |
| 39 23 | 71 01 | 56 | 8/20/70 | 2509.0 | 2394.0 | -0.048 | -2.40 | -0.010 | -0.50 |
| 39 20 | 70 00 | Unknown | Unknown | 2640.0 | 2000.0 | -0.032 | -1.60 | -0.002 | -0.10 |

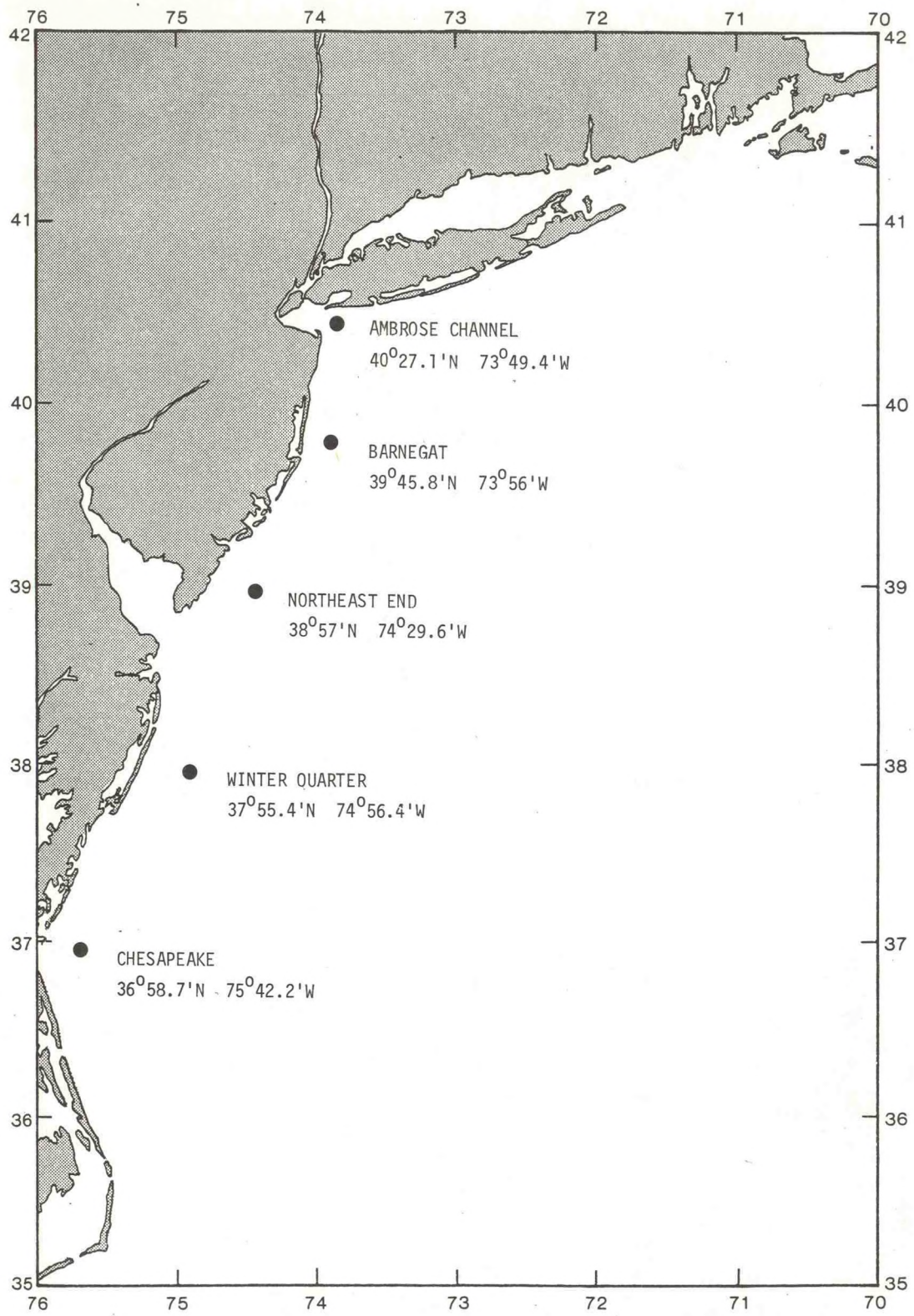


Figure 5.22.--Locations of Haight's (1942) current measurements.

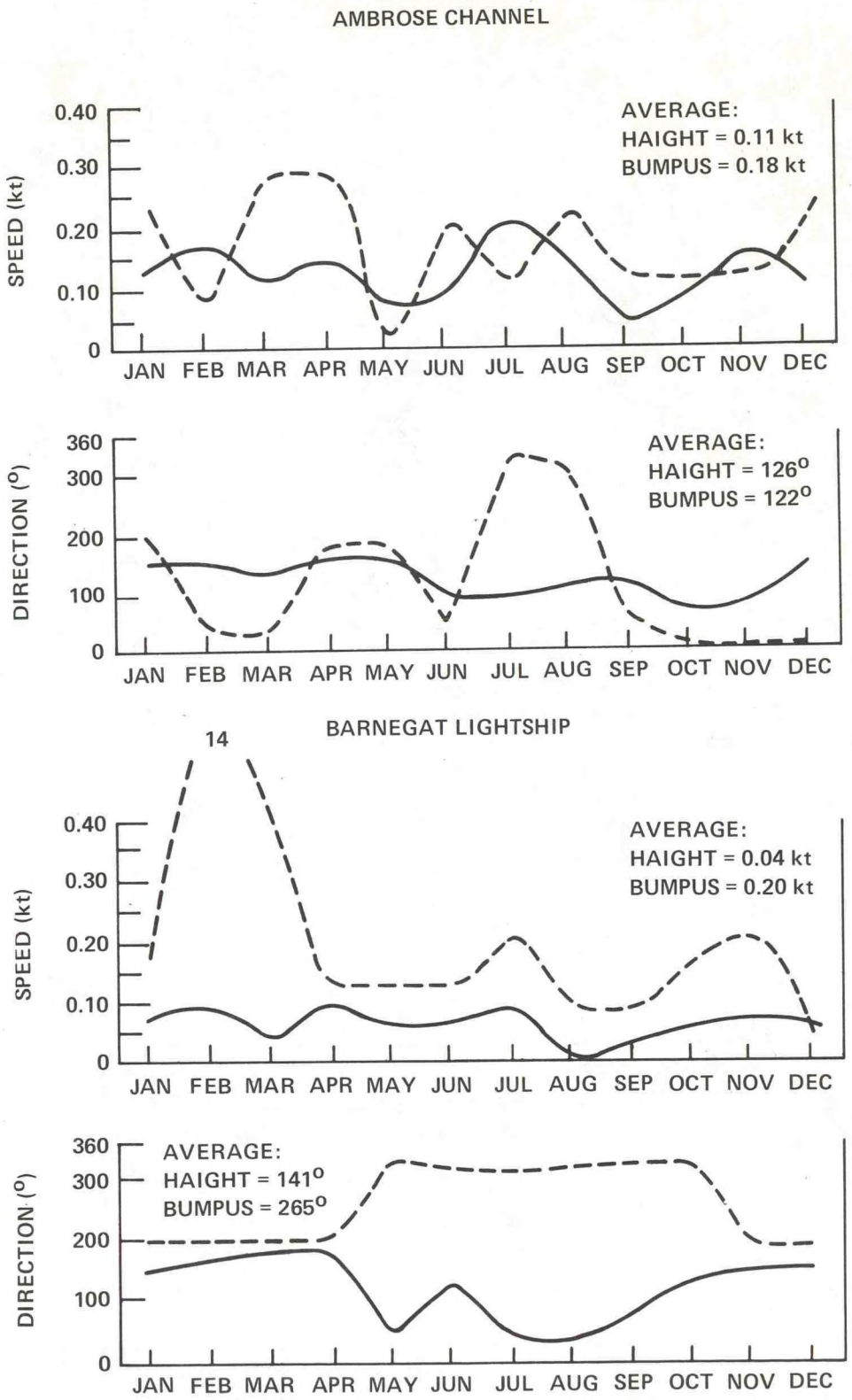


Figure 5.23.--Comparison of current measurements by Haight (solid line) and Bumpus and Lauzier (dashed line).

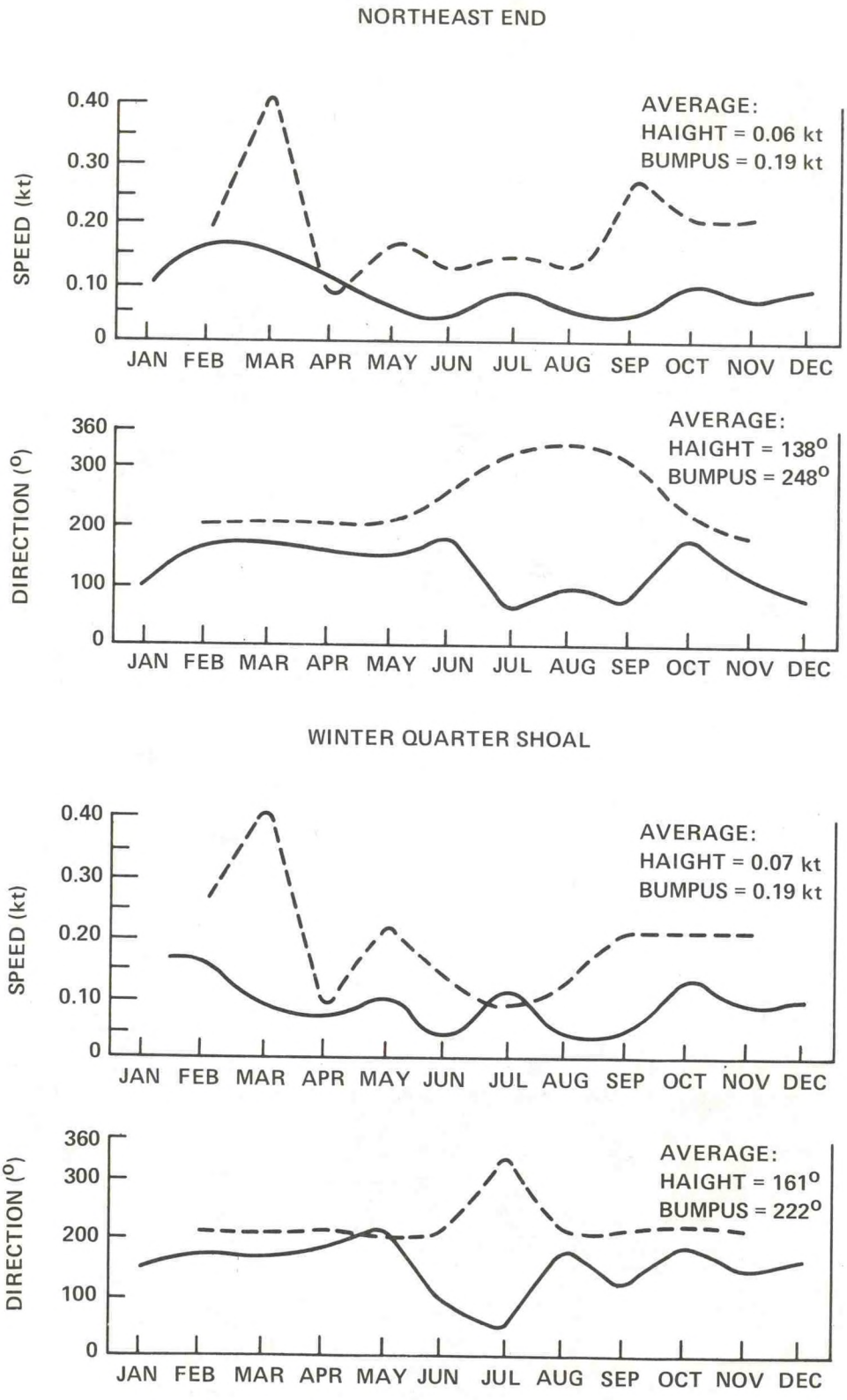


Figure 5.23 (cont.).--Comparison of current measurements by Haight (solid line) and Bumpus and Lauzier (dashed line).

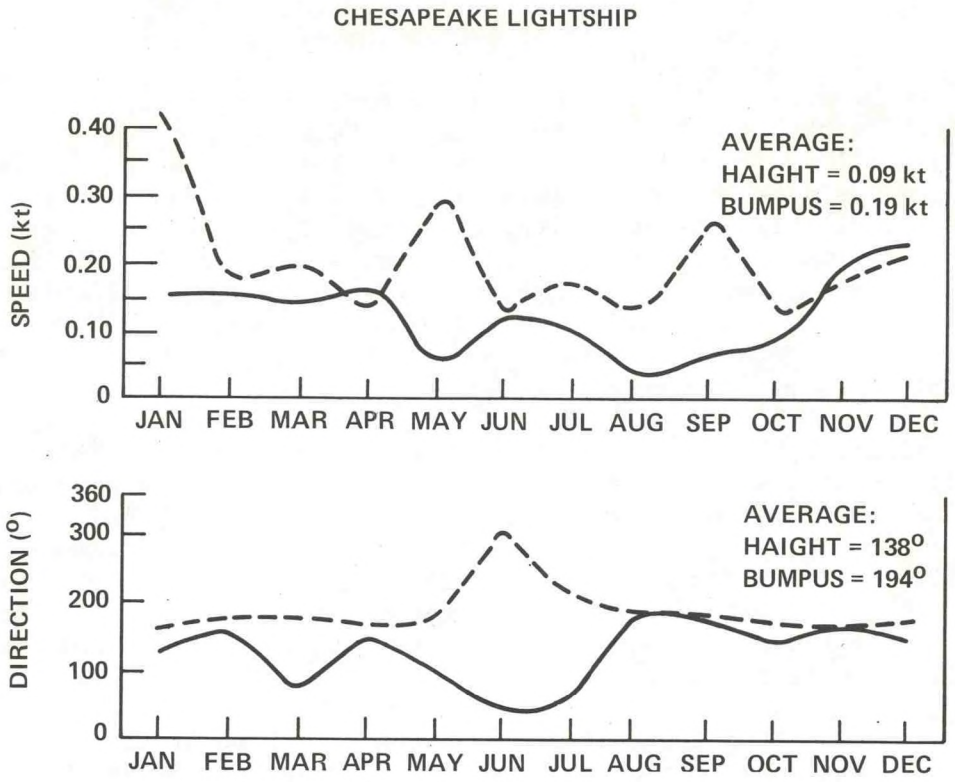


Figure 5.23 (cont.).--Comparison of current measurements by Haight (solid line) and Bumpus and Lauzier (dashed line).

## 5.4 Analysis of Current Meter Data

As noted earlier, 18 current meter records from the tapes provided by the MESA Program Office and acquired through NODC were selected for analysis on the basis of location and length of record. Three of these were found to contain erroneous data and were eliminated from further consideration. A fourth (station 13) was retained although some sections of the data appeared questionable. Summary statistics of these data are given in table 5.2. Mean currents are seen to be a few centimeters per second, while variability is much higher (0.15 to 0.52 kt, or 7.5 to 26.0 cm/s), with maximum currents ranging from 1.2 to 1.4 kt (60 to 70 cm/s) to as high as 3.6 kt (180 cm/s). Note that in some cases mean currents are larger at greater depths.

The amplitude histograms of the currents shown in figure 5.24 indicate that the distributions are generally bimodal near the shelf and approach unimodal shape in locations farther offshore (stations 6 and 13). A bimodal distribution of the velocity components is typical in coastal waters where strong bidirectional tides prevail. Most of the distributions show low kurtosis, i.e., a wide spread, and, although the mean currents are very small, the number of instances in which measured currents are considerably larger than the mean is proportionately high.

Figure 5.25 shows the complete spectrum from 0 to Nyquist frequency (3 cycles/hr) for station 4 after heavy smoothing, 38 values having been used in obtaining the average. The spectrum contains high energy at very low frequencies, and is relatively flat just under the Nyquist frequency, which may indicate introduction of errors by high frequency variations in, for example, ocean wind waves.

The tidal and subtidal variance in all 15 records was examined by estimating the spectra using less smoothing (12 values) to increase the spectral resolution. Sections showing the most energetic part of the spectral band are presented in figure 5.26.

Figure 5.26 shows peaks of both the semidiurnal tidal and inertial frequencies at station 1 at shallow depths. The magnitude of the inertial peak is perhaps surprising, as Beardsley et al. (1976) have indicated that the inner shelf is relatively free from inertial energy. The current spectrum for station 2, at the same mooring location but at greater depth, is also shown in figure 5.26. There is little indication of significant inertial energy, and the semidiurnal tide is predominant in this record. A hydrographic station near this location on September 18, 1973, showed that the first current meter record was acquired in the mixed layer, while the deeper record was acquired at the base of the pycnocline. Since the energy in the u and v components is roughly equal in this record, both the inertial and tidal currents were probably oriented from northeast to southwest.

In the spectra for station 3 (fig. 5.26) at 14-m depth slightly to the northeast, based on a longer record, the semidiurnal tide is again a major component of the current. Some inertial energy is indicated in the v component. A lower frequency constituent, at 0.0085 cycle/hr (4.9 days) is indicated, but the level of confidence is low. The spectra for station 4, south of station 3 and also plotted in figure 5.26, show considerable inertial and semidiurnal energy.

Table 5.2.--Statistical summary of current meter records

| Beginning (date) | (hr) | Ending (date) | (hr) | Depth instr./water (m) | Mean u comp. (kt) | (cm/s) | Stand. dev. (kt) | (cm/s) | Mean v comp. (kt) | (cm/s) | Stand. dev. (kt) | (cm/s) | Max. u comp. (kt) | (cm/s) | Max. v comp. (kt) | (cm/s) |
|---|---|---|---|---|---|---|---|---|---|---|---|---|---|---|---|---|
| | | | | Station 1, 40°25'N, 73°45'W* | | | | | | | | | | | | |
| 9/24/73 | 1637 | 10/11/73 | 1610 | 17.4/28.4 | 0.13 | 6.65 | 0.38 | 18.87 | 0.09 | 4.62 | 0.34 | 17.00 | 0.86 | 42.84 | 0.88 | 44.00 |
| | | | | Station 2, 40°25'N, 73°45'W* | | | | | | | | | | | | |
| 9/24/73 | 1643 | 10/11/73 | 1643 | 25.6/28.4 | 0.03 | 1.52 | 0.18 | 8.84 | 0.09 | 4.32 | 0.15 | 7.52 | 0.86 | 42.84 | 0.88 | 44.00 |
| | | | | Station 3, 40°28'N, 73°40'W* | | | | | | | | | | | | |
| 10/24/73 | 1520 | 12/10/73 | 1503 | 14.3/23.2 | 0.23 | 11.59 | 0.52 | 26.22 | 0.01 | 0.35 | 0.39 | 19.43 | 1.31 | 65.36 | 1.30 | 64.91 |
| | | | | Station 4, 40°10'N, 73°24'W* | | | | | | | | | | | | |
| 9/04/73 | 1928 | 10/10/73 | 2005 | 21.0/36.3 | -0.11 | -5.68 | 0.23 | 11.66 | -0.10 | -4.76 | 0.22 | 10.77 | 0.86 | 42.84 | 0.88 | 44.00 |
| | | | | Station 5, 40°33'N, 73°10'W* | | | | | | | | | | | | |
| 9/04/73 | 2103 | 10/10/73 | 1553 | 14.9/23.8 | 0.01 | 0.31 | 0.41 | 20.54 | -0.04 | -1.89 | 0.28 | 14.16 | 1.14 | 56.73 | 1.10 | 54.92 |
| | | | | Station 6, 39°38'N, 72°38'W* | | | | | | | | | | | | |
| 2/23/75 | 1807 | 4/29/75 | 1400 | 4.3/75.9 | 0.05 | 2.44 | 0.30 | 14.77 | 0.03 | 1.57 | 0.30 | 14.80 | 3.78 | 188.78 | 3.80 | 190.13 |
| | | | | Station 7, 39°38'N, 72°38'W | | | | | | | | | | | | |
| 2/23/75 | 1807 | 4/29/75 | 1400 | 26.2/75.9 | -0.09 | -4.65 | 0.44 | 22.06 | -0.01 | -0.60 | 0.45 | 22.54 | 3.78 | 188.78 | 3.80 | 190.13 |
| | | | | Station 8, 39°38'N, 72°38'W | | | | | | | | | | | | |
| 2/23/75 | 1752 | 4/29/75 | 1252 | 41.2/75.9 | -0.07 | -3.68 | 0.40 | 19.96 | -0.02 | -0.73 | 0.42 | 21.15 | 3.78 | 188.78 | 3.80 | 190.13 |

Table 5.2.--Statistical summary of current meter records (continued)

| Beginning (date) | (hr) | Ending (date) | (hr) | Depth instr./water (m) | Mean u comp. (kt) | (cm/s) | Stand. dev. (kt) | (cm/s) | Mean v comp. (kt) | (cm/s) | Stand. dev. (kt) | (cm/s) | Max. u comp. (kt) | (cm/s) | Max v comp. (kt) | (cm/s) |
|---|---|---|---|---|---|---|---|---|---|---|---|---|---|---|---|---|
| | | | | Station 9, 39°38'N, 72°38'W | | | | | | | | | | | | |
| 2/23/75 | 1750 | 4/29/75 | 1250 | 75.0/75.9 | -0.05 | -2.31 | 0.12 | 5.80 | 0.01 | 0.672 | 0.18 | 9.07 | 3.78 | 188.78 | 3.80 | 190.13 |
| | | | | Station 10, 40°08'N, 73°38'W | | | | | | | | | | | | |
| 2/27/75 | 2207 | 4/01/75 | 1407 | 8.2/58.9 | 0.07 | 3.37 | 0.38 | 18.86 | -0.11 | -5.24 | 0.21 | 10.48 | 1.31 | 65.36 | 1.30 | 64.91 |
| | | | | Station 11, 40°08'N, 73°38'W | | | | | | | | | | | | |
| 2/27/75 | 2207 | 4/01/75 | 1407 | 39.0/58.9 | -0.14 | -7.06 | 0.28 | 13.90 | 0.08 | 3.91 | 0.28 | 13.73 | 1.31 | 65.36 | 1.30 | 64.91 |
| | | | | Station 12, 40°08'N, 73°38'W | | | | | | | | | | | | |
| 2/27/75 | 2207 | 4/01/75 | 1407 | 57.9/58.9 | -0.06 | -3.13 | 0.15 | 7.49 | 0.04 | 1.75 | 0.09 | 4.54 | 1.31 | 65.36 | 1.30 | 64.91 |
| | | | | Station 13, 39°38'N, 73°34'W* | | | | | | | | | | | | |
| 2/27/75 | 1833 | 4/02/75 | 1233 | 26.8/34.8 | -0.04 | -2.07 | 0.24 | 12.04 | -0.07 | -3.49 | 0.26 | 12.78 | 1.40 | 70.13 | 1.43 | 71.66 |
| | | | | Station 14, 39°47'N, 72°58'W | | | | | | | | | | | | |
| 2/23/75 | 0100 | 4/30/75 | 2233 | 7.3/77.2 | -0.05 | -2.71 | 0.41 | 20.3 | -0.06 | -3.19 | 0.42 | 21.05 | 1.55 | 77.42 | 1.60 | 79.90 |
| | | | | Station 15, 39°47'N, 72°58'W | | | | | | | | | | | | |
| 2/23/75 | 1400 | 5/01/75 | 1000 | 62.2/77.2 | -0.05 | -2.65 | 0.23 | 11.68 | -0.02 | -0.77 | 0.31 | 15.26 | 3.78 | 188.78 | 3.80 | 190.13 |

*Indicates records analyzed in figures 5.24 to 5.26.

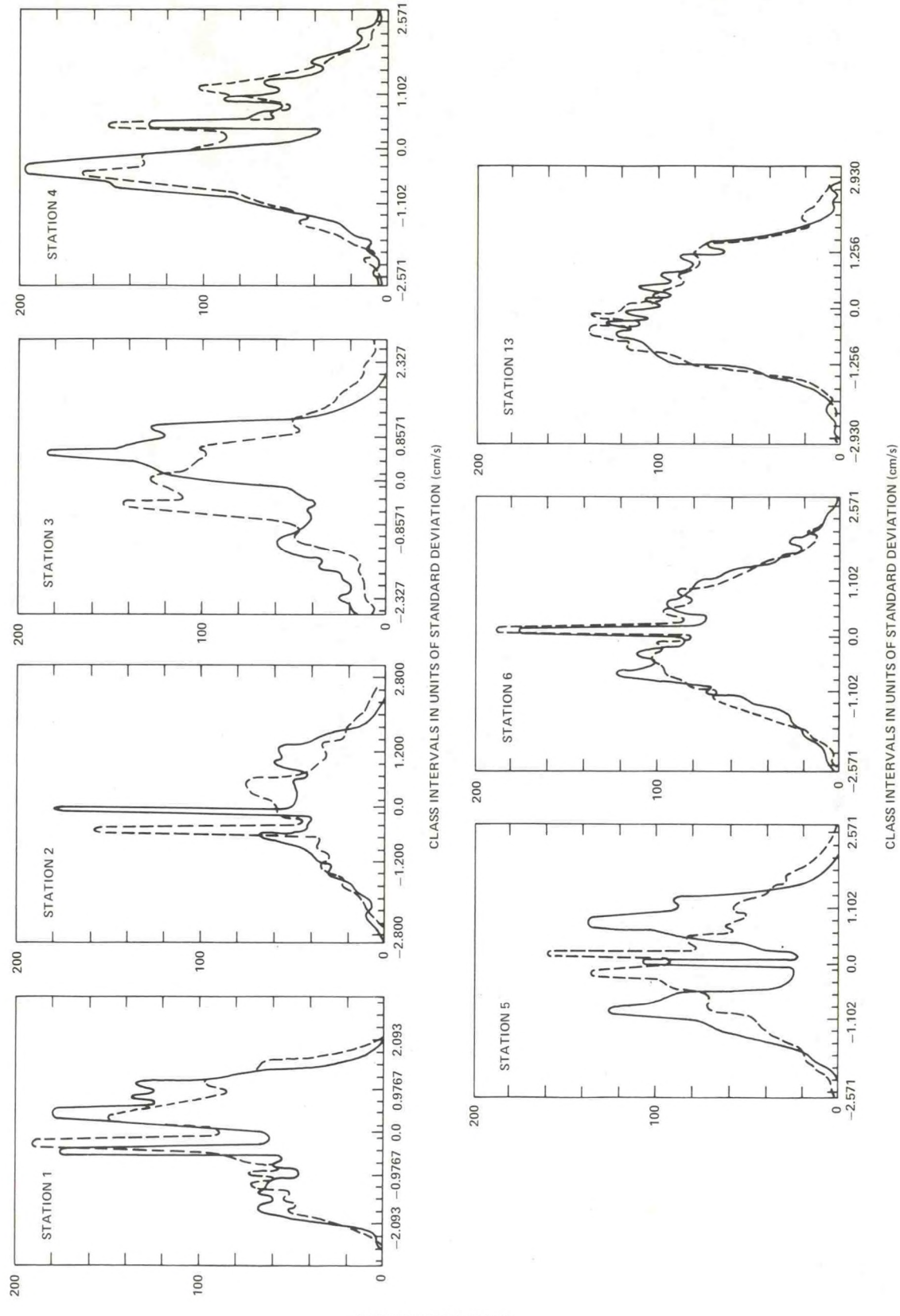


Figure 5.24.--Histograms of u component (solid line) and v component (dashed line) of current velocity.

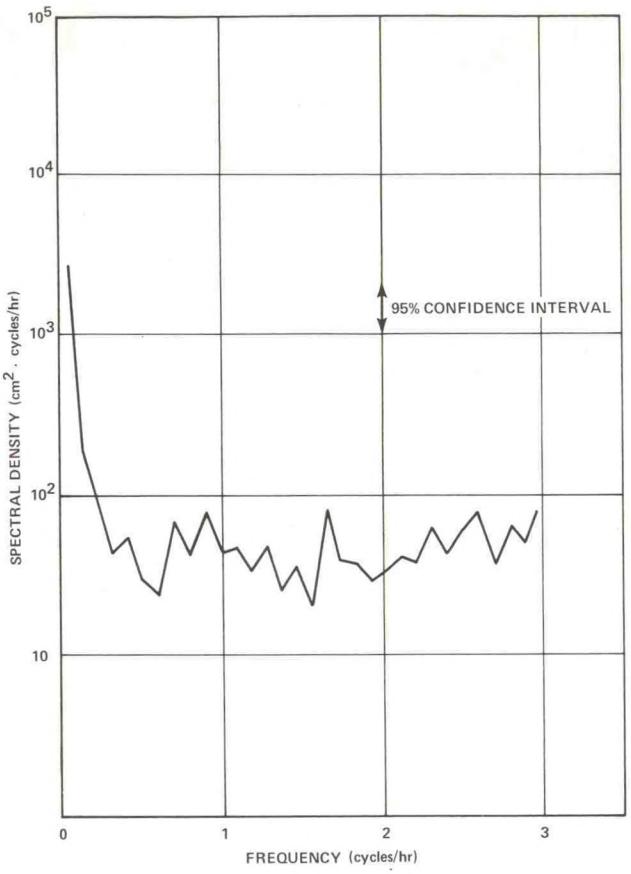


Figure 5.25.--Energy spectrum of u component of current velocity, station 1, at a depth of 17.4 m.

Station 5 in figure 5.26 is illustrative of very nearshore conditions, showing a large peak in the v component at the inertial frequency, while station 6 in the same figure gives an example of the spectra farthest offshore. The energy at tidal or inertial frequencies in the latter case does not exceed the background noise level of random processes. Most of the energy appears at lower frequencies, and could be the result of meteorological forcing. The spectra for station 13, about 40 mi east of Atlantic City, are very similar to those for station 6. Here again, most of the energy appears at the subtidal frequencies, but the largest peak is seen at 0.16 cycle/hr (6.25 hr). Examination of the u and v time histories in this record revealed considerable noise in some portions of the record, possibly as a result of instrument malfunction.

In summary, the current meter records analyzed above show the following:

(1) Mean current components are of the same order of magnitude and direction as the currents derived from ship-drift data.

(2) Variability is usually much larger than the mean value.

(3) Maximum currents are generally an order of magnitude larger than the vector mean currents.

(4) Most frequently observed current speeds are larger than the mean vector currents.

(5) Semidiurnal tides are a major component of the current close to shore, the magnitude of these tides decreasing rapidly with distance from the coast.

(6) Inertial currents appear to be prominent in the very shallow layers of nearshore mooring stations, in contrast to some findings by other investigators (e.g., Beardsley et al., 1976).

(7) There is evidence of current shear with depth under stratified conditions.

(8) Current spectra offshore reveal that most of the energy occurs at subtidal frequencies.

(9) The quality of the data appears good, although quality control procedures used during the observations cannot be readily judged from the documentation available.

More sophisticated analysis than that performed here would help resolve the detail in the spectrum, and much longer records are needed to resolve the tidal, subtidal, and inertial components of flow. For example, to separate the diurnal tidal from the inertial currents, a resolution of better than 0.0012 cycle/hr is needed, which requires a record length of 35 days. For this length of record, however, there would be only 2 degrees of freedom in

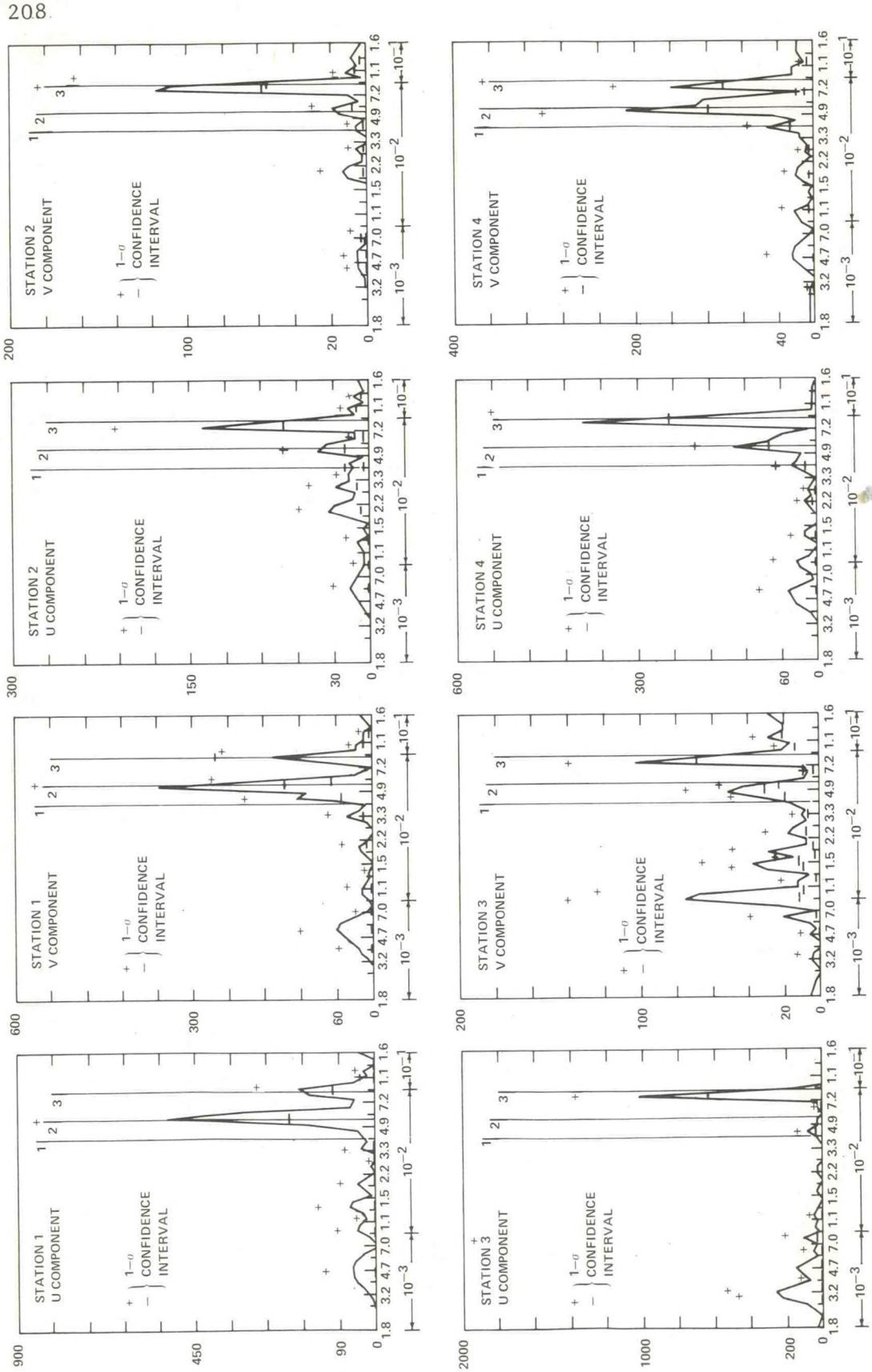


Figure 5.26.--Spectral density of u and v components of current velocity.

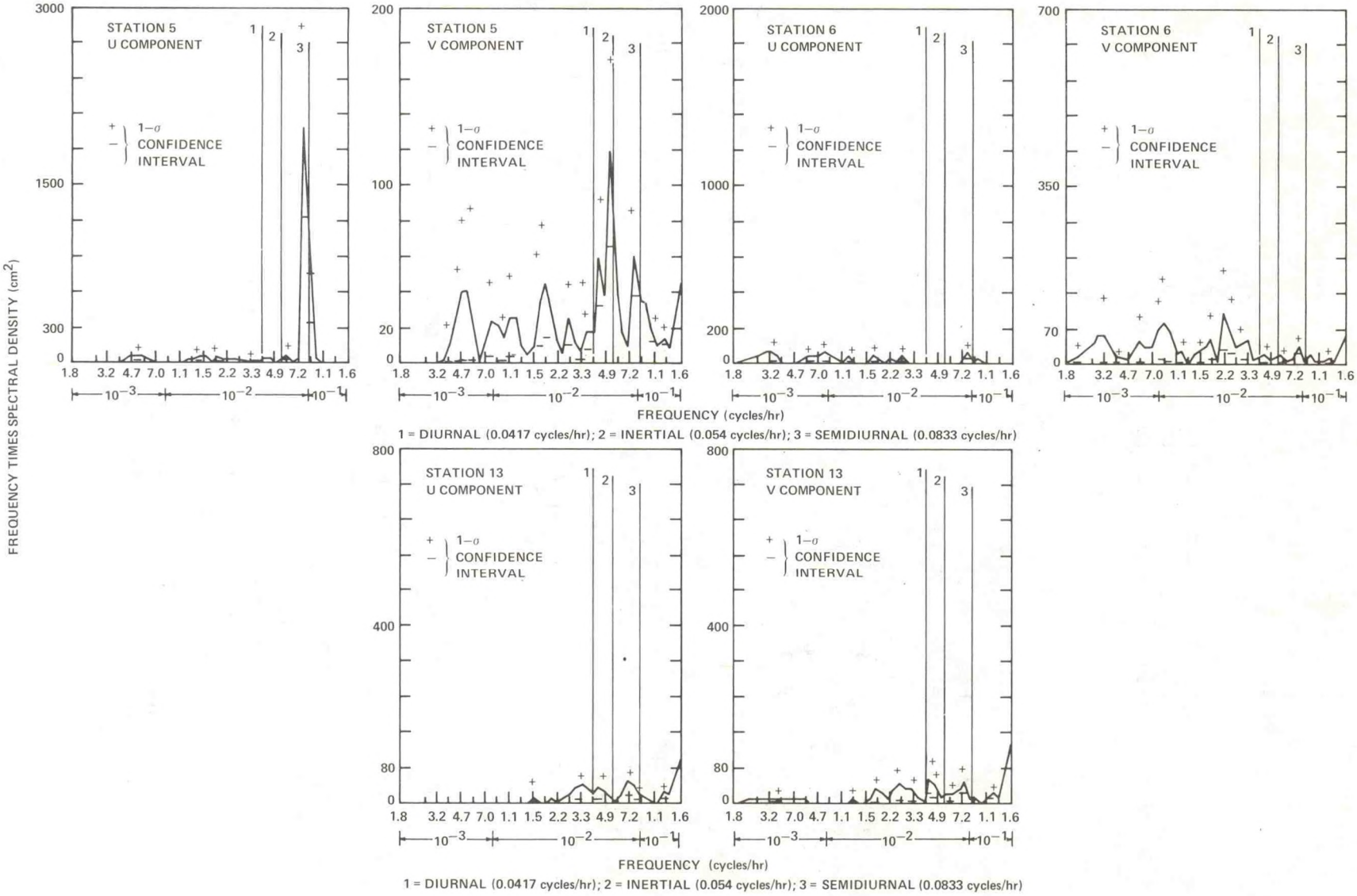


Figure 5.26 (cont.).--Spectral density of u and v components of current velocity.

the spectral estimate, making it almost impossible to distinguish a genuine spectral peak from random statistical fluctuations. A record length on the order of 350 days is needed to satisfactorily resolve these components with confidence, as well as to resolve lower frequency components due to either meteorological forcing, or forcing from the deep ocean.

Many more current meter records are needed for all areas, except the inner New York Bight, than were available at the time of this analysis. Particularly in the middle and outer shelf regions, there is a strong requirement for more data.

## 5.5 Tidal Currents

Most of the historical information available on tidal currents in the Mid-Atlantic Bight has been summarized by Haight (1942). More recent work on tidal curents in the area has been presented by Swanson (1976).

In embayments and shoal areas near the coast, tidal velocities can be quite high (2 to 3 kt, or 100 to 150 cm/s). Offshore open-sea tidal velocities are generally less than 0.1 kt (5 cm/s). Tides near the coast are generally bidirectional, while offshore the tidal flow is rotary and shows no period of slack water. The rotary tidal currents undergo periodic variations related to astronomical changes of the moon and sun, and meteorologically forced currents can also occur at near-tidal periods to produce an increase in apparent tidal variations.

The predominant tide in the Mid-Atlantic Bight is semidiurnal. A diurnal tide exists, but it is much smaller and its detailed characteristics are not well known.

Beardsley et al. (1976) found relatively sharp peaks of energy at the semidiurnal and diurnal frequencies, and noted that the amplitude of the semidiurnal peaks increased shoreward across the shelf. They observed the semidiurnal and diurnal tidal components to be weakest on the continental rise.

Current meter observations at Texas Tower 4, 70 mi southeast of New York City (Griscom, 1968), showed that semidiurnal tidal currents accounted for over 70 percent of the variance in the data at 30-m depth. The major axis of the tide ellipse was oriented 303 to 123°. Mean maximum tidal currents were about 0.3 kt (15 cm/s). Spring streams were about 45 to 50 percent stronger than neap streams.

Recent measurements of tidal currents have been carried out in the New York Bight as part of NOAA's MESA Program. Based on these measurements, tidal ellipses for the major constituents of the tidal currents have been computed by Patchen et al. (1976), who reported semidiurnal tidal current speeds ranging from 0.4 kt (20 cm/s) off New York City to 0.2 kt (10 cm/s) along the New Jersey coast close to the bottom. Maximum diurnal tidal speeds were 0.1 to 0.16 kt (5 to 8 cm/s) at 4 to 8 m above the bottom.

## 5.6 Transient Currents

Seasonal mean current speeds in the Mid-Atlantic region are low (>0.2 kt, or <10 cm/s), but the current variability is several times larger. This variability is caused by (1) tidal components that result in relatively small net movement of water, and (2) transient components that can result in large movements of water within a period of days (Boicourt and Hacker, 1976). Transient currents can be classified as follows:

(1) Inertial currents, which are excited by fast-moving meteorological disturbances.

(2) Subtidal oscillations, with durations of several days, which are believed to be excited by synoptic-scale atmospheric disturbances; examples are shelf and edge waves, although not all these disturbances are wavelike.

(3) Long-period oscillations on the order of 30 days, which are possibly forced by topographic Rossby waves, Gulf Stream meanders, or anticyclonic eddies.

### 5.6.1 Inertial Currents

Inertial currents have been measured and studied extensively on the continental slope at "site D" (39°20'N, 70°W) by Webster (1969). He found these currents to be highly intermittent in character, with amplitudes varying widely (0.1 to 0.6 kt, or 5 to 30 cm/s) without a consistent pattern. Webster points out that single 2-month time series of current measurements should be interpreted cautiously, since conditions during other 2-month periods might be very different. He demonstrates that the inertial currents observed had very low vertical coherence, but high horizontal coherence out to at least 3-km separation.

The MESA current meter records discussed in section 5.4 show evidence of inertial currents on the continental shelf, but in many of these records it is not possible to clearly differentiate between inertial energy and diurnal tidal energy because of insufficient record length.

### 5.6.2 Subtidal Currents

Subtidal current oscillations associated with strong winds lasting from one to several days have been observed by many investigators.

Beardsley and Butman (1974) made observations of surface winds at Block Island and of currents 70 km southeast of the island from March 8 to April 10, 1973. They found that west-to-east wind stresses produced major current oscillations with little net water displacement, but two storms with wind stress from east-to-west ("northeasters") resulted in mean current speeds of 0.8 kt (45 cm/s) and 0.6 kt (30 cm/s), with westward displacements of 75 km and 40 km, respectively. These two storms produced 67 percent of the total westward transport observed.

Boicourt and Hacker (1976) in 1974 deployed current meter arrays along lines perpendicular to the shelf between Cape May, New Jersey, and Cape Henry, Virginia. They observed predominantly longshore flow, with the major percentage of water displacement occurring during the passage of strong winds. High correlation was observed between current meters separated by 135 km in the longshore direction. They point out that these current records are dominated by transient atmospheric events and not by periodic signals. Boicourt and Hacker also noted the development of a high velocity jet flowing southward along the Virginia-North Carolina coasts during periods of high northerly wind stress.

Scott and Csanady (1976) observed currents 11 km south of Long Island in 32 m of water at three levels. They found that strong nontidal flow developed almost immediately in response to eastward wind stress, and that the responses of the three water layers to variable wind stress was often quite different, indicating stratification of currents of different directions during wind stress toward the east. They noted that, although wavelike analytical models are often invoked to explain transient current behavior, these models are not appropriate to their measurements, because the observed rapid response of the water column to wind stress suggests frictionally controlled flow rather than an ocillatory system. Charnell and Mayer (1975) and Patchen et al. (1976), on the other hand, from their measurements in the Mid-Atlantic Bight, observed delay in ocean response on the order of 12 to 18 hr to strong atmospheric events of a few days duration.

Extensive current measurements made by EG&G (1974) at the site of the proposed public service nuclear generating station off Atlantic City in 1972-73 showed that variances in the current spectrum at subtidal range over 2 or more days were correlated with strong surface winds.

### 5.6.3 Long-Period Oscillations

Long-period oscillations (30 days) at 100-m depth have been measured with buoys at "site D" by the Woods Hole Oceanographic Institution (Beardsley et al., 1976). The cause of these oscillations is not known, but they may be related to the interaction between the deep ocean and coastal waters--possibly to the passage of anticyclonic eddies over the eastern edge of the Bight.

Chamberlin (1977) describes an intrusion of a warm-core Gulf Stream eddy into the eastern edge of the Bight between March 1974 and May 1974. This eddy moved unusually close to the coast along the continental slope, and resulted in an abrupt warming, followed by gradual cooling during March over most of the width of the continental shelf and downward on the continental slope to just below 360-m depth.

The above observations show that transient features of long period do occur in the shelf break region, and that these features cause significant departures from mean conditions on the outer continental shelf.

## 5.7 Bottom Currents

From statistics on the recovery of seabed drifters, Bumpus (1973) and Norcross and Stanley (1967) report a general south and southwest bottom current flow, regardless of season, with definite flow toward the mouths of estuaries. This residual drift shows large variations, at times nearly reversed in direction, but the general flow pattern is consistent.

There appears to be, according to Bumpus (1973), a line of divergence, one-half to three-quarters of the way from the beach to the 100-m isobath. Shoreward of this line the drift is toward the coast; seaward, it is away from the coast (fig. 5.27). Norcross and Stanley (1967) also obtained some evidence for this line of divergence. The residual drift toward the mouths of estuaries produces an influx of shelf water of higher salinity along the bottom. The rate of residual flow above the bottom is very small, 0.0028 to 0.02 kt (0.14 to 1.00 cm/s).

The small number of bottom current meter measurements available (sec. 5.4, table 5.1), indicate high variability in bottom current, but in general speeds are considerably less than surface current speeds. Shonting (1969) measured a mean surface current speed of 0.416 kt (20.8 cm/s), and a near-bottom current speed of 0.178 kt (8.9 cm/s) in the region between Block Island and Martha's Vineyard during late July and early August 1967.

## 5.8 Summary

Currents in the Mid-Atlantic region have been analyzed based on a review of the literature, ship-drift observations, and a small number of subsurface current meter records. The analysis shows that the current regime in the region to consists of the following:

(1) The Gulf Stream, a "permanent" current flowing northeast at speeds on the order of 2 kt (100 cm/s) at the eastern boundary of the region.

(2) A mean surface current flowing generally southwest onshore of the 100-m isobath during all seasons at speeds on the order of 0.1 to 0.2 kt (5 to 10 cm/s).

Weak seasonal variations in the current, in response to changes in surface winds and river runoff, amount to about 0.1 kt (5 cm/s) in the midshelf area, but to somewhat more near the shelf break. Surface current constancy was found to be low: on the order of 20 to 40 percent in the midshelf area, and about 10 to 20 percent over the shelf break. Only large-scale features of bottom circulation are known, indicating a net southwesterly flow during all seasons of the year. In winter, bottom currents are generally in the direction of surface currents, but in summer, when vertical stability is high, they appear to be fairly independent on the surface flow. There is evidence of a shoreward flux of water close to the bottom.

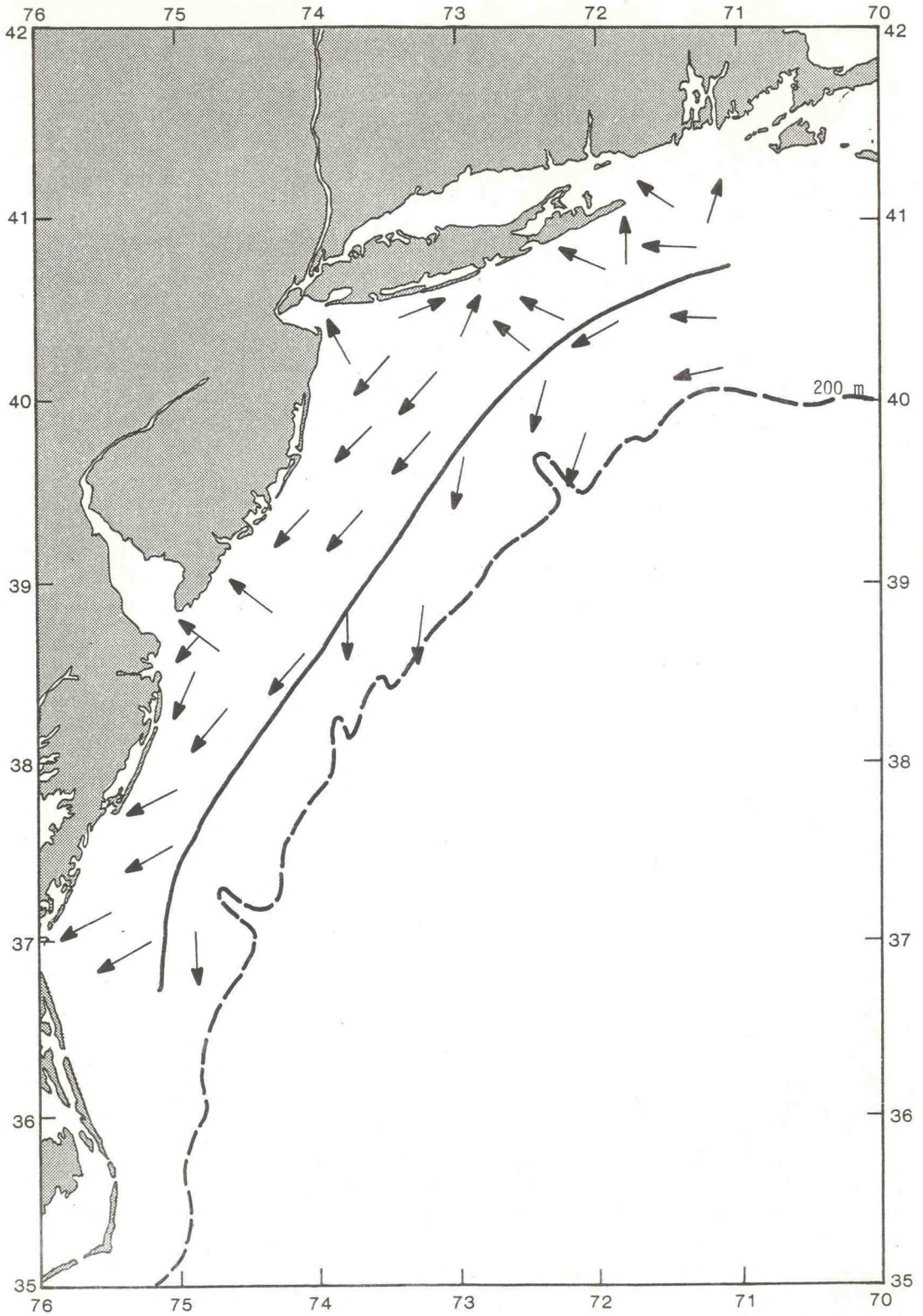


Figure 5.27.--Mean bottom currents from drifter measurements, showing line of divergence (solid line).

(3) Strong bidirectional semidiurnal tides, found near the coast with speeds as high as 2 to 3 kt (100 to 150 cm/s).

Offshore, this tide is rotary with speeds of a few tenths of a knot. A diurnal tide occurs, but is much smaller in magnitude, and its characteristics are not well known. Analysis of subsurface current meter records indicates that tidal constituents frequently account for most of the kinetic energy in the subsurface flow near the coast, but the percentage of tidal energy drops off rapidly with distance from shore.

(4) Transient currents, occurring on three major time scales: (a) inertial (18.5 hr), (b) subtidal (more than 1 day), and (c) long period (30 days or more).

Inertial currents with amplitudes of 0.1 to 0.6 kt (5 to 30 cm/s) have been observed consistently at one site on the continental slope. Current meter records give evidence of inertial currents on the inner shelf, which are believed to be excited by the passage of fast-moving meteorological disturbances. Subtidal flows, apparently resulting from synoptic-scale atmospheric disturbances produce large water mass transports on the order of tens of kilometers within only a few days. These currents appear to be highly coherent in the longshore direction for distances of over 100 km, and they could effect large spreading and dispersal of pollutants. Speeds as high as 0.9 kt (45 cm/s) have been observed from this type of flow.

(5) Long-period flows of 30 days or more, which include anticyclonic eddies moving southwest along the shelf break at 0.1 to 0.2 kt (5 to 10 cm/s) with current speeds of up to 1.6 kt (80 cm/s) within the eddy.

Long-term current moorings at 39°20'N, 70°00'W indicate considerable current energy, which may be due to these eddies or to topographic Rossby waves propagating up the continental slope. In at least one instance, an anticyclonic eddy was observed to have a major impact on the physical environment and on the biota of the continental shelf. The dispersion of a pollutant on time scales of days to weeks could be significantly aided by the presence of an eddy, since the eddies contribute greatly to the variability of the current field, although probably not much to the total water mass balance of the region.

The ship-drift data archived at NODC were found to be very useful for studying seasonal coastal currents. In some areas of the Mid-Atlantic region, comparison between currents derived from ship-drift data and currents measured by other means, such as drift bottles or surface floaters, do not show good agreement. Surface currents obtained from ship-drift observations do not show as strong seasonal variations nor the rather steady increase in current strengh with distance from the coast as do currents obtained from surface-drifter studies. On the whole, however, agreement between current patterns derived from the different types of measurement is good.

Although the state of knowledge of tidal currents appears to be adequate for estimating the horizontal dispersion rate of pollutants, one aspect not yet sufficiently known is the vertical velocity shear resulting from tidal currents flowing up the continental slope. This shear may be a key variable in

the "calving" process (bubbles detaching from the cold shelf water and moving into the slope water) and in the generation of internal waves and production of vertical turbulence.

The importance of the transient current fields is only now beginning to emerge from the few direct measurements of subsurface currents made to date, and the observations available now are enough to whet the appetite of even the most conservative investigator. Many more observations are needed, however, before the time and space scales of flow and the magnitudes of the horizontal and vertical velocity shears can be reliably delineated for use in trajectory models.

## 6. VERTICAL MIXING

The probable vertical distribution of spilled pollutants can be an important factor in environmental risk assessment. In the case of oil, for example, weathering and the inclusion of sand or other particulate matter can increase the density of the oil and result in lumps floating below the sea surface (e.g., Neumann and Pierson, 1966). These residues can sink into the sediments, with possible harm to the benthic fauna.

Vertical mixing in the ocean can occur by convective processes, by mechanical stirring, such as surface wind-wave mixing, by tidal current mixing, or by diffusion. Vertical mixing is therefore a function of the density stratification and of the vertical turbulence. Mixing processes in estuaries have been studied extensively (e.g., Bowden, 1976), but few major studies have been made of mixing in open coastal waters. One reason is that the geometry and dynamics of estuaries often permit simplifying assumptions in the interpretation of the data that would not be valid for the open ocean. For example, in the case of estuaries, advection can sometimes be neglected, concentration gradients can be specified in only one dimension, and boundary conditions can be simplified. In the open ocean, the problem is fundamentally three-dimensional and the precise statement of boundary conditions is difficult.

A quantitative formulation of vertical mixing for incorporation in pollution dispersion models applicable to the Mid-Atlantic region would require both an extension of theoretical work performed in conjunction with estuarine studies (e.g., Officer, 1976), as well as dedicated field experiments. Efforts in this direction are now being made, for example, by Christodoulou et al. (1976).

Perhaps the most important quantity required to parameterize vertical mixing is the flux Richardson number, which can be defined as the ratio between the increase in potential energy due to mixing and the kinetic energy of turbulent flow (Officer, 1976). Evaluation of the flux Richardson number is difficult, and can be subject to large fluctuations resulting from relatively small experimental errors. It can be done by dividing the product of the vertical density gradient and the acceleration due to gravity by the product of mean water density and the square of the vertical velocity shear, and then multiplying this result by the ratio of the eddy diffusivity coefficient to the eddy viscosity coefficient. The flux Richardson number varies between 0 and 1, where small values indicate a well-mixed condition, and values closer to 1 indicate a stratified condition in which mixing is suppressed. The eddy viscosity and diffusivity coefficients can be evaluated from spatial and temporal distributions of such conservative properties as salinity and from the velocity distribution. These coefficients, and the vertical shear of horizontal velocity, vary in general with depth and location so that a large number of synoptic measurements at several locations over the four seasons are required.

Archived data in support of the evaluations mentioned above are not available at present, but individual investigators have performed experiments that give insight into the vertical mixing problem in the Mid-Atlantic region (e.g., Voorhis et al., 1976). Also, now emerging from NOAA's MESA program are data that may add to the data base required for model evaluation. Since all

types of mixing produce changes in the vertical density profile, some deductions from the seasonal march of the vertical density gradient and the depth of the vertically mixed layers are presented below.

## 6.1 Method of Analysis

Implications regarding the extent of vertical mixing are drawn from the analysis of water "stability", E, defined by Hesselberg and Sverdrup (1914) to be the vertical density gradient. Large positive values of E imply strong vertical stratification, which inhibits vertical mixing; small positive values of E imply deep vertical mixing, as caused, for example, by strong winter winds. Here, E will be closely approximated by $\Delta\sigma_t/\Delta z$, the vertical gradient of density, $\sigma_t$, multiplied by $10^3$, to provide a convenient numerical range.

To reduce the noise level, $E \equiv (\Delta\sigma_t/\Delta z) \times 10^3$ was computed by a smoothing procedure in which the vertical density gradient for each level was calculated from the slope of the least-squares line fit to five adjacent standard level density values.

## 6.2 Seasonal March

Values of stability for areas 5, 6, 8, 9, and 12 are given in table 6.1 for all seasons.

Winter. In the mid-shelf areas 5, 6, and 8, stability is low, and variability is high. The water column for area 6 in winter, shown in figure 6.1, is nearly homogeneous, with only a slight increase in density from surface to bottom. This is associated with strong wind mixing and surface cooling. The offshore areas 9 and 12 show similar characteristics in the first 100 m, but stability below 100 m decreases smoothly to near zero in the bottom layers. Seasonal density changes in the upper 100 m for area 9 are shown in figure 6.2. During winter, density increases very gradually with depth, and mixing occurs throughout the water column on the shelf and down to the depth of penetration of seasonal influence on the slope (> 200 m).

Spring. Warming and river runoff in the surface layers combine to decrease density in the surface layers, and thus increase stability. Figures 6.1 and 6.2 show the decrease in density on both the shelf and the slope, and table 6.1 shows the slight increase in stability. Under these conditions, vertical mixing will not be as strong as during winter, but there is no "barrier" to vertical mixing.

Summer. Surface heating and inflow of river water are associated with a further increase in the near-surface stability on the shelf (fig. 6.1). Stability is also high in the top 30 m on the slope, as seen in table 6.1, with increasing values toward the south. Area 9 shows evidence of a definable mean mixed layer 15 m deep (fig. 6.2). Area 10 does not have a mixed density layer, but rather a steady increase of density with depth as illustrated in figure 6.3. This may be due to the rather steady increase of salinity with depth, or it could be the result of averaging over a near-discontinuity which fluctuates widely in depth. The increase of density with depth in the shelf

Table 6.1--Vertical stability $E \equiv (\Delta\sigma_t/\Delta z) \times 10^3$

| Depth (m) | Winter | | Spring | | Summer | | Fall | |
|---|---|---|---|---|---|---|---|---|
| | Mean | Stand. dev. | Mean | Stand. dev. | Mean | Stand. dev. | Mean | Stand. dev. |
| | | | | Area 5 | | | | |
| 10 | 9.1 | 20.6 | 54.1 | 51.5 | 100.0 | 43.4 | 8.0 | 13.0 |
| 20 | 15.2 | 3.2 | 49.3 | 36.7 | 92.8 | 41.6 | 6.27 | 13.8 |
| 30 | 2.2 | 6.7 | 23.5 | 14.6 | 61.5 | 22.9 | 6.3 | 8.3 |
| 40 | 1.7 | 2.8 | 14.4 | 8.4 | 33.2 | 16.7 | 13.0 | 12.1 |
| 50 | | | | | 30.0 | 7.15 | | |
| | | | | Area 6 | | | | |
| 10 | 5.3 | 20.5 | 74.5 | 108.8 | 167.0 | 123.2 | 16.1 | 28.6 |
| 20 | 17.4 | 36.2 | 74.5 | 85.6 | 125.4 | 81.1 | 44.1 | 68.8 |
| 30 | 6.2 | 14.2 | 29.0 | 42.1 | 65.3 | 45.3 | 26.6 | 32.1 |
| 40 | 2.0 | 6.0 | 9.6 | 10.1 | 31.6 | 19.5 | 38.4 | 13.1 |
| | | | | Area 8 | | | | |
| 10 | 24.7 | 74.5 | 147.9 | 164.7 | 226.4 | 225.5 | 50.2 | 104.7 |
| 20 | 2.6 | 5.8 | 38.4 | 45.9 | 119.8 | 102.0 | 14.8 | 27.2 |
| | | | | Area 9 | | | | |
| 10 | 2.5 | 4.8 | 5.0 | 28.9 | 50.2 | 49.2 | 9.5 | 29.3 |
| 20 | 3.1 | 5.0 | 30.0 | 19.6 | 64.4 | 36.4 | 10.9 | 19.5 |
| 30 | 4.3 | 6.3 | 22.3 | 23.4 | 63.8 | 19.8 | 15.2 | 19.7 |
| 40 | 4.3 | 5.3 | 19.8 | 9.6 | 48.6 | 17.3 | 16.8 | 18.0 |
| 50 | 4.0 | 4.3 | 14.3 | 7.2 | 32.8 | 11.2 | 16.7 | 13.8 |
| 60 | 3.5 | 4.0 | 8.3 | 13.7 | 23.0 | 8.3 | 16.8 | 12.6 |
| 70 | 3.6 | 3.6 | 8.9 | 12.1 | 16.5 | 6.5 | 14.5 | 9.4 |
| 80 | 3.6 | 4.5 | 6.7 | 8.5 | 12.8 | 5.3 | 12.9 | 10.0 |
| 90 | 3.7 | 4.1 | 7.3 | 6.6 | 9.6 | 4.3 | 11.5 | 7.8 |
| 100 | 3.2 | 3.2 | 7.1 | 8.2 | 7.6 | 3.6 | 10.1 | 5.1 |
| | | | | Area 12 | | | | |
| 10 | 0.13 | 13.8 | 53.3 | 84.2 | 123.6 | 148.7 | 26.3 | 52.5 |
| 20 | 2.5 | 5.7 | 36.6 | 35.4 | 130.3 | 95.0 | 26.6 | 31.0 |
| 30 | 2.8 | 7.2 | 19.3 | 22.0 | 58.2 | 50.4 | 34.9 | 28.0 |
| 40 | 2.5 | 4.4 | 18.4 | 15.3 | 36.1 | 24.8 | 29.6 | 22.4 |
| 50 | 1.9 | 2.8 | 15.0 | 11.5 | 25.8 | 17.8 | 22.9 | 17.8 |
| 60 | 2.6 | 4.2 | 13.0 | 9.6 | 18.2 | 16.3 | 18.4 | 17.4 |
| 70 | 2.9 | 2.9 | 10.3 | 8.3 | 15.8 | 14.6 | 18.5 | 12.2 |
| 80 | 3.4 | 2.7 | 9.0 | 6.8 | 16.0 | 11.4 | 20.7 | 17.5 |
| 90 | 3.5 | 3.9 | 8.2 | 5.5 | 11.9 | 7.3 | 14.9 | 8.5 |
| 100 | 3.8 | 4.8 | 6.6 | 4.5 | 8.1 | 5.4 | 11.4 | 8.1 |

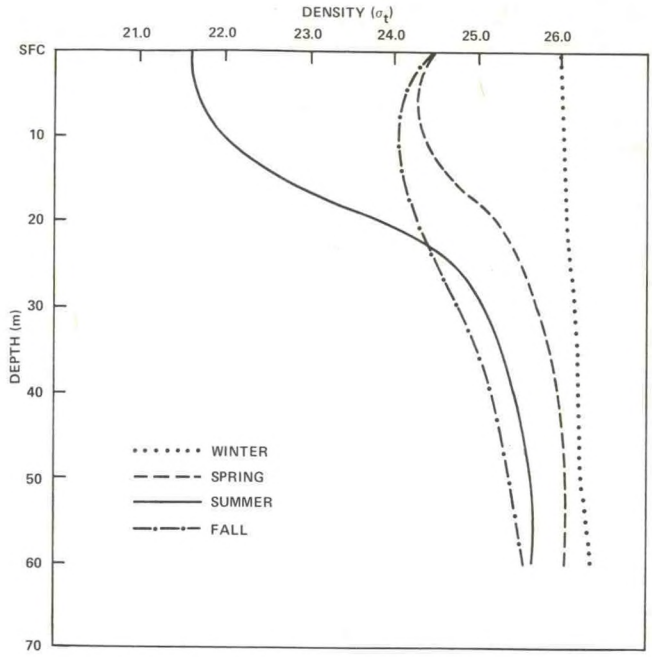


Figure 6.1.--Mean vertical density profiles, area 6.

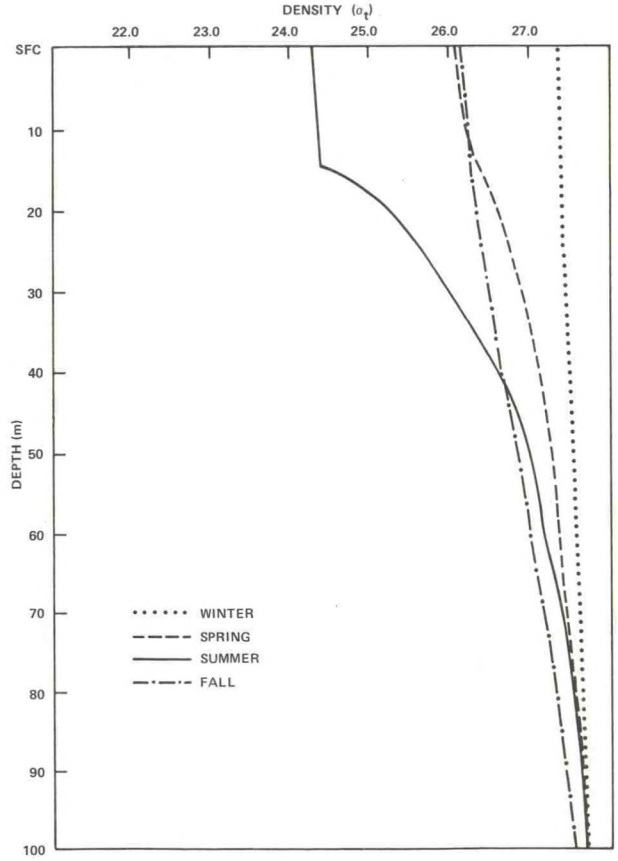


Figure 6.2.--Mean vertical density profiles, area 9.

and slope waters opposes vertical mixing, and facilitates the generation and propagation of internal waves.

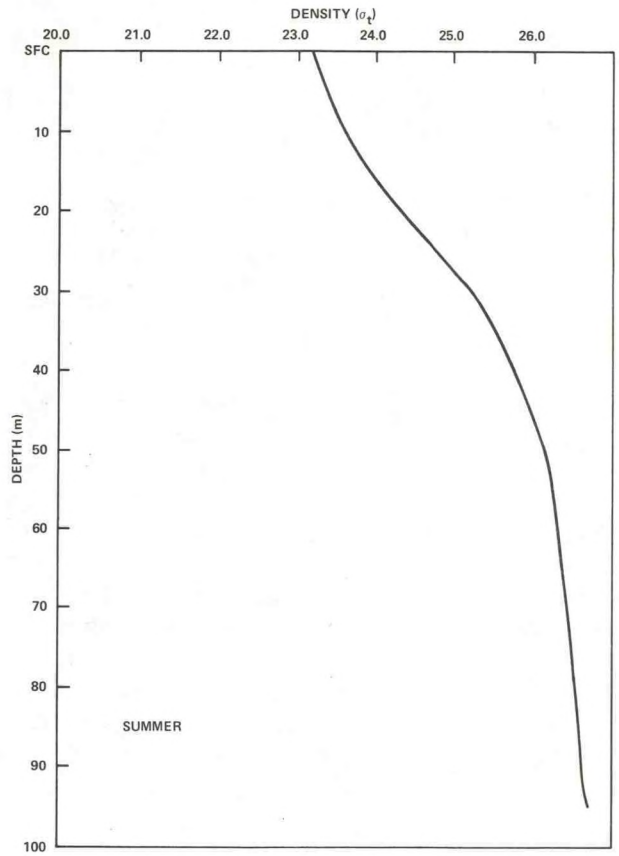


Figure 6.3.--Mean summer vertical profile, area 10.

In section 5 of this report, reference was made to cases of apparent decoupling of near-surface and bottom currents (e.g., Shonting, 1967; Scott and Csanady, 1976). MESA data archived at NODC also indicate that inertial currents do not seem to extend beneath the pycnocline. Hence, the strong vertical density stratification, as well as the weaker winds and waves, in summer tend to result in differences in speed and direction between surface and bottom currents. This difference would produce a current shear that would enhance turbulent mixing, i.e., increase the flux Richardson number. Since mean density generally increases steadily with depth, however, it would be difficult to prepare a chart of mean mixed layer depth.

The distribution of nutrients is often useful for drawing inferences regarding patterns of oceanic mixing. For example, the analysis of dissolved phosphate concentration in area 6 in summer (sec. 4.5.2) shows the effect of the Hudson River plume in reducing surface water density and thus increasing

near-surface stability. The concentration in the surface water of area 5 is similar, suggesting that land runoff may be important in determining near-surface water characteristics in these areas. As another example, the dissolved oxygen distribution for area 9 in March (sec. 4.5.2) appears to show the effects of strong vertical mixing, which corroborates the stability data for this area in winter (table 6.1). For the most part, however, there is insufficient nutrient data in the Mid-Atlantic region to infer the intensity of vertical mixing.

Fall. Surface cooling and evaporation increase density both on the shelf and on the slope, as seen in figures 6.1 and 6.2, resulting in lowered stabilities of both shelf and slope water (table 6.1). Autumn convective overturn on the shelf in the fall, with subsequent return to winter conditions, can be quite rapid (within a week) and dramatic, as has been shown by Shonting et al. (1966).

## 6.3 Summary

The time and space scales over which important mixing processes occur have not been adequately documented. The data available from the NODC archive make it possible only to infer a description of seasonal mixing in general, qualitative terms from stability profiles. In summer, high surface temperature, low bottom temperature, low surface salinity, and high bottom salinity, coupled with generally weak southwesterly winds, produce large vertical density gradients over the entire shelf and slope. The resulting strong buoyancy force would oppose the mechanical downward mixing of surface pollutants. The presence of a seasonal pycnocline on the shelf is prima facie evidence that there is a barrier to vertical mixing in summer. However, turbulent diffusion enhanced by vertical current shear and turbulent flow fields associated with internal gravity waves can produce some vertical mixing under such conditions.

In winter, strong northwesterly winds and weak stratification would facilitate the mixing of a pollutant rapidly throughout the entire water column, and to a depth of 200 m or more on the slope. The surface and bottom flows appear to be relatively uniform under these conditions.

Mixing over time scales of days or even hours, and space scales of meters in the vertical, may bring about changes that may be locally as large as the seasonal variation, as seen from case studies and experiments conducted by Boicourt and Hacker (1976) and Voorhis et al. (1976). Some of these important mixing processes have only just begun to be identified. Officer (1976) notes that estuaries are generally found in one of two preferred states, either vertically well mixed or noticeably stratified. These two states seem to correspond to winter and summer conditions, respectively, in the inner and midshelf regions, with spring and fall belonging in one or the other category, depending on the weather patterns of a particular year.

In summary, although the historical data base is useful for developing a qualitative description of seasonal mixing patterns based on T-S characteristics and mean vertical density profiles, it is of limited value for establishing a climatology of specific scales of dispersion of pollutants on time scales of days to weeks. Further model development and dedicated field experiments are required for delineating these scales.

# 7. OCEAN WAVES

## 7.1 Data Sources

The major source of data on surface wave direction, height, and period in the Mid-Atlantic region are the Marine Deck observations on file at the National Climatic Center.

Visual observation of waves from ships is very difficult and can lead to biased data (Gutman, 1976). Apparent wave heights depend on, for example, the height of the observer above water, visibility conditions, the stability of the platform, and the skill and motivation of the observer. Also, instructions for wave observations have changed over the years. In 1929, the Douglas scale was used for reporting swell waves. A new wave observation code adopted by the World Meteorological Organization came into general use in 1949, which was changed again in 1968 to try to correct difficulties encountered when observers converted visual wave observations to code for data logging and transmission.

The National Climatic Center has instituted various quality control procedures to attempt to correct some of the errors apparently due to misunderstanding of the coding instructions. Some of these procedures, however, may not be suitable for application to shallow coastal areas, such as the Mid-Atlantic Bight.

Previous studies have shown that visual observations, especially of wave periods, do not compare well with concomitant observations by wave recorder (Pierson, 1956 and 1977; Harris, 1972). In addition, some important characteristics of the wave field cannot be determined from visual observations, most important of which is the spectrum. Pierson (1974) has suggested procedures whereby reasonably correct visual estimates of wave height and period can be obtained, but these procedures have not been in common use except on a few research or ocean station vessels, nor are they incorporated in the current "National Weather Service Observing Handbook" No. 1 (U.S. Department of Commerce, 1974). Because of the rarity of surface wave observations with instruments, visual observations will of necessity continue to play a role in studies of the wave climatology of the Mid-Atlantic Bight.

Theoretical wave hindcasting models, based on limited data sets, have been used by oceanographers in the past, but application of an appropriate hindcast model for this study was prevented by the lack of suitable wind data. A limited comparison of wave height and wave period statistics for climatological area 7 (see fig. 2.1, sec. 2) in summer with height and period data produced by a hindcast model applied to the Longbranch, New Jersey, area (Saville, 1954) indicated that model results compare favorably with wave statistics obtained from observations.

## 7.2 Analysis

Most of the analyses presented in this section are based on summaries of surface wave observations. In the analysis of extreme wave height, however, estimated wave conditions were used, derived from both empirical and theoretical relationships between wind speed, wind fetch, and wind duration. This was done because shipping has in the past avoided areas of heavy seas, resulting in biased observation records. Also, maximum wave height is associated with a single wave within a whole field of waves and may not be seen by an observer even if a ship were in the region of maximum waves.

### 7.2.1 Wave Roses and Wave Height-Period Diagrams

Statistics on wave direction, and wave height vs. wave period are important inputs to wave refraction models, to platform design computations, and to marine operations in general. Height-period relationships, for example, determine ships' pitch and roll.

As wave trains approach the shore from deep water, they are refracted by the rapidly shoaling bottom, thus modifying the deepwater behavior of the waves. In general, as water depth decreases, so does the speed of the wave crests, which results in refraction of wave trains, especially over submarine ridges and valleys. When the shoreward-moving wave trains arrive in very shallow water, increasing bottom friction results in the waves' breaking along the shoreline or over shoals. In addition to refraction and breaking, interference and diffraction of wave trains are caused by bottom topography. This high dependence of the surface field in shallow areas on local geography and topography underscores the need for analytical and numerical modeling (Goldsmith et al., 1974) and for use of instruments in obtaining lengthy records on surface waves at carefully selected sites.

With recognition of the possible bias in visual surface wave observations, these observations are used here to give a general description of wave conditions in areas 4, 6, 9, and 11, shown in figure 7.1. Areas 4 and 6 represent typical shallow water conditions on the shelf, while areas 9 and 11 represent conditions along the continental slope, where depth increases rapidly seaward. It is hoped that the wave climatology for these areas can provide guidance for the design of experiments to more accurately quantify surface wave parameters needed for engineering applications.

Area 4 has a representative depth on the order of 50 m. It is severely fetch-limited to the west and north, and very high waves would not be expected when the wind is from these directions. Monthly wave roses for winter (November to April) for this area are shown in figure 7.2, and for summer (May to October) in figure 7.3. It is seen that seas are higher in winter, and that the predominant wave direction from November to February is from west to northwest. The highest waves, from 6 to 7.5 m, are observed in December, January, and February, but for only a very small percentage of the time. Thirty percent of the time, the waves propagate from a westerly direction and are less than 1.5 m in height. In June and July, the waves are almost exclusively from the southwest and south and less than 1.5 m high. Height-period histograms for area 4 for winter and summer, shown in figure 7.4, indicate that waves as high as 9 m have been observed in winter, although

rarely, whereas in summer the maximum height is 5 m.

In deep water, higher waves are generally expected to have longer periods, but in shallow water, when refraction affects the waves, the height of the waves is expected to decrease without significant modification of the wave period (Kinsman, 1965). Therefore, wave height-period statistics for shallow water areas cannot be expected to show the expected association between long (short) period waves and high (low) height.

In area 6, much the same conditions were found as in area 4, except that waves were higher, as seen in figures 7.5 to 7.7. The lack of resolution between the range of wave periods associated with various wave heights for both areas 4 and 6 (figs. 7.4 and 7.7) may be attributed to shallow water affects. According to Gutman (1976), as noted earlier, ship observations of wave periods are commonly biased toward short periods, which may also explain the height-period statistics shown here. Note, however, the relatively strong component of waves in area 6 from the northeast in September. Also, the difference between winter and summer is more pronounced than for area 4. As seen in figure 7.7, in summer very few waves higher than 3 m are observed, whereas in winter such waves are not uncommon, particularly waves with a period of 6 s or more.

Area 9 represents an essentially deepwater area in a generally more exposed position than areas 4 and 6, i.e., longer fetches from the southwest and north, but shorter fetches to the west than in area 6. The wave statistics in figures 7.8 to 7.10 indicate that observed wave heights and directions are very similar to those in area 6 (figs. 7.5 to 7.7), with slightly higher waves observed in area 6.

The wave climatology in areas 9 and 11 appear to be very similar, although the occurrence of long-period waves ($\geq$ 6 s) is slightly more frequent in area 11. Wave directions are similar to those in the other areas (figs. 7.11 to 7.13).

The wave height-period diagrams for the deepwater areas 9 and 11 (figs. 7.10 and 7.13) do not show the expected wave-period differences between different wave heights. As in the shallow-water areas, observer error may have affected these statistics; however, a low "ground swell" with a period of 6 to 9 s and a wave height of less than 0.7 m is often observed in eastern coastal waters. The fact that these wave roses indicate waves approaching predominantly from the west despite the nearly unlimited fetch to the east is of particular interest when one considers that the energetic wave fields that would be detrimental to marine operations usually occur during hurricanes, when the winds are from the southeast, or during "northeasters," when the winds are from the northeast (Pierson, 1977). It appears likely, as Goldsmith et al. (1974) have suggested that there is a bias in the visual ship observations toward fair weather, since ships tend to avoid severe weather conditions or not to make observations during such conditions because of hazardous conditions on deck. This bias in the Marine Deck observations has also been found in a study by Quayle (1974), who compared transient-ship records with those from ocean weather stations.

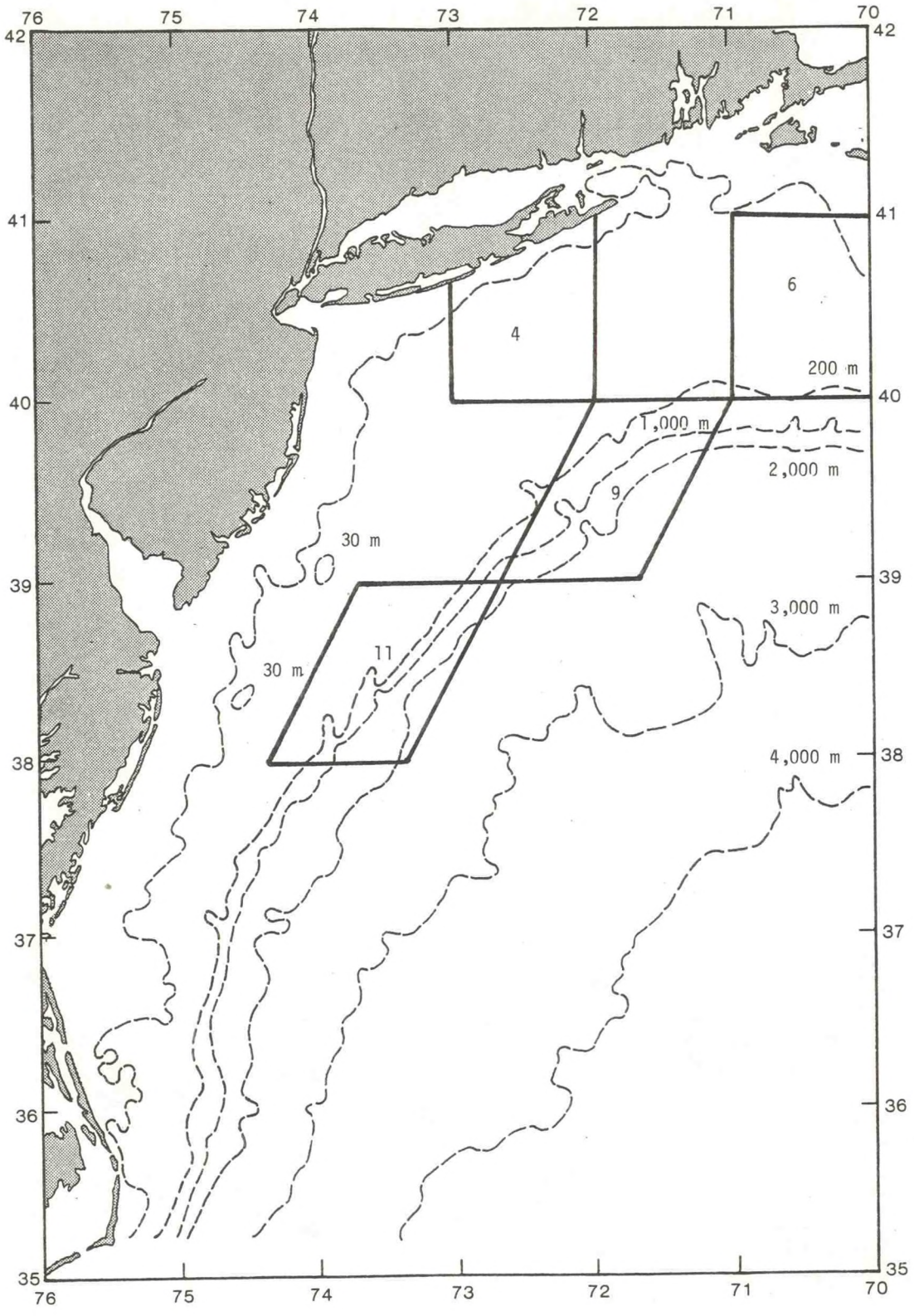


Figure 7.1.--Climatological areas analyzed, showing bottom topography.

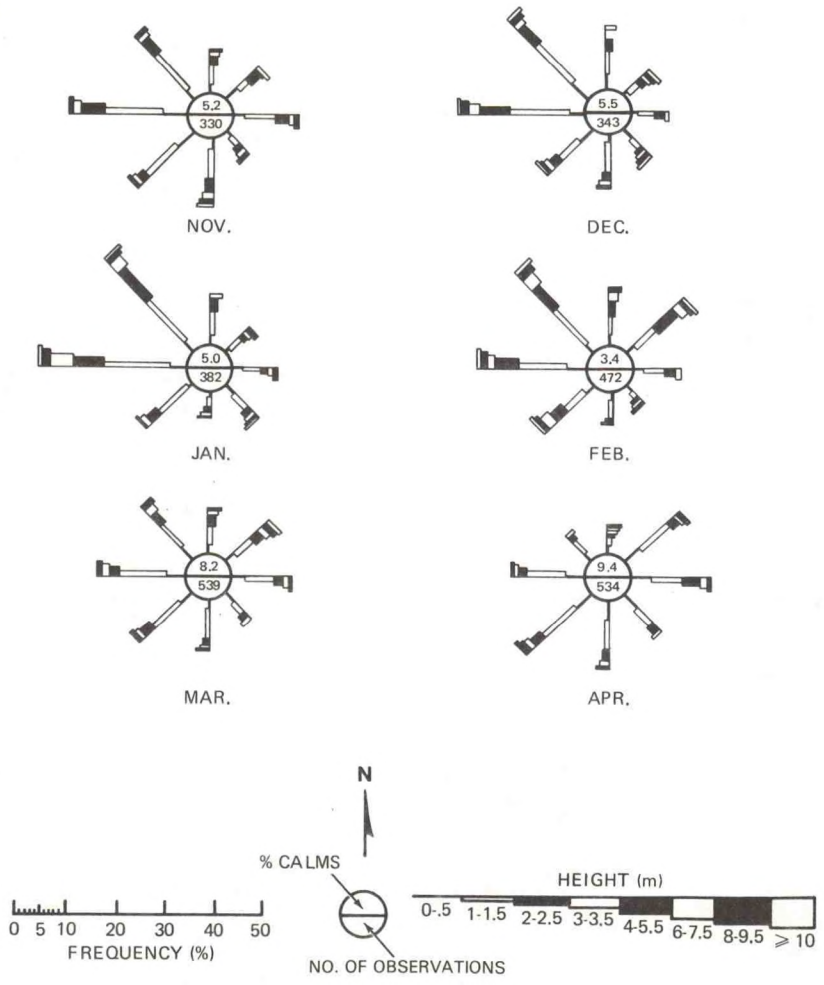


Figure 7.2.--Winter wave roses, area 4.

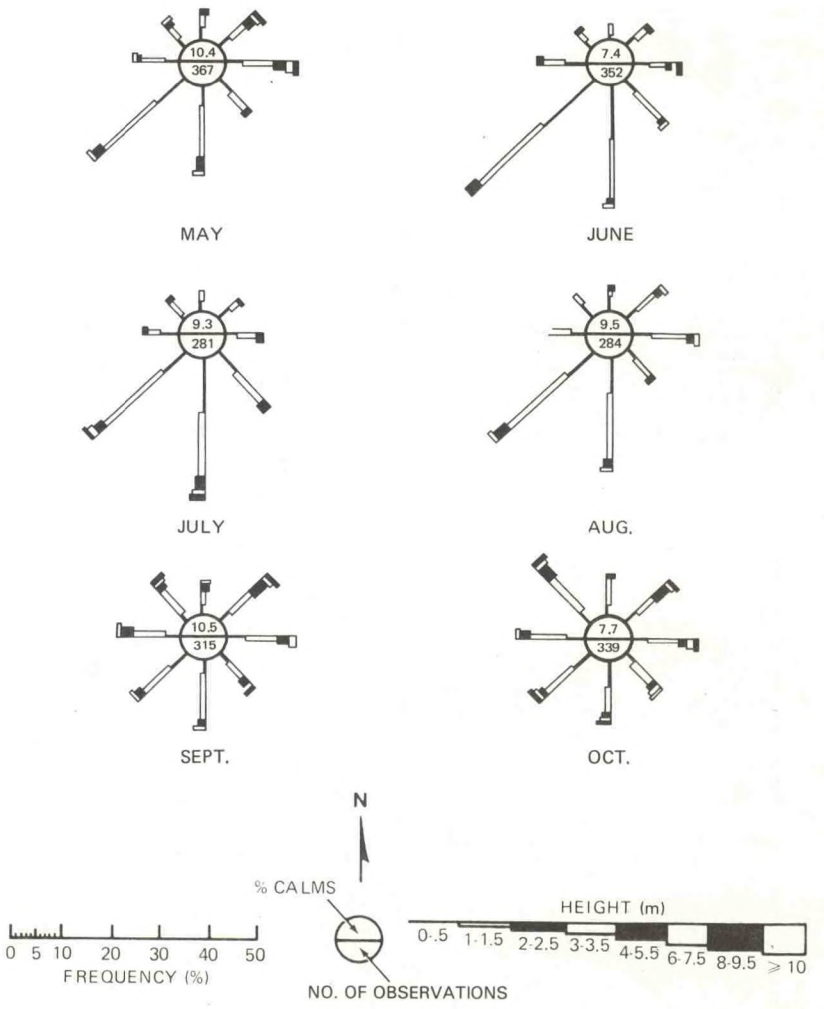


Figure 7.3.--Summer wave roses, area 4.

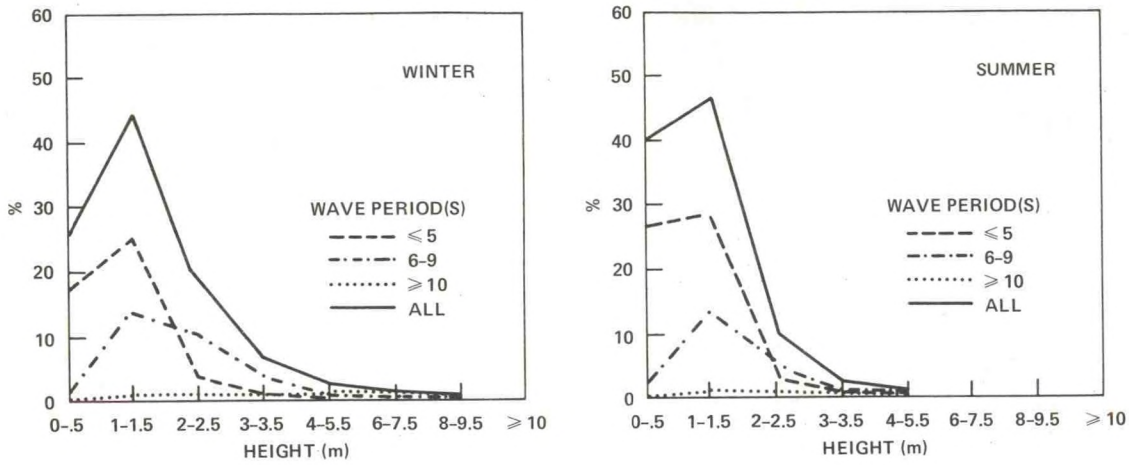


Figure 7.4.--Wave height-period histograms, area 4.

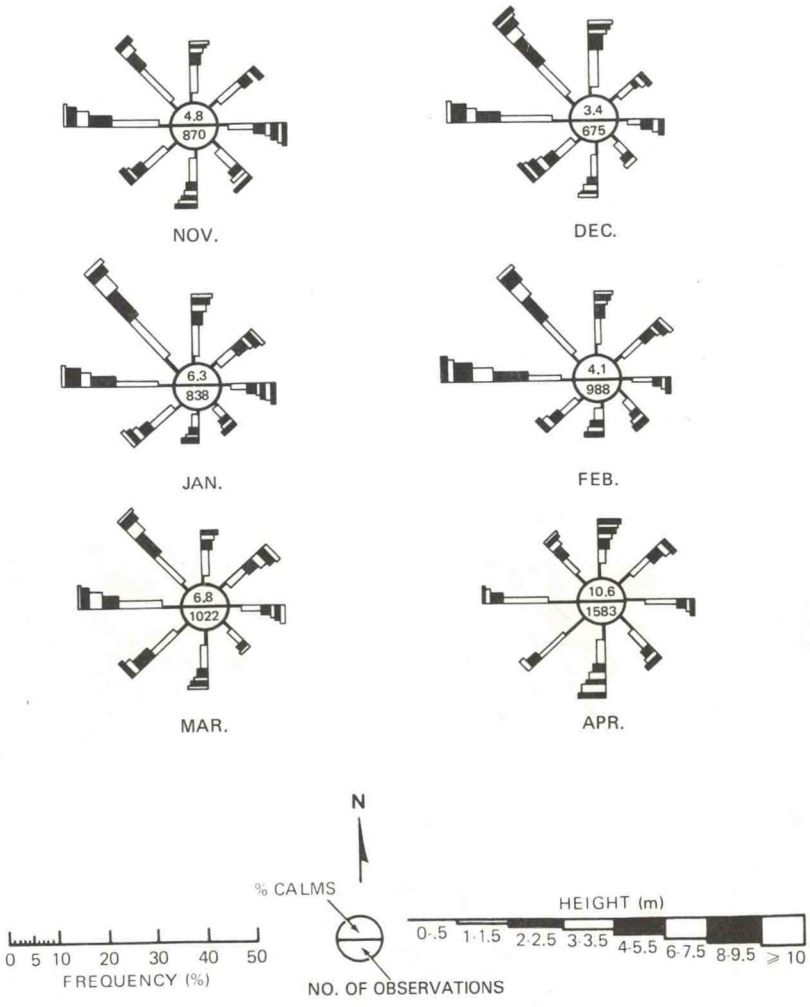


Figure 7.5.--Winter wave roses, area 6.

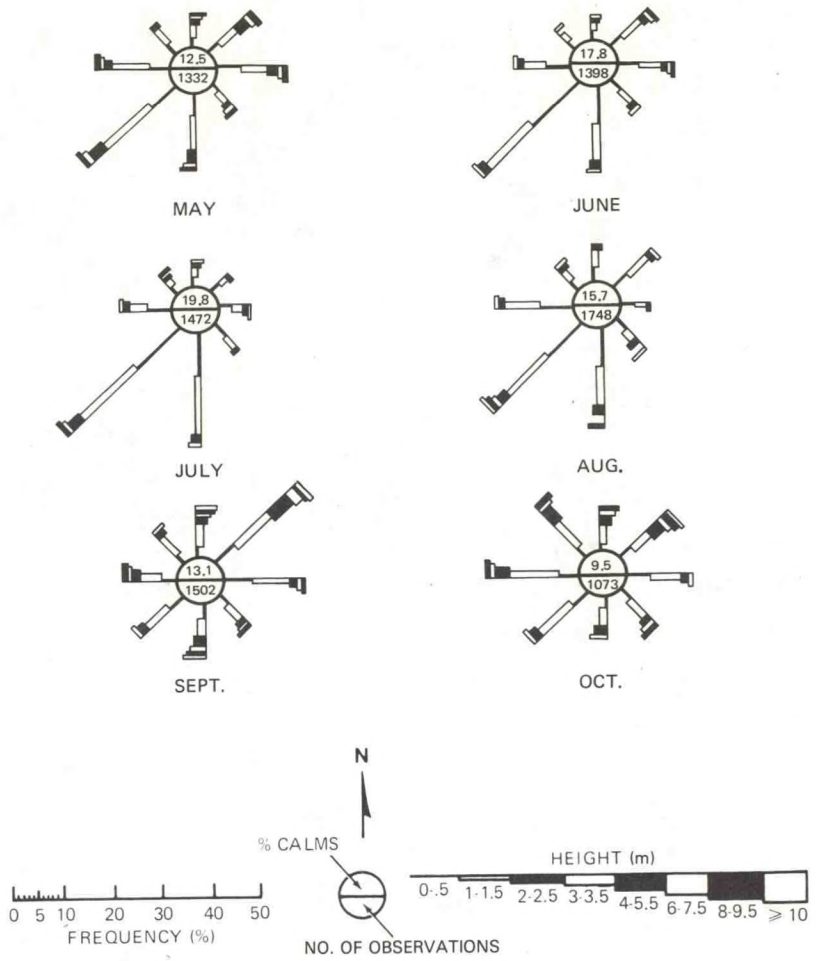


Figure 7.6.--Summer wave roses, area 6.

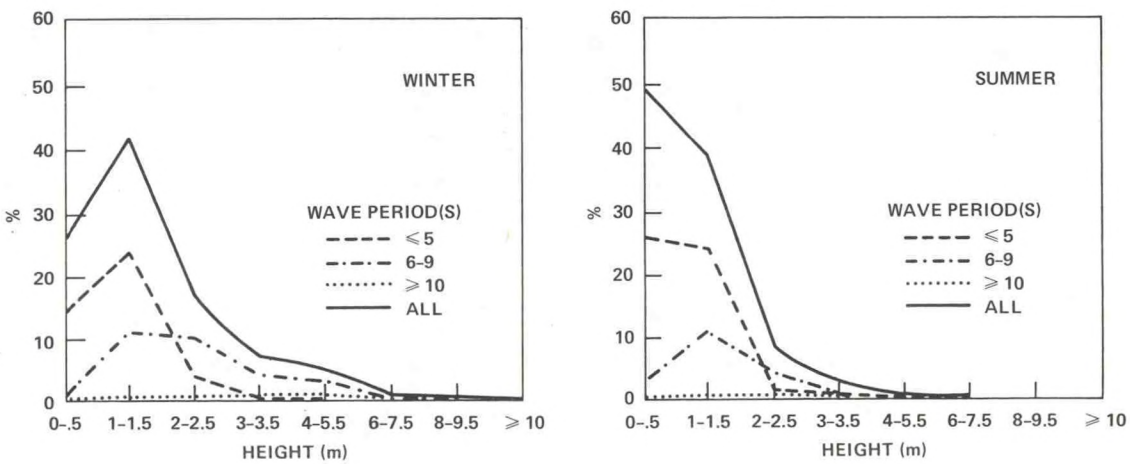


Figure 7.7.--Wave height-period histograms, area 6.

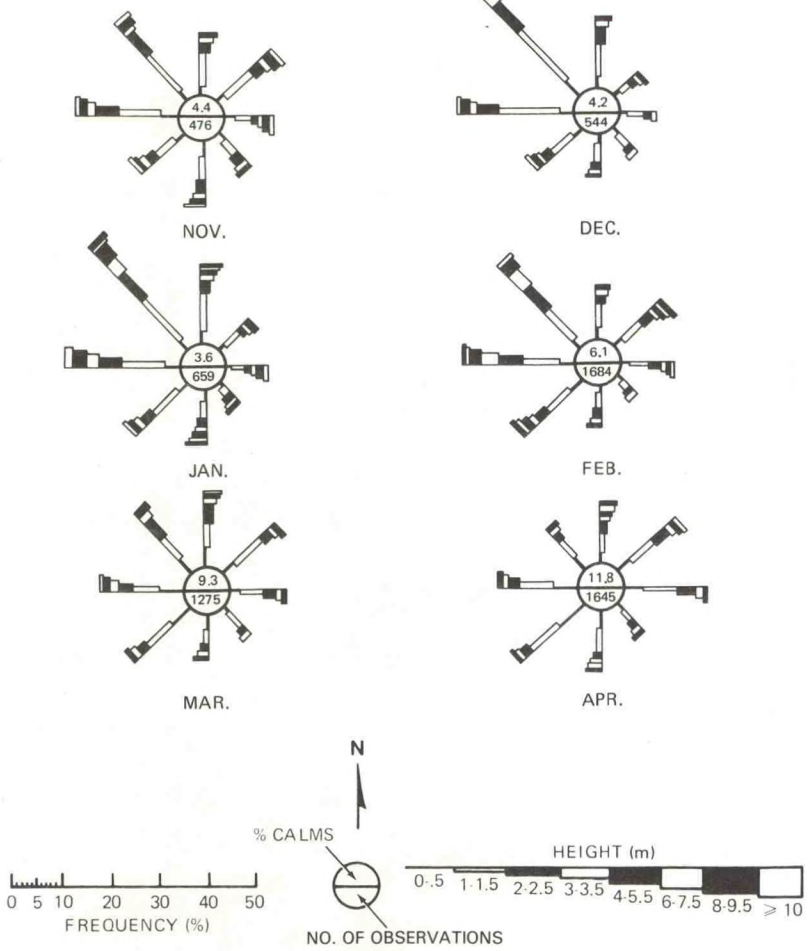


Figure 7.8.--Winter wave roses, area 9.

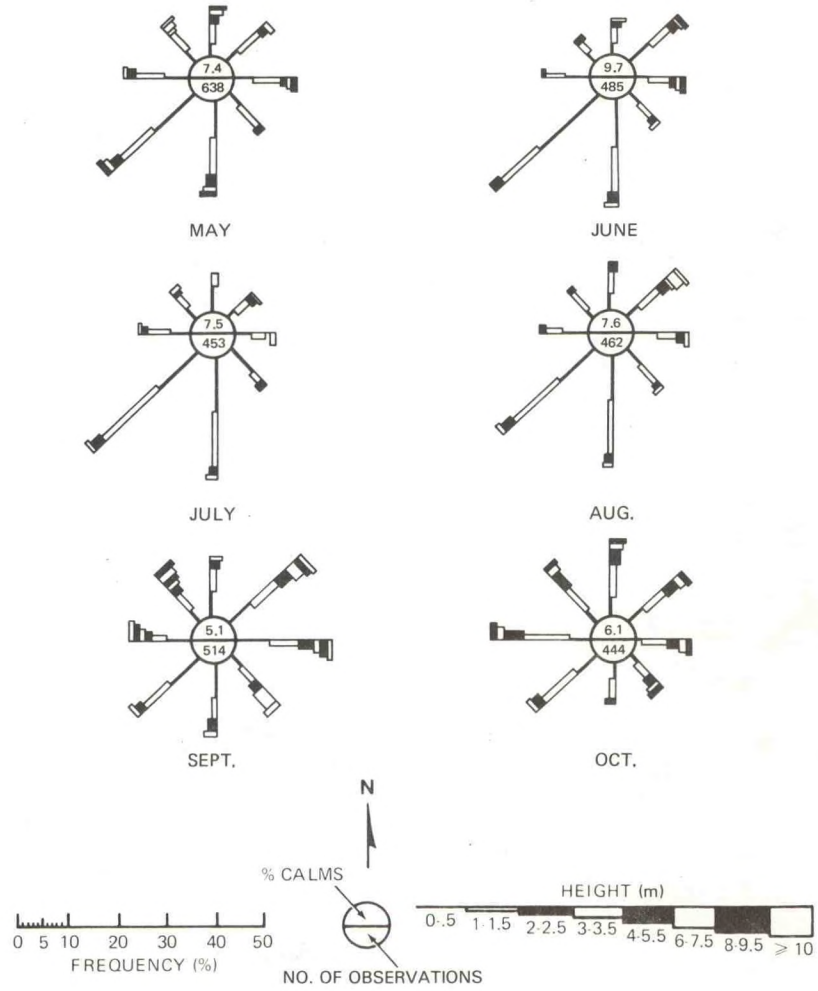


Figure 7.9.--Summer wave roses, area 9.

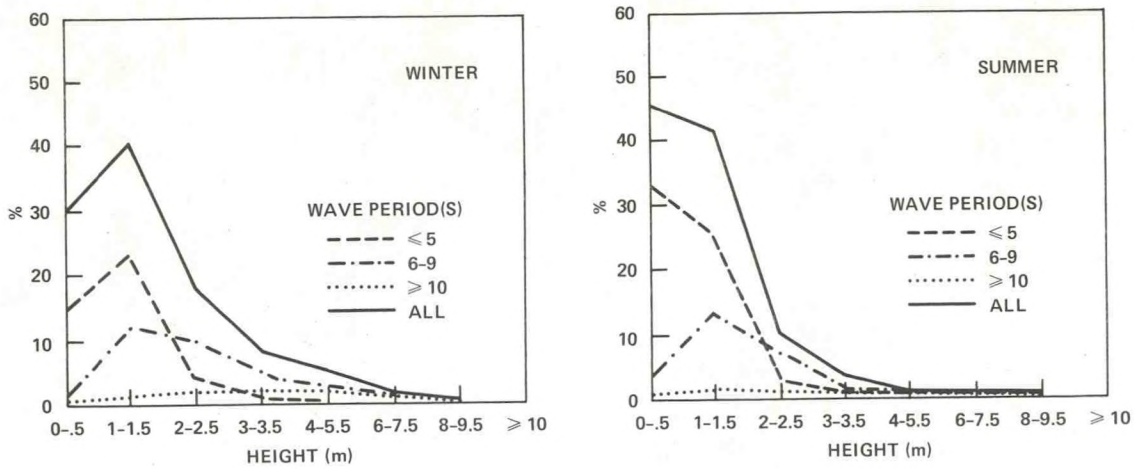


Figure 7.10.--Wave height-period histograms, area 9.

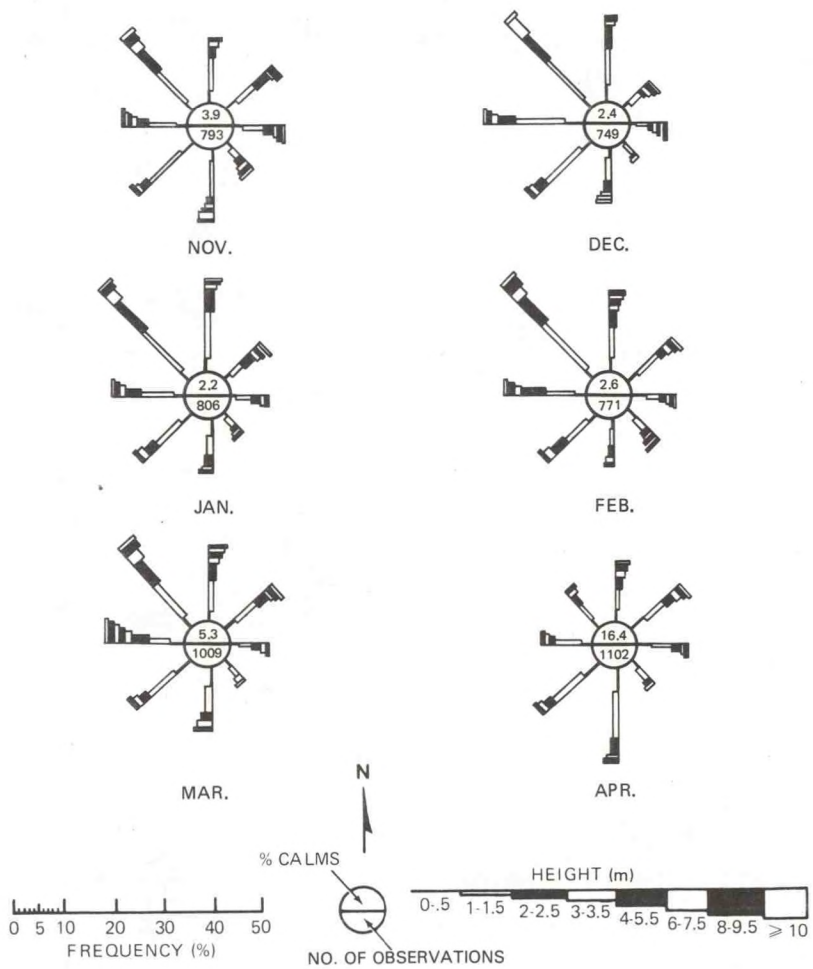


Figure 7.11.--Winter wave roses, area 11.

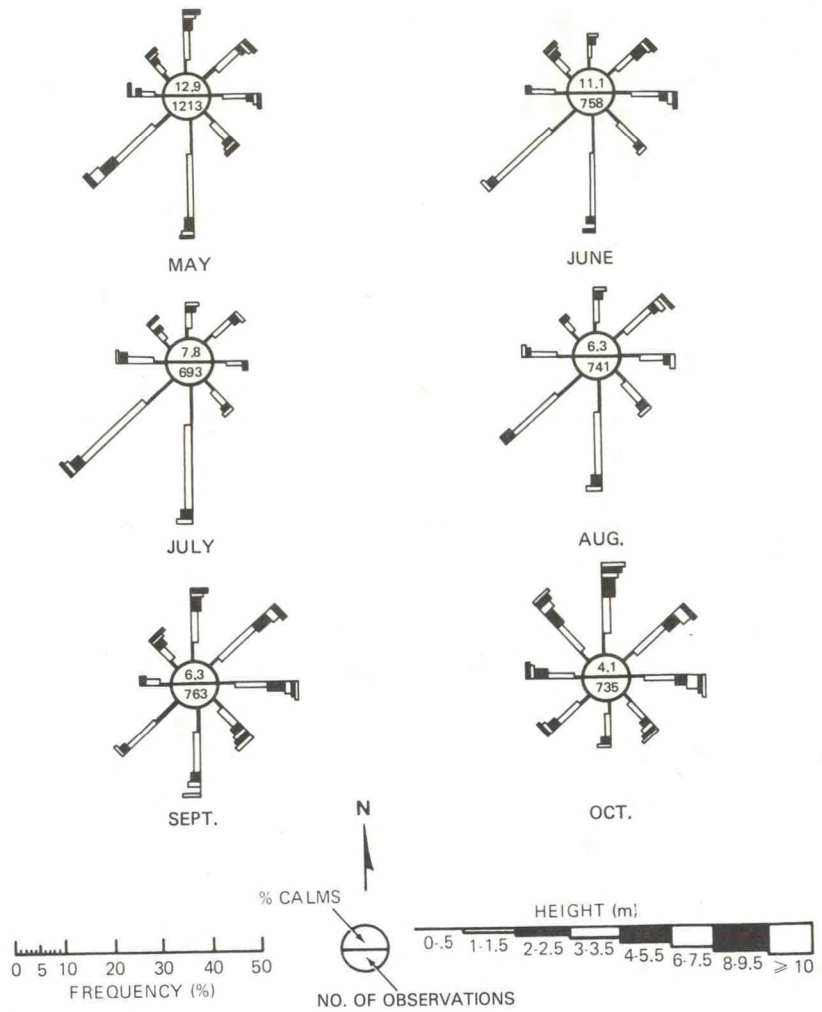


Figure 7.12.--Summer wave roses, area 11.

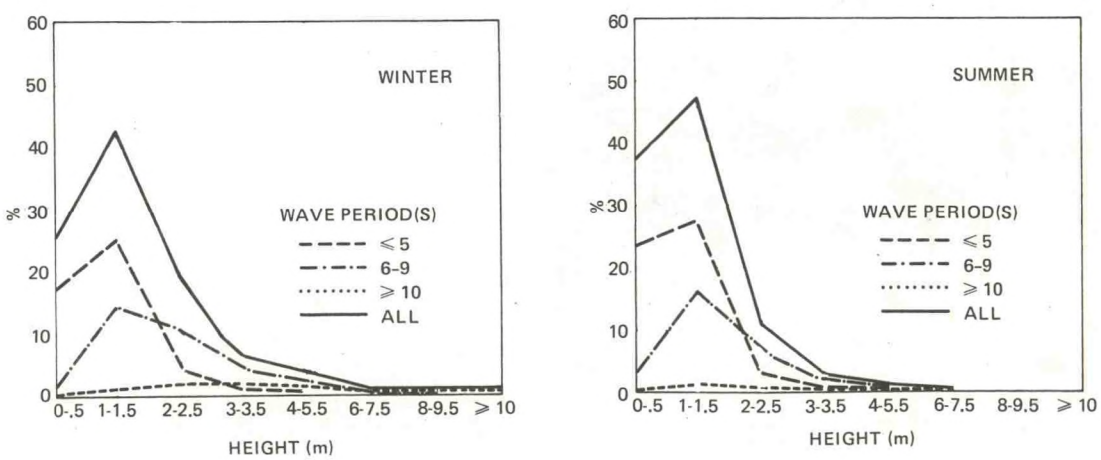


Figure 7.13.--Wave height-period histograms, area 11.

7.2.2 Extreme Wave Height

Wave height is dependent upon wind speed, wind fetch, and the duration of time that wave-building conditions prevail. In shallow water, water depth affects wave development and storm surge, and astronomical tides may increase the water level in these areas when locally generated waves and swells are superimposed. Extreme wave height usually is not estimated directly from the distribution of observed wave heights, because ships avoid areas of maximum wave height and because heights are difficult to estimate accurately from the deck of a ship. One method is to estimate extreme wave height from the extreme values of wind speed, approximating extreme distributions of both wind and wave height by a Fisher-Tippette Type II distribution, as has been done by Thom (1973). Another accepted practice in design studies for offshore structures is to determine past wave conditions based on known meteorological data and to statistically analyze these wave conditions to determine the probability and characteristics of extreme wave conditions. Such an approach, however, is beyond the scope of this study. The tacit assumptions of deep water and unrestricted fetch that underlie Thom's technique are not valid for the Mid-Atlantic region. Therefore, the estimates of extreme wave height made here by that method will be given with qualifications, indicating limited fetch or water-depth effects.

In the Marine Deck observations, significant wave height, $H_{sig}$, is reported, i.e., the height that is exceeded by only one-third of the highest waves in the observation area. Estimates of significant wave height, maximum wave height, $H_{max}$, and return period based on Thom's method are given in table 7.1, where $H_{max} = 1.86\ H_{sig}$.

The representative water depth in each of the 15 climatological areas and maximum depth-limited wave height are given in table 7.2. The depth is the central depth in the area subjectively estimated from isobaths on U.S. Coast and Geodetic Survey charts (scale 1:400,000). The maximum wave height given in the table is the height that theoretically may develop before waves break, and is obtained from $H_{max}$ = water depth x 0.78.

Since the depth-limited wave height for the shallowest of the 15 areas is 29 m, Thom's method used in obtaining the $H_{max}$ values (table 7.1) has some applicability in all areas, but in the areas bounded by the shore these values pertain only to the deeper portions.

The coastal areas of the Mid-Atlantic region have wind fetch restrictions in the north and west quadrants. The fetch lengths from the center of each area for each of eight compass directions are given in table 7.3. Fetch length over 300 nmi was considered unrestricted fetch.

In table 7.3, only the geographic restrictions to fetch have been considered. In a practical sense, the fetch is determined to be the distance over which the wind stress acts on the water surface to increase and build the wave height. According to fetch-speed nomograms published by the U.S. Navy Hydrographic Office (Pierson et al., 1955), fetch less than 100 nmi will permit $H_{max}$ of about 13 m with hurricane winds; fetch of 200 nmi, $H_{max}$ of about 20 m; and fetch of 300 nmi, $H_{max}$ of about 23 m. Hurricanes have a return

Table 7.1.--Significant and maximum wave heights

| Area | Significant height (m) | Maximum height (m) | Return period (yr) | Area | Significant height (m) | Maximum height (m) | Return period (yr) |
|---|---|---|---|---|---|---|---|
| | 13.1 | 23.5 | 5 | | 12.2 | 22.0 | 5 |
| | 14.9 | 26.5 | 10 | | 13.7 | 24.7 | 10 |
| 1 | 17.4 | 31.1 | 25 | 9 | 16.2 | 29.0 | 25 |
| | 19.5 | 35.1 | 50 | | 18.0 | 32.6 | 50 |
| | 22.0 | 39.3 | 100 | | 20.4 | 36.6 | 100 |
| | 12.2 | 22.3 | 5 | | 11.9 | 21.3 | 5 |
| | 14.0 | 25.0 | 10 | | 13.4 | 24.4 | 10 |
| 2 | 16.5 | 29.6 | 25 | 10 | 15.9 | 28.4 | 25 |
| | 18.3 | 33.2 | 50 | | 17.7 | 32.0 | 50 |
| | 20.7 | 37.2 | 100 | | 19.8 | 36.0 | 100 |
| | 12.2 | 22.0 | 5 | | 11.9 | 21.3 | 5 |
| | 13.7 | 24.7 | 10 | | 13.4 | 24.1 | 10 |
| 3 | 16.2 | 29.0 | 25 | 11 | 15.9 | 28.4 | 25 |
| | 18.6 | 32.6 | 50 | | 17.7 | 31.7 | 50 |
| | 20.4 | 36.6 | 100 | | 19.8 | 35.7 | 100 |
| | 12.5 | 22.3 | 5 | | 12.2 | 22.0 | 5 |
| | 14.0 | 25.3 | 10 | | 14.0 | 25.0 | 10 |
| 4 | 16.5 | 29.6 | 25 | 12 | 16.2 | 29.3 | 25 |
| | 18.6 | 33.2 | 50 | | 18.3 | 32.9 | 50 |
| | 20.7 | 37.5 | 100 | | 20.4 | 36.9 | 100 |
| | 12.5 | 22.6 | 5 | | 11.3 | 20.4 | 5 |
| | 14.0 | 25.3 | 10 | | 12.8 | 23.2 | 10 |
| 5 | 16.5 | 29.9 | 25 | 13 | 15.2 | 27.1 | 25 |
| | 18.6 | 33.5 | 50 | | 17.1 | 30.5 | 50 |
| | 20.7 | 37.5 | 100 | | 19.2 | 34.5 | 100 |
| | 13.1 | 23.8 | 5 | | 11.6 | 21.0 | 5 |
| | 14.9 | 26.8 | 10 | | 13.1 | 23.8 | 10 |
| 6 | 17.4 | 31.4 | 25 | 14 | 15.6 | 27.7 | 25 |
| | 19.5 | 35.4 | 50 | | 17.4 | 31.4 | 50 |
| | 22.0 | 39.6 | 100 | | 19.5 | 35.1 | 100 |
| | 11.6 | 20.7 | 5 | | 12.2 | 22.3 | 5 |
| | 13.1 | 23.5 | 10 | | 14.0 | 25.0 | 10 |
| 7 | 15.2 | 27.4 | 25 | 15 | 16.2 | 29.3 | 25 |
| | 17.1 | 30.8 | 50 | | 18.3 | 32.9 | 50 |
| | 19.2 | 34.5 | 100 | | 20.7 | 37.2 | 100 |
| | 12.8 | 23.2 | 5 | | | | |
| | 14.6 | 26.2 | 10 | | | | |
| 8 | 17.1 | 30.8 | 25 | | | | |
| | 19.2 | 34.5 | 50 | | | | |
| | 21.7 | 38.7 | 100 | | | | |

Table 7.2.--Representative water depth and maximum depth-limited wave heights by areas

| Area | Representative water depth (m) | Maximum depth-limited wave height (m) |
|---|---|---|
| 1 | 37 | 29 |
| 2 | 38 | 30 |
| 3 | 42 | 30 |
| 4 | 55 | 30 |
| 5 | 73 | 30 |
| 6 | 91 | 30 |
| 7 | 37 | 29 |
| 8 | 73 | 30 |
| 9 | 91 | 30 |
| 10 | 37 | 29 |
| 11 | 64 | 30 |
| 12 | 91 | 30 |
| 13 | 37 | 29 |
| 14 | 91 | 30 |
| 15 | 91 | 30 |

Table 7.3.--Wind fetch length (nmi)

| | Direction | | | | | | | |
|---|---|---|---|---|---|---|---|---|
| Area | N | NE | E | SE | S | SW | W | NW |
| 1 | 15 | 35 | UR | UR | UR | 145 | 35 | 10 |
| 2 | 15 | 30 | 10 | UR | UR | 270 | 70 | 5 |
| 3 | 17 | 25 | UR | UR | UR | 28 | 25 | 18 |
| 4 | 25 | 97 | UR | UR | UR | 105 | 65 | 23 |
| 5 | 50 | 75 | UR | UR | UR | 200 | 105 | 35 |
| 6 | 50 | UR | UR | UR | UR | UR | 165 | 70 |
| 7 | 65 | 170 | UR | UR | UR | 80 | 25 | 20 |
| 8 | 80 | 160 | UR | UR | UR | 195 | 65 | 70 |
| 9 | 120 | UR | UR | UR | UR | 215 | 110 | 100 |
| 10 | 50 | UR | UR | UR | UR | 25 | 13 | 35 |
| 11 | 130 | UR | UR | UR | UR | 150 | 75 | 75 |
| 12 | 145 | UR | UR | UR | UR | 200 | 125 | 12 |
| 13 | 35 | UR | UR | UR | UR | 33 | 23 | 25 |
| 14 | 130 | UR | UR | UR | UR | 100 | 75 | 80 |
| 15 | 195 | UR | UR | UR | UR | 150 | 120 | 125 |

UR - unrestricted

period of 5 years; therefore, since fetch directions in the 15 areas is unrestricted (> 300 nmi) we estimate that 23-m waves have a return period of about 5 years (table 7.1).

The highest wind speeds are associated with hurricane winds that flow in circular paths around the hurricane. Since, in effect, the length of associated fetch is restricted by the curvature of the wind trajectory, an estimate of the attendant practical fetch length is required. It has been noted, however, that hurricanes sometimes travel with a speed that will keep the field of maximum wind up with the advancing waves Earle (1975). The effective fetch for continuous wave building can, therefore, be larger than the diameter of the storm area of hurricane winds. According to Earle (1975), who gives wave height data for hurricanes for a 30-year period of record in the Diamond Shoals area, hurricanes producing a significant wave height of 9 m or greater have occurred five times. The largest significant hurricane-generated wave height in the 30-year record period was reported to be 11 m.

Fetch lengths of 500 nmi associated with extratropical storm winds (>25 kt; 1.3 m/s) are commonly observed, and some as long as 1,400 nmi have been observed in the Mid-Atlantic region. Fetch length of maximum winds in "northeasters" has been found to extent to 340 nmi (Peterson et al., 1964), and a maximum wave associated with maximum wind (>56 kt; 2.9 m/s), and fetch (>340 nmi) is estimated from the fetch-speed nomograms (Pierson et al., 1955) to be about 24 m.

If the return period for "northeasters" of a size to generate 24-m wave heights is assumed to be equal to the observation frequency of once in 50 years, a rough straight-line graph of return period vs. maximum wave height can be plotted from storm climatology data and for estimates derived by Thom's Fisher-Tippette Type II distribution method. Such a graph for area 5 is shown in figure 7.14, which is representative of the entire region, since there is little difference in the return period frequency distributions of maximum wave height from one area to another. Comparison of the two lines in this figure indicates a considerable difference between the return period frequency estimates obtained by Thom's method and estimates based on storm climatology data.

## 7.3 Summary

In the published literature on ocean wave statistics, reports of errors in shipboard wave observations are commonly found. In the Mid-Atlantic region area few observations have been made that can be compared with wave statistics from passing ships. A recently published atlas of the New York Bight (Lettau et al., 1976) gives monthly wave statistics based on comparable data sets from the Ambrose and Barnegat lightships and from the immediate surrounding ocean areas. Examination of the data in that publication revealed no difference in the records that could be attributed to shipboard observer error.

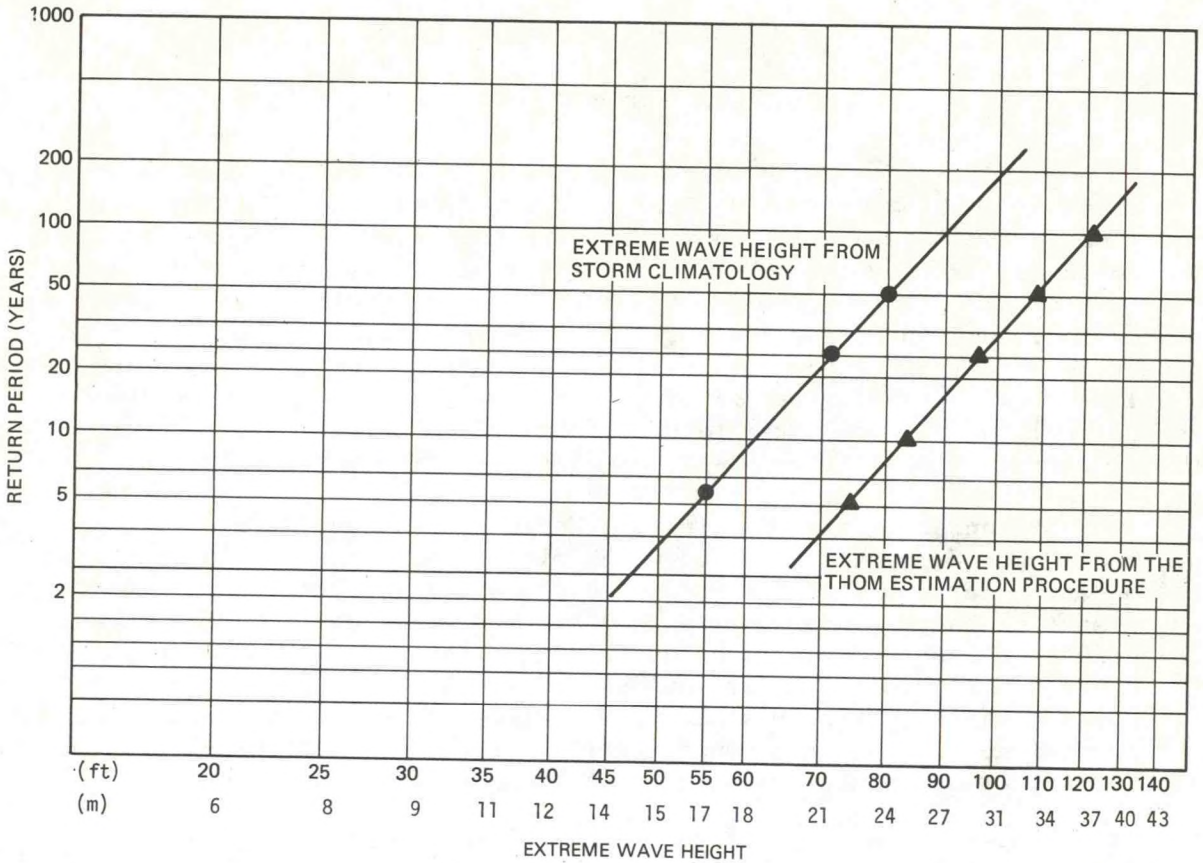


Figure 7.14.--Extreme wave heights and return periods.

Published results of coastal wave measurements compared with passing ship reports, however, has indicated considerable differences, but because of shallow-water effects these reported differences may not be entirely attributable to observation error. Therefore, although there may be considerable error in the Marine Deck data summarized here, the effects of these errors are not readily discernible.

In the absence of suitable wave measurements and data for wave hindcasting, estimates of maximum wave height must be based on projections from theoretical distributions. Although the limitations of fetch length and shallow water on maximum wave height in the Mid-Atlantic region have been considered here in using Thom's method for estimating return periods of maximum wave heights, the wave height estimates seem to be too large. This may be attributable to such factors as the existence of fetch limitations due to curvatures of wind trajectory paths, limited wave building durations, and the effects of wind fields that are counter to moving wave fields.

Accurate estimates of the return periods of extreme waves are required for risk assessment connected with potential oil spills. Such estimates could best be derived from numerical wave models, i.e., from hindcasts of waves based on wind, fetch, and duration data for actual storms that have passed through the region.

# 8. CONCLUSIONS AND RECOMMENDATIONS

## 8.1 Meteorological Factors

The broad-scale atmospheric surface circulation as analyzed on the basis of passing-ship, or "Marine Deck," observations is similar to that documented in the literature. In winter, the mean flow field over the Mid-Atlantic region is from the WNW-NW, with winds at around 7.0 to 9.0 kt; in summer, winds are from the SSW-SW at 3.3 to 4.5 kt. Variability of the surface wind, described in terms of wind "constancy," is highest during these two seasons. Apart from the possibility of a systematic bias toward low wind speeds, as shown by comparison with both ocean weather station data and buoy observations, the Marine Deck data were found to be quite adequate for defining the major statistical features of the surface wind field.

Comparison of coastal-station and Marine Deck observations were also made, and a method was developed by which wind speed and direction adjustment factors can be derived from the Marine Deck observations and applied to coastal station data to approximate conditions over adjoining ocean areas. Such computations were found to be useful over short periods of time in areas where winds are of similar distributions. Only short records of buoy observations were available for this study, but time-series data now being acquired by buoys deployed in the area, when paired with synoptic coastal-station data, will allow a more complete description of land-sea wind differences.

Adjustment factors, based on the method mentioned above, were also applied to 10 years of coastal wind data for computation of wind trajectories, which can be used to simulate the motion of drifting oil on the sea surface under the effect of wind alone. The computed trajectory climatology indicates that the spatial distribution of the trajectories is similar to a "random walk" process superimposed on a large-scale transport vector.

Extreme wind speed return periods were estimated by use of a method developed by Thom (1966) and adjusted for return periods of hurricanes. Better estimates of extreme wind speeds and return periods depend on many more years of wind records or on improved statistical estimation techniques.

Calculation of monthly frequencies, in percent, of poor visibility ranges of $\leq$ 1 mi and $\leq$ 1/4 mi indicates that visibility is often restricted in early spring because of advection fog. Another hazard, that of ice accretion on the superstructures of ships in the area, was found to be slight.

## 8.2 Water Masses

Classification of water masses in the Mid-Atlantic region by temperature-salinity correlation, based on STD/Nansen cast data, yielded useful results, with six characteristic water groups having been identified. Primary in determining the distribution is the tendency for low-salinity shelf water to flow seaward in the surface layers, and high salinity oceanic water to flow landward in the deeper layers. The boundary between shelf water and

slope water, the shelf-slope water front, is generally located above the 200-m isobath, and is a major hydrographic feature of the area. The front has been clearly delineated in all seasons on individual cruises, but its location tends to be blurred when historical data are averaged by season. Its seasonal variations can be described only in very general terms from these data. These variations of the shelf-slope water front correspond to the seasonal march of temperature and salinity, and the ensuing changes in water density structure. In winter, isopleths of temperature, salinity, and density tend to be vertical, clustering together in the vicinity of the front. All three variables increase seaward. The density increase is due to the effect of the salinity gradient, which is on the order of 2 ppt in 20 mi, and which overrides the effect of the temperature increase. In winter, a vertically well-mixed regime prevails in the shelf and upper slope water, where salinity, and often temperature, increase with depth in most areas. This increase is more rapid with depth in the upper part of the water column in the vicinity of the shelf-slope water front.

With the onset of spring warming, the orientation of the isotherms evolves from near-vertical (horizontally stratified) in early spring, to near-horizontal (vertically stratified) in summer. The near-surface horizontal temperature gradient across the front is thus greatly reduced, and the seasonal thermocline, another principal feature of the hydrography in the area, becomes prominent. With the development of the thermocline, which is usually located at 15- to 25-m depth, internal waves, generally of tidal period, often occur and propagate landward from the shelf-break region. The thermocline persists into fall, when winds and surface cooling return the water column once again to its well-mixed state. The salinity distribution also attains maximum vertical stratification in summer, when spring runoff from the major rivers has had sufficient time to spread out over the shelf and lower near-surface salinity, while bottom salinity remains high.

These temperature and salinity effects combine to enhance the vertical density stratification in summer, when density increases rapidly with depth because of decreasing temperature and increasing salinity. In winter, density is controlled mainly by the salinity, increasing with depth and with distance from the coast, corresponding to the salinity gradient.

Analysis of nutrient data demonstrated seasonal and spatial variation in concentration of dissolved oxygen, phosphates, and silicates. Surface layer concentrations of dissolved oxygen vary seasonally because of changing water temperature, but the water in the surface layer is always saturated. Vertical water mass stratification, caused by river runoff and heating of the surface by insolation, produces large vertical differences in dissolved oxygen concentration in the midshelf area. Pronounced variation in dissolved phosphate concentration from summer to winter is found in longshore water masses. Low summer concentrations are attributed to biological uptake; high winter concentrations, to reduced biological uptake and increased decay. It is apparent that land and river runoff is a significant factor in determining phosphate and silicate concentrations in the Mid-Atlantic shelf area. Low silicate concentrations in the surface layers in summer are attributed to biological uptake and low volume of river flow.

Regarding the adequacy of the data for the Mid-Atlantic region, the following was concluded:

(1) The Marine Deck observations provide a good description of the surface temperature field.

(2) The MBT and XBT data constitute by far the largest source of subsurface temperatures, and are useful after careful editing. Significant mean temperature differences were found between these data, as well as between them and the STD Nansen cast data. These differences are believed to result from large natural variability, including possible long-term trends in continental shelf temperatures and temperature gradients; sampling biases; instrumental biases and random errors; and errors in reporting or processing procedures, leading to, for example, position, date-time, and reference temperature errors. Because of these differences, the STD Nansen cast data, which are inherently more accurate than the MBT and XBT data, were used for subsequent analyses.

(3) The STD Nansen data are adequate for identifying the major water masses of the area and for delineating their approximate boundaries. They are also adequate for documenting seasonal, but not monthly, means and variabilities in most cases. The number of these observations is not sufficient for delineating the shelf-slope water front.

(4) Salinity data for most of the Mid-Atlantic region cannot be used to reliably describe the physical processes taking place, a problem compounded by year-to-year variability and by the fact that intraseasonal variability is often larger than mean seasonal variability.

(5) For summer and fall, the number of observations of specific volume anomaly is inadequate for determining the mean fields of mass and pressure at a spatial resolution of less than about 100 km. Hence, the historical data base is of limited use in objectively estimating mean seasonal geostrophic currents in the Mid-Atlantic region. Its use as input to circulation models, other than those employing the vertically integrated mass fields, is also limited because of the poor spatial and temporal distributions of the data. Geostrophic computations could best be made from these data on a quasi-synoptic (cruise-by-cruise) basis, rather than from seasonal averages.

(6) Data on dissolved oxygen and nutrients are adequate for defining seasonal means in some areas but only differences between summer and winter are easily delineated. These data are not adequate for establishing a benchmark of water quality with which future water quality measurements could be compared.

## 8.3 Circulation

Mean southwesterly surface flow is on the order of 5 cm/s (0.1 kt) in the Mid-Atlantic region during all seasons of the year. Seasonal variability of surface currents, as determined from ship-drift data was found not to be

so pronounced as variability reported in the literature from surface-drifter observations. Recent evidence from direct current measurements indicates that seasonal surface variability may, indeed, be small. The ship-drift data analyzed in this study do not show the uniform increase in mean surface current strength with distance from the coast inferred by others from tracking of surface drifters and from direct current measurements.

An attempt to relate surface wind climatology to surface currents from the ship-drift data produced inconclusive results, and these data were therefore "validated" only through comparison with surface-drifter and a few direct current measurements. Differences in speed and direction of surface current were generally small, with some large differences found in a few areas.

Analysis of subsurface currents based on current-meter records showed the following:

(1) Mean subsurface current components are of the same order of magnitude as those derived from ship-drift data.

(2) Variability is much larger than the mean value.

(3) Maximum subsurface currents are generally an order of magnitude larger than the mean vector magnitude.

(4) The most frequent values of subsurface current speed are larger than the mean vector magnitude.

(5) Semidiurnal tides are a major component of the current close to shore, decreasing in magnitude rapidly with distance from the coast.

(6) Inertial currents appear to be present in shallow, nearshore areas, in contrast to results reported in the literature.

(7) Under conditions of strong vertical density gradients, bottom currents are often decoupled from surface currents.

(8) Most of the energy occurs at subtidal frequencies in the midshelf and outer shelf areas.

The ship-drift data base was found to be a good source of data for study of seasonal mean surface currents in the Mid-Atlantic region at $1/2^{o}$ resolution, but the number of observations is deemed insufficient for generating reliable monthly summaries.

The number and duration of direct current measurements are inadequate for resolving reliably the time and space scales of motion in the region, except in the New York Bight apex. In experimental studies, simultaneous measurements of current and wind have seldom been made. The wind data used in such studies have been obtained at land stations or other fixed sites many miles away and at sampling rates incompatible with the current measurements. This lack of systematic approach to studies of ocean response to atmospheric forcing precludes documentation of the spatial and temporal characteristics

of the response of the ocean, and severely limits prediction modeling. The assumption made in many studies, that net water movement past a single observation point can be used to infer net transport of water over the period of observation, should be verified by simultaneous current-meter and current-drogue studies.

## 8.4 Vertical Mixing

Vertical mixing in the Mid-Atlantic region is strong in winter when nearly homogenous water is found from the surface to the bottom. Vernal warming and, in some nearshore areas, surface layer intrusion by river flow and land runoff create vertical density gradients that inhibit vertical mixing. Although the gradual, seasonal changes in water mass characteristics at depths below 15 to 20 m indicate that small-scale turbulence and internal waves produce vertical mixing, these mixing processes cannot be analyzed based on existing data. The data are useful for indirect assessment of vertical mixing on a seasonal time scale, but do not lend themselves to direct study of the problem on smaller space and time scales.

## 8.5 Ocean Waves

The seasonal surface wave climatology compiled from visual shipboard observations shows that sea states in the Mid-Atlantic region are maximum in winter and minimum in summer. Strong northwest winds in winter produce waves that increase in height and length with distance from the coast. Weak southwest summer winds produce a predominant southwest direction for ocean waves, with wave heights and periods again increasing with distance from the coast. The data appear to be biased toward low sea states in both winter and summer, since the highest waves propagate into the region from the northeast-to-southeast quandrant, but the relative frequency of high waves from the east is lower than expected.

Visual shipboard observations are useful in providing general background climatology of "typical" wave conditions, but return periods of extreme wave heights cannot be estimated reliably without an adequate storm climatology for the Mid-Atlantic region, and a wave hindcasting model that includes the effects of refraction and limited fetch. The extreme wave heights estimated in this study by the method developed by Thom (1966) are thought to be too high.

## 8.6 Recommendations

The hydrographic data base currently available does not reliably document the variability at time scales smaller than seasonal or space scales smaller than the ocean areas delineated for this study. The ship-drift data do not reliably define the flow field on time scales smaller than seasonal. Yet, it is over time periods of days and weeks and smaller space scales than those used here that major transport and mixing of spilled pollutants occur.

A primary task facing the water trajectory modeler today is to identify and estimate relative magnitudes of the atmospheric forcing functions and the magnitudes and phase delays of the ocean response. Documentation of this forcing and the response of shelf waters should have highest priority, followed by similar analysis of the slope water and of the exchanges between shelf and slope water, and the associated dynamics of the shelf-slope water front.

Deployment of observation networks to empirically determine the probability distribution of oceanographic and meteorological parameters on all time and space scales of interest to a study such as this one would be prohibitively costly. The only practical approach appears to be the careful design of systematic, coordinated experiments of increasing scope and complexity that would provide the information on various time and space scales and on the exchanges across the open boundaries that is necessary in the development of diagnostic and prognostic circulation models. To that end, the following program is proposed, to be carried out over approximately a 5-year period in three phases.

The highest priority is the collection of long time-series data to (1) resolve energetic time scales of motion and forcing at limited spatial separations, (2) to obtain statistics on intermittent and transient events, and (3) to identify trends on the continental shelf. Since case studies indicate that the most energetic flows occur generally in the longshore direction, and that horizontal coherence is high in that direction for time scales longer than a day, it is recommended that meteorological-oceanographic buoys be deployed along the continental shelf, each buoy containing sensors at depth intervals of 10 m or less for measuring air temperature, surface wind, barometric pressure, ocean hydrostatic pressure, surface wave height, current speed and direction, sea temperature, and salinity.

The buoys should be deployed about 200 km apart parallel to the coast in the midshelf area and should be maintained for 5 years. The buoys should be serviced by oceanographic vessels that would make closely spaced hydrographic sections to, from, and between buoys, taking an STD cast every 10 km, and an XBT every 5 km. While in transit, the ships should operate acoustic sounders to monitor internal wave activity, and record continuously surface temperature and salinity, barometric pressure, and wind velocity.

In the initial phase, covering 1 year, two buoys should be deployed: one off Long Island, the second off Cape May. Exact positions would have to be determined after consideration of shipping lanes and fishing grounds.

After this first phase, two buoys should be added: one off Cape Charles, the other off Nantucket. Servicing and oceanographic runs by two ships should be made at least every 2 months. During the second phase, a cluster of three to five buoys should also be deployed around the Cape May buoy and a 2-month intensive experiment should be performed to study internal waves and mixing processes in summer, e.g., intrusion of slope water in response to wind shift.

The third phase of the program would see an extension of the experiment to the continental slope, to examine cross-shelf gradients and

shelf-slope water interactions. Buoys should be deployed along the 2,000-m isobath and midway between the 2,000-m isobath and the buoys deployed during the first phase. A third ship should be added for oceanographic survey and buoy maintenance, which would run tracks around and through the area defined by the buoys. During ship operations, aircraft overflights should be made to monitor eddy activity through the area by ART and IR scanning and by surface and subsurface Lagrangian current meters drifted through the array.

These experiments would provide the data needed for deducing the time-space correlation functions of water velocity and water mass characteristics. The intense, short-term experiments during the second phase would provide the data required for documenting mixing scales and internal wave characteristics.

The program outlined above is presented as a concept only at this time. The specific design should be developed with the participation of a number of scientists, who would take responsibility for planning the various data analyses and specify the data requirements for those analyses. The program should be designed to also provide initialization and verification data for water circulation models.

REFERENCES

Amos, A.F., "The New York Bight & Hudson Canyon in October 1974: Hydrography, Nephelometry, Bottom Photography, Currents, VEMA Cruise 32 Leg 1 Data," Prepared for the United States Energy Research and Development Administration under Contract No. E(11-1)-2185, Lamont-Doherty Geological Observatory, Palisades, New York, 1976, 192 pp.

Apel, J.R., H.M. Byrne, R.R. Proni, and R. Charnell, "Observations of Oceanic Internal Surface Waves From the Earth Technology Satellite," Journal of Geophysical Research, Vol. 80, No. 6, 1975a, pp. 865-881.

Apel, J.R., J.R. Proni, H.M. Byrne, and R.L. Sellers, "Near-Simultaneous Observations of Intermittent Internal Waves on the Continental Shelf From Ship and Spacecraft," Geophysical Research Letters, Vol. 2, No. 4, 1975b, pp. 128-131.

Armstrong, F.A.J., "Silicon," Chemical Oceanography, J.P. Riley and G. Skirrow, Ed., Academic Press, London, 1965, pp. 409-432.

Beardsley, R.C., and B. Butman, "Circulation on the New England Continental Shelf: Response to Strong Winter Storms," Geophysical Research Letters, Vol. 1, No. 4, 1974, pp. 181-184.

Beardsley, R.C., and C.N. Flagg, "The Water Structure, Mean Currents, and Shelf-Water-Slope-Water Front on the New England Continental Shelf," Memoires de la Societe Royale des Sciences de Liege, Continental Shelf Dynamics, Seventh Liege Colloquium on Ocean Hydrodynamics, University of Liege, May 5-9, 1975, J.C.J. Nihoul, Ed., Siege de la Societe: Universite Liege, Belgium, 1976, pp. 209-225.

Beardsley, R.C., W.C. Boicourt, and D.V. Hansen, "Physical Oceanography of the Middle Atlantic Bight," Proceedings of the Symposium, American Museum of Natural History, New York City, 3, 4, 5 November 1975, Special Symposia, Vol. 2, M. Grant Gross, Ed., American Society of Limnology and Oceanography, Inc., Allen Press, Lawrence, Kansas, 1976, pp. 20-34.

Bigelow, H.B., and M. Sears, "Studies of the Waters on the Continental Shelf, Cape Cod to Chesapeake Bay, Part II, Salinity," Papers in Physical Oceanography and Meteorology, Vol. IV, No. 1, Contribution No. 7 from the Woods Hole Oceanographic Institution, Massachusetts Institute of Technology, Cambridge, Massachusetts, 1935, 94 pp.

Bisagni, J.J., "Passage of Anticyclonic Gulf Stream Eddies Through Deepwater Dumpsite 106 During 1974 and 1975," NOAA Dumpsite Evaluation Report 76-1, National Oceanic and Atmospheric Administration, U.S. Department of Commerce, Washington, D.C., 1976, 39 pp.

Boicourt, W.C., and P.W. Hacker, "Circulation on the Atlantic Continental Shelf of the United States, Cape May to Cape Hatteras," Memoires de la Societe Royale des Sciences de Liege, Vol. X, Continental Shelf Dynamics, Seventh Liege Colloquium on Ocean Hydrodynamics, University of Liege, May 5-9, 1975, J.C.J. Nihoul, Ed., Siege de la Societe, Universite Liege, Belgium, 1976, pp. 187-200.

Bowden, K.F., "Turbulence," Sec. VI, The Sea, M.N. Hill, Ed., Vol. 1, Physical Oceanography, Interscience Publishers, New York, 1962, pp. 802-817.

Bumpus, D.F., "A Description of the Circulation on the Continental Shelf of the East Coast of the United States," Progress in Oceanography, B.A. Warren, Ed., Vol. 6, Pergamon Press, New York, 1973, pp. 111-157.

Bumpus, D.F., and L.M. Lauzier, "Surface Circulation on the Continental Shelf off Eastern North America Between Newfoundland and Florida," Serial Atlas of the Marine Environment, Folio 7, American Geographical Society, New York, 1965, 4 pp.

Chamberlin, J.L., "Bottom Temperatures on the Continental Shelf and Slope South of New England During 1975," In "Ocean Variability: Effects on U.S. Marine Fishery Resources 1975," NOAA Technical Report, National Marine Fisheries Service, National Oceanic and Atmospheric Administration, U.S. Department of Commerce, Washington, D.C., 1977, pp. 271-292 (in press).

Charnell, R.L., and D.A. Mayer, "Water Movement Within the Apex of the New York Bight During Summer and Fall of 1973," NOAA Technical Memorandum ERL MESA-3, Marine Ecosystems Analysis Program Office, Environmental Research Laboratories, National Oceanic and Atmospheric Administration, U.S. Department of Commerce, Boulder, Colorado, 1975, 29 pp.

Christodoulou, George C., Jerome J. Connor, and Bryan R. Pearce, "Mathematical Modeling of Dispersion in Stratified Waters," Report No. MITSG 76-14, MIT Sea Grant Program, Massachusetts Institute of Technology, Cambridge, Massachusetts, 1976, 308 pp.

Cresswell, G.M., "Quasi-Synoptic Monthly Hydrography of the Transition Region Between Coastal and Slope Water South of Cape Cod, Massachusetts," Reference No. 67-35, Woods Hole Oceanographic Institution, Woods Hole, Massachusetts, 1967, 47 pp. + illus.

Csanady, G.T., "Mean Circulation in Shallow Seas," Journal of Geophysical Research, Vol. 81, No. 30, 1976, pp. 5389-5399.

Earle, M.D., "Oceanographic Design Conditions for Diamond Shoals Light Tower," Technical Note No. 6110-3-75, Naval Oceanographic Office, Washington, D.C., 1975, 47 pp.

EG&G Corporation, "Summary of Oceanographic Observations in New Jersey Coastal Waters Near 39°28'N Latitude and 74°15'W Longitude During the Period March 1974 Through May 1974," Waltham, Massachusetts, 1974, 231 pp.

Gaul, R.D., "Observations of Internal Waves Near Hudson Canyon," Journal of Geophysical Research, Vol. 66, No. 11, 1961a, pp. 3821-3820.

Gaul, R.D., "The Occurrence and Velocity Distribution of Short-Term Internal Temperature Variations Near Texas Tower No. 4," Technical Report TR-107, U.S. Naval Oceanographic Office, Washington, D.C. 1961b, 45 pp.

Griscom, C., "An Analysis of Subsurface Currents and Temperatures at Six Sites on the Continental Shelf of the Northeast United States," Technical Report to ONR, contract N00014-68-C0201, General Dynamics Corporation, 1968.

Fieux, M., and H. Stommel, "Preliminary Look at Feasibility of Using Marine Reports of Sea Surface Temperatures for Documenting Climatic Change in the Western North Atlantic," Journal of Marine Research, Vol. 33, Supplement, 1975, pp. 83-95.

Flagg, C.N., and R.C. Beardsley, "Report on the 1974 M.I.T. New England Shelf Dynamics Experiment (March 1974), Part I: Hydrography," Report 75-1, Department of Meteorology, Massachusetts Institute of Technology, Cambridge, Massachusetts, and the Woods Hole Oceanographic Institution, 1975, 87 pp.

Flagg, C.N., J.A. Vermersch, and R.C. Beardsley, "Report on the 1974 M.I.T. New England Shelf Dynamics Experiment (March 1974), Part II: The Moored Array," Report 76-1, Department of Meteorology, Massachusetts Institute of Technology, Cambridge, Massachusetts, and the Woods Hole Oceanographic Institution, 1976, 22 pp.

Franklin, B., A Letter from Dr. Benjamin Franklin to Mr. Alphonsus le Roy, Member of Several Academics, at Paris, Containing Sundry Maritime Observations, Transactions, American Philosophical Society, Vol. 2, 1786, pp. 294-329.

Goldsmith, V., W.D. Morris, R.J. Byrne, and C.H. Whitlock, "Wave Climate Model of the Mid-Atlantic Shelf and Shoreline (Virginian Sea)," NASA SP-358, National Aeronautics and Space Administration, Washington, D.C., 1974, 146 pp.

Gutman, A.L., "Delineation of a Wave Climate for Dam Neck, Virginia Beach, Virginia," Special Report in Applied Marine Science and Ocean Engineering No. 125, Virginia Institute of Marine Science, Gloucester Point, Virginia, 1976, 38 pp.

Haight, F.J., "Coastal Currents Along the Atlantic Coast of the United States," Special Publication No. 230, Coast and Geodetic Survey, U.S. Department of Commerce, Washington, D.C., 1942, 73 pp.

Halpern, D.F., "Semi-Diurnal Internal Tides in Massachusetts Bay," Journal of Geophysical Research, Vol. 76, No. 27, 1971, pp. 6573-6584.

Hamilton, D., and Jalickee, J.B., "An Objective Method of Classifying Oceanographic Data," EDS, Environmental Data Service, National Oceanic and Atmospheric Administration, U.S. Department of Commerce, Washington, D.C., 1977, pp. 12-17.

Harris, D.L., "Characteristics of Wave Records in the Coastal Zone," C. Meyer, Ed., Waves on Beaches, Academic Press, New York, 1972.

Hesselbert, T., and H.U. Sverdrup, "Die Stabilitatsverhaltnisse bei vertikalen Verschlebungen in der Atmosphare und in Meer, Bergens Museums Aarbok, Nos. 14 and 15, Bergen, Norway, 1914.

Horne, R.A., Marine Chemistry, Wiley Interscience, New York, 1969, pp. 230-337.

Jalickee, J.B., and D.B. Hamilton, "Objective Analysis and Classification of Oceanographic Data," 1978 (to be published in Tellus).

Ketchum, B.H., and D.J. Keen, "The Accumulation of River Water Over the Continental Shelf Between Cape Cod and Chesapeake Bay," Deep Sea Research, Supplement to Vol. 3, 1955, pp. 346-357.

Ketchum, B.H., and N. Corwin, "The Persistence of "Winter" Water on the Continental Shelf South of Long Island, New York," Limnology and Oceanography, Vol. IX, No. 9, 1974, pp. 467-475.

Kinsman, B., Wind Waves: Their Generation and Propagation on the Ocean Surface, Prentice-Hall, Englewood Cliffs, New Jersey, 1965, 676 pp.

Koblentz-Mishke, O.J., V.V. Volkovinsky, and J.G. Kabanova, "Plankton Primary Production of the World Ocean," Scientific Exploration of the South Pacific, W.S. Wooster, Ed., National Academy of Sciences, Washington, D.C., 1970, pp. 183-193.

Lettau, B., W.A. Brower, Jr., and R.G. Quayle, "Marine Climatology," MESA New York Bight Atlas, Monograph No. 7, New York Sea Grant Institute, Albany, New York, 1976, 239 pp.

Mamayev, O.I., "Temperature-Salinity Analysis of World Ocean Waters," Elsevier Oceanography Series, 11, Elsevier Scientific Publishing Company, Amsterdam, 1975, 374 pp. (Translated from the Russian.)

Minsk, L.D., "Ice Accumulation on Fixed and Floating Ocean Structures," Corps of Engineers, U.S. Army, Hanover, New Hampshire, 1975, pp. 37-39.

Montgomery, R.B., "Circulation in Upper Layers of the Southern North Atlantic Deduced With Use of Isentropic Analysis," Papers, Physical Oceanography and Marine Meteorology, Massachusetts Institute of Technology and the Woods Hole Oceanographic Institution, Vol. 6, No. 2, 1938.

Moore, W.J., Physical Chemistry, Third ed., Prentice-Hall, Englewood, New Jersey, 1962, pp. 232-238.

Morgan, C.W., J.M. Bishop, and F.F. Mulher, "Oceanography of the New York Bight, August 1974," United States Coast Guard Oceanographic Report, CG 373-71, Washington, D.C. 1976, 89 pp.

Neumann, G., "On the Dynamical Structure of the Gulf Stream as an Equivalent - Barotropic Flow," Journal of Geophysical Research, Vol. 65, No. 1, 1960, pp. 239-247.

Neumann, G., and W.J. Pierson, Principles of Physical Oceanography, Prentice-Hall, Englewood Cliffs, New Jersey, 1966, 545 pp.

Neumann, G., and A. Schumacher, "Oberflachen Stromungen und Dichte der Meeresoberflache vor der Ostkuste Nord Amerikas," Annalen der Hydrographie und Maritimen Meteorologie, Vol. 72, 1944, pp. 277-279.

Norcross, J.J., and E.M. Stanley, "Inferred Surface and Bottom Drift, June 1973 through October 1964," In "Circulation of Shelf Waters Off Chesapeake Bight," Professional Paper No. 3, Environmental Science Services Administration, U.S. Department of Commerce, Washington, D.C., 1967, pp. 11-42.

Officer, Charles B., Physical Oceanography of Estuaries (and Associated Coastal Waters), John Wiley & Sons, New York, 1976, 465 pp.

Otto, L., "Environmental Factors in Operations To Combat Oil Spills," Reports on Marine Science Affairs, Report No. 9, WMO - No. 359, World Meteorological Organization, Geneva, Switzerland, 1973, 25 pp.

Ownbey Jr., J.W., "A Synoptic Comparison of Wind and Wave Reports From Ocean Weather Station (OWS) Hotel and Ships-in-Passage," M.S. Thesis, North Carolina State University, Raleigh, North Carolina, 1975 (unpublished manuscript).

Patchen, R.C., E.E. Long, and C.B. Parker, "Analysis of Current Meter Observations in the New York Bight Apex, August 1973-June 1974," NOAA Technical Report ERL 368-MESA 5, Environmental Research Laboratories, U.S. Department of Commerce, National Oceanic Atmospheric Administration, Boulder, Colorado, 1976, 24 pp.

Panofsky, H.A., and G.W. Brier, Some Applications of Statistics to Meteorology, Pennsylvania State University Press, University Park, Pennsylvania, 1958, 224 pp.

Peterson, K.R., and H.V. Goodyear, and Staff, "Criteria for a Standard Project Northeaster for New England North of Cape Cod," National Hurricane Research Project, Report No. 68, Weather Bureau, U.S. Department of Commerce, 1964, 66 pp.

Pierson, W.J., "Visual Wave Observations," Miscellaneous Publication No. 15921, U.S. Navy Hydrographic Office, Washington, D.C., 1956, 50 pp.

Pierson, W.J., "Wave Conditions," MESA New York Bight Atlas, Monograph No. 5, New York Sea Grant Institute, Albany, New York, 1977 (in press).

Pierson Jr., W.J., G. Neumann, and R.W. James, "Practical Methods for Observing and Forecasting Ocean Waves by Means of Spectra and Statistics," H.O. Publication No. 603, U.S. Navy Hydrographic Office, Washington, D.C., 1955, 284 pp.

Proni, J.R., and J.R. Apel, "On the Use of High Frequency Acoustics for the Study of Internal Waves and Microstructure," Journal of Geophysical Research, Vol. 80, No. 9, 1975, pp. 1147-1151.

Quayle, R.G., "A Climatic Comparison of Ocean Weather Stations and Transient Ship Records," Mariners Weather Log, Vol. 18, No. 5, pp. 307-311.

Riley, J.P., and R. Chester, Introduction to Marine Chemistry, Academic Press, New York, 1971, 173 pp.

Royer, T.C., "A Note Comparing Historical Sea Surface Temperature Observations at Ocean Station P," Journal of Physical Oceanography, Vol.6,1976,pp.969-971.

Saville Jr., T., "North Atlantic Coast Wave Statistics Hindcast by Bretschneider - Revised Sverdrup-Munk Method," Technical Memorandum No. 55, Beach Erosion Board, Office of the Chief of Engineers, Department of the Army, 1955.

Schwartzberg, H.G., "Spreading and Movement of Oil Spills," Water Pollution Control Research Report, L5080-EPA 04/70, 1970, 21 pp.

Scott, J.T., and G. Csanady, "Near Shore Currents off Long Island," Journal of Geophysical Research, Vol. 81, 1976, pp. 181-184.

Shonting, D.H., "Rhode Island Sound Square Kilometer Study, 1967: Flow Patterns and Kinetic Energy Distribution," Journal of Geophysical Research, Vol. 74, No. 13, 1969, pp. 3386-3395.

Shonting, D.H., G.S. Cook, and F.G. Wyatt, Jr., "Oceanographic Observations in Rhode Island Sound 1963-64: A Data Report," Consecutive Report No. 423, U.S. Naval Underwater Ordnance Station, Newport, Rhode Island, 1966, 4 pp. + illus.

Simpson, H.J., D.E. Hammond, B.L. Deck, and S.C. Williams, "Nutrient Budgets in the Hudson River Estuary," Marine Chemistry in the Coastal Environment, T. M. Church, Ed., American Chemical Society, Washington, D.C., 1975, pp. 618-635.

Stommel, H., and A. Leetmaa, "Circulation of the Continental Shelf," Proceedings, National Academy of Sciences, Washington, D.C., Vol. 69, No. 11, 1973, pp. 3380-3384.

Sturges, W., "Longshore Slope of Sea Level Along the New England Coast," EOS Transactions, Vol. 58, No. 4, 1977.

Swanson, R.L., "Tides," MESA New York Bight Atlas, Monograph No. 4, New York Sea Grant Institution, Albany, New York, 1976, 34 pp.

Thom, H.C.S., "Some Methods of Climatological Analysis," Technical Report No. 81, WMO-No. 199.TP.103, World Meteorological Organization, Geneva, Switzerland, 1966, pp. 26-38.

Thom, H.C.S., "Extreme Wave Height Distribution Over Oceans," Journal of Waterways, Harbors, and Coastal Engineering Division, Proceedings of the American Society of Civil Engineers, August 1973, pp. 355-374.

Thompson, E.F., "Results From the CERC Wave Measurement Program," Proceedings of the International Symposium on Ocean Wave Measurement and Analysis, American Society of Civil Engineers, New Orleans, Louisiana, 1974, pp. 836-855.

U.S. Department of Commerce, "Marine Surface Observations," Weather Service Observing Handbook No. 1, Silver Spring, Maryland, 1974, 101 pp.

U.S. Department of the Interior, "Outer Continental Shelf Oil and Gas Lease Sale Offshore the Mid-Atlantic States, OCS Sale No. 40," Final Environmental Statement, Vol. 1, 1976, 621 pp.

U.S. Naval Oceanographic Office, "Oceanographic Atlas of the North Atlantic Ocean," Publication No. 700, Sec. 1, Washington, D.C., 1947.

U.S. Naval Oceanographic Office, "Pilot Charts of the North Atlantic Ocean," Washington, D.C., 1971-1976.

Von Arx, W.S., "Notes on the Surface Velocity Profile and Horizontal Shear Across the Width of the Gulf Stream," Tellus, Vol. 4, 1952, pp. 211-214.

Voorhis, A.D., D.C. Webb, and R.C. Millard, "Current Structure and Mixing in the Shelf Slope Water Front South of New England," Journal of Geophysical Research, Vol. 81, No. 21, 1976, pp. 3695-3708.

Walford, L.A., and R.I. Wicklund, "Monthly Sea Temperature Structure From the Florida Keys to Cape Cod," Serial Atlas of the Marine Environment, Folio 15, American Geographical Society, New York, 1968, 27 pp.

Waters, W., "New Surface Current Data Available," EDS, Environmental Data Service, National Oceanic and Atmospheric Administration, U.S. Department of Commerce, Washington, D.C., 1976, pp. 21-22.

Webster, F., "On the Representativeness of Direct Deep-Sea Current Measurements," Progress in Oceanography, Vol. 5, M. Sears, Ed., Pergamon Press, New York, 1969, pp. 3-15.

Whitcomb, V.L., "Oceanography of the Mid-Atlantic Bight in Support of ICNAF," United States Coast Guard Oceanographic Report No. 35, CG373-35, Washington, D.C., 1970, 157 pp.

Wright, W.R., "The Limits of Shelf Water South of Cape Cod, 1941 to 1972," Journal of Marine Research, Vol. 34, 1976.

Wright, W.R., and D.C.E. Parker, "A Volumetric Temperature/Salinity Census for the Middle Atlantic Bight Area," Limnology and Oceanography, Vol. 21, No. 4, 1976, pp. 563-571.

Wyrtki, K. "Oceanographic Atlas of the International Indian Ocean Expedition," Prepared under grants to the University of Hawaii, U.S. National Science Foundation, Washington, D.C., 1971.

Wunsch, C., and R. Hendry, "Array Measurements of the Bottom Boundary Layer and the Internal Wave Field on the Continental Slope," Geophysical Fluid Dynamics, Vol. 4, 1972, pp. 101-145.

Yentsch, C.S., "New England Coastal Water," Marine Chemistry in the Coastal Environment, T.M. Church, Ed., American Chemical Society, Washington, D.C., 1975, pp. 608-617.

# APPENDIX A

## A WIND ESTIMATION PROCEDURE

Wind climatology is commonly given in the form of wind roses or tabular summaries that give the observation frequency of wind speed observations within specified speed categories and direction ranges. These summaries can be produced from observations available at regular time intervals from a fixed location, such as a coastal meteorological station, or from observations collected within a specified geographical area by, for example, passing ships. As an illustration, table A.1 gives the January monthly wind summary for the Westhampton, Long Island, coastal station and for the ocean area $40^{o}$-$41^{o}$N, $72^{o}$-$73^{o}$W, based on passing ship reports. These summaries were used to estimate wind speed and direction adjustment factors that characterize vector differences between the mean winds from the two sites. Calms, which were listed separately in the original summary tables, were distributed evenly over all directions in the column for 0-3 kt in table A.1 to facilitate the calculations.

Table A.1--January wind speeds for Westhampton, L.I., and the ocean area 40-41°N, 72-73°W (% frequency)

| Direction | Wind Speed (kt) | | | | | | | | | |
|---|---|---|---|---|---|---|---|---|---|---|
| | 0-3 | 4-6 | 7-10 | 11-16 | 17-21 | 22-27 | 28-33 | 34-40 | 41-47 | >47 |
| | | | | A. Westhampton, L.I. | | | | | | |
| N | 2.6 | 3.1 | 4.7 | 4.1 | 1.0 | 0.3 | | | | |
| NE | 2.3 | 1.8 | 2.5 | 2.3 | 0.6 | 0.5 | 0.1 | | | |
| E | 1.8 | 1.3 | 1.3 | 1.1 | 0.3 | | | | | |
| SE | 1.8 | 0.7 | 0.8 | 0.5 | | | | | | |
| S | 2.0 | 1.0 | 1.2 | 0.9 | 0.1 | | | | | |
| SW | 2.2 | 2.8 | 4.7 | 3.4 | 0.4 | 0.1 | 0.1 | | | |
| W | 3.3 | 5.0 | 5.9 | 4.7 | 0.9 | 0.3 | 0.1 | | | |
| NW | 3.1 | 4.1 | 6.9 | 7.8 | 2.7 | 0.9 | 0.3 | | | |
| | | | | B. Ocean area | | | | | | |
| N | 0.4 | 0.3 | 2.1 | 2.8 | 2.3 | 1.0 | 0.9 | 0.3 | | |
| NE | 0.5 | 0.6 | 0.9 | 1.9 | 0.9 | 0.8 | 0.4 | 0.8 | | |
| E | 0.9 | 0.5 | 1.6 | 1.7 | 0.5 | 0.8 | 0.7 | 0.2 | | |
| SE | | 0.9 | 1.6 | 2.1 | 0.5 | 0.2 | 0.1 | 0.4 | | |
| S | | 1.6 | 0.9 | 1.3 | 0.6 | 0.7 | 0.4 | | | |
| SW | 0.4 | 1.1 | 1.4 | 4.3 | 2.4 | 1.1 | 0.6 | 0.1 | | |
| W | 1.0 | 0.6 | 3.8 | 7.0 | 5.0 | 4.7 | 3.9 | 1.0 | | |
| NW | 0.4 | 0.4 | 3.7 | 6.7 | 6.8 | 3.2 | 3.3 | 1.0 | | |

With $\rho_k$ defined as the mean speed of the kth wind speed interval and $\theta_\ell$ as the mean of $\ell$th direction interval, the entry appearing in the $\ell$th row and the kth columns of the Westhampton summary (A in table A.1) is represented by the complex number

$$A_{k\ell}\rho_k e^{i\theta_\ell} \quad , \tag{A-1}$$

where $A_{k\ell}$ is the percent frequency of observations found in that category, and i is the square root of -1. Using this representation, the average vector wind for the A table is given by averaging over all the k x $\ell$ entries in the table, i.e.,

$$\vec{V}_A = \frac{1}{k \times \ell} \sum_{k=1}^{k} \sum_{\ell=1}^{\ell} A_{k\ell}\rho_k e^{i\theta_\ell} \quad . \tag{A-2}$$

The ocean area summary (B in table A.1) is represented in an identical manner, and its average is denoted by $\vec{V}_B$.

Next, the two summary tables are related in the least-squares sense through the adjustment factors $\eta$ for speed and $\phi$ for direction by introducing the modified coastal mean wind defined by

$$\hat{\vec{V}}_A = \eta e^{i\phi} \vec{V}_A \quad ,$$

and the values of these quantities are determined by requiring that

$$\sum_{k=1}^{k} \sum_{\ell=1}^{\ell} \left| B_{k\ell}\phi_k e^{i\phi_\ell} - \hat{\vec{V}}_A \right|^2 = \text{Minimum}(\eta,\phi) \quad .$$

It can be shown that the required values satisfy the relation

$$\hat{\vec{V}}_A = \eta e^{i\phi} \vec{V}_A = \vec{V}_B \quad ,$$

which is easily solved for $\eta$, $\phi$.

Adjustment factors for estimates of offshore wind in the ocean area 40°-41°N, 72°-73°W (table 3.5, sec. 3.1.2.4) were applied to the Westhampton wind summary (A in table A.1). Results of this application are estimates of the January wind climatology for the ocean area. The differences between these estimates and the observed wind values in summary table B is given in table A.2.

Table A.2.--Differences between estimated and observed climatology

| Direction | Wind speed (kt) | | | | | | | | | |
|---|---|---|---|---|---|---|---|---|---|---|
| | 0-3 | 4-6 | 7-10 | 11-16 | 17-21 | 22-27 | 28-33 | 34-40 | 41-47 | >47 |
| N | 0.9 | 0.3 | 0.6 | 0.6 | 0.7 | 1.1 | 0.7 | 0.5 | 0.2 | 0.2 |
| NE | 0.6 | 0.0 | 0.9 | -0.1 | 0.7 | 0.4 | 0.5 | -0.3 | 0.3 | 0.4 |
| E | -0.1 | -0.1 | -0.3 | -0.6 | 0.3 | -0.3 | -0.3 | 0.0 | 0.0 | 0.0 |
| SE | 0.6 | -0.5 | -0.7 | -1.5 | 0.0 | 0.1 | 0.1 | -0.4 | 0.0 | 0.0 |
| S | 0.7 | -1.1 | 0.3 | -0.4 | 0.2 | -0.3 | -0.1 | 0.1 | 0.0 | 0.0 |
| SW | 0.7 | -0.6 | 1.0 | -1.0 | 0.5 | 0.6 | 0.6 | 0.2 | 0.1 | 0.1 |
| W | 0.6 | 0.2 | 0.4 | -2.4 | -1.3 | -2.4 | -2.2 | -0.3 | 0.2 | 0.3 |
| NW | 1.1 | 0.4 | -0.2 | -1.9 | -2.1 | 0.7 | -0.2 | 1.2 | 0.3 | 0.4 |

In the derivation of the wind speed and wind direction adjustment factors, it was assumed that differences between the wind climatologies obtained from coastal-station and ocean-area measurements were the result of a uniform bias over all compass directions and over the entire observed range of speeds. This may not be true for all coastal wind estimates, however. Very low wind speeds are probably not estimated with precision because of common inaccuracies in measurement of such speeds and because of possible influence of local climatic conditions, i.e., terrain near the coastal station. In addition, very high winds for offshore areas are probably not estimated as accurately as lesser speeds because high winds are usually associated with frontal systems and storm centers within limited areas. The derivation of offshore wind estimates from a coastal station should be confined to an area within 200 to 300 mi from the coast.

# APPENDIX B

## ASYMPTOTIC SINGULAR DECOMPOSITION (ASD)

### Objective Analysis and Classification of Oceanographic Data *

John B. Jalickee
Center for Experiment Design and Data Analysis
Environmental Data Service
National Oceanic and Atmospheric Administration

Douglas B. Hamilton
National Oceanographic Data Center
Environmental Data Service
National Oceanic and Atmospheric Administration

Abstract. A new approach to the analysis and classification of oceanographic data is presented. The technique is an empirical one, based on the singular decomposition theorem, for characterizing temperature-salinity-depth profiles as in water-mass analysis. Complementary to the profiles are station or cast-dependent coefficients, which show similarities and differences according to the space-time distributions of the individual stations in the data set. These coefficients are used for classifying the individual stations into groups having similar profiles. Results of applying the new method to a set of data from ocean stations off the coast of Oregon are given.

## Introduction

Studies related to the oceans often require a precise, objective description or characterization of the physical nature of the region of interest. Such a characterization is usually in the form of expected values and variations of one or more parameters within several geographic areas, time periods, and depths. Statistics describing a data population are most accurate and useful if the population is homogeneous, but it is difficult to identify homogeneous populations in the dynamic ocean. One approach often used is to choose geographic subareas and seasonal time periods in such a way that each exhibits a unique set of attributes. Inherent in this approach, however, is the assumption that oceanographic features conform to static geographic and time boundaries.

---

* Although this paper (to be published in Tellus, 1978) refers to temperature-salinity analysis of the Columbia River outflow area, the methodology is the same as that applied to the Mid-Atlantic Bight.

Another possible approach is to group data according to similarity of various features, such as the shape of temperature-salinity-depth (T-S-Z) curves, as in water-mass analysis. If this can be done, the variability within each group is minimized, and the expected values of the parameters in each group are more reliable than the expected values of the total population. Also, if the grouping succeeds in characterizing oceanographic regions, natural boundaries or transition zones in time and space will be apparent in time and location plots of the stations of each group.

Described here is a numerical technique, called Asymptotic Singular Decomposition (ASD), which has been developed at the National Oceanic and Atmospheric Administration for the analysis of complex data sets.

## Singular Decomposition

The basic mathematical concept on which the analysis is based is the singular decomposition of a matrix. Let $A = \{A_{ij}\}$ be an N x M matrix $N \leq M$, then the singular decomposition of A is

$$A_{ij} = \lambda_1 f_i^{(1)} g_j^{(1)} + \lambda_2 f_i^{(2)} g_j^{(2)} + \ldots + \lambda_N f_i^{(N)} g_j^{(N)}. \tag{B.1}$$

The numbers $\lambda_1, \lambda_2, \ldots, \lambda_N$ are the singular values of A, with

$$\lambda_1 \geq \lambda_2 \geq \ldots \geq \lambda_N \geq 0. \tag{B.2}$$

Elements $f_1^{(\ell)}, f_2^{(\ell)}, \ldots, f_N^{(\ell)}$ and $g_1^{(\ell)}, g_2^{(\ell)}, \ldots, g_M^{(\ell)}$ form the $\ell$th left and right singular vectors of A respectively. These vectors are mutually orthonormal:

$$\sum_{i=1}^{N} f_i^{(\ell)} f_i^{(m)} = \sum_{j=1}^{M} g_j^{(\ell)} g_j^{(m)} = \begin{cases} 0 & \ell \neq m \\ 1 & \ell = m. \end{cases} \tag{B.3}$$

The value of the singular decomposition in this study lies in the fact that the first k terms in the expansion form an optimal approximation to the original matrix in the sense of the least squares. Let $\hat{A}_{ij}^{(k)}$ denote an approximation comprised of the first k terms:

$$\hat{A}_{ij}^{(k)} = \sum_{\ell=1}^{k} \lambda_\ell f_i^{(\ell)} g_j^{(\ell)}. \tag{B.4}$$

Then

$$\sum_{i,j} \left( A_{ij} - \hat{A}^{(k)}_{ij} \right)^2 = \text{Minimum} \qquad \text{(B.5)}$$

with respect to all possible choices of the elements of the terms in expansion of $\hat{A}^{(k)}_{ij}$. These terms are also ordered in terms of the variance each explains.

$$\left( \lambda_\ell^2 / \sum_{k=1}^{N} \lambda_k^2 \right) * 100\%$$

of the total variance of the entire array is explained by the $\ell$th term and since the $\lambda$'s are ordered, so are the individual variances explained by them.

This scheme of successive approximations can be shown to be equivalent to principal component analysis (Whittle, 1952), but differs in two respects: (1) the conjugate pairs of vectors are on an equal footing and both can be given physical interpretation, and (2) the computational methods for calculating the terms in the singular expansion are considerably more accurate and reliable than those commonly used in principal component analysis. Good (1969) has made these points and described other uses of singular decomposition Golub and Reinsch (1971) have pointed out the pitfalls of calculating the terms of the expansion by "equivalent" methods and have developed an efficient and accurate method for calculating the terms directly. The Asympotic Singular Decomposition (ASD) method, however, which has been described in detail by Jalickee (1976), is especially designed for calculating the leading terms of the expansions of very large matrices.

## Model of Ocean Data

For the analysis of T-S-Z data the basic definition of the data matrix was modified as follows: Let $T_{d,c}$ and $S_{d,c}$ denote the temperature and salinity respectively at depth level d, d = 1, 2, .... , N for the cth station, c = 1, 2, .... , M. The the T-S-Z matrix A is defined by:

$$A_{1,d,c} = T_{d,c} ,$$

$$A_{2,d,c} = S_{d,c} . \qquad \text{(B.6)}$$

and the singular decomposition is written in the form:

$$A_{i,d,c} = \sum_{\ell=1}^{2N} \lambda_\ell \, f^{(\ell)}_{i,d} \, g^{(\ell)}_{c} . \qquad \text{(B.7)}$$

This matrix is then considered as a 2N x M matrix and is decomposed by an appropriate computational procedure.

Now if we define

$$T_d^{(\ell)} = \lambda_\ell f_{1,d}^{(\ell)} , \tag{B.8a}$$

and

$$S_d^{(\ell)} = \lambda_\ell f_{2,d}^{(\ell)} , \tag{B.8b}$$

we can rewrite eq. (B.7) in a more descriptive form:

$$(T_{d,c}, S_{d,c}) = \sum_{\ell=1}^{2N} (T_d^{(\ell)}, S_d^{(\ell)}) g_c^{(\ell)} , \tag{B.9}$$

where the new left singular vector suggest characteristic T-S-Z profiles. The $g_c$'s will be called station coefficients.

To show how these characteristic functions are optimum we denote by $(\hat{T}_{d,c}^{(k)}, \hat{S}_{d,c}^{(k)})$, the kth approximation, the sum of the first k terms of eq. (B.9). Then the approximation satisfies:

$$\sum_{d,c} \delta_{d,c}^2 = \text{Minimum} ,$$

where

$$\delta_{d,c}^2 = \left( (T_{d,c} - T_{d,c}^{(k)})^2 + (S_{d,c} - S_{d,c}^{(k)})^2 \right). \tag{B.10}$$

The minimum is over all possible choices of the characteristic profiles and station coefficients. This is shown graphically in figure B.1.

Because the elements in the model are determined empirically, they contain physically significant information related to ocean conditions as embodied in the temperature-salinity data. Also, the terms in the expansion are orthogonal to one another; hence each term represents independent information. Since the terms are ordered according to the variance explained, the higher order terms generally describe finer details of the data set.

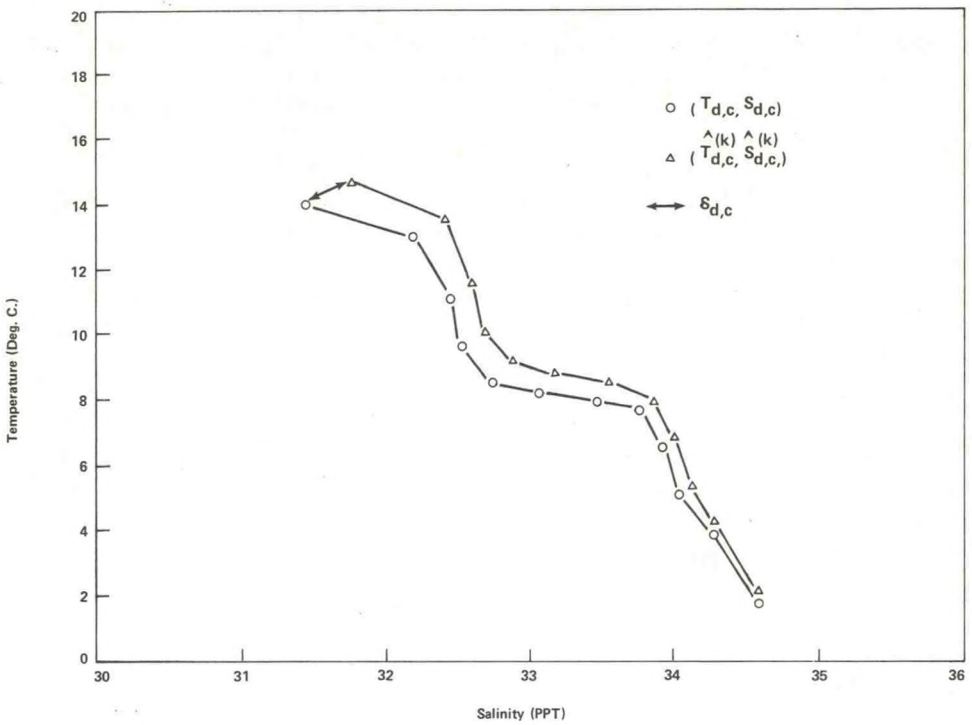


Figure B.1.--Example of the minimizing function described in eq. (B.1).

The first characteristic profile, $(T_d^{(1)}, S_d^{(1)})$, effectively constitutes the typical profile, since it alone best describes the entire collection of original profiles. Subsequent terms modify the collection of previous terms in describing next-most-important variations, The station coefficients in the expansion modify these profile values to produce a unique approximation to each of the stations. Therefore, a unique set of coefficients exists for each different station. Because the characteristic profiles are the same for all stations, the unique T-S-Z characteristics of a particular station are reflected in the coefficients of that station. The sets of coefficients for stations with similar T-S-Z profiles will be similar, while the sets corresponding to different profiles will be diverse. This property of the coefficients make them useful as indicators of similarities and differences between casts and constitutes the basis for the objective classification scheme described later.

## Data Used in the Analysis

Data obtained from a group of stations located off the coast of Oregon were selected from the ocean station data archive at the National Oceanographic Data Center to examine characteristics of the ASD technique using oceanographic data. One requirement to applying this technique is that the data must be in matrix form, with all cells filled. For

this analysis, the matrix was made up of temperature and salinity values at standard depth levels. Thus, depths are not directly a part of the analysis, but the depth of each datum is known indirectly by its position in the array.

To obtain a sufficient number of stations with enough depth for a meaningful analysis, stations with temperature and salinity values at each standard depth between the surface and 900 m were accepted. This yielded a total of 95 stations in the region 45° to 46° north latitude and 125° to 127° west longitude (fig. B.2). The matrix constructed from these stations consists of 36 rows (18 depths for both temperature and salinity) and 95 columns (one for each station).

The temperature-salinity-depth distributions of the data used in the analysis are shown in figures B.3 and B.4. These stations exhibit characteristics typical of the coastal subarctic Pacific Ocean as described by Dodimead, Favorite, and Hirano (1963). The problem now is to identify groups within this data set, each of which has a unique temperature-salinity relationship. Before discussing the results of the ASD classification, however, we will examine the information obtained from the model functions and coefficients.

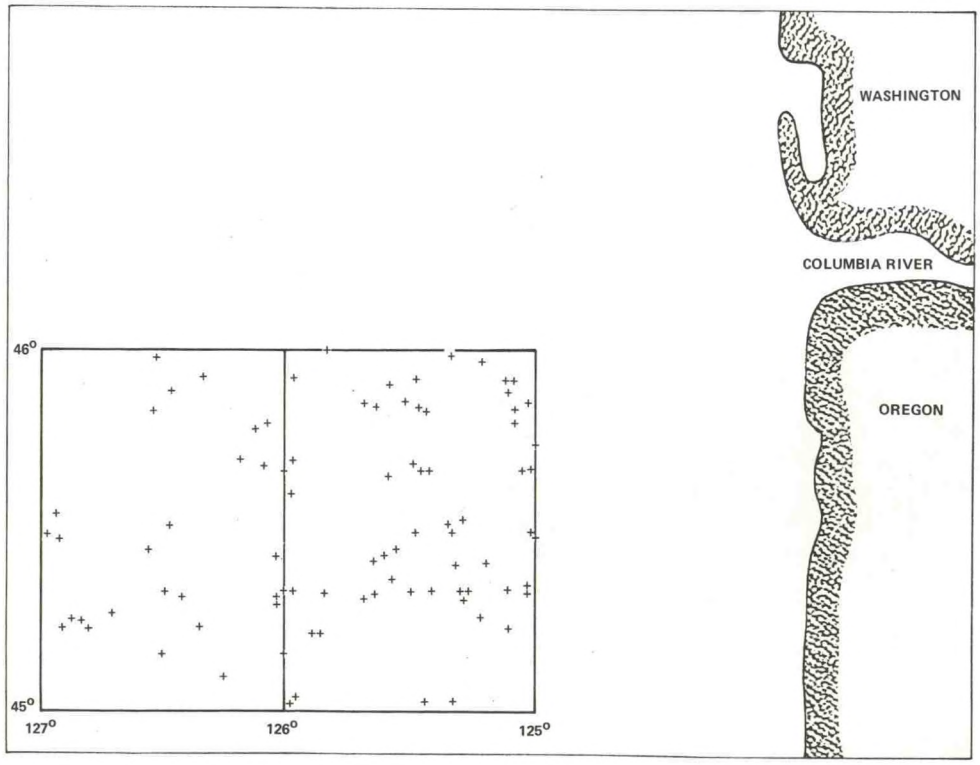


Figure B.2.--Locations of station data used in the analysis.

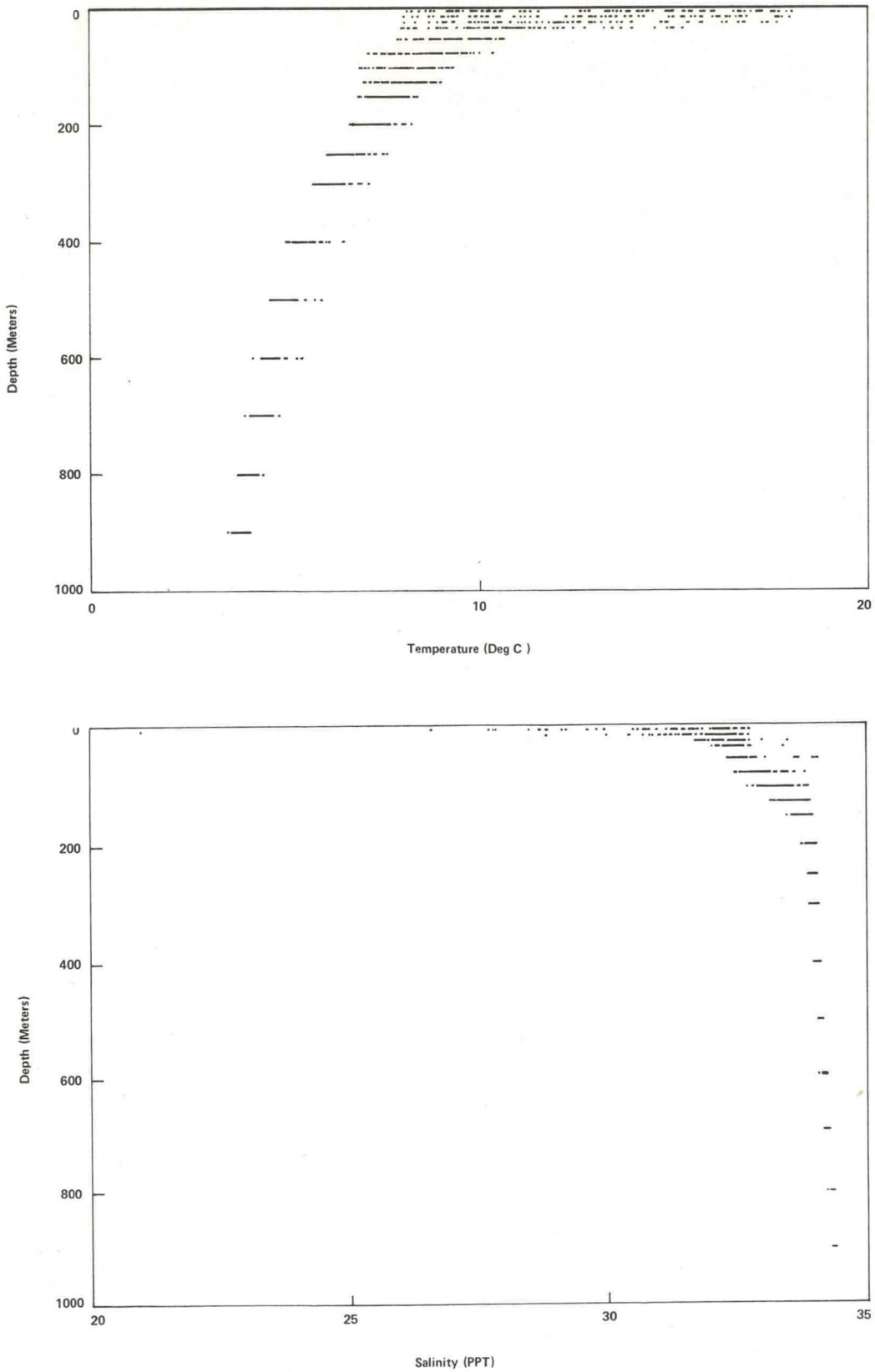


Figure B.3.--Temperature-depth (top) and salinity-depth (bottom).

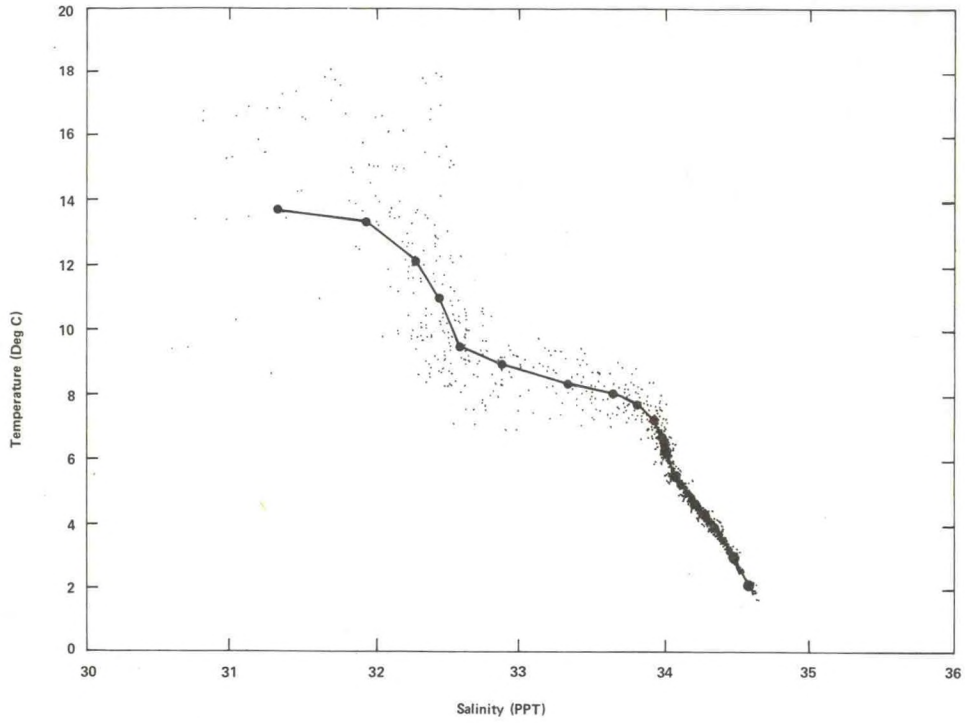


Figure B.4.--Temperature-salinity data with the first characteristic T-S-Z profile superimposed.

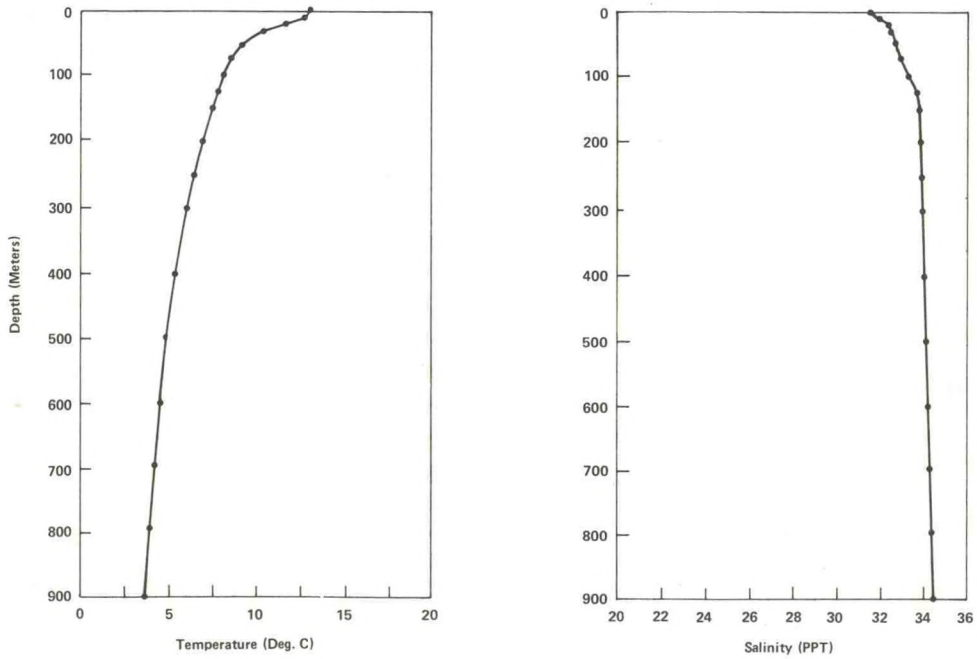


Figure B.5.--First characteristic profiles representing the typical depth dependence of temperature and salinity.

## Physical Information Obtained from Model Elements

### Functions

Features of the vertical distributions of temperature and salinity of the 95 stations are shown in the profiles computed by ASD. The first profile ($T_d^{(1)}$, $S_d(1)$), when multiplied by the average station-coefficient $\bar{g}_c^{(1)}$, representative of all stations, provides an estimate of expected average values of temperature and salinity at each depth level, as shown in figure B.5. These values are also shown in figure B.4., superimposed on the data used in the analysis. Succeeding functions (fig. B.6) give information about the most significant variations of actual profiles from the first estimate. Each of these, when multiplied by a station coefficient and added to the first function, makes a slight change in the approximation to produce an estimate of a particular station. Estimates of the profiles comprising the data set become more accurate with the addition of each successive term.

Of greatest interest are the second and third functions. The second function contributes a large negative salinity at the surface and fairly large negative temperature values between 20 and 900 m. The third function, on the other hand, primarily modififes temperature values, especially in the upper 20 m. The fourth function contributes a small correction to both salinity and temperature in the uppermost layers. The functions act together in an infinite number of possible combinations to add to or subtract from each other at each depth level.

### Coefficients

Coefficients of these functions, computed for this analysis, reveal the similarities and disparities of stations. The first coefficient, when applied to the first function, determines the magnitude of temperature and salinity values in the first approximation, and can therefore be used as an index to the relative magnitudes of individual stations. Similarly, subsequent coefficients determine the magnitude and sign of modifications to the first approximation. The second coefficient of each station is an indicator of the presence or absence of low surface salinity; a station with normal surface salinity (about 3.25 °/₀₀) would have a second coefficient near zero, but the coefficient of a station with extremely low surface salinity will have a large negative value.

Turning now to the distribution of individual coefficients of all stations as a function of the Julian Day of year of each station, we find that the sine curve pattern of the third coefficients (fig. B.7) is reasonable, since changes made by the third function are mostly to temperature in the upper 20 to 30 m. Obviously, this distribution reflects seasonal temperature change in the surface layer. On the other hand, the distribution of the second coefficient, shown in figure B.8, is uniform during most of the year, with the exception of a rather sharp

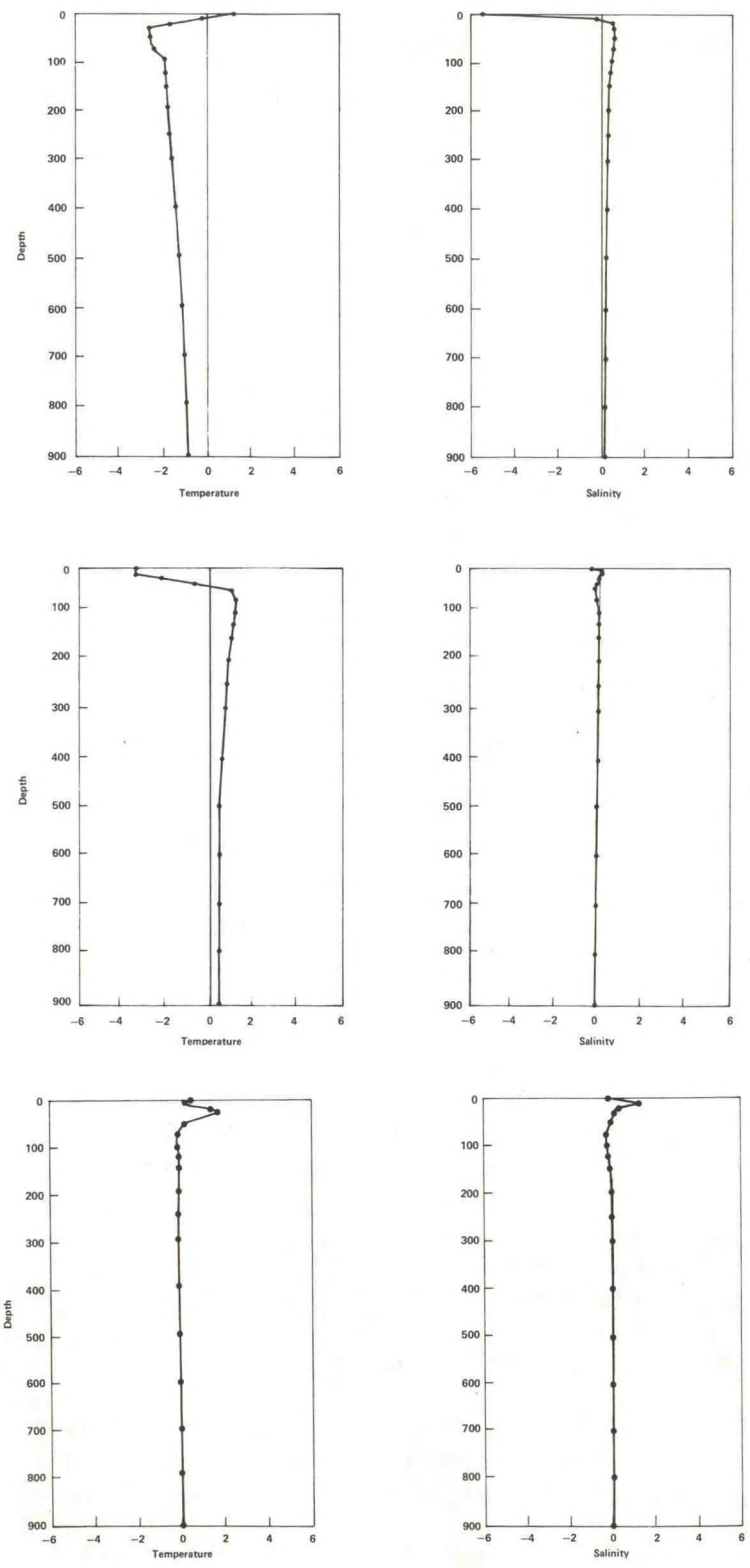


Figure B.6.--Characteristic profiles two (top), three (center), and four (bottom).

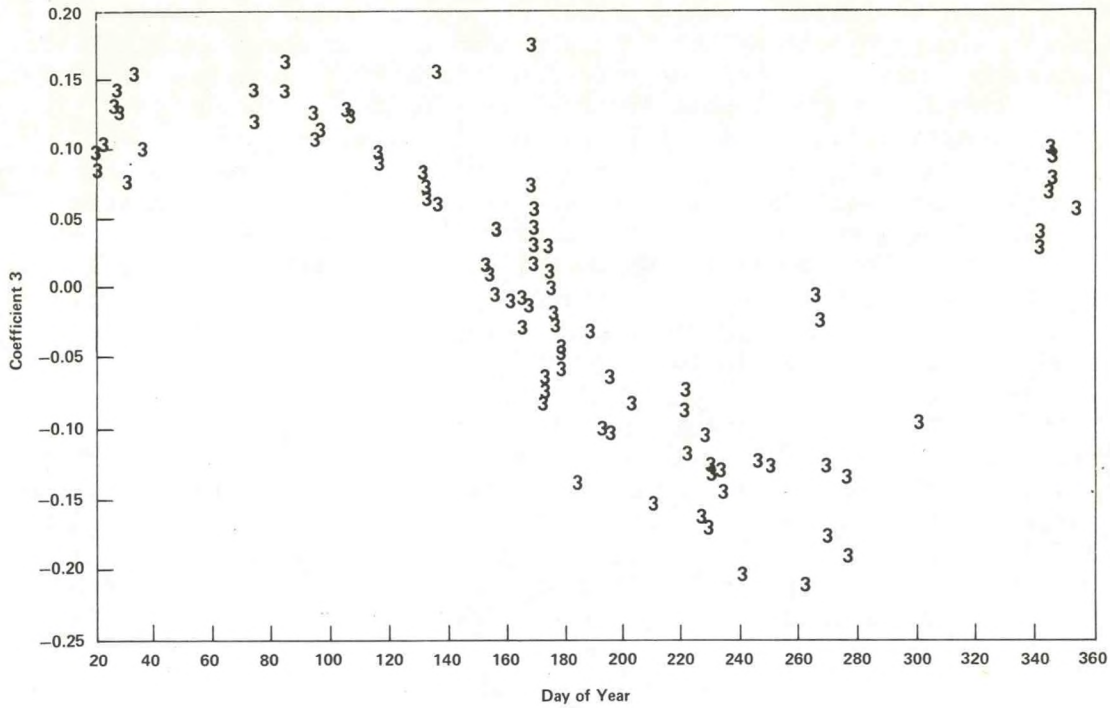


Figure B.7.--Day-of-year dependence of station coefficient 3.

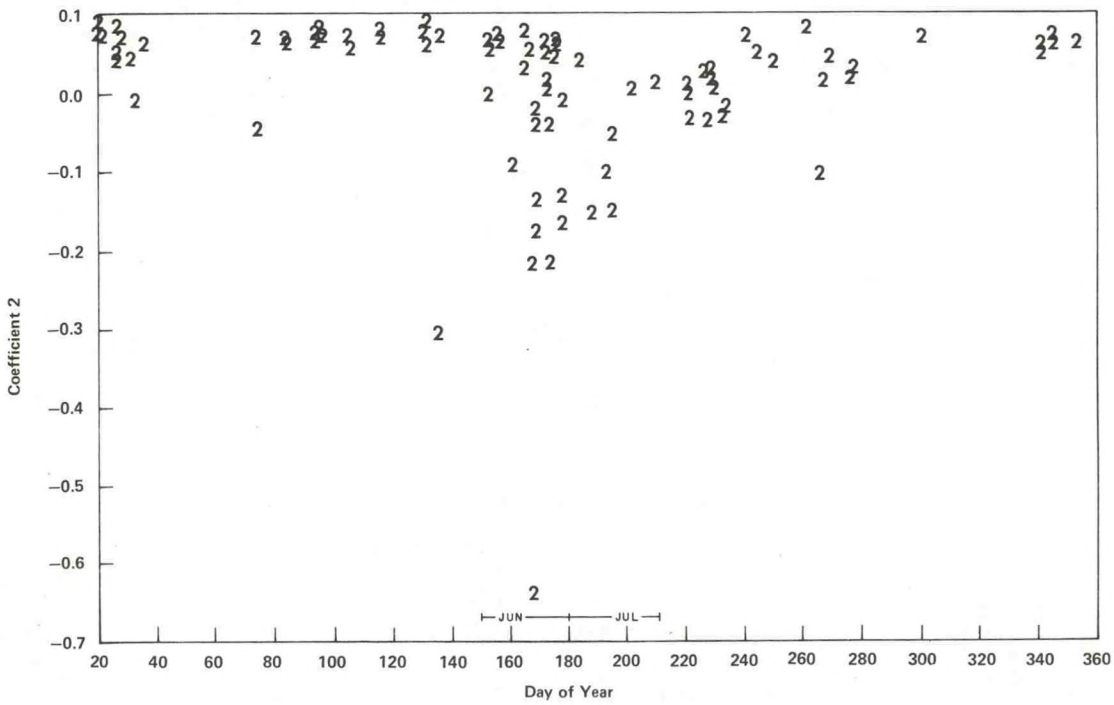


Figure B.8.--Day-of-year dependence of station coefficient 2.

peak in June and July. Recalling that the second function modifies surface salinity values and that this region is near the Columbia River, we can assume that the large negative coefficients in June belong to stations taken in the Columbia River plume. In fact, the 15-year (1953-1967) mean of river outflow at Astoria, Oregon, indicates that the normal discharge volume of the river is about 7,500 $m^3/s$ during most of the year, but in mid-June there is a peak of about 17,500 $m^3/s$. There is also a minor peak during February, due to coastal river runoff into the Columbia River, but the plume is generally turned northward along the coast by southerly winds during winter. In summber, however, the plume flows southwestward through the region being studied because of the predominant northerly winds (Barnes, Duxbury, and Morse, 1972).

In addition to time distributions of coefficients, geographic distributions can be useful in the analysis. For example, a plot of the second coefficients during June and July (fig. B.9) shows a correlation of large negative values with the northeast portion. Translating this into salinity, we would not expect to find low surface salinities in regions with positive second coefficients because the second function would add rather than subtract salinity at the surface.

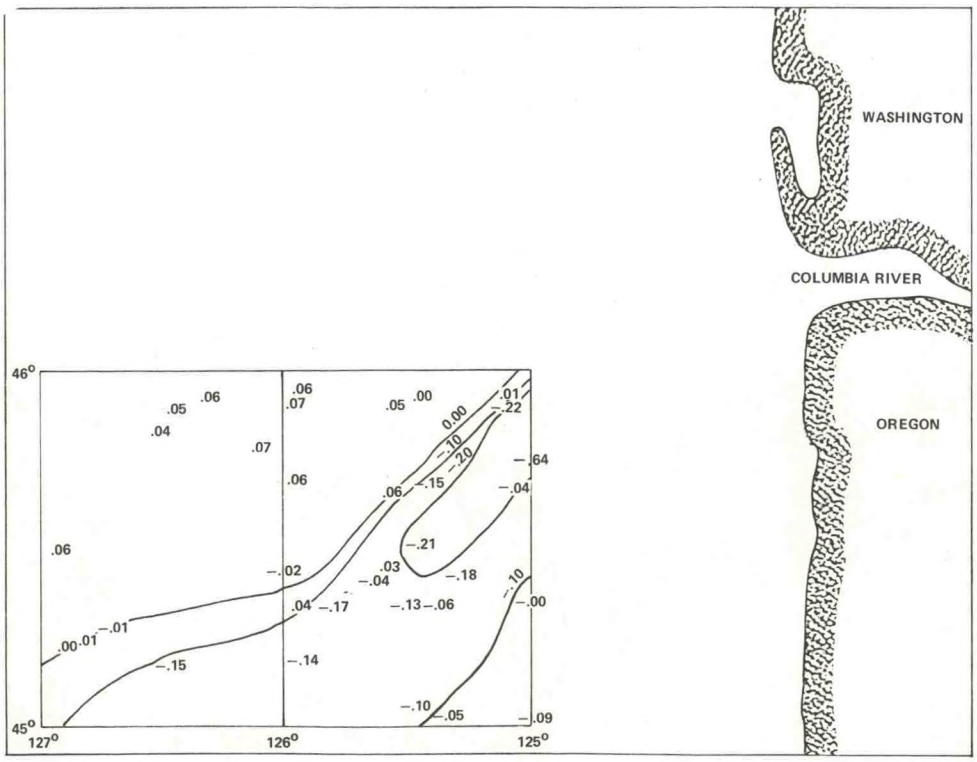


Figure B.9.--Contour map of station coefficients for June and July.

## Other Uses of Model Elements

The model elements are potentially useful for solving a number of other types of problems. In the approximation of data from the model elements, for example, minor irregularities of individual T-S profiles are eliminated. Therefore, smooth data fields can be developed from reconstructed data.

Distributions of coefficients in time and space provide the possibility of data validation, and interpolation on time and location fields. If a station shows values that exceed the normal range of variation, the coefficients of that station will obviously be different from coefficients of normal stations, particularly on plots of coefficient distributions. If there is a period of time or a geographic area for which no data exist, it is possible to interpolate coefficients from existing distributions and create an expected T-S-Z profile. Of course, the reliability of that profile will depend on the continuity of actual ocean conditions and the amount of data surrounding the region of interpolation.

All T-S-Z profiles in the original data set can, of course, be approximated by the model. Therefore, the model can be used as a compressed version of the original data. In this analysis, there were 18 temperature and salinity values per station and 95 stations, or a total of 3,420 data values. The model consists of four singular terms, four functions, each having 36 values, and four coefficients for each station, or a total of 528 values. This represents an almost sixfold reduction, and reduction would be even greater for larger data sets.

## Classification of T-S-Z Profiles

In order to determine homogeneous groups within the data set, the model elements are rearranged to form a different expansion, consisting of new functions and station coefficients that are particular linear combinations of the original ones. These new functions and coefficients not only approximate each T-S profile, but also represent each of the homogeneous groups. In the original model, the first function was a first order estimate of temperature-depth and salinity-depth profile shapes for all stations in general. In the new model, however, each function represents the temperature-depth and salinity-depth profiles of one of the groups, the second function being a first order estimate of T-S-Z in group 2, and so forth. The station coefficients of the new model indicate the degree of association of each station with each of the groups. The T-S-Z profile of a station is most similar to the group whose coefficient is largest in magnitude for that station. Thus, the new model functions provide representative T-S-Z profiles for each group, and the new coefficients indicate the group to which each station belongs.

The expansion, eq. (B.9), rewritten in terms of the new component is

$$(\hat{T}^{(k)}_{d,c}, \hat{S}^{(k)}_{d,c}) = \sum_{\ell=1}^{k} (\tilde{T}^{(\ell)}_{d}, \tilde{S}^{(\ell)}_{d})\, \tilde{g}^{(\ell)}_{c} . \qquad (B.11)$$

Here the new station coefficients, $\tilde{g}_c^{(\ell)}$, are defined in terms of the old coefficients through the transformation defined by the elements $\{\alpha_{\ell,m}\}$:

$$\tilde{g}_c^{(\ell)} = \sum_{m=1}^{k} \alpha_{\ell,m} g_c^{(m)}. \tag{B.12}$$

We require these new coefficients to retain the normalization of the old, so that

$$\sum_{c=1}^{M} \left(\tilde{g}_c^{(\ell)}\right)^2 = 1, \tag{B.13}$$

which implies

$$\sum_{m=1}^{k} \alpha_{\ell,m}^2 = 1. \tag{B.14}$$

The new T-S-Z profiles are described from the old using the inverse transformation described by the elements $\{\beta_{\ell m}\}$. That is, with

$$\sum_{\ell=1}^{k} \beta_{\ell,n} \alpha_{\ell,m} = \begin{cases} 0 & n \neq m \\ 1 & n = m \end{cases}, \tag{B.15}$$

we have

$$(\tilde{T}_d^{(\ell)}, \tilde{S}_d^{(\ell)}) = \sum_{n=1}^{k} (T_d^{(n)}, S_d^{(n)}) \beta_{\ell,n}. \tag{B.16}$$

Using the definition of the new factors and the transformations, one can show that eqs. (B.9) and (B.11) are in fact identical. We have merely rearranged the terms and not changed the actual approximation.

Our choice of transformation elements is made under the requirement that the new station coefficients be as mutually exclusive as possible. To this end, consider the product

$$\left(\tilde{g}_c^{(\ell)} * \tilde{g}_c^{(m)}\right)^2, \quad \ell \neq m.$$

We see that this number is non-negative and identically zero when the groups are exactly mutually exclusive. If one and only one station coefficient, $g_c^{(3)}$ say, is different from zero for a given station, that station belongs to one and only one new characteristic profile or group; in this case, the third group. This is not generally the case, but we attempt to approach this condition by minimizing the sum of all such possibilities through

$$\sum_c \left\{ \sum_{\substack{\ell \\ \ell \neq m}} \sum_m \left( g_c^{(\ell)} * g_c^{(m)} \right)^2 \right\} = \text{Minimum} \qquad \text{(B.17)}$$

with respect to the set of $\alpha$'s under the conditions of normality in eq. (B.14). This method is quite similar to methods of factor rotations in factor analysis. The procedure developed by Powell (1964) was used to achieve the minimization.

Transformation of the original model produced four homogeneous groups, which are discussed below.

## Results

The ideal classification would be one in which the group of every station is clearly identifiable. In reality, however, some stations will have characteristics that overlap between two or more groups. Therefore, each group may include some stations that do not seem to belong, but each is, in general, an entity with unique characteristics. The temperature-salinity traits of the first group (fig. B.10a) are typical of winter coastal subarctic waters, with a relatively cool, low salinity (32.0 to 32.5 °/oo) mixed layer about 50 m deep. Stations in this group are found in all parts of the region from December through the early part of June.

Stations in the second group (fig. B.10b) are typical of summer coastal subarctic waters. The salinity-depth distribution is similar to that of the first group, but the temperature-depth distribution shows higher values in the surface mixed layer. Stations with these characteristics are distributed throughout the area from June through October (and perhaps into November, although no station data are available for that month). The first two groups represent normal seasonal T-S conditions in this region; there is no geographic correlation of any consequence in these groups, and together they span all months of the year. Groups 3 and 4, however, reflect departures from the norm due to the influx of Columbia River water.

Salinity values of stations in the third group (fig. B.10c) are extremely low at the surface (less than 30 °/oo) and nearly normal at 10 m, which indicates the presence of a thin layer of relatively fresh water. Stations in this group cover almost exclusively the month of June and are located in a fairly well-defined northeast-to-southwest band.

Temperature-salinity-depth characteristics of stations in the fourth group (fig. B.10d) indicate the presence of modified Columbia River outflow. Both temperature and salinity profiles show a mixed layer of 10-m depth in which water is warm and of moderately low salinity (about 30 °/oo). At 20-m depth, however, salinity values are generally higher than 32 °/oo. Although the stations in group 4 are geographically more

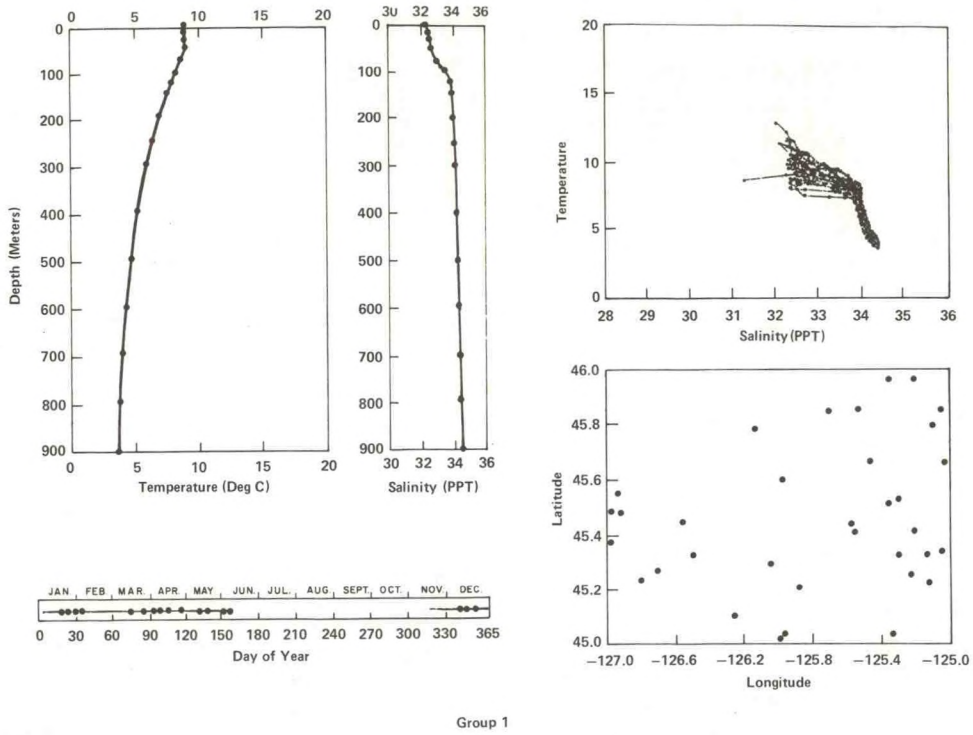


Figure B.10a.--Results of classification, group 1.

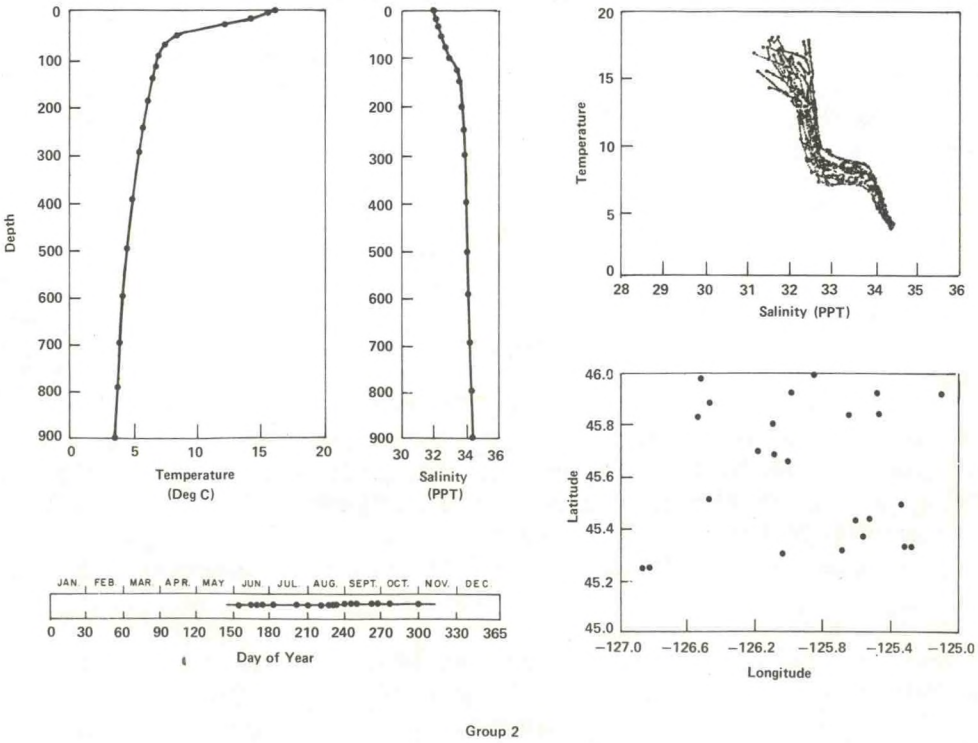


Figure B.10b.--Results of classification, group 2.

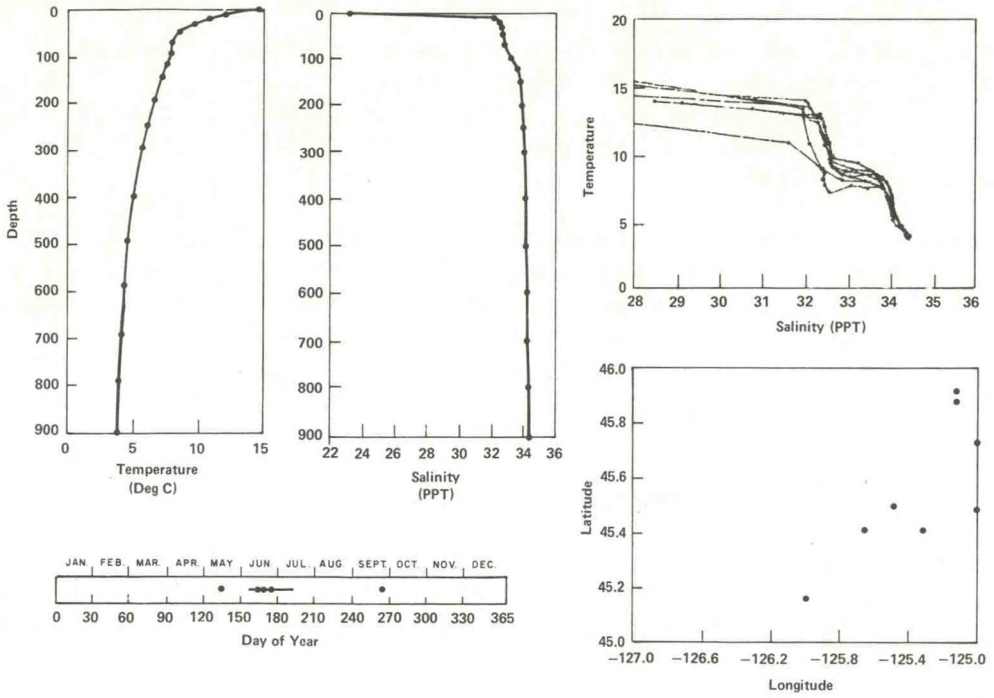


Figure B.10c.--Results of classification, group 3.

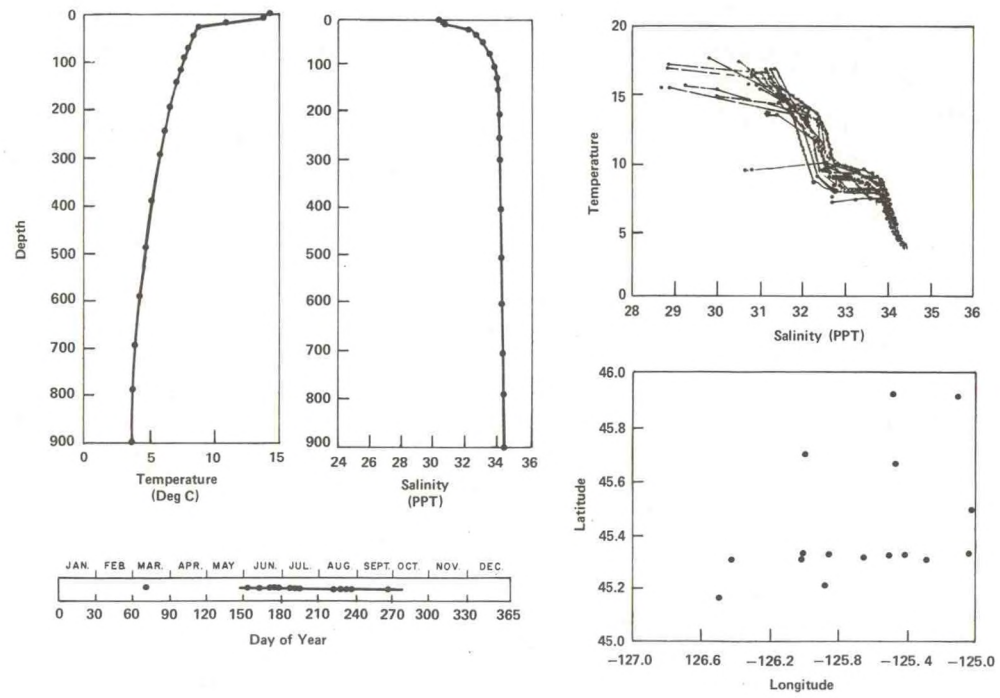


Figure B.10d.--Results of classification, group 4.

widespread than those in group 3, they tend to be located primarily in the eastern part of the region. The distribution of these stations in time is also more widespread, covering the months June through September. The presence of one station in March is perhaps the result of the winter peak in Columbia River outflow.

Examination of the T-S plots of the four groups in figure B.10 shows that the stations have been successfully classified into homogeneous groups by the ASD method. Furthermore, as a result of the classification, the region of interest can be definitively described in terms of the T-S-Z characteristics and the geographic and time distributions of stations in each of the four groups.

## Summary and Conclusions

We have described and illustrated an approach to the analysis and classification of oceanographic data. Using the technique of singular decomposition, important features of the data are extracted and represented in the form of optimum characteristic profiles and station-related coefficients. The classification scheme makes use of station coefficients, which were shown to be important indicators of T-S characteristics, and the rotation of characteristic profiles, a procedure closely related to factor rotation in factor analysis.

By applying the ASD technique, we were able to objectively classify the original 95 stations into 4 groups, according to temperature-salinity-depth traits. Furthermore, the groups produced by ASD are supported by environmental factors, such as time, location, and river outflow.

The value of the ASD technique lies in its ability to reduce the original data, consisting of a complex mass of numbers, to a smaller, more important set of numbers. The end result of the analysis, however, depends on the skill with which the products of the technique are assembled in order to uncover significant relationships.

## References

Barnes, C. A., A. C. Duxbury, and B. Morse, 1972. Circulation and selected properties of the Columbia River effluent at sea. The Columbia River Estuary and Adjacent Ocean Waters. Chapt. 3, pp. 41-80. Bioenvironmental Studies. A. T. Pruter and D. L. Alverson, ed. University of Washington Press, Seattle, p. 868.

Dodimead, A. J., F. Favorite, and T. Hirano, 1963. Review of oceanography of the Subartic Pacific region. Salmon of the North Pacific Ocean, Part II. International North Pacific Fisheries Commission, Bull. No. 13. Vancouver, Canada, p. 195.

Good, I. J., 1969. Some applications of the singular decomposition of a matrix. Technometrics, Vol. 11, No. 4, pp. 823-831.

Golub, G. H., and C. Reinsch, 1970. Singular value decomposition and least squares solutions. Numer. Math. Vol. 14, pp. 403-420.

Jalickee, J. B., 1976. Asympotic singular decomposition of large matrices, in preparation.

Powell, M. J. D., 1964. An efficient method for finding the minimum of a function of several variables without using derivatives. Comp. J. London, Vol. 7, No. 2, pp. 155-162.

Whittle, P., 1952. On principal components and least square methods of factor analysis. Skand. Aktuar., Vol. 35, pp. 223-239.

# APPENDIX C

## DATA EDITING AND VALIDATION

The following data were acquired in support of the historical physical oceanographic summary for the Mid-Atlantic Bight region:

| Source | No. of Casts |
|---|---|
| NODC STD Data File . . . . . | 2,460 |
| Virginia Institute of Marine Science | 3,806 |
| Chesapeake Bay Institute . . . . . | 346 |
| MESA . . . . . | 875 |
| MIT . . . . . | 277 |
| Total | 7,764 |

Subsequent review resulted in a large number of deletions for the following reasons:

| Source | No. Deleted and Reason |
|---|---|
| NODC STD Data File | Of the 2,460 casts, 137 were deleted because only 2,323 actually fell within the area of interest, which was specified to the nearest tenth of a degree, a level of precision not available in the information inventory systems used at NODC. |
| Virginia Institute of Marine Sciences | Of the 3,806 casts, 543 were eliminated by NODC, because they were largely bucket temperatures with no valid salinity measurements. Of the remaining 3,263 casts, 1,306 fell within the Mid-Atlantic study area; the rest fell either just south of it or within Chesapeake Bay. |
| Chesapeake Bay Institute | Of 335 casts submitted to NODC, 256 were taken in the project area, and 79 either in the mouth of the Chesapeake Bay or in the Bay itself. |
| MESA | Of the 875 casts, 129 were taken in the estuaries. |
| MIT | This was the last data set received, and because of format difficulties, they could not be processed in time. Therefore, these data were used only in generating the ASD contour plots, and not in the bulk of the statistical summaries. |

## Data Editing

The initial compilation of area statistics revealed numerous outliers and a very large scatter in the data that exceeded the bounds of reasonable physical expectation. In editing these data, a procedure based on asymptotic singular decomposition (ASD) was developed by the Applications Design Branch at NODC.

Application of this procedure required that the casts contain at least a specific minimum number and density of data points, and, since the ASD method requires rectangular data arrays, was complicated by the fact that depth decreases rapidly as the shoreline is approached. Criteria established for minimum distance between the observation points and minimum cast depth by area were as follows:

| Area | Minimum Data Interval (m) | Minimum Depth (m) |
|---|---|---|
| 1 | 3 | 18 |
| 2 | 2 | 10 |
| 3 | 4 | 40 |
| 4 | 4 | 40 |
| 5 | 8 | 40 |
| 6 | 8 | 80 |
| 7 | 8 | 80 |
| 8 | 8 | 80 |
| 9 | 10 | 100 |
| 10 | 10 | 100 |
| 11 | 10 | 100 |
| 12 | 10 | 100 |

The depth increments thus established the "standard depths" used to build the data matrix for each area. Subsequent processing revealed that even these criteria were too strict. Therefore, casts were incorporated into the data base if they reached at least 40 percent of the minimum established depth, and if sampling frequency was at least 60 percent of the minimum standard. These casts were accepted as input to an interpolation-extrapolation routine, by which linear interpolation between points increased the density of observed points to the minimum standard, and extrapolation extended the casts in depth, based on the vertical space derivative. These restructured casts were then written to a direct access file and processed through the ASD program. Printed plots of ASD coefficients were reviewed, outliers were identified, and casts containing outlying points were then displayed as T-S diagrams on the NODC interactive computer system. Casts that showed large instabilities or unusual values were excluded from further processing. Subsequent compilation of area statistics revealed the continued presence of erroneous data in four areas. All data for these areas were manually reviewed, and erroneous data were eliminated.

# APPENDIX D

## MONTHLY CURRENT VECTORS

Figures D.1 to D.12 show monthly current vectors for the Mid-Atlantic region. Shown also are current constancy, speed, and direction.

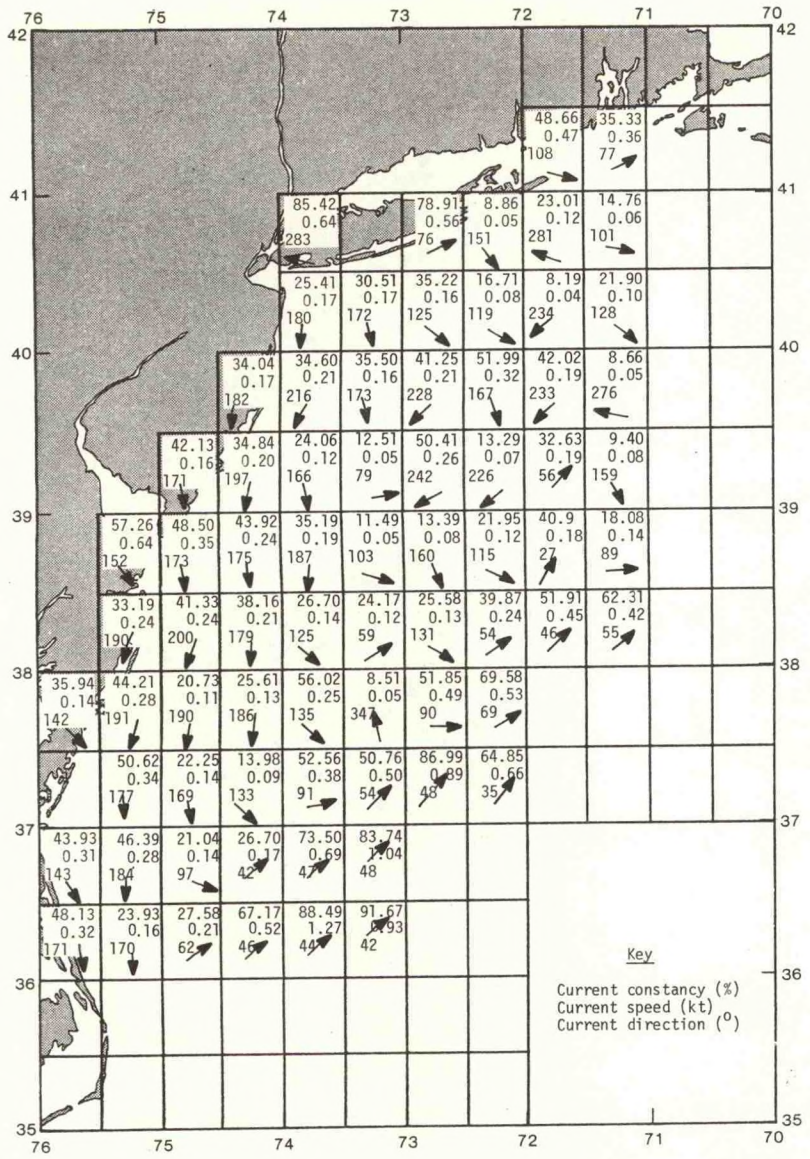


Figure D.1.--January mean current vectors.

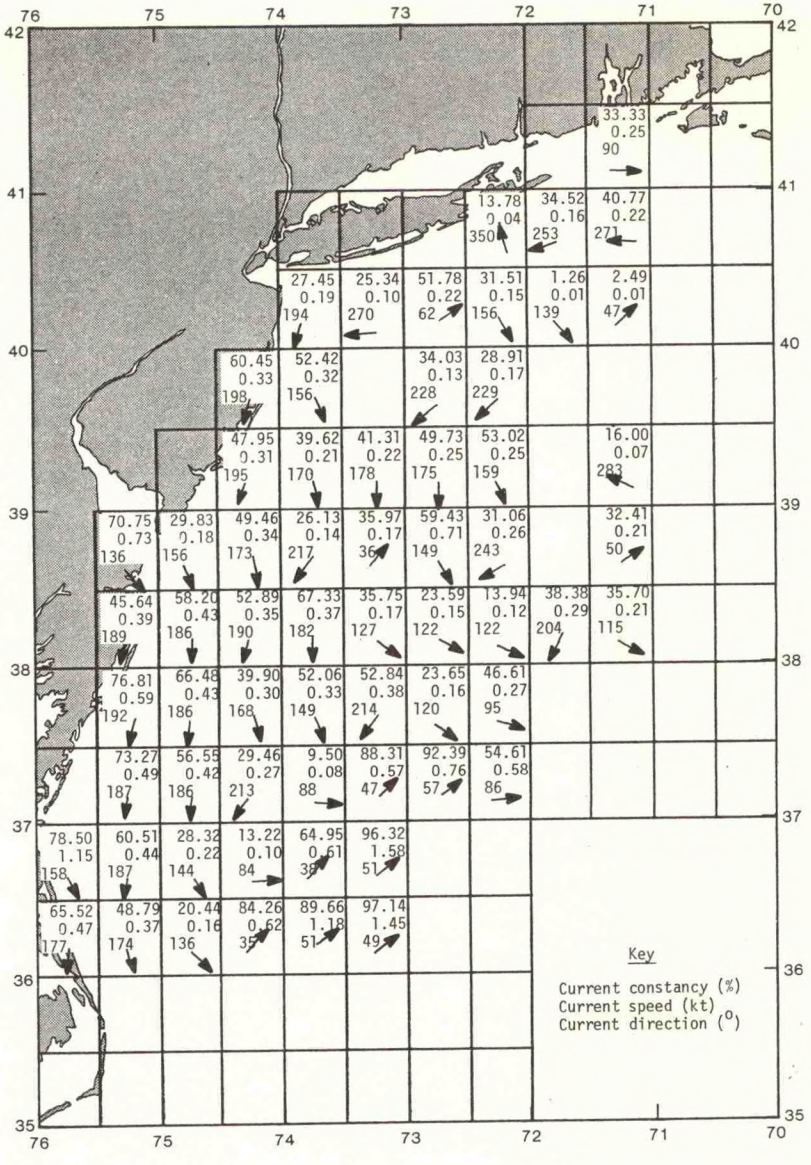


Figure D.2.--February mean current vectors.

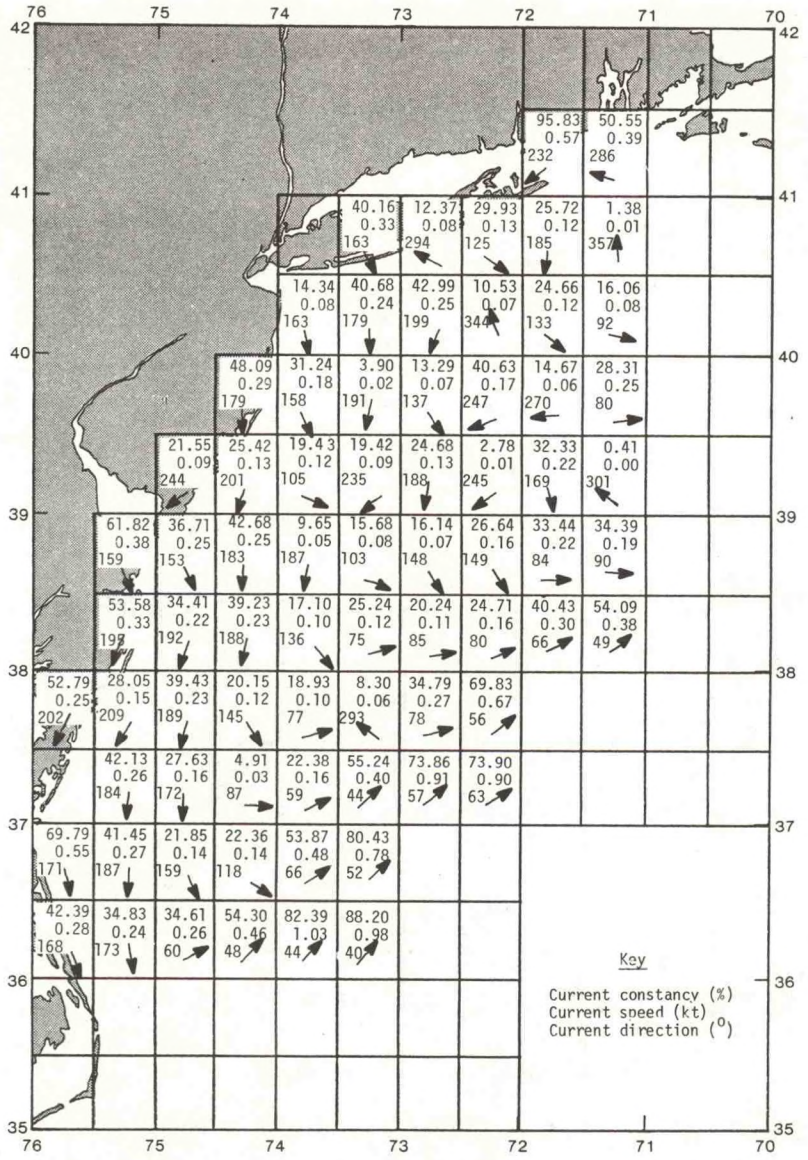


Figure D.3.--March mean current vectors.

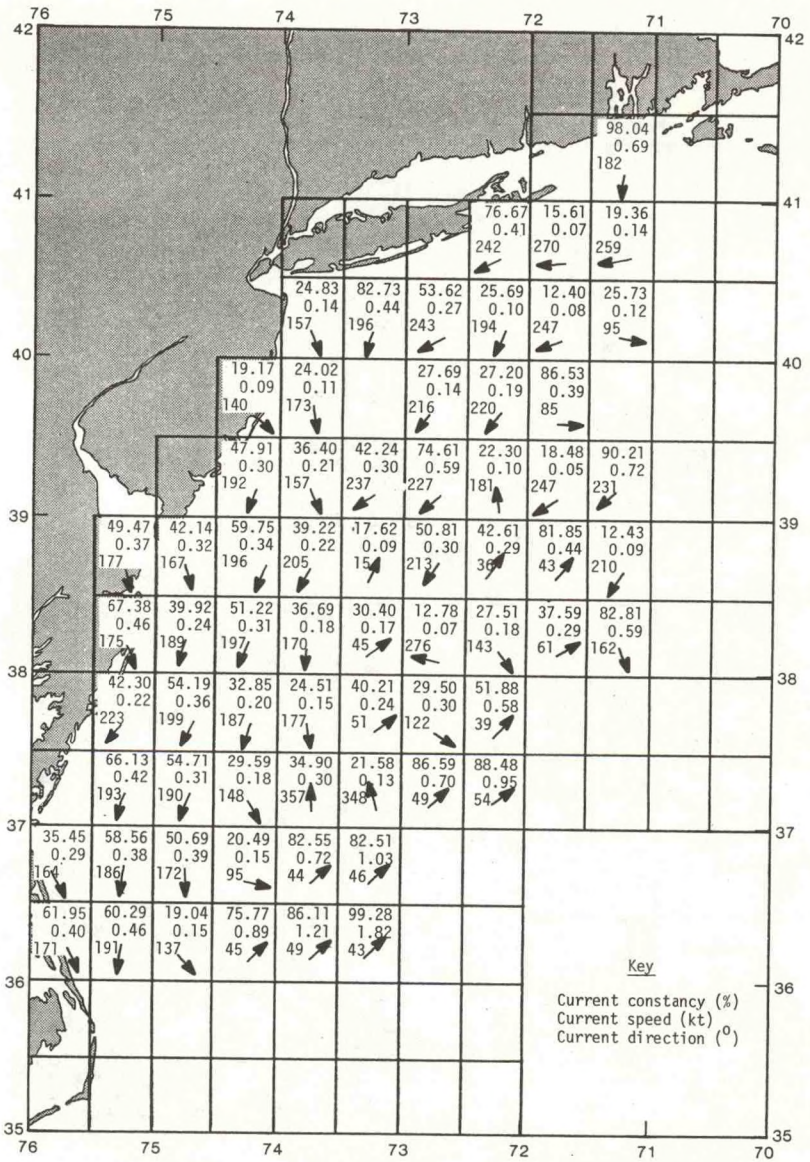


Figure D.4.--April mean current vectors.

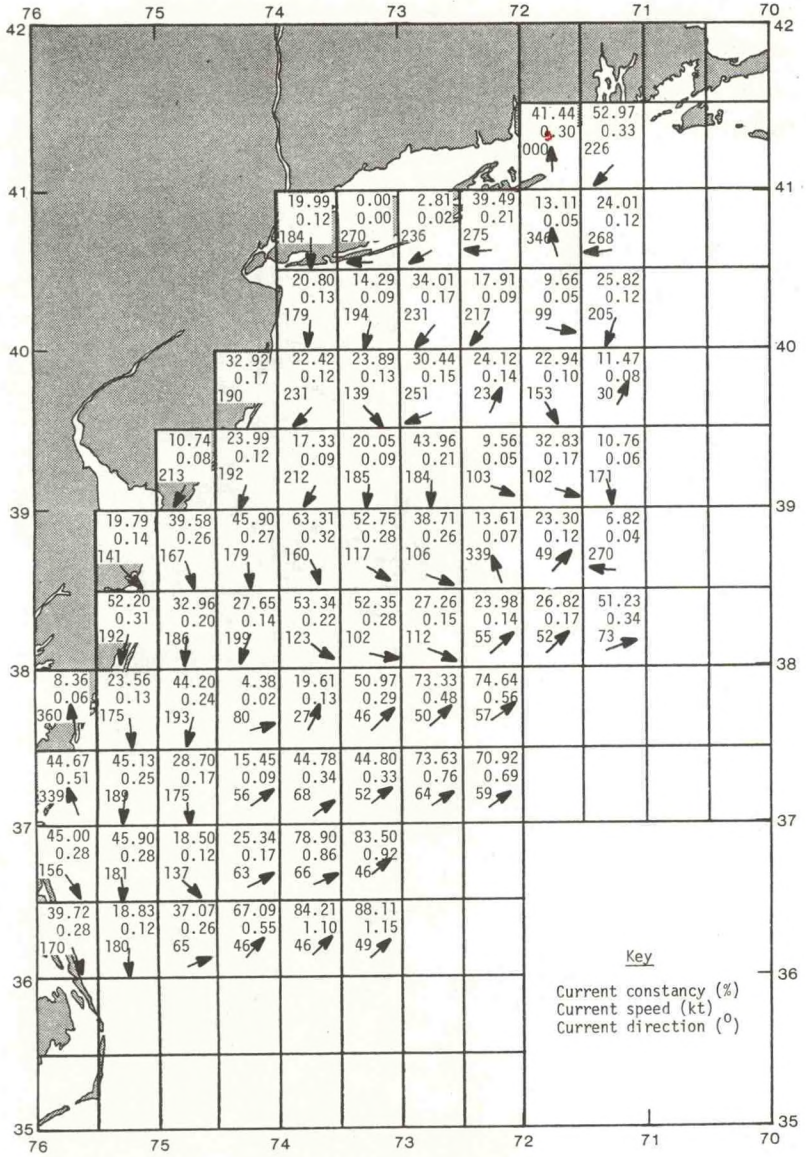


Figure D.5.--May mean current vectors.

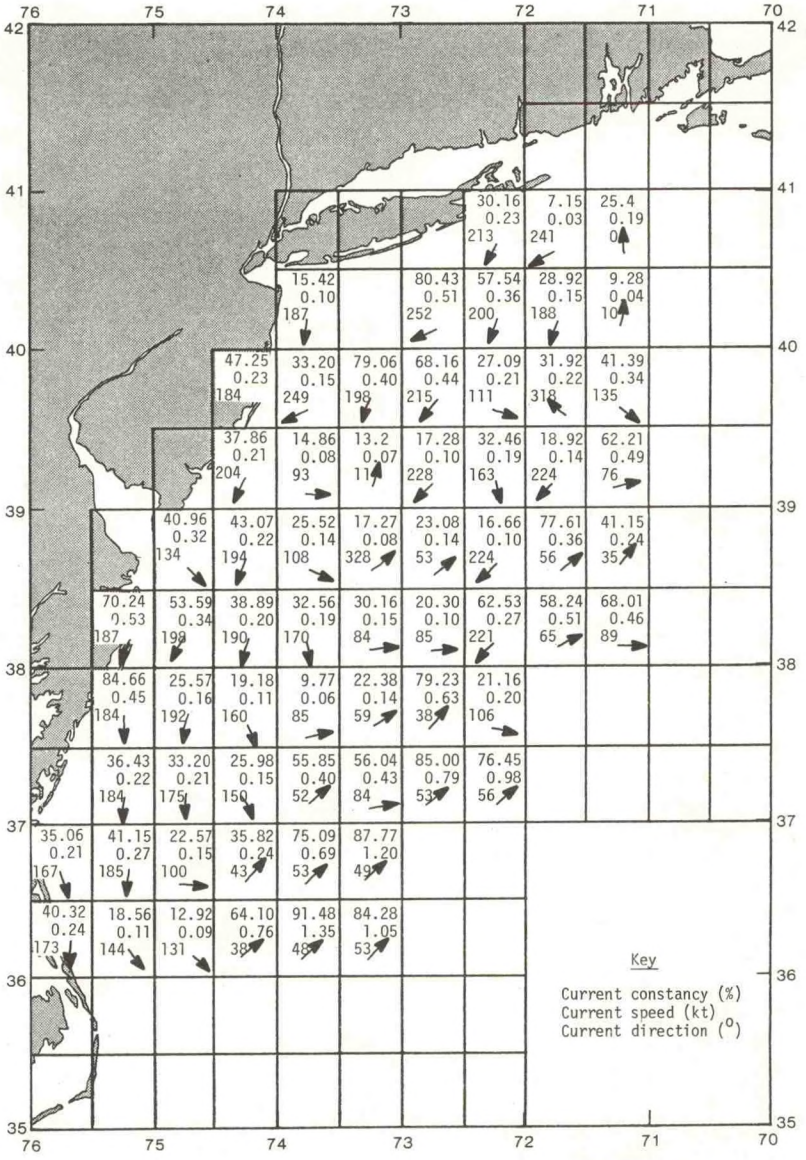


Figure D.6.--June mean current vectors.

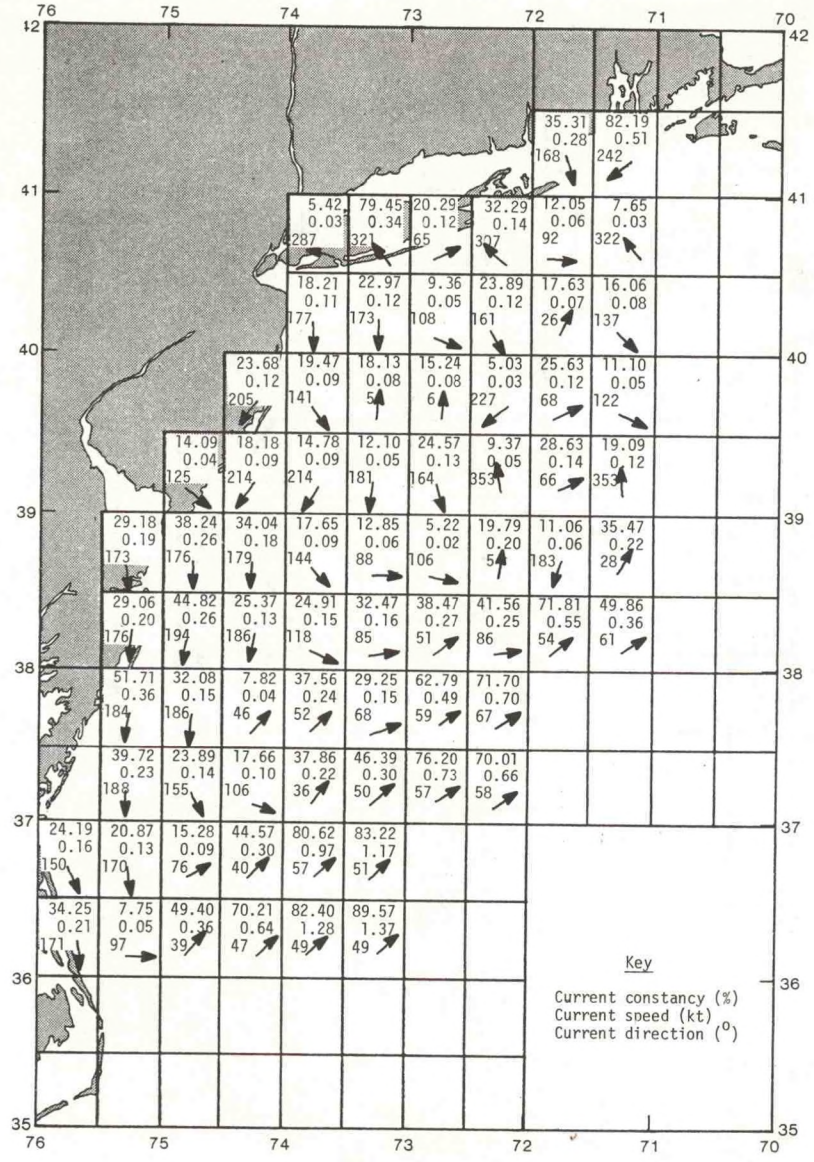


Figure D.7.--July mean current vectors.

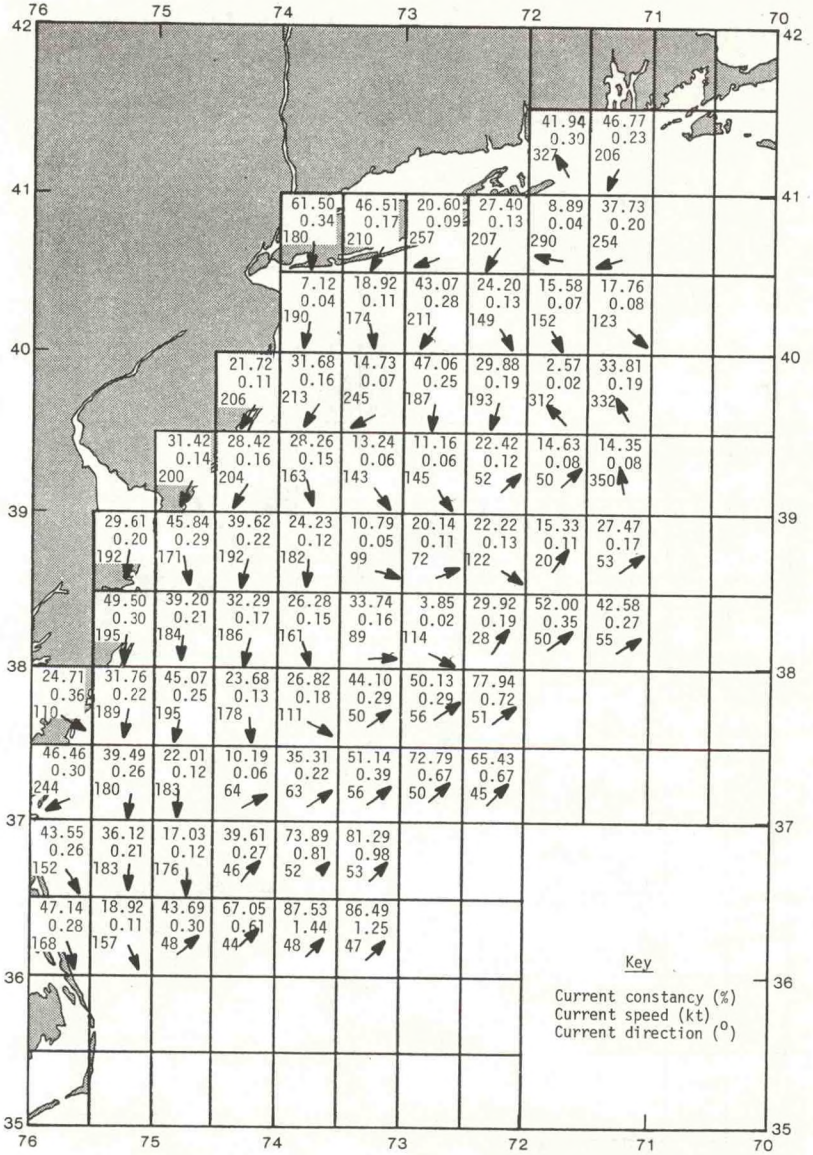


Figure D.8.--August mean current vectors.

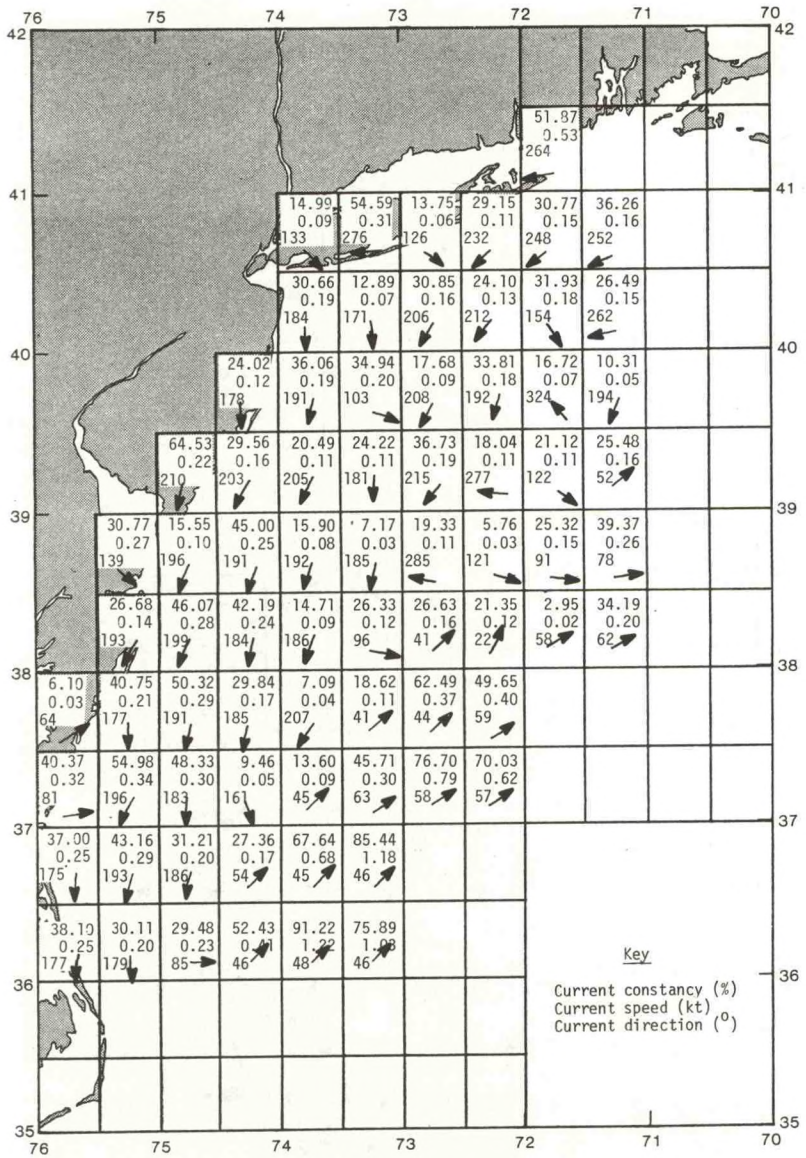


Figure D.9.--September mean current vectors.

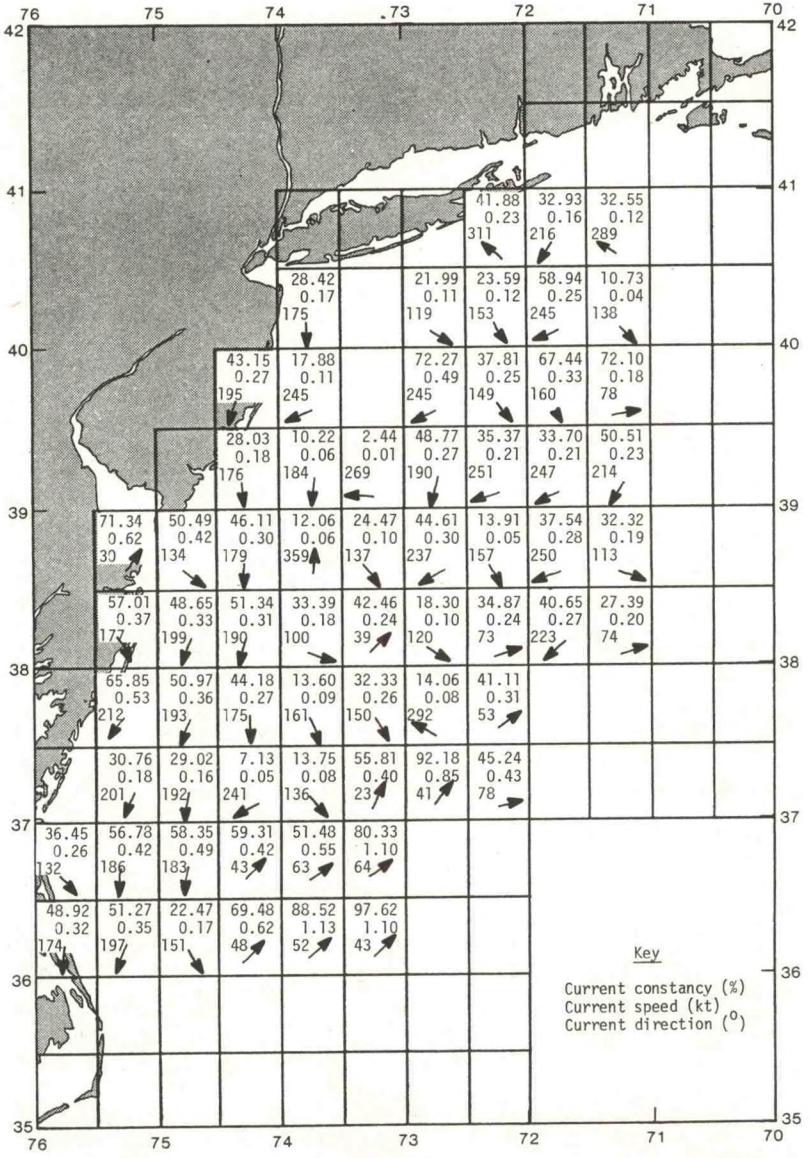


Figure D.10.--October mean current vectors.

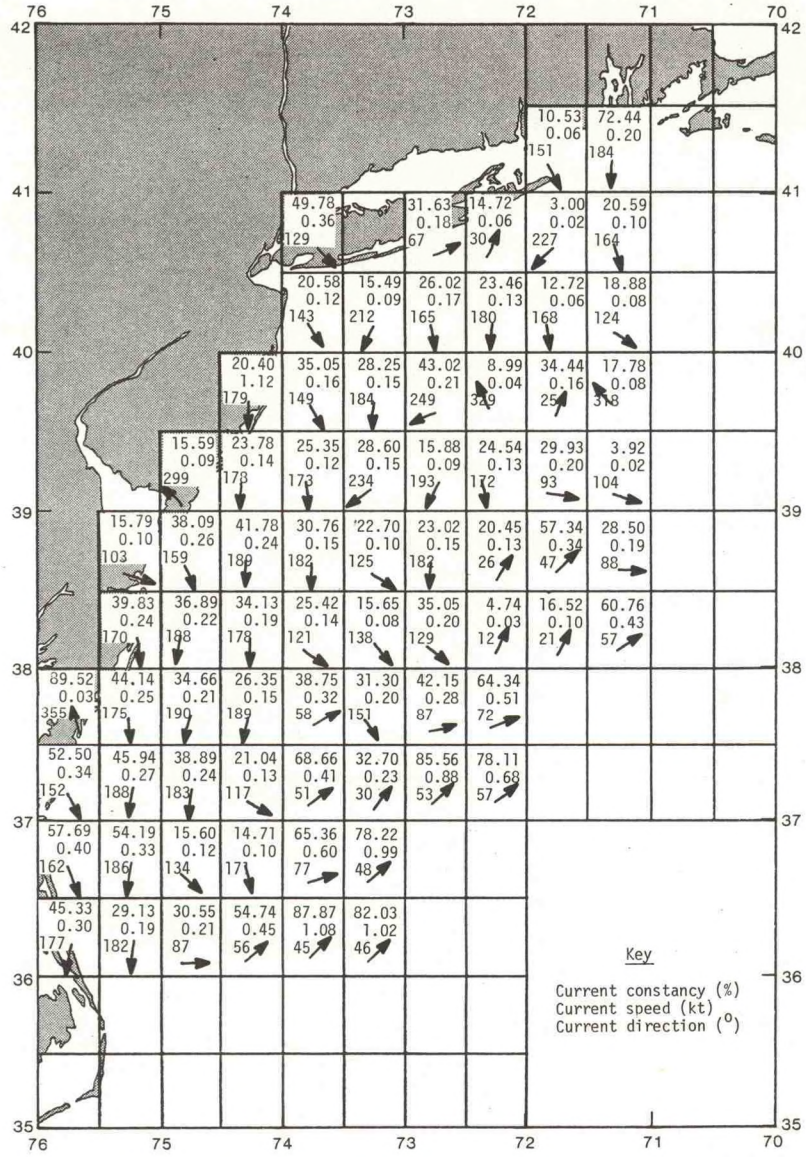


Figure D.11.--November mean current vectors.

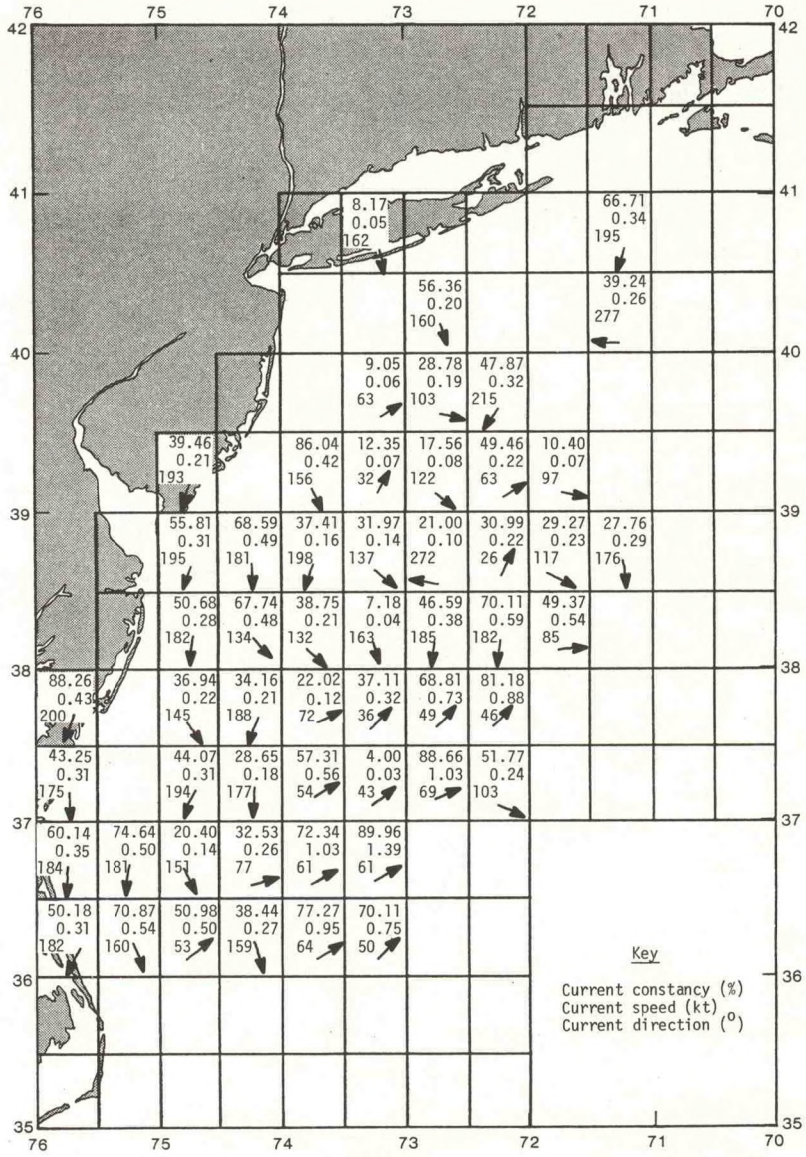


Figure D.12.--December mean current vectors.

# APPENDIX E

## ANTICYCLONIC GULF STREAM EDDIES THAT AFFECT THE MID-ATLANTIC BIGHT

Although the main portion of the Gulf Stream is well removed from the Mid-Atlantic Bight region, periodic, at present unpredictable, perturbations occur in the flow that allow a portion of the Gulf Stream water to break away and drift in the water of the continental slope. These "bubbles" of warm, saline Gulf Stream water were detected as early as the 1930's (Iselin, 1936), but little research was done on them until the mid-1960's. They transfer heat, momentum, and mass from the Gulf Stream, and cause shelf water to intrude over the slope as they pass along the continental edge. With the passage of a "bubble," there is also a modification of current and thermohaline structure over the outer portions of the shelf.

As the Gulf Stream moves into the Atlantic Ocean between Cape Hatteras and the Grand Banks, it has a tendency to develop meanders of varying scale. Observations by Hansen (1969) and Saunders (1971) indicate that when a meander becomes enlarged, the base narrows and tends to close off, leaving, on the north side, a "bubble" of warm, saline water floating in the cooler, less saline water of the continental slope. This "bubble" is commonly referred to as a Gulf Stream "eddy," or, in some cases, a "ring."

Most Gulf Stream eddies are first detected in an area south of Nova Scotia, roughly bounded by 39 to 41°N and 60 to 65°W, although they have occasionally been found farther east, and west, of this area. The life cycle of an eddy is 6 to 12 months as determined both by observation and by theoretical considerations of heat loss and dissipation of kenetic energy (Saunders, 1971). From five to eight anticyclonic eddies are generally found on the north side of the Gulf Stream each year. One to four of them pass into the Mid-Atlantic Bight and remain in the area from 3 and 6 months. The rest of the eddies either dissipate as a result of small water mass discontinuities or become entrained with another Gulf Stream meander.

An eddy normally has an elongated shape and, when newly formed, its long axis is oriented east-west. This axis rotates with time, and has a general north-south orientation when the eddy reaches 70 to 71°W. At this point, the eddy shape becomes more rounded and the elongation is not as pronounced.

The diameter of an eddy varies from about 100 to 200 km at the surface, as determined by airborne radiation thermometer observations and temperature gradients. At the 200-m isobath (an eddy normally being defined by the 15°C isotherm at this isobath), the diameter is 70 to 120 km, with means of 150 and 100 km, respectively. There is a tendency for an eddy to decrease somewhat in size once it crosses 70°W.

When newly formed, eddies drift toward the north and northwest until they are deflected by the topographical influences of the continental shelf. Part of this deflection process is the increased density gradient set up on the

north side of the eddy when the warm, saline Gulf Stream water comes in close proximity with cold and fresh shelf water (21°C and 36 ppt vs. 12°C and 33 ppt). Once deflected, the eddy tends to follow the shelf edge toward the west and southwest until it either dissipates or rejoins the Gulf Stream, most often in an area northeast of Cape Hatteras near 36°N. The speed of movement, i.e., translation of the center, is generally 0.1 to 0.2 kt (5 to 10 cm/s) with accelerated speeds up to 0.4 kt (20 cm/s) west of 70°W (Bisagni, 1976). Figure E.1 shows 13 eddy tracks from September 1970 to October 1976 (U.S. Naval Oceanographic Office, 1970-1976). Shown are the mean and extreme tracks, the maximum shelf area that may be affected by the extreme northern track, the general eddy shape and axis orientation, and the average diameter at the surface and at the 200-m isobath.

Eddies that occur north of the Gulf Stream have an anticyclonic (clockwise) current flow of 0.6 kt to 1.6 kt (30 to 80 cm/s) at the surface, with the maximum current ring (1.2-1.6 kt, or 60-80 cm/s) located approximately midway between the eddy center and the outer edge. The circulation gradually decays with depth, and near the 1000-m isobath the speed has decreased to 0.04 to 0.1 kt (2 to 5 cm/s). Although some circulation may be found as deep as 2000 m, it is so weak as to be negligible.

As an eddy progresses westward along the continental slope, a wedge of shelf water is drawn down behind it along the eastern side. This wedge may extend out over the slope to a distance of 150 km or more. The wedge appears to begin its outward movement over the slope around 70°W, and generally follows the eddy for the remainder of its journey to the Gulf Stream. Figure E.2 shows the track of one eddy center from the time it was first located to the time of its reentry into the Gulf Stream.

Figure E.3 shows the surface current speed and circulation of the eddy tracked in figure E.2, and figure E.4 indicates some of the intrusions of shelf water with the southward progression of the eddy.

The sea-surface temperature associated with the same eddy as determined from airborne radiation thermometer measurements is illustrated in figure E.5. Note the warm water on the western side, the cooler shelf water on the eastern side of the eddy, and the increased temperature gradient around the northern side along the shelf edge.

The vertical temperature structure in an eddy resembles an inverted pyramid, with the isotherms gradually becoming less sharp with depth, being almost flat by 1000 m depth. An idealized vertical temperature field along the transect A-B shown in figure E.5 is illustrated in the inset within the figure.

Figure E.6 is a reproduction of a "Weekly Sea Current Chart" (U.S. Coast Guard Oceanographic Unit, 1976), showing the eddy center, the circulation, and the water mass boundaries. The chart covers the same time frame as figure E.5, and was compiled from aircraft and satellite infrared data. Although there are some differences between the figures, notably in the shelf water intrusion area, figure E.6 is representative of the flow patterns in the Mid-Atlantic Bight.

Between January and July 1974 a rather anomalous eddy passed through the Mid-Atlantic Bight (Chamberlin, 1976). The eddy was unusually close to the continental edge, and also irregular in its movement in the region south of New England near 39°20'N, 71°W from early March until mid-May. The closeness of its path to the continental edge affected water temperatures over a larger portion of the shelf and slope and, because of its very slow forward motion, for a longer period of time than is usual. The effect was a rise in the temperature of the water column from a few to several degrees Celsius over the continental slope and outer shelf area.

In summary, Gulf Stream eddies affect the outer portion of the continental shelf by modifying current flow and thermohaline distribution. Although eddies tend to follow the pattern outlined, each eddy has its own characteristics and must be treated on an individual basis.

The clockwise circulation around the eddies and the offshore flux of shelf water behind them would tend to move spilled pollutants out over the slope and away from the coast. If a pollutant became trapped in the eddy itself, the length of time involved in the eddy movement would afford a long period for degradation to occur, and the probability of the pollutant remaining with the eddy until it reaches the Gulf Stream is high. This would result in a movement away from the coast and a reduction of adverse environmental impact.

## References

Bisagni, James J. 1976. Passage of anticyclonic Gulf Stream eddies through deepwater dumpsite 106 during 1974 and 1975. NOAA Dumpsite Evaluation Report 76-1, National Oceanic and Atmospheric Administration, U.S. Department of Commerce, pp 1-39.

Chamberlin, J. L. 1976. Bottom temperatures on the continental shelf and slope south of New England during 1974. Marine Resources Monitoring, Assessment, and Prediction Program (MARMAP) Contribution No. 104, National Marine Fisheries Service, National Oceanic and Atmospheric Administration, U.S. Department of Commerce, Sec. 18, pp. 18-2 to 18-5.

Hansen, Donald V. 1970. Gulf Stream meanders between Cape Hatteras and the Grand Banks. Deep Sea Research, Vol. 17, No. 3, pp 495-511.

Iselin, C. O'D. 1936. A study of the circulation of the Western North Atlantic. Papers Physical Oceanography and Meteorology 4(4), pp 1-101.

Saunders, P. M. 1971. Anticyclonic eddies formed from shoreward meanders of the Gulf Stream. Deep Sea Research, Vol. 18, No. 12, pp 1207-1219.

U.S. Coast Guard Oceanographic Unit, 1976. Weekly Sea Current Charts.

U.S. Naval Oceanographic Office - National Oceanic and Atmospheric Administration, Gulfstream, 1966-1976.

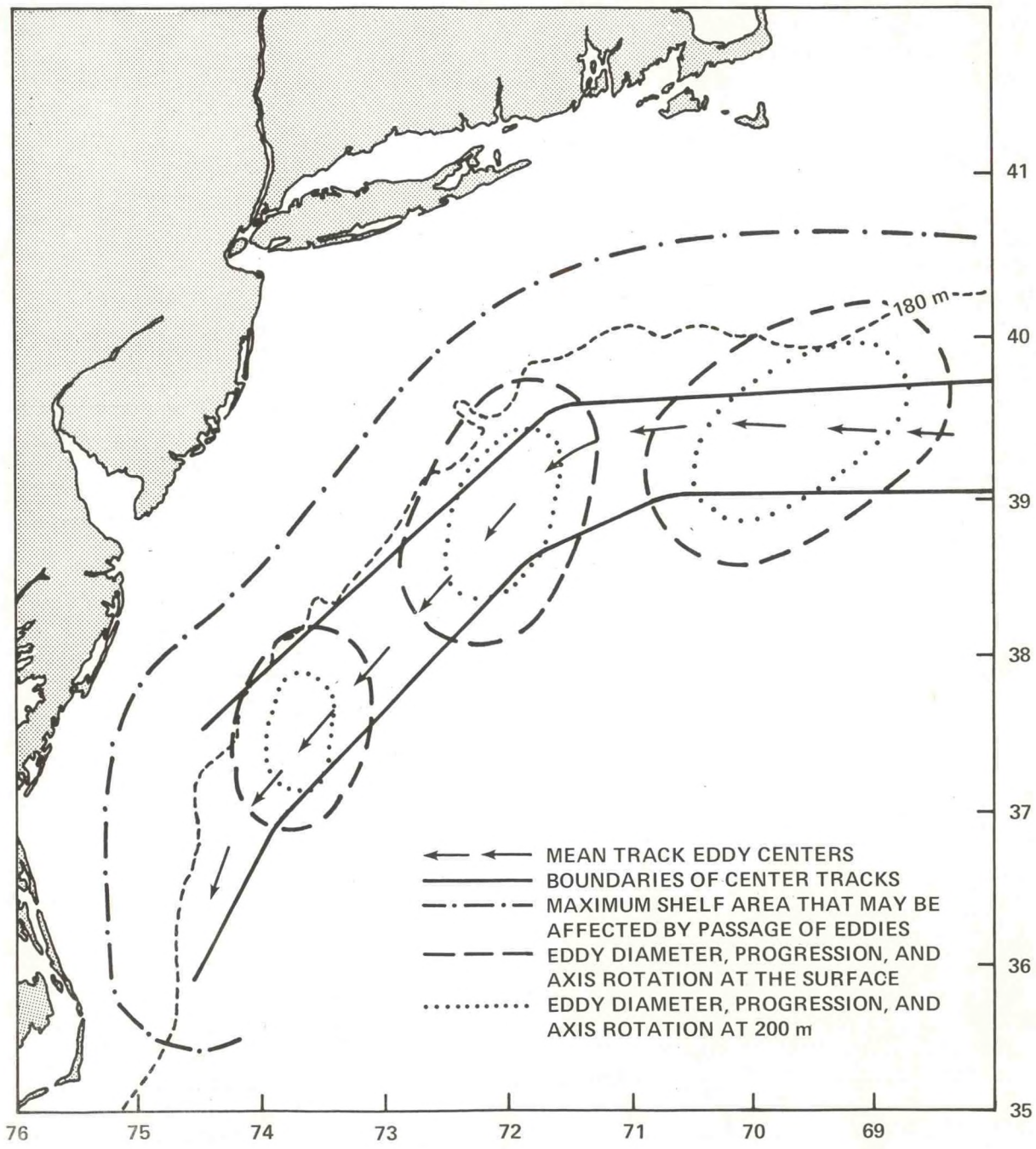


Figure E.1.--Gulf Stream eddy tracks, based on 13 tracks from September 1970 to October 1976.

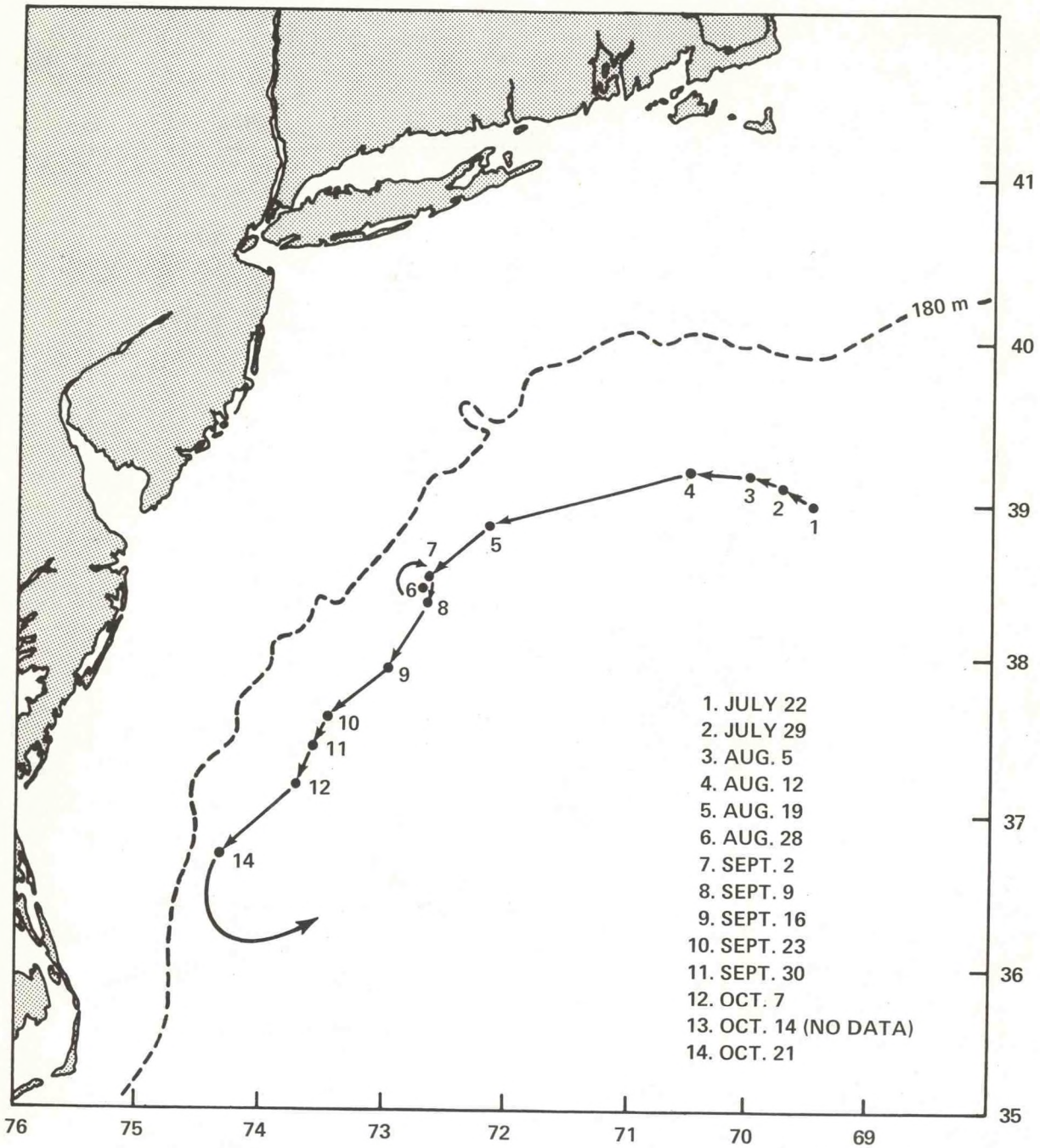


Figure E.2.--Gulf Stream eddy track, showing successive positions of the eddy center from July to October 1976.

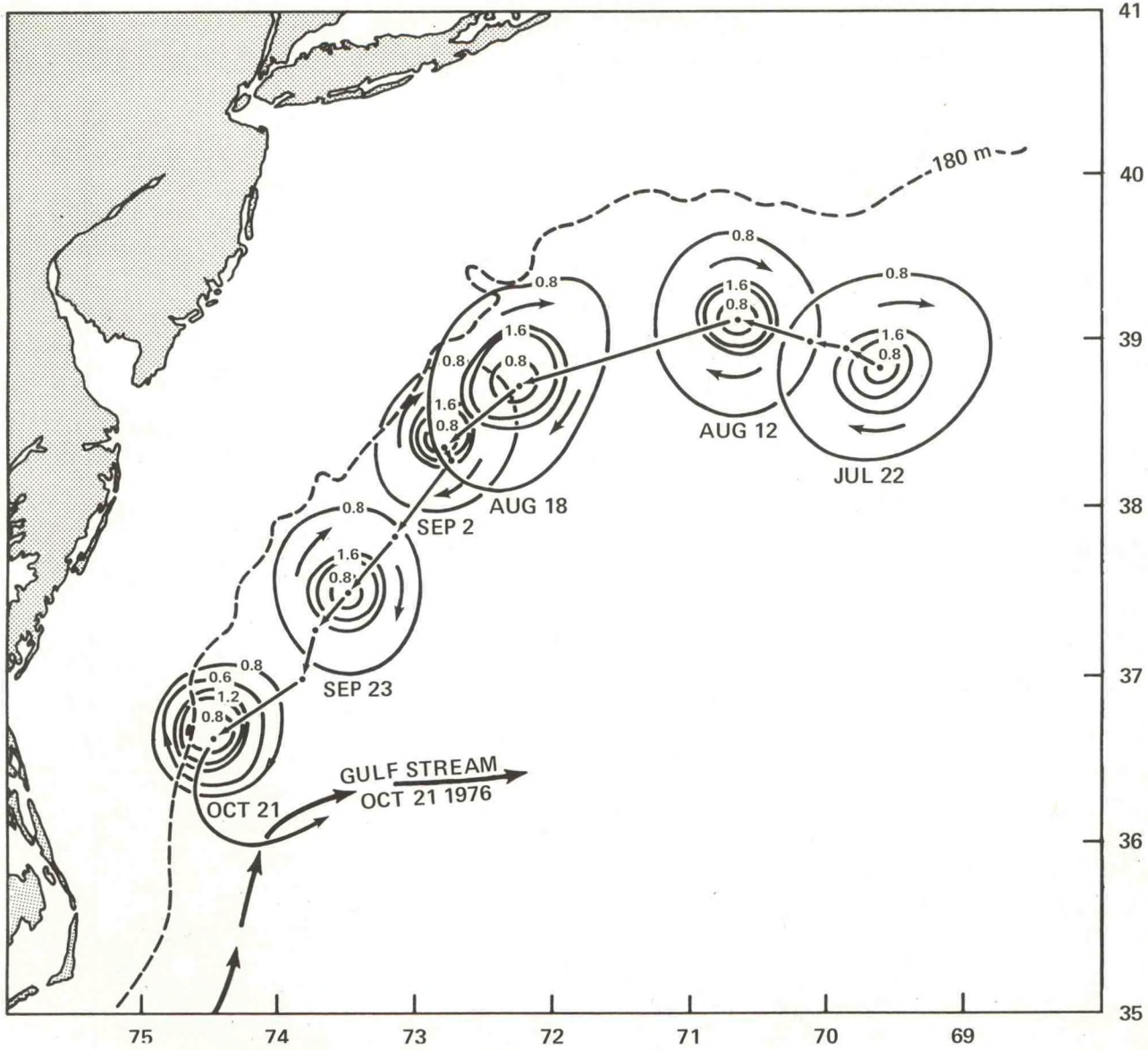


Figure E.3.--Surface current speed (kt) and circulation associater with the eddy in figure E.2.

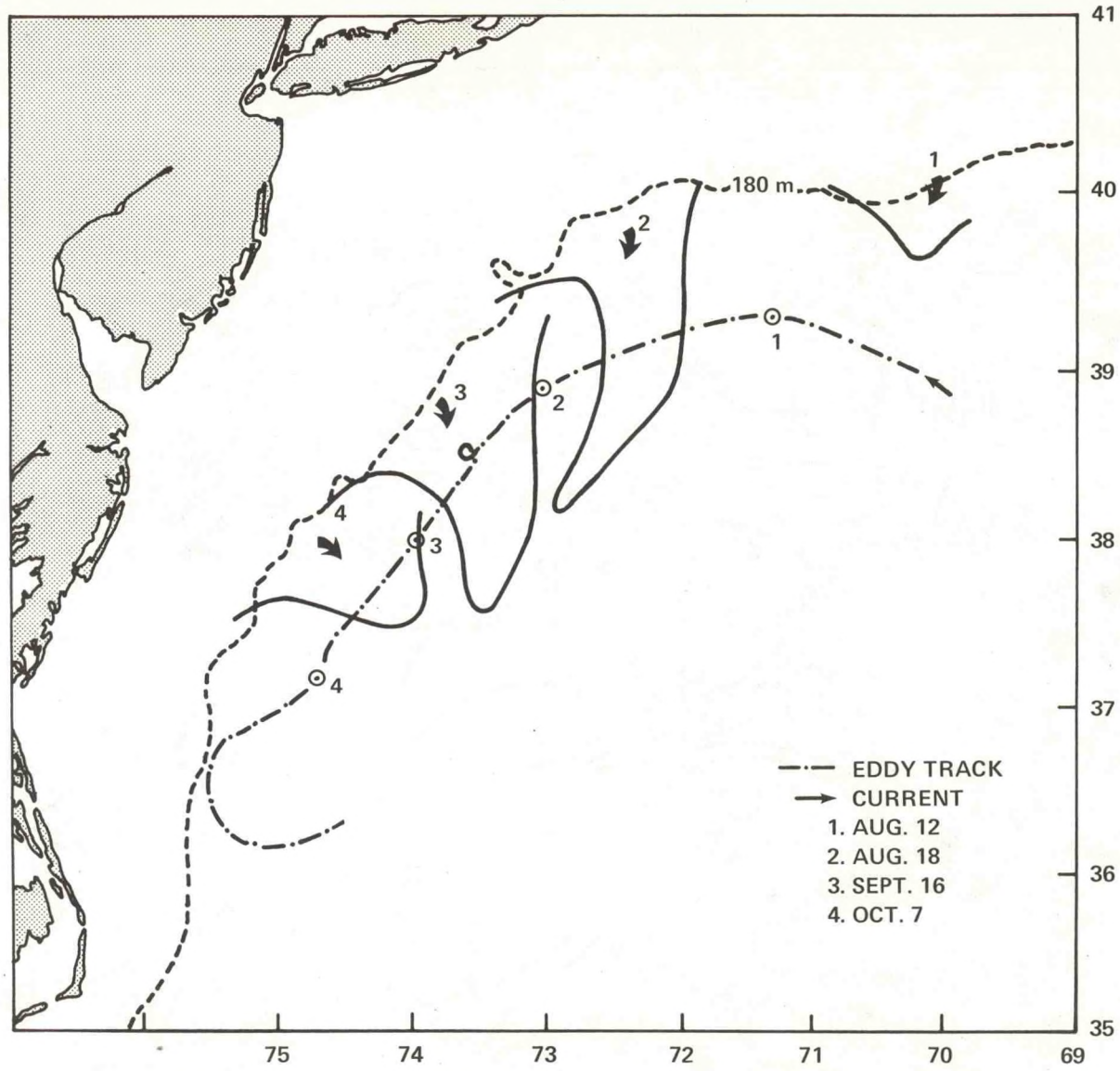


Figure E.4.--Intrusion of shelf water over the slope associated with the eddy in figure E.2.

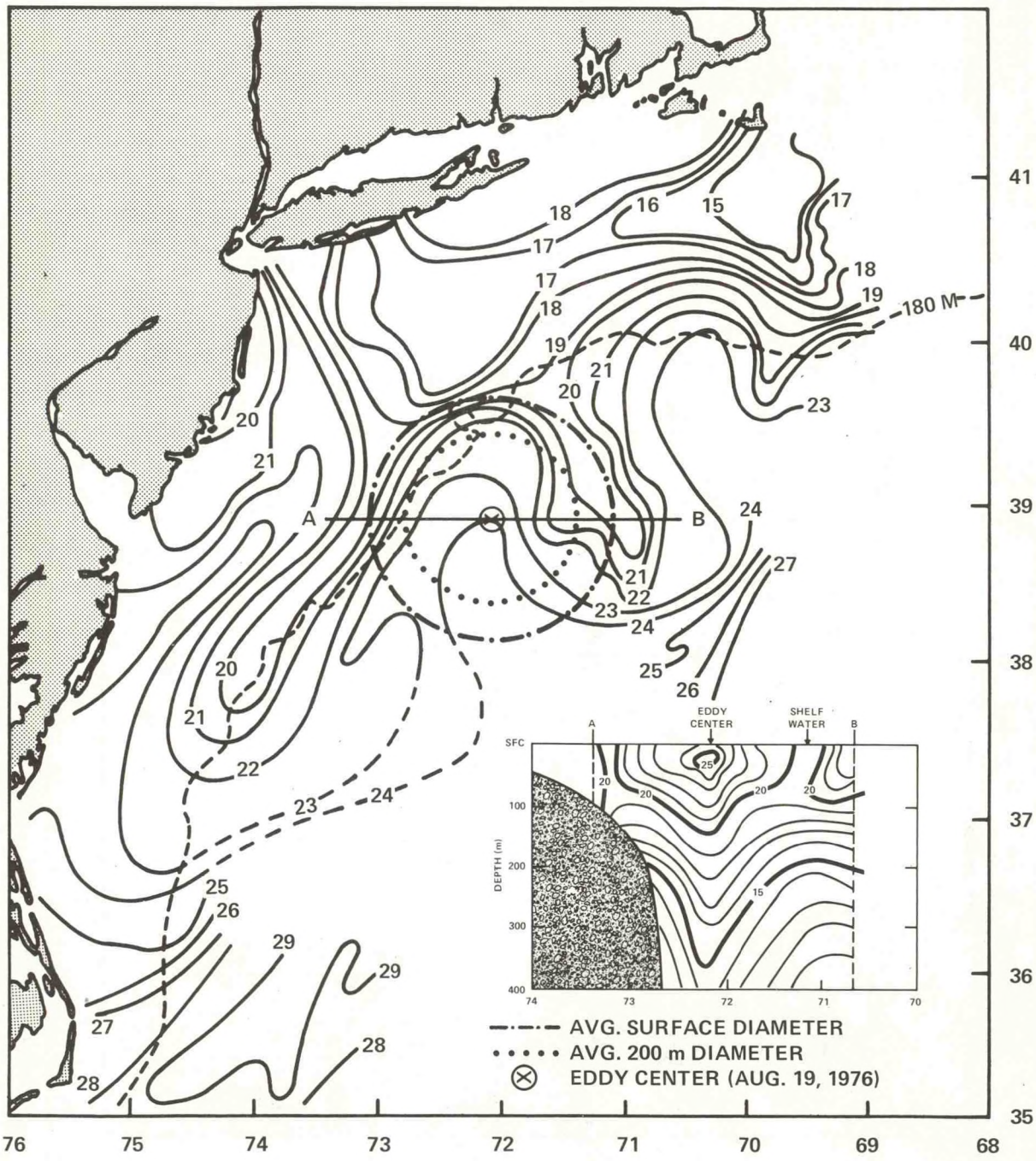


Figure E.5.--Sea-surface isotherms (°C), August 17-19, 1976, with eddy center and average surface and 200-m diameters. An idealized vertical temperature structure along transect A-B is shown in the inset.

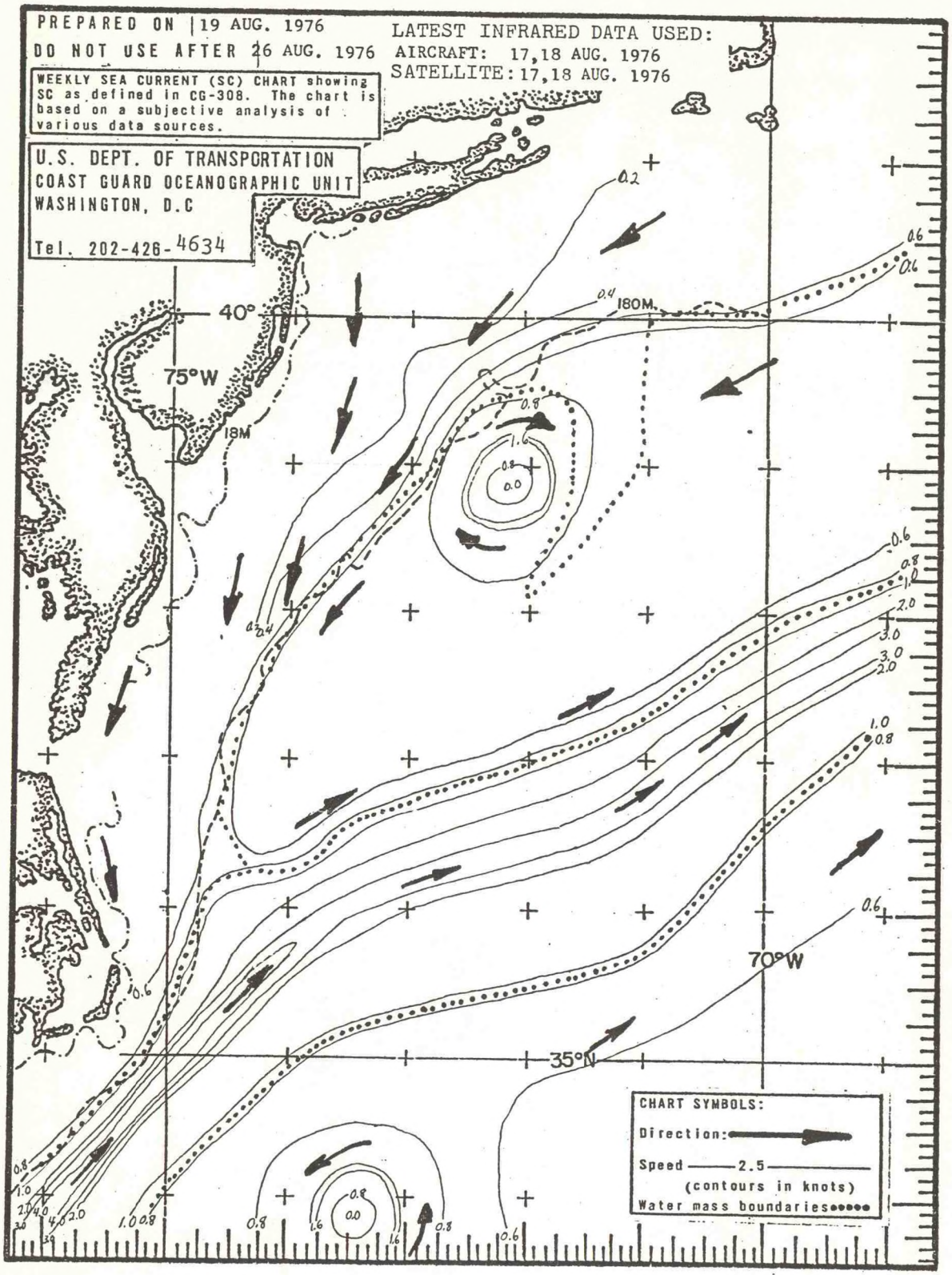


Figure E.6.--Sea current chart as published weekly by the U.S. Coast Guard.

☆ U. S. GOVERNMENT PRINTING OFFICE : 1977--261-238/410

NOAA--S/T 77-2804